British Geological Survey
NATURAL ENVIRONMENT RESEARCH COUNCIL

The Mersey estuary: sediment geochemistry

Coastal Geoscience and Global Change Impacts Programme
Research Report RR/10/02

BRITISH GEOLOGICAL SURVEY

RESEARCH REPORT RR/10/02

Keywords

Estuaries, geochemistry, contamination, sediment, geology, hydrography, bathymetry.

Front cover

Collection of cores in the Mersey estuary (P746939).

Bibliographical reference

Ridgway, J, Bee, E, Breward, N, Cave, M, Chenery, S, Gowing, C, Harrison, I, Hodgkinson, E, Humphreys, B, Ingham, M, Jarrow, A, Jenkins, G, Kim, A. Lister R, Milodowski, A, Pearson, S, Rowlands, K, Spiro, B, Strutt, M, Turner, P and Vane, C. 2012. The Mersey estuary: sediment geochemistry. *British Geological Survey Research Report*, RR/10/02.

ISBN 978 0 85272 711 9

The Mersey estuary: sediment geochemistry

J Ridgway, E Bee, N Breward, M Cave, S Chenery, C Gowing, I Harrison, E Hodgkinson, B Humphreys, M Ingham, A Jarrow, G Jenkins, A Kim, R T Lister, A Milodowski, S Pearson, K Rowlands, B Spiro, M Strutt, P Turner, and C Vane

Keyworth, Nottingham British Geological Survey 2012

BRITISH GEOLOGICAL SURVEY

The full range of our publications is available from BGS shops at Nottingham, Edinburgh, London and Cardiff (Welsh publications only) see contact details below or shop online at www.geologyshop.com

The London Information Office also maintains a reference collection of BGS publications, including maps, for consultation.

We publish an annual catalogue of our maps and other publications; this catalogue is available online or from any of the BGS shops.

The British Geological Survey carries out the geological survey of Great Britain and Northern Ireland (the latter as an agency service for the government of Northern Ireland), and of the surrounding continental shelf, as well as basic research projects. It also undertakes programmes of technical aid in geology in developing countries.

The British Geological Survey is a component body of the Natural Environment Research Council.

British Geological Survey offices

BGS Central Enquiries Desk
Tel 0115 936 3143 Fax 0115 936 3276
email enquires@bgs.ac.uk

Environmental Science Centre,
Keyworth, Nottingham NG12 5GG
Tel 0115 936 3241 Fax 0115 936 3488
email sales@bgs.ac.uk

Murchison House, West Mains Road,
Edinburgh EH9 3LA
Tel 0131 667 1000 Fax 0131 668 2683
email scotsales@bgs.ac.uk

BGS London, Natural History Museum, Cromwell Road,
London SW7 5BD
Tel 020 7589 4090 Fax 020 7584 8270
Tel 020 7942 5344/45 email bgslondon@bgs.ac.uk

Columbus House, Greenmeadow Springs,
Tongwynlais, Cardiff CF15 7NE
Tel 029 2052 1962 Fax 029 2052 1963

Maclean Building, Crowmarsh Gifford,
Wallingford OX10 8BB
Tel 01491 838800 Fax 01491 692345

Geological Survey of Northern Ireland,
Colby House, Stranmillis Court, Belfast BT9 5BF
Tel 028 9038 8462 Fax 028 9038 8461
www.bgs.ac.uk/gsni/

Parent Body

Natural Environment Research Council, Polaris House,
North Star Avenue, Swindon SN2 1EU
Tel 01793 411500 Fax 01793 411501
www.nerc.ac.uk

Website www.bgs.ac.uk
Shop online at www.geologyshop.com

Acknowledgments

In addition to the BGS staff listed as authors, many others have contributed to this study of the Mersey estuary. Members of staff from the sample preparation and analytical laboratories, cartography and the library are thanked for their hard work behind the scenes. During the sample collection programme Dr P S Balson, Dr D Brew, D Entwisle, P M Green, Dr J G Rees and Dr P Wilby helped with the fieldwork in the estuary.

The sample collection programme would not have been possible without the assistance of the Environment Agency at Warrington who provided invaluable advice and information, the means of accessing the intertidal and tidal reaches of the estuary and also temporary storage space for cores and samples. The captain and crew of the Coastal Guardian are thanked for their help in the grab sampling of bottom sediments and in particular we would like to acknowledge the major contributions made by Dr P D Jones and Mr K Sharpes in the collection of cores using the EA launch and hovercraft. The EA also made available the LIDAR data on which Figure 1.5 is based.

Earlier versions of the report were reviewed by Ms F Fordyce of BGS, Dr A J Plater of the University of Liverpool and Dr J Kirby of Liverpool John Moores University. Their detailed critiques of the report are gratefully acknowledged, but any remaining shortcomings are the responsibility of the authors.

Contents

TABLES

PLATES

FIGURES

Summary

This report describes a study of the geochemistry of the Mersey estuary carried out between April 2000 and December 2002. The study was the first in a new programme of surveys of the geochemistry of major British estuaries aimed at enhancing our knowledge and understanding of the distribution of contaminants in estuarine sediments.

The report first summarises the physical setting, historical development, geology, hydrography and bathymetry of the Mersey estuary and its catchment. Details of the sampling and analytical programmes are then given followed by a discussion of the sedimentology and geochemistry. The chemistry of the water column and suspended particulate matter have not been studied, the chief concern being with the geochemistry of the surface and near-surface sediments of the Mersey estuary and an examination of their likely sources and present state of contamination.

1 Introduction

The Mersey estuary drains into Liverpool Bay in the south-east of the eastern Irish Sea (Figure 1.1). Its catchment covers some 5000 km^2 of Merseyside, Greater Manchester, Cheshire, Derbyshire and Lancashire and includes the major conurbations of Manchester and Merseyside, with the port of Liverpool lying on its north-eastern bank, near the estuary mouth. Along or adjacent to the banks of the estuary, major manufacturing centres are found at Liverpool, Birkenhead, Bromborough, Ellesmere Port, Stanlow, Runcorn, Widnes and Warrington. The Mersey catchment has a population of over 5 million people and in excess of 830 000 people live within 1 kilometre of the estuary shoreline (NRA, 1995). Further inland the industrial centres of south-east Lancashire, including Manchester, Rochdale, Bury, Bolton, Stockport and St Helens, are drained by rivers which feed into the Mersey. With such an industrialised and urbanised drainage basin, it is not surprising that the Mersey estuary is widely regarded as one of the most polluted estuaries in Europe (NRA, 1995; Jones, 2000).

The general topography of the Mersey basin reflects its underlying geology. The Mersey valley is eroded in relatively low-lying Triassic marls and sandstones. The majority of the area, except in Liverpool and some parts of the Wirral, is covered by glacial till and postglacial alluvial deposits, which serve to mantle the underlying geology and produce a smooth or gently undulating topography. The Wirral peninsula has a generally smooth topography, with low hills in the north and west, reaching 65 m at Bidston Hill and 110m at Poll Hill. On the Liverpool side of the Mersey, the land rises smoothly to about 50 m above sea level (Wedd et al., 1923) (Figures 1.2 and 1.3).

Although the Environment Agency (EA) and the National Monitoring Programme (NMP) carry out monitoring work on estuarine contamination in England and Wales, the overall distribution of contaminants, thickness of contaminated sediment and relationships to the sedimentary regime and naturally varying background concentrations are inadequately documented. A systematic survey approach, such as that described here for the Mersey, provides a way to remedy these deficiencies and aid the authorities concerned in compliance with international agreements, such as the OSPAR Action Plan 1998–2003 with regard to Hazardous Substances (OSPAR, 1998) and the EU Water Framework Directive, which sets out standards for water quality and aquatic habitats.

1.1 ORIGIN OF THE ESTUARY

The present-day Mersey river system has developed since the retreat of the Devensian ice sheet. Preglacial drainage of the area was modified by glacial activity, with some channels becoming in-filled and new rock-cut channels becoming established. It is generally accepted that the major drainage channels of the region were established during the Tertiary, and subsequently modified during the Pleistocene, with the Mersey/Weaver system being incised into the till-covered plain by meltwater streams. The modern-day rivers broadly followed the glacially modified pattern in the upland areas, with a new system cut into the lowland tills. In addition to the River Mersey itself, a number of rivers flow into the estuary. Inputs to the northern side of the estuary include Sankey Brook and Ditton Brook. The southern side of the estuary has inputs from: the Manchester Ship Canal (including River Weaver), Holpool Gutter, River Gowy, Dibbinsdale Brook and River Birket (NRA, 1995) (Figure 1.2). The estuary was formed as sea level rose to near its present level by about 5000 BP (Harvey, 1985). Geomorphologically, the early Holocene saw gradual stabilisation of an unstable postglacial landscape, with destabilisation reintroduced during the later Holocene under the increasing influence of human activity.

The origin of the Mersey estuary has been a topic of considerable debate over the past 40 years. Its unusual banana-shaped profile does not conform to the typical funnel shape common to estuaries in England and Wales (e.g. Severn, Thames). Therefore it is unlikely that its present course is a purely a result of marine incursion into incised valleys. Present-day channel morphology probably reflects the influence of the pre-Pleistocene bedrock geology and the Pleistocene deposits.

In the Merseyside–Dee region, boreholes have shown that the Carboniferous and Permo-Triassic basement rocks that underlie the Pleistocene deposits have a very uneven topography, yielding a number of deep ungraded channels. Within these channels the glacial deposits locally reach thicknesses of up to 92 metres (Bathurst and Brenchley, 1975).

Gresswell (1964) initially postulated that these features, and thus the morphology of the Mersey and Dee estuaries, are a result of the formation of "ice-ways"—"ice eroded features that result from the escape of ice from a lowland ice-sheet when it is otherwise hemmed in by more elevated ground." He proposed that these features formed because of the movement of ice from the Irish Sea into the Cheshire–Shropshire plain, their pathways cutting deep valleys into the Permo-Triassic bedrock.

However, Howell (1973) reinterpreted the subdrift features to represent a number of erosional events during the Tertiary and Quaternary. The river-like distribution of these valley systems suggests that they are of fluvial origin. However, when the valleys in the subdrift surface are examined in detail, fluvial processes alone cannot account for their origin. The longitudinal profiles of the valleys are ungraded, with depths approaching nearly 92 m below present-day sea level. Low eustatic sea levels were experienced during the Pleistocene glaciations throughout the world, falling by more than 100 m. Despite this, the presence of rock barriers at about 30 m below present sea level places an important constraint on the form of any graded profile upstream of these barriers (Howell, 1973). Therefore, although it was very likely that parts of the original river systems were eustatically rejuvenated during one or more of the Pleistocene retreats of the Irish Sea, the areas of the subdrift surface that reach depths lower than 30m must be of a different origin. During certain parts of the Pleistocene, glaciers would have been present over the area. Meltwater flowing beneath the glacier would have led to the formation of tunnel valleys, which in turn would have channelled within existing valleys, causing local scouring of the bedrock. The Triassic sandstones are known to be

friable and would therefore have been very susceptible to scouring.

Howell therefore proposes that the subdrift features that have influenced the present day morphology of the Mersey estuary have formed through of a combination of erosional events, thus accounting for the unique profile of the Mersey estuary.

1.2 URBAN DEVELOPMENT, CONSTRUCTION, RECLAMATION AND HABITATS

1.2.1 Human influence: AD 1000 to AD 1700

The development of the landscape of the Mersey basin prior to the Industrial Revolution resulted from the interaction of social, demographic, climatic and economic factors (Philpott and Lewis, 1999). By the mid 17th century, the landscape of the basin and the counties of Lancashire and Cheshire had become significantly modified by human activity, and heavily partitioned. The Mersey basin at the time of Domesday (about AD 1086) had few villages in the classic sense of a nucleated settlement with church and manor house, instead largely consisting of singular farms and small hamlets. The Roman settlement of Chester formed the only major town in the region, although townships were established in some areas, due to their local importance as administrative centres. Each township consisted of variable proportions of waste, woodland, meadow and arable land. Total population was probably less than 10 000 in each county (Philpott and Lewis, 1999).

The late 11th to mid 14th century, saw a major growth in population, mirroring that experienced throughout Britain during this time, with a three-fold population growth at Burton in Wirral, presumably reflecting growth elsewhere throughout the region (Philpott and Lewis, 1999). Existing settlements increased in size, with new settlement developing on the edges of existing townships. A rise in cash over service-based transactions stimulated trade, exchange, and the establishment of towns. Although they were relatively small in extent (with Liverpool having no more than seven streets by the 1660s (Nicholson, 1981), and retaining a strong agricultural component), towns played a major role in the development of the medieval and postmedieval landscape (Philpott and Lewis, 1999).

Settlement and population growth probably reached a maximum in the late 13th and early 14th centuries, declining thereafter because of a sudden climatic worsening, a series of bad harvests and disease. Following the outbreak of bubonic plague during AD 1348/9 (which may have reduced the population by as much as 25–30 per cent (Philpott and Lewis, 1999)), less labour-intensive pastoral farming became more widespread. Climate change also had an impact on settlement patterns and farming practices in low-lying coastal and riverine regions. Dune instability, for example, led to inundation and impoverishment of cultivatable soil with sand. Land was lost to the sea in the early 13th century on the Wirral and at Ince, whilst on the Sefton coast, the settlement of Argarmeols had disappeared by AD 1346 The Cistercian abbey at Stanlow, founded in AD 1178, was subjected to several inundations and finally moved to Whalley in AD 1296 (Philpott and Lewis, 1999). Severe flooding was recorded along the Mersey marshes and Formby coast during the 14th and 15th centuries.

By the beginning of the 18th century the landscape was heavily enclosed, with pastoral farming dominant and Cheshire having an established reputation as a dairying area. The majority of the population still depended on agriculture for their livelihood, although industries, such as clay digging for pottery and coal mining, which were to become hugely important later during the 18th and 19th centuries, were already underway. These industries began as part-time activities for smallholders during medieval and postmedieval times but with little associated impact on the landscape, only gaining significant capital investment during the 17th century. Salt was already an established urban-based industry with extensive trade networks, production of which was fuelled during the 17th century by the demand from dairying and the provision of salt food for shipping. The textile industry was also strongly emerging in south-east Lancashire at this time, although the development of these industries was hampered to some extent by poor communications until improvements to major road routes and the development of the canal network in the second half of the 18th century.

1.2.2 Industrial development

By 1700, the stage was set for the major changes of the Industrial Revolution. Key to the early development was the application of waterpower to processes other than flour milling (Jarvis and Reed, 1999). The production of silk and cotton in the Cheshire and Lancashire mills were the prototypes of factory production, in which the process was broken down into stages carried out by specialised machinery. The River Goyt provided the power source for the important silk mills of Macclesfield, with water continuing to be the main driver of factory production until well in to the 19th century. Ultimately, restrictions to the size of operations from using water as the power source led to the adoption of the rotative steam engine, which whilst more expensive, was gradually adopted as continued expansion ensured that it became profitable. The steam engine ensured that, it was now possible to produce almost any amount of power in any location that had an economic supply of coal (Jarvis and Reed, 1999). Expansion of the textile industry highlighted the need for a port to supply raw materials from overseas and to serve export markets, as well as to serve other coastal shipping. The Port of Liverpool grew rapidly during the 18th century, with a sixteen-fold increase in vessel traffic between 1757 and 1857. In 1757, the dock area covered 8 acres, increasing to 290 acres by 1857, with a further 160 acres in Birkenhead. The last dock, at Bidston, was opened in 1937 (Bennett et al., 1995). A series of satellite ports grew up around the Mersey, including Runcorn, Widnes, and Ellesmere Port, linking Liverpool to the hinterland canal network. The latter half of the 18th century saw widespread improvements to the road network and the building of most of the countries principal canals, many of which were geared to serving the industrial needs of south Lancashire and north Cheshire, and connected with the River Mersey. A number of industrial links developed alongside the textile industry, based around the ancillary processes of bleaching, dying, and printing, with demand rapidly increasing in proportion to the output from textile production. The adoption of chlorine-based bleaching, and increasing demand for alum as a caustic, proved important in the development of the chemical industry. The advent of steam printing of The Times newspaper in 1814, led to the adoption of the process for bulk printing of textiles. Gas lighting was introduced in the early 1800s to enable the factories to adopt shift working, with rapid expansion of the gas industry accompanying the 1847 ‘ten hours act’, which encouraged the adoption of two shorter shifts in place of one longer one. Flour mills, sugar refineries, animal feed mills, edible oil mills, tobacco factories, soap making, margarine manufacture and metal ore processing have all at one time featured on or near the estuary. Much of the port activity has diminished as containerisation and the use of larger ships has increased, so that most of the Mersey trade is now handled at the Royal Seaforth Dock, opened in 1973 (Bennett et al., 1995).

While the cotton trade declined after the First World War, oil became more important with tanker berths constructed on the Manchester Ship Canal at Stanlow (1922 and 1933), Queen Elizabeth Dock (1954) and Tranmere (1960). Refineries have been constructed at Ellesmere Port (1934) and Stanlow (1949) and this has attracted a fertiliser works and an oil-fired power station at Ince (Bennett et al., 1995). At Widnes, an alkali industry developed from the middle of the 19th century using the Leblanc process and chemical waste has been dumped on the salt marshes beside the estuary. A major chemical works has also been established at Weston Point, Runcorn, staring in 1885, and in 1897 the Castner Keller works, using the electrolysis process, was opened beside the Manchester Ship Canal (Bennett et al., 1995). Widnes also had a copper industry based on the extraction of copper from the pyrites used at the Leblanc works, whilst Warrington was a base for iron-founding, wire-working, brewing and tanning, all contributing pollutants to the estuarine system (Porter, 1973).

Shipbuilding has also been a feature of industrial development on Merseyside since the early 19th C, some based in Liverpool–Bootle, but the major development being in Birkenhead at the Cammel Laird site. This industry has now suffered a severe decline (Bennett et al., 1995).

The Mersey basin also played a key role in the development of railways, with the Liverpool and Manchester Railway, being the first real main-line railway. The railway's initial impact was in passenger transport, making it possible to do business in person on a daily basis. Eventually railways became part of the supply and production chain for virtually every local industry.

1.2.3 Urban development

Along with the rapid development of industry, came a corresponding rapid increase in population and equally rapid urbanisation. Towns such as Oldham, almost entirely dominated by mills and factories, developed rapidly alongside industry. This speed of urbanisation ultimately led to overpopulation and squalor in many of the urbanised areas, aiding the spread of epidemic diseases on a scale unknown since the Black Death in the 14th century (Jarvis and Reed, 1999). Compiled population statistics for the Mersey basin as a whole are difficult to find, but the figures for Liverpool give an indication of the type of rapid increase that took place (Table 1.1). Figures for the whole of the Merseyside area (Table 1.2) suggest that the decline in Liverpool's population from a peak in 1931 was not matched by an overall decrease in Merseyside as a whole, where numbers increased up to 1961 before starting to fall. Detailed analysis of urban development in the Mersey basin is beyond the scope of this study, but maps showing the pattern of urban growth in Manchester and Merseyside are given in Handley and Wood (1999).

The expansion of both industry and urban development was accompanied by increases in the discharge of sewage effluent to the Mersey, which has been a major contributor to the pollution of the estuary (Jones, 2000).

Table 1.1 Population statistics for Liverpool (internet information).

Year	Population	Year	Population
1272	840	1871	493 405
1662	775	1881	552 425
1720	11 833	1901	684 947
1760	25 787	1931	855 539
1801	77 708	1961	745 750
1821	118 972	1971	610 000
1841	286 487	1981	510 000
1861	437 740	1991	477 000

1.2.4 Construction and reclamation

A number of anthropogenic activities have significantly influenced the configuration of the shoreline of the outer part of the estuary (LBCG, 1999). Thomas et al. (2002) noted several major civil engineering works that have been undertaken in the estuary and Liverpool Bay area that may have contributed to changes in estuary morphology. Within Liverpool Bay these included:

- dredging of the bar at the seaward end of Queens Channel beginning in 1890 to a depth of –6.4 m Liverpool Bay Datum (LBD), increased to –9 m LBD by 1895. By 1908 1Mt of material was being removed from the bar annually
- dredging of the sea approach channels, starting with the removal of 10 Mt of sediment in 1908 and increasing to a maximum of 17 Mt per year between 1910 and 1917
- construction of training walls, commencing with a 3.6 km length on the outside of Crosby Channel bend, extended to the west and augmented between 1914 and 1935 by training walls on both the east and west sides of Crosby Channel. Between 1945 and 1957 the training walls were extended in a seawards direction.

Sections of the open coast have been altered by the construction of man-made features including promenades and coastal protection works. Between Meols and New Brighton, there has been a historical landward movement of the high water mark halted only by the construction of the Wallasey Embankment (1840–1900), Leasowe Revetment (1920s) and King's Parade (1935/6). Along the King's Parade frontage (reclaimed in the 1930s), beach levels in front of the sea wall fell by up to 3.5 m between 1935 and 1975. The intertidal zone of the shoreline near Crosby has been significantly affected by the dredging, disposal, training, and dock construction that have been carried out along this section of coastline. Onshore sediment transport has led to a growth in height of the Formby Bank, pushing the exit of the River Alt southward. This has led to foreshore lowering and erosion of the Crosby frontage, which has continued since construction of a sea wall during the 1970s. Accretion of the Formby Bank has further provided a barrier to landward sand replenishment near Crosby, requiring rubble protection (Figure 1.1).

Within the estuary itself, several civil engineering operations have had an effect on the morphology of the Mersey. They include:

- construction of piers for the Runcorn Railway Bridge, completed in 1865

Table 1.2 Population statistics for the Merseyside area (after Potter, 1973).

Year	1901	1911	1921	1931	1951	1961	1971
Total	1 133 000	1 262 800	1 363 100	1 474 000	1 538 000	1 580 500	1 527 900

- construction of the Manchester Ship Canal, with its associated reclamation of river and tidal water, completed in 1894. This resulted in a large area of saltmarsh being separated from the Mersey between 1887 and 1893 (e.g. Helsby marshes), and reclaimed for industry and the dumping of canal dredgings (Bennett et al., 1995; EAU, 1987) (Figure 1.2). The canal also affected sediment movement in the Upper Estuary, with deposition of sediment in the canal on the flood tide

- diversion of the River Weaver, completed in 1896

- tipping of slag to form an embankment on the north-east side of the estuary between Runcorn and Hale Head, completed in 1896

- construction of piers for the Runcorn transporter bridge, completed in 1902

- dredging of estuary channels carried out intermittently from the 1890s and culminating in the average annual extraction of 2.75 x 10 Mm^3 from the Eastham Channel during the latter part of the 1950s (Thomas et al., 2002).

Channel modification, including straightening for navigation, bank protection and canalisation in urban areas has led to changes in river hydrology. Many of the Mersey headwaters around the Manchester basin have been dammed for water supplies, with the effect of reducing river flow and modifying the flow regime to the estuary (Harvey, 1985).

Between 1906 and 1977 dredging within the estuary was largely overridden by the effects of a greater net flux of sediment into the estuary. As the estuary has moved towards a state of dynamic equilibrium, the net flux of sediment into the estuary has decreased. Thus dredging has exerted a greater influence upon net morphological change in recent years. Although estuary volume may now be increasing as a consequence of sediment removal via dredging, this only represents the net estuary trend with localised patterns of erosion and accretion within the estuary maintaining the requirement for dredging (Thomas et al., 2002).

1.2.5 Habitats

The effects of pollution and land use from industrial and urban development are strongly evident in the habitats of the Mersey basin. In particular, domestic and industrial pollution, and reclamation of lowland areas has exerted pressure on the flora and fauna of the waterways, with very few having escaped human influence. Despite this, the Mersey estuary is of considerable importance for nature conservation, with large areas internationally or nationally designated for the protection of their ecology. In addition, certain areas are covered by local policies, which protect the biological and geological, or landscape and amenity value (EAU, 1987). Useful information on designated habitat sites in the Mersey can be found on the Joint Nature Conservation Committee website at www.jncc.gov.uk.

Important terrestrial coastal habitats within the basin include the sand dunes of the coast north of Liverpool. Only the southern half of the dune system lies within the basin area proper, but the whole comprises approximately 2,100 ha (Weekes et al., 1999). At Seaforth Dock, on the southern end of the dune system, building development is confined to the surviving dune in a narrow strip at the top of the beach, but the wider dune system provides an example of calcareous dunes of national and European importance, which is important for migrating birds and other rare species such as the sand lizard and natterjack toad (Taylor and Parker, 1993). This is recognised by the designation of the majority of the dune system as a Site of Special Scientific Interest (SSSI), along with two National Nature Reserves (NNR), Local Nature Reserves (LNR) and National Trust land designations. Dunes also exist on the Wirral Coast, including Red Rocks SSSI and Wallasey dunes (Doody, 1999).

The Mersey estuary hosts a number of important intertidal estuarine habitats, including saltmarshes and mudflats. The benthic fauna of the estuary consists primarily of the bivalve mollusc *Macoma balthica*, which is widely distributed. Smaller numbers of *Hydrobia ulvae* are localised in the muddy region around Weaver sluices, but are becoming more abundant. The polychaetes *Neries diversicolor* and *Nephtys hombergii* appear in low densities in the Inner Estuary, with *Capitella capitata* abundant in the organic-rich muds near the north bank of the Inner Estuary (EAU, 1987). An improvement in water quality resulting from the treatment of sewerage effluent since the 1960s has meant that planktonic and benthic life has increased. The Mersey continues to support higher densities of wildfowl and waders than adjacent estuaries, which may result from greater invertebrate productivity as a result of the high organic load. The area of saltmarsh available for feeding may also have increased during the same period (Bennett et al., 1995; Weekes et al., 1999). Areas of saltmarsh have developed at Ince and Stanlow, which are of ecological importance for feeding and roosting birds. Other areas of saltmarsh at Hale and above the Runcorn Bridge have little botanical or ornithological value (EAU, 1987). The saltmarsh plant, *Spartina anglica*, artificially introduced during the 1930s, can be found at Stanlow Point, although its spread has been limited compared with adjacent areas such as the Dee estuary. The intertidal growth of seaweed is restricted in the Mersey estuary by high turbidity. Green algae, such as *Enteromorpha*, are found on the dock walls in the upper tidal areas. Mussels (*Mytilus edulis*) are also found in this zone, along with other invertebrates such as shore crabs and barnacles *Balanus balanoides* and *B. cretanus* (EAU, 1987).

In recent decades, the importance of the Mersey estuary for bird life has increased substantially. Large numbers of birds use the Mersey and other north-west coast estuaries during migration and as overwintering grounds. A key contributing factor has been the increased loss of European overwintering grounds, ensuring that birds have moved to the west coast estuaries as an alternative. The Mersey estuary is of international significance for wildfowl, particularly shelduck (*Tadorna tadorna*), wigeon (*Anas Penelope*), teal (*A. crecca*) and pintail (*A. acuta*). Waders are also present at internationally important levels, with dunlin (*Calidris alpina*) being most numerous, and oystercatcher (*Haematopus ostralegus*) and knot (*C. canutus*) also significant. Redshank (*Tringa totanus*) are recorded at nationally important levels, as are curlew (*Numenius arquata*) and turnstone (*Arenaria interpres*) which are found on the rocky shore of the north Wirral coast and near New Brighton. Gulls also feed and roost on the estuary in large numbers, with the black headed gull (*Larus ridibundus*) most numerous, and the common gull (*L. canus*), herring gull (*L. argentatus*) and lesser black-backed gull (*L. fusca*) also present. Large mixed flocks of terns (Sterna) are present at Formby Point (EAU, 1987).

Because of the importance of the estuary for wildlife, 24 Sites of Biological Importance (SBI) have been designated, along with one NNR, three SSSIs, two Special

Protection Areas (SPA), and two Ramsar sites (Weekes et al., 1999). Figure 1.4 shows some of the important sites of environmental importance in the Mersey estuary.

1.3 THE MODERN ESTUARY

The estuary itself covers approximately 8 900 ha, with an intertidal area of 5,600 ha and shoreline length of 102.6 km (Weekes et al., 1999).

Buck (1993) classified the Mersey estuary as a coastal plain geomorphological type, but it has also been termed a ria without spits (Halcrow, 2002) because of the geological constraint of the narrow mouth between rocky shores. Clearly, the estuary has features of both types. Four main sections are usually recognised (NRA, 1995): the **Upper Estuary**, between the tidal limit at Howley Weir, Warrington (occasionally overtopped during high tides) and Runcorn Gap; the **Inner Estuary**, between Runcorn Gap and Otterspool (on the NE bank); the **Narrows**, between Otterspool and Egremont (on the SW bank); and the **Outer Estuary**, seawards of Egremont and taking in part of Liverpool Bay (Figure 1.2). The distance from Howley Weir to the opening into Liverpool Bay is approximately 47 km and in the Inner Estuary a maximum width of approximately 5 km is attained. With a mean maximum tidal range of almost 9 m (Table 1.3), the estuary is macrotidal. In terms of the mixing of fresh and saline waters, the estuary is considered partially mixed (Halcrow, 2002).

The **Upper Estuary** is a narrow, meandering channel that widens from less than 100 m near Warrington to just over 1 km near Widnes before being constricted to 250 m at the Runcorn Gap, by a north–south trending sandstone ridge. For much of this 12 km distance, the Mersey is constrained to the south by the Manchester Ship Canal (MSC) and to the north by the St Helens Canal. Extensive sand and mud banks are exposed at low water. A disposal ground for material dredged from the MSC is located on both sides of the river, near the confluence with Sankey Brook (Figure 1.2) (Clift, 2000).

From Runcorn Gap, where the estuary is constricted by a north–south oriented sandstone ridge, the estuary widens rapidly into the large basin of the **Inner Estuary**, most of which is exposed at low tide as sand and mud banks. Saltmarsh has developed on both shores of the estuary, but is most extensive on the south bank between Mount Manisty and the Frodsham Score (Figure 1.2). However, the saltmarsh is accreting on the northern shore at Oglet Bay, but eroding on the southern shore. In this region, between Speke and Ellesmere Port, the estuary achieves its maximum width of just less than 5 km, before progressively narrowing seawards towards Otterspool.

Between Otterspool (on the north-east bank) and Egremont (on the south-east bank) the estuary becomes a straight, narrow channel, the **Narrows** (Figure 1.2), with depths of over 20 m, even at low tide (DSIR, 1938; NRA, 1995) and strong tides of up to 3 m s^{-1} (NRA, 1995; Thomas, 1999). Due to tidal scour, there is only a thin veneer of bottom sediment in this region. The nearshore zone between New Brighton and Seacombe Ferry, is characterised by a low, narrow boulder foreshore with patches of intertidal rock platform, from which the majority sand has been eroded. The northern side of the estuary mouth is heavily developed with dockland, but with some mud accumulations at the level of low tide.

From Egremont out into Liverpool Bay, the **Outer Estuary** consists of extensive intertidal sand and mud banks, with the Crosby and Queens Channel's constrained by training walls for a distance of 16 km out into Liverpool Bay. The channels are dredged to maintain a navigable entrance to the estuary (Figure 1.2). The intertidal banks have formed as a result of an easterly feed of sediment along the Wirral coastline. Notable among these are the North Bank and Great Burbo Bank (Figure 1.1). These are exposed to constant reworking by wave action, and are subject to seasonal variation, which can increase or decrease the rate of supply of fine material to the estuary (LBCG, 1999). The Mersey estuary is constricted near its mouth, leading to local tidal scour. The banks of the Mersey are formed of low till slopes, with a few bedrock outcrops. Much of the Mersey coastline is defended and natural processes have been considerably altered as a result.

Some parts of the northern shore are formed of boulder clay cliffs, which have freshwater seepages and are subject to periodical slumping. There are also areas of rocky shore at Garston Rocks, Bromborough and New Brighton.

According to the estuary classification scheme in use in 1995, based on biological, aesthetic and chemical quality, the Narrows and the Inner Estuary are predominantly poor (class C), whilst upstream of Runcorn, the Upper Estuary is bad (class D) (NRA, 1995).

Table 1.3 Summary statistics for the Mersey estuary (NRA, 1995; Buck, 1993).

Parameter	Value
Total area	89.14 km^2
Intertidal area	56.07 km^2
Subtidal area	33.03 km^2
Saltmarsh area	8.48 km^2
Sandflat & mudflat area	47.59 km^2
Shore length	102.6 km
Tidal range (mean maximum)	8.9 m
Extreme spring	10.4 m
Extreme neap	4.0 m
Estuary volume (high water spring tide)	6.5 x 108 m^3
Population of Mersey basin	> 5 million
Population living within 1 km of the shore	834 000

1.3.1 Bathymetry

Bathymetric surveys of the Mersey, largely by the Mersey Dock and Harbour Company, have been carried out regularly since 1861, firstly at 10 yearly intervals and from 1881 onwards, every 5 years. The last detailed surveys were in 1997 and 2002. The 2002 bathymetry and the coastline used on Ordnance Survey maps are shown in Figure 1.5, which is based on a combination of data collected at low tide by LIght Detection And Ranging techniques (LIDAR) and at high tide by sonar bathymetry. The 2002 data were made available by the Environment Agency.

Elevation ranges between heights of 0 to 10 metres above Ordnance Datum (OD) on Figure 1.5 have been chosen to approximate the position of the coastlines on Admiralty charts, set at mean high water spring tidal level (MHWS), and Ordnance Survey maps, set at mean high water level (MHW). Tidal levels for places in the estuary are given in Table 1.4, from which it can be seen that MHWS lies

Table 1.4 Tidal heights (metres) above Ordnance Datum (Newlyn) for places in the estuary from Gladstone Dock, at the mouth, to Warrington, near the tidal limit, based on data given on Admiralty Charts 3478 and 3490 (HO,1994a;HO,1994b). MHWS = mean high water springs, MHW = mean high water.

Station	MHWS	MHW
Gladstone Dock	4.3	3.3
Alfred Dock	4.4	3.4
Eastham	4.8	3.8
Hale Head	4.9	3.9
Widnes	5.1	4.1
Fiddler's Ferry	5.4	4.3
Warrington	5.6	

at approximately 5 m OD and MHW at 4 m OD in the Inner Estuary (Hale Head). Thus the boundaries at 4 and 5 m OD on Figure 1.5 can be expected to represent the chart and map coastlines most accurately within the Inner Estuary. In practise, the area between the two coastlines should correspond very closely to the area of saltmarsh development, particularly within the Inner Estuary.

In general the map and chart coastlines and corresponding bathymetric boundaries are very similar in the outer and Upper Estuary areas, but considerable deviation is apparent on the southern shore of the Inner Estuary, reflecting the dynamic nature of erosion and deposition in this part of the system. Morphological change in the Inner Estuary has been discussed by several workers (e.g. Bennett et al., 1995; Thomas et al., 2002) and will be considered further later in this report.

From the mouth of the estuary, the deep-water channel occupying the Narrows extends southwards to Bromborough. Near the Cheshire shore, the Eastham Channel provides deep water access as far as the entrance to the Manchester Ship Canal, whilst near the north-eastern shore the Garston Channel extends deeper water beyond Garston. Near Garston another deeper channel splits off southwards and can be traced turning eastward towards Ince Banks, where it abuts against the present MHW line at 4 m OD and swings to the north-east to join another deeper water channel that runs across the central part of the Inner Estuary towards Hale Head (Figure 1.5). The erosion of the western side of Ince Banks can presumably be attributed to the migration of the channel on its north-western flank.

Elevations on Figure 1.5 relate to Ordnance Datum, which in the region of the Narrows is 4.93 m above the local chart datum. Thus actual water depths in the Narrows are somewhat shallower than might be deduced from Figure 1.5, averaging 15 m (Prandle and Lane, 2000). Upstream, almost the whole of the Inner Estuary dries out at low water on spring tides, with drying heights of over 5 m shown on Admiralty charts between Eastham and Garston (Figure 1.6).

1.3.2 Tides and currents

Mean tidal heights and ranges for various stations within the Mersey estuary are given in Table 1.5. The maximum tidal range is in excess of 10 m (Table 1.3) and the largest ranges occur at the seaward end of the Inner Estuary. Mean spring and neap tidal curves for some of the stations detailed in Table 1.5 are shown in Figure 1.7. The asymmetry of the tidal curves increases dramatically in the Upper Estuary, with a short flood period and a long steady ebb. Time differences between local high water times and those at Princes Pier are given in Table 1.6. The effects of tides and tidal currents on the movement of sediment will be dealt with later in the report.

Tidal stream data, based on near surface measurements, for four stations in the Narrows, all approximately central in the channel, are given in Table 1.7. Using current dominance as a simple measure of asymmetry, the Narrows

Table 1.5 Tidal heights and ranges in the Mersey estuary, based on data given in Price and Kendrick (1963). Low water, and hence range, data for Warrington are not guaranteed to be reliable.

Metres above Liverpool Bay datum									
Station	**Means springs**			**Mean**			**Mean neaps**		
	HW	LW	Range	HW	LW	Range	HW	LW	Range
Gladstone Dock	8.7	0.5	8.2	7.9	1.4	6.4	7.0	2.3	4.6
Princes Pier	8.8	0.5	8.4	7.9	1.4	6.5	7.0	2.3	4.7
Eastham	9.1	0.3	8.9	8.2	1.3	6.9	7.3	2.3	5.0
Widnes	9.5	5.0	4.5	8.5	4.9	3.6	7.5	4.8	2.7
Fiddler's Ferry	9.8	6.9	2.9	8.7	6.9	1.8	7.6	6.8	0.8
Warrington	10.0	7.9	2.1	8.8	7.6	1.1	7.5	7.3	0.2
Metres above Liverpool Bay Datum									
Station	**Means springs**			**Mean**			**Mean neaps**		
	HW	LW	Range	HW	LW	Range	HW	LW	Range
Gladstone Dock	4.3	-3.9	8.2	3.4	-3.0	6.4	2.5	-2.1	4.6
Princes Pier	4.4	-4.0	8.4	3.5	-3.0	6.5	2.6	-2.1	4.7
Eastham	4.7	-4.2	8.9	3.8	-3.2	6.9	2.9	-2.2	5.0
Widnes	5.1	0.6	4.5	4.1	0.5	3.6	3.1	0.3	2.7
Fiddler's Ferry	5.4	2.5	2.9	4.3	2.4	1.8	3.2	2.4	0.8
Warrington	5.6	3.5	2.1	4.3	3.2	1.1	3.1	2.9	0.2

Table 1.6 Time differences (in minutes) between local high water times and those at Princes Pier (after Pugh, 1975).

Station	MHWS	MHWN
Gladstone Dock	-9	-6
Princes Pier		
Eastham	+21	+27
Hale Head	+31	+27
Widnes	+40	+43
Fiddler's Ferry	+59	+75
Warrington	+68	

appears to be flood dominated, although the measurements for Egremont suggest ebb dominance. Observations by DSIR (1938) also indicate flood dominance, particularly for the Upper Estuary above Runcorn, where it is particularly pronounced. Some maximum current velocities for the Inner Estuary are shown in Table 1.8. DSIR (1938) noted that in the inner and Upper Estuary, especially above Dungeon Point, current conditions do not normally remain constant for more than a day or two, due to the frequent movement of banks and channels. It was also observed that stream velocities were highest in the channels before the banks were covered, after which there was no large difference between current speeds over the banks and channels. Recent assessments of tidal currents suggest flood dominance, although this appears to have been diminishing over recent times as intertidal area has increased (Halcrow, 2002).

The intrusion of saline waters pushed upstream by the tides also has an effect on currents. On small tides, saline water only penetrates to just beyond Widnes, but on higher ones it can reach almost to the tidal limit at Warrington (NRA, 1995). A number of studies have examined salinity gradients in the Mersey over several tidal cycles, particularly in the Narrows e.g. (e.g. Bowden and Sharaf El Din, 1966; Bowden and Gilligan, 1971), but also extending into the inner and Upper Estuary (Price and Kendrick, 1963). These studies confirm the presence of a residual density current circulation pattern leading to net landward movement of saline water near the bed and net seaward movement of fresher water near the surface. Price and Kendrick (1963) found that the salinity gradient had the effect of increasing flood velocities near the bed and decreasing the ebb velocities, whilst at the same time increasing the period of flood tide near the bed at the expense of the ebb. Current measurements in the Narrows have showed a residual current of about 12 cm^{-1} seaward in the upper layer and 10 cm^{-1} landwards in the lower layer, values being approximately the same at spring and neap tides (Bowden, 1975). This residual density circulation, which persists from the Narrows to the vicinity of Dingle–Eastham, greatly influences the movement of sediment in the estuary and implies that sediment is effectively trapped in the estuary and can only escape into Liverpool Bay during exceptionally wet weather and large spring tides, if at all (Halliwell and O'Connor, 1975).

Tidal action is fundamental to water quality in the Mersey estuary because water-borne pollutants discharged into the estuary, directly or through a tributary, may remain in the estuary for many days oscillating to and fro in the water body between high and low waters. This movement of a water body between high and low waters is known as the tidal excursion, the magnitude of which can be calculated from bathymetric and tidal height and time data. Figure 1.8 shows the calculated volumes of water seawards of Howley Weir at high and low water for a spring tide of 9.3 m and a neap tide of 7.4 m. The volume of water entering through the Narrows during such tides is 450 x 106 m^3 and 260 x 106 m^3 respectively (NRA, 1995). At low water on a spring tide the volume of the body of water upstream of a point 30 km from Howley Weir is just less than 10 x 106 m^3 (point A) and for a neap tide it is just over this figure. If this volume of water remains as a single body it will be pushed by the tide to point B, about 12 km from the Weir. This body of water now occupies a shorter length of river with an increased depth. The distance between points A and B, approximately 19 km, is the tidal excursion. For a neap tide the corresponding excursion is 10 km (after NRA, 1995). An interesting feature of Figure 1.8 is that in the Upper Estuary, the volume of water at spring low tide is greater than at neap low tide. This implies that spring low water is higher

Table 1.7 Tidal stream velocity in m s^{-1} and direction in degrees (D), for spring (S) and neap (N) tides at four stations in the centre of the Narrows. Times are in hours before high water at Liverpool (Alfred Dock) are prefixed by -. Based on Admiralty Chart 3490 (HO, 1994a,b).

	Gladstone Dock			Egremont			Tranmere Beach			Dingle		
Hours	D	S	N	D	S	N	D	S	N	D	S	N
-6	319	0.46	0.26	335	0.36	0.21	313	0.31	0.15	300	-.41	0.21
-5		0.00	0.00	165	0.15	0.10		0.00	0.00		0.00	0.00
-4	146	0.98	0.51	172	1.29	0.72	159	0.82	0.46	142	0.46	0.26
-3	146	2.26	1.23	172	2.16	1.18	167	2.47	1.34	144	1.75	0.98
-2	145	1.95	1.08	175	2.06	1.13	164	2.68	1.44	147	2.42	1.29
-1	145	1.65	0.93	172	1.34	0.72	164	2.11	1.13	147	1.54	0.87
0	136	0.51	0.26	165	0.46	0.26	161	0.62	0.31	147	0.51	0.26
1	324	1.23	0.67	348	1.34	0.72	329	1.29	0.72	312	1.08	0.57
2	327	2.16	1.18	348	2.73	1.49	325	2.26	1.23	311	2.06	1.13
3	331	1.70	0.93	346	2.31	1.23	328	1.95	1.08	313	1.75	0.98
4	329	1.34	0.72	344	1.85	1.03	331	1.54	0.87	319	1.23	0.67
5	328	0.98	0.51	342	1.23	0.67	328	1.03	0.57	324	0.87	0.46
6	325	0.62	0.31	341	0.62	0.31	324	0.51	0.26	306	0.57	0.31
Max Flood		2.26	1.23		2.16	1.18		2.68	1.44		2.42	1.29
Max Ebb		2.16	1.18		2.73	1.49		2.26	1.23		2.06	1.13

Table 1.8 Maximum current velocities in m s^{-1} at stations in the Inner Estuary (after DSIR, 1938).

	Max
Dingle	1.65
Bromborough	1.95
Oglet	1.71
Hale Head	2.50
Weston	2.87
Runcorn Docks	1.10

than neap low water, in contrast to the more normal situation found near the mouth of the estuary (see Figure 1.7). This is most probably due to there being insufficient time during spring tides for the water entering on the flood to leave on the ebb before the start of the next flood (NRA, 1995).

The seaward movement of water in an estuary is governed by the input of fresh water at its head, from tributaries entering along its length and from effluent outfalls. The rate at which the fresh water, which brings in and carries most of the contaminant load, passes out to sea depends largely on the size of the estuary and the volume of fresh water discharging into it. The freshwater flow into the Mersey estuary is relatively small for the its size and this affects the period, the flushing time, that materials spend in the estuary, or any part of it. The major freshwater inputs to the Mersey estuary are summarised in Table 1.9 and Figure 1.2 and calculated average flushing times are given in Table 1.10. There are considerable discrepancies in the freshwater flow rates quoted by different authors. Actual flow rates will clearly vary and flows at Howley Weir, the River Mersey input, are reported to lie between extremes of less than 10 m^3s^{-1} and 600 m^3s^{-1} with more typical flows in the range 20–40 m^3s^{-1}. Flushing time for water flowing over Howley Weir to reach New Brighton has been calculated at over 30 days. At times of high and low flow this can be reduced to less than 20 days or increased to over 50 days respectively (NRA, 1995).

Table 1.9 Estimated daily flow rates for freshwater inputs to the Mersey estuary (after Cashin, 1949; DSIR, 1938; NRA, 1995; Shaw, 1975). MSC = Manchester Ship Canal.

	Mean daily flow in m^3s^{-1}			
	DSIR	**NRA**	**Shaw**	**Cashin**
Mersey (Howley Weir)	27.52	18.75	42	
Sankey Brook	2.75	3.98		
MSC+ R Weaver	9.63	11.69	13	
Ditton Brook		0.98	0.7	
Holpool Gutter	0.23	0.22		
R Gowy	1.31	1.25	1.1	
Dibbinsdale Brook		0.38		
R Birkett		0.46		
Rainfall in sewers/sewers	2.05		4	
Surface rain on Esuary + MSC	2.42			
Other streams etc	6.91		5	
TOTAL	52.82	37.71	65.8	52.62

Table 1.10 Average flushing times in the Mersey estuary (NRA, 1995).

Reach	**Days**
Warrington to Widnes	2.0
Widnes to Hale	3.5
Hale to Mount Manisty	9.5
Mount Manisty to Dingle	12.3
Dingle to Rock Light	5.1
Warrington to Rock Light	32.4

The bathymetric evolution of the Mersey estuary over the period 1906–1997 and its relationship to tides and currents has been discussed by Lane (2004).

1.3.3 Sedimentology

1.3.3.1 General features

As will be described in more detail later, the Mersey is predominantly a sandy estuary, with fine sediment occurring in places along its inner margins (Figure 1.9). Because of the large tidal range a large area of the estuary lies within the intertidal zone. The tidal asymmetry is flood-dominated and the estuary is a net sink for sand and mud. The ebb and flood currents follow different courses within the estuary, resulting in a complex, evolving pattern of channel courses, and shifting sandbanks.

Dredging of sediment in the mouth of the estuary has long occurred to maintain the navigation channels and docks, with the dredged material being subsequently deposited in Liverpool Bay (Norton et al., 1984). In the early part of the last century, the volumes of dredged sediment exceeded the natural sediment volume changes within the estuary. As dredging volumes have since reduced from their annual peak of about 10 million tonnes to about 1 million tonnes recently (Prandle, 2000), natural sediment fluxes are now more significant again in controlling the geomorphology of the Inner Estuary.

Monitoring of bathymetric changes across the estuary indicates that a significant amount of accretion occurred between 1900 and 1977, reducing the capacity of the estuary by about 10 per cent (Spearman et al., 2000). The Mersey experiences stronger velocities on the flood tide causing net movement of sediment into the estuary, because the net direction of bedload sand transport is determined by the direction of peak tidal current speed. Great Burbo Banks in Liverpool Bay has been identified by particle tracking techniques as the principal source of sand moving into the estuary (Spearman et al., 2000). The rate of transport of sediment from Liverpool Bay into the inner Mersey has increased since the construction of the training walls between1906 and 1948 as a measure to stabilise the main navigation channel between sand banks in the Outer Estuary.

Sediment transport budgets and fluxes therefore control the development of banks and intertidal flats in the Inner Estuary. The influx of sand into the Inner Estuary allows the area of intertidal flats to increase, which in turn has a morphological feedback in reducing the period of the ebb tide, increasing the ebb current velocity and subsequently reducing the landward transport of sand. Excluding anthropogenic influences, the driving forces for the morphological changes within the estuary are the current

circulation and sediment availability within Liverpool Bay. Unlike nearby estuaries, such as the Dee, with a fully open aspect to the sea, the Mersey has a narrow opening and significant freshwater inputs from its 5000 km^2 catchment area. However, construction of the Manchester Ship Canal totally disrupted the natural discharge of rivers from the Mersey catchment, and freshwater now enters the Inner Estuary in pulses during opening of the lock gates at the end of the canal. Only the seaward or Outer Estuary is representative of full marine conditions. The reduced salinity across much of the estuary impacts on the abundance and variety of benthic fauna, and thus the level of biogenic disturbance of the estuarine sediments and their included contaminants. Pollutants are incorporated in the sediment by physical, biological and chemical processes.

Due to the shape of the Mersey estuary, narrow at its mouth, but widening further upstream, the growth of intertidal banks occurs upstream of Rock Ferry (Figures 1.2 and 1.6). Sand is carried through the Narrows by strong tidal currents, leaving largely gravel-rich sediments on the estuary floor (Figure 1.9).

The dock walls on the Liverpool side of the estuary reflect wave energy onto the littoral shoreline between New Brighton and Seacombe causing beach erosion. Foreshore volumes have decreased by 100 000 m^3 in the past 15 years along this stretch of coast, equivalent to a 25 cm drop in level of the intertidal zone (LBCG, 1999, P.211).

Sidescan sonar data, collected during a shallow seismic survey as part of a study of the evolution of the estuary, exist only for the outer part of the estuary, north-west of Mount Manisty (Figure 1.10). This is because water depths in the Inner Estuary limited the access of the survey vessel. The large expanse of sand extending from Eastham Sands to The Sloyne, consists of asymmetric megaripples and sand waves, suggesting active sediment transport, with a net landward movement towards Eastham Sands and a net seaward movement beyond New Ferry. The sand body off New Brighton at the mouth of the Mersey estuary is megarippled with ripple asymmetry suggesting a net seaward sediment movement. There thus are indications of an ebb tidal delta seaward of the mouth of the estuary and a flood delta landwards of the Narrows.

1.3.3.2 Intertidal sand banks

Substantial intertidal sandbanks occur in the Inner Estuary, upstream from Rock Ferry, and in the Upper Estuary immediately east of Runcorn Bridge (Figures 1.2 and 1.6). These sandbanks are the product of dissection of sandflats by migrating channels, and are distinguished from the adjacent sandflats by their higher sand content due to winnowing of fines, and by the bed forms that migrate over their surfaces during the ebb and flood tides. The surface shape of the banks is subject to repeated slight modification by these migrating bed forms. Major changes in the bank positions occur over a longer time scale, caused by laterally shifting tidal channels. The occurrence and development of the banks needs to be considered in the context of the reduced estuary volume since the construction of the Manchester Ship Canal, and the net sediment accretion that occurred within the estuary between 1906 and 1977 (Thomas et al., 2002).

The behaviour of the low water channel since the middle of the 19th century can be divided into three phases (Kendrick and Stevenson, 1985; Thomas, 1999). It was able to meander unimpeded across the Inner Estuary prior to 1900, channel activity was high with wide fluctuations. Construction of the Manchester Ship Canal within the last decade of the 19th century reduced the capacity of the estuary and the inflow of freshwater from its tributaries. Subsequent dredging of the Eastham Channel helped to stabilise the position of the low water channel close to the northern shore between Hale Head and Oglet for the first sixty years of the 20th century. During this period of relative stability, a large area of intertidal sandbanks developed within the middle of the Inner Estuary (especially in the vicinity of Ince and Stanlow). Since about 1960 the low water channel has again actively migrated within the Inner Estuary, leading to frequent modification of the shape and position of the mid-estuary sandbanks and erosion of salt marshes (Figure 1.11).

Little is known about the internal structure of the banks because there are no deep boreholes through the mid-estuary banks. Large-scale cross-bedding is not evident from cores recovered in this study on top of the banks. Instead, sediments from the upper surfaces of the banks show abundant plane parallel lamination and horizons of reworked mud clasts, both indicative of high-energy current flows in a subtidal setting. Also commonly seen are apparently structureless units of sand, typically in the order of 10 cm thick, which were also in all likelihood deposited rapidly by tidal currents. Grading of beds is sometimes detected, consistent with deposition in single event waning-energy flows. Interestingly, the dune bed forms seen on the surface of the banks during low tides are not commonly recorded by cross-bedding in the sediment record, although ripple cross-lamination is abundant.

1.3.3.3 Dune and bed forms

Ripple dunes are observed on the periphery of most of the large sandbanks in the Inner Estuary. For example, sandbanks are covered with dunes/megaripples near the slipway at Speke airfield. Here the steeper (lee) faces of the bed forms point towards the Outer Estuary, indicative of ebb current flows near the estuary margin. The dunes have large arcuate crestlines with small forms superimposed on the stoss slope. These ripples probably reflect late-stage run-off of the ebb tide.

Trains of ripples cover the flattened top surfaces of the banks either side of Runcorn Bridge. Low amplitude symmetrical ripples with sinuous crestlines and interference ripples (irregular linguoid forms) were the dominant bed forms observed in this part of the Inner Estuary. Rounding of ripple crests was noted at several localities, a result of reworking of ripples during the process of emergence. Falling water levels can produce ripples with double crests. X-ray photographs (see section 2.4 for methodology) commonly reveal wave ripple cross-lamination, distinguished from current ripples by internal laminae that are discordant with the surface ripple form, laminae which are often but not solely bidirectional, and undulatory ripple bases. The ripple cross-laminated beds are never more than a few centimetres thick and are generally sandwiched between plane-parallel laminated beds.

1.3.3.4 Sand waves

In the Outer Estuary, and in the main channel of the Inner Estuary seaward of Garston, sand waves have been detected on side-scan sonar records (Figure 1.10). These bed forms are distinct from the smaller linguoid dunes observed on the surface of the sand banks.

From the direction of the lee slopes of the sandwaves, a zone of bedload parting is indicated to occur at the New Ferry – Dingle end of the Narrows.

1.3.3.5 Intertidal and supratidal flats

From Weston eastwards along the Upper Estuary, the bedding exposed in eroding banks and channel banks is

essentially horizontal with sand layers of varying thickness. The higher intertidal flats have been colonised by saltmarsh vegetation.

Cores taken by BGS (see later) through Ince Marshes (at +5.08 to +5.42 m OD) record Holocene sequences from 7.4 m to in excess of 11.1 m where the underlying Pleistocene sands and till were not reached. The Holocene sequences comprise units of dark grey silt-rich mud and yellowish brown very fine-grained sand with individual beds of peat up to 1.5 m thick, containing wood fragments. Upward-fining sequences, from very fine sand to peat, are observed, representing progradation of the saltmarsh over intertidal flat sediments. Erosive tops to the peat beds and occasional reworked lumps of peat indicate inundation and reworking of the marsh sediments by tidal waters.

The Holocene history of the Helsby and Ince Marshes, as recorded in the BGS cores, has been discussed by Wilson et al. (2005a and 2005b).

1.3.3.6 Biota and surface bioturbation

Trace fossils identify the activities of certain organisms. As a general rule, biogenic structures preserved within sediments will be biased towards those formed by deeply burrowing (>30 cm) infauna and will not represent accurately the original faunal densities or diversities.

Despite numerous surface trails, especially bird footprints, worm feeding/dwelling tubes, and faecal pellets, bioturbation is hard to discern within shallow pits dug on the intertidal banks and flats of the Mersey estuary. Detection of biogenic traces is hindered by the water-saturated state of the surface sediments and homogeneity of many sand beds. Non-preservation of biogenic activity in homogeneous sediments is a common problem. The paucity of biogenic traces within the subsurface sediments is corroborated by an X-radiographic study of over 20 cores collected from the estuary. Evidence of bioturbation in the cores, if present, is generally restricted to the upper 30 cm of sediment. It would seem that frequent reworking of the sediments by tidal currents has destroyed many biogenic structures in the sediment record.

However, two other issues come into play; the salinity trends within the estuary and the impacts of pollution. The upstream tidal limit is Howley Weir in Warrington, but reductions in salinity due to freshwater dilution are such that the Inner Estuary sediments seem unable to support some intertidal molluscan species. The variety and abundance of invertebrate species diminishes up estuary in response to the natural decrease in salinity of the estuary waters. The inner zone of the estuary has the most impoverished benthic communities (Ridgway et al., 2001).

The effects of pollution are probably mainly responsible for the paucity of intertidal molluscs. As a result, shell lags are comparatively uncommon within the inner Mersey sediments, in contrast to more pristine estuaries such as the Solway Firth. The impacts of pollution on fauna have been described by Bennett et al. (1995).

The earliest estuarine invertebrate fauna surveys were undertaken after the estuary sediments were already polluted. For instance, Bassindale (1938) sampled 100 sites and provided a useful reference point before the onset of some of the worst pollution in the estuary between about 1940 and 1970. Some of the most chronic pollution incidents occurred during the Second World War when pollution controls were relaxed. There was a general trend of diminishing species abundance and diversity from the 1930s onwards (Hawkins et al., 1999). There was a temporary loss of benthic fauna from the inner and middle estuary during the 1960s as a consequence of pollution and the development of anoxic bottom conditions (Hawkins et al., 1999).

Recent evidence, however, indicates that a burrowing fauna, including the common ragworm, has recolonised the intertidal flats along the margins of the estuary, where sediments are comparatively stable, and some of the intertidal banks. The sporadic reappearance of mussels in some middle estuary sites occurred in the mid 1980s and the lugworm, *Arenicola marina*, has reappeared recently in the Inner Estuary (NRA, 1995). By the late 1990s a fairly typical estuarine fauna dominated by the Baltic Tellin, common cockle and common ragworm were present within the estuary. Polychaete worms (*Capitella capitata*) are now the dominant infaunal species.

All factors considered, the paucity of burrow traces in the cores is best explained in terms of the frequent reworking of sediments on the intertidal banks which obliterates most burrow traces, but also partly reflects a sparse benthic fauna in the recent past as a result of the effects of pollution, and also salinity changes in the Inner Estuary.

1.3.3.7 Mud clasts and faecal pellets

Mud-rich oblate clasts and mud balls were commonly observed on rippled sand flats. These are preserved in the sediment cores as mud flake horizons. Mud pebble conglomeratic horizons are seen in cores M38C and M55C (see Figure 2.1)

The mud clasts are mainly rounded, with some elongate and subangular varieties. They typically range in size from 1 cm to 15 cm in maximum dimension.

Sediments containing layers of mud and mud pebbles occur on some present-day tidal flats. For example, mud-pebble beds derived from mud layers are widespread in the deposits of the Dutch Wadden Sea (Straaten, 1954).

The origin of the Mersey mud clasts is not clear. They could have formed due to the erosion of mud layers by: meandering channels; tidal currents during phases of high tide; or by strong wave action. Alternatively, they may result from surface desiccation and cracking of mud layers, and subsequent current transport of mud flakes.

Burrowing organisms can defaecate both at the sediment surface or within the burrow depending on the species involved. Material transported up and down a burrow will often be in the form of faecal pellets. The excretory matter of organisms can be an important constituent of some sediments. Faecal pellets can be transported and deposited as granular clay with hydraulically equivalent quartz sand grains (Reineck and Singh, 1980).

Transported faecal pellets were noted in ripple troughs during the present study. The faecal pellets are both rounded and tubiform. The sand flats near Runcorn showed good examples of faecal pellets.

1.3.3.8 Reworking of estuarine sediments

During the sample collection programme it was observed that the position and morphology of bed forms showed frequent modification due to strong tidal influence. The pattern of sediment movement, and in particular the position of the edges of intertidal sandbanks varied considerably, with morphological changes reflecting the frequent and significant movement of sediment around the margins of the banks.

This intensive history of civil engineering has had a significant effect on the capacity and channel migration within the estuary (Kendrick and Stevenson, 1985; Thomas, 1999), particularly in the Inner Estuary. From 1870 to the late 1950s, the natural position of the low water channel was on the Lancashire shore. During this time large sand

banks (e.g. Eastham Sands and Dungeon Banks) formed in the middle of the estuary, with mud banks forming on the Cheshire shore. An area of 19 km^2 of sand and mud banks was present in 1958. However, between the mid 1950s and 80s, the low water channel migrated towards the Cheshire shore. In the process, significant loss of saltmarsh appears to have taken place from the western part of Ince Banks and from Stanlow Banks, with new saltmarsh developing to the east of Ince Banks. In 1984 the low water channel had begun to move northwards again to the Lancashire shore, and by 1988 the channel was approximately central within the estuary (Bennett et al., 1988) (Figure 1.11). The estuary is apparently now entering a new phase of dynamic equilibrium, where the low water channel will meander within its present constraints.

The frequent reworking of sediments affects the preserved sedimentary record. Surface features such as ripple marks are under-represented in the sedimentary record, with horizontal plane parallel lamination predominating. Most significantly, the reworking of intertidal sediment by tidal flows obliterates most traces of the benthic fauna within the estuary.

1.4 PREVIOUS WORK ON SEDIMENT CHEMISTRY AND CONTAMINATION

The Mersey estuary has a long-standing history of pollution, beginning with the industrial revolution of the 18th century. Recognised as least as far back as the mid 19th centuary, contamination was probably at its worst in the mid 1960s, when sewage effluent was combined with a complex mixture of inorganic and organic chemicals originating from factories in the Mersey catchment and along the estuary shores (NRA, 1995; Jones, 2000). Major improvements have taken place in recent years (Jones, 2000), but considerable quantities of organic and inorganic contaminants are still present in the estuarine sediments.

1.4.1 Inorganic contaminants

A study of heavy metals in surface sediments of the Mersey, monitored over a period of 25 years (Harland, 2000), has shown that metal concentrations are strongly correlated with organic matter and particle size, resulting in distribution patterns which reflect sediment characteristics and dynamics rather than the position of input sources. Although a general decline in metal concentrations was observed, in line with reducing inputs, remobilisation of previously consolidated saltmarsh sediments was considered responsible for significant perturbations in the overall reduction trend (NRA, 1995; Harland et al., 2000; Harland et al., 2001). This view is supported by the work described in this report, which indicates that the position of the mean high water mark on the south bank of the estuary has changed, in comparison with the 1992 1:25 000 scale map of the area (Ordnance Survey, 1992), as a result of the erosion of a significant part of the Ince Banks saltmarsh development. In contrast, Jemmett (1991) found that saltmarsh on the northern bank of the estuary near Hale Head had undergone continuous, but variable rate, accretion since 1911. He also found the saltmarsh here to be contaminated with elevated concentrations of the heavy metals Cd. Cu, Pb and Zn in comparison with a saltmarsh at Foryd Bay on the Menai Strait in North Wales.

In order to examine the contamination history of the Mersey estuary, Fox et al. (1999) determined DDT and a series of heavy metals and radionuclides in 3 cm slices of 1 m cores of saltmarsh sediments from Widnes Warth and Ince Banks. They considered ^{210}Pb dating, a common technique for recent sediments (e.g. Appleby et al., 1988), unsuitable because of relatively low concentrations of "unsupported" ^{210}Pb. Instead, "event dating" based on the relationships of the output of contaminants (e.g. DDT, ^{137}Cs, ^{239}, ^{240}Pu, Hg) to documented dateable events (e.g. start and reduction of emissions) was employed. On the basis of core depth alone, the contamination histories of the two marshes appeared different, but using the event dating technique the similar lengths of core at the two sites were shown to represent different periods of sedimentation in which contamination histories were compatible. The Widnes Warth core covers a 120-year time span, whilst that from Ince Bank represents a little over the last 50 years of sedimentation (Fox et al., 1999). Contamination profiles for selected metals in the Widnes Warth core (NRA, 1995) are shown in Figure 1.12 and can be linked to specific industrial activities. The start of Cu smelting in NW England in 1870 and the use of Hg cathodes in the production of chlorine from 1897 are clearly shown in the gradual rise in concentrations of these elements after the late 19th century. Similarly, the rise in the importance of Zn as an anticorrosion agent in the 20th century and the output of As as a by-product of smelting Cu concentrates from SW England and the Americas in the early 1900s are matched by increased levels in the sediments (NRA, 1995). Taylor (1986) depicts Hg levels in 2 cores of 5 m length from Ince Marsh and Mount Manisty and a core of 30 m from Randle Marsh in the Inner Estuary. He reports that elevated levels of Hg are restricted to the topmost 2 m of the cores, but his data suggest that the rise in Hg concentrations might start as deep as 5 m.

The cores studied by Fox et al. (1999) were of essentially constant sediment composition, but the potential for misinterpretation of contamination records if grain size is ignored is demonstrated in Figure 1.13, which shows how normalisation to Ga as a proxy for grain size alters the profile to show the highest levels of contamination at core depths of 30–50 cm instead of at 5–10 cm in the non-normalised data (Ridgway et al., 2003). The overall decrease in contaminant levels in the Mersey is not apparent if grain-size variation is ignored.

Isotope geochemistry can be used to help trace the origin of Pb in the Mersey estuary and its catchment. The Pb isotope ratios in surface sediment samples from the estuary, the Manchester Ship Canal, which runs along its southern shore, and the Mersey catchment form an array between those typical of Pb from Pennine ores and others characteristic of Pb from Broken Hill Type (Australia) ores (BHT), the latter of which are used extensively in the petrochemical industry. Samples taken from near an oil terminal on the western shore of the estuary, near the Stanlow oil refinery on the Manchester Ship Canal and near Runcorn on the Canal, all display high concentrations of the BHT end-member in comparison with other samples from the area. A similar high BHT content is shown by a sample from the River Tame upstream in the catchment, but close to a motorway flyover where petroleum products could be washed into the drainage course. The high relative BHT content in these samples is independent of the absolute Pb concentration, reflecting only the source of the Pb (Ridgway et al., 2001) (Figure 1.14).

Despite the overall improvement in sediment quality in the modern Mersey, comparison of the average chemistry of 13 surface sediment samples from throughout the estuary with model values for the catchment, based on BGS stream sediment geochemical data (BGS, 1997),

indicates that levels of Cr, Zn, As are significantly higher in the estuary (Fig. 1.15; Ridgway et al., 2003). The trace for an offshore sample is very similar to that of the estuary average indicating a significant impact on the Irish Sea. In comparison with other major UK estuaries, the Mersey has relatively high levels of Hg (not all samples), Cd and Pb (CEFAS, 1998), but compares favourably for most metals (MPMMG, 1998).

1.4.2 Organic contaminants

The situation with regard to organic contaminants in Mersey sediments is less well documented, most studies concentrating on waters and suspended particulates. In this context, the portioning of organic compounds between sediment and water column is of considerable interest. In a study of bird mortalities in the Mersey, Wilson et al. (1986) found that the alkyl lead species considered to be responsible apparently were not scavenged by particulate material and that, consequently, no evidence of alkyl lead was found in the sediments. Blackburn et al. (1999) showed that alkylphenol concentrations in the Mersey (one of only two out of nine estuaries in which alkylphenols were detected) water and sediments were broadly correlated, whilst Preston and Prodduturu (1992) report somewhat higher carbohydrate concentrations in suspended particulate matter than in the underlying sediments. Preston and Al-Omran (1986) found that phthalates were enriched in the sediment relative to suspended material at the same site by a factor of about 5. The data of Osborne et al. (1997) suggest that the suspended/bottom sediment ratios for azaarene concentrations in the Mersey can vary considerably with the time of collection, either phase having the highest levels.

Total polycyclic aromatic hydrocarbon (PAH) data in surface sediments are given in CEFAS (1998) and MPMMG (1998) where the level of contamination in the Mersey is seen to compare well with that of other UK estuaries. A general amelioration of hydrocarbon contamination is suggested if these results are judged against the presence of heavily weathered or biodegraded oil recorded in MAFF (1992) and the exceptionally high background hydrocarbon levels reported by Davies and Wolff (1990).

Both PAHs and azaarenes are introduced into the marine environment largely through the burning of fossil fuels, but Osborne et al. (1997) found negligible correlation between the two groups of chemicals in surface sediments from the Mersey and tributary canals, with azaarenes having quite different environmental mobility and showing seasonal variability that could be related to levels of fuel combustion. Osborne et al. (1997) also note that PAHs show little reactivity after deposition, whereas azaarenes showed significant and selective loss of two ring compounds down estuary.

Data summarised in MPMMG (1998) show that polychlorobiphenyls (PCBs), hexachlorodimethanonaphthalene (dieldrin), dichlorodiphenyltrichloroethane (DDT) compounds and hexachlorobenzene (HCB) are not significant contaminants in surface sediments of the Mersey estuary. However, most of the samples were of sandy sediment with a low organic carbon content and finer grained sediments might show higher concentrations.

Cores from the same salt marshes as used by Fox et al. (1999) to study inorganic contaminant histories (above) have been analysed to provide a record of organochlorine contamination in the Mersey estuary (Fox et al., 2001). Coring and dating techniques were the same as for the inorganic study. Only HCB, hexachlorocyclohexane (HCH), DDT compounds and the 7 PCB congeners most commonly used to monitor PCBs in marine systems were examined. For total DDT concentrations, time/depth profiles for both Ince and Widnes Warth marshes show a take-off around 1945, reflecting the onset of DDT production in the Mersey basin. After a peak in the mid 1960s, when legislation banning the manufacture and use of DDT was introduced, concentrations decrease to relatively low levels in modern sediments. Profiles from both marshes indicate that contamination by PCBs began in the 1940s, peaked around 1970 and subsequently declined. However, levels at the surface are higher than would be expected for substances whose use was discontinued in the late 70s, probably as a result of environmental persistence of some congeners and continuing dispersion from residues within old transformers and other dielectric fluids in landfill sites. A more complex situation is found for HCH and HCB in particular, with the two marshes having different time profiles and peak concentrations. Levels of dieldrin are low at both sites.

The 1 m core from Widnes Warth penetrates to below the depth of significant organochlorine (and also metal) contamination, but that from Ince Marsh does not (Fox et al., 2001). The work of Taylor (1986), cited above, suggests that metal contamination may extend down to 5 m. Such features are of importance for the planning of sampling campaigns aimed at the calculation of total contaminant loads and prediction of the likely environmental impact of salt marsh erosion.

The Environment Agency (EA, 2001) studied organotin levels in both sediment and water samples and organotin concentrations are also reported by OSPAR (OSPAR, 2000) and CEFAS (CEFAS, 2000). These studies suggest that, in common with other contaminants, organotins are effectively scavenged from water by suspended particulate matter and then deposited in estuarine areas where fine material accretes and in docks and marinas. Both dibutyltin (DBT) and tributyltin (TBT) show correlation with particle size. The EA report a general increase in both TBT and DBT in the middle and Upper Estuary, with the exception of a few anomalous sites where the high fine-grained sediment content leads to high organotin concentrations (EA, 2001). Concentrations of TBT in sediment range from <2 to 25 ppb in Mersey sediments and 54 to 11730 ppb in the Liverpool and Birkenhead Docks according to the EA (EA, 2000), who also report values from CEFAS of 140 to 8840 ppb. Dibutyltin in Mersey sediments ranged from <2 to 75 ppb (EA, 2000).

2 Sampling and analytical programmes

2.1 SAMPLING METHODOLOGY

Sampling of the estuary of the River Mersey for this study was carried out over a period of 30 months, with initial orientation samples collected in May 2000, and the final drill cores from Widnes Warth, collected in November 2002. The majority of the samples were collected in the period May 2000 to June 2001 in an attempt to get a 'snapshot' of the estuarine geochemistry and minimise long-term variation effects. Sample locations are shown on Figure 2.1.

In the Inner Estuary, and Outer Estuary where access could be gained from the shore, the principal method of sample collection was by plastic tubes, manually driven into the exposed sediment and extracted to recover the core material. Generally between 0.75 m and 1.25 m of continuous core was recovered, however in some instances near-surface bedrock prevented deep penetration of the core tubes. At three locations, deep, anoxic mud allowed cores in excess of 1.60 m to be recovered. A surface sample, collected with a stainless-steel trowel, was also taken at each core site. Samples were collected by this method from 238 sites, with an approximate grid spacing of 500 m between sites. Sampling was generally carried out under spring tide conditions, during which the estuary bed was exposed to the maximum degree. Sampling sites in the Inner Estuary were accessed by the Environment Agency hovercraft 'Sea Spray', using predetermined GPS co-ordinates to accurately locate each position (Plate 2.1). Typically, a working window of 4–5 hours over a low tide allowed the collection of 10–15 samples.

In the Outer Estuary, the Environment Agency vessel 'Coastal Guardian' was used to collect surface grab samples from the submerged estuary bed. Predetermined GPS co-ordinates were used to accurately locate each site. Deployment of a 'Day' grab from the rear of the vessel enabled the collection of 41 samples over a two-day period in February 2001 (Plate 2.2).

At 8 locations near the margins of the Narrows it was possible to collect cores using a Mackereth corer (Plate 2.3). The corer was deployed from the Environment Agency vessel 'Sea Jet'. Using compressed air, a plastic core tube was forced into the submerged sediment, enabling cores of up to 1 m to be recovered.

Following interpretation of the geochemical data from analysis of the initial core samples, several target sites were selected for further investigation. Over a three-day period in November 2001, a large hovercraft was leased to transport a mechanically powered 'Vibrocore' rig to 12 previously sampled sites (Plate 2.4). At 10 of these locations, penetration to greater depth was possible using the Vibrocorer. Unfortunately, strong winds prevented the hovercraft from operating for the duration of one day.

Core samples were collected from Ince Bank salt marshes over a three-day period in July 2002. A mechanically powered 'Marlow' corer was transported by barge, via the Manchester Ship Canal, and unloaded onto Ince Bank.

Cores were recovered from three locations, with penetration and recovery of material from depths of 8.31 m, 7.00 m and 9.00 m respectively in each of the three holes drilled (Plate 2.5).

The final samples to be collected were from Widnes Warth, where 6 holes were drilled using the 'Marlow' corer. Samples were collected during two visits, the first over two days in October 2002, and the second over three days in November 2002. Mechanical failure of the drill shoe during the first visit allowed only one core to a depth of 5.00 m and a second to a depth of 2.00 m to be collected. The second visit enabled collection of a further three 2.00 m cores and a fourth core penetrating to a depth of 6.58 m.

Throughout the sampling operation, duplicate samples were collected from a number of sites in order to quantify any systematic errors introduced during the sampling and analytical processes. A number of sample locations were also revisited after approximately 18 months when a second sample was collected. This exercise was designed to indicate any short-term dynamic movements within the estuarine sediment. Quality control procedures are dealt more fully in Appendix 1.

Cores and samples were frozen as soon as possible after collection to minimise post collection chemical change and later split to allow sampling. The longer cores from Ince Bank and Widnes Warth were logged using the protocol set out in Ridgway et al. (1998) and then sampled on the basis of recognisable sedimentary units as also described in Ridgway et al. (1998). The shorter cores were sampled over 10 cm intervals (e.g. 0–10 cm, 10–20 cm etc).

As part of a parallel programme to study the evolution of the Mersey estuary, several cores were drilled, using the Marlow rig, in the Ince Marshes area, to the south of the Manchester Ship Canal (Figure 2.1).

Table 2.1 Numbers of samples collected by different methods.

Equipment	Sample type	Number
Manual – plastic tube and trowel	Estuarine sediment core and surface sediment	238
Day grab	Estuarine bed sediment	41
Mackereth corer	Estuarine sediment core	8
Marlow corer	Salt marsh sediment core	13
Portable vibrocorer	Estuarine sediment core	10

2.2 CHEMICAL ANALYSIS PROGRAMME

The analytical programme included both organic and inorganic determinations, the former dealing with a relatively small number of samples because of the high costs involved in organic geochemical analysis. Details of the sample preparation, analytical and quality control procedures employed are set out in Appendix 1. In common with many marine and estuarine sediment studies, determinations were carried out on the < 2 mm fraction of material. Where sieving was necessary, samples for organic determinations were treated using a brass sieve and those for major and trace elements using nylon sieve cloth.

As a general aid to interpretation and a preliminary to more focused investigations of their organic geochemistry 87 sediment samples collected from the Mersey estuary had both their total organic carbon (TOC) and loss on ignition (LOI) at 450°C determined on the freeze-dried < 2 mm fraction. The latter provides a relatively cheap estimate of TOC. The TOC determinations were outsourced from BGS to ALcontrol Geochem Laboratories, Chester, UK, who hold UKAS accreditation for this technique.

Polycyclic aromatic hydrocarbons (PAHS) were determined in 20 samples, polychlorinated biphenyls (PCBs) in 26 samples, organo tin, organo lead and saturates/ biomarkers in 10 samples (Table 2.2), organic carbon and nitrogen content in 66 samples and natural organic matter compounds in a single core.

Major and trace elements were determined mainly by wavelength dispersive x-ray fluorescence spectrometry (WDXRF) on 1410 pressed powder pellets. Additional elements were determined by energy dispersive x-ray flouresence (EDXRF). Mercury was determined in 216 samples by vapour generation atomic fluorescence spectrometry.

Table 2.2 Summary of samples used for the determination of organic compounds. See text for further explanation.

Sample No.	PAH	PCB	Org. Sn, Pb & saturates	Sample No.	PAH	PCB	Org. Sn, Pb & saturates
M34 0-10		X		M102 50-60	X		
M34 10-20		X		M102 60-70	X		
M34 20-30		X		M102 70-80	X		
M34 30-40		X		M102 90-100	X		
M34 40-50		X		M122 0-10	X		
M34 50-60		X		M122 10-20	X		
M34 60-70		X		M122 20-30	X		
M34 70-80		X		M122 30-40	X		
M34 80-90		X		M122 40-50	X		
M38 50-60	X			M122 50-60	X		
M39 60-70		X	X	M122 60-70		X	X
M42 10-20		X	X	M160 10-20		X	X
M43 Bulk		X	X	M165 0-10		X	
M45 60-70	X	X	X	M16510-20		X	
M45 70-80	X			M165-20-30		X	
M55 50-60	X			M165 30-40		X	
M55 60-70	X	X	X	M165 40-50		X	
M55 90-100	X			M165 50-60		X	
M102 0-10	X	X	X	M165 60-70		X	
M102 10-20	X			M168 20-30		X	X
M102 20-30	X			M170 10-20		X	X
M102 40-50	X						

2.3 PARTICLE SIZE ANALYSIS (PSA)

Two methods of sieving for particle size analysis were undertaken: wet sieving for the separation of the cohesive sediment and for the collection of the <63 µm fine fraction; and dry sieving for the analysis of the coarse fraction containing insignificant quantities of silt and clay. A SediGraph 5100 was used for determining the size distribution of particles less than 63 µm in diameter by sedimentation, in which the density of the sediment suspension at various intervals is measured. By combining data from the sieving and sedimentation procedures, a continuous particle-size distribution curve of the sediment could be plotted for each sample, from the coarsest particles down to the clay fraction. In total 56 samples were subjected to PSA.

2.4 X-RADIOGRAPHY

The sedimentary characteristics of the sediments within the estuary have been determined by X-radiography of 19 selected cores, undertaken by NDT Services Ltd at East Midlands Airport. Although some sedimentary structures and lithological changes can be observed under good lighting in slabbed sediment cores, the styles of bedding and any biological or physical disturbance to the sediments can often be revealed in much greater detail using X-radiography. The cores were slabbed in a frozen state to prevent artificial disruption to the bedding, and subsequently X-rayed in a partially defrosted state to avoid an impaired image due to the presence of ice crystals. X-ray intensity was varied to reveal the maximum information on sedimentary structures.

2.5 MINERALOGY

Mineralogical studies were carried out on a limited number of Mersey cores and river sediment samples from the catchment of the Mersey to provide more information on the characteristics of the sediments, their provenance, and the chemical speciation of their constituents.

2.5.1 Clay mineralogy

The clay mineralogy of 22 estuarine and 11 river sediments was characterised by X-ray diffractometry (XRD) (Table 2.3). The bulk sediments were wet-sieved to separate out the <63 µm fraction and then a nominal less than 2 µm fraction was further separated from this by gravitational settling according to Stoke's Law. The less than 0.5 µm fraction of three samples was also studied.

2.5.2 Petrography

Detailed petrographical observations were made on three sampling sites in the Mersey estuary, selected because they showed high concentrations of heavy metal contamination (as indicated by bulk geochemical analyses, described elsewhere in this report). Petrographical analyses were undertaken on cores which had been preserved by sealing and freezing immediately after core recovery in order to limit any mineralogical alteration of the

Table 2.3 Details of samples used in mineralogical studies.

Estuary site	Sample type	Depth (cm)	River site	Sample type	Depth (cm)
M7	grab	0–10	Irwell centre river	grab	0–10
M28	half-core	0–10	Irwell 2 central	grab	0–10
“	“	30–40	Bollin 1	grab	0–10
“	“	60–70	Bollin 2	grab	0–10
M42	grab	0–10	Tame 1	grab	0–10
M42	half-core	30–40	Weaver 1	grab	0–10
“	“	58–68	Goyt 1 centre bar	grab	0–10
M48	grab	0–10	Roch 1	grab	0–10
M48	half-core	30–40	Croal 1 left bank	grab	0–10
M69	grab	0–10	Mickerbrook 1	grab	0–10
M95	half-core	0–10	Etherow 1	grab	0–10
“	“	30–40			
“	“	60–70			
“	“	90–100			
M101	half-core	0–10			
“	“	30–40			
“	“	60–70			
M167	half-core	0–10			
“	“	30–40			
M193	grab	0–10			
M205	grab	0–?			
M232	grab	0–?			

anoxic sediments by oxidation that might occur during sample storage. Subsamples of frozen core material were examined using cryogenic scanning electron microscopy (cryoSEM) (Dodd, 2000; Large et al., 2001; Dodd et al., 2003). Mineralogical identifications made during cryoSEM observation were based on microchemical information obtained by semiquantitative energy-dispersive X-ray microanalysis (EDXA), carried out simultaneously during cryoSEM. Some quantitative compositional information for authigenic sulphides was also obtained using EDXA during cryoSEM observation. Additional petrographical information was obtained by conventional SEM observation of the surfaces and alteration characteristics of separated heavy ‘mineral’ fractions (see also below).

2.5.3 Heavy mineralogical components

Heavy liquid (bromoform, specific gravity = 2.95) separation was carried out on 17 sediment samples from different depths at six sites (M28, M42, M48, M95, M101 and M167), in order to concentrate discrete heavy metal phases that might be present as trace components in the sediments. These concentrates were then characterised mineralogically and chemically by scanning electron microscopy (SEM) and EDXA.

2.5.4 Sequential chemical extraction and chemometric analysis

The distribution of trace metals within the different physico-chemical phases found in sediments can provide an insight into their transport and fate within the environment. This study aims to investigate the solid phase distribution of trace elements that are considered as markers for anthropogenic pollution (As, Cd, Co, Cr, Cu, Ni, Pb, V and Zn). The proposed methods for determining the distribution is a new methodology called Chemometric Identification of Substrates and Metal Distributions (CISMeD) recently described by Cave et al. (2004).

The four core samples used for the study were selected to be representative of the variety of environments encountered over the length of the estuary. Table 2.4 shows the core numbers and sample depths. M42 comes from near the mouth of the Mersey estuary and M48 comes from close to the tidal limit of the estuary. For core M101 three samples were taken to look for depth trends; this core was taken from the north bank of the estuary in the central region where most of the past and present industrial activities have taken place. M167 was taken from the south bank in the central industrialised region of the estuary.

The data from the CISMeD extraction test were subjected to the chemometric data processing procedure described by Cave et al., (2004).

Table 2.4 List of core samples tested for CISED extraction.

Core	Sample depth (cm)
M42	30–40
M48	30–40
M101	0–10
M101	30–40
M101	60–70
M167	30–40

3 The Mersey estuary sediment geochemistry geographical information system (GIS)

As much as possible of the available spatial data relevant to the study of sediment geochemistry in the Mersey estuary has been assembled in the Mersey Geographical Information System (MGIS), built in ESRI's ArcGIS. Its principle role has been to provide a means for viewing and querying spatially attributed data within the extent of the Mersey estuary. The GIS provides a wealth of information for use in assessing the evolutionary characteristics of the estuary as well as sediment and contaminate sources and sinks.

This data is in British National Grid coordinate system. This has a Transverse Mercator projection with an Airy spheroid and an OSGB 1936 datum.

The Mersey GIS holds the following data layers.

- ***Mersey sampsites*** – this point layer shows the locations of core and grab samples collected in the Mersey estuary by BGS during the study.

- ***Tin contour*** – this is a model of the land surface and was created from Ordnance Survey Landline data that BGS holds in DXF format. The data was gridded and an ArcInfo grid file created. This was saved as a triangulated irregular network file (TIN) and was contoured.

- ***Bathymetry*** – The bathymetric dataset is a combination of LIDAR data at low tide and Sonar bathymetry data at high tide. The LIDAR instrument records the heights of all objects that the laser pulse hits, regardless of whether it is ground surface or a building. Data derived in this way is termed a Digital Surface Model (DSM) or a Digital Elevation Model (DEM). The data was passed through a classification and filtering process that attempts to identify all of the surface objects (i.e. buildings, vegetation etc) and remove them from the model. This should give a good estimate to the bare earth measurement. This model is called a Digital Terrain Model (DTM).

Both the DTM and DSM data were provided by the Environment Agency in the form of 50m spaced spot heights in OSGB projection. A Triangulated Irregular Network (TIN) was the created from this point data using the elevation (Z) values. The TIN surface was then classified into 15 categories divided by Natural Breaks in the data.

- ***Satellite images*** – Satellite imagery of the Mersey estuary is incorporated. Nigel Press Associates supplied the images. Four images of the estuary are included, three using Landsat 5 on 31st May 1985, October 30th 1988 and May 31st 1994 respectively, and one using Landsat 7 on September 11th 2002. The images use bands 2 (Green), 3 (Red) and 4 (near infra red) of the electromagnetic spectrum. Band 2 has been coloured blue, band 3 has been coloured green and band 4 has been coloured red. Red areas on the imagery depict salt marsh/vegetation. Brown areas indicate mud and silt, green areas depict sands and brown/green areas indicate intermixed sand and silts.

- ***Geochemistry samples*** – Geochemical Baseline Survey data (GBASE) is high-resolution geochemical data derived principally from stream sediments at an average density of 1 sample every 1–2 square kilometre of the UK land surface. Soil samples have also been collected in urban areas. The data is stored in the BGS data holdings. The geochemistry of sediments and soils is related to factors such as bedrock geology, drift cover, land use, climate and topography.

- ***Geochemistry grids*** – illustrations of the concentrations of various chemical elements from the GBASE samples.

- ***Geological information*** – This shows BGS geology data from the BGS data holdings. This has the most up to date geology maps for the UK. Any scale of map not required can be deleted from the layer. Scales of maps included are the 625k superficial and bedrock layers, 250k bedrock layer and 50k superficial, bedrock, mass movement and artificial layers.

- ***Topographic vector layers*** – These layers are vector topographic features from the Ordnance Survey Strategi and Sysdata data sets. The data includes layers such as coastline, county boundary, place names and roads.

- ***Topographic raster layers*** – These layers are raster topographic images from the Ordnance Survey. They are loaded using the topographic base maps from BGS data holdings. There are several scales of map included and the base map displayed is that which is appropriate to the map scale.

- ***XRF images*** – This grouped layer is the XRF images. This includes 16 raster grid files that are stored in ArcInfo format. They show a raster representation at each sample point for element values both at the surface, 0–10cm, and at depth, 30–40 cm.

- ***Historical OS maps*** – Georectified historical maps obtained from the Ordnance Survey are available within the GIS. These maps, when compared with current OS data, give insight into the evolution of the shape of the estuary. The historical maps date back as far as 1844 in the Merseyside area.

4 Particle size distribution

A modified Folk classification is used to describe the nature of the estuary sediments (Figure 1.9). The predominantly sandy nature of the Mersey estuary is illustrated in Figure 1.9, drawn up on the basis of particle size data collected during this study. The sand is predominantly fine-grained, becoming medium-grained towards the middle of the estuary where flow velocities are higher. Towards the Narrows, where the channel becomes constricted and is scoured by fast flowing tides, the estuary floor is covered by gravelly sand. However, over a large area of the Narrows, velocities are so high that no sediment is deposited, and underlying bedrock is exposed.

As a general rule, mud is most prevalent along the margins of the Inner and Upper Estuary, occurring on intertidal flats at Ince Banks, including to the west of Stanlow Point, the inner part of Dungeon Banks, and along the estuary flanks from the Runcorn bridges to Howley Weir, Warrington. Mud also accumulates within the enclosed areas of the dockyards along the sides of the Outer Estuary.

Mud is also deposited from suspension on the larger banks within the middle of the estuary, but is prone to reworking by subsequent tides and consequently is underrepresented in the sediment cores. The common occurrence of mud clasts within cores sunk through the estuary sediments testifies to destruction of the mud layers by tidal current action.

5 Organic geochemistry

5.1 TOTAL ORGANIC CARBON AND LOSS ON IGNITION

As a preliminary to more focused investigations of their organic geochemistry 87 samples of core sediments collected from the Mersey estuary had both their Total Organic Carbon (TOC) and Loss On Ignition (LOI) determined (Table 5.1). A plot of TOC versus LOI (Figure 5.1) exhibits a strong correlation ($R^2 = 0.9406$) between the two parameters indicating that LOI can be employed to provide a crude estimate of the organic matter content of the sediments. However, it should be borne in mind that LOI measurements tend to overestimate the amount of organic matter since the loss of strongly bonded structural water (e.g. water of crystallization) and carbon dioxide from mineral bicarbonates and some carbonates, together with loss of nonorganic volatile material, also occurs during the process (Goldin, 1987). The equation presented in Figure 5.1 may be rearranged to calculate the TOC in terms of the LOI such that $TOC \approx 0.336\ LOI - 0.15$. In other published data the correlating coefficient tends to be closer to 0.4 (Ball, 1964; Goldin, 1987). However, Ball acknowledges that substantial variations in reported organic carbon/organic matter ratios are found to occur in the literature.

Loss On Ignition determinations are listed with the main inorganic chemistry dataset, but a tabulation of LOI determinations carried out specifically to inform the organic geochemistry programme is presented in Appendix 2 (a–h), together with brief descriptions of the samples. In general, the LOI values were found to be in the range 0 to 11 per cent with three notable exceptions. These occurred for:

- M51 where material from 70–80 cm down the core gave an LOI of 19.72 per cent in contrast to the remainder of the core where LOI varied between 1.74 and 7.71 per cent.
- M142 where material from 10–20 cm down the core gave an LOI of 20.15 per cent in contrast to remainder of the core where LOI varied between 3.33 and 6.98 per cent.

Table 5.1 Comparison of TOC (per cent by wt) and LOI (per cent by wt) in Mersey estuary sediments. Depths in cores are in cm. nd = not detected.

Sediment core	TOC	LOI	Sediment core	TOC	LOI	Sediment core	TOC	LOI	Sediment core	TOC	LOI
M31 0–10	0.09	0.69	M45 20–30	0.06	0.70	M55C 40–50	0.11	0.78	M104 40–50	0.06	0.50
M31 10–20	0.09	0.67	M45 30–40	0.08	0.75	M55C 50–60	0.68	2.16	M104 50–60	0.06	0.67
M31 20–30	0.19	1.01	M45 40–50	0.12	0.62	M55C 60–70	0.57	1.49	M104 60–70	0.06	0.86
M31 30–40	0.28	1.32	M45 50–60	0.44	1.53	M55C 70–80	0.13	1.12	M104 70–80	0.10	0.76
M31 40–50	0.13	0.82	M45 60–70	0.77	1.74	M55C 80–90	0.17	0.78	M104 80–90	0.07	0.56
M31 50–60	0.09	0.88	M45 70–80	0.60	2.04	M55C 90–100	0.83	2.08	M105 0–10	0.28	1.26
M31 60–70	0.08	0.54	M47 0–10	0.26	1.18	M56 0–10	0.09	1.11	M105 10–20	0.15	1.59
M31 70–80	0.06	0.55	M47 10–20	0.09	0.50	M56 10–20	0.07	1.10	M105 20–30	0.30	1.62
M31 80–90	0.16	0.74	M47 20–30	0.07	0.70	M56 20–30	0.07	0.96	M105 30–40	0.21	1.38
M31 90–100	0.11	0.64	M47 30–40	0.19	0.93	M56 30–40	0.10	0.86	M105 40–50	0.20	1.14
M31 100–110	0.06	0.52	M47 40–50	0.50	1.75	M56 40–50	0.07	0.96	M105 50–60	0.27	1.41
M38 0–10	0.09	0.51	M47 50–60	0.37	1.45	M56 50–60	0.06	0.69	M105 60–70	0.14	0.97
M38 10–20	0.08	0.65	M47 60–70	0.36	1.22	M56 60–70	0.10	0.80	M105 70–80	0.10	1.09
M38 20–30	0.06	0.64	M47 70–80	0.15	0.86	M56 70–80	0.21	0.82	M105 80–90	0.09	1.11
M38 30–40	0.07	0.59	M47 80–90	0.33	1.33	M102 0–10	1.67	6.56	M108 0–10	0.09	0.81
M38 40–50	0.37	1.27	M50 0–10	0.06	0.52	M102 10–20	0.97	3.67	M108 10–20	0.05	0.71
M38 50–60	1.48	4.34	M50 10–20	0.05	0.48	M102 20–30	0.63	2.87	M108 20–30	0.07	0.77
M38 60–70	0.20	1.15	M50 20–30	0.16	0.72	M102 30–40	0.47	1.76	M108 30–40	0.05	0.86
M38 70–80	0.19	0.77	M50 30–40	nd	nd	M102 40–50	1.06	3.19	M108 40–50	0.06	0.93
M39 0–10	0.08	0.85	M50 40–50	0.06	0.76	M102 50–60	1.16	3.01	M108 50–60	0.08	0.70
M39 10–20	0.06	0.83	M50 50–60	0.09	0.61	M102 60–70	0.77	2.23	M108 60–70	0.05	0.78
M39 20–30	0.07	1.06	M50 60–70	0.08	0.41	M102 70–80	0.61	2.03	M108 70–80	0.05	0.64
M39 30–40	0.05	0.50	M50 70–80	0.15	0.57	M102 80–90	0.56	1.76	M122 0–10	2.14	7.33
M39 40–50	0.06	0.72	M50 80–90	nd	nd	M102 90–100	0.67	1.96	M122 10–20	1.79	6.35
M39 50–60	0.10	0.75	M50 90–100	nd	nd	M102 100–110	0.34	1.34	M122 20–30	1.81	7.18
M39 60–70	0.49	1.21	M55 0–10	0.21	1.12	M104 0–10	0.06	0.85	M122 30–40	1.64	5.04
M39 70–80	0.06	0.73	M55 10–20	0.15	1.10	M104 10–20	0.05	0.76	M122 40–50	1.43	4.21
M45 0–10	0.08	0.93	M55 20–30	0.18	1.10	M104 20–30	0.05	0.52	M122 50–60	1.56	5.02
M45C 10–20	0.07	0.75	M55 30–40	0.21	1.03	M104 30–40	0.05	0.74	M122 60–70	0.47	1.92

- SJ47NE80 7.50–7.74 INCE 4–10 where material from 7.50–7.74 m down the core gave an LOI of 27.88 per cent in contrast to remainder of the core where LOI varied between 1.02 and 3.53 per cent.

In the last case, the field sampling notes recorded a peat horizon between 7.10–8.10 m whilst the rest of the core consisted essentially of sand, silt and clay. It is possible that in the two other cores the high LOI values also correspond with discrete horizons of high organic matter content, but this is not explicitly recorded in the sampling notes.

Two main observations emerge from a review of the LOI data:

- In general, there was not a large variation of LOI with depth. For the organic geochemistry programme it was thus deemed acceptable to calculate average LOI values for each core and employ these to give an estimate of TOC (per cent by weight) for the various sampling locations. The results are presented in Table 5.2. The validity of this operation relies on the strong correlation found to exist between LOI and TOC for these sediments (Figure 5.1).
- Overall, there was found to be a close relationship between sediment type and LOI estimated TOC (Table 5.3).

The predominantly muddy cores came largely from the banks of the estuary with the majority of the sandy cores originating in mid estuary. Contaminants predicted to associate with the natural organic matter content of the Mersey sediments, e.g. polycyclic aromatic hydrocarbons (PAHs), polychlorinated biphenyls (PCBs) and other anthropogenic organic pollutants, might thus be expected to occur at much higher concentrations nearer the margins of the estuary.

5.2 POLYCYCLIC AROMATIC HYDROCARBONS

5.2.1 Introduction

As a class of organic compounds, polycyclic aromatic hydrocarbons (PAHs) are characterised by two or more fused aromatic rings and as environmental contaminants give cause for concern because some display toxic, mutagenic and carcinogenic activity (Lehr and Jerina, 1977). In general, low molecular weight two- and three-ringed PAHs have a significant acute toxicity, whereas four- to six-ringed PAHs tend to display a greater carcinogenicity.

Table 5.2 Estimated TOC (per cent by weight) in Mersey estuarine sediments based on LOI (per cent by weight).

Sample	TOC %	Sample	TOC %	Sample	TOC %	Sample	TOC %	Sample	TOC %	Sample	TOC %	Sample	TOC %	Sample	TOC %
M2	0.27	M62	0.18	M156	0.14	M215 Grab	0.12	M258	1.76	1IB6	3.17	2IB7	1.70	INCE2–1	0.32
M4	0.55	M64	1.61	M157	0.20	M216 Grab	0.20	M260	0.54	2IB6	2.54	3IB7	1.84	INCE2–2	0.19
M6	0.25	M66	0.24	M158	0.22	M217 Grab	0.20	M261	0.16	3IB6	2.37	4IB7	1.93	INCE2–3	0.41
M7	0.20	M67	1.77	M160	0.12	M218 Grab	0.12	M262	0.14	4IB6	1.99	5IB7	1.83	INCE2–4	0.97
M12	1.63	M70	0.58	M162	0.00	M219 Grab	0.12	M263	0.12	5IB6	2.52	6IB7	1.97	INCE2–5	0.98
M15	0.70	M71	1.46	M163	0.10	M220 Grab	0.15	M264	0.14	6IB6	2.42	7IB7	1.87	INCE2–6	0.55
M16	0.17	M72	0.37	M164	1.12	M221 Grab	2.76	M265	1.27	7IB6	2.77	8IB7	1.72	INCE2–7	0.59
M17	0.31	M76	1.37	M165	1.78	M222 Grab	0.25	M266	1.33	8IB6	2.66	9IB7	1.68	INCE3–1	1.04
M20	0.11	M77	1.97	M166	2.69	M223 Grab	0.45	M267	0.22	9IB6	2.34	10IB7	1.72	INCE3–2	0.65
M22	0.19	M80	0.81	M167	3.24	M224 Grab	0.09	M268	1.41	10IB6	1.99	11IB7	1.67	INCE3–3	0.33
M23	0.19	M82	0.33	M168	1.77	M225 Grab	0.06	M269	0.14	11IB6	1.64	12IB7	1.50	INCE3–4	0.36
M26	1.82	M84	1.75	M170	0.17	M227 Grab	1.18	M270	0.40	12IB6	1.56	13IB7	1.58	INCE3–5	0.45
M28	2.02	M86	0.29	M177	0.77	M228 Grab	1.36	M271	0.71	13IB6	1.78	14IB7	1.57	INCE3–6	0.36
M30	1.00	M92	0.12	M181	2.69	M229	0.93	M272	0.76	14IB6	1.54	15IB7	2.01	INCE3–7	0.46
M31	0.11	M95	1.31	M182	2.40	M230	0.38	M273	0.34	15IB6	1.91	16IB7	0.79	INCE3–8	0.54
M34	1.74	M97	0.01	M183	1.60	M231	1.53	M274	0.96	16IB6	1.86	17IB7	0.57	INCE4–1	1.00
M36	0.16	M98	0.21	M185	0.64	M232	1.57	M275	0.93	17IB6	1.96	18IB7	0.85	INCE4–2	0.29
M37	0.07	M99	0.40	M186	1.23	M233	1.62	M276	1.80	18IB6	1.69	19IB7	0.62	INCE4–3	0.15
M38C	0.27	M101	2.43	M188 Grab	0.31	M234	1.30	M277	1.64	19IB6	1.74	20IB7	0.23	INCE4–4	0.32
M39C	0.13	M102	0.78	M189 Grab	0.17	M236	0.99	M278	1.85	20IB6	2.05	21IB7	0.25	INCE4–5	0.69
M42	1.15	M104C	0.08	M190 Grab	0.29	M238	0.18	M279	1.97	21IB6	2.04	22IB7	0.09	INCE4–6	1.01
M45C	0.23	M105C	0.28	M192 Grab	0.17	M239	0.42	M280	2.32	22IB6	1.39	23IB7	0.17	INCE4–7	0.43
M47	0.22	M106	1.38	M195 Grab	0.23	M241	0.14	M281	2.03	23IB6	0.61	24IB7	0.30	INCE4–8	0.42
M48	0.80	M108C	0.11	M196 Grab	0.18	M243	0.11	M282	1.61	24IB6	0.61	25IB7	0.20	INCE4–9	0.87
M50	0.46	M122	1.63	M199 Grab	0.20	M244	0.63	M283	1.59	25IB6	0.65	26IB7	0.21	INCE4–10	9.22
M51	1.81	M126	2.74	M200 Grab	0.20	M245	2.10	M287	2.32	26IB6	0.56	27IB7	0.32	INCE4–11	0.01
M55C	0.28	M131	0.21	M201 Grab	0.18	M248	1.67	M288	1.41	27IB6	0.26	29IB7	0.19	INCE5–1	0.22
M56	0.16	M142	2.27	M202 Grab	0.16	M249	1.85	M289	1.56	28IB6	0.30	1IB8	0.16	INCE5–2	0.31
M57	0.23	M146	2.24	M205 Grab	0.22	M250	1.64	M290	2.00	29IB6	0.02	2IB8	0.29	INCE5–3	0.34
M58	0.33	M149	0.09	M206 Grab	0.63	M251	1.52	M293	0.65	30IB6	0.07	3IB8	0.12	INCE5–4	0.32
M59	0.19	M150	0.17	M207 Grab	0.15	M253	0.09	M294	0.83	31IB6	0.08	4IB8	0.18		
M60	0.29	M151	0.18	M210 Grab	0.12	M255	0.17	M297	0.80	32IB6	0.08	5IB8	0.15		
M61	0.33	M155	1.77	M211 Grab	0.12	M257	0.13	M298	0.66	1IB7	3.04	6IB8	0.25		

Table 5.3 Relationship between sediment type and LOI-estimated TOC.

Core	Highest	Lowest	Average	Std. dev.	No. of type Samples
	est. TOC %	est. TOC %	est. TOC %	est. TOC %	
Sandy	0.70	0.00	0.21	0.13	56
Sand/mud	1.81	0.20	0.64	0.37	23
Muddy	3.24	0.54	1.76	0.52	51

The presence of PAHs in the environment is the result of a variety of anthropogenic and biogenic activities with incomplete combustion and pyrolysis of fossil fuels serving as the major source (McCready et al., 2000). This pyrolitic input may be supplemented by PAHs originating from grass and forest fires. In specific locations there may also be a petrogenic contribution of PAHs to estuarine sediments from crude oil, coal and various refinery products. Normally, anthropogenic in origin and typically arising from run-off, industrial and sewage discharges, spillage, shipping activities etc. this source can in some cases be natural as for instance oil seepage from depth. Additionally, though to a lesser extent, natural petrogenic PAHs in sediments can originate from the diagenesis of natural precursors like terpenes, pigments and steroids.

PAHs are ubiquitous, even tainting sediments from formerly pristine regions like the Beaufort and Barents Seas of the Arctic (Yunker et al., 1996). Many hundreds of PAHs exist in the environment, but the US Environmental Protection Agency (USEPA) has listed sixteen as "Consent Decree" priority pollutants and these are most frequently monitored for regulatory purposes. The distributions and ratios of some of these, (e.g. phenanthrene:anthracene and fluoranthene:pyrene), can provide information on the likely sources of anthropogenic PAH contamination (Readman et al., 2002).

Because PAHs are extremely nonpolar and hydrophobic they tend to partition strongly into sediment organic matter leaving low concentrations of PAH in equilibrium with any surrounding aqueous phase. Often, PAH concentrations in the porewaters of sediment cores are very much lower than predicted by equilibrium partioning models (even by as much as 100 times) because of the presence of soot particles (Bucheli and Gustafsson, 2000). Generated concomitantly with PAHs during incomplete combustion processes, sediment soot particles increase the partition of PAH into the particulate phase. This impacts the bioavailability of PAHs as microrganisms can only degrade them as dissolved species.

Details of the PAH content of 20 samples of sediment obtained from a variety of locations within the Mersey estuary are given in Table 5.4. The samples chosen were those displaying the highest TOCs of the 116 for which TOC was actually determined (see Table 5.1). It was assumed that these would have an appreciable PAH content and accordingly be representative of the higher levels of PAH pollution that might be expected in the estuary.

Using the chromatographic data it was possible to draw some conclusions concerning the likely origins of the PAH in the sediments.

5.2.2 Total PAH concentrations

The chromatographically determined values for the concentrations of 15 PAHs appear in Table 5.4. The PAH concentrations for each sample have been summed to give the total PAH for that sample. It should be borne in mind that this 'total', though useful for facilitating comparisons, is likely to underestimate the actual total concentration of PAHs as it consists of only parental (i.e. non-alkylated) PAHs in the two- to seven-ringed range. Also, the focus on these non-alkylated species can detract from the recognition of petrogenic PAHs where lower molecular weight alkylated homologues and sulphur heterocyclics abound (Bouloubassi and Saliot, 1993). That said, most sediment PAH studies are based on the determination of a limited number of individual PAHs — typically between 9 and 28 (Readman et al., 2002) and the use of the 15 or 16 USEPA PAHs has been universally adopted at the present for contaminated land assessment.

Total PAH concentrations in the samples were found to range between 626 µg/kg and 3766 µg/kg. A relatively recent survey of UK estuarine PAHs (conducted between 1993 and 1996) revealed a PAH range for the summed concentrations of 15 USEPA PAHs in Mersey mud samples of 1811 µg/kg to 6230 µg/kg (i.e. a comparable analysis to this study), with a much lower range of 6 µg/kg to 220 µg/kg for sandy samples (Woodhead et al., 1999). The much lower concentrations of PAHs in sandy samples primarily stems from their lower organic matter content. Because PAHs are extremely hydrophobic they tend to sorb strongly to the organic content of sediments rather than associate with the more hydrophilic mineral constituents. Our determinations of TOC (Total Organic Carbon) and LOI (Loss on Ignition) on a very large number of Mersey estuarine sediments invariably showed that a much lower organic matter content was associated with sandy samples than with muddy samples (see Section 5.1 Total Organic Carbon and Loss On Ignition).

Additionally, a degree of correlation between the TOC and the total PAH concentration of the sediments was found as shown in Table 5.4 and illustrated graphically in Figure 5.2. When PAHs originate, as most do, from pyrolitic sources, the high temperature combustion process leads to their usually being bound to very fine "supersorbent" soot particles. In such a form they can be transported great distances by the wind, hence their global ubiquity. The fine soot fraction has been found to comprise 2–30 per cent of total organic carbon in coastal sediments (Bucheli and Gustafsson, 2000). The PAHs in the samples analysed, were probably bound largely to soot particles that constituted a variable proportion of the total organic phase of the sediments, leading to a weakly positive but nevertheless significant correlation. These conclusions are of course based on the premise that the PAHs found in the sediments are primarily of a pyrolitic origin. That this was essentially the case was demonstrated by examination of the distribution patterns of the PAHs in the sediments (see below). Notwithstanding, the examination also indicated the presence of some petrogenic input (see section 5.2.3).

The highest total PAH concentrations found by Woodhead et al. (1999), i.e. 6230 µg/kg and 5740 µg/kg, were for sediments obtained from Eastham Lock, located at the western end of the Manchester Ship Canal. This value correlates well with an earlier sample from the same site where PAH concentration for a total of 13 PAHs was found to be 5310 µg/kg (Readman et al., 1986).

In a later study (1998) of UK estuarine PAH, a much larger number of sediments from the Mersey estuary were analysed and total PAH in the range 664 µg/kg to 11229 µg/kg for the summed concentrations of 22 PAHs and 265 µg/kg to 6629 µg/kg for the 4–6 ring members was discovered (Rogers, 2002). The highest concentrations were in sediment from Oglet and it was in this vicinity that the highest concentrations in this study were found, at sample location M122 (about 1 km east of Oglet).

Table 5.4 PAH data and limits of detection for Mersey core samples. Abbreviations:

Ace.	Acenaphthene	Anth.	Anthracene	Chrys.	Chrysene
Fanth.	Fluoranthene	Fluor.	Fluorene		Phen.
	Phenanthrene Pyr.	Pyrene		Naph.	Naphthalene
B(a)anth.	Benzo(a)anthracene	B(a)pyr.	Benzo(a)pyrene		
B(b)fanth.	Benzo(b)fluoranthene	B(k)fanth.	Benzo(k)fluoranthene		
B(ghi)per.	Benzo(ghi)perylene	DB(ah)anth.	Dibenzo(ah)anthracene		

I(123cd)pyr. Indeno(1,2,3-cd)pyrene.

Sample	Weight of sediment extracted	Naph.	Ace.	Fluor.	Phen.	Anth.	Fanth.	Pyr.	B(a) anth.	Chrys.	B(b) fanth.	B(k) fanth.	B(a) pyr.	DB(ah) anth.	B(ghi) per.	I(123cd) pyr.	Total	TOC
	g	µg/kg	µg/kg	µg/kg	µg/kg	µg/kg	µg/kg	µg/kg	µg/kg	µg/kg	µg/kg	µg/kg	µg/kg	µg/kg	µg/kg	µg/kg	µg/kg	%
M38C 50–60	16.795	45.7	28.4	36.9	94.4	28.4	61.1	112.9	58.4	83.1	114.5	54.4	107.0	27.4	93.6	89.7	1036	1.48
M45C 60–70	22.573	19.3	12.5	17.8	69.5	25.3	113.7	112.6	55.8	79.0	77.9	45.3	86.7	21.7	27.8	68.1	833	0.77
M45C 70–80	24.097	17.8	24.3	30.3	77.7	31.8	98.5	157.9	83.1	107.0	144.2	73.3	138.2	46.2	115.1	115.3	1261	0.60
M55C 50–60	26.926	28.7	16.0	18.9	44.8	13.4	59.6	157.9	53.2	69.3	94.1	48.8	80.8	28.5	62.3	64.3	793	0.68
M55C 60–70	20.214	8.5	13.6	14.3	34.9	13.8	38.2	66.3	35.0	47.2	80.5	41.3	76.3	20.4	67.4	68.0	626	0.57
M55C 90–100	27.507	38.5	38.4	11.6	155.0	60.0	184.4	284.3	150.4	198.8	200.3	105.0	218.1	62.5	131.5	166.1	2005	0.83
M102 0–10	13.950	48.3	58.3	64.6	180.3	60.0	220.0	342.9	207.3	302.6	425.0	197.7	315.1	102.6	303.5	370.3	3207	1.67
M102 10–20	16.114	31.0	31.3	22.0	120.3	42.8	221.6	201.8	115.5	164.8	227.7	115.9	201.3	50.1	186.5	188.7	1921	0.97
M102 20–30	30.478	29.3	30.4	39.7	126.8	43.7	119.7	204.4	102.4	134.0	154.1	81.0	144.3	38.9	127.4	124.9	1501	0.63
M102 40–50	27.155	46.2	47.4	56.1	238.4	71.4	359.6	378.2	192.8	248.0	306.6	158.5	300.8	103.4	223.0	258.1	2989	1.06
M102 60–70	25.348	45.6	54.6	71.1	236.5	93.2	246.5	395.8	303.2	474.4	279.1	137.8	289.3	97.7	214.7	226.2	3166	1.16
M102 70–80	28.705	49.2	39.0	35.7	224.8	70.0	226.7	356.8	165.7	222.1	245.5	126.5	251.0	63.6	188.6	191.8	2457	0.77
M102 50–60	24.457	39.3	32.2	45.4	140.4	50.4	152.3	206.1	121.6	164.5	199.3	112.1	227.0	59.4	172.0	180.2	1902	0.61
M102 90–100	21.153	45.2	41.7	58.6	225.3	87.5	257.7	255.9	206.1	155.9	290.0	165.7	332.2	89.3	219.9	252.4	2683	0.67
M102 0–10	13.909	48.5	47.7	60.9	166.5	61.5	300.7	261.1	189.5	268.6	392.3	204.3	367.9	88.3	339.8	366.3	3164	2.14
M122 10–20	24.679	57.1	52.9	74.0	211.0	78.3	278.0	306.3	192.3	296.8	418.5	205.5	348.1	108.5	332.2	353.6	3313	1.79
M122 20–30	18.230	37.2	56.8	75.0	234.8	80.4	308.4	378.2	227.8	344.4	432.7	212.9	439.7	109.9	352.6	475.3	3766	1.81
M122 30–40	31.163	21.4	47.7	75.0	213.8	78.3	362.4	363.6	194.0	295.7	247.4	163.7	349.5	93.4	266.8	429.3	3202	1.64
M122 40–50	30.119	57.0	51.8	45.2	238.3	79.5	392.2	341.7	192.4	294.6	382.0	382.0	363.4	90.3	90.3	304.9	3306	1.43
M122 50–60	31.545	55.8	51.1	61.4	251.1	81.6	261.2	330.7	200.6	293.1	360.8	184.8	331.6	84.8	300.6	345.0	3194	1.56
Limit of detection	0.21	40		0.04	0.05	0.03	0.17	0.16	0.05	0.06	0.19	0.04	0.04	0.35	0.37	0.21		
RSD %	4.7	5.3		2.9	6.2	2	3.7	11.9	3.8	2.9	3.2	1	2.3	0.35	6.8	2.5		

The Woodhead et al. (1999) study produced ranges for the 15 USEPA PAHs in other estuaries whose environments are highly industrialised and where similar activities to those in the Mersey region occur, e.g. River Tyne (260 µg/kg to 43470 µg/kg), River Wear (205 µg/kg to 31715 µg/kg) and River Tees (653 µg/kg to 26549 µg/kg). These may be contrasted with the total for the 15 USEPA PAH in the Solway estuary, a nonindustrialised area, where the concentration range is much lower, i.e. 12 µg/kg to 1512 µg/kg (Harrison, 2002). The Mersey estuary sediments would thus seem to suffer a lesser degree of PAH contamination than the estuaries of the north east of England. However, the study of Rogers (2002) contains an assessment of sediment toxicity (based on an equilibrium partitioning – toxic unit approach), which indicates that in the UK it is the Clyde and Mersey estuaries together with Southampton Water that possess the highest mean toxicities to aquatic organisms. The study also found that the toxicity in Mersey sediments displayed a clear decline towards the mouth, with maximum toxicity evident at Widnes West Bank (near the Runcorn–Widnes Bridge) in immediate proximity to discharges from chemical works.

It is interesting to contrast the two available depth profiles for cores taken from the estuary, i.e. for M102 and M122, shown in Figure 5.3. There is quite a wide variation in total PAHs concentration with depth for M102 and very little variation for M122. It becomes plain, however, from the TOC information, that this largely explicable in terms of a variation in the organic matter content of the sediments. Although both cores were taken from the Dungeon Banks they were about 1 km apart and so had somewhat differing constitutions. M122 was described as a brown/grey mud, whereas M102 was referred to as muddy sand (see Table 5.6).

5.2.3 PAH distribution patterns

Column charts that display the concentrations and distributions of the PAHs appear in Figure 5.4. Inspection of these reveals that, in the main, the relative proportions of PAHs are roughly similar in all the samples, regardless of sampling location and total concentration. The pattern corresponds with one that is typical globally and epitomises PAH assemblages that result from high temperature combustion processes (McCready et al., 2000). It is characterised by an abundance of the high molecular weight PAHs, (i.e. the 4-, 5-, 6- and 7-ringed members), eight of which tend to

Table 5.5 PAH relative abundance order.

Sample	Naph.	Ace.	Fluor	Phen.	Anth.	Fanth.	Pyr.	B(a) anth.	Chrys.	B(b+k) fanth.	B(a) pyr	DB(ah) anth.	B(ghi) per	I(123cd) pyr
M38C 50–60				4		8	2	9	7	1	3		5	6
M45C 60–70				6		2	3	8	5	1	4		9	7
M45C 70–80				9		7	2	8	6	1	3		5	4
M55C 50–60				9		7	2	8	4	1	3		6	5
M55C 60–70				9		7	5	8	6	1	2		4	3
M55C 90–100				7		5	2	8	4	1	3		9	6
M102C 0–10				9		7	3	8	6	1	4		5	2
M102C 10–20				8		2	3	9	7	1	4		6	5
M102C 20–30				6		7	2	8	4	1	3		5	7
M102C 40–50				7		3	2	9	6	1	4		8	5
M102C 50–60				7		6	3	4	1	2	5		9	8
M102C 60–70				5		4	2	9	6	1	3		8	7
M102C 70–80				8		7	3	9	6	1	2		5	4
M102C 90–100				6		3	4	8	9	1	2		7	5
M122C 0–10				9		5	7	8	6	1	2		4	3
M122C 10–20				8		7	5	9	6	1	3		4	2
M122C 20–30				8		7	4	9	6	1	3		5	2
M122C 30–40				8		4	3	9	6	2	5		7	1
M122C 40–50				8		2	4	9	6	1	3		7	5
M122C 50–60				8		7	4	9	6	1	3		5	2
Typical pyrolitic source				9		3	2	6	7	1	4		5	8
(McReady et al., 2000)														

predominate. These, in descending order, are benzo(b+k) fluoranthenes, pyrene, fluoranthene, benzo(a)pyrene, benzo(ghi)perylene, benz(a)anthracene, chrysene, and indeno(1,2,3-cd)pyrene. Phenanthrene, the most thermodynamically stable of the 3-ringed PAHs, may be prominent also, although if it is present in large amounts, i.e. so that the phenanthrene:anthracene ratio is greater than 10, then this may be indicative of a petrogenic origin (Budzinski et al., 1997). The relative abundances of the PAHs in the sediments were ranked and tabulated (Table 5.5). The eight high molecular weight pyrolitic PAHs together with phenanthrene were ranked in order of their prevalence. It will be observed that there were no divergences from the nine pyrolitic PAHs being exclusively the predominant species. That said, there are some differences in PAH distributions between the samples (see Figure 5.4), even from those within the same core, reflecting multiple sources of PAH input. This is perhaps not surprising given the diverse nature of the industries located in the region, i.e. chemical works, power stations, sewage works, docks, boat dismantlers, oil refineries, paper works etc., all probably making some greater or lesser discharge to the estuary. Rogers (2002) noted that for the Mersey estuary the sediments exhibited a 'mixed PAH source profile throughout its tidal range' and ascribed this to mixed petrogenic/combustion inputs from many discharges together with the continuous resuspension and mixing of historically contaminated surficial sediments during tidal mixing.

Another approach for the ascription of petrogenic/pyrolitic PAH origin is the use of molecular indices criteria based on isomeric ratios (Readman et al., 2002). The criteria arise from thermodynamic considerations of the behaviour of pairs of PAH isomers. For instance, phenanthrene is more thermodynamically stable than its isomer anthracene. Accordingly, the phenanthrene/anthracene ratio is found to be temperature dependent. At low temperature, (e.g. the slow thermal maturation of organic matter in petroleum), the phen./anth. ratio is high (50 at 100°C) but at higher temperatures, (e.g. the combustion of fossil fuels), it is much lower (4 to 10). The criteria of phen./anth. >10 for petrogenic and <10 for pyrolitic inputs emerges. It must be borne in mind that this is not rigorous and borderline values need to be treated with caution. For example, phen./anth. ratios <15 usually relate to incomplete combustion of organic matter, yet the analysis of some petroleum products, can produce ratios as low as 4 to 10 for gas-oils and about. 14 for crude oils before combustion (Budzinski et al., 1997). Similar logic may be applied to the fluor./pyr. ratio, where values >1 are classically related to pyrolitic origins, but again there are exceptions. A combination of these two ratios graphically provides a more reliable estimate of PAH source (Baumard et al., 1998). The ratio of another pair of isomers, i.e. benz(a)anth./chrys. has also been used to provide the criteria: >0.9 (pyrolitic) and ≤ 0.4 (petrogenic) with the same caveat of caution, particularly in the intermediate zone (Gschwend and Hites, 1981). Yet another pair of isomers can be used in the form of the ratio of indeno(1,2,3-cd)pyrene to indeno(1,2,3-cd) pyrene plus benzo(ghi)perylene. The criteria that emerge are that if this ratio is <0.2 a petroleum source is indicated, 0.2 to 0.5 implies liquid fossil fuel (vehicle and crude oil) combustion, and ratios >0.5 betoken coal, grass or wood combustion (Yunker et al., 2002.)

Table 5.6 presents the molecular indices for the sediments. It will be observed that all the phen/anth. ratios are <10 indicating pyrolytic PAH origin. However, fourteen of the fluoranth./pyr. ratios are <1, many

Table 5.6 Sediment data (descriptions, locations, molecular indices, summed PAHs and TOC).

Sample	Sample description	Possible sources/pathways	Phen/ Anth	Fanth/ Pyr	Phen/ Anth	B(a)A/ Chrys	I(123cd)pyr / I(123cd)pyr + B(ghi)per	Total mg/kg	TOC %
M38C 50–60	Coarse rippled sand	Located mid channel between	3.32	0.54	3.32	0.7	0.49	1036	1.48
	in stratified dunes	ex-Liverpool airport (North Bank)							
	with thin organic layers.	and oil storage depot							
		and paper works (South Bank)							
M45C 60–70	Flat sand wet	Adjacent to chemical works	2.75	1.01	2.75	0.71	0.71	833	0.77
M45C 70–80	exposed mud on surface	/ Manchester ship canal	2.44	0.62	2.44	0.78	0.5	1261	0.6
M45C 50–60	Flat sand wet	Adjacent to chemical works	3.34	0.54	3.34	0.77	0.51	793	0.68
M55C 60–70	exposed mud on surface	(Hale bank)	2.53	0.58	2.53	0.74	0.5	626	0.57
M45C 90–100			2.58	0.65	2.58	0.76	0.56	2005	0.83
M102C 0–10	Shallow,	Close to ex-Liverpool airport	2.62	0.64	2.62	0.69	0.55	3207	1.67
M102C 10–20	creeked,		2.81	1.1	2.81	0.7	0.5	1921	0.97
M102C 20–30	muddy	Downstream from several	2.9	0.59	2.9	0.76	0.5	1501	0.63
M102C 40–50	sands.	chemical works and a power	3.34	0.95	3.34	0.78	0.54	2989	1.06
M102C 50–60	Thin algae	station at Widnes	2.54	0.62	2.54	0.64	0.51	3166	1.16
M102C 60–70	on surface.		3.21	0.64	3.21	0.75	0.5	2457	0.77
M102C 70–80			2.79	0.74	2.79	0.74	0.51	1902	0.61
M102C 90–100			2.57	1.01	2.57	1.32	0.53	2683	0.67
M122C 0–10			2.71	1.15	2.71	0.71	0.52	3164	2.14
M122C1 0–20	Brown-grey	Close to ex-Liverpool airport	2.69	0.91	2.69	0.65	0.52	3313	1.79
M122C 20–30	mud		2.92	0.82	2.92	0.66	0.57	3766	1.81
M122C 30–40		Downstream from several	2.73	1	2.73	0.66	0.62	3202	1.64
M122C 40–50		chemical works and a power	3	1.15	3	0.65	0.52	3306	1.43
M122C 50–60		station at Widnes	3.08	0.79	3.08	0.68	0.53	3194	1.56

quite substantially so. Additionally when the benz(a) anth./chrys. ratio criteria are applied then only one sample (M120 90–100) would be strictly of pyrolitic origin, though conversely none would fall into the purely petrogenic category. All samples give ratios >0.5 when the isomers indeno(1,2,3-cd)pyrene and benzo(ghi)perylene are considered, implying a pyrolitic contribution that is primarily from solid fuel (presumably coal) combustion.

Plotting the phen./anth. ratio against the fluoranth./pyr. ratio gives the plot that appears in Figure 5.5. It can be seen from this that only six of the samples plot within the purely pyrolitic quadrant of the graph but none plot within the purely petrogenic quadrant. The molecular indices information, taken overall, points to a mainly pyrolitic PAH signature for the samples which has been supplemented to some extent with petrogenic PAHs.

On balance, it may be concluded that in the Mersey estuary the muds, which are predominantly located close to the banks of the river as delineated at high tide, are the principal sinks for PAH as a consequence of their higher TOC cf. the mid-estuarine sands. These can be quite strongly contaminated with PAH; our study revealed up to 3766 µg/kg for the combined 15 USEPA PAH. Other studies (Readman et al., 1986; Woodhead et al., 1999; Rogers, 2002) have disclosed even higher totals for some locations within the estuary. There would appear to be diverse PAH inputs and the distributions are indicative of a primarily pyrolitic input, augmented with a variety of industrial petrogenic inputs. This is typical for a region characterised by a large conurbation, (contributing combustion and run-off PAHs from traffic, coal burning etc.) and a high density of riverside industry (contributing both combustion-related and industry-specific PAHs).

Although the suites of 15 or 16 USEPA PAH are commonly encountered in contaminated land assessment they do not usually provide sufficiently detailed information on PAH distributions to permit definitive links to be made between specific sources of PAH contamination and observed sediment loads. Their principle value is in providing an estimate of total and individual PAH concentrations. However, even when greater detail is obtained by increasing the number of PAHs determined (e.g. Rogers, 2002), specific source identity is still invariably hindered by the complexity and diversity of inputs. Thus, estuarine system dynamics involving the tidal resuspension of bed sediments, which are themselves inhomogeneous, usually renders specific source identification difficult.

The PAH data presented here augment the comparatively sparse information currently available in published literature concerning PAH concentrations in the sediments of the Mersey estuary.

5.3 POLYCHLORINATED BIPHENYLS

5.3.1 Introduction

Polychlorinated biphenyls (PCBs) were widely used as plasticisers and heat-transfer fluids. Because of their high toxicity release to the environment is prohibited, but residues persist and significant amounts continue to enter this region through rivers, ocean currents and the atmosphere. As commercial PCB formulations comprise a series of closely related substances (congeners), and analytical techniques applied vary with respect to the number of congeners measured, datasets from different laboratories are often not directly comparable.

In this current study, the concentrations of total PCBs and 7 congeners were determined in 10 unsieved sediment samples from various depths and locations in the Mersey estuary (Table 5.7). The PCB concentrations obtained for the certified reference material (LGC 6114 harbour sediment) were in agreement within the confidence limits of the certified values.

The samples were chosen to be representative of the Mersey estuary (Table 5.7, Appendix 2), and ranged from "upstream" near Runcorn to approximately 16 km west "downstream" near the Birkenhead–Liverpool ferry port. In order to investigate the type and concentration of organic contaminants, a variety of sediment types (and TOC contents) were chosen close to potential sources (Figure 2.1). These sources included:

a) Chemical works at Hale Bank near the Ditton Brook outlet (core M55)

b) Weaver Sluices near Runcorn (core M45)

c) Airport (cores M102, M122, M160)

d) Refinery at Ellesmere Port (cores M168, M170)

e) Manchester Ship Canal outlet (M43)

f) Shipping docks at East Float Ferry Port (core M42)

These sites were also used for the organo-tin, organo-lead and saturates/biomarkers studies.

5.3.2 PCBs v TOC

The concentration of PCBs in sediments tends to be positively correlated with TOC (Figure 5.6, r2 = 0.44). This is in agreement with a study by Camacho-Ibar et al. (1996), who found a strong TOC–PCB correlation (r2 = 0.775) and demonstrated that TOC had a highly significant second order relationship with the percentage of fine sediments (r2 = 0.947) and a linear relationship with the aluminium content (r2 = 0.931). The correlation with the amount of fine particulates is a common feature of natural organic matter in bulk estuarine and marine sediments (Mayer, 1993; Keil et al., 1994).

In the current study, the lowest PCB concentration (36 ng/g) was found in mid estuary, at Stanlow Bank, in sandy sediment with a low organic matter content compared with silt or mud. Some of the highest concentrations (1409 and 113 ng/g) were found in muddy cores from Ellesmere Port (core M168, per cent TOC not determined) and Hale Village (core M102, TOC = 0.97 per cent) respectively (Table 5.8). This relationship suggests a surface area control on the TOC concentrations, which indicates the TOC in estuarine sediments is mostly present as an absorbed coating (onto which PCBs are bound), rather than as discrete organic particles (Mayer, 1993; Keil et al., 1994; Mayer, 1994).

Table 5.7 Representative samples from the Mersey estuary selected for PCB analysis.

Sample site No.	Depth interval (cm)	Description	Grid ref.	Sample ID	Type
M39	60–70	Eastham Sands, mid estuary	3382 3802	06845-00026	Brown-grey clay
M42	10–20	East Float Ferry Port,	3295 3900	06905-00026	Grey clay
M43	n/a	Manchester Ship Canal	3347 3804		Light grey clay
M45C	60–70	Weaver Sluices near Runcorn	3492 3793	06845-00034	Grey clay
M55	60–70	Hale Bank, Chemical Works near Ditton Brook outlet	3507 3833	06845-00061	Brown-grey clay
M102	10–20	150 m SSE of Hale village	3452 3803	06845-00074	Brown-grey clay
M122	60–70	Liverpool Airport, eastern end of runway	3441 3808	06845-00166	Brown clay
M160	10–20	Liverpool airport (north bank)	3407 3806	06922-00067	Medium grain sand
M168	20–30	Ellesmere Port refinery	3412 3768	06905-00076	Grey-brown clay
M170	10–20	Stanlow Bank, mid estuary	3413 3781		Fine sand

5.3.3 Total PCB concentrations

The concentrations of seven individual PCB congeners are presented in Table 5.8. The 10 sediments analysed contain a mean total PCB concentration of 231 ng/g, but there is a wide range in total values from 36.1 ng/g to 1409 ng/g.

The significance of these values is difficult to assess since there is currently much international debate with respect to maximum permitted concentrations of specified organic toxins in marine/estuarine sediments. Concentrations in the Mersey for the seven congeners can be compared with the background values presented by OSPAR (1997) shown in Table 5.9 and the Swedish Environment Protection Agency (2001) in Table 5.10. These reference values were selected for comparison because they were "normalised" to 0.5–1.0 per cent TOC which is in the same range as the TOC in the Mersey estuary samples. Under the OSPAR criteria for Norwegian Sea sediments, the Mersey estuary sediments would be classed as approximately 100–5000 times above that of background (Table 5.9). However using the Swedish model, the Mersey sediments would be classed as having "moderate to very high levels" of both total and individual PCB congeners (Table 5.10).

The range of total concentrations for the 10 Mersey sediments would be provisionally classed by OSPAR (2000) as concentrations indicating a potential area of concern. According to OSPAR (2000), un-normalised concentrations at sandy sites are generally below the detection limits (0.2–0.5 ng/g) whereas in some muddy areas, such as the north-western Irish Sea, concentrations are typically 1000–10 000 ng/g dry weight (for the sum of ten individual congeners).

5.3.4 PCB source fingerprinting

To provide a PCB "type" fingerprint for each sediment sample, PCB groups were identified on the basis of their level of chlorination, i.e. total tri-tetra-penta-hexa-hepta chlorinated congeners (Figure 5.7).

Visual inspection of the patterns (Figure 5.7) shows that sediments from some specific sites seem to have different (individual) fingerprints, although this cannot be verified on the basis of a unified depth horizon. The cores that seem to be distinctive were from Eastham Lock on the Manchester Ship Canal (M43), near Liverpool

Table 5.8 Concentrations of PCBs in the Mersey estuary. Standard error is <5 per cent.

Sample	TOC (%)	PCB 28 (ng/g)	PCB 52 (ng/g)	PCB 101 (ng/g)	PCB 118 (ng/g)	PCB 153 (ng/g)	PCB 138 (ng/g)	PCB 180 (ng/g)	Total PCBs (ng/g)
M39C (60–70)	0.49%	1.43	0.87	0.51	2.26	<0.15	0.38	<0.2	54.9
M42 (10–20)		0.68	1.58	1.05	2.94	2.15	1.55	<0.2	62.5
M43		1.33	1.84	1.22	3.43	1.31	2.50	1.17	336.3
M45C (60–70)	0.77%	4.17	1.11	0.64	2.42	3.18	0.88	<0.2	58.2
M55 (60–70)	0.57%	1.77	0.92	0.55	2.48	2.01	0.71	0.49	71.2
M102 (10–20)	0.97%	2.37	2.32	1.59	3.63	4.81	2.69	1.39	112.6
M122C (60–70)		0.78	0.78	0.40	2.02	<0.15	0.61	0.36	50.5
M160 (10–20)		<0.1	<0.1	0.13	<0.1	<0.15	<0.15	<0.2	118.5
M168 (20–30)		5.74	40.41	58.68	70.40	53.79	95.80	14.98	1409
M170 (10-20)		<0.1	<0.1	0.15	<0.1	<0.15	<0.15	<0.2	36.1
LGC 6114, SRM, PCBs in harbour sediment, determined		17.26	298.2	605.6	693.9	408.9	694.3	118.8	7354
LGC 6114, SRM, PCBs in harbour sediment, certified values		15 (±8)	335 (±57)	810 (±193)	688 (±200)	537 (±127)	648 (±164)	119 (±22)	-

Airport (M160) and off Stanlow Point (M168). With a larger sample set it might be possible to use such distinctive fingerprints to identify changes in pollutant sources with time and movement of contaminants in the estuary.

5.3.5 Down-core PCB levels

Core M34 was collected from the north bank of the estuary near Liverpool Airport and M165 was collected from the southern part of the estuary near Ellesmere Port (Figure 2.1). Because PCB concentrations in sediments are closely correlated with TOC, the down core variations in Figures 5.8 and 5.9 are all normalised to 1 per cent TOC. These data are also presented in Tables 5.11 and 5.12. Core M34 (Figures 5.8 and 5.9) shows a distinct maximum at a depth of 0.5 m, which could be related to: (a) varying sedimentation rates, i.e a slower rate at the peak; (b) particle size and surface area influencing the absorbance of PCBs, i.e. smaller particle size (larger surface area) at the peak; and/or (c) the beginning (0.8 m) and phasing out (0.5–0.2 m) of PCB production. Commercial PCB production began in 1929 and increased dramatically as their use as, inter alia, dielectric fluids in capacitors and transformers, became more widespread. By the time production in the UK ceased, the national output was estimated at 6.7 x 104 t with 1 per cent remaining in the UK environment (Harrad et al., 1994). In addition, M34 displays a second, smaller peak in total PCBs at 0.2 m (Figures 5.8c and 5.9), for which sedimentation rate or particle size variation seem to offer the best explanation. In contrast, core M165 has lower overall concentrations with no pronounced maxima, showing instead a slight increase down core from 0.35 to 0.65 (Figures 5.8b, 5.8d, and 5.9). This contrast between the two cores may be due to: (a) the location of M165 further out in the estuary, where it would be subjected to greater sedimentary turbation (e.g. by currents and channel migration) than M34, which is located very close to the north bank; (b) different original sources and concentrations of PCBs for the two cores; and/or (c) different grain-size distributions in the cores, M34 being finer-grained overall.

5.4 ORGANO-TINS

5.4.1 Introduction

Tributyltin (TBT) is a widespread contaminant of coastal waters and sediments due to its use as an antifouling agent on marine structures, nets and vessel hulls. It can be very persistent in the environment and demonstrates high toxicity to marine organisms, notably endocrine disruption in gastropod molluscs. Although the use of TBT is now restricted to vessels in excess of 25 m in length, residues persist in many coastal locations. Recent surveys have shown that TBT is common near ports, shipping channels and smaller harbours and marinas where there are facilities for small boat maintenance. The UK has set an Environmental Quality Standard for TBT in sea water of 2 ng/L. Concentrations in some busy waterways such as Milford Haven and the Mersey estuary have exceeded the UK Environmental Quality Standard by as much as a factor of ten, whilst concentrations in coastal and offshore waters are generally below the detection limit (OSPAR, 2000).

5.4.2 Results

OSPAR recently (OSPAR, 2000) reported that typical concentrations of TBT in sediments of estuaries on

Table 5.9 Ranges of background concentrations (in ng/g dry wt.) of PCB congeners in surface sediments for application in specific regions of the OSPAR Convention Area, (OSPAR, 1997).

Substances	Norwegian Sea	Iceland Sea/ Norwegian Sea	South Norway/Skagerak
TOC (%)	0.5	0.5	0.6
PCB 28	<0.01	<0.01	0.030
PCB 52	<0.01	<0.01	0.035
PCB 101	0.012	0.016	0.065
PCB 153	0.025	0.020	0.090
PCB 138	0.025	0.026	0.120
PCB 180	0.015	<0.01	0.060

Table 5.10 Classification of organic environmental toxins in sediments (Swedish EPA, 2001). Concentrations of PCBs are based on samples taken in connection with Swedish environmental monitoring programmes.

	Class 1	Class 2	Class 3	Class 4	Class 5
Substances	Null	Low level	Moderate level	High level	Very high level
	ng/g dry weight; corrected for 1% organic carbon				
PCB 28	0	0–0.06	0.06–0.2	0.2–0.6	> 0.6
PCB 52	0	0–0.06	0.06–0.2	0.2–0.8	> 0.8
PCB 101	0	0–0.16	0.16–0.6	0.6–2	> 2
PCB 118	0	0–0.15	0.15–0.6	0.6–2	> 2
PCB 153	0	0–0.03	0.03–0.3	0.3–3.5	> 3.5
PCB 138	0	0–0.3	0.3–1.2	1.2–4.1	> 4.1
PCB 180	0	0–0.1	0.1–0.4	0.4–1.9	> 1.9
PCB (sum of 7)	0	0–1.3	1.3–4	4–15	> 15
Total PCB	0	0–5	5–20	20–75	> 75

current study (Table 5.13) where TBT was found in all the sediments studied, both core and surface samples, with concentrations ranging from 0.4–2.4 µg/g (mean = 1.3 µg/g). Monobutyl and dibutyl tin compounds were also found at slightly lower concentrations (Table 5.13). The dibutyltin:tributyltin ratio was 50:50 in all the sediments with the exception of that from mid estuary at Eastham Sands (M39, 60–70 cm), which contained the highest concentration of TBT of the sample set.

5.5 ORGANO-LEADS

5.5.1 Introduction

Until recently lead was added to fuel in varying proportions of five tetra-aklyllead compounds as antiknocking agents and today it is still used under specified circumstances (USEPA, 2000). The environmental relevance of organo-lead compounds has been reviewed by Craig (1986). Such compounds are highly neurotoxic through skin absorption, inhalation and ingestion (Waldron and Stöfen, 1974). They have been found to be present in air, water, sediments and biota, with higher concentrations in urban areas. There is evidence that $Pb2^{+}$ salts can be microbially alkylated in natural aquatic sediments (Craig, 1986).

5.5.2 Results

In this current study, the lowest concentrations for trimethyllead and triethyllead were 0.49 and 0.15 ng/g (as Pb) respectively in core M43 from Eastham lock at the outlet of the Manchester Ship Canal. The highest concentrations for the same organo-lead compounds were 13.34 and 52.22 ng/g (as Pb) in core M102, 10–20 cm from near Hale village on the north shore of the estuary. The mean concentrations for the other sediments were 5.7 and 13.9 ng/g (as Pb) (Table 5.13).

5.6 SATURATES/BIOMARKERS

5.6.1 Introduction

Crude oil is a complex mixture of tens of thousands of compounds. Most of the compounds (> 75 per cent) are types of hydrocarbons in the classes n-alkanes, branched alkanes, cycloalkanes, triterpanes, aromatics, naphthenoaromatics and PAHs with up to ten condensed aromatic rings. In addition, organosulphur compounds, acids, phenols, pyridine and pyrroles are present, as are highly complex asphaltenes (Killops and Killops, 1993).

Petrogenic hydrocarbons arise from natural oil seeps, emissions, spillages or effluents, during the production and transportation of crude oil, from the refining and petrochemical industries, from general shipping activities and from the dumping of oil-contaminated dredged materials. River inputs of oil constitute a significant part of the overall load of oil entering the maritime area. 'Oil' occurs naturally in the marine environment, but not necessarily everywhere, and consequently, when it is present it is more likely to be there due to human activity than to natural causes.

5.6.2 Results

The concentrations of the hexane-extractable organic compounds are presented in (Table 5.13). The mean value was 0.56 mg/g and the maximum concentration (34.3 mg/g) was located near Ellesmere Port refinery (M168, 20–30). To our knowledge, no figures have been promulgated for maximum permitted concentrations of hydrocarbons in marine sediment. This is not surprising since many coastal areas are in direct contact with oil source rocks, for example the Kimmeridge Bay area (Dorset, UK), where the shale contains up to 20 per cent TOC, mainly as saturated organic compounds.

All the chromatograms of these extracts show very similar distributions of the organic compounds (Figure 5.10), specifically:

a) They are mainly composed of n-C21-34 alkanes, i.e. saturated organic compounds of mid to high chain length.

b) There is no odd-over-even predominance of the n-alkanes (this would suggest no significant leaf-wax input).

c) There is no predominance of n-C21 or n-C23 alkanes (this would suggest no significant marine algal input).

These 3 factors strongly indicate that the organic extract is of anthropogenic origin, probably discharged from marine craft and local industrial activity (i.e. fuel oil and lube oil).

The ratios of the biomarkers (pristane:n-C17, phytane:n-C18 and pristane:phytane) varied greatly which reflects multiple sources and mixing within the Mersey estuary (Table 5.13).

The presence of bis (2)-methylpropyl ester hexandioic acid, diisooctyl ester phthalic acid and 2,4-bis(dimethylbenzyl)-6-T-butylphenol are indicative of plastisisers which could have come from 2 possible sources: (1) the plastic core casing whilst the core was cut, or (2) anthropogenic input into the sediment from industrial or sewerage waste.

Table 5.11 Absolute PCB concentrations (ng/g) down two selected cores in the Mersey estuary. Standard error is <5 per cent; n.d. = not detected.

Core	Core depth (m)	TOC (%)	PCB 28	PCB 52	PCB 101	PCB 118	PCB 153	PCB 138	PCB 180	Total of 7 PCBs	Tri-Cl	Tetra-Cl	Penta-Cl	Hexa-Cl	Hepta-Cl	Sum of all PCBs	Extraction efficiency	
																	Tri-Cl	Hexa-Cl
M34	0.0–0.1	1.48	2.51	2.07	2.39	1.83	1.30	2.23	0.84	**13.15**	5.37	10.93	8.18	5.12	1.25	**30.8**	29%	58%
M34	0.1–0.2	1.39	2.65	1.46	2.17	0.30	1.56	2.36	1.20	**11.71**	7.90	9.62	10.38	4.25	1.90	**34.1**	48%	61%
M34	0.2–0.3	1.52	5.65	2.91	4.29	<0.15	2.89	4.24	2.22	**22.20**	18.97	21.14	23.63	11.08	4.22	**79**	72%	59%
M34	0.3–0.4	1.60	8.31	4.86	5.38	3.71	2.52	3.19	<0.20	**24.27**	19.10	28.85	10.38	6.55	n.d.	**64.9**	16%	31%
M34	0.4–0.5	1.80	12.18	4.98	5.90	4.84	3.62	5.25	3.07	**39.85**	47.28	39.27	44.51	18.20	11.42	**161**	97%	73%
M34	0.5–0.6	2.03	11.67	6.04	7.67	7.27	1.80	6.85	3.68	**44.98**	45.77	46.67	57.48	23.56	13.01	**186**	117%	67%
M34	0.6–0.7	1.90	1.63	1.29	0.45	<0.15	0.38	0.54	<0.20	**4.29**	1.63	4.08	1.40	0.33	n.d.	**7.4**	34%	74%
M34	0.7–0.8	0.96	<0.1	<0.1	<0.1	<0.15	<0.15	<0.15	<0.20	**n.d.**	n.d.	n.d.	n.d.	n.d.	n.d.	**n.d.**	24%	85%
M34	0.8–0.9	0.64	<0.1	<0.1	<0.1	<0.15	<0.15	<0.15	<0.20	**n.d.**	n.d.	n.d.	n.d.	n.d.	n.d.	**n.d.**	30%	74%
M165	0.0–0.1	1.78	3.35	1.30	2.16	2.15	1.83	2.46	1.19	**11.11**	13.72	9.28	12.37	6.72	3.27	**45.4**	65%	66%
M165	0.1–0.2	1.66	3.21	1.26	2.04	1.84	1.70	2.53	1.33	**10.75**	10.48	10.09	11.84	7.24	2.85	**42.5**	71%	40%
M165	0.2–0.3	1.61	2.95	1.29	2.13	1.71	1.86	2.35	0.99	**10.58**	11.79	8.98	11.93	6.10	1.90	**40.7**	49%	34%
M165	0.3–0.4	1.63	2.96	1.57	2.65	2.19	1.96	2.74	1.40	**11.89**	13.78	12.44	16.72	7.99	4.34	**55.3**	67%	65%
M165	0.4–0.5	1.30	3.15	1.70	2.33	2.01	1.81	2.69	1.38	**11.67**	13.29	9.13	15.27	8.45	2.77	**48.9**	93%	77%
M165	0.5–0.6	0.72	1.59	1.03	1.24	1.21	1.06	1.73	0.79	**6.64**	9.13	6.07	7.71	3.73	0.79	**27.4**	84%	62%
M165	0.6–0.7	1.40	3.61	1.55	2.67	2.03	1.90	2.28	1.45	**12.01**	14.56	12.19	14.84	8.62	3.10	**53.3**	18%	17%
Procedural blank (silica)			<0.1	<0.1	<0.1	<0.15	<0.15	<0.15	<0.20	**n.d.**	n.d.	n.d.	n.d.	n.d.	n.d.	**n.d.**	19%	48%
Average determined values, CRM, LGC 6113, PCBs in soil			14.78	10.91	24.18	29.63	31.86	44.42	25.23	**181.01**	–	–	–	–	–	–	7%	18%
Std. dev. values, CRM, LGC 6113, PCBs in soil			1.00	0.90	0.63	3.34	1.60	1.68	1.18	**3.48**	–	–	–	–	–	–	–	–
Certificate values, CRM, LGC 6113, PCBs in soil			14 (±3)	11 (±3)	23 (±6)	28 (±9)	42 (±12)	43 (±13)	29 (±8)	**None given**	–	–	–	–	–	–	–	–

5.7 NATURAL ORGANIC MATTER

5.7.1 Introduction

The fate of organic carbon (OC) in estuarine sediments is essential to understanding the flux of terrigenous material discharged from rivers to the coastal shelf. Sorption and desorption of many hydrophobic organic contaminants by altered organic matter are important processes controlling the fate and transport of pollutants. Elucidation of biological sources and geographical distributions of terrestrial organic matter (TOM) in estuaries is difficult given multiple origins of vascular plants, variations of biochemical stabilities and protective sorption of organic molecules on mineral surfaces (Hedges, 1997; Louchouarn, 1997; Hedges, 1999). These complexities are compounded by physical processes such as the daily turbulence of tides resulting in resuspension of OM and mixing of fresh and salt water that can generate significant changes in salinty, pH, density, temperature. Such dynamic physical conditions result in approximately 50 per cent of the sedimentary materials in deltas and estuaries being continually resuspended and redeposited in sediments along continental margins (Hedges and Keil, 1999).

Accumulation of vascular plant detritus in estuaries is due in part to riverine transport and deposition of organic matter from soils, marshes, cultivated land, grasslands and woodlands (Hedges et al., 1997; Hedges and Oades, 1997). Other sources of vascular plant detritus in estuaries include autochthonous Spartina marsh (salt tolerant) and aquatic higher plant communities such as sea grasses which grow on subtidal mudbanks (Opsahl and Benner, 1995; Klap et al., 1998; Klap et al., 2000). Lignin, the aromatic macromolecule found in terrestrial higher plant tissues, has been used as an indicator of land-derived organic matter in rivers, estuaries, and coastal marine sediments (Cowie and Hedges, 1992; Goni and Thomas, 2000). In comparison to cellulose, xylans and amino acids, lignin is resistant to biodegradation. The recalcitrant nature of lignin is attributed in part to the wide variety of ether and carbon–carbon bonds, which link phenylpropanoid monomers (Kirk and Farrell, 1987). The most abundant linkage in extant lignins are the aryl-alkylether types, depending on the model and lignin type these represent between 69 and 80 per cent of all inter unit linkages and are therefore crucial to the preservation of the lignin structure (Cody and Saghi-Szabo, 1999).

Tetramethylammonium hydroxide (TMAH) thermochemolysis is an analytical method that has been applied to the characterization of lignin in fungally degraded wheat straw, fresh and decomposing Spartina anglica, TOM in the Delaware estuary and near shore sediments off the coast of Newfounland (Mannino, 2000; Mannino and Harvey, 2000; Vane et al., 2001; Pulchan et al., 2003). Decomposition

Table 5.12 PCB concentrations (ng/g) normalised to 1 per cent TOC down 2 selected cores in the Mersey estuary. Standard error is <5 per cent; n.d. = not detected.

Core	Core depth (m)	TOC (%)	PCB 28	PCB 52	PCB 101	PCB 118	PCB 153	PCB 138	PCB 180	Total of 7 PCBs	Tri-Cl	Tetra-Cl	Penta-Cl	Hexa-Cl	Hepta-Cl	Total of all PCBs
M34	**0.0–0.1**	1.48	1.70	1.40	1.61	1.24	0.88	1.50	0.57	**8.89**	3.6	7.4	5.5	3.5	0.8	**20.8**
M34	0.1–0.2	1.39	1.91	1.05	1.56	0.22	1.12	1.70	0.86	**8.42**	5.7	6.9	7.5	3.1	1.4	**24.5**
M34	0.2–0.3	1.52	3.72	1.91	2.82	<0.15	1.90	2.79	1.46	**14.60**	12.5	13.9	15.5	7.3	2.8	**52.0**
M34	0.3–0.4	1.60	5.19	3.04	3.37	2.32	1.57	1.99	<0.2	**15.17**	11.9	18.0	6.5	4.1	n.d.	**40.6**
M34	0.4–0.5	1.80	6.77	2.77	3.28	2.69	2.01	2.92	1.70	**22.14**	26.3	21.8	24.7	10.1	6.3	**89.3**
M34	0.5–0.6	2.03	5.75	2.98	3.78	3.58	0.89	3.38	1.81	**22.16**	22.5	23.0	28.3	11.6	6.4	**91.9**
M34	0.6–0.7	1.90	0.86	0.68	0.24	<0.15	0.20	0.28	<0.2	**2.26**	0.9	2.1	0.7	0.2	n.d.	**3.9**
M34	0.7–0.8	0.96	<0.1	<0.1	<0.1	<0.15	<0.15	<0.15	<0.2	**n.d.**	n.d.	n.d.	n.d.	n.d.	n.d.	**n.d.**
M34	0.8–0.9	0.64	<0.1	<0.1	<0.1	<0.15	<0.15	<0.15	<0.2	**n.d.**	n.d.	n.d.	n.d.	n.d.	n.d.	**n.d.**
M165	0.0–0.1	1.78	1.88	0.73	1.21	1.21	1.03	1.38	0.67	**6.24**	7.7	5.2	7.0	3.8	1.8	**25.5**
M165	0.1–0.2	1.66	1.94	0.76	1.23	1.11	1.02	1.53	0.80	**6.47**	6.3	6.1	7.1	4.4	1.7	**25.6**
M165	0.2–0.3	1.61	1.84	0.80	1.32	1.06	1.16	1.46	0.61	**6.57**	7.3	5.6	7.4	3.8	1.2	**25.3**
M165	0.3–0.4	1.63	1.82	0.96	1.63	1.34	1.20	1.68	0.86	**7.29**	8.5	7.6	10.3	4.9	2.7	**33.9**
M165	0.4–0.5	1.30	2.42	1.31	1.79	1.55	1.39	2.07	1.06	**8.98**	10.2	7.0	11.7	6.5	2.1	**37.6**
M165	0.5–0.6	0.72	2.21	1.43	1.72	1.67	1.47	2.40	1.09	**9.22**	12.7	8.4	10.7	5.2	1.1	**38.1**
M165	0.6–0.7	1.40	2.58	1.11	1.91	1.45	1.35	1.63	1.03	**8.58**	10.4	8.7	10.6	6.2	2.2	**38.1**
Procedural blank (silica)			<0.1	<0.1	<0.1	<0.15	<0.15	<0.15	<0.2	**n.d.**	n.d.	n.d.	n.d.	n.d.	n.d.	**n.d.**

of lignin during the base catalyzed reactions caused by tetramethylammonium hydroxide thermochemolysis only occurs where propyl-aryl ether linkages are adjacent to hydroxyl groups on the alkyl side chain (Filley et al., 1999). Methylation of hydroxyl groups results in the formation of mono-, di- or tri-methoxybenzenes with either a one- two-or three-carbon side chain, which can be subsequently analysed by gas chromatography-mass spectrometry (GC-MS) (Clifford et al., 1995). Increases in the relative intensity ratios of 3, 4-dimethoxybenzoic acid methyl ester to 3, 4-dimethoxybenzaldehyde (Ad/Al)G and 3, 4, 5-trimethoxybenzoic acid methyl ester to 3, 4, 5-trimethoxybenzaldehyde (Ad/Al)S provide an excellent indicator of oxidative fungal decay (Hatcher, 1995; Hatcher and Minard, 1995; Vane et al., 2001; Vane et al., 2003). Summation of mono-, di- and trimethoxybenzene derivatives provides a measure of the amounts of labile ether linked lignin and cinnamic acid units if normalised to 100 mg of organic carbon (Λ)(McKinney and Hatcher, 1996).

Pollution of the Mersey estuary has been studied extensively but little is known about the origin, cycling and early diagenesis of particulate organic matter (POM) within the estuary inlet despite the fact that the properties of organic matter are ideally suited understanding dynamic estuarine processes (Hedges and Keil, 1999). The application of TMAH thermochemolysis can aid the characterization of organic matter in the Mersey.

5.7.2 Organic C and total N of surface sediments

The organic carbon (per cent OC) and total nitrogen composition (per cent TN) of 52 surficial sediments (0–10 cm) are presented in Figure 5.11. Concentrations of OC (per cent dry wt) ranged from 0.06 to 4 per cent (Figure 5.11). The overall highest concentrations of organic carbon were in fine muds and the lowest concentrations were from mid-channel medium sands. Total nitrogen contents of sediments (per cent dry wt) ranged from 0.003 to 0.4 per cent. General trends in per cent TN were similar to those of per cent OC in that nitrogen contents were highest in muds and lowest in sands. The C/N ratio of surface sediments ranged from 0.2 to 47 (Figure 5.12). Vascular plant cell walls are composed of nitrogen poor, carbon rich macromolecules such as lignin, tannin, suberin, cellulose and xylans, which exhibit C/N values of 20–500 (Hedges and Oades, 1997; Goni and Thomas, 2000; Vane et al., 2003). In contrast, protein rich fungi (C/N~8–10), phytoplankton (C/N~8–10), algae (C/N~3–7) and bacteria (C/N~4) are composed of molecules depleted in carbon and enriched in nitrogen (Cowie and Hedges, 1992).

The mean C/N value of 14 for surface sediments is consistent with organic matter from predominantly planktonic remains, which suggests that the estuary is a sink for marine derived OM. The fact that the average C/N value of 14 is somewhat higher than that of fresh plankton is explained by accumulation of degrading marine plankton, which tend to preferentially lose nitrogen relative to carbon. An alternative hypothesis is that a low concentration of terrestrial OM contributes to the background pool of organic carbon in the estuary. Figure 5.12 shows that six surficial sediments have C/N values greater than 20 which suggests incorporation of vascular plant debris. Several areas of salt marsh namely, Ince bank, Wigg Island, Halton Moss, Stanlow banks bound the Mersey river and these are dominated by nonwoody angiosperm flora which have C/N values in the range 35–55. Therefore, the origin of OM at locations with C/N greater than 20 probably reflects input from salt marsh plant debris. Although C/N values of fungally decayed woods range from 20–100 it is highly improbable that these materials contribute to the pool of OM. This is supported by the absence of sediments with C/N values that indicate fresh or moderately decayed woody debris (Vane et al., 2003). A comparison of C/N values down core at the M106 site (salt marsh) (Figure 2.1) revealed changes with depth (Figure 5.13). The highest C/N value was 35 at 30–40 cm depth and the lowest C/N value was 5 at 60–70 cm. These data suggest that there

Table 5.13 Concentration of organotins, organoleads, and saturates in the Mersey estuary. Standard error is <5 per cent; n.d. = not detected.

Sample	Mono butyl-tin µg/g as Sn or (µg/g as tri-chloride)	Dibutyl-tin µg/g as Sn or (µg/g as di-chloride)	Tributyl-tin (µg/g as Sn) or (µg/g as chloride)	Trimethyl-lead chloride (ng/g as Pb)	Triethyl-lead chloride (ng/g as Pb)	Saturates (mg/g)	Pristane/ n-C17	Phytane/ n-C18	Pristane/ Phytane
M39C (60–70)	<0.02 (<0.05)	0.23 (0.58)	0.89 (2.43)	<0.05	0.45	0.20	1.62	0.49	2.65
M42 (10–20)	<0.02 (<0.05)	0.15 (0.37)	0.15 (0.41)	<0.05	<0.05	0.91	0.72	0.44	1.12
M43	0.09 (0.21)	0.61 (1.56)	0.58 (1.58)	0.49	0.15	0.62	1.09	1.12	1.35
M45C (60–70)	0.05 (0.13)	0.34 (0.85)	0.33 (0.91)	1.29	2.82	0.49	1.61	0.78	1.82
M55 (60–70)	<0.02 (<0.05)	0.41 (1.03)	0.36 (0.99)	7.56	<0.05	0.33	1.12	0.77	1.32
M102 (10–20)	<0.02 (<0.05)	0.56 (1.43)	0.54 (1.46)	13.34	52.22	0.22	0.53	0.67	0.52
M122C (60–70)						1.47	1.88	0.96	1.39
M160 (10–20)						0.32	0.42	0.64	0.93
M168 (20–30)						34.23	n.d.	n.d.	n.d.
M170 (10–20)						0.49	2.21	1.20	1.34
PACS-1, CRM, Organotins in harbour sediment, determined	0.40 (0.94)	1.04 (2.64)	1.04 (2.84)						
PACS-1, CRM, Organotins in harbour sediment, certified value	0.28 (±0.17)	1.16 (±0.18)	1.27 (±0.22)						
BCR-CRM-605, trimethyllead in road dust, determined				6.82					
BCR-CRM-605, trimethyllead in road dust, certified value				7.9 (±1.2)					

is considerable temporal variation in the contribution of marine versus terrestrial OM in salt marshes. However, further bulk ^{13}C isotope data would be required to further constrain the contributions of OM sources.

Wilson et al. (2005a and 2005b) provide further discussion of ^{13}C isotope data and C/N studies in Mersey saltmarsh cores.

5.7.3 Assessment of biochemical precursors using thermochemolysis with TMAH

Figure 5.14 (a and b) shows the total ion chromatograms of the TMAH thermochemolysis products of sediments from a single core (M106) at 10 cm depth intervals (peak assignments are listed in Table 5.14). Generally, the first portion of the chromatograms contains poorly resolved peaks from precursor polysaccharides and proteinaceous compounds, the second portion consists of methylated phenolic compounds from lignin and the third section contains fatty acid methyl esters from fatty acid-containing lipids (Figure 5.14). The presence of methylated lignin phenols such as 4-methoxystyrene (P3) 3, 4-dimethoxybenzaldehyde (G4) 3, 4-dimethoxyacetophenone (G5), 3, 4-dimethoxybenzoic which are mainly indicative of terrestrial plant input in the upper sections of the core (M106) was expected since the study site is located on Ince Banks salt marsh. However, the amount and distribution of lignin phenols detected was very limited at all depths due in part to the low TOC content of the sediment (Figure 5.14 a and b).

Increases in the relative acid to aldehyde intensity ratios of 3, 4-dimethoxybenzoic acid methyl ester to 3, 4-dimethoxybenzaldehyde provide an indicator of oxidative microbial decomposition (Vane et al., 2001; Vane et al., 2003). The absence of a significant increase in 3, 4-dimethoxybenzoic acid methyl ester concentrations with depth (Figure 5.14 a and b) suggests that bacterial and particularly fungal decay was severely limited under waterlogged (O limited) estuarine conditions. In addition, there is no evidence of input from allochthonous plant material during tidal inundation events (spring tides) since these would cause variation in amounts and distribution of lignin derivatives. This observation is consistent with the

Table 5.14 Identification of thermochemolysis products shown in Figure 5.14.

Peak number	Assignment/TMAH nomenclature	Possible origin
1	4-methoxystyrene (P3)	Lignin
2	1-(1,1-dimethylethyl)-4-methoxy benzene	Lignin
3	3,4-dimethoxystyrene (G3)	Lignin
4	3,4-dimethoxybenzaldehyde (G4)	Lignin
5	3,4-dimethoxyacetophenone (G5)	Lignin
6	3,4-dimethoxybenzoic acid methyl ester (G6)	Lignin
7	Tetradecanoic acid methyl ester	Lipid
8	Triacetonoic acid methyl ester	Lipid
9	Nonanoic acid methyl ester	Lipid
10	7-hexadecanoic acid methyl ester	Lipid
11	9-octadecanoic acid methyl ester	Lipid

moderate vascular plant input from the urban/industrial Mersey catchment. On the other hand, such tidal events may not supply enough organic matter to rise above background levels.

The major thermochemolysis products from core M106 were tentatively identified as tetradecanoic acid methyl ester (Peak 7), triacetonoic acid methyl ester (Peak 8), nonanoic acid methyl ester (Peak 9), 7-hexadecanoic acid methyl ester (Peak 10) and 9-octadecanoic acid methyl ester (11) (Figure 5.14 a and b). The abundance of fatty acid methyl esters was higher than lignin moieties throughout the length of the core (0–80 cm). Fatty acids are present in wide variety of biochemical precursors including but not limited to bacterial membranes, terrestrial plants (seeds and oils), animal fats and fish oils. Although the biological precursor origin of the fatty acids is outside the scope of this study previous studies have shown that marine sediments are comprised of significant amounts of fatty acids (Pulchan et al., 1997; Pulchan et al., 2003). The total ion chromatograms of selected surface sediments (0–10 cm) up and down stream of Ince Banks (M92, M102, M104, M168) are presented in Figure 5.15. In general, distinctions can be made between these sandy surface samples with only a few/ no TMAH products (M92, M102, M104) and those at salt marsh site M106. These show that the standard offline thermochemolysis method appears ineffective at releasing substantial amounts of GC amenable products from medium sands with moderate TOC values (mean 0.32 per cent). This paucity of products can be explained in part by the fact that thermochemolysis with TMAH was developed as a tool for characterising plant biomass with 50 per cent organic carbon content (wt/wt). The concentration of detectable amounts of lignin derivatives in sediments with moderate TOC contents represents an important analytical challenge. One plausible solution may be to use offline continuous flow through methods that would enable thermochemolysis of larger samples.

5.8 SUMMARY AND CONCLUSIONS

Organic geochemical analyses on sediment samples were undertaken to assess total organic carbon (TOC), polycyclic aromatic hydrocarbons (PAH), polychlorinated biphenyls (PCB), organotin, organolead, saturated aliphatic hydrocarbons and natural organic material (OM).

Total organic carbon (TOC) was either determined directly, or estimated from loss on ignition measurements with which it was found to correlate strongly (r2 = 0.941). TOC was found to be in the range 0 to 11 per cent for 1355 of the 1358 samples taken from a total of 144 cores and 28 grab samples. Of the three samples with higher TOC, one was from a core in which a peat horizon had been identified at a depth that corresponded with the sample and for this a TOC of about 28 per cent was determined. For the remainder of that core TOC ranged between 1 and 4 per cent. For the other two high TOC values of about 20 per cent no explicit mention was made of peat horizons but again other samples from within these cores had comparatively low TOCs of between 2 and 8 per cent.

Total PAH concentrations in 20 sediment samples from various locations were found to range between 626 ng/g and 3766 ng/g, comparable with other studies of Mersey sediment and also with studies of sediments from other UK estuaries in highly industrialised environments. Some degree of correlation between the TOC and the total PAH concentration of the sediments was discernible and provided a rational explanation of PAH variations in depth profiles. From the PAH data, it was possible to conclude that the muds, predominantly located close to the banks of the river, with their higher TOC cf. the mid-estuarine sands, were the principal sinks for PAH.

The distribution patterns of the PAHs, examined in a number of ways (bar charts, isomeric ratios, prevalence ranking etc) revealed that pyrolitic inputs (from incomplete fossil fuel combustion) were the primary source of sediment PAH, although in some samples this was augmented by the presence of some petrogenic input (from refinery products, crude oil etc.). This is typical for a region characterised by a large conurbation, (contributing combustion and run-off PAHs from traffic, coal burning etc.) and a high density of riverside industry, e.g. chemical works, power stations, sewage works, docks, boat dismantlers, oil refineries, paper works etc., (contributing both combustion-related and industry-specific PAHs). Differences in PAH distributions between the samples, even from those within the same core, reflected the diversity of PAH input and are in accord with a separate study that notes a mixed PAH source profile throughout the Mersey's tidal range and tidal mixing that results in the resuspension and redeposition of contaminated sediments. The latter observation on estuarine dynamics forms part of the reason for the difficulties associated with specific PAH source identification, a detailed examination of which was not possible with our relatively limited PAH data.

The principal value of the PAH data presented is to supplement the comparatively sparse information currently available in published literature concerning PAH concentrations in the sediments of the Mersey estuary.

For PCBs the mean total concentration was 231 ng/g (range 36–1409 ng/g). Under the OSPAR criteria for Norwegian Sea sediments, both total and individual PCB concentrations found in this study would be classed as approximately 100–5000 times above that of background or "moderate to very high levels" using the Swedish model. PCBs (presented as groups depending on the level of chlorination) provided a PCB "type" fingerprint for each sediment sample, this indicated that sediments from some specific sites may have different (individual) fingerprints. With a larger sample set, these different fingerprints could be used to help identify changes in pollutant sources with time and movement of contaminants in the estuary. Unfortunately, this was not possible with the 10 sediments analysed during this study.

PCB concentrations were determined down two cores to a depth of 1m and all concentrations were normalised to 1 per cent TOC. The first core showed a distinct double PCB peak profile down core possibly due to one, or a combination of, the following influences: varying sedimentation rates, particle size/surface area sorption effects and the beginning and end of PCB production. The second core (located mid estuary) had a lower PCB concentration and did not show such a trend, only a slight increase in PCB concentrations was observed, which may be due to greater sedimentary turbation (by water currents) compared with the first core (located on the estuary bank and subsequently affected less by physical disturbance), and/or the PCBs originated from a different source.

Tributyltin (TBT) was found in all sediments, where the concentrations ranged from 0.4–2.4 μg/g (mean = 1.3 μg/g). In addition, the mean concentration for trimethyllead was 5.7 ng/g as Pb (range = 0.49–13.34 ng/g) and the mean concentration for triethyllead was 13.9 ng/g as Pb (range = 0.15–52.22 ng/g).

The bulk of the extractable organic saturated compounds are from fuel oil and/or lube oil which probably come from multiple sources within the Mersey estuary. Biomarker distributions indicate that there is an insignificant proportion

of natural-source input of these compounds compared with anthropogenic input.

The question of flux and source(s) of natural organic matter (OM) in the Mersey estuary was addressed using C/N values as well as thermochemolysis with TMAH as a molecular tracer technique. A plot of 52 C/N values from surface sediments (0–10 cm) revealed that natural organic matter was predominantly derived from planktonic remains. This is consistent with the view that the Mersey estuary is a net sink for marine-derived OM. However, the average C/N value of 14 was somewhat higher than that expected for purely marine-derived OM, probably indicating that a low concentration of terrestrial OM contributes to the background pool of natural organic carbon in the estuary. This surmise was confirmed in part by the observation that locations adjacent to a salt marsh habitat yielded C/N values of greater than 20 reflecting input from salt marsh plant debris. A comparison of C/N values down core at a salt marsh site revealed considerable temporal variation in the contribution of marine versus terrestrial OM. The major thermochemolysis products from another salt marsh core, sampled at 10 cm intervals, were characterised using GC/MS. This showed that the organic matter was mainly composed of products derived from polysaccharide, lignin, protein and fatty acids. The absence of a significant increase in the ratio of dimethoxybenzoic acids to dimethoxybenzaldehyde with depth suggested that bacterial and particularly fungal decay was severely limited under waterlogged (oxygen-limited) estuarine conditions. In general the TMAH thermochemolysis technique was found to offer considerable potential as a tool for terrestrial organic matter source assessment.

6 Inorganic geochemistry

6.1 SURFACE SEDIMENTS

6.1.1 Introduction

A total of 238 cores of various lengths and 41 surface grab samples were taken from the sub- and intertidal areas of the estuary during the course of the Mersey survey. For the purposes of this review, maps were made for selected elements from the analytical data from the top 10 cm of 165 cores and the 41 surface grab samples to show the spatial geochemical distribution within the estuary.

6.1.2 Results

Gridded surface maps for CaO, SiO_2, Na_2O, Zr, Cr, Cu, Pb, V, and Zn are shown in Figures 6.1–6.14 as examples of geochemical behaviour within the Mersey estuary. Locations of samples analysed for Hg and a variable size symbol plot of values are shown in Figures 6.15 and 6.16. The most striking feature of the data generally is the similarity of distribution of many of the elements, but this is explained partly by grain-size variation between the samples, which were analysed without sieving, or sieving only to <2 mm (see Chapter 2). Consequently, there is a strong positive correlation of concentration of many elements with the proportion of fine-grained material (such as clay minerals and precipitated iron and manganese oxides) and a negative correlation with the proportion of coarse, clean sand (compare distribution maps with Figure 1.9)

This strong grain-size control may mask variations due to, for example, increased contaminant inputs to the system, so some form of compensation is required. This is most easily achieved by normalisation to an element that is strongly associated with the clay mineral content and shows little other control from natural or anthropogenic inputs. Elements such as aluminium (expressed as the oxide Al_2O_3) or gallium (Ga) are frequently used for this purpose, and in this case elements have been normalised, when considered necessary, by dividing by the Al_2O_3 value and multiplying by five (the mean Al_2O_3 value, 5 per cent).

As an example of the effect of normalisation to aluminium, scatter plots showing the correlation of Cr and V with Al_2O_3 before and after normalisation are given in Figures 6.17 and 6.18

In each case a very strong positive correlation breaks down completely leaving a noncorrelated scatter above a natural baseline, which clearly reflects differences in metal inputs. All of the heavy metals and many other elements show a similar pattern, including major elements such as MgO and K_2O. Silica, not surprisingly, shows a negative correlation with Al_2O_3 and almost everything else. Calcium, however, shows little correlation with Al_2O_3 (see below) suggesting that its principal mineral host is biogenic carbonate from detrital shell fragments, plus variable amounts of inorganic calcium.

Sodium likewise shows little correlation with Al_2O_3, probably due to variable amounts of halite crystallising out from saline pore waters.

The percentile-based colour-classified geochemical maps (Figures 6.1–6.14) show the general spatial distributions and the effect of normalisation where this has been applied. Calcium as CaO, SiO_2, Na_2O and Zr have not been normalised to Al_2O_3 because they are not associated with the clay fraction of the sediments and show poor correlation with Al. They are dealt with first.

For **Calcium** (Figure 6.1), the main feature of note is the nearshore effect, which is shown by a number of elements. A more significant anomaly can be observed near Birkenhead, where mussel shell beds and associated debris are present.

Silica (Figure 6.2) clearly shows the presence of the main sand bars within the central belt of the estuary and the dominant areas of silica-poor mud notably against the north shore between Garston and Hale (Dungeon Banks), and in the south, offshore from Ellesmere Port (Stanlow and Ince Banks). Many metals show high concentrations in these areas prior to normalisation.

Sodium (Figure 6.3) shows high values off Hale Head and on Ince Bank that, in surface samples, can only be due to locally saline pore waters in the muds at these sites. The more sandy sediments in the centre of the estuary generally show low Na_2O values.

Zirconium (Figure 6.4), which shows an excellent 'normal distribution' histogram, is a good example of a resistate element that may be expected to concentrate in coarser-grained sediments in higher-energy environments. Comparison with SiO_2 indicates that there is not a direct correlation with the highest SiO_2 levels, but the Zr levels are higher in the sands of the central channels as expected.

For the heavy metals where normalisation has been applied, some more general points can be made. Firstly, examination of the histograms on the normalised maps shows that, with the exception of Zn, normalisation produces a much tighter 'bellcurve' normal distribution than does the raw data. Secondly, some high-concentration areas are still prominent after normalisation, remaining anomalously high, indicating that these are not solely related to grain size.

Chromium (Figures 6.5 and 6.6) and **Vanadium** (Figures 6.11 and 6.12) show similar patterns with both natural mineralogical associations and similar anthropogenic sources, for example, from steel alloys. The latter may be the source of the high values shown in the normalised patterns in the sandy areas of the northern part of the estuary, offshore from the former shipyards at Birkenhead. High levels of both metals in the normalised data can be seen off Hale Head. This may be related to contaminated sediment brought in by the polluted Speke Brook (BGS, 1997), or to the tipping of slag in 1896 to form and embankment between Hale Head and Runcorn (see Section 1.4.1). Vanadium is enriched relative to Cr in some heavy crude oils (Pearson and Green, 1993), and some low-level contamination from the refineries at Stanlow may be responsible for the elevated V levels at Ince Banks.

Copper (Figures 6.7 and 6.8) and **Lead** (Figures 6.9 and 6.10) also show significant elevations in the 'normalised' data in the sediments off Hale Head, presumably for the same reasons as above. Normalised levels are also relatively high at Ince Banks and the Weaver outfall, though the latter is only a single-site anomaly of about 50 ppm Pb. The line of very low Pb values in the centre of the estuary is

Table 6.1 Background levels in salt marsh cores.

INCE MARSHES		ppm							%	
Normalisation	Ni	Cr	Cu	Pb	Zn	As	Ba	P_2O_5	MnO	
	Max	48	117	21	31	94	16	428	0.17	0.138
None	Min	5	18	2	8	7	2	262	0.03	0.005
	Mean	24.66	77.03	10.45	14.52	52.41	8.97	312.59	0.11	0.07
	Range	43	99	19	23	87	14	166	0.14	0.133
	Max	3.53	8.65	1.54	1.89	5.74	1.12	65.81	0.01	0.01
Al_2O_3	Min	1.16	4.19	0.47	1.04	1.63	0.37	22.80	0.01	0.00
	Mean	2.17	7.06	0.93	1.33	4.58	0.80	30.43	0.01	0.01
	Range	2.37	4.47	1.08	0.85	4.12	0.75	43.01	0.01	0.01
	Max	17.65	43.26	7.72	9.45	28.72	5.61	329.07	0.07	0.05
Al_2O_3*5	Min	5.81	20.93	2.33	5.21	8.14	1.85	114.02	0.03	0.01
	Mean	10.86	35.29	4.63	6.63	22.92	4.00	152.17	0.05	0.03
	Range	11.83	22.33	5.40	4.24	20.58	3.76	215.05	0.04	0.04
INCE BANK										
Normalisation		Ni	Cr	Cu	Pb	Zn	As	Ba	P_2O_5	MnO
	Max	39	101	36	66	113	29	394	0.16	0.133
None	Min	4	23	3	8	13	5	177	0.05	0.019
	Mean	18.97	62.72	11.64	20.54	49.36	11.36	269.10	0.09	0.06
	Range	35	78	33	58	100	24	217	0.11	0.114
	Max	2.77	12.44	4.08	9.18	18.57	5.92	58.38	0.02	0.01
Al_2O_3	Min	1.14	5.71	0.71	1.13	3.33	0.70	21.70	0.01	0.00
	Mean	2.01	8.01	1.34	2.72	5.74	1.65	39.69	0.01	0.01
	Range	1.62	6.72	3.37	8.06	15.24	5.22	36.68	0.01	0.01
	Max	13.83	62.20	20.41	45.92	92.86	29.59	291.89	0.10	0.07
Al_2O_3*5	Min	5.71	28.57	3.57	5.64	16.67	3.49	108.50	0.04	0.02
	Mean	10.07	40.03	6.68	13.59	28.71	8.27	198.46	0.06	0.04
	Range	8.12	33.62	16.84	40.28	76.19	26.10	183.39	0.06	0.04
WIDNES WARTH										
Normalisation		Ni	Cr	Cu	Pb	Zn	As	Ba	P_2O_5	MnO
	Max	49	121	40	53	176	17	415	0.17	0.159
None	Min	7	25	3	8	15	3	239	0.06	0.021
	Mean	23.88	74.13	13.90	19.78	60.60	9.05	307.40	0.11	0.06
	Range	42	96	37	45	161	14	176	0.11	0.138
	Max	3.07	13.80	9.60	13.75	39.60	5.45	54.00	0.02	0.01
Al_2O_3	Min	1.40	5.00	0.57	1.42	3.06	0.49	22.68	0.01	0.00
	Mean	2.10	7.22	1.38	2.07	5.86	0.94	32.40	0.01	0.01
	Range	1.67	8.80	9.04	12.33	36.54	4.96	31.32	0.01	0.01
	Max	15.34	69.00	48.01	68.75	198.01	27.27	270.00	0.08	0.07
Al_2O_3*5	Min	7.00	25.00	2.83	7.09	15.31	2.45	113.39	0.04	0.02
	Mean	10.52	36.10	6.90	10.35	29.28	4.71	161.98	0.05	0.03
	Range	8.34	44.00	45.18	61.66	182.71	24.82	156.61	0.04	0.05

Table 6.2 Preferred natural background levels for the Mersey.

INCE MARSHES									
Normalisation		Ni	Cr	Cu	Pb	Zn	As	P_2O_5	MnO
	Max	48	117	21	31	94	16	0.17	0.138
None	Min	5	18	2	8	7	2	0.03	0.005
	Mean	24.66	77.03	10.45	14.52	52.41	8.97	0.11	0.07
	Range	43	99	19	23	87	14	0.14	0.133
	Max	3.53	8.65	1.54	1.89	5.74	1.12	0.01	0.01
Al_2O_3	Min	1.16	4.19	0.47	1.04	1.63	0.37	0.01	0.00
	Mean	2.17	7.06	0.93	1.33	4.58	0.80	0.01	0.01
	Range	2.37	4.47	1.08	0.85	4.12	0.75	0.01	0.01
	Max	17.65	43.26	7.72	9.45	28.72	5.61	0.07	0.05
Al_2O_3*5	Min	5.81	20.93	2.33	5.21	8.14	1.85	0.03	0.01
	Mean	10.86	35.29	4.63	6.63	22.92	4.00	0.05	0.03
	Range	11.83	22.33	5.40	4.24	20.58	3.76	0.04	0.04
Normalisation		Ba	Fe_2O_3	V	Co	Nb	Cd	Sn	Sb
	Max	428	7.82	117	14.6	16	1	5	1
None	Min	262	0.57	14	0.6	3	0.5	2	0.5
	Mean	312.59	3.59	65.21	8.10	10.97	0.98	3.48	0.84
	Range	166	7.25	103	14	13	0.5	3	0.5
	Max	65.81	0.58	8.31	1.07	1.43	0.23	0.63	0.23
Fe_2O_3	Min	22.80	0.13	3.26	0.14	0.70	0.05	0.21	0.03
	Mean	30.43	0.32	5.74	0.71	1.03	0.10	0.34	0.08
	Range	43.01	0.44	5.05	0.93	0.73	0.19	0.43	0.20
	Max	329.07	2.88	41.54	5.37	7.14	1.16	3.17	1.16
Al_2O_3*5	Min	114.02	0.66	16.28	0.70	3.49	0.23	1.03	0.17
	Mean	152.17	1.58	28.68	3.54	5.14	0.50	1.68	0.42
	Range	215.05	2.21	25.27	4.67	3.65	0.93	2.15	0.99

prominent in both raw and normalised maps, and appears as a mirror image of the SiO_2 map.

Zinc (Figures 6.13 and 6.14) is unusual in that the histogram of the normalised data shows a similar spread to that of the 'raw' data and a multimodal rather than normal distribution. This suggests a weaker relationship with grain size than for the other heavy metals, and indeed the correlation of raw Zn with Al_2O_3, although strong at R2 = 0.6739, is much weaker than, say V-Al_2O_3, at R2 = 0.9001. The normalised data, where the Zn–Al correlation gives R2 <0.04, shows a regular uncorrelated background of around 150 ppm with just a few anomalies above 300 ppm which are clearly of anthropogenic origin. These can again be seen at Garston, Hale Head, Ince Banks and the Weaver outfall.

Mercury (Figures 6.15 and 6.16) was determined by atomic fluorescence techniques on a smaller number of samples than used in the XRF programme. In grab samples and core tops, the highest mercury (Hg) levels are present in the samples from the Ince Banks saltmarshes, with rather lower, but still high, levels present on the mudflats off Ellesmere Port (sites M245 and M183), Runcorn (site M64) and Widnes (site M268); and also near the Bootle docks near the entrance to the estuary at Liverpool. Given the high concentrations of industry surrounding the Mersey estuary, and in the catchments of its main feeder rivers including the Mersey, Irwell and Weaver, high metal levels in the estuary sediments should be no great surprise. However, Hg levels of >2 mg/kg are still exceptional, and the high concentration of chemical factories in the Widnes–Runcorn area are probably historically responsible, especially as the alkali, bleaching and detergents industries developed in this area in the mid 19th century and included the Castner–Kellner process for large-scale sodium hydroxide and bleach production. This is notable as it uses a flowing liquid mercury cathode in an electrolytic reaction cell. Losses and discharges from such plants, plus releases from other

Table 6.3 Background levels for mercury.

Hg ppm			
Normalisation	None	Al_2O_3	Al_2O_3*5
Max	0.43	0.07	0.34
Min	0.01	0.00	0.00
Mean	0.15	0.02	0.10
Range	0.43	0.07	0.34

industries and domestic coal-burning, may have released many tonnes of Hg to the estuary over several decades. The high levels found near the docks may represent the outfall muds derived by reworking of material in the Upper Estuary, or historical contamination from imported material.

Other elements: Maps for Al (as Al_2O_3), As, Ba, Br, Co, Fe_2O_3, Ga, Ge, K_2O, La, MgO, Mn, Nb, Ni, Sc, Sn and Sr are shown in Figures 6.19–6.36. As noted previously, many elements show very similar distribution patterns, these being controlled largely by the sediment grain-size distribution, which may be at least partly compensated for by normalisation to aluminium. Such distribution patterns are similar to those already described and there would be little point in repeating the same description many times over. With the exception of Sn, normalised maps for these elements are not shown.

Aluminium (Figure 6.19) is of course the 'typical' element of the group most directly controlled by clay mineral content (for which grain size is a good first estimate) and of the above list Ba, Fe_2O_3 Ga, K_2O, MgO, Ni and Sc show distributions which are very similar to that of Al_2O_3.

Arsenic (Figure 6.20) shows a broadly similar distribution to Al_2O_3 but there are notable low-As areas upstream of Runcorn and in the central area between Hale Head and Frodsham marshes, whilst Br also shows low levels upstream of Runcorn, perhaps related to its dominantly marine source.

Germanium (Figure 6.26) broadly follows the Al_2O_3 pattern but is more 'noisy' due to its low abundance and the lower end of the data distribution being close to the analytical limit of detection. Cobalt, La and Nb distributions are again broadly similar to the Al_2O_3 pattern, but lack the prominent line of low values along the central channel of the estuary. This implies a heavy resistate-mineral component for these elements, which is present within the coarser quartz-rich sands of this area.

Manganese (Figure 6.30) shows a strong anomaly off Stanlow Banks, for which the origin is obscure.

Tin (Figures 6.34 and 6.35) The spatial distribution of Sn concentrations (non-normalised) in surface sediments generally follows that of many of the other metals, with a strong mud–sand grain size bias. Very low levels (1–2 ppm) occur over the sandbanks in the channel centre and higher levels, up to 59 ppm, over the nearshore muds and the saltmarshes, e.g. at Ince Banks and Widnes Warth. With a natural background in terrestrial stream sediments of the Mersey catchment of around 5 ppm, it is clear that the estuary sediments are generally a 'sink' for Sn (median = 9.2 ppm) and that the high values represent an order of magnitude concentration. This degree of concentration is rather less than for metals such as Pb, but is still significant. The pattern of Sn concentrations normalised to 5 per cent Al_2O_3 shows a broadly similar pattern to the 'raw' data with major concentrations at Ince Banks, Widnes Wharfe and Hale Head, implying that there is a significant anthropogenic component as well as a grain size/clay control. The correlation of the raw Sn data with aluminium is strong at R2 = 0.6726 (n = 176), dropping to R2 = 0.1659 on normalisation, but there remains sufficient non-clay-related variation to show the genuine enrichment of the 'anomaly' sites.

Higher Sn levels are present at depth in some of the cores, notably those from the salt marshes at Ince Banks and Widnes Wharfe. Values up to nearly 200 ppm Sn are present at 1 m depth in one Mackereth core near Liverpool docks, but the 15 samples showing the highest anomalous 'raw' values from Ince Banks and Widnes Wharfe are in the 80–140 ppm range. On normalisation, this falls to about 25–60 ppm, still a substantial figure but not surprising given the highly industrialised nature of the Mersey catchment.

Strontium (Figure 6.36) shows a mainly Al_2O_3–like pattern but there is only a weak anomaly at the Weaver outfall, and stronger enrichment over the shell-sand beds at Tranmere, where Sr follows the high CaO levels.

6.2 INTERTIDAL SEDIMENT CORE PROFILES

Sediment data for seven selected cores, namely M28, M39, M42, M48, M95, M101 and M181, are shown as depth-profile graphs in Figures 6.37–6.43. These cores cover a wide spatial range extending from Upper Estuary to sea and from nearshore to mid channel, and sediment type ranging from mainly sand (M39) to mainly mud (M101). The data are arranged in four graphs per page, with Ga and LOI showing clay mineral and organic matter content, the major elements (Na_2O, MgO, Al_2O_3, P_2O_5, K_2O, CaO, TiO_2, MnO and Fe_2O_3), the heavy metals (V, Cr, Co, Ni, Cu, Pb and Zn) and a selection of 'others' (Br, Rb, Sr, Y and Zr). The cores are discussed in turn.

Core M28. [340937, 382725] (Figure 6.37)

This is a nearshore core from near Liverpool Airport. Gallium and LOI both show a down-core decline with silica increasing, showing an increase in the proportion of sand at depth. A high Na_2O value in the 10–20 cm section suggests an evaporitic salt horizon within the core but otherwise the major elements show little variation. Zinc shows a sharp increase in the 40–60 cm section but is low at the >60 cm core base. Copper and lead show a similar but less marked rise at the 40–60 cm section suggesting an anthropogenic source at the time of deposition. Zirconium shows a clear rise at 30–40 cm depth and remains relatively high to the core base.

Core M39. [339897, 381025] (Figure 6.38)

This is a sand-dominated core within the sandbanks of the central channel, and not surprisingly has a very high silica level with low levels of most other elements. Both Ga and LOI values are notably low, and there is little down-profile variation in these or in the major elements. Most heavy metal levels are also low, but the elements hosted by resistate minerals, such as Cr and Zr, are relatively enriched in the middle parts (20–60 cm) of the core. Only in the 60–70 cm section is Zn significantly higher than the other heavy metals.

Core M42. [332633, 390194] (Figure 6.39)

The most seaward of the examples chosen, taken from the shore near Tranmere, core M42 is a more complex core with a sandy part between 10 and 30 cm and generally higher than usual CaO levels, typically 5 per cent, reaching 10 per cent in the 50–60 cm section. The Ga and LOI trends are closely followed by those of the heavy metals,

especially Zn and Cr, and also Zr. The trend for Sr closely follows that of CaO, indicating their combined source in shell detritus derived from the nearby mussel beds.

Core M48. [357432, 386699] (Figure 6.40)

Core M48 is the furthest upstream of the cores, taken from a mid-river sandbank near Warrington, and might therefore be expected to show the greatest riverine rather than marine influence. Both Ga and LOI fall steadily with depth as silica rises from 60 to 68 per cent while CaO remains steady at about 7 per cent. With the exception of Zn, most heavy metals are relatively low and decline with depth on a similar trend to Ga and LOI. Zinc is relatively high, and although it, too, follows the same trend, the 250–380 ppm levels suggest some current anthropogenic input. High Sr levels reflect the elevated CaO content due to biogenic carbonate (shell fragments).

Core M95. [346800, 379000] (Figure 6.41)

Core M95, taken to the east of the Ince Banks, shows relatively little variation with depth, other than a shallow peak in Ga levels in the 20–30 cm section, probably indicating a particularly muddy horizon, which is reflected by the high Zn level (~ 570 ppm). The only other peak of note is an elevated sodium level (10 per cent) in the 80–90 cm section. Calcium levels are relatively high but steady at around 5 per cent, and this is reflected by the high Sr level. Other than Zn, heavy metal levels are unremarkable.

Core M101. [346119, 381708] (Figure 6.42)

Core M101, located just offshore from Hale Head on the Dungeon Banks, shows Ga and LOI both falling steadily with depth, but is most notable for high levels of sodium due to evaporitic halite at a number of horizons, with corresponding troughs in the SiO_2 and Al_2O_3 trends. Heavy metal levels, notably Pb, Cu, Cr and especially Zn, are high in all but the sub-60 cm sections. Conversely, Zr shows an opposite trend, with low levels in the upper sections and elevated levels below 60 cm. The very high Zn levels (up to 1180 ppm), even in fine-grained sediment, suggest that there is a major anthropogenic component of this (plus Cu and Pb), at least in the top half metre of the core. Although almost the whole of the Mersey estuary is surrounded by industrial and urban centres, the sources for these heavy metals are most probably the Speke Brook, which enters the estuary to the east of Hale Head, and to a lesser extent the Ditton Brook which enters a further 2 km upstream. Both of these streams show high levels of heavy metals in stream sediments in the regional geochemical atlas (BGS, 1997).

Core M181. [341565, 377370] (Figure 6.43)

Core 181 is a dry-land core from the saltmarshes near the heavily industrial Ellesmere Port and Stanlow centres, but collected in the same manner as the other short cores. Gallium and LOI levels are both relatively high and decline steadily with depth, but there are two major high-sodium horizons, with associated SiO_2 and Al_2O_3 troughs in the trend lines, due to evaporitic horizons. There is remarkably little variation in the heavy metals or the Br–Zr group with depth. Zinc levels are high, but not anomalously so, while Zr levels are low, similar to those of Sr.

6.2.1 Mercury (Figure 6.44)

Mercury was determined using a different methodology and a different range of samples to the other elements, and is thus dealt with separately. Concentration profiles with respect to depth are shown for three shallow (≤ 1 m) cores. In the shallow cores, both M64 and M245 show a clear reduction in Hg by about 50 per cent in the top 40 cm of core relative to the deeper material. This suggests that incorporation of Hg is falling as industrial emissions have been tightened and some industries have declined and closed. However, even the more recent values of around 1 mg/kg are still high enough to be of some environmental concern if this material is potentially biochemically active. At site M232, near the docks, a slight overall rise in values from deeper to shallower material, except for the top 10 cm, implies a slight increase in Hg source material, possibly from the erosion of sediment from Ince Banks (see Section 6.5).

6.3 SALT MARSH CORES

6.3.1 Sampling

A number of drill cores were collected from salt marsh sediments at Widnes Warth on the north side of the estuary and from Ince Bank and Ince Marshes on the south side. The cores were analysed for inorganic chemical constituents in order to document changes in contamination with time and to allow natural background levels for the Mersey to be promulgated.

Widnes Warth

At Widnes Warth on the right bank of the estuary, three holes were drilled in October and November 2002. Hole WW1 penetrated to 5 m and WW2 to 2 m in the lower salt marsh; in November 2002 hole WW7, from a slightly higher location than in the earlier visit, reached a depth of 6.94 m, the first 2.7 m of which were through 'made ground'. Sampling was carried out using intervals of approximately 20 cm, variations in this interval being based on changes in sediment characteristics (Appendix 3).

Ince Bank

Three cores were collected from the Ince Bank salt marshes on the left bank of the estuary in July 2002. The 'Marlow' corer was transported by barge, via the Manchester Ship Canal, and unloaded onto Ince Bank. The cores (IB6, 7 and 8) reached depths of 8.3, 7.0 and 9.0 m respectively. The first 2 m or so of the cores were sampled at 10 cm intervals in order to examine recent changes in some detail, whilst deeper levels were sampled on the basis of recognisable sedimentary units (Appendix 3).

Ince Marshes

The cores from Ince Marshes are from old saltmarsh on the landward side of the Manchester Ship Canal and were drilled and sampled as part of a study of the Holocene evolution of the region. Sampling was on the basis of recognisable sedimentary units, as described in Ridgway et al. (1998), and not narrow depth intervals, but data from the cores is useful for geochemical studies related to natural background values. Four cores, Ince 2–5, were drilled in June 2000, attaining depths of 11.07 m, 8.70 m, 9.07 m and 8.07 m respectively. Sampling intervals and sediment type are given in Appendix 3.

6.3.2 Geochemistry

The geochemistry of the cores is depicted in a series of spidergrams (Figures 6.45–6.54), which allows multi-element comparisons of the downhole samples to be seen. This is achieved by normalising element values to the upper crustal average of Wedepohl (1995) and plotting these on a logarithmic scale on the y-axis against element position on the x-axis. Further normalisation to Al minimises the effects

of variation in grain size of the sediment samples. Only the WDXRF data were used in the spidergrams.

Widnes Warth

Figure 6.45 (compare with Appendix 3) shows sample signatures for core WW1. Contamination by Cr, Cu, Zn, As and Pb is evident from 0.82 m upwards, the highest levels occurring in the interval 0.40–0.60 m with a drop in the topmost 23 cm. There is also evidence of contamination in these upper levels by P, Mn and Ba. Mercury values are available for samples WW1/1–WW1/11 only, but contamination again is evident from 0.82 m upward, where Hg values jump from 0.04 to 0.99 ppm. From 0.60 m upwards, Hg values are greater than 4 ppm (Figure 6.55).

A similar pattern is seen in WW2 (Figure 6.46 and Appendix 3), which penetrated to only 2 m. Here contamination (P, Mn, Cr, Cu, Zn, As, Pb, Ba) is clear from 0.88 m upwards, with the highest levels found between 0.12 and 0.50 m. Again a fall in concentrations is seen near the surface (0.00–0.12 m). The deepest sample (1.80–2.00 m) also shows evidence of contamination.

Sampling in WW7 started at 2.68 m depth, where made ground ended and true salt marsh sediment was reached. The pattern of contamination here is more complex than at the other Widnes Warth sites (Figure 6.47 and Appendix 3) with the topmost 52 cm of salt marsh material showing clear evidence of contamination, particularly by Cu, Zn, As and Pb, but with some deeper samples also appearing to be contaminated, notably from 4.00–4.20 m (Cu, Zn, As and Pb) and 5.00–5.24 m (As and Pb only). As with WW1 and WW2, the topmost sample (2.68–2.94 m) shows a fall in contaminant levels from their peak at 3.00–3.20 m.

In WW1, Sn concentrations of 11–77 ppm are found between 1.16 and 2.00 m, over 1 m deeper than contamination in other metals, although a low value of 2 ppm occurs in the interval 1.00–1.16 m. The maximum Sn value occurs between 0.4 and 0.6 m above which concentrations fall, reaching 33 ppm in the topmost sample (Figure 6.56). The full depth of WW2 appears to host Sn contamination with 111 ppm being found at 1.80–2.00 m. The lowest Sn value is found at 1.0–1.2 m, but the topmost sample again shows a fall from peak levels (Figure 6.56). Core WW7 also shows evidence of Sn contamination over its full depth although concentrations are generally lower than in WW1 and WW2. In the deepest levels, below 6.40 m, values range only from 3 to 6 ppm and the topmost sample again shows a reduction from the maximum concentration of 141 ppm at 3.0–3.2 m. In all three cores the patterns of variation with depth are erratic (Figure 6.56).

Cadmium values in the Widnes Warth cores reach a maximum of 3.0 ppm (WW7, 3.00–3.20 m) and Cd contamination is generally, at a low level, reaching a maximum of 3 ppm in core WW7.

The topmost parts of all three cores show evidence of Sb contamination at the same depths as recorded for other metals. Maximum values are 13 ppm in WW1, 20 ppm in WW2 and 24 ppm in WW7. In WW2 and WW7 contamination is sporadically present at deeper levels.

6.3.3 Ince Bank

Of the three holes drilled in Ince Bank (IB 6–8) the westernmost core (IB7) shows the clearest distinction between contaminated and uncontaminated sediment, contamination by P, Mn, Co, Ni, Cr, Cu, Zn, As, Pb and Ba extending to a depth of 1.10 m (Figure 6.48). The situation in IB6, approximately 1 km east-north-east of IB7 is less clear cut, but contamination by Cu, Zn, As and Pb appears to extend to a depth of 4.96 m, although the spidergram traces can be separated into two groups (0.10–2.83 m and 2.96–4.96 m). Below this depth the variations in concentrations may be natural with one deeper sample (5.56–5.66 m) showing signs of contamination (Figure 6.49). In IB8, a further 1 km east-north-east, contamination may extend to a depth of 3.60 m, but as with IB6 the cut off point is not entirely clear (Figure 6.50). In common with the Widnes Warth cores, all three from Ince Banks show a lessening in concentration of contaminants in the topmost parts of the sequence, possibly from as deep as 30 cm.

Mercury in the Ince Banks sites, IB6–IB8, shows several features of interest (Figure 6.57). Very low Hg levels (< 0.5 mg /kg) occur at depth (below 3.46 m in IB6, below 1.1 m in IB7). In both cores, Hg levels rise rapidly to around 3–6 mg /kg and remain high except for the top 10 cm, which shows a fall in both cases. Mercury contamination in IB6 starts at a shallower depth than for other metals (3.46 m instead of 4.96 m). Core IB8 differs in that it shows a more steady rise from very low levels at depth (>2.5 m) reaching a peak of 5.7 mg /kg at >20 cm before falling sharply to around 2 mg /kg (ppm) in the top 20 cm. As with IB6, Hg contamination in IB8 starts at a shallower depth than for other metals (2.5 m instead of 3.6 m).

Tin in the Ince Bank cores shows similar patterns to other metals, although low level contamination seems to extend a little deeper in all three (Figure 6.56). In IB6 Sn values of 11 to 69 ppm occur above 4.96 m with 10 ppm being recorded in the interval 5.56–5.66 m. Core IB7 has values between 38 and 59 ppm above 1.10 m, the main interval of contamination in other metals, but Sn values of 10–17 ppm are found as deep as 1.30 m with an isolated value of 19 ppm between 21.0 and 2.32 m. Easily recognised contamination in IB8 is restricted to the same depth levels as for other metals with a range of 12 to 139 ppm.

There is evidence of contamination by Cd and Sb in all three cores (2–7 ppm Cd and 2–8 ppm Sb), but except in IB7 this starts 1–2 m higher than for other metals.

6.3.4 Ince Marshes

Downhole variations in the Ince Marshes cores (Ince 2–5) are shown in Figures 6.51–6.54 (see Appendix 3 for sampling intervals). Only the topmost 0.6 m of core Ince 4 shows any sign of contamination (including Sn and possibly Sb). Three peats from Ince 4 have been dated giving conventional radiocarbon ages of 800±40 BP (between Ince 4-4 and Ince 4-5), 3220±40–5940±40 BP (between Ince 4-5 and Ince 4-6) and 6800±50–7350±60 BP (between Ince 4-10 and Ince 4-11). The medium sand layer of Ince 4-11 is considered to be Pleistocene in age and samples deeper than Ince 4-5 are clearly pre-industrial era. Indeed, Wilson et al. (2005) believe that the 800 BP age is too young for its stratigraphic position (depths in Wilson et al. are at variance with those given here as a result of using a different logging protocol). The close comparison between the geochemistry of Ince 4-2 and Ince 4-3 and the deeper Ince 4 samples suggest that they too are of pre-industrial in age.

6.3.5 Discussion

The spidergrams of Figures 6.45–6.54 allow contaminated samples to be distinguished from uncontaminated 'background' samples. If contaminated samples are ignored, it is possible to determine the range of 'natural background'

concentrations in the cores. These concentrations can be normalised to Al to reduce the effects of varying grain size. Maximum background concentrations from the Widnes Warth and Ince Bank cores are generally higher than in the Ince Marshes cores for Cr, Cu, Pb, Zn and As, particularly in normalised values (Table 6.1). It is possible that this is due to postdepositional downward diffusion of these metals under the influence of rising and falling tidal water levels. The chemistry of this process is beyond the scope of this paper, but downward diffusion of metals has been noted in other aquatic sediments (Farmer, 1991). In these circumstances, the background values from the Ince Marshes cores are the most reliable and should be adopted as the 'natural background' levels for the Mersey. The Ince Marshes cores also provide the best estimates for background values for Cd, Sn and Sb. However, in order to compare like with like and minimise variations due to grain size effects it is advisable to use normalised values to define the background levels. The results of this exercise can be seen in Table 6.2 in which preferred natural background levels for various metals are shown. Concentrations above the maximum values can be considered to be due to contamination.

Mercury values are available for selected samples from core WW1 and cores IB6–8 only. Background values based on these samples are shown in Table 6.3.

The depth to which contamination extends is much less in the Widnes Warth cores than in those from Ince Bank and indicates that sediment accumulation rates were greater at Ince Bank. This agrees with the findings of Fox et al. (1999; 2001), who also recorded greater accumulation rates at Ince Bank (termed Ince Marsh by Fox et al.). It is also noticeable that contamination penetrates to different depths in the Ince Bank cores suggesting variable sedimentation rates at the sites, perhaps related to the evolution of the salt marshes, accretion rates decreasing as the marsh surface gets closer to the high tide level and is inundated less frequently by sediment-bearing water (Long and Mason, 1983).

Tin contamination is found at deeper levels than for other metals and suggests that Sn processing in the Mersey catchment began earlier than the onset of major industrial development.

Bathymetric surveys of the Mersey, largely by the Mersey Dock and Harbour Company, have been carried out regularly since 1861. The last detailed surveys were in 1997 and 2002. The 2002 bathymetry (made available by the Environment Agency), which is based on a combination of data collected at low tide by LIght Detection And Ranging techniques (LIDAR) and at high tide by sonar bathymetry, coupled with sample location data from the Mersey geochemical survey, show that the position of the mean high water mark on the south bank of the estuary has changed, in comparison with the 1992 1:25 000 scale map of the area (Ordnance Survey, 1992), as a result of the erosion of a significant part of the Ince Bank saltmarsh development (Figures 1.5 and 2.1). This erosion of the western side of Ince Bank and Stanlow Bank, with new saltmarsh developing to the east of Ince Banks, can be attributed to the migration of the main channel of the estuary on its north-western flank. Morphological change in the Inner Estuary has been discussed by several workers (e.g. Bennett et al., 1995; Thomas et al., 2002) emphasising the dynamic nature of erosion and deposition in this part of the system. These changes are important because of the considerable quantities of contaminants held in the Ince Bank salt marsh sediments that could be released into the estuarine system through erosion.

As an example, the amount of Hg present in the Ince Banks sediments, assuming that the cores are representative and the distribution is fairly homogenous, can be calculated through multiplying the probable volume of sediment in the top 3 m of saltmarsh by the mean of approximately 3 mg/kg of Hg and sediment density of around 2.5 g/cm^3. Thus with a salt marsh area of approximately six square kilometres, an estimated 135 tonnes of Hg are held in this sediment reservoir. As parts of Ince Bank are currently being eroded, this potentially represents a significant current input of Hg to the active sediments of the Mersey irrespective of any 'new' industrial input.

6.4 INTERPRETATION OF THE MERSEY ESTUARY TOTAL ELEMENT DATA USING SELF-MODELLING MIXTURE RESOLUTION

6.4.1 Introduction

Data from all the Mersey sediments have been subjected to a multivariate statistical analysis. Chemical composition and spatial variation in the Mersey estuary sediments can be considered to be made up from a number of geochemical inputs: underlying geology; riverine and marine sediments being deposited as a result of river and tidal flows; biogenic inputs from plants and animals; and anthropogenic inputs from industrial or other man made activities. The distribution and mixing of these inputs along the length of the estuary are primarily driven by the tidal and river water flow. Particle size and density of the sediment will play an important role, with the finer, less dense particles being held in suspension in areas of high water flow, e.g. the central channel of the Mersey, leaving only the heavier particles behind e.g. coarse sand. Where the flow of water is low, e.g. near banks of the river or at the turn of the tide on saltmarshes and/or mudflats, the finer particles can fall out of suspension. Understanding how these different inputs are distributed over the Mersey estuary provides vital information on how these dynamic estuarine environments are formed and how pollution sources are incorporated.

Element concentration plots of the chemical composition of the sediments over the estuary can provide some insight into how the various geochemical inputs are distributed. However, no single element can act as a pathfinder for a particular input as they are usually found to be associated with more than one source. Multivariate methods, in which all of the variables (in this case element concentrations) are considered have the ability for to resolve complex mixtures into source components (Malinowski, 2002). Recently, Cave et al. (2004) described a self modelling algorithm specifically designed for elucidating the intrinsic underlying components in geochemical data sets. In the case of the estuarine samples, the modelling method assumes that any given sample is made up of a mixture of intrinsic components (referred to here as assemblages) each having a chemically distinct composition. The algorithm relies on the fact that the proportion of each of the assemblages will vary from sample to sample. This variation allows the algorithm to estimate the number of assemblages present, the chemical composition of each assemblage present and, the amount of each assemblage in each sample. The data analysis algorithm is based on an iterative fitting procedure whereby the original data consisting of the chemical compositions of each individual samples is modelled as the product of a compositions matrix (containing the compositions of the estimated assemblages) and a matrix containing the relative proportions of each assemblage in each sample. During the data processing the fit of the model over a range

of different number of assemblages is calculated and the model predicted data is compared to the predicted data for each assemblage number. Figure 6.58 shows that the minimum average difference between actual and modelled data reaches a minimum for 18 of the assemblages. This number has been subsequently used for the interpretation of the data.

6.4.2 Data presentation

The results of the mixture resolution approach are shown in Figures 6.59–6.112. Figures 6.59 and 6.60 give an overall picture of how each of the identified assemblages contribute to the model in terms of the amount of variance explained by each assemblage (Figure 6.59) and the range of mass contributions that each assemblage makes to each sample (Figure 6.60). Figure 6.61 shows model fit plots for the four worst case elements and will be discussed in more detail later.

For each individual assemblage the following information is provided:

i) a bar plot summarising the major and trace element composition of the assemblage

ii) a bar plot summarising enrichment factors for each major and trace element (where the enrichment factor for a particular element is calculated as the ratio of the concentration in the assemblage divided by the median concentration for that element for all of the samples collected in this study)

iii) a 3D scatter plot showing the concentration of each the assemblage in each sample represented by a colour scale.

The information on the composition/relative enrichment, combined with the distribution of the assemblage over the estuary provides information that can be used to give a geochemical/ physical interpretation of the assemblage, e.g. if the assemblage is mainly made up of SiO_2 and it is predominantly in the centre of the estuarine channel then it is probably coarse grained sand.

An initial review of the 18 assemblages showed that they all had distinctive distributions and chemical compositions apart from assemblages 11, 12, 15 and 17 whose chemical compositions only varied slightly and had very similar distributions over the estuary (see Figures 6.62–6.76). Consequently, these assemblages are discussed together and the remaining assemblages are discussed individually.

In addition to the discussion on each assemblage, summary plots for each element (Figures 6.77–6.111) have also been produced as follows:

i) a bar plot of the explained single element variance in each assemblage

ii) a box and whisker plot showing the variation in element concentration for each sample within each assemblage

iii) a scatter plot of the actual element concentration found in each sample vs the amount in each sample predicted by the mixture model

iv) a bar plot of the concentration of the element found within each assemblage.

The bar plots of the element variance and concentrations and the box and whisker plot provide information on which assemblages are important sources of particular elements. This is particularly helpful in understanding the source and fate of potentially harmful elements within the estuary, e.g. As, Cd, Cu, Pb and Sn. The plot of the measured element concentration against the modelled concentration provides a measure of how well the mixture model fits the original data. From these plots it is possible to calculate the uncertainty of the fit of the model to any particular element based on the root mean square (rms) difference between the actual and predicted values for all samples. Table 6.4 gives a summary of the 95 per cent uncertainty limits (based on twice the rms value) for each element.

Table 6.4 Ninety-five per cent confidence limits on the modelled element data.

Majors		**Traces**			
	%		**mg kg^{-1}**		**mg kg^{-1}**
Na_2O	*2.3*	Sc	0.6	Ga	1.0
MgO	0.32	V	8.3	As	29.0
Al_2O_3	0.85	Cr	14.2	Br	13.4
SiO_2	16.3	Co	2.0	Rb	5.2
P_2O_5	0.02	Ba	187.4	Sr	30.4
K_2O	0.18	La	2.3	Y	2.2
CaO	1.8	Ce	6.4	Zr	63.4
TiO_2	0.06	Nd	1.8	Hf	1.3
MnO	0.04	Ni	3.4	Pb	53.8
Fe_2O_3	0.38	Cu	24.6	Th	0.5
LOI	1.8	Zn	138.8	Ag	0.4
				Sn	14.0
				I	8.1

The data in Table 6.4 can be used to aid the interpretation of the data for each assemblage to show whether the concentration of a particular element within any assemblage is significant.

For the majority of elements (Figures 6.77–6.111) the plot of actual element concentration follows the line of equivalence with the measured data apart from a few outliers. Figure 6.61, however, shows the scatter for Si, Ca, Ba and, to a certain extent Mn, where there is significant deviation from equivalence. The reason behind the poorer fit for these elements is thought to be that the proportion of these elements within any one assemblage is more variable than for other elements and it is therefore difficult to assign a single value for their composition. Despite this, it is thought that the mixture model provides a reasonable representation of the overall mixture processes occurring in the Mersey estuary.

6.4.3 Data selection

Analytical data for 1410 samples were used for the mixture modelling. Elements, where the data were mostly below or close to detection limit, were not included in the data processing. A total of 35 elements was used (see Table 6.4). Where data were missing (i.e. below detection limit or had not been analysed) imputed values were calculated using the method of Schneider (2001).

6.4.4 Results and discussion

The results are summarised in Figures 6.62 to 6.76.

Assemblage 1 (Figure 6.62) has a relatively low mass contribution of about 5 per cent (Figure 6.60) and accounts

for about 10 per cent of the total variance in the data. The fact that the highest concentrations are found on the banks of the estuary and the chemical composition is dominated by Al, Fe and Mg suggests this is a clay material (possibly chlorite, illlite or smectite) also containing some fine-grained iron oxide (e.g. haematite). The organics content is quite high (about 15 per cent) and V, La, Ce, Nd, Ni, Ga Y and Th are all enriched by a factor of about 10 in this assemblage.

Assemblage 2 (Figure 6.63) has a very low mass contribution of <1 per cent (Figure 6.60) and accounts for <1 per cent of the total variance in the data (Figure 6.59). The highest concentrations, up to about 3 per cent, are found in the surface samples along Ince Banks with lower concentrations, about 1 per cent, along the banks of the estuary. The chemical composition suggests it a fine-grained mixture of Mn and Fe oxide/oxyhydroxides in combination with organics and is probably formed as the result of oxic reactions and the decomposition of plant material. It is highly enriched in Cu, Zn, As, Pb and Sn, and accounts for a large proportion of the variance of these elements (Figures 6.96–6.110).

Assemblage 3 (Figure 6.64) has a very low mass contribution (about <1 per cent) and accounts for about 1 per cent of the total variance in the data. The highest concentrations are found on the southern bank of the mouth of the estuary (about 8–12 per cent) with lower concentrations (about 2–6 per cent) spread intermittently along the banks of the whole length of the estuary. The high content of Ca suggests this is shell debris with Na, Ca and Sr showing enrichment factors of 10 or higher. Other trace metals occur at relatively low concentrations

Assemblage 4 (Figure 6.65) has a very low mass contribution (about 1 per cent) and accounts for about 1 per cent of the total variance in the data. The highest concentrations of this component are found along the banks of the central region of the estuary and on the northern bank of the estuary mouth. As with assemblage 3 the high carbonate content suggest this is derived from a shelly material. Unlike assemblage 3, however, assemblage 4 is enriched in Cu, Zn and Pb and is highly enriched in Br and I (about 50 and 100 times respectively), which could suggest a marine origin.

Assemblage 5 (Figure 6.66) has a very low mass contribution (less than 1 per cent) and accounts for <1 per cent of the total variance in the data. The highest concentrations (about 2.5–3 per cent) occur in the middle of channel. It is Ca rich but low in LOI suggesting that it is not a carbonate. It is enriched in Na, Ca and Ti (enrichment factor >10) and highly enriched in Zr and Hf (enrichment factor >80) and shows medium enrichments (enrichment factor around 10–20) in Cr, Ce, Cu, Zn, Sr, Y, Pb, Th and Sn. This suggests that this assemblage is of heavy mineral origin.

Assemblage 6 (Figure 6.67) has a very low median mass contribution (less than 1 per cent) but accounts for about 8 per cent of the total variance in the data with some very high individual contributions (>60 per cent). Assemblage 6 has a very high Na content appearing at point locations along both the north and south banks in the centre of the estuary; it shows enrichment in Na, Br and I. It may represent saline spring sources or it could be derived from a sampling artefact since some cores were observed to contain salt crystals at the ends possibly due to pooling of saline water collected with the core.

Assemblage 7 (Figure 6.68) has a relatively low mass contribution (about 5 per cent) and accounts for about 7 per cent of the total variance in the data. The highest concentrations (up to about 20–25 per cent) occur at the eastern end of the estuary and over the north and south banks of the centre portion of the estuary. As it occurs predominantly on the banks and is principally made up of Si it is probably fine-grained sand or silt. It also contains percent concentrations of P, Ca, Fe and LOI suggesting the present of coatings on the quartz grains. It is particularly enriched in P (enrichment factor of about 10) and to a lesser extent Cu, Zn, As, Pb and I (about 5–10 per cent). The high phosphate and Zn content of this Assemblage suggests an anthropogenic source. Figure 6.68 shows three possible sources near where the assemblage appears in relatively high concentration. The site of the car plant on the north bank which could account for high Zn concentrations from metal galvanisation processes, the Procter and Gamble factory on the south bank where soap products waste could account for high phosphate or the Weaver Sluice where waste sediments from the Manchester ship canal have been deposited. Alternatively, the distribution pattern could suggest a riverine source (possibly from sewage or fertiliser input), which is carried down river (Figure 6.68 shows high concentrations of assemblage 7 in the upstream section of the estuary) and deposited on the banks in the mid section of the estuary.

Assemblage 8 (Figure 6.69) has a very low mass contribution (<1 per cent) and contributes < 1 per cent to the overall variance in the data. The spatial plot shows some point sources going up to about 2 per cent in concentration but it occurs both on the banks and in the central channel. Assemblage 8 is predominantly made up from LOI (i.e probably organic material) with Ca, Mg, and Na. It is highly enriched in Co (>150 enrichment factor) and to a high but lesser extent with Cu, Sn and I (>50 enrichment factor). The source of this assemblage is not clear.

Assemblage 9 (Figure 6.70) has a relatively low mass contribution (about 5 per cent) and contributes about 2 per cent to the overall variance in the data. It is fairly evenly distributed along the length of the estuary. It is predominantly made up of SiO_2(about 60 per cent). It is probably a natural residual sand with some clay and shell debris (possibly feldspar and clay) and is not an important pollution source. Cr is the only element that shows significant enrichment (factor of about 5).

Assemblage 10 (Figure 6.71) has a very low mass contribution (less than 1 per cent) and contributes < 1 per cent to the overall variance in the data. It is made up of over 80 per cent SiO_2 this is probably a sand but has very high silver enrichment (about 150) it appears in point sources (around 5–7 per cent) it could possibly be an artefact of the data processing.

Assemblage 13 (Figure 6.72) has a relatively low mass contribution (about 2 per cent) and contributes about 2 per cent to the overall variance in the data. The highest concentrations occur in the centre of the estuary on the southern bank. It principally consists of SiO_2 (about 70 per cent) with smaller concentrations of Al, K and Fe. This suggests that this is a fine-grained sediment with clay. This component has the highest As content of all assemblages and it is also enriched in Co, Ga, Pb and Sn suggesting a high anthropogenic input.

Assemblage 14 (Figure 6.73) has a medium low mass contribution (about 5 per cent) and contributes about 2 per cent to the overall variance in the data. It is principally composed of SiO_2, Al and Ca (>20 per cent) with smaller amounts of K, Mg and Na. The highest concentrations are to be found along the banks of the estuary (the highest values are found in the deep cores on Ince banks (up to about 18 per cent) possibly coming from the river end of the

Table 6.5 Summary of the assemblage descriptions and qualitative assessment of contamination.

Assemblage number	Brief description	Level of anthropogenic contamination	Enriched elements
1	Fine-grained clay with iron oxides and organics	High	Cr, Ni, Pb, V, Cu, Sn
2	Fe/Mn oxides with organics	High	Cu, Zn, As, Pb, Sn
3	Ca-rich shell debris	Low	Na, Ca, Sr
4	Ca-rich shell debris with Fe and Mn	High	Cr, Cu, Zn, Pb, Br, I
5	Heavy mineral	Low	Zr, Hf
6	Na salt (possible artefact)	Low	Na, Br, I
7	Fine silty sand with P,Ca,Fe and organics	High	P, Cu, Zn, As, Pb, I
8	Organics with ?	Medium	Sn, As, Cu, Co, I
9	Natural residual sand with clay and shell debris	Low	Cr
10	Sandy material with Ag	Medium/high	Ag
11	Coarse well-washed sand	Low	-
12	Coarse well-washed sand	Low	-
13	Fine-grained sediment with clay	High	As, Co, Ga, Pb, Sn
14	Glacially derived Ca rich clay	Low	Sc, Rb, Sr
15	Coarse well-washed sand	Low	-
16	Organic-rich fine sandy clay	Low	-
17	Coarse well-washed sand	Low	-
18	Fine sandy clay	Medium	Sc, Cr, As, I

estuary. This suggests that this is a glacially derived Ca rich clay (derived from rock fragments) possibly from riverine source. It has relatively low trace metal content and only Sc, Rb and Sr show significant enrichment (around 4–5 times).

Assemblage 16 (Figure 6.74) has a medium mass contribution of about 12 per cent and contributes to about 18 per cent to the overall variance in the data. The highest concentrations (30–60 per cent) are found along the banks of the estuary. It consists principally, of SiO_2 (about 80 per cent) with smaller concentrations (about 1–5 per cent) of all of the other majors showing a three-fold enrichment in LOI. This suggests an organic rich fine sandy clay. It has a low trace element content with the majority of elements showing depletion with respect to their median values apart from Br which shows a slight enrichment.

Assemblage 18 (Figure 6.75) has a medium mass contribution of about 8 per cent and contributes about 8 per cent to the overall variance in the data. The highest concentrations are found along the central portion of the southern bank of the estuary (25–30 per cent) although it is also found at lower concentrations (15–20 per cent) fairly evenly distributed along the whole length of both the north and south banks. In a similar way to assemblage 16, it consists principally of SiO_2 (about 80 per cent), with smaller concentrations (1–5 per cent) of all other majors, but all of the majors are very close to their overall median values. This suggests a fine sandy clay material, which, unlike assemblage 16, shows around 2–3 fold enrichment factors for Sc, Cr, As and I, suggesting an anthropogenic input.

Assemblages 11, 12 15 and 17 (Figure 6.76) have been combined together as they all consist predominantly of SiO_2 (more than 95 per cent) with only very minor differences in trace metal content which is low in all of the these assemblages. It is found in high concentrations (45–70 per cent) in the central channel of the estuary and is most likely to represent coarse well-washed sand. It is interesting to note that high concentrations are also found in the deeper core samples taken on Ince Bank suggesting the presence of an old river channel in this area.

Figure 6.112 shows how the total amount of 10 selected elements in all of the samples is distributed between the assemblages. These 10 elements have been chosen as possible markers for anthropogenic pollution. In addition to this, Table 6.5 gives summary descriptions of each of the assemblages and indicates which are likely to be the main sources of contamination. Spatially, most highly polluted areas appear to be on the banks of the central portion of the estuary and on the banks of the mouth of the estuary. These areas have been sites for industrial inputs and are at points in the estuary where the water flow is lower and therefore finer material can settle out into the sediment. The majority of the contamination is associated with fine-grain material, which is deposited on the banks (Table 6.5 and Figures 6.62–6.75). These contaminated sediments can be classified into three types:

i) fine clay/iron oxide material with high organic content (Assemblages 1 and 2)

ii) Ca-rich shelly debris (Assemblage 4)

iii) fine sand with coatings (Assemblages 7, 13 and 18).

It is difficult to associate particular sources with these contaminated assemblages but it appears that they are acting as sinks for any pollution that is released into the estuary. It is evident, however, that there are a number of fine-grained assemblages containing very little contamination (e.g. 3, 9, 14 and 16) and these possibly represent older (pre-industrial) inputs into the estuarine system.

This relatively new approach to the interpretation of geochemical data as a mixture resolution problem has been successful in identifying a number of distinct geochemical assemblages and identifying their spatial distributions. This approach also allows the distribution of trace metals between the different assemblages to be estimated and hence a detailed geochemical interpretation of the estuarine environment to be made.

7 Detailed mineralogical and chemical investigations

7.1 GENERAL CHARACTERISTICS OF THE MERSEY ESTUARY SEDIMENTS

The estuarine sediments subjected to detailed mineralogical and chemical investigation comprise organic-rich fine muddy sand (Plate 7.1) to silty mud (Plate 7.2). They are dominantly composed of very fine sand-grade to mud-grade major detrital quartz, with minor amounts of detrital clay minerals, muscovite, biotite, chlorite, potassium feldspar and albite, and accessory detrital minerals, including rutile, zircon, apatite, monazite, amphibole, garnet, and iron and titanium oxides (probably magnetite and ilmenite). The detrital grains are typically very angular (Plate 7.3).

In addition to siliclastic material, the sediments also contain a significant amount of biogenic silica in the form of diatom remains (Plates 7.4 and 7.5). Several species of diatoms contribute to the sediment, with cylindrical and discoid forms being most common. They are composed of pure silica, and both complete and highly fragmented diatom skeletons are present. The diatomaceous material shows little sign of dissolution or alteration.

7.1.1 Clay mineralogy

7.1.1.1 Estuarine sediments

The XRD analyses of the nominal <2 μm size fractions of selected estuarine samples are summarised in Table 7.1, and example XRD traces are shown in Figures A4.1 and A4.2 in Appendix 4.

The estuarine samples were found to have almost identical 'clay' mineral assemblages. In every sample, the <2 μm assemblage consists of quartz, illite mica, chlorite and kaolinite. Feldspar (albite) was tentatively identified as a trace constituent of one sample. Quartz is the most abundant phase in every sample. In fact, the samples are all unusually quartz rich. The chlorite is interpreted to be Fe rich, based on observation of the relative heights of the 00l and 002l peaks, and since its much larger 002l peaks overlap with the kaolinite 00l peaks, it is hard to estimate relative abundances from the peak heights. Nevertheless, an estimate has been made, based on the height of the tallest peak identifiable of each mineral phase. The three phyllosilicates all appear to be present in roughly equal amounts.

The <0.5 μm size fraction was examined from three samples (sites M42, M48 and M167) to try to refine the identification of the clay mineralogy in the estuary sediments. The XRD traces are shown in Figures A4.3 to A4.5 (air-dried, glycolated and heated trace of each <0.5 μm sample) in Appendix 4. Also shown in Figures A4.6 to A4.8 in Appendix 4 are the air-dried traces obtained from both the <0.5 and <2 μm fractions of the same samples for comparison. The analytical results are summarised in Table 7.2.

The <0.5 μm fractions consist of mostly the same assemblage as the <2 μm fractions: i.e. quartz, illite, kaolinite and chlorite. In addition, a swelling clay was identified in the <0.5 μm fraction that was not discriminated in the <2 μm material. This clay mineral appears to be a randomly interstatified mixed-layer smectite-chlorite. The amount of quartz appears to be much reduced in the <0.5 μm fraction relative to the <2 μm fraction. However, comparison with the <2 μm fraction shows that the low angle end of the diffraction trace is increased in intensity while the high angle end is reduced. This suggests that the large amount of quartz present in the coarser size fraction material may have been disrupting the physical orientation of the clays in the XRD mount. It is therefore difficult to assess whether the proportions of the different phyllosilicates in the <0.5 μm samples are significantly different from those in the <2 μm samples.

Table 7.1 Summary of XRD analyses of <2 μm fractions.

Sample No.	Depth (cm)	Major	Minor	Trace
M7	0	quartz	Illite, kaolinite, chlorite	
M28	0–10	quartz	Chlorite, iillite, kaolinite	
M28	30–40	quartz	Chlorite, iillite, kaolinite	?Albite
M28	60–70	quartz	Kaolinite, illite, chlorite	
M42	0	quartz	Chlorite, illite, kaolinite	
M42	30–40	quartz	Illite, chlorite, kaolinite	
"	58–68	quartz	Illite, kaolinite, chlorite	
M48	0	quartz	Chlorite, iillite, kaolinite	
M48	30–40	quartz	Kaolinite, illite, chlorite	
M69	0	quartz	Kaolinite	Illite, chlorite
M95	0–10	quartz	Kaolinite, illite, chlorite	
"	30–40	quartz	Illite, kaolinite, chlorite	
"	60–70	quartz	Illite, chlorite, kaolinite	
"	90–100	quartz	Chlorite, kaolinite, illite	
M101	0–10	quartz	Illite, kaolinite, chlorite	
"	30–40	quartz	Illite, kaolinite, chlorite	
"	60–70	quartz, illite, kaolinite	Chlorite	
M167	0–10	quartz	Chlorite, illite, kaolinite	
"	30–40	quartz	Illite, kaolinite, chlorite	
M193	0	quartz	Illite, kaolinite, chlorite	
M205	0	quartz	Chlorite, iillite, kaolinite	
M232	0	quartz	Illite, kaolinite, chlorite	

Major = >400 cps; Minor = 100–400 cps; Trace = <100 cps; ? = presence uncertain (cps = counts per second)

7.1.1.2 Interestuarine variations

There is little variation in the clay mineralogy of the sediments between the different sites studied. Only one sample differs in terms of the fine-grained minerals present, in that it contains detectable levels of albite feldspar (M28/30–40 cm). There are minor variations between samples in the relative peak heights of different minerals, principally with respect to the total clay mineral content present relative to quartz, but the relative amounts of the three clay minerals vary only slightly. It was not possible to determine whether the phyllosilicate assemblage varies with depth or location however: the observed variations are so small that no real significance can be ascribed to them without a much more detailed study.

Table 7.2 Summary of XRD traces from <0.5 μm size fractions of Mersey estuary sediments.

Sample	Major (>200 cps)	Minor (50–200 cps)
M167, 30–40 cm	Illite mica	Quartz, smectite-chlorite (random layer), chlorite, kaolinite
M42, 0 cm	Illite mica	Quartz, smectite-chlorite (random layer), chlorite, kaolinite
M48, 0 cm	Illite mica	Smectite-chlorite (random layer), quartz, chlorite, kaolinite

7.1.1.3 River sediments

The XRD analyses of the <2 μm size fractions of the tributary river samples are summarised in Table 7.3. Typical XRD traces are shown in Figures A4.9 to A4.11 in Appendix 4.

The <2 μm fractions of the tributary river samples (see Table 7.3) all have a mineralogical assemblage consisting of quartz with lesser amounts of illite (mica), kaolinite and Fe-rich chlorite. Kaolinite is the major clay mineral in many of the river sediments, particularly in those rivers whose catchment area is at least partly underlain by Carboniferous strata (e.g. rivers Bollin, Croal, Etherow, Irwell, Roch and Tame). Illite is present in minor to trace concentrations, and chlorite is always a trace constituent. In one sample (Weaver 1), calcite is also present in significant amounts.

7.1.2 Heavy minerals

Although a detailed quantitative analysis of the heavy mineral assemblage in the estuarine sediments was outside the scope of the present study, some limited SEM-EDXA observations of the natural heavy mineral fraction were undertaken (see Appendix 1).

Despite significant differences in anthropogenic heavy 'mineral' components, the six sites (M28, M42, M48, M95, M101 and M167), which are discussed in Section 7.2 all displayed similar natural heavy mineral characteristics. The major heavy mineral species present in all of the samples examined are zircon, apatite, rutile, monazite, garnet (of variable iron, manganese, titanium and calcium compositions), and iron and titanium oxides (probably magnetite and ilmenite and their alteration products). Biotite, chlorite, and minerals tentatively identified as tourmaline and amphibole are present to a lesser extent. Rare xenotime was also identified in some samples.

Zircon, monazite, xenotime, rutile, ilmenite and magnetite, and most apatites show little evidence of corrosion or alteration, and most grains appear to be fairly fresh. However, some amphibole and garnet grains may have slightly pitted or etched surfaces (Plates 7.6 and 7.7), but overall the degree of heavy mineral dissolution is very minor.

Angular grains of barite and rhombs of ankeritic dolomite form a very significant proportion of the heavy mineral fraction separated in bromoform. Anhydrite grains are also present in many of the samples. These grains have very angular morphology and in the particular, the ankerite grains typically display good euhedral rhombic crystal forms (e.g. Plates 7.8 and 7.9). The degree of angularity, lack of abrasion, and lack of corrosion of these relatively soft and/or relatively soluble minerals suggests that they have not been transported far. It is therefore possible that these particular minerals may be derived from industrial sources (e.g. barite may be derived from paint manufacture – where it may be used as a filler, or from drilling mud used in offshore gas field operations), rather than derived from natural sources. Some of the ankerite grains do show corrosion effects (Plate 7.10). However both corroded and fresh ankerite grains are found together in the same sample.

Table 7.3 Summary of XRD analyses of <2 μm fractions.

Sample No.	Depth (cm)	Major	Minor	Trace
Irwell centre river	0	Quartz, kaolinite	Illite	?Chlorite
Irwell 2 central	0	Quartz	Kaolinite	Illite, chlorite
Bollin 1	0	Quartz	Kaolinite, illite	Chlorite
Bollin 2	0	Quartz, kaolinite	Illite	Chlorite
Tame 1	0	Quartz, kaolinite	Illite	Chlorite
Etherow 1	0	Quartz, kaolinite	Illite	Chlorite
Goyt 1 centre bar	0	Quartz	Kaolinite, illite	Chlorite
Roch 1	0	Quartz, kaolinite	Illite	Chlorite
Croal 1 left bank	0	Quartz	Kaolinite, illite	Chlorite
Weaver 1	0		Quartz, calcite	Kaolinite, illite, chlorite
Mickerbrook 1	0	Quartz		Kaolinite, illite, chlorite

Major = >400 cps; Minor = 100–400 cps; Trace = <100 cps; ? = presence uncertain (cps = counts per second)

7.1.3 Implications for sediment sources

7.1.3.1 Provenance of river sediments

The bedrock of the entire Mersey catchment area is made up dominantly of Carboniferous limestones and siliclastic rocks, and Permo-Triassic sandstones and mudstones, which are overlain by a cover of Quaternary glacial drift.

Carboniferous rocks surround the Cheshire basin on the west, south and east sides and continue north beyond Manchester and Bolton. The rivers Croal, Irwell, Roch, Tame, Etherow and Goyt have their catchments almost entirely on the Carboniferous, and the upper parts of the Bollin also drains a terrain of Carboniferous strata. These rocks are made up mostly of limestones, sandstones, siltstones and shales (Jones et al., 2003). The clay mineralogy of the Carboniferous mudrocks comprises major illite, illite–smectite mixed-layer clays and kaolinite, with chlorite as a minor to rare component (Smart and Clayton, 1985; Jones et al., 2003). It is also worth noting that authigenic kaolinite (formed by diagenetic and weathering alteration of detrital feldspars) is common in Carboniferous rocks (e.g.;Cliff et al., 1991) and much of the kaolinite found in the tills and modern sediments of the Irish Sea is considered by some authors to be derived locally from the Carboniferous strata (Kelly and Emptage, 1992).

The sediments in rivers draining catchment terrains developed on Carboniferous strata (Irwell, Tame, Etherow, Goyt and Croal) were all found to have a similar clay mineralogy: of kaolinite, illite and chlorite, with kaolinite usually being present in much larger amounts than the other phyllosilicates. This is very similar to the clay mineralogy of the underlying Carboniferous strata, and the relatively high kaolinite content appears to reflect the kaolinite-rich clay mineralogy of the bedrock. However, mixed-layer clay minerals, which are also present in the bedrock, appear to be absent in the river sediments.

The Permo-Triassic strata within the Mersey catchment are dominated by the Mercia Mudstone Group and the Sherwood

Sandstone Group. The Mercia Mudstone Group covers an area stretching from the Mersey river south beyond Whitchurch, almost exactly corresponding to the catchment of the river Weaver. Its clay mineralogy is dominated by two assemblages: (i) an assemblage of illite, corrensite (a regularly interstatified smectite-chlorite mixed-layer clay mineral) and minor chlorite; and (ii) an illite and chlorite dominated assemblage (Plant et al., 1996). The Sherwood Sandstone Group surrounds the Mercia Mudstone Group on all sides and extends south of the Mersey estuary beyond Chester and north of the estuary beyond Liverpool. It underlies most of the Mickerbrook and some of the Irwell and Bollin catchments. Clay mineral assemblages in the Sherwood Sandstone Group are comprised of illite, smectite and variable amounts of chlorite (Plant et al., 1999).

The samples taken from the rivers draining the Permo-Triassic terrain (rivers Weaver and Mickerbrook) appear to have a clay fraction dominated by quartz, with a clay mineralogy consisting of illite, kaolinite and chlorite, all at similarly low levels. This differs significantly from the mineralogy of the underlying Permo-Triassic rocks, which corrensite and smectite as major components, and in which kaolinite is largely absent.

Overall, the two main differences between the river sediments and their catchment bedrocks are:

(i) swelling clays (smectite, corrensite) are absent in the river sediments, despite their presence in many bedrocks;

(ii) kaolinite is seen in the sediments of the two rivers on Permo-Triassic terrain, whereas it is absent in the bedrock.

The presence of kaolinite in the river sediments of the Weaver and Mickerbrook suggests that their clay minerals may be sourced from the Quaternary glacial drift deposits (which are elsewhere known to contain kaolinite; (Jones et al., 2003)), and which may (at least partially) ultimately be derived from the erosion of the underlying kaolinite-bearing Carboniferous strata. The absence of swelling clays in the river sediments is more difficult to explain. One possibility is that the swelling clay minerals may somehow become physically separated during erosion and transport through the river system. Smectitic minerals are often much finer grained, and therefore may remain in suspension longer than the other clay minerals. Consequently, they may get preferentially washed downstream rather than deposited in the river system. Their apparent absence in the XRD analyses of the river sediments may also in part be an experimental artefact caused by the presence of unusually large amounts of quartz in the fine grained fraction. Oriented mounts are made to enhance the basal (00/) reflections of phyllosilicate minerals, but if large amounts of fine-grained quartz are present it may (i) dilute the clays, thus reducing the intensity of their reflections; and (ii) disrupt the orientation of clays in the mount itself, thus preferentially reducing their 00l reflections. One way to test all these possibilities further would be to try to separate out the <0.5 m size fraction by centrifuging, and characterise it by XRD. This might possibly remove most of the quartz and as a result, might enhance the reflections of the clay minerals.

7.1.3.2 Provenance of the Mersey estuary sediments

The clay fraction of the estuarine sediments (Table 7.1) has a broadly similar mineralogical assemblage to that seen in the tributary rivers, comprising mainly quartz, with illite, mica, kaolinite and Fe-rich chlorite clay minerals, with only very minor amounts of mixed-layer chlorite-smectite. However, there are differences between the fluvial and estuarine sediments in terms of the relative proportions of the different clay mineral species:

- The estuarine clays contain a much greater proportion of chlorite than any of the river sediments, which by contrast contain chlorite only in trace quantities.

- The estuarine sediments also differ from those of the rivers draining the Carboniferous terrain in that kaolinite is not the most abundant clay mineral.

Thus, whilst the rivers draining both Carboniferous and Permo-Triassic catchments may contribute sediment to the Mersey estuary, they cannot solely account for the higher proportions of chlorite seen in the estuarine sediments.

Sea-bed sediments from the Irish Sea west of Cumbria have been studied in detail by several previous workers (see Jones et al., (2003), and references therein). These studies showed that their clay mineralogy is similar across the East Irish Sea area; comprising chlorite, illite and kaolinite. Mixed-layer clay minerals (or 'swelling clays') are absent, or form only a relatively minor component of the clay fraction. However, mixed-layer clay minerals have been identified in estuarine sediments of the Cumbrian coast (Kelly and Emptage, 1992).

The Mersey estuary sediments have a broadly similar clay mineral assemblage to that reported from the Irish Sea sea-bed sediments. These observations would therefore be consistent with the movement of sediment into the Mersey estuary from the Irish Sea. Studies of other estuaries in the Irish Sea area (West Cumbria (Kelly and Emptage, 1992) and Cardigan Bay (Moore, 1968)) also concluded that their sediments were largely derived from the Irish Sea, rather than being contributed by rivers draining into these estuaries.

The limited heavy mineral data also supports the concept that much of the sediment in the Mersey estuary is probably derived mainly from reworking of the Irish Sea sea-bed sediments. The Mersey estuary sediments have quite a diverse assemblage of heavy minerals. In contrast, the heavy mineral assemblage in the Permo-Triassic strata is very restricted (Plant et al., 1999), comprising largely zircon, rutile monazite and tourmaline. There is a paucity of modern heavy mineral data for the late Carboniferous clastic rocks within the Mersey Catchment area, which prevents comparison with the Mersey sediments. The only comparable data available are from the Namurian sandstones of the Lancaster area (Hallsworth, 1991). These rocks have a broadly similar assemblage to the Permo-Triassic strata, although monazite is more abundant (c.f. Plant et al., 1999). This implies that the Carboniferous and Permo-Triassic strata are probably not the principal source of the estuarine sediments.

The presence of apatite, garnet and amphibole implies derivation ultimately from a relatively high-grade metamorphic terrain. Furthermore, the lack of, or limited, alteration of these minerals suggests that they have not been recycled through the erosion of the regional Carboniferous bedrock in the catchment area, since these minerals would have been expected to have been dissolved during deep burial diagenesis. It seems most likely that the heavy minerals in the Mersey estuary sediments are sourced by reworking of the Quaternary glacial drift forming the sea bed of the Irish Sea, and which was deposited by the Devensian ice sheets which eroded the Scottish metamorphic terrain.

7.1.4 Sediment diagenesis

The sediments are undergoing early diagenetic sulphide and iron reduction, with the formation of principally authigenic iron sulphides. The authigenic sulphides occur in a variety of forms from ultrafine or 'amorphous' or structureless films of iron sulphide (Plate 7.11) coating detrital grains or replacing organic material, to spherical protoframboids with indistinct

crystal form (Plate 7.12), and well-developed framboids composed of tightly interlocking minute octahedral crystals (Plate 7.13). All these different iron sulphide forms occur together in the same sediment sample but petrographical observations suggest that the early 'amorphous films' progressively coarsen and recrystallise to protoframboids and eventually framboidal sulphide. Two of the sites studied (Site M42 and Site M101) had very high concentrations of copper, zinc and lead. The authigenic sulphides found growing in the sediment correspondingly were found to be iron–copper–zinc–nickel bearing, rather than iron sulphide.

EDXA shows that the composition of the authigenic sulphide is variable and often non-stoichiometric (Table 7.4). The compositional variation closely reflects the authigenic sulphide morphology. Amorphous sulphide films have a relatively low S:Metal ion ratio (0.72–1.30) and are close in composition to the iron monosulphide, mackinawite (Figure 7.1). The intermediate protoframboids have a higher S:Metal ion ratio (1.25–1.70), approximately similar to greigite (Figure 7.1). The more crystalline framboids have the highest S:Fe ion ratio (1.69–1.97) and some may reach a composition similar to pyrite (Figure 7.1). The types of authigenic sulphide and the sequence of sulphide authigenesis observed in the Mersey estuary are very similar to those described during the sulphide reduction in modern canal sediments by Large et al. (2001).

The copper and nickel content of the authigenic sulphides from the metal-contaminated sediments from Sites M42 and M101 varies antithetically to the S:Fe ratio, with the highest copper and nickel concentrations found in the least crystalline (low S:Fe) sulphide (Figure 7.2). This suggests that the more evolved pyrite-like authigenic phases is less able to incorporate metals such as copper and nickel, and that these metals are re-released back into the sediment porewaters as the authigenic minerals evolve.

7.2 MINERALOGY OF ANTHROPOGENIC CONTAMINATION

7.2.1 General

Whole sediment geochemical analysis (see section 6 in this report) identified higher levels of heavy metals (Cr, Zn, Cu, Pb, As, Sn) in sediments from Inner Estuary sites (Zn 500 to >1000 ppm; Cu 120 to 240 ppm; Pb 180 to 380 ppm; Cu 120 to 200 ppm; Sn 20 to 30 ppm, Cd up to 449 ppm) than in sites at the estuary mouth or in the upper reaches of the estuarine system. In particular, sediments from site M101, near Hale on the central north shore, were found to have particularly high concentrations of Zn, Cu, Cd and Cr. These elements would appear to be 'marker elements' for potential anthropogenic contamination. The mineralogical characteristics and mineral-chemical association of anthropogenic contaminants in these sediments were examined and characterised from six of the estuarine sample sites (Figure 2.1):

- Estuary mouth (Birkenhead) represented by site M42;
- Central estuary region (north bank) represented by sites M28 and M101;
- Central estuary region (south bank) represented by sites M95 and M167;
- Upper reaches (upstream of Widnes and Runcorn) represented by site M48

CryoSEM-EDXA and SEM-EDXA examination of intact sediment and heavy mineral separates identified a wide range of contaminant phases which are probably related to industrial processing and other anthropogenic origins. These are discussed below:

Table 7.4 The composition of authigenic iron and polymetallic sulphides in sediments from the Mersey estuary, measured by EDXA.

Description	Atom %							Site and sample depth (cm)
	Fe	Co	Ni	Cu	Zn	S	S/metal	
Iron sulphides								
Framboid	33.70	0.00	0.00	0.00	0.00	66.30	1.97	M42, 58–68
Framboid	34.59	0.00	0.00	0.00	0.00	65.41	1.89	M42, 58–68
Framboid	35.75	0.00	0.00	0.00	0.00	64.25	1.80	M42, 58–68
Framboid	37.24	0.00	0.00	0.00	0.00	62.76	1.69	M42, 58–68
Protoframboid	41.47	0.00	0.00	0.00	0.00	58.53	1.41	M42, 58–68
Protoframboid	41.88	0.00	0.00	0.00	0.00	58.12	1.39	M42, 58–68
Protoframboid	42.32	0.00	0.00	0.00	0.00	57.68	1.36	M28, 30–40
Protoframboid	42.91	0.00	0.00	0.00	0.00	57.09	1.33	M42, 58–68
Protoframboid	44.40	0.00	0.00	0.00	0.00	55.60	1.25	M28, 30–40
Amorphous film	45.46	0.00	0.00	0.00	0.00	54.54	1.20	M42, 58–68
Amorphous film	48.66	0.00	0.00	0.00	0.00	51.34	1.06	M42, 58–68
Ultrafine/amorphous film	50.05	0.00	0.00	0.00	0.00	49.95	1.00	M42, 30–40
Ultrafine/amorphous film	58.14	0.00	0.00	0.00	0.00	41.86	0.72	M42, 30–40
Polymetallic sulphides								
Framboid–protoframboid	35.55	0.00	1.45	0.00	0.00	63.01	1.70	M101, 30–40
Framboid–protoframboid	36.25	0.00	1.26	0.48	0.00	62.01	1.63	M101, 30–40
Framboid–protoframboid	41.73	0.00	2.35	0.00	0.00	55.91	1.27	M101, 30–40
Ultrafine/ amorphous film	29.99	0.00	2.85	6.76	3.83	56.56	1.30	M42, 0–10
Ultrafine/ amorphous film	33.82	0.00	4.22	5.96	3.76	52.24	1.09	M42, 0–10
Ultrafine/ amorphous film	48.85	0.00	2.48	0.00	0.00	48.66	0.95	M101, 30–40
Ultrafine/ amorphous film	55.69	0.00	4.99	0.00	0.00	39.32	0.65	M101, 30–40
Ultrafine/ amorphous/film	62.30	0.00	7.00	0.00	0.00	30.70	0.44	M101, 30–40
Ultrafine/ amorphous/film	30.80	0.00	10.28	20.28	10.58	28.06	0.39	M42, 0–10

7.2.2 Ferrous and heavy metal phases

7.2.2.1 Iron phases

Iron oxide particles (excluding common natural detrital minerals such as magnetite and ilmenite) are the most abundant 'heavy mineral' particles. Typically, they are spongy or microporous oxide grains, or occur as spongy Fe oxide coatings on other grains (normally obscuring the underlying host particle (e.g. Plate 7.14). Spongy Fe oxide particles are very abundant in sediments at the mid-estuarine Site M101, particularly in sediment above 40 cm depth. Although present, these particles are relatively rare in sediments examined from the other sites. EDXA shows that the Fe oxide particles often contain detectable P, Al and Si. Ca and Mg are also sometimes detectable by EDXA. Many of the Fe oxide particles from Site M101 are enriched in Zn, with Pb and Cu sometimes detectable by EDXA (Figure 7.3).

Metallic particles

Rare fragments of partially corroded steel (Fe–Ti alloy) and Fe metallic particles were identified in near-surface sediments at the mid-estuarine Site M101. Rare steel particles were also found at 58–68 cm depth in sediments from Site M42 near Birkenhead docks. In this case, the particles appear to be composite fragments of steel 'bonded' to fibrous asbestos (Plates 7.15 and 7.16). Qualitative EDXA suggests that the asbestos is chrysotile-like in composition. These particles are clearly of industrial origin, and their proximity to the docks may indicate a derivation from some ship-related processes.

7.2.2.2 Zinc phases

Zinc-rich particles are very abundant in heavy mineral separates from above 40 cm depth at Site M101. Sphalerite (ZnS) grains are particularly abundant. They range in size from <1 to 200 μm in size, are typically angular and fresh-looking, and show little or no evidence of alteration (Plate 7.17). Sphalerite would be expected to oxidise and weather readily in the natural environment, and therefore it would not be expected to be of detrital origin in these sediments. The common presence of chalcopyrite and galena grains, in addition to sphalerite, in heavy mineral separates from sediments at Site M101 suggests that these minerals are derived from ore processing wastes, or from ore material dumped or spilled in the estuary.

Sediments from above 40 cm depth at Site M101 also contain grains of Zn-bearing Fe aluminosilicate slag. These are probably derived from base metal smelting processes, and may be derived from the same source as the sphalerite, galena and chalcopyrite.

Zinc is also present in many spongy Fe oxide particles found at Site M101 (which have been described previously in Section 7.2.2.1, above).

7.2.2.3 Lead phases

Lead-rich particles, ranging from <1 to 200 μm in size, were identified in sediments from above 60 cm depth at Site M101. These particles include grains of galena (PbS), anglesite ($PbSO_4$) lead oxide, slaggy particles, and Pb-rich spongy Fe oxide grains. These lead particles show little evidence of alteration. The particles are closely associated with Zn- and Cu-bearing particles in sediments from Site M101, and are probably contaminants derived from base-metal smelting, although they have been found to greater depth than particles of Zn and Cu phases.

Lead oxide and Pb phosphate coated particles were also found in heavy mineral separates from near-surface (0–10 cm depth) sediments at site M95. However, at this site they are only a very minor component of the heavy mineral fraction and are not seen to be associated with Zn and Cu phases.

7.2.2.4 Copper phases

Chalcopyrite was identified as a minor component in heavy mineral separates from sediments above 40 cm depth at Site M101. The chalcopyrite occurs as fresh, angular grains ranging from 20 to 200 μm in size. They show no evidence of alteration. Copper was also detected in spongy Fe oxide particles from the same sample site. These Cu-rich particles are closely associated with Zn- and Pb-bearing particles in sediments from Site M101, and are probably contaminants derived from base-metal ore processing and smelting wastes.

7.2.2.5 Tin phases

Rare grains coated with Sn oxide were found in near-surface sediments (0–10 cm depth) from Site M95. The Sn oxide forms small (0.2–5 μm), euhedral crystals, which appear to have nucleated on the surface of detrital quartz grains (Plate 7.18). Their euhedral morphology suggests that these particles have not been transported far, and they may be of authigenic origin within the sediments. However, authigenic Sn mineralisation would not normally be anticipated in natural sedimentary systems. Therefore, it is possible that the precipitation of this Sn phase is related to the alteration of anthropogenic Sn contamination during the early diagenetic modification of these muddy sediments.

7.2.3 Fly ash and slag components

Fly ash and slaggy grains are very common accessory components in the estuarine sediments at all sites examined. Slaggy grains are particularly common in sediments from above 60 cm depth at Site M101.

Fly-ash particles occur as glassy spherules with surfaces variously ornamented by dendritic and microcrystalline intergrowth fabrics probably formed by devitification (Plates 7.19–7.22). Several types of fly ash are present, but the most abundant compositional types are Ca-Mg-Al-Si-silicate-dominated, Ca-Al-Fe-P-silicate-dominated and Al-Fe-Ti K-Ca-Na-Mg-silicate. Most of the glassy spherules show delicate surface ornamentation that probably represents a devitification texture. Many fly-ash particles are fresh and unaltered but many also show evidence of corrosion and dissolution, with preferential dissolution of the glassy matrix phase often proceeding along the grain boundaries of crystalline Al-Fe oxide phases (Plates 7.21 and 7.22). In some cases, the glass appears to be altering to a delicate secondary smectitic clay-like alteration product. Both altered and unaltered fly ash particles may be present in the sediment at any given depth in the different sampling sites.

Slag particles are also common. These are typically angular, vesicular glassy silicate grains of variable composition but usually containing Fe, Al, Ti, Mn, Ca, Mg and sometimes P and K (Plate 7.23). The slaggy particles found in sediments from Site M101 often contained Zn at a sufficient concentration to be detectable by EDXA. The slag particles vary from fresh angular grains with little evidence of alteration or dissolution, to grains that are highly corroded or coated with smectitic clay-like or Fe oxide alteration rinds (Plate 7.24). The Fe oxide associated with altered slag from Site M101 contains significant Zn.

7.2.4 Asbestiform and fibrous mineral components

Asbestiform or very fibrous minerals/particles are present in most of the sediment samples examined, although usually as very minor or trace components. The fibres range from

<2 μm to >1 mm in length, although most of the fibrous particles are <50 μm long. Chrysotile-like asbestiform particles, associated with fragments of steel were identified in sediment from Site M42 (Birkenhead docks). Fibrous or asbestiform particles are particularly common in the sediments from Site M101 (Plate 7.25), and a variety of fibrous phases have been differentiated by SEM-EDXA, including Mg-rich silicate fibres, calcium silicate fibres, and Mg-Fe-rich silicate fibres.

7.2.5 Other anthropogenic components

Dolomite, barite and anhydrite are common accessory components in the heavy mineral separates from the estuarine sediments (see Section 7.1.3). Anhydrite, barite and dolomite are either very soluble and/or very soft minerals. Therefore, it seems unlikely that these would survive in a marine or estuarine environment. Since many of these particles are fresh, they are probably of anthropogenic origin, rather than present as natural detrital minerals.

7.3 MINERAL–CHEMICAL ASSOCIATIONS IN THE SEDIMENTS

7.3.1 Bulk trace metal compositions

Figure 7.4 shows a comparison of selected trace element concentrations found in contaminated bulk core samples (the data for the three core samples for M101 have been averaged). These elements are considered to be markers of anthropogenic contamination. In general, the cores from the Inner Estuary (M101 and M167) have higher marker element contents than those from either end of the estuary with M101 having the highest concentrations. Core M48 from the Upper Estuary tends to have a lower marker element content than M42 from nearer the mouth of the estuary (apart from Zn and Cd). This fits in with the Inner Estuary being most highly industrialised, the mouth being the next most industrialised and finally the Upper Estuary being the least industrialised.

7.3.2 CISMeD marker element distribution

For each core sample the CISMeD test (see Appendix 1) identifies physico-chemical components that are dissolved out of the core material and can be tentatively identified by their chemical composition and the range of acid extraction conditions over which they have been dissolved. The data processing also gives the distribution of the anthropogenic pollution marker elements (As, Cd, Co, Cr, Cu, Ni, Pb, V and Zn) among the identified physico-chemical components (Tables 7.5 to 7.12).

Figure 7.5 shows how much of the total marker element in each core was leached by the CISMeD extraction. CISMeD extraction profiles for each sediment core are shown in Figures 7.6 to 7.9. As, Cu, Pb and Zn show the highest recoveries (ca. 50–100 per cent) and core samples M101 and M167 tend to show higher amounts of extractable elements than the samples from the extreme ends of the estuary.

Table 7.5 Composition of the physico-chemical components found in Core M48 (per cent).

		Carbonate	Carbonate	Carbonate	Carbonate			
Element	**Pore-water**	**1**	**2**	**3**	**4**	**Fe-Mg-P**	**Fe-Mg-S**	**Fe-K-Na**
Al	0.00	0.00	0.00	0.00	0.64	3.37	7.24	8.44
As	0.02	0.01	0.00	0.00	0.02	0.05	0.05	0.33
Ba	0.00	0.07	0.04	0.05	0.02	0.20	0.19	0.00
Ca	0.00	87.72	97.07	95.74	96.78	7.98	0.00	0.00
Cd	0.00	0.00	0.00	0.01	0.00	0.00	0.00	0.02
Co	0.00	0.00	0.00	0.00	0.00	0.02	0.03	0.00
Cr	0.00	0.00	0.00	0.00	0.01	0.08	0.24	0.00
Cu	0.00	0.00	0.00	0.01	0.08	0.01	0.09	0.00
Fe	0.00	0.00	0.08	0.00	0.84	38.32	42.37	14.84
K	6.27	2.05	0.00	0.00	0.03	0.00	0.00	18.35
Li	0.01	0.01	0.00	0.00	0.00	0.00	0.00	0.24
Mg	0.91	8.58	1.12	0.91	0.00	31.78	14.90	0.00
Mn	0.00	0.28	0.79	0.42	0.33	2.18	0.49	0.00
Na	86.72	0.00	0.17	0.51	0.00	0.00	0.00	46.48
Ni	0.00	0.00	0.00	0.00	0.00	0.02	0.05	0.01
P	0.62	0.00	0.05	0.00	0.69	11.49	0.00	2.73
Pb	0.01	0.00	0.00	0.00	0.21	0.08	0.01	0.00
S	5.21	0.00	0.18	0.50	0.00	1.32	29.11	3.85
Se	0.00	0.00	0.00	0.00	0.00	0.00	0.02	0.13
Si	0.22	0.83	0.10	0.00	0.00	2.98	4.72	4.48
Sr	0.00	0.45	0.36	0.27	0.22	0.00	0.00	0.00
V	0.00	0.00	0.00	0.00	0.00	0.01	0.02	0.10
Zn	0.00	0.00	0.03	1.55	0.12	0.11	0.45	0.00

Table 7.6 Distribution of extracted marker elements in core M48.

			Carbonate		Carbonate		Carbonate
Element	**Pore-water**	**Element**	**1**	**Element**	**2**	**Element**	**3**
As	2	V	5	Co	14	Cd	93
V	1	As	5	Ni	14	Zn	83
Cd	1	Co	3	Zn	2	Co	14
Pb	0	Cd	1	Cd	0	Cu	10
Cu	0	Ni	1	Pb	0	Ni	9
Zn	0	Cu	0	As	0	Pb	0
Cr	0	Cr	0	Cu	0	As	0
Co	0	Pb	0	Cr	0	Cr	0
Ni	0	Zn	0	V	0	V	0
Element	**Carbonate 4**	**Element**	**Fe-Mg-P**	**Element**	**Fe-Mg-S**	**Element**	**Fe-K-Na**
Pb	84	Cr	51	Cr	33	V	12
Cu	75	Ni	45	Ni	22	As	9
V	34	Co	43	V	19	Cd	4
As	33	As	40	Co	12	Ni	1
Cr	15	V	29	As	10	Co	0
Co	14	Pb	15	Cu	8	Pb	0
Ni	9	Cu	6	Zn	3	Zn	0
Zn	9	Zn	3	Pb	0	Cu	0
Cd	0	Cd	0	Cd	0	Cr	0

Table 7.7 Composition of the physico-chemical components found in Core M101 (per cent).

Element	Pore-water	Carbonate 1	Na-K	Carbonate 2	Carbonate 3	Fe-Mg-Al-Si	Fe oxide 1	Fe-Ca	S-Fe
Al	0.00	0.00	0.05	1.00	2.07	12.26	4.19	2.14	6.96
As	0.00	0.00	0.10	0.00	0.09	0.02	0.28	0.19	0.03
Ba	0.00	0.10	0.13	0.10	7.72	0.41	0.00	0.00	0.18
Ca	0.00	76.93	0.00	89.65	52.81	0.00	14.30	39.82	0.00
Cd	0.00	0.00	0.00	0.02	0.00	0.00	0.00	0.00	0.00
Co	0.00	0.00	0.00	0.01	0.00	0.04	0.00	0.02	0.01
Cr	0.00	0.00	0.00	0.00	0.27	0.42	0.07	0.95	0.23
Cu	0.00	0.00	0.03	0.32	0.06	0.00	0.47	0.03	0.14
Fe	0.00	1.67	0.00	0.00	8.19	58.97	44.63	41.99	10.48
K	3.35	2.87	11.20	0.00	1.87	0.00	1.47	0.56	0.00
Li	0.00	0.00	0.02	0.00	0.00	0.03	0.00	0.00	0.02
Mg	3.17	16.40	4.65	2.68	0.00	17.14	10.10	3.18	0.00
Mn	0.00	1.60	0.00	3.43	4.34	0.00	0.93	0.07	0.96
Na	87.17	0.00	80.47	0.00	0.00	0.00	11.39	0.00	0.00
Ni	0.00	0.00	0.00	0.02	0.04	0.04	0.01	0.03	0.04
P	0.01	0.00	0.38	0.00	7.43	0.00	7.82	0.00	2.32
Pb	0.00	0.03	0.00	0.19	0.60	0.00	1.07	0.00	0.30
S	6.23	0.00	0.00	0.00	3.09	0.00	1.41	0.00	77.87
Se	0.00	0.00	0.01	0.00	0.00	0.00	0.00	0.03	0.00
Si	0.06	0.00	2.80	0.00	9.32	10.46	1.68	9.66	0.00
Sr	0.00	0.38	0.01	0.20	0.37	0.00	0.00	0.00	0.03
V	0.00	0.00	0.03	0.06	0.00	0.03	0.05	0.02	0.03
Zn	0.00	0.02	0.11	2.31	1.71	0.19	0.14	1.31	0.39

Table 7.8 Distribution of extracted marker elements in Core M101 (per cent).

Element	Fe-Ca 1	Element	Carbonate 1	Element	Pore-water
As	77	Cd	95	As	0
Pb	71	Zn	80	V	0
Cu	50	V	52	Cd	0
V	30	Co	45	Pb	0
Cr	18	Cu	45	Cu	0
Ni	11	Ni	43	Zn	0
Zn	4	Pb	17	Cr	0
Cd	0	As	0	Ni	0
Co	0	Cr	0	Co	0
Element	**S-Fe**	**Element**	**Fe-Ca 2**	**Element**	**Carbonate 2**
Cr	10	Cr	21	Cr	13
Ni	10	Co	5	Ni	10
Pb	4	As	5	Zn	8
Co	4	Ni	3	Pb	7
Cu	3	Zn	3	As	5
Zn	2	V	1	Co	1
As	2	Cd	0	Cd	1
V	0	Cu	0	Cu	1
Cd	0	Pb	0	V	0
Element	**Carbonate 3**	**Element**	**Na-K**	**Element**	**Fe-Mg-Al-Si**
Co	8	As	8	Cr	39
Ni	3	V	6	Co	37
Pb	1	Cd	1	Ni	19
Zn	0	Cu	1	V	8
Cu	0	Zn	1	As	2
As	0	Ni	1	Zn	2
V	0	Pb	0	Cd	2
Cr	0	Cr	0	Pb	0
Cd	0	Co	0	Cu	0

Table 7.9 Composition of the physico-chemical components found in Core M167 (per cent).

Element	Pore-water	Fe-oxide	Carbonate	S-Fe	K-Ca-S-Mg-Si
Al	0.00	7.61	0.00	4.24	4.15
As	0.01	0.16	0.00	0.00	0.27
Ba	0.00	0.29	0.09	0.16	0.12
Ca	0.94	7.87	85.55	2.41	20.70
Cd	0.00	0.00	0.00	0.00	0.00
Co	0.00	0.02	0.01	0.03	0.00
Cr	0.00	0.17	0.00	0.38	0.00
Cu	0.01	0.30	0.03	0.00	0.00
Fe	0.00	43.45	0.00	38.71	0.00
K	4.66	0.07	1.99	0.00	29.35
Li	0.00	0.01	0.00	0.01	0.09
Mg	4.66	9.86	9.14	0.00	13.25
Mn	0.00	0.69	2.43	0.75	0.01
Na	87.93	13.17	0.00	3.56	0.00
Ni	0.00	0.02	0.01	0.03	0.05
P	0.20	6.64	0.00	0.00	0.01
Pb	0.01	0.56	0.06	0.00	0.00
S	1.55	3.08	0.00	45.99	18.38
Se	0.00	0.00	0.00	0.00	0.06
Si	0.00	5.36	0.09	3.55	12.65
Sr	0.02	0.00	0.31	0.00	0.77
V	0.00	0.06	0.01	0.00	0.14
Zn	0.00	0.63	0.27	0.18	0.00

Table 7.10 Distribution of extracted marker elements in Core M167 (per cent).

Element	Pore-water	Element	Fe-oxide	Element	Carbonate
As	1.83	As	90.09	Cd	80.26
Cu	1.53	Pb	81.13	Zn	46.61
Pb	1.11	Cu	80.60	Co	33.24
V	0.52	Cr	59.77	V	32.57
Zn	0.00	V	59.45	Ni	29.99
Cd	0.00	Zn	49.01	Cu	17.86
Ni	0.00	Co	40.63	Pb	17.75
Co	0.00	Ni	40.62	As	0.00
Cr	0.00	Cd	12.53	Cr	0.00
Element	**S-Fe**	**Element**	**K-Ca-S-Mg-Si**		
Cr	40.23	As	8.07		
Co	25.43	V	7.46		
Ni	23.34	Ni	6.06		
Cd	7.22	Co	0.69		
Zn	4.37	Cu	0.00		
Cu	0.00	Pb	0.00		
Pb	0.00	Zn	0.00		
V	0.00	Cd	0.00		
As	0.00	Cr	0.00		

Table 7.11
Composition of the physico-chemical components found in Core M42 (per cent).

Element	Pore-water	Na	Carbonate 1	Carbonate 2	Carbonate 3	Fe-Ca	Ca-Fe-Mg	Na-Si-Mg-Fe	S-Fe
Al	0.00	0.00	0.00	0.43	0.05	3.60	8.47	1.04	5.81
As	0.00	0.02	0.00	0.00	0.00	0.10	0.02	0.09	0.06
Ba	0.00	0.00	0.07	0.05	0.01	0.00	0.15	0.67	0.00
Ca	0.00	0.00	97.35	95.33	70.02	25.44	34.10	0.00	0.00
Cd	0.00	0.00	0.00	0.00	0.00	0.00	0.00	0.00	0.00
Co	0.00	0.00	0.01	0.01	0.00	0.01	0.03	0.03	0.01
Cr	0.00	0.00	0.00	0.00	0.00	0.09	0.01	0.52	0.42
Cu	0.00	0.00	0.00	0.09	0.00	0.09	0.03	0.00	0.09
Fe	0.00	0.00	0.00	0.00	0.02	45.33	30.78	16.65	23.60
K	4.00	7.78	0.00	0.00	7.64	0.00	0.00	5.66	3.47
Li	0.00	0.01	0.00	0.00	0.00	0.00	0.02	0.01	0.02
Mg	3.27	0.46	0.26	1.68	20.09	7.02	13.77	15.32	0.00
Mn	0.00	0.00	1.76	1.15	0.81	0.06	0.68	1.29	0.10
Na	86.85	85.34	0.00	0.40	0.00	7.94	0.00	37.51	0.00
Ni	0.00	0.00	0.00	0.01	0.00	0.00	0.03	0.01	0.03
P	0.02	0.94	0.00	0.00	0.00	5.50	0.79	3.31	0.00
Pb	0.00	0.00	0.00	0.10	0.01	0.43	0.07	0.00	0.00
S	5.86	3.77	0.00	0.00	0.00	2.16	7.50	0.00	63.57
Se	0.00	0.01	0.00	0.00	0.00	0.00	0.00	0.01	0.08
Si	0.00	1.63	0.11	0.01	0.89	2.12	3.21	17.27	2.53
Sr	0.00	0.00	0.36	0.28	0.45	0.01	0.00	0.00	0.10
V	0.00	0.04	0.00	0.03	0.00	0.04	0.02	0.03	0.01
Zn	0.00	0.00	0.08	0.45	0.00	0.08	0.33	0.60	0.12

Table 7.12
Distribution of extracted marker elements in Core M42 (per cent).

Element	Pore-water	Element	Na	Element	Carbonate 1
Cd	0	V	6	Co	13
Ni	0	Cd	4	Ni	11
Zn	0	As	4	Zn	5
Pb	0	Ni	1	Cd	2
As	0	Cu	0	Pb	0
V	0	Cr	0	As	0
Cu	0	Pb	0	V	0
Co	0	Zn	0	Cu	0
Cr	0	Co	0	Cr	0
Element	**Carbonate 2**	**Element**	**Carbonate 3**	**Element**	**Fe-Ca**
Cd	77	Cd	5	As	69
Zn	66	Pb	1	Pb	57
Cu	64	Cu	0	Cr	33
V	56	As	0	V	23
Pb	38	Zn	0	Cu	22
Co	38	V	0	Co	8
Ni	28	Co	0	Zn	4
As	0	Cr	0	Ni	4
Cr	0	Ni	0	Cd	0
Element	Ca-Fe-Mg	Element	Na-Si-Mg-Fe	Element	S-Fe
Ni	42	Cr	37	Cr	30
Co	30	As	12	Ni	10
Zn	14	Cd	7	As	8
As	12	Co	6	Cu	4
V	10	Zn	6	Co	2
Pb	8	V	3	V	2
Cu	7	Ni	2	Zn	1
Cr	4	Pb	0	Cd	0
Cd	0	Cu	0	Pb	0

8 Summary and environment issues

Estuarine sedimentation is an active, dynamic process. Old deposits, possibly hosting industrial contamination, are re-worked, new sediments are brought in, and others are removed by current and tidal action. This study of the sediments of the Mersey estuary has concentrated on the spatial distribution of chemical elements and organic compounds, solid phase-speciation geochemistry and environmental mineralogy. The most important features revealed by these studies are summarised here.

Comparison of sedimentology and spatial mapping of element distributions shows clear relationships between sediment type and heavy-metal content within estuary. The highest metal concentrations are found in the finer-grained sediments reflecting strong grain-size control related to clay mineral and organic matter contents. Normalisation to Al_2O_3 content as a proxy for grain-size differences suggests that grain-size is generally a more important control on geochemistry than organic matter content. Such normalisation reveals the geochemical variation that can be considered to more closely reflect anthropogenic inputs. High heavy-metal loading is seen to be located near the north and south banks of the Inner Estuary, particularly near Hale Head on the north shore and Weaver Sluices, Ince Bank and Stanlow Bank on the south shore. Other 'hot spots' are off Tranmere on the left bank in the Narrows, off the dock area on the right bank at the mouth of the estuary, and in the Inner Estuary near Widnes. Industrial sources likely to have contributed most metals to the sediments include the towns of Warrington, Widnes and Runcorn with chemical (originally mainly alkali and bleaching), petrochemical, paint manufacture, metal ore smelting, engineering and shipbuilding operations, and the general industry of the ports and docks. Slag dumped on the north bank of the estuary between Hale Head and Runcorn may also have contributed to high metal values. The Manchester Ship Canal has also been a source of contaminants to the estuary because the process of 'levelling', when lock gates are opened, releasing water which, particularly in the past, may have been highly contaminated.

Major geochemical associations or assemblages were identified by multivariate statistical analysis of the sediment data. Of these the most clearly defined and important, in order of increasing metal loading, are: clean quartz sand (mainly of marine origin), fine sands with organic-rich coatings, shell fragment beds, and organic-rich mud. These assemblages match closely with the observed spatial mapping in both the surface sediments and core profiles.

Organic geochemical data collected in the course of this study are too few to allow any firm conclusions to be drawn. However, there is a degree of correlation between TOC and PAH contents and mud, predominantly located close to the banks of the estuary, appears to be the principal sink for PAHs. Pyrolitic inputs, from the incomplete combustion of fossil fuel, form the main source of PAHs, although in some cases this is augmented by a petrogenic component from refinery products and crude oil. The PCB data show that, in comparison with the OSPAR criteria for Norwegian Sea sediments (OSPAR, 2000), Mersey levels are of the order of 100–5000 above background. Organotin compounds are present throughout the sediments studied. Natural organic matter in the sediments has a predominantly marine origin. The presence of salt-rich horizons at depth within some of the cores was a little surprising, as the general rather moist climate of Merseyside is hardly conducive to extensive evaporite formation. It is possible that these were formed by ingress from local groundwater brine springs, rather than by surface evaporation, but an alternative explanation is that post-collection precipitation of salt from pore water or otherwise pooled saline is responsible.

Mineral grain analysis suggests a mainly marine origin for the heavy mineral assemblage and therefore implies a major marine component to the estuary sediments (cf. natural organic matter). The variety of clay minerals suggests a greater input of the fine-grained material from the river catchment. Anthropogenic sources are responsible for the ore minerals, slags, metallic particles and asbestos found in the surface sediments and cores.

Much of the interest in the geochemistry of the Mersey Estuary sediments centres on the present and potential environmental impacts of contamination. This study has identified the areas of the estuary with the highest metal loadings and their relationship to sediment type. It has been shown that salt marsh sediments at Widnes Warth and Ince Bank are contaminated with As, Ba, Cr, Cu, Mn, Ni, P, Pb and Zn in their upper parts, with the implication that the fine-grained sediment of the estuary in general must be similarly contaminated. Further, the old salt marsh sediments at Ince Marshes could provide good indicators of 'natural background' values for the Mersey Estuary. Table 6.2 gives some of these 'natural background' background values in both 'raw' and Al normalised form, the maximum values being the critical levels for the definition of contamination. Comparison of these values with those shown on the element distribution maps confirms that for Cr, Cu, Pb and Zn the whole of the Mersey estuary contains sediment with concentration levels above the Al normalised 'natural background' level. These findings are comparable with those of Harland et al. (2000). Given the industrial setting of the Mersey estuary and its catchment such widespread contamination is not unexpected, particularly since much of the surface and near surface sediment is subject to mixing, erosion and redeposition processes. Sediment reworking during tidal cycles and channel migration removes most evidence of time-related change in the short, intertidal sediment cores collected during this study. However, the cores taken from the more stable saltmarsh environments show a decrease in metal levels in the topmost parts, suggesting that contamination in the Mersey estuary is on the decline.

Pollution of the Mersey estuary has been a cause of concern for over 150 years (Jones, 2000), but was more recently brought to the fore in the 1980s when the UK Department of the Environment published "A consultation paper on tackling the water pollution in the rivers and canals of the Mersey catchment and improving the appearance of their banks" and convened a Mersey conference in 1983 to pursue the issues (Jones, 2006). Subsequently, in 1985, the Mersey Basin Campaign was launched with the objectives of improving water quality, encouraging waterside regeneration and engaging public, private, community and

voluntary sectors in these activities (EKOS, 2006). As a result of the measures put in place, water quality in the Mersey has improved significantly and the variety of fish species and their abundance have increased, including the return of salmonids to the estuary (EKOS, 2006; Jones, 2006). These improvements are paralleled by the lessening of contamination in the topmost parts of the Widnes Warth and Ince Bank salt marsh sediments as described above and by implication also in the fine-grained sediment of the estuary in general. A decrease in sediment metal contamination is likely to lead to a concomitant decrease in dissolved metals (Martino et al., 2002).

The improvements in water quality have largely been due to a decrease in the quantities of effluent entering the estuary and increased dissolved oxygen levels. The impacts of metal levels, particularly in sediment, on biota are less well known. Reductions in the input of Hg to the estuary have lead to lower concentrations of the metal in sediments, mussels and angler fish, and concentrations of Pb and Hg in eels and flounder decreased significantly between 1992 and 1996 (Jones, 2000). The salt marsh sediments of Ince Marshes and elsewhere contain large quantities of Hg that could be re-released into the estuary by erosion to the detriment of environmental quality. However, the erosion of large areas of the Ince Banks in the latter part of the 20th C does not appear to have had a significant impact on the environment or biota, although the effects on metal levels in fish are not well documented. Equally, the constant reworking of metal contaminated sediment by tidal currents and channel migration does not seem to have had any great affect on ecosystems. The only well-documented case of contaminant-related bird mortality in the estuary was caused by alkyl lead species that were not scavenged by particulate material and consequently not found in the sediments (Wilson et al., 1986).

Although levels of most contaminant metals decrease in the topmost layers of the saltmarsh sediments, showing the general improvement in the environment, there must still be concern that the large quantities of metal stored in the sediments could be released into the Mersey as a result of erosion, either through natural causes or man-made interference. There are also thought to be high levels of contaminants, including asbestos, in the slag used to form an embankment between Hale Head and Runcorn on the northern shore of the estuary. The potential impact of sea-level rise is important in these respects.

References

British Geological Survey holds most of the references listed below, and copies may be obtained via the library service subject to copyright legislation (contact libuser@bgs.ac.uk for details). The library catalogue is available at: http://geolib.bgs.ac.uk

APPLEBY, P G, NOLAN, P J, OLDFIELD, F, RICHARDSON, N, and HIGGIT, S R. 1988. Pb-210 dating of lake sediments and ombrotrophic peats by gamma assay. *The Science of the Total Environment*, Vol. 69, 157–177.

AYRIS, S, CURRADO, G M, SMITH, D, and HARRAD, S. 1997. GC/MS procedures for the determination of PCBs in environmental matrices. *Chemosphere*, Vol. 35, 905–917.

BALL, D F. 1964. Loss-on-ignition as an estimate of organic matter and organic carbon in non-calcareous soils. *Journal of Soil Science*, Vol. 15, 84–92.

BASSINDALE, R. 1938. The intertidal fauna of the Mersey estuary. *Journal of the Marine Biological Association of the UK*, Vol. 23, 83–98.

BATHURST, R G C, and BRENCHLEY, P J. 1975. Liverpool Bay: an assessment of present knowledge compiled by members of the Liverpool Bay Study Group. NERC Publication Series 'C' No.14.

BAUMARD, P, BUDZINSKI, H, MCHIN, Q, GARRIGUES, P, BURGEOT, T, and BELLOCQ, J. 1998. Origin and bioavailability of PAHs in the Mediterranean Sea from mussel and sediment records. *Estuarine, Coastal and Shelf Science*, Vol. 47, 77–90.

BENNETT, C, CURTIS, M S, and FAIRHURST, C. 1988. The Mersey estuary – naturally ours. (Warrington: Mersey Estuary Conservation Group.)

BENNETT, C, CURTIS, M S, and FAIRHURST, C. 1995. Recent changes in the Mersey estuary 1958–1988. 12–23 in *The Mersey estuary – naturally ours*. CURTIS, M S, NORMAN, D, and WALACE, I D (editor). (Warrington: Mersey Estuary Conservation Group.)

BGS. 1997. *Regional geochemistry of parts of North-west England and North Wales*. (British Geological Survey, Keyworth, Nottingham.)

BGS. 2000. *Regional geochemistry of Wales and part of west-central England: stream sediment and soil*. (Keyworth, Nottingham: British Geological Survey.)

BLACKBURN, M A, KIRBY, S J, and WALDOCK, M J. 1999. Concentrations of alkyphenol polyethoxylates entering UK estuaries. *Marine Pollution Bulletin*, Vol. 38, 109–118.

BOULOUBASSI, I, and SALIOT, A. 1993. Investigation of anthropogenic and natural organic inputs in estuarine sediments using hydrocarbon markers (NAH, LAB, PAH). *Oceanologica Acta*, Vol. 16, 145–161.

BOWDEN, K F. 1975. Circulation and mixing. 17–21 in *Liverpool Bay: An Assessment of Present Knowledge*. No. 14. (Natural Environment Research Council.)

BOWDEN, K F, and GILLIGAN, R M. 1971. Characteristic features of estuarine circulation as represented in the Mersey Estuary. *Limnology and Oceanography*, Vol. 16, 490–502.

BOWDEN, K F, and SHARAF EL DIN, S H. 1966. Circulation, salinity and river discharge in the Mersey estuary. *Geophysical Journal of the Royal Astronomical Society*, Vol. 10, 383–399.

BUCHELI, T D, and GUSTAFSSON, Ö. 2000. Quantification of the soot–water distribution coefficient of PAHs provides mechanistic basis for enhanced sorption observations. *Environmental Science and Technology*, Vol. 34, 5144–5151.

BUCK, A L. 1993. An inventory of UK estuaries. Volume 3. North-west Britain. (Peterborough: Joint Nature Conservation Committee.)

BUDZINSKI, H, JONES, I, BELLOCQ, J, PIÉRARD, C, and GARRIGUES, P. 1997. Evaluation of sediment contamination by polycyclic aromatic hydrocarbons in the Gironde estuary. *Marine Chemistry*, Vol. 58, 85–97.

CAMACHO-IBAR, V F, and MCEVOY, J. 1996. Total PCBs in Liverpool Bay sediments. *Marine Environmental Research*, Vol. 41, 241–263.

CASHIN, J A. 1949. Engineering works for the improvement of the Mersey. *Journal of the Institute of Civil Engineers*, Vol. 32, 296–355.

CAVE, M R, MILODOWSKI, A E, and FRIEL, E N. 2004. Evaluation of a method for identification of host physico-chemical phases for trace metals and measurement of their solid-phase partitioning in soil samples by nitric acid extraction and chemometric mixture resolution. *Geochemistry: Exploration, Environment, Analysis*, Vol. 4, 71–86.

CEFAS. 1998. Monitoring and surveillance of non-radioactive contaminants in the aquatic environment and activities regulating the disposal of wastes at sea, 1995 and 1996. *Centre for Environment, Fisheries and Aquaculture Science*. Report No. 51. (Lowestoft: Centre for Environment, Fisheries and Aquaculture Science.)

CEFAS. 1998. Monitoring and surveillance of non-radioactive contaminants in the aquatic environment and activities regulating the disposal of wastes at sea, 1997. *Aquatic Environment Monitoring Report*, No. 52. (Lowestoft: Centre for Environment, Fisheries and Aquaculture Science.)

CLIFF, R A, DREWERY, S E, and LEEDER, M R. 1991. Sourcelands for the Carboniferous Pennine river system: constraints from sedimentary evidence and U–Pb geochronology using zircon and monazite. 137–159 in Developments in sedimentary provenance studies. MORTON, A C, TODD, S P, and HAUGHTON, P D (editors). *Geological Society of London Special Publication*, No. 57.

CLIFFORD, D J, CARSON, D M, MCKINNEY, D E, BORTIATYNSKI, J M, and HATCHER, P G. 1995. A new rapid technique for the characterization of lignin in vascular plants – thermochemolysis with tetramethylammonium hydroxide (TMAH). *Organic Geochemistry*, Vol. 23, 169–175.

CLIFT, F. 2000. Navigation of the River Mersey (1999). *Department of the Environment, Transport and the Regions*.

CODY, G D, and SAGHI-SZABO, G. 1999. Calculation of the C-13 NMR chemical shift of ether linkages in lignin derived geopolymers: constraints on the preservation of lignin primary structure with diagenesis. *Geochimica et Cosmochimica Acta*, Vol. 63, 193–205.

COWIE, G L, and HEDGES, J I. 1992. Sources and reactivities of amino-acids in a coastal–marine environment. *Limnology and Oceanography*, Vol. 37, 703–724.

CRAIG, P J. 1986. Chemical species in industrial discharges and effluents. 443–464 in *The importance of chemical 'speciation' in environmental processes*. BERNHARD, M, BRINKMAN, F E, and SADLER, P J (editors). (Berlin: Springer-Verlag.)

DAVIES, N J, and WOLFF, G A. 1990. The Mersey oil spill, August 1989: A case of sediments contaminating the oil. *Marine Pollution Bulletin*, Vol. 21, 481–484.

DODD, J S. 2000. An investigation of the geochemistry and petrology of canal sediments. Unpublished PhD Thesis, University of Nottingham.

DODD, J S LARGE, D J, FORTEY, N J, KEMP, S, STYLES, M, WETTON, P, and MILODOWSKI, A. 2003. Geochemistry and petrography of

phosphorus in urban canal bed sediment. *Applied Geochemistry*, Vol. 18, 259–267.

DOODY, J P. 1999. Saltmarshes and sand dunes – natural or not. 167–174 in *Ecology and landscape development: a history of the Mersey Basin*. GREENWOOD, E F (editor). (Liverpool: Liverpool University Press.)

DSIR. 1938. Estuary of the River Mersey. *His Majesty's Stationary Office, Water Pollution Research Technical Paper*, No. 7.

EAU. 1987. The Dee and Mersey estuaries: environmental background. Environmental Advisory Unit, Liverpool University. Report compiled for Shell UK Ltd.

EKOS. 2006. An evaluation of the Mersey Basin Campaign: Final Report. EKOS Consulting, Government Office North West.

FARMER, J G. 1991. The perturbation of historical pollution records in aquatic sediments. *Environmental Geochemistry and Heath*, Vol. 13, 76–83.

FILLEY, T R, MINARD, R D, and HATCHER, P G. 1999. Tetramethylammonium hydroxide (TMAH) thermochemolysis: proposed mechanisms based upon the application of C-13-labeled TMAH to a synthetic model lignin dimer. *Organic Geochemistry*, Vol. 30, 607–621.

FÖRSTNER, U, and SALOMONS, W. 1980. Trace metal analysis on polluted sediments Part 2. Evaluation of environmental impact. *Environmental Technology Letters*, 506–517.

FOX, W M, JOHNSON, M S, JONES, S R, LEAH, R T, and COPPLESTONE, D. 1999. The use of sediment cores from stable and developing salt marshes to reconstruct historical contamination profiles in the Mersey estuary, UK. *Marine Environmental Research*, Vol. 47, 311–329.

FOX, W M, CONNOR, L, COPPLESTONE, D, JOHNSON, M S, and LEAH, R T. 2001. The organochlorine contamination history of the Mersey estuary, UK, revealed by analysis of sediment cores from salt marshes. *Marine Environmental Research*, Vol. 51, 213–227.

GOLDIN, A. 1987. Reassessing the use of loss-on-ignition for estimating organic matter content in non-calcareous soils. *Communications in Soil Science and Plant Analysis*, Vol. 18, 1111–1116.

GONI, M A, AND THOMAS, K A. 2000. Sources and transformations of organic matter in surface soils and sediments from a tidal estuary (north inlet, South Carolina, USA). *Estuaries*, Vol. 23, 548–564.

GRESSWELL, R K. 1964. The Origin of the Mersey and Dee estuaries. *Geological Journal*, Vol. 4, 77–86.

GSCHWEND, P M, and HITES, R A. 1981. Fluxes of polycyclic aromatic hydrocarbons to marine and lacustrine sediments in the north-eastern United States. *Geochimica et Cosmochimica Acta*, Vol. 45, 2359–2367.

HALCROW. 2002. Futurecoast. Department for Environment, Food and Rural Affairs CD ROM.

HALLIWELL, A R, and O'CONNOR, B A. 1975. Water and sediment movement in the Mersey Estuary and Liverpool Bay. 33–36 in Liverpool Bay: *An Assessment of Present Knowledge*. No. 14. (Natural Environment Research Council.)

HALLSWORTH, C. 1991. Heavy minerals from the Millstone Grit of the 1:50 000 Sheet 59 (Lancaster): implications for provenance. *British Geological Survey Technical Report*, WH/91/399R.

HARLAND, B J, TAYLOR, D, and WITHER, A. 2000. The distribution of mercury and other trace metals in the sediments of the Mersey estuary over 25 years 1974–1998. *The Science of the Total Environment*, Vol. 253, 45–62.

HARLAND, B J, TAYLOR, D, and WITHER, A. 2001. Corrigendum to 'The distribution of mercury and other trace metals in the sediments of the Mersey estuary over 25 years 1974–1998 [The Science of the Total Environment, 253 (2000) 45–62]. *The Science of the Total Environment*, Vol. 279, 231.

HARRAD, S J, SEWART, A P, ALCOCK, R, BOUMPHREY, R, BURNETT, V, DUARTE-DAVIDSON, R, HALSALL, C, SANDERS, G, WATERHOUSE, K, WILD, S R, and JONES, K C. 1994. Polychlorinated-biphenyls (PCBs) in the British environment – sinks, sources and temporal trends. *Environmental Pollution*, Vol. 85, 131–146.

HARRISON, I. 2002. Determination of polycyclic aromatic hydrocarbons (PAHs) in sediments from the Irish Sea. *British Geological Survey Internal Report*, IR/02/029.

HARVEY, A M. 1985. The river sytems of North-west England. xxx–xxx in *The Geomorphology of North-west England*. JOHNSON, R H (editor). (Manchester: Manchester University Press.)

HATCHER, P G, and MINARD, R D. 1995. Comment on the origin of benzenecarboxylic acids in pyrolysis methylation studies. *Organic Geochemistry*, Vol. 23, 991–994.

HAWKINS, S J, ALLEN, J R, FIELDING, N J, WILKINSON, S B, and WALLACE, I D. 1999. Fifteen: Liverpool Bay and the estuaries: human impact, recent recovery and restoration. 155–166 in *Ecology and landscape development: a history of the Mersey Basin*. Greenwood, E F (editor). (Liverpool: Liverpool University Press.)

HEDGES, J I, and KEIL, R G. 1999. Organic geochemical perspectives on estuarine processes: sorption reactions and consequences. *Marine Chemistry*, Vol. 65, 55–65.

HEDGES, J I, and OADES, J M. 1997. Comparative organic geochemistries of soils and marine sediments. *Organic Geochemistry*, Vol. 27, 319–361.

HEDGES, J I, and STERN, J H. 1984. Carbon and nitrogen determinations of carbonate-containing solids. *Limnology and Oceanography*, Vol. 29, 657–663.

HEDGES, J I, KEIL, R G, and BENNER, R. 1997. What happens to terrestrial organic matter in the ocean? *Organic Geochemistry*, Vol. 27, 195–212.

HO. 1994a. Mancester Ship Canal and Upper River Mersey. Chart 3478. (UK Hydrographic Office.)

HO. 1994b. West coast, part of Liverpool. Chart 3490. (UK Hydrographic Office.)

HOWELL, F T. 1973. The sub-drift surface of the Mersey and Weaver catchment and adjacent areas. *Geological Journal*, Vol. 8.

INGHAM, M N, and VREBOS, B A R. 1994. High productivity geochemical XRF analysis. *Advances in X-ray Analysis*, Vol. 37, 717–724.

JARVIS, A E, and REED, P N. 1999. Where there's brass there's muck: the impact of industry in the Mersey Basin c. 1700–1900. 57–64 in *Ecology and landscape development: a history of the Mersey Basin*. GREENWOOD, E F (editor). (Liverpool: Liverpool University Press.)

JEMMET, A W L. 1991. An investigation into the heavy metals, sediment and vegetation of a Mersey Estuary saltmarsh. Unpublished Ph D Thesis, University of Liverpool.

JONES, D G, DAVIES, A M, HIGGO, J J W, JAMES, J W C, LANGSTON, W J, METCALFE, R, MILDOWSKI, A E, PEARCE, J M, RIDGWAY, J, and WEST, J M. 2003. Review of the relative importance of biological, physical and chemical processes on the transport and speciation of pollutants, particularly radionuclides, in the Irish Sea. *British Geological Survey Technical Report*, WP/99/17.

JONES, P D. 2000. The Mersey Estuary–Back from the Dead. Solving a 150-Year Old Problem. *Journal of the Chartered Institution of Water and Environmental Management*, Vol. 14, 124–130.

JONES, P D. 2006. Water quality and fisheries in the Mersey estuary, England: A historical perspective. *Marine Pollution Bulletin*, Vol. 53, 144–154.

KEIL, R G, TSAMAKIS, E, FUH, C B, GIDDINGS, J C, and HEDGES, J I. 1994. Mineralogical and textural controls on the organic composition of coastal marine-sediments–hydrodynamic separation using SPLITT-fractionation. *Geochimica et Cosmochimica Acta*, Vol. 58, 879–893.

KELLY, M, and EMPTAGE, M. 1992. Distribution of radioactivity in the Esk Estuary and its relationship to sedimentary processes. *Department of the Environment*, DoE/HMIP/RR/92/015.

KILLOPS, S D, and KILLOPS, V J. 1993. *An introduction to organic geochemistry*. (Longman Group Ltd.)

KENDRICK , M P, and STEVENSON, T. 1985. Changes in the tidal capacity of the River Mersey. Report on studies made in 1984–85. *HR Wallingford*, Report SR 43.

KIRK, T K, and FARRELL, R L. 1987. Enzymatic combustion–the microbial degradation of lignin. *Annual Review of Microbiology*, Vol. 41, 465–505.

KLAP, V A, BOON, J J, HEMMINGA, M A, and VAN SOELEN, J. 1998. Chemical characterization of lignin preparations of fresh and decomposing Spartina anglica by pyrolysis mass spectrometry. *Organic Geochemistry*, Vol. 28, 707–727.

KLAP, V A, HEMMINGA, M A, and BOON, J J. 2000. Retention of lignin in seagrasses: angiosperms that returned to the sea. *Marine Ecology–Progress Series*, Vol. 194, 1–11.

LANE, A. 2004. Bathymetric evolution of the Mersey estuary, UK, 1906–1997: causes and effects. *Estuarine, Coastal and Shelf Science*, Vol. 59, 249–263.

LARGE, D J, FORTEY, N J, MILODOWSKI, A E, CHRISTY, A G, and DODD, J. 2001. Petrographic observations of iron, copper and zinc sulphides in freshwater canal sediment. *Journal of Sedimentary Research*, Vol. 71, 61–79.

LBCG. 1999. Liverpool Bay Shoreline Management Plan, Sub-cell 11a: Great Ormes Head to Formby Point. Liverpool Bay Coastal Group Context Report.

LEHR, R E, and JERINA, D M. 1977. Metabolic activations of polycyclic hydrocarbons: Structure–activity relationships. *Archives of Toxicology*, Vol. 39, 1–6.

LOBINSKI, R, DIRKX, W M R, CEULEMANS, M, and ADAMS, F C. 1992. Optimization of comprehensive speciation of organotin compounds in environmental–samples by capillary gas-chromatography helium microwave-induced plasma emission-spectrometry. *Analytical Chemistry*, Vol. 64, 159–165.

LONG, S P, and MASON, C F. 1983. *Salt march ecology*. (Glasgow: Blackie.)

LUOMA, S N. 1983. Bioavailability of trace metals to aquatic organisms: a review. *The Science of the Total Environment*, Vol. 28, 1–22.

MAFF. 1992. Monitoring and surveillance of non-radioactive contaminants in the aquatic environment and activities regulating the disposal of wastes at sea 1990. *Ministry of Agriculture, Fisheries and Food: Directorate of Fisheries Research*, Report No. 30.

MALINOWSKI, E R. 2002. *Factor analysis in chemistry*. (John Wiley & Sons Inc.)

MANNINO, A, and HARVEY, H R. 2000. Terrigenous dissolved organic matter along an estuarine gradient and its flux to the coastal ocean. *Organic Geochemistry*, Vol. 31, 1611–1625.

MAYER, L M. 1993. Organic matter at the sediment–water interface. 171–184 in *Organic Geochemistry*. ENGEL, M, and MACKO, S (editors). (New York: Plenum Press.)

MARTINO, M, TURNER, A, NIMMO, M, and MILLWARD, G E. 2002. Resuspension, reactivity and recycling of trace metals in the Mersey Estuary, UK. *Marine Chemistry*, Vol. 77, 171–186.

MAYER, L M. 1994. Surface-area control of organic-carbon accumulation in continental-shelf sediments. *Geochimica et Cosmochimica Acta*, Vol. 58, 1271–1284.

MCCREADY, S, SLEE, D J, BIRCH, G F, and TAYLOR, S E. 2000. The distribution of polycyclic aromatic hydrocarbons in surficial sediments of Sydney Harbour, Australia. *Marine Pollution Bulletin*, Vol. 40, 999–1006.

MCKINNEY, D E, and HATCHER, P G. 1996. Characterization of peatified and coalified wood by tetramethylammonium hydroxide (TMAH) thermochemolysis. *International Journal Of Coal Geology*, Vol. 32, 217–228.

MOORE, J R. 1968 Recent sedimentation in northern Cardigan Bay, Wales. *Bulletin of the British Museum (Natural History), Mineralogy*, Vol. 2, 19–31.

MORTON, A C. 1984. Stability of detrital heavy minerals in Cainozoic sandstones of the North Sea Basin. *Clay Minerals*, Vol. 19, 287–308.

MPMMG. 1998. *National Monitoring Programme: survey of the quality of UK coastal waters*. (Aberdeen: Marine Pollution Monitoring Management Group.) ISBN 0 9532838 3 6

NICHOLSON, S (editor). 1981. *The changing face of Liverpool 1207–1727*. (Liverpool: Merseyside Archaeological Society.)

NORTON, M G, ROWLATT, S M, and NUNNY, R S. 1984. Sewage-sludge dumping and contamination of Liverpool Bay sediments. *Estuarine Coastal and Shelf Science*, Vol. 19, 69–87.

NRA. 1995. The Mersey Estuary: a report on environmental quality. *National Rivers Authority Water Quality Series*, 23.

OPSAHL, S, and BENNER, R. 1995. Early diagenesis of vascular plant tissues–lignin and cutin decomposition and biogeochemical implications. *Geochimica et Cosmochimica Acta*, Vol. 59, 4889–4904.

ORDNANCE SURVEY. 1992. Ellesmere Port (East). Pathfinder 757. 1:25 000. (Southampton: Ordnance Survey.)

OSBORNE, P J, PRESTON, M R, and CHEN, H Y. 1997. Azaarenes in sediments, suspended particles and aerosol associated with the River Mersey estuary. *Marine Chemistry*, Vol. 58, 73–83.

OSPAR. 1997. Agreed background / reference concentrations for contaminants in sea water, biota and sediment. Oslo and Paris Conventions for the Prevention of Marine Pollution Joint Meeting of the Oslo and Paris Commissions, 2–5 September 1997, Brussels.

OSPAR. 1998. OSPAR strategy with regard to hazardous substances. *Summary Record of the Ministerial Meeting of the OSPAR Commission, Sintra*, Portugal, Oslo and Paris Commissions, Vol. OSPAR 98/14/1, Annex 34, 20 pp.

OSPAR. 2000. *Commission for the Protection of the Marine Environment of the North-East Atlantic, Quality Status Report 2000 Region III – Celtic Seas*. (London: OSPAR Commission.) ISBN 0 946956 49 9.

PEARSON, C D, and GREEN, J B. 1993. Vanadium and nickel comlexes in petroleum residue acid, base and neutral factions. *Energy Fuels*, Vol. 7, 338.

PHILPOTT, R A, and LEWIS, J M. 1999. Five: The human influence: the Norman Conquest–Industrial Revolution. 45–56 in *Ecology and landscape development: a history of the Mersey Basin*. GREENWOOD, E F (editor). (Liverpool: Liverpool University Press.)

PIRAZZOLI, P A. 1991. World atlas of Holocene sea-level changes. (Amsterdam: Elsevier.)

PLANT, J A, JONES, D G, and HASLAM, H W. 1996. Basin evolution, fluid movement and mineral resources in a Permo-Triassic rift setting: the Cheshire Basin. *British Geological Survey Technical Report*, WP/96/14R.

PLANT, J A, JONES, D G A, and HASLAM, H W E. 1999. *The Cheshire Basin: Basin evolution, fluid movement and mineral resources in a Permo-Triassic rift setting*. (Keyworth, Nottingham: British Geological Survey.)

PORTER, E. 1973. *Pollution in four industrialised estuaries. Studies in relation to changes in population and industrial development*. (London: Her Majesty's Stationary Office.)

PRANDLE, D. 2000. Database for EMPHASYS Project – Mersey Estuary. 13 *in* Modelling estuary morphology and process. Final Report for MAFF Project FD1401. Estuaries Research Programme, Phase 1, Report TR 111. (EMPHASYS Consortium.)

PRANDLE, D, and LANE, A. 2000. Modelling tide and marine sediments in the Mersey with 1D, 2D and 3D models – a critique of their respective capabilities and limitations. 27–33 *in* Modelling estuary morphology and process. Final Report for MAFF Project FD1401. Estuaries Research Programme, Phase 1, Report TR 111. (EMPHASYS Consortium.)

PRESTON, M R, and AL-OMRAN, L A. 1986. Disolved and particulate phthalate esters in the River Mersey estuary. *Marine Pollution Bulletin*, Vol. 17, 548–553.

PRESTON, M R, and PRODDUTURU, P. 1992. Tidal variations of particulate carbohydrates in the Mersey estuary. *Estuarine, Coastal and Shelf Science*, Vol. 34, 37–48.

PRICE, W A, and KENDRICK, M P. 1963. Field and model investigations into the reasons for siltation in the Mersey estuary. *Proceedings of the Institution of Civil Engineers*, Vol. 24, 413–517.

PUGH, D T. 1975. Tides, tidal steams and storm surges in Liverpool Bay. 22–28 in Liverpool Bay—an assessment of present kowledge compiled by the members of the Liverpool Bay Study Group. *Natural Environment Research Council Publications Series*, C14.

PULCHAN, J, ABRAJANO, T A, and HELLEUR, R. 1997. Characterization of tetramethylammonium hydroxide thermochemolysis products of near-shore marine sediments using gas chromatography mass spectrometry and gas chromatography combustion/isotope ratio mass spectrometry. *Journal of Analytical and Applied Pyrolysis*, Vol. 42, 135–150.

PULCHAN, K J, HELLEUR, R, and ABRAJANO, T A. 2003. TMAH thermochemolysis characterization of marine sedimentary organic matter in a Newfoundland fjord. *Organic Geochemistry*, Vol. 34, 305–317.

READMAN, J W, PRESTON, M R, and MANTOURA, R F C. 1986. An integrated technique to quantify sewage, oil and PAH pollution in estuarine and coastal environments. *Marine Pollution Bulletin*, Vol. 17, 298–308.

READMAN, J W, FILLMANN, G, TOLOSA, I, BARTOCCI, J, VILLENEUVE, J-P, CATINNI, C, and MEE, L D. 2002. Petroleum and PAH contamination of the Black Sea. *Marine Pollution Bulletin*, Vol. 44, 48–62.

REINECK, H-E, and SINGH, I B. 1980. Depositional sedimentary environments. (Berlin: Springer-Verlag.)

RIDGWAY, J, REES, J G, GOWING, C J B, INGHAM, M N, COOK, J M, KNOX, R W O B, BELL, P D, ALLEN, M A, and MOLINEUX, P J. 1998. Land–Ocean Evolution Perspective Study (LOEPS) Core Programme: Geochemical Studies– 1: Methodology. *British Geological Survey Technical Report*, WB/98/55.

RIDGWAY, J, LANGSTON, W J, ROWLATT, S M, BREWARD, N, BURT, G R, CAMPBELL, S, CHENERY, S R, CHESMAN, B S, GOWING, C J, INGHAM, M N, LISTER, R, POPE, N D, and REES, J G. 2001. Distinguishing between natural and anthropogenic sources of metals entering the Irish Sea. *British Geological Survey Commissioned Report*, CR/01/15.

RIDGWAY, J, BREWARD, N, LANGSTON, W J, LISTER, R, REES, J G, and ROWLATT, S M. 2003. Distinguishing between natural and anthropogenic sources of metals entering the Irish Sea. *Applied Geochemistry*, Vol. 18, 283–309.

ROGERS, H R. 2002. Assessment of PAH contamination in estuarine sediments using the equilibrium partitioning–toxic unit approach. *The Science of the Total Environment*, Vol. 290, 139–155.

SCHNEIDER, T. 2001. Analysis of incomplete climate data: Estimation of mean values and covariance matrices and imputation of missing values. *Journal of Climate*, Vol. 14(5), 853–871.

SHAW, D F. 1975. Water inputs to Liverpool Bay. 11–12 *in* Liverpool Bay, an assessment of present knowledge compiled by the members of the Liverpool Bay Study Group. *Natural Environment Research Council Publications Series*, C14.

SMART, G, and CLAYTON, T. 1985. The progressive illitization of interstratified illite-smectite from Carboniferous sediments of northern England and its relationship to organic maturity indicators. *Clay Minerals*, Vol. 20, 455–466.

SPEARMAN, J, TURNBULL, M, THOMAS, C, and COOPER, A. 2000. Two and three dimensional modelling of sediment transport mechanisms in the Mersey estuary. 21–26 *in* Modelling estuary morphology and process. Final Report for MAFF Project FD1401. Estuaries Research Programme, Phase 1, Report TR 111. (EMPHASYS Consortium.)

STRAATEN, L M J U V. 1954. Composition and structure of recent marine sediments in the Netherlands. *Leidse Geologische. Medel edlingen*, Vol. 19, 1–110.

SWEDISH-EPA. 2001. Assessment of contamination level. Swedish Environmental Protection Agency.

TAYLOR, D. 1986. Changes in the distribution patterns of trace metals in sediments of the Mersey Estuary in the last decade (1974–83). *The Science of the Total Environment*, Vol. 49, 257–295.

TAYLOR, P M, and PARKER, J G E. 1993. *The coast of North Wales and North West England: An environmental appraisal*. (London: Hamilton Oil Company.)

THOMAS, C. 1999. Analysis of bathymetric surveys of the Mersey Estuary. *HR Wallingford*, Report IT 469.

THOMAS, C G, SPEARMAN, J R, and TURNBULL, M J. 2002. Historical morphological change in the Mersey estuary. *Continental Shelf Research*, Vol. 22, 1775–1794.

USEPA. 2000. Draft PBT national action plan for alkyl-lead", persistent bioaccumulative and toxic pollutants (pbt). USEPA Office of Pollution Prevention and Toxins.

VANE, C H, MARTIN, S C, SNAPE, C E, and ABBOTT, G D. 2001. Degradation of lignin in wheat straw during growth of the oyster mushroom (Pleurotus ostreatus) using off-line thermochemolysis with tetramethylammonium hydroxide and solid-state C-13 NMR. *Journal of Agricultural and Food Chemistry*, Vol. 49, 2709–2716.

VANE, C H, DRAGE, T C, and SNAPE, C E. 2003. Biodegradation of oak (*Quercus alba*) wood during growth of the shiitake mushroom (*lentinula edodes*):a molecular approach. *Journal of Agricultural and Food Chemistry*, Vol. 51, 947–956.

VICKERS, B P, PEACHEY, D, and ROBERTS, J L. 1992. Geochemical methods handbook, 1: Rapid geochemical methods for use in geochemical surveys overseas. *British Geological Survey Research Report*, SI/92/1.

WALDRON, H A, and STÖFEN, D. 1974. *Subclinical Lead Poisoning*. (London: Academic Press.)

WEDD, C B, SMITH, B, SIMMONS, W C, and WRAY, D A. 1923. The geology of Liverpool, with Wirral and part of the Flintshire Coalfield. *Memoir of the Geological Survey of Great Britain*, Sheet 96 (England and Wales).

WEDEPOHL, K H. 1995. The composition of the continental crust. *Geochimica et Cosmochimica Acta*, Vol. 59, 1217–1232.

WEEKES, L, MITCHAM, T, MORRIES, G, and BUTTERILL, G. 1999. Natural habitats of the Mersey Basin: what is left? 65–72 in *Ecology and landscape development: a history of the Mersey Basin*. GREENWOOD, E F (editor). (Liverpool: Liverpool University Press.)

WILSON, G P, LAMB, A L, LENG, M J, GONZALEZ, S, and HUDDART, D. 2005a. $\delta^{13}C$ and C/N as potential coastal palaeoenvironmental indicators in the Mersey Estuary, UK. *Quaternary Science Reviews*, Vol. 24, 2015–2029.

WILSON, G P, LAMB, A L, LENG, M J, GONZALEZ, S, and HUDDART, D. 2005b. Variability of $\delta^{13}C$ and C/N in the Mersey Estuary, U.K. and its implications for sea-level reconstruction studies. *Estuarine, Coastal and Shelf Science*, Vol. 64, 685–698.

WILSON, K W, HEAD, P C, and JONES, P D. 1986. Mersey estuary (UK) bird mortalities–causes, consequences and correctives. *Water Science and Technology*, Vol. 18, 171–180.

WOLFF, W J. 1980. Biotic aspects of the chemistry of estuaries. 263–295 in *Chemistry and biogeochemistry of estuaries*. OLAUSSON, E, and CATO, I, (editors). (New York: Wiley-Interscience.)

WOODHEAD, R J, LAW, R J, and MATTHIESSEN, P. 1999. Polycyclic aromatic hydrocarbons in surface sediments around England and Wales, and their possible biological significance. *Marine Pollution Bulletin*, Vol. 38, 773–790.

YUNKER, M B, SNOWDON, L R, MACDONALD, R W, SMITH, J N, FOWLER, M G, SKIBO, D N, MCLAUGHLIN, F A, DANYUSHEVSKAYA, A I, PETROVA, V I, and IVANOV, G I. 1996. Polycyclic aromatic hydrocarbon composition and potential sources for sediment samples from the Beaufort and Barents Seas. *Environmental Science and Technology*, Vol. 30, 1310–1320.

YUNKER, M B, MACDONALD, R W, VINGARZAN, R, MITCHELL, R H, GOYETTE, D, and SYLVESTRE, S. 2002. PAHs in the Fraser River basin: a critical appraisal of PAH ratios as indicators of PAH source and composition. *Organic Geochemistry*, Vol. 33, 489–515.

Appendix 1 Analytical methods

TOTAL ORGANIC CARBON (TOC) AND LOSS ON IGNITION (LOI)

As an aid to interpretation and a preliminary to more focused investigations of their organic geochemistry some of the sediments collected from the Mersey estuary had both their Total Organic Carbon (TOC) and Loss On Ignition (LOI) determined. The LOIs were determined at an ignition temperature of 450°C on freeze-dried sediment that had been ground in an agate Tema mill to <200 µm, then subsampled and ground further in an agate ball mill to <40 µm. The TOCs were determined on freeze-dried sediment samples that had been ground to <50 µm in an agate ball mill. The TOC determinations, were outsourced from BGS to ALcontrol Geochem Laboratories, Chester, UK, who hold UKAS accreditation for this technique. At ALcontrol the samples were initially washed with dilute acid to remove inorganic carbonates (e.g. calcium, magnesium etc.) prior to their analysis on a LECO CS444 elemental analyzer where their organic carbon content was obtained by a combination of combustion and infra-red spectrometry.

LOI determinations were conducted at BGS and involved heating known weights of sample (dried at 105°C overnight) to 450°C in a muffle furnace for a minimum of 4 hours (Vickers et al., 1992). After cooling the samples were reweighed and the percentage loss in weight (LOI) calculated. Quality control was achieved through the use of two in-house QC standards, i.e. LLC (low level control) and S3B (high level control) with LOIs of 3.5 per cent and 12.5 per cent respectively. These were run alternately in each batch of forty samples.

POLCYCLIC AROMATIC HYDROCARBONS (PAHS)

Sample preparation

Sediments for PAH analysis were freeze-dried and then sieved to < 2 mm using a brass mesh. The < 2 mm fraction material was homogenised and stored in clean glass jars, whose screw caps had been lined with aluminium foil, ready for extraction and PAH analysis.

In order for the samples to be in a form suitable for chromatographic analysis it was necessary to leach the PAHs into solution by means of solvent extraction. This was accomplished by extracting a known weight of dried, sieved sediment into 150 ml of refluxing HPLC-grade dichloromethane in a conventional Soxhlet apparatus for 24 hours. The Soxhlet system is designed to wash samples repeatedly with hot solvent recirculated by a process of evaporation, condensation and siphoning. The resultant extract was treated with 2 ml of an internal standard solution (i.e. 5 mg/l p-terphenyl in acetonitrile), to aid in quantification of the PAHs, before being injected into the HPLC system.

Quality control was achieved by subjecting a well-characterised, low-level PAH proficiency testing material (LGC Contest Sediment Sample 31.3c) to the above procedure and analysing it by the same method as for the samples. Results obtained for the quality control material are shown in Table 1. A procedural blank prepared from white quartz sand (Sigma Aldrich, UK) – a material devoid of PAH – was treated in a similar fashion.

PAH analysis

Following solvent extraction of the PAHs from the sediments, high performance liquid chromatography (HPLC) was used for their separation and fluorescence detection applied for their individual quantification. Fluorescence detection is a selective and sensitive means of determining PAHs, however, it will only allow 15 of the 16 PAHs specified in the US Environmental Protection Agency (USEPA) methods to be quantified. This is because one of the 16 USEPA PAHs, viz. acenapthylene, is not a fluorescent compound. Nevertheless, sufficient data can be generated to gain a meaningful assessment of the PAH content and distribution in the samples without necessarily having knowledge of the acenaphthylene concentrations.

A small aliquot, ca. 50 µL, was taken from each sample extract (including that for the QC and the procedural blank) by an HPLC syringe and used to completely rinse and

Appendix Table 1 Concentrations of 15 USEPA PAHs in quality control material (LGC Contest 31.3c).

LGC (Laboratory of the Government Chemist) Contest Soil 31.3c	PAH in soils Laboratory intercomparison material															
	Naph. mg/kg	Ace. mg/kg	Fluor. mg/kg	Phen. mg/kg	Anth. mg/kg	Fanth. mg/kg	Pyr. mg/kg	B(a)anth. mg/kg	Chrys. mg/kg	B(b)fanth. mg/kg	B(k)fanth. mg/kg	B(a)pyr. mg/kg	DB(ah)anth. mg/kg	B(ghi)per. mg/kg	I(123cd)pyr. mg/kg	Total mg/kg
LGC Assigned Value	4.08	8.00	8.54	63.40	7.20	45.50	24.41	13.20	16.30	11.50	7.63	6.60	2.30	7.43	7.25	233
LGC Assigned Uncertainty	1.45	3.11	2.20	23.43	2.64	10.68	6.51	3.71	4.85	2.97	3.25	1.36	1.50	1.65	1.85	
Permissible Max.	5.53	11.11	10.74	86.83	9.84	56.18	30.92	16.91	21.15	14.47	10.88	7.96	3.80	9.08	9.10	
Permissible Min.	2.63	4.89	6.34	39.97	4.56	34.82	17.90	9.49	11.45	8.53	4.38	5.24	0.80	5.78	5.40	
Value obtained	3.40	10.00	6.40	49.20	6.20	35.30	19.90	11.60	17.80	13.20	8.90	6.60	2.00	8.30	9.10	208

fill the 5 µL sample loop installed on the HPLC (Waters 600E). This was then connected into the flow of eluent (1mL/min) from the HPLC pump and swept through the chromatographic separation column (Hypersil®PAH 100 mm x 4.6 mm i.d.). Baseline separation of the 15 PAHs was achieved within 40 mins by gradient programming the eluent i.e. increasing its eluotropic strength with time according to a defined programme. Thus, far-UV HPLC grade acetonitrile (Rathburn Ltd.) with a high eluotropic strength, and HPLC grade water (Milli-Q) with a low eluotropic strength were pumped as a 50/50 mix at the start of each chromatographic run. This condition was maintained for 5 minutes into the run. Thereafter, up to 27 minutes, the proportion of acetonitrile was continuously and steadily increased from 50 to 100 per cent. From 27 minutes until the end of the run (40 mins.) elution with 100 per cent acetonitrile was maintained.

As each individual PAH exited the column, with its own distinctive retention time, it was directed into the scanning fluorescence detector (Varian 363 Pro-Star). The detector was programmed so that optimised excitation and emission wavelengths for each PAH were selected based on their retention times. Table 2 shows the parameters found to produce the optimum chromatography: Abbreviations employed throughout the report for the fifteen PAHs that were determined and the limits of detection based on the minimum concentrations that gave clearly defined peaks, i.e. signal-to-noise ratio ≈ 4 are displayed in Table 5.4 in the main text.

POLYCHLORINATED BIPHENYLS (PCBS)

Sample preparation

Samples for PCB analysis, as for PAH and other organic compounds, were frozen after collection and freeze dried prior to analysis.

All glassware was cleaned in chromic acid (24 hours), rinsed with deionised water (4 times), dried at 100°C for 12 hours and rinsed with HPLC grade dichloromethane (DCM) Prior to use, anhydrous Na_2SO_4, antibumping granules and quartz wool were cleaned by Soxhlet extraction using DCM for 24 hours. The reagents used in this study are presented in Table 3.

The method used is based on that described by Ayris et al, (1997). PCBs standards (dissolved in n-hexane) were added to the samples, the solvent was allowed to evaporate away, vigorously shaken and stored for 24 hours at room temperature in a sealed glass container prior to extraction. Accurately weighed of portions sediment and silica procedural blank (4–25 g) were mixed with an equal amount of anhydrous sodium sulphate and Soxhlet extracted for >18 hours using hexane:acetone (40:60 v/v). Acetone was removed from the crude extracts with 2 x 50 mL aliquots of de-ionised water. Elemental sulphur was removed from the "acetone free extracts" by the addition of solvent-cleaned copper wire and the volume reduced to approximately 2 mL using rotary evaporation and a steam of nitrogen gas. To remove any humic material and release any humic bound PCBs, all extracts were washed with an equivalent volume of concentrated sulphuric acid. The organic layer was then dried by passing it through a Pasteur pipette containing precleaned anhydrous sodium sulphate (1 g) and the volume reduced to approximately 2 mL using a steam of nitrogen gas. Subsequently all extracts were then eluted through a Pasteur pipette containing precleaned Florisil (1 g, activated, 60–100 mesh) with n-hexane (10 mL). To remove aliphatic material from QA2 and the harbour sediment, the eluant from this column was extracted with dimethylsulphoxide (DMSO, 2 x 12 mL). The DMSO extracts were combined and diluted with de-ionised water (25 mL) prior to "back-extraction" with n-hexane (2 x 50 mL). The hexane "back-extracts" were combined and the volume reduced to approximately 5mL using rotary evaporation. This was then dried by passing it through a Pasteur pipette containing 1 g precleaned anhydrous sodium sulphate and the volume reduced to approximately <0.1 mL using a stream of nitrogen gas.

Appendix Table 2 Wavelength programming of the fluorescence detector.

Time from run start (mins)	Excitation (nm)	Emission (nm)
0.0–14.2	275	325
14.2–16.2	253	373
16.2–21.5	240	425
21.5–35.2	254	395
35.2–40.0	302	506

PCB analysis

Following extraction, a "Fisons MD 800" Gas Chromatograph Mass Spectrometer (GCMS) was used to determine a range of PCBs with the following settings:
Mass range – full scan ion monitoring (m/z: 39–600), with electron impact and quadrupole analyser.

On-column injection – DB-1 column (60 m length x 0.32 mm i.d. x 0.25 µm film thickness). Oven temperature programme – 100°C (1 min. isothermal) to 200°C (at 5°C / min.) to 280°C (at 2.4°C / min.) to 320°C (at 20°C / min.) and isothermal at 320°C for 5 minutes.
Carrier gas – helium at 16 p.s.i.

ORGANO-TIN COMPOUNDS

Sample preparation

The method used is based on that described by Łobiński et al, (1992). A 1–5 g sediment sample was placed in a 100 mL glass centrifuge tube, an internal standard added (dipropyltin dichloride 1.3 ng/g as Sn), shaken, and air-dried for 24 hours. The following were then added: concentrated acetic acid (20 mL), deionised water (10 mL), DDTC solution in pentane (3 mL) and n-hexane (25 mL). The mixture was then shaken and ultrasonicated for 30 minutes, centrifuged and the organic / n-hexane layer removed. The aqueous sediment mixture was extracted twice with fresh n-hexane (25 mL). The organic extracts were combined and reduced in volume (2–3 mL) using rotary evaporation and a steam of nitrogen gas. The organic extract was dried using a glass Pasture pipette filled with anhydrous Na_2SO_4, reduced to <1.0 mL using a steam of nitrogen gas. The extract was derivatised with 0.5 M n-pentyl magnesium bromide (1 mL) followed by gentle agitation for 2 minutes. To destroy the excess Grignard reagent n-hexane (5 mL) was added to the extract, transferred to a separating funnel and shaken with 0.5 M H_2SO_4 (10 mL). The aqueous phase was discarded and the organic layer rinsed with deionised water (10 mL). The aqueous phase was discarded and the organic layer

Appendix Table 3 Reagents used for PCB, organotin, organolead and saturates extraction and sample clean-up.

Name	Grade	Comments
Acetic acid (glacial)	Analytical grade	
Acetone	HPLC grade	Rathburn Chemical Company, Peebleshire, UK
Aluminium oxide	Analytical grade	90 active neutral, 70–230 mesh, 100% activated, Merck, Leicestershire, UK
Butyl magnesium chloride, (C4H9)MgCl (2M in tetrahydrofuran)	Analytical grade	Sigma-Aldrich, Poole, Dorset, UK
Bromotrimethyllead	97%	Sigma-Aldrich, Library of Rare Chemicals, Poole, Dorset, UK
Copper wire	Analytical grade	Cleaned with c.HNO_3, deionised water, methanol, DCM, hexane
Dichloromethane (DCM)	HPLC grade	Rathburn Chemical Company, Peebleshire, UK
Diethyldithiocarbamaic acid, sodium salt trihydrate (DDTC)	Analytical grade	Sigma-Aldrich, Poole, Dorset, UK
Dimethylsulpoxide (DMSO)	Analytical grade	Sigma-Aldrich, Poole, Dorset, UK
Diphenyllead dichloride,		
$(C_6H_5)_2$ Pb Cl_2	99% technical grade	Sigma-Aldrich, Poole, Dorset, UK
Dipropyltin dichloride,		
$(C_3H_7)_2$ Sn Cl_2	Analytical grade	QmX Laboratories Ltd., Thaxted, Essex, UK.
Florisil	Analytical grade	100 % activated, 60–100 mesh, Sigma-Aldrich, Poole, Dorset, UK
Helium	CP grade	BOC Speciality Gases Ltd., Guildford, Surrey, UK.
n-hexane	HPLC grade	Rathburn Chemical Company, Peebleshire, UK
Methanol	HPLC grade	Rathburn Chemical Company, Peebleshire, UK
Pentylmagnesium chloride, (C_5H_{11})MgCl (2M in diethyl ether)	Analytical grade	Sigma-Aldrich, Poole, Dorset, UK
PCB-19 (100 µg/mL in hexane)	Analytical grade	Promochem, Welwyn Garden City, UK
PCB-34 (100 µg/mL in hexane)	"	"
PCB-29 (100 µg/mL in hexane)	"	"
PCB-62 (100 µg/mL in hexane)	"	"
PCB-119 (100 µg/mL in hexane)	"	"

was dried by passing it through a glass Pasture pipette filled with anhydrous Na_2SO_4 and reduced to 1.2 mL using a steam of nitrogen gas. The organic phase was cleaned by passing it through a glass Pasture pipette filled with Al_2O_3. The resulting eluant was reduced to approximately 0.1 mL using a steam of nitrogen gas and stored at <-10°C in darkness prior to GCMS analysis.

Organo-tin analysis

Analysis was carried out by GCMS using the same setting as described above for PCBs. The organotin concentrations obtained for the certified reference material (PACS-1 harbour sediment) were in agreement within the confidence limits of the certified values.

ORGANO-LEAD COMPOUNDS

Sample preparation

A 1–5 g sediment sample was placed in a 100 mL glass centrifuge tube, an internal standard added (diphenyllead dichloride 3.84 ng/g as Pb), shaken, and air-dried for 24 hours. Tetrahydrofuran (10 mL) was added and 5 mL of Grignard reagent (butyl magnesium chloride) was sequentially added, shaken, ultrasonicated for 30 minutes and left for 2 hours. The excess Grignard was deactivated using H_2SO_4 (25 mL, 0.5 M) and the resulting aqueous solution extracted with n-hexane (3 x 10 mL). The organic extract was dried using a glass Pasture pipette filled with anhydrous Na_2SO_4. The organic extract was cleaned in 2 sequential steps: (1) using a microcolumn (glass Pasture pipette) filled with 1 g aluminium oxide (eluted with 10mL n-hexane) and reduced to <0.5 mL using a steam of nitrogen gas; (2) using a microcolumn (glass Pasture pipette) filled with 1 g Florisil (eluted with 10 mL n-hexane) and reduced to <0.05 mL using a steam of nitrogen gas. The purified extracts were stored at <-10°C in darkness prior to GCMS analysis.

Organo-lead analysis

Analysis was carried out by GCMS using the same setting as described above for PCBs. The trimethyllead concentration obtained for the certified reference material (BCR-CRM-605 road dust) was in agreement within the confidence limits of the certified values.

SATURATES/BIOMARKERS

Sample preparation

A 3 g sediment sample was placed in a 7 mL glass vial, and extracted with n-hexane (3 x 5 mL). The organic extracts were combined, elemental sulphur removed using fresh copper wire, dried using a glass Pasture pipette filled with anhydrous Na_2SO_4 and reduced to "dryness" using a steam of nitrogen gas in a preweighed glass vial. The extract was stored at <-10°C in darkness prior to GCMS analysis.

Saturates/biomarkers analysis

Analysis was carried out by GCMS using the same setting as described above for PCBs.

NATURAL ORGANIC MATTER

Elemental analysis

Crucibles containing 100 mg of previously frozen powdered sample were flushed through twice with 50 per cent HCl in order to remove inorganic carbon and then rinsed four times with distilled water (Hedges and Stern, 1984). Organic carbon and nitrogen content was determined using a Carlo Erba 1106 elemental analyzer. Blanks and samples were

interchanged in order to account for possible instrumental drift.

Off-line thermochemolysis

For each experiment, borosilicate glass tubing (o.d. 5 mm, i.d. 4 mm), was sealed at one end with a natural gas/oxygen flame to give a vessel of length 13 cm. Each vessel was rinsed with methylene chloride, and oven dried for 12 h at approximately 75 °C. Mersey sediment samples (0.5–1 mg) were placed in individual reaction vessels with 100 μL of tetramethylammonium hydroxide (TMAH) solution (25 % w/w in methanol). The TMAH preparations were left overnight in a vacuum desiccator in the presence of P_2O_5 in order to facilitate thorough mixing prior to the removal of methanol under vacuum. The dried mixtures were sealed under vacuum and heated in an oven at a temperature of 250 °C for 30 min. After cooling the reaction vessels were opened, the inner surfaces of the tubes were washed five times with 1 mL of dichloromethane. The combined extracts were dried under a stream of N2 and dissolved in 100 μL of dichloromethane.

Gas chromatography-mass spectrometry

GC-MS was performed using a Fisons MD-800 operated at 70 eV with a mass range of m/z 30–600 with helium carrier gas. The GC was fitted with a 30 m × 0.2 mm id × 0.11 °m HP-5 coated fused silica column coated with a 5 % phenylmethylsilicone bonded stationary phase The oven temperature was programmed from 30 °C to 300 °C at 4 °C / min and held isothermally at 300 °C for 5 min.

MAJOR AND TRACE ELEMENTS

Sample preparation

Core samples

All core samples were initially frozen soon after collection, and stored in a freezer at the BGS. Samples selected for analysis were removed from the freezer and, in the first instance, allowed to partially thaw for approximately 2–3 hours. The partially frozen core, still within the plastic core tube and sealed with end caps, was then cut lengthwise into halves. One half section was immediately wrapped in aluminium foil then sealed inside heavy duty polythene, before being refrozen and stored for organic analysis.

The remaining half section of core was then measured and marked at 10 cm intervals from the top to the base. The core was then cut across each 10 cm mark to produce a number of down-profile subsamples. The number of subsamples was dependant upon the length of the core.

Each subsample was carefully removed from the plastic core tube and transferred into appropriately labelled Kraft porous paper bags. All bagged subsamples from individual cores were then placed into a seal-again polythene bag, labelled with the core number and number of subsamples, and returned to the freezer to await the next stage of preparation.

Core subsamples in Kraft bags were collected from the freezer before being freeze-dried in preparation for multi-element inorganic analysis. The material was then disaggregated and sieved to –2 mm. All samples were coned and quartered and a 50 g split ground in an agate planetary ballmill (Fritsch P5) until 95% of the material was less than 53 m. Excess ground material was retained and stored for future reference.

Samples were prepared by grinding 12 g of sample and 3 g of Elvacite 2013 binder (n-butyl methacrylate copolymer, Dupont & Co) in an agate planetary ballmill for 30 minutes. The mixture was then pressed at 25 t load into 40 mm diameter pellets using a Herzog (HTP-40) semi-automatic press.

Grab and surface samples

All grab and manually collected samples were initially frozen soon after collection, and stored in a freezer at the BGS. Samples selected for analysis were removed from the freezer and, in the first instance, allowed to partially thaw for approximately 2–3 hours. Sample splits were then taken for the various analyses to be carried out, and any remaining material was immediately returned to the freezer for storage. Grab and surface samples selected for multi-element inorganic analysis were freeze-dried and prepared in the same manner as core samples. Sample splits for organic analysis were transferred into labelled glass jars before being refrozen.

Sample type	Samples collected	Sample locations
Manual Core	238	Estuary bed exposed at low tide
Manual Surface	208	Estuary bed exposed at low tide
Day Grab	41	Lower estuary (Eastham - Bootle)
Mackereth Piston Core	8	Lower estuary docks
Vibrocorer Core	10	Selected from pre-sampled locations
Marlow Core	9	Ince Banks & Widnes Warth

X-ray fluorescence spectrometry

The general principles of the laboratory-based XRF system used by BGS are described by Ingham and Vrebos (1994). The system enables elements in the range F to U to be determined with a higher degree of accuracy and precision than is possible with the portable instrument.

Analyses were carried out using three sequential, fully automatic wavelength dispersive X ray fluorescence spectrometers, each fitted with automatic sample changers (2 x Philips PW2400 and 1 x PW1480/10, Plate 4). The PW2400 spectrometers are fitted with 60 kV generators and 3 kW rhodium (Super Sharp) end-window X-ray tubes. The PW1480 is fitted with a 100kV generator and a 3kW tungsten side-window X-ray tube. The emitted fluorescent x-rays are counted using gas flow and scintillation detectors, measuring sequentially the intensity of characteristic x-ray peaks and backgrounds. Each spectrometer is controlled via a PC running the Philips X40 (version 4.0E) and SuperQ (version 2.0) XRF application packages. Data are stored on a PC before transfer into spreadsheets for further data processing.

Analyte angles were determined using 1000 mg/kg single element standards in a silica matrix. Background factors, where applicable, are calculated by either angular difference (2) or from regression values from ‘high purity’ oxide blanks. Line-overlap factors were calculated from high concentration single element standards of the interfering analyte. Internal ratio was used for matrix correction where applicable. Synthetic and natural multi element standards (Certified Reference Materials (CRM), Reference Materials (RM) and in house reference materials) were used for calibration purposes. The Philips calibration algorithm was used to fit calibration curves, deriving saved calibration constants (intercept, slope and alpha coefficient of the element interference upon itself). All backgrounds and

peaks were drift corrected using an external ratio monitor. Drift correction intensities from the monitor were stored on hard disc and used to monitor instrumental stability and detect machine faults. The lower limits of detection (LLDs) for the trace elements in geological matrices are in the range 1–3 ppm (these are theoretical values for the concentration equivalent to 3 times the standard deviation above background count rate for the analyte in a silica matrix; high instrumental stability results in practical values for these materials approaching the theoretical).

The study elements (Na, Mg, Al, Si, P, K, Ca, Ti, Cr, Mn, Fe, Sc, V, Cr, Co, Cs, Ba, La, Ce, Nd, Sm, Ni, Cu, Zn, Ga, Ge, As, Se, Br, Rb, Sr, Y, Zr, Nb, Mo, Hf, Ta, W, Tl, Pb, Bi, Th, U) were determined using the appropriate tube anode to obtain optimum detection limits and precision. Calibration intercepts were checked weekly and adjusted where necessary. Routine calibrations cater for rocks, soils, stream sediments, panned concentrates, tills and panned tills. Additional elements (Ag, Cd, Sn, Sb, Te, I) were determined by energy-dispersive X-ray fluorescence spectrometry.

The BGS XRF Section operates under quality assurance (QA) procedures to BS EN ISO 9000. For quality control (QC) purposes, the spectrometer goniometer and collimator alignment is checked weekly using an in-house 1000 ppm Sr standard and Sr Kα. Instrumental drift is corrected for approximately every 8 hours by measurement of stable glass monitors, one of high concentration (≈2000 ppm traces) and the other ≈0 ppm. Pressed powder major and trace element calibration concentration intercepts are checked at least once a week by analysing high purity SiO_2. At the same time a glass monitor sample containing 47 elements is analysed and the results entered into run charts for statistical analysis using a QC package (QI Analyst). An in-house standard is analysed with every 100 unknowns and the results entered into run charts for statistical analysis using the QC package.

Additional quality control checks were carried out through a programme in which cores were resampled some weeks after the original sampling, fresh pressed powder pellets prepared and the analytical programme rerun. Results of this exercise are shown in Figure 5 and confirm the suitability of the sampling and analytical techniques for the purposes of the LOEPS geochemical programme.

Determination of mercury

A 0.5 g (±0.01 g) portion of sample was weighed into a calibrated test tube to which 5 ml of deionised water and 5 ml of aqua-regia (3HCl:1HNO3) were added. This was placed in a heating block and left overnight at room temperature. It was then taken to gentle boiling and maintained at this temperature for 2 hours. After cooling the solution was diluted to 50 ml volume with deionised water, shaken and allowed to settle. The clear solution was decanted and Hg determined by Atomic Fluorescence Spectrometry (AFS). Appropriate reference materials were run with each analytical batch.

Data quality control

In order to monitor analytical instrument performance, a number of internal reference materials were analysed throughout the entire period of analysis of the Mersey estuary samples.

Reference ID	Number of analyses	Sample type
MB1	9	Bulk Alluvial Sand
MB3	9	Bulk Stream Sediment
MSB1	7	Bulk Estuarine Sediment

All reported analytical data for reference material is presented in Tables 4–7

These data show a consistently high level of reproducibility for the majority of major and trace elements reported by the BGS XRF laboratory, and included in this report.

Throughout the sampling operation, duplicate samples were collected from a number of sites in order to quantify any systematic errors introduced during the sampling and analytical processes.

A number of sample locations were revisited after approximately 18 months, when a second sample was collected in order to establish any short-term dynamic movements within the estuarine sediment. At several revisited sites, a duplicate sample was also collected. Location details of duplicated sites are contained in Table 8.

Analytical data from all fourteen duplicated/replicated sites are presented graphically as individual 'spidergrams' for each site. A broken line represents sites sampled during the initial sampling phase in 2000. Solid lines show revisited and duplicated sites sampled in 2001. The element concentrations have been plotted using a log scale on the Y-axis to allow all elements to be plotted simultaneously on a single spidergram.

PARTICLE SIZE ANALYSIS

All the particle size analysis for the Mersey estuary has been carried out in accordance with BS1377: Part 2: 1990.

Two methods of sieving for particle size analysis were undertaken; wet sieving for the separation of the cohesive sediment and for the collection of the <63 μm fine fraction and dry sieving for the analysis of the coarse fraction containing insignificant quantities of silt and clay. The SediGraph 5100 was used for determining the size distribution of fine particles less than 63 μm by sedimentation, in which the density of the soil suspension at various intervals is measured. Combined sieving and sedimentation procedures enable a continuous particle size distribution curve of the soil to be plotted, from the coarsest particles down to the clay fraction.

Initially at least 150 g of sample for coarse fraction analysis and a sub sample of at least 50 g for fine fraction analysis were placed on the mixer for 24 hours, with a sodium hexametaphosphate and distilled water solution at a concentration of 2.5 g/L. The actual amount of sample and sub sample needed differed depended on the estimated <63 μm content.

After mixing, the sample for coarse fraction analysis was wet sieved, until the water ran clear, through the 2 mm and 63 μm aperture sieves. Material passing the 63 μm sieve was left to run to waste. The retained material above 63 μm was oven dried and then passed though a selection of nested sieves for percentage analysis.

The subsample for the analysis of the fine fraction was also wet sieved through the 2 mm 63 μm aperture sieves using as little water as possible however the material passing the 63 μm sieve was collected in a large beaker and oven dried to be analysed by the SediGraph 5100. A standard concentration of 5 g of sample to 50 ml 0.05 % sodium hexametaphosphate solution was used thought out the SediGraph analysis. The ultrasonic probe was also used for 30 seconds, on each sample, in order to prevent flocculation and aid dispersion of the finer particles.

X-RADIOGRAPHY

The sedimentary characteristics of the sediments within the estuary have been determined by X-radiography of 19 selected

Appendix Table 4 Internal Reference Material – Analytical Data: Na_2O_3–Cr.

Standard ID	Na_2O	MgO	Al_2O_3	SiO_2	P_2O_5	K_2O	CaO	TiO_2	MnO	Fe_2O_3	Sc	V	Cr
	%	%	%	%	%	%	%	%	%	%	ppm	ppm	ppm
MB1	1.2	1.9	7.2	68.8	0.09	1.92	3.92	1.286	0.058	6.49	9	108	55
MB1	1.1	1.6	6.3	76	0.08	1.72	3.24	1.379	0.062	7.23	10	121	58
MB1	1.1	1.7	6.6	79	0.08	1.79	3.33	1.429	0.064	7.43	9	117	59
MB1	1.1	1.6	6.3	77.2	0.08	1.74	3.23	1.406	0.06	7.21	8	123	58
MB1	1.1	1.6	6.6	78.3	0.08	1.8	3.31	1.408	0.061	7.18	9	121	58
MB1	1.1	1.6	6.6	77.8	0.08	1.79	3.36	1.404	0.059	7.29	9	120	66
MB1	1.1	1.7	6.9	76.6	0.08	1.84	3.48	1.383	0.059	7.08	9	119	58
MB1	1.1	1.7	6.7	76.8	0.08	1.82	3.4	1.383	0.061	7.17	9	122	59
MB1	1.1	1.6	6.5	78.7	0.08	1.8	3.29	1.418	0.062	7.29	9	119	54
Mean MB1	1.1	1.7	6.6	76.6	0.08	1.8	3.4	1.388	0.061	7.15	9	119	58
Standard ID	**Na_2O**	**MgO**	**Al_2O_3**	**SiO_2**	**P_2O_5**	**K_2O**	**CaO**	**TiO_2**	**MnO**	**Fe_2O_3**	**Sc**	**V**	**Cr**
MB3	2.1	2.7	15.9	56.9	0.11	3.06	1.35	0.705	0.119	7.02	14	112	66
MB3	2.2	2.5	15.3	57.4	0.11	3.02	1.3	0.709	0.119	7.12	15	113	70
MB3	2.3	2.5	15.5	60.7	0.11	3.05	1.28	0.721	0.118	7.24	17	113	74
MB3	2.3	2.6	16	61	0.11	3.11	1.31	0.724	0.12	7.16	16	114	71
MB3	2.4	2.6	16.3	62.1	0.11	3.14	1.3	0.722	0.124	7.27	16	117	70
MB3	2.3	2.5	15.6	59.8	0.11	3.06	1.27	0.715	0.121	7.04	16	109	71
MB3	2.3	2.5	16.2	61.7	0.11	3.13	1.29	0.726	0.121	7.26	16	113	71
MB3	2.3	2.6	16.3	61.2	0.11	3.14	1.29	0.727	0.122	7.23	16	116	73
MB3	1.8	2.4	14.4	53.7	0.11	3	1.28	0.699	0.12	5.95	16	115	70
MB3	2.2	2.5	15.7	59.4	0.11	3.08	1.3	0.716	0.12	7.03	16	114	71
Standard ID	**Na_2O**	**MgO**	**Al_2O_3**	**SiO_2**	**P_2O_5**	**K_2O**	**CaO**	**TiO_2**	**MnO**	**Fe_2O_3**	**Sc**	**V**	**Cr**
MSB1	1.2	1.8	7.4	74.6	0.24	1.64	5.55	0.411	0.088	2.6	9	44	77
MSB1	1.2	1.8	7.6	73	0.26	1.7	5.78	0.41	0.086	2.63	10	42	84
MSB1	1.2	1.8	7.5	76	0.24	1.67	5.56	0.411	0.087	2.62	8	46	77
MSB1	1.2	1.8	7.8	73.9	0.27	1.7	5.8	0.416	0.089	2.62	8	46	78
MSB1	1.2	1.9	7.8	73.4	0.26	1.72	5.83	0.412	0.089	2.62	9	47	76
MSB1	1.2	1.8	7.5	74	0.25	1.69	5.68	0.412	0.087	2.62	9	46	93
MSB1	1.1	1.6	6.8	62.6	0.26	1.66	5.87	0.401	0.089	2.16	9	44	76
Mean MSB1	1.2	1.8	7.5	72.5	0.25	1.68	5.72	0.41	0.088	2.55	9	45	80

cores, undertaken by NDT Services Ltd at East Midlands Airport. Although some sedimentary structures and lithological changes can be observed under good lighting in slabbed sediment cores, the styles of bedding and any biological or physical disturbance to the sediments can often be revealed in much greater detail using X-radiography. The cores were slabbed in a frozen state to prevent artificial disruption to the bedding, and subsequently X-rayed in a partially defrosted state to avoid an impaired image due to the presence of ice crystals. X-ray intensity was varied to reveal the maximum information on sedimentary structures. Uniformity of texture causes a lack of contrasting sediment density for radiography and results in a relatively uniform radiograph.

X-RAY DIFFRACTION ANALYSIS

The clay mineralogy of the Mersey estuary sediments was determined by X-ray diffraction (XRD) analysis. The estuarine grab samples had already been separated into different grain size fractions for the purposes of sediment grain size analysis, prior to mineralogical examination. Consequently, the <63 µm grain size fraction material was used for the separation of the clay minerals and their characterisation by XRD.

Separation and preparation of <2 µm grain size fraction

Several hundred grams of each sample was placed in a plastic bottle with de-ionised water (DIW) and manually shaken to disaggregate the material. It was then subjected to 3 minutes of ultrasonic agitation, to further disaggregate the clay minerals. The sample was manually shaken briefly, left to stand for a few minutes, and then some of the material remaining in suspension was decanted into a tall, thin gas jar and topped up with DIW. After mixing to homogenise the grain size distribution, the material was left to settle under gravity. At this stage, most of the samples flocculated, and so they were further diluted with DIW, each time adding a few drops of 0.1 M Calgon (sodium hexametaphosphate) until flocculation no longer occurred. The homogenised suspension was then left for a time determined by Stoke's Law of gravitational settling such that after that time, all the material remaining in suspension should have a nominal grain size of 2 µm or less. The suspension was then decanted and oven-dried at 55°C. 100 mg of this <2 µm material was then resuspended in a minimal amount of distilled water and pipetted onto a ceramic tile. The water was drawn through the tile under vacuum to leave an oriented mount of clay on the tile. The clay mounts were

Appendix Table 5 Internal Reference Material – Analytical Data: Co–As.

Standard ID	Co	Cs	Ba	La	Ce	Nd	Sm	Ni	Cu	Zn	Ga	Ge	As
	ppm	ppm	ppm	ppm	ppm	ppm	ppm	ppm	ppm	ppm	ppm	ppm	ppm
MB1	4	<4	978	28	54	26	8	13	17	46	7	1	11
MB1	8	<4	952	29	62	29	6	10	18	51	8	<1	12
MB1	9	<5	962	27	60	23	<5	14	19	51	8	1	12
MB1	6	<5	950	28	63	24	10	12	18	51	9	1	11
MB1	8	<5	963	26	54	30	6	13	17	50	8	1	10
MB1	7	<5	967	27	67	25	<5	12	18	51	7	2	10
MB1	9	<5	951	27	62	23	<5	13	18	49	8	<1	10
MB1	8	<5	937	27	59	24	<5	13	18	49	7	<1	12
MB1	8	<5	939	28	62	32	<5	13	20	50	8	<1	11
Mean MB1	7	<5	955	27	60	26	8	13	18	50	8	1	11
Standard ID	**Co**	**Cs**	**Ba**	**La**	**Ce**	**Nd**	**Sm**	**Ni**	**Cu**	**Zn**	**Ga**	**Ge**	**As**
MB3	13	ND	852	27	66	27	<5	18	57	198	18	3	93
MB3	15	<4	864	30	61	26	<5	18	57	194	19	1	93
MB3	15	<5	871	30	66	31	9	18	59	197	19	1	94
MB3	17	ND	854	35	63	28	<5	18	59	195	19	2	96
MB3	14	ND	874	30	68	26	<5	17	60	199	19	<1	94
MB3	12	<5	846	34	64	23	<5	17	56	193	18	<1	92
MB3	13	<5	863	37	67	28	<5	18	59	198	19	1	95
MB3	16	<5	874	33	61	24	<5	17	60	197	17	1	95
MB3	8	<5	834	34	66	25	10	15	47	164	14	2	78
MB3	14	N/A	859	32	65	26	10	17	57	193	18	2	92
Standard ID	**Co**	**Cs**	**Ba**	**La**	**Ce**	**Nd**	**Sm**	**Ni**	**Cu**	**Zn**	**Ga**	**Ge**	**As**
MSB1	5	ND	381	17	42	14	<5	18	32	271	7	2	14
MSB1	7	ND	394	18	39	17	<5	19	34	274	8	2	13
MSB1	7	ND	373	19	39	18	<5	18	34	274	7	2	14
MSB1	6	ND	369	12	35	21	<5	17	35	274	8	1	14
MSB1	8	ND	387	19	36	19	10	18	34	275	8	2	14
MSB1	10	ND	386	19	38	23	<5	18	33	273	8	2	14
MSB1	5	ND	386	19	37	19	<5	13	27	226	6	1	12
Mean MSB1	7	N/A	382	18	38	19	10	17	33	267	7	2	14

then Ca-saturated using 2 ml 1 M $CaCl_2.6H_2O$ solution and washed twice to remove excess reagent before being allowed to air-dry.

Separation and preparation of <0.5 µm grain size fraction

Each of the dried bulk samples was placed in de-ionised water and disaggregated on a shaker table overnight. It was then subjected to about 5 minutes of ultrasonic agitation to break up the clay particles. Dilute suspensions of the material were placed in tall gas jars and left for a short time (either 4 or 17 hours) to allow the largest particles to settle out. According to Stoke's Law of gravitational settling this would nominally have removed particles greater than 4 or 2 µm (respectively) in diameter, depending on the time. The remaining suspension was decanted and then placed in a centrifuge at 300 rpm. Stoke's Law was again used to calculate the time it would take at this speed to settle out all but the <0.5 µm fraction, and this was done. The remaining suspensions were decanted and oven-dried at ~50 ºC.

The resulting <0.5 µm powders were then prepared as oriented mounts and analysed by XRD analysis using the methods described above. XRD analysis was carried out sequentially on the samples following air-drying, glycolation and heating to 550 ºC for two hours.

XRD analysis

XRD analysis of the oriented clay mineral mounts was carried out using a Phillips PW1700 series diffractometer using Co–K radiation and operating at 45 kV and 40 mA. The oriented mounts were scanned over the range 1.5–32 °2 at a scanning speed of 0.5°2/minute. They were sequentially analysed by XRD after air-drying, then after ethylene glycol solvation and finally after heating at 500°C for 2 hours. Diffraction data were analysed using Phillips X'Pert software coupled to a International Centre for Diffraction Data (ICDD) database.

SCANNING ELECTRON MICROSCOPY

Samples and sample preservation

Petrographical analysis was undertaken on samples taken from selected preserved sediment cores. The sediment cores were taken in plastic tubes, which were then capped

Appendix Table 6 Internal Reference Material – Analytical Data: Se–Pb.

Standard ID	Se	Br	Rb	Sr	Y	Zr	Nb	Mo	Hf	Ta	W	Tl	Pb
	ppm	ppm	ppm	ppm	ppm	ppm	ppm	ppm	ppm	ppm	ppm	ppm	ppm
MB1	<1	1	51	375	27	1109	26	<1	22	1	2	<1	13
MB1	<1	1	50	371	28	1215	28	<1	24	2	<1	<1	14
MB1	<1	2	50	378	28	1231	27	<1	25	2	<1	<1	15
MB1	<1	1	49	373	26	1199	27	<1	25	<1	1	<1	14
MB1	<1	<1	48	371	27	1205	27	<1	23	2	1	<1	15
MB1	<1	<1	50	377	28	1226	27	<1	24	<1	1	<1	14
MB1	<1	1	49	372	27	1212	27	<1	25	2	1	<1	14
MB1	<1	<1	48	373	27	1214	27	<1	24	2	2	<1	14
MB1	<1	1	51	379	27	1244	27	<1	26	<1	<1	<1	14
Mean MB1	N/A	1	50	374	27	1206	27	N/A	24	2	1	N/A	14
Standard ID	**Se**	**Br**	**Rb**	**Sr**	**Y**	**Zr**	**Nb**	**Mo**	**Hf**	**Ta**	**W**	**Tl**	**Pb**
MB3	<1	4	106	191	22	528	14	<1	10	2	2	<1	33
MB3	<1	4	106	193	24	557	14	<1	13	<1	3	<1	33
MB3	<1	4	106	190	23	558	15	<1	11	<1	3	<1	34
MB3	<1	3	106	189	25	560	15	<1	12	<1	2	<1	32
MB3	<1	3	107	192	24	566	15	<1	13	<1	1	<1	33
MB3	<1	3	103	185	24	547	14	<1	12	<1	3	<1	33
MB3	<1	3	105	192	24	562	14	<1	12	<1	3	<1	34
MB3	<1	4	106	191	24	555	14	<1	11	<1	4	<1	33
MB3	<1	2	87	156	19	442	12	<1	10	<1	3	<1	28
MB3	N/A	3	104	187	23	542	14	N/A	12	2	3	N/A	33
Standard ID	**Se**	**Br**	**Rb**	**Sr**	**Y**	**Zr**	**Nb**	**Mo**	**Hf**	**Ta**	**W**	**Tl**	**Pb**
MSB1	<1	45	56	190	19	345	9	<1	6	<1	1	<1	59
MSB1	<1	44	56	193	17	336	9	<1	6	1	3	<1	58
MSB1	<1	44	54	193	20	349	9	<1	7	<1	2	<1	59
MSB1	<1	46	56	190	19	345	9	<1	8	<1	2	<1	60
MSB1	<1	45	56	191	18	340	9	<1	6	<1	1	<1	58
MSB1	<1	47	55	193	17	343	9	<1	6	<1	2	<1	60
MSB1	<1	37	45	158	13	272	8	<1	5	<1	2	<1	48
Mean MSB1	N/A	44	54	187	18	333	9	N/A	6	1	2	N/A	57

immediately after recovery. In order to prevent or limit drying and postcoring chemical alteration (e.g. oxidation of iron sulphides) the capped tubes were sealed under nitrogen within 'crimp-welded' aluminised plastic flat-roll tubing, and stored as soon as possible at approximately -40 °C within a deep-freeze. The samples were maintained in a frozen state prior to petrographical and mineralogical analysis.

Petrographical analysis of preserved samples by cryogenic scanning electron microscopy

Petrographical observation of the sediments were undertaken by cryogenic scanning electron microscopy (cryoSEM). This technique has been used previously by the BGS to successfully examine mineralogical fabrics within preserved unconsolidated modern sediment samples, enabling them to be examined directly in the scanning electron microscope (SEM) instrument without the need for sample drying, and thereby preventing any alteration of unstable minerals such as early diagenetic sulphides (Dodd et al., 2000; 2003; Large et al., 2001).

CryoSEM analyses were performed using a LEO 435VP variable pressure digital scanning electron microscope fitted with an Oxford Instruments CT1200 cryogenic sample preparation, transfer unit and SEM cold-stage. 10 mm sized sub-samples were taken from the frozen core by fracturing with a hammer, and the frozen fragments immediately placed in liquid nitrogen to cool them to very low temperature. These were then fixed onto purpose-made brass cryoSEM mounts with a droplet of water (which froze on contact) with the very cold frozen sample fragment. The frozen SEM mounts were then placed onto the cold-stage within the SEM instrument, via the vacuum airlock of the Oxford Instruments CT1200 cryogenic transfer unit. The time that the frozen sample surfaces were in contact with air was minimised as far as possible in order to reduce the development of a 'hoar-frost' coating (formed by condensation of atmospheric water vapour) on the sample surfaces (which hinders SEM observation). Once placed on the SEM cold-stage within the SEM chamber (at a low vacuum of about 0.3 torr), the samples were very slowly warmed until the ice on the surface was observed to start to sublime (at approximately -80 ºC). The surface of the sample was then very carefully 'developed' so as to expose and reveal the mineralogical fabrics from the interstitial frozen porewater matrix (which comprised

Appendix Table 7 Internal Reference Material – Analytical Data: Bi–I.

Standard ID	Bi	Th	U	Ag	Cd	Sn	Sb	Te	I
	ppm	ppm	ppm	ppm	ppm	ppm	ppm	ppm	ppm
MB1	<1	8	3	<1	<1	2	1	<2	5
MB1	<1	10	4	<1	<1	3	1	<2	6
MB1	<1	9	4	<1	<1	2	<1	<2	<2
MB1	<1	10	5	<1	<1	2	1	<2	<2
MB1	1	10	3	<1	<1	1	1	<2	<2
MB1	<1	10	4	<1	<1	2	1	<2	<2
MB1	<1	9	4	<1	<1	3	1	<2	<2
MB1	<1	8	3	<1	<1	1	2	<2	<2
MB1	<1	11	4	<1	<1	2	<1	<2	<2
Mean MB1	1	9	4	N/A	N/A	2	1	N/A	6
Standard ID	**Bi**	**Th**	**U**	**Ag**	**Cd**	**Sn**	**Sb**	**Te**	**I**
MB3	<1	20	5	<1	<1	4	6	<2	7
MB3	<1	19	5	1	<1	3	7	<2	8
MB3	<1	20	4	1	<1	2	7	<2	<2
MB3	1	19	5	2	<1	1	7	<2	<2
MB3	<1	20	5	<1	<1	2	7	<2	<2
MB3	<1	19	4	<1	<1	2	7	<2	<2
MB3	<1	21	6	<1	<1	2	6	<2	<2
MB3	<1	20	5	<1	<1	3	7	<2	<2
MB3	<1	17	4	<1	<1	1	6	<2	<2
MB3	1	19	5	1	N/A	2	7	N/A	8
Standard ID	**Bi**	**Th**	**U**	**Ag**	**Cd**	**Sn**	**Sb**	**Te**	**I**
MSB1	<1	6	1	<1	<1	9	<1	<2	20
MSB1	<1	6	2	1	<1	9	<1	<2	20
MSB1	<1	7	1	<1	<1	8	<1	<2	21
MSB1	<1	6	2	<1	<1	9	<1	<2	18
MSB1	<1	7	2	<1	<1	9	<1	<2	21
MSB1	<1	6	1	<1	<1	9	<1	<2	20
MSB1	<1	5	3	1	<1	7	<1	<2	17
Mean MSB1	N/A	6	2	1	N/A	9	N/A	N/A	20

up to 90 % of the sediment volume in some cases). Once the surface was 'developed' to the desired extent, the sample was recooled to <160 ºC to prevent further sublimation, and to maintain the sample intact. SEM observations were then carried in the low-vacuum mode, using backscattered electron imaging (BSEM), thereby allowing observations to be made without the need for coating the sample with an electrically-conductive gold coating. SEM observations were made using a 10–20 kV electron beam, and 100–800 pA beam current as appropriate.

Mineralogical and chemical characterisation of features observed under the SEM was aided by semi-quantitative energy-dispersive X-ray microanalysis (EDXA) using an Oxford Instruments ISIS 300 digital EDXA system fitted to the electron microscope. In some cases, the EDXA system was used to quantitatively determine the metal-to-sulphur ratios of the authigenic sulphides, although the accuracy of the quantitative EDXA was limited by the unpolished surface of the samples. EDXA spectra for quantitative analysis were acquired using a 20 kV electron beam and beam currents of 300–500 pA, and processed using the Oxford ISIS 300 SEMQUANT standardless EDXA software package.

HEAVY MINERAL/HEAVY PARTICLE ANALYSIS

Subsamples of sediment were wet-sieved to pass successively through 250 µm, 125 µm and 63 µm mesh sieves. The 125–250 µm and 63–125 µm size fractions were then dispersed in bromoform (specific gravity = 2.95) and placed in separating funnels. The heavy fraction (specific gravity = >2.95) – 'sinking fraction' – was then separated and washed with acetone, and dried.

The heavy mineral/heavy particle concentrates were characterised by SEM observation, using semi-quantitative EDXA to aid phase identification. The heavy mineral grains mounted on a 0.5 inch pin-type SEM stub using electrically conductive double-sided adhesive carbon 'sticky-tabs'. The SEM mounts were then coated with a thin film of carbon (approximately 250 Å thick) to make their surface electrically conductive. These were then examined by conventional 'high vacuum' SEM.

SEM-EDXA analysis was carried out using a LEO 435VP variable pressure digital scanning electron microscope, fitted with an Oxford Instruments ISIS 300 digital EDXA microanalysis system. Observations were made in high vacuum mode (<1 x 10-4 torr), using a 20 kV electron beam and 100–300 pA beam currents (as appropriate).

Appendix Table 8 Duplicate samples collected.

Sample	Date	East	North	Depth	Recovery	Compaction	Dup Site 1	Dup Site 2	Comments
M26	07-Jun-00	341305	382382	0.95	68	0.27	M276	M277	Fine organic rich mud. 50 m upstream from yacht club slipway at Speke, 60 m from shoreline.
M30	08-Jun-00	338914	379400	1.27	0.89	0.28	M293	M294	Thin runny surface mud over layers of brown sand and muddy sand. White plastic bag at 1.27.
M34	08-Jun-00	340405	383085	1.14	0.89	0.25	M250	M251	Very muddy black surface sediment consistant to depth. 200 m SE Garston ship dismantlers.
M70	24-Jul-00	331347	394251	NR	NR	NR	M238		Adjacent to Life Guard post at New Brighton. Sampled from shore.
M72	25-Jul-00	331511	393893	1.04	0.86	0.18	M239		Medium beach sand.
M106	27-Jul-00	345650	378739	1.26	0.94	0.32	M282	M283	Mud in area of eroded salt marsh.
M146	22-Sep-00	343207	377806	1.24	0.99	0.25	M280	M281	Mud flat on western edge of Ince Bank. Organic rich mud at surface, black sand at base.
M165	06-Oct-00	341991	378016	1.22	0.70	0.52	M288	M289	Thick organic mud on expansive raised mud flat. Thin oxidised surface layer ~10 cm.
M167	06-Oct-00	342519	377519	1.30	0.45	0.85	M287		Very soft anoxic mud close to shore at Stanlow Point.
M238	16-Feb-01	331348	394247	1.16	1.03	0.13	M70		Duplicate of M70. New Brighton. Fine sand, organic content towards base of core.
M239	16-Feb-01	331510	393893	1.16	1.03	0.13	M72		Duplicate of M72. End of N breakwater to S of New Brighton coastguard station. Fine sand, organic content at base of core.
M248	08-May-01	342020	381992	1.24	0.99	0.25	M249		Duplicate of M159 and M249. Thick anoxic mud with organic rich base
M249	08-May-01	342020	381992	1.27	0.98	0.29	M248		Duplicate of M159 and M248. Thick anoxic mud with organic rich base
M250	09-May-01	340424	383100	1.20	1.00	0.20	M34	M251	Duplicate of M251 and M34. Creeked thick mud c.200m S of Garston ship dismantling yard
M251	09-May-01	340424	383100	1.19	0.99	0.20	M34	M250	Duplicate of M250 and M34. Creeked thick mud c.200m S of Garston ship dismantling yard
M265	10-May-01	339264	384192	1.25	0.82	0.43	M266		Duplicate of M266. Fine silt on anoxic mud at Garston Lock
M266	10-May-01	339264	384192	1.18	0.92	0.26	M265		Duplicate of M265. Fine silt on anoxic mud at Garston Lock
M271	11-May-01	355676	384711	1.32	1.14	0.18	M272		Duplicate of M272. C.35 m W of "old" W–E drain entrance. Area of mud over dark fine sand. 30 cm v soft mud on surface.
M272	11-May-01	355676	384711	1.31	1.09	0.22	M271		Duplicate of M272. C.35 m W of "old" W–E drain entrance. Area of mud over dark fine sand. 30 cm v soft mud on surface.
M276	11-Jun-01	341305	382386	1.02	NR	NR	M26	M277	Muddy core. Very dark grey. Duplicate of M277 and M26
M277	11-Jun-01	341305	382386	1.01	NR	NR	M26	M276	Muddy core. Very dark grey. Duplicate of M276 and M26
M278	11-Jun-01	344174	381384	0.97	NR	NR	M279		Very black mud. Duplicate of M279 and M139
M279	11-Jun-01	344174	381384	0.97	NR	NR	M278		Very black mud, finer at depth Duplicate of M278 and M139
M280	11-Jun-01	343206	377817	0.96	NR	NR	M146	M281	Fine grey mud on large mud bank. Duplicate M281 and M146
M281	11-Jun-01	343206	377817	0.97	NR	NR	M146	M280	Fine grey/black mud. Duplicate M280 and M146
M282	12-Jun-01	345654	378737	1.31	0.98	0.33	M106	M283	Fine silt on thick anoxic mud. Duplicate of M283 and M106
M283	12-Jun-01	345654	378737	1.30	0.88	0.42	M106	M282	Fine silt on thick anoxic mud. Duplicate of M282 and M106
M287	12-Jun-01	342525	377527	2.42	1.68	0.73	M167		Thick black anoxic mud to depth @ 150w Stanlow point. Duplicate of M286 and M167
M288	13-Jun-01	341990	378023	1.24	0.94	0.30	M165	M289	Thick black mud @ Stanlow. Duplicate of M289 and M165
M289	13-Jun-01	341990	378023	1.24	0.94	0.30	M165	M288	Thick black mud @ Stanlow. Duplicate of M288 and M165
M293	14-Jun-01	338918	379402	1.19	0.89	0.30	M30	M294	Sandy mud. Duplicate of M294 and M30.
M294	14-Jun-01	338919	379402	1.25	1.05	0.20	M30	M294	Sandy mud. Duplicate of M293 and M30.
M297	14-Jun-01	338913	379401	1.29	1.05	0.24	M298		Sandy mud. Duplicate of M298.
M298	14-Jun-01	338912	379398	1.15	0.89	0.26	M297		Sandy mud. Duplicate of M297.

SEQUENTIAL CHEMICAL EXTRACTION AND CHEMOMETRIC IDENTIFICATION OF SUBSTRATES AND METAL DISTRIBUTIONS (CISMED SEQUENTIAL EXTRACTION)

Total digestion

Some 0.1 g of the dried and core samples was accurately weighed into a Teflon digestion tube. 1.0 ml of concentrated HF was added and the sample left overnight at room temperature to break down the soil matrix. 0.4 ml of concentrated perchloric acid and 0.8 ml of concentrated HNO_3 were added and digestion took place on a temperature controlled hot-block. The temperature of the hot-block used for the digestion is increased at time intervals by a controller unit until it reaches 190°C. The stages involved are five hours at 100°C, followed by one hour at 140°C with the final stage reaching 190°C for six hours. The hot-block temperature was then taken down to 50°C where 1.0 ml of 50% HNO_3 was added and the samples are left for one hour.

On removal from the hot-block 9.0 ml of freshly prepared de-ionised water was added to the resulting digestion solution. If any organic matter was still present in the digestion solution 1.0 ml of hydrogen peroxide was added.

In all cases the supernatent solution was decanted and stored at 4°C prior to analysis by ICP-AES. All calibration standards and quality control solutions were matrix matched to each extraction media and spike tests performed prior to analysis.

CISMED sequential extraction

The extraction vessels employed were Schleicher and Schuell® 'Centrex MF-25' polypropylene centrifuge tubes with filter inserts. The filter is a regenerated cellulose membrane (pore size 0.45 μm). Approximately 2 g of sample was accurately weighed into the filter tube insert. Ten ml aliquots of extractant were sequentially added to the insert. The extractants used for this technique were de-ionised water (extract 1 and 2), 0.01(extracts 3 and 4), 0.05 (extracts 5 and 6), 0.1 (extracts 7 and 8), 0.5 (extracts 9 and 10), 1 (extracts 11 and 12) and 5 (extracts 14 and 15) M aqua regia. For the 0.1, 0.5, 1 and 5 M aqua regia extracts, hydrogen peroxide was added in the amounts 0.25, 0.50, 0.75 and 1 ml, with the remaining volume made up to 10 ml with the appropriate strength acid. The sample was leached with two 10 ml aliquots of each extractant. Each vessel was centrifuged for 10 minutes at 1034 g.

Analysis of the extraction leachates

Each 10 ml aliquot from the CISMeD test was analysed for Al, As, Ba, Ca, Cd, Co, Cr, Cu, Fe, K, Mg, Mn, Na, Ni, P, Pb, S, Se, Si, Sr, V, Zn by ICP-AES.

Data processing

The data from the CISMeD extraction test were subjected to the chemometric data processing procedure described by Cave et al., (2002).

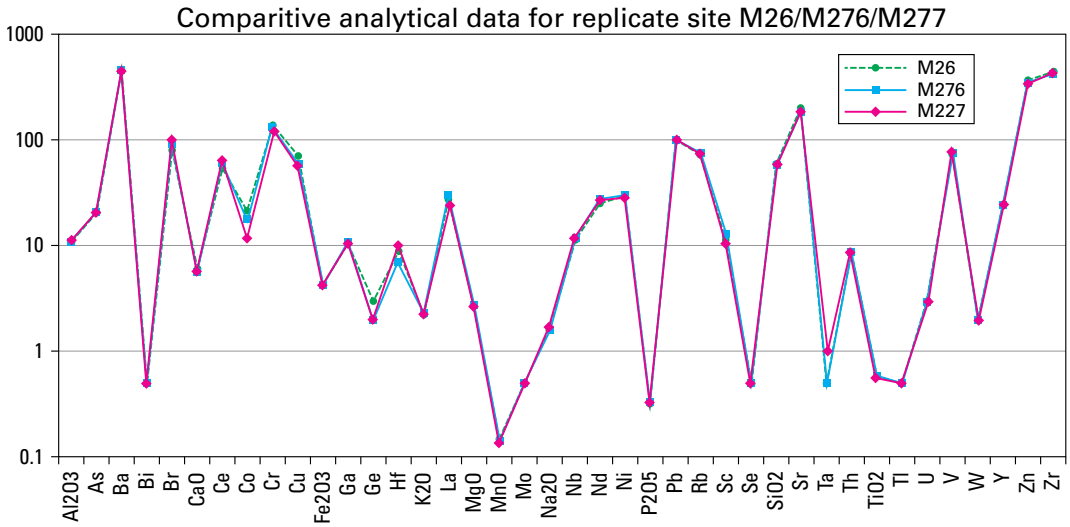
Comparitive analytical data for replicate site M26/M276/M277
1000
100
10
1
0.1
M26
M276
M227
Al2O3 As Ba Bi Br CaO Ce Co Cr Cu Fe2O3 Ga Ge Hf K2O La MgO MnO Mo Na2O Nb Nd Ni P2O5 Pb Rb Sc Se SiO2 Sr Ta Th TiO2 Tl U V W Y Zn Zr

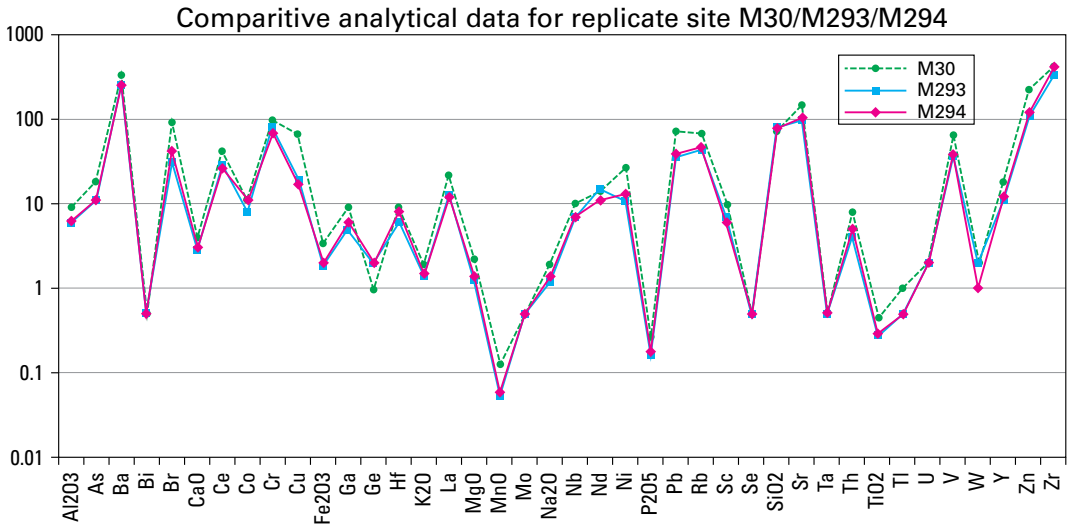
Comparitive analytical data for replicate site M30/M293/M294
1000
100
10
1
0.1
0.01
M30
M293
M294
Al2O3 As Ba Bi Br CaO Ce Co Cr Cu Fe2O3 Ga Ge Hf K2O La MgO MnO Mo Na2O Nb Nd Ni P2O5 Pb Rb Sc Se SiO2 Sr Ta Th TiO2 Tl U V W Y Zn Zr

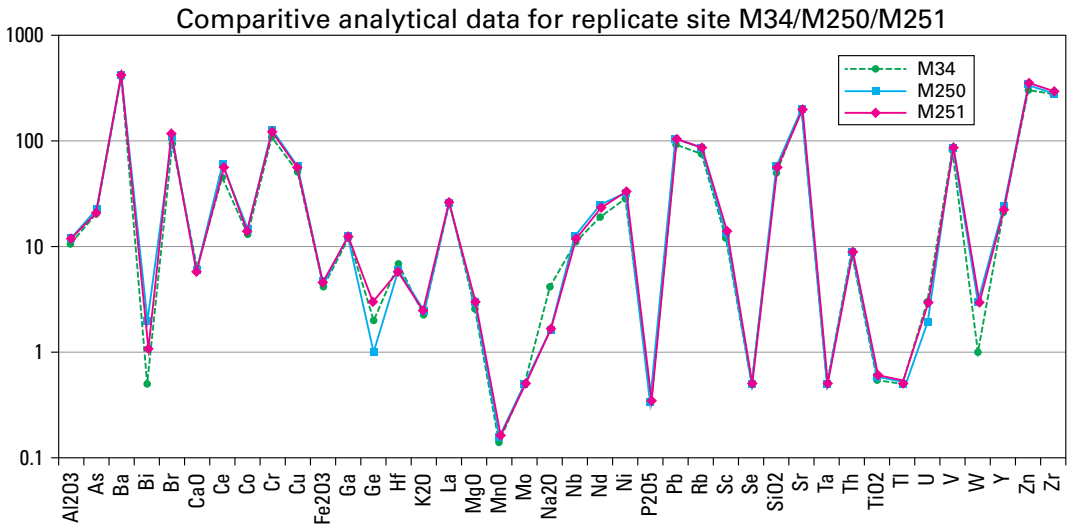
Comparitive analytical data for replicate site M34/M250/M251
1000
100
10
1
0.1
M34
M250
M251
Al2O3 As Ba Bi Br CaO Ce Co Cr Cu Fe2O3 Ga Ge Hf K2O La MgO MnO Mo Na2O Nb Nd Ni P2O5 Pb Rb Sc Se SiO2 Sr Ta Th TiO2 Tl U V W Y Zn Zr

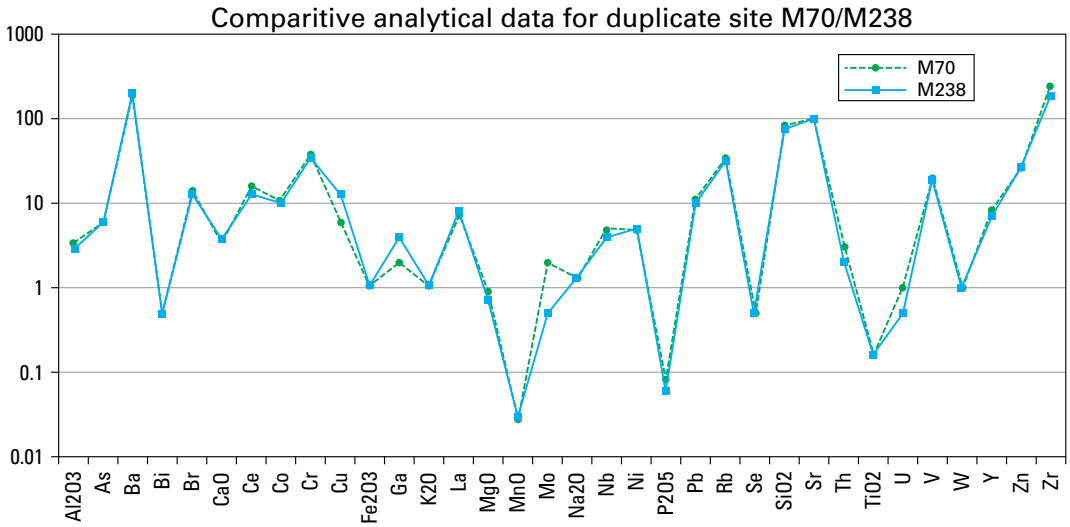
Comparitive analytical data for duplicate site M70/M238
1000
100
10
1
0.1
0.01
M70
M238
Al2O3 As Ba Bi Br CaO Ce Co Cr Cu Fe2O3 Ga K2O La MgO MnO Mo Na2O Nb Ni P2O5 Pb Rb Se SiO2 Sr Th TiO2 U V W Y Zn Zr

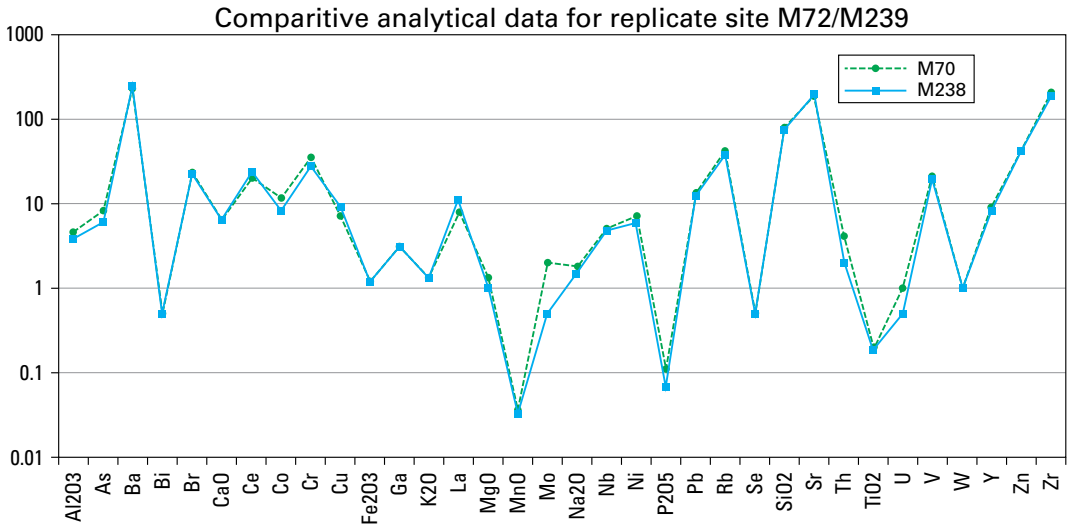
Comparitive analytical data for replicate site M72/M239
1000
100
10
1
0.1
0.01
M70
M238
Al2O3 As Ba Bi Br CaO Ce Co Cr Cu Fe2O3 Ga K2O La MgO MnO Mo Na2O Nb Ni P2O5 Pb Rb Se SiO2 Sr Th TiO2 U V W Y Zn Zr

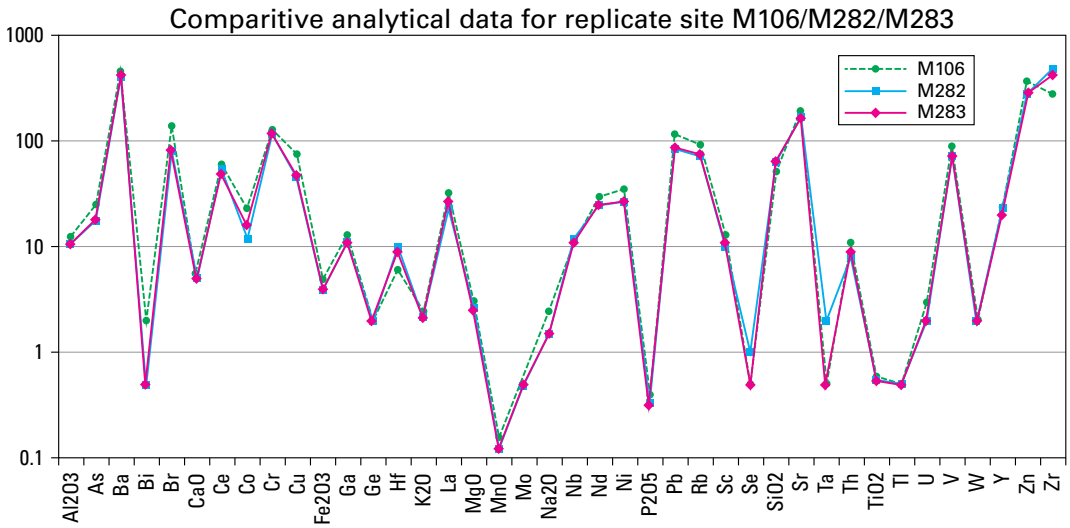
Comparitive analytical data for replicate site M106/M282/M283
1000
100
10
1
0.1
M106
M282
M283
Al2O3 As Ba Bi Br CaO Ce Co Cr Cu Fe2O3 Ga Ge Hf K2O La MgO MnO Mo Na2O Nb Nd Ni P2O5 Pb Rb Sc Se SiO2 Sr Ta Th TiO2 Tl U V W Y Zn Zr

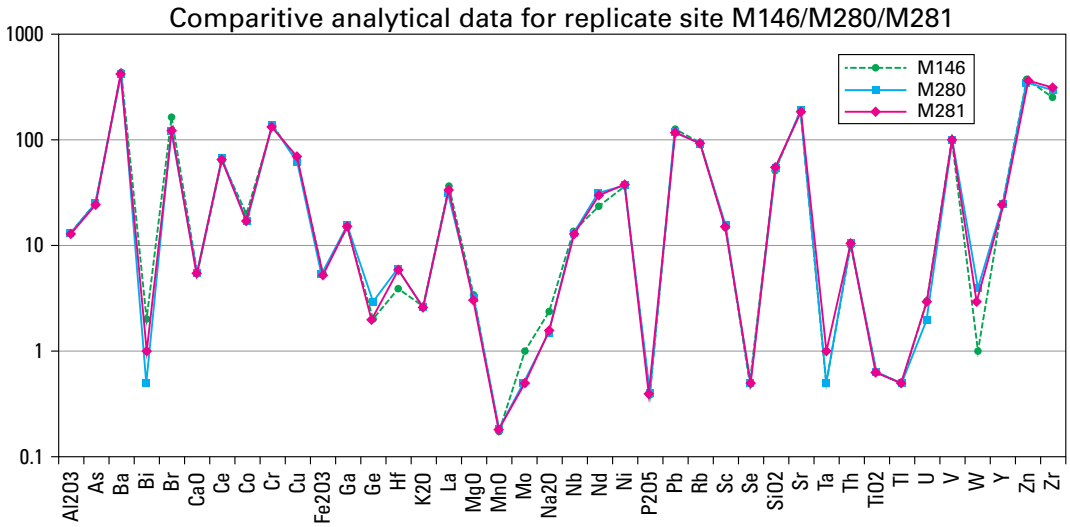
Comparitive analytical data for replicate site M146/M280/M281
M146
M280
M281
1000
100
10
1
0.1
Al2O3 As Ba Bi Br CaO Ce Co Cr Cu Fe2O3 Ga Ge Hf K2O La MgO MnO Mo Na2O Nb Nd Ni P2O5 Pb Rb Sc Se SiO2 Sr Ta Th TiO2 Tl U V W Y Zn Zr

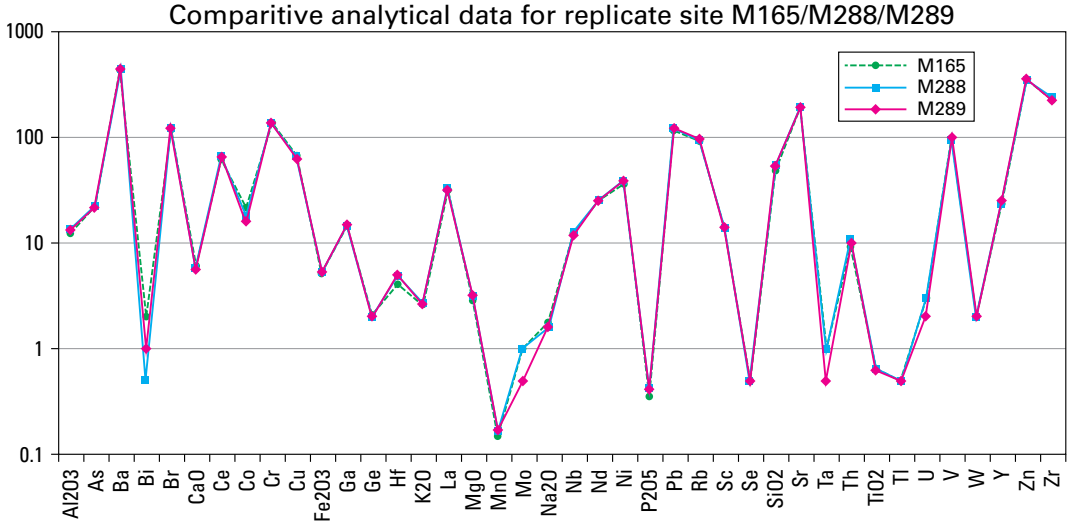
Comparitive analytical data for replicate site M165/M288/M289
M165
M288
M289
1000
100
10
1
0.1
Al2O3 As Ba Bi Br CaO Ce Co Cr Cu Fe2O3 Ga Ge Hf K2O La MgO MnO Mo Na2O Nb Nd Ni P2O5 Pb Rb Sc Se SiO2 Sr Ta Th TiO2 Tl U V W Y Zn Zr

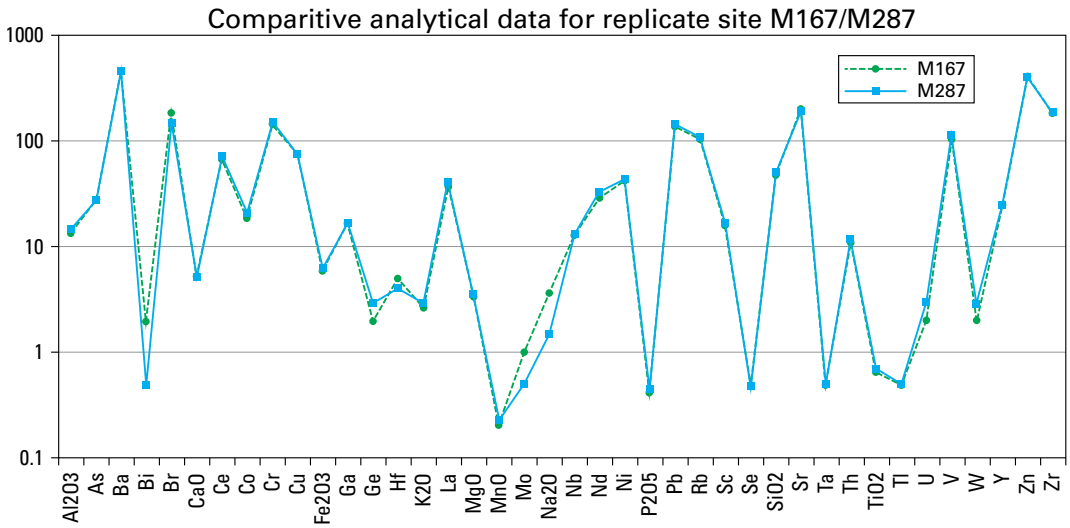
Comparitive analytical data for replicate site M167/M287
M167
M287
1000
100
10
1
0.1
Al2O3 As Ba Bi Br CaO Ce Co Cr Cu Fe2O3 Ga Ge Hf K2O La MgO MnO Mo Na2O Nb Nd Ni P2O5 Pb Rb Sc Se SiO2 Sr Ta Th TiO2 Tl U V W Y Zn Zr

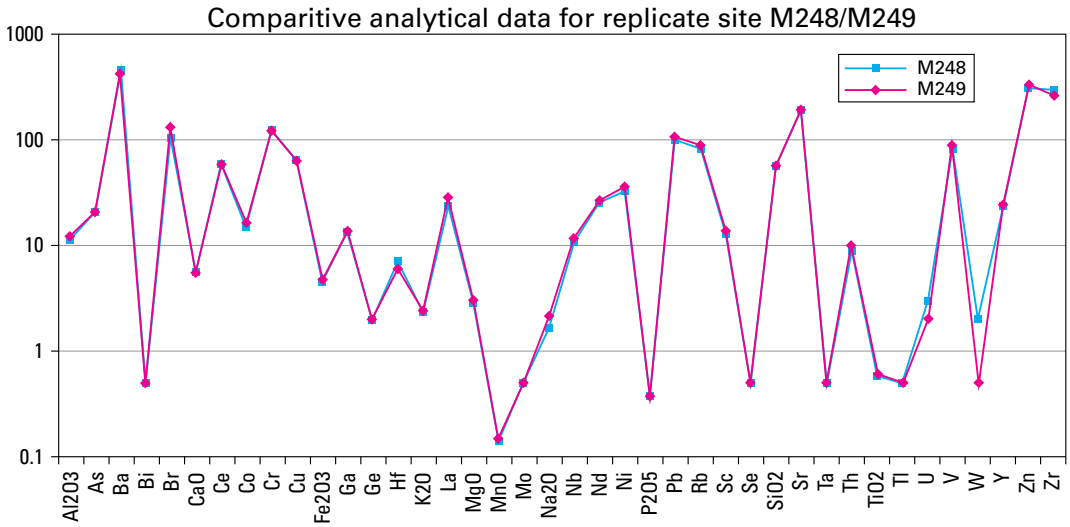
Comparitive analytical data for replicate site M248/M249
M248
M249
1000
100
10
1
0.1
Al2O3 As Ba Bi Br CaO Ce Co Cr Cu Fe2O3 Ga Ge Hf K2O La MgO MnO Mo Na2O Nb Nd Ni P2O5 Pb Rb Sc Se SiO2 Sr Ta Th TiO2 Tl U V W Y Zn Zr

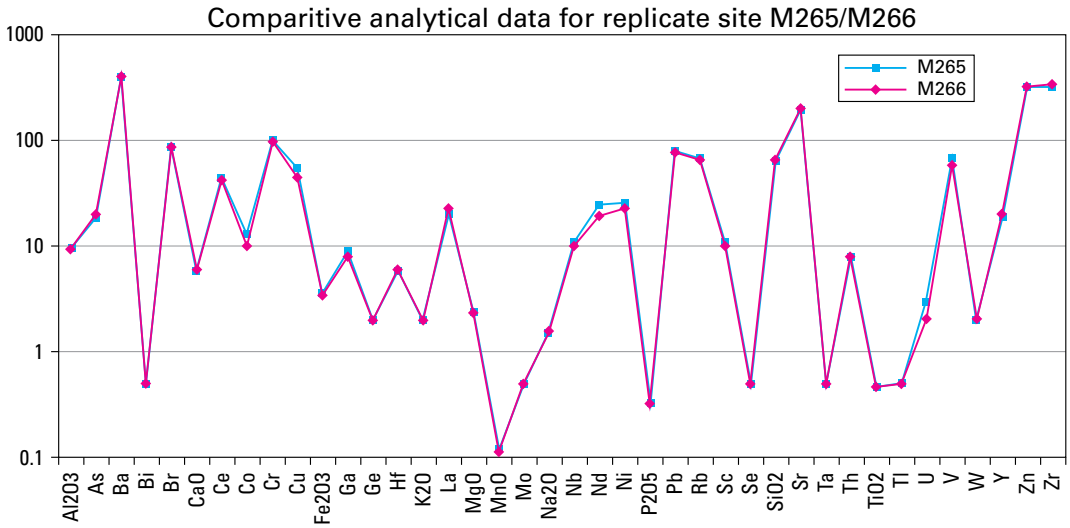
Comparitive analytical data for replicate site M265/M266
M265
M266
1000
100
10
1
0.1
Al2O3 As Ba Bi Br CaO Ce Co Cr Cu Fe2O3 Ga Ge Hf K2O La MgO MnO Mo Na2O Nb Nd Ni P2O5 Pb Rb Sc Se SiO2 Sr Ta Th TiO2 Tl U V W Y Zn Zr

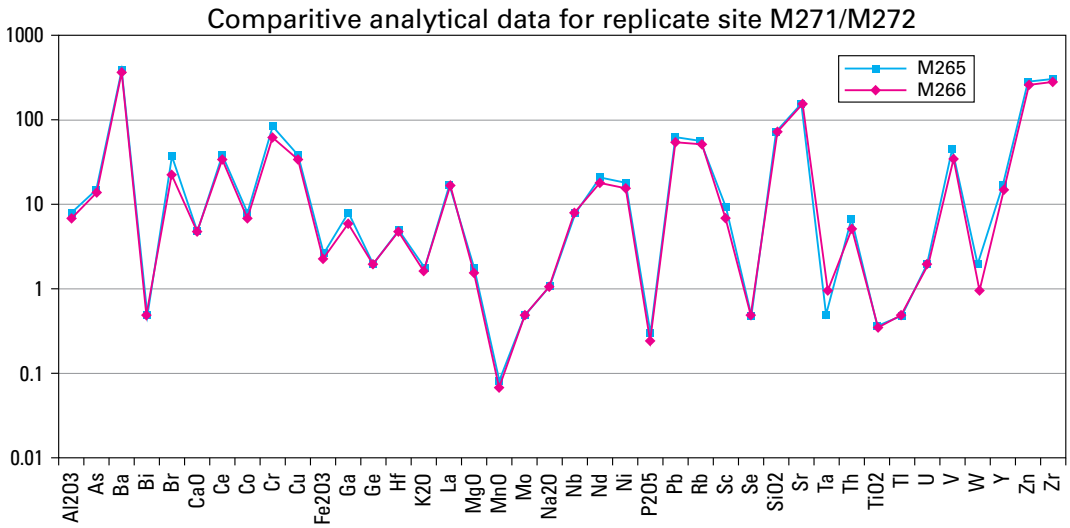
Comparitive analytical data for replicate site M271/M272
M265
M266
1000
100
10
1
0.1
0.01
Al2O3 As Ba Bi Br CaO Ce Co Cr Cu Fe2O3 Ga Ge Hf K2O La MgO MnO Mo Na2O Nb Nd Ni P2O5 Pb Rb Sc Se SiO2 Sr Ta Th TiO2 Tl U V W Y Zn Zr

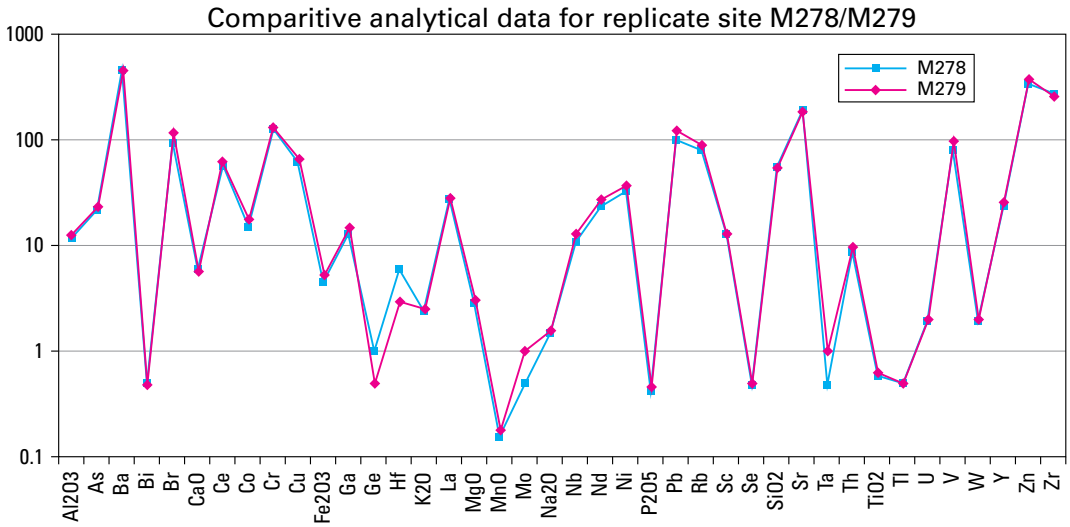
Comparitive analytical data for replicate site M278/M279
M278
M279
1000
100
10
1
0.1
Al2O3 As Ba Bi Br CaO Ce Co Cr Cu Fe2O3 Ga Ge Hf K2O La MgO MnO Mo Na2O Nb Nd Ni P2O5 Pb Rb Sc Se SiO2 Sr Ta Th TiO2 Tl U V W Y Zn Zr

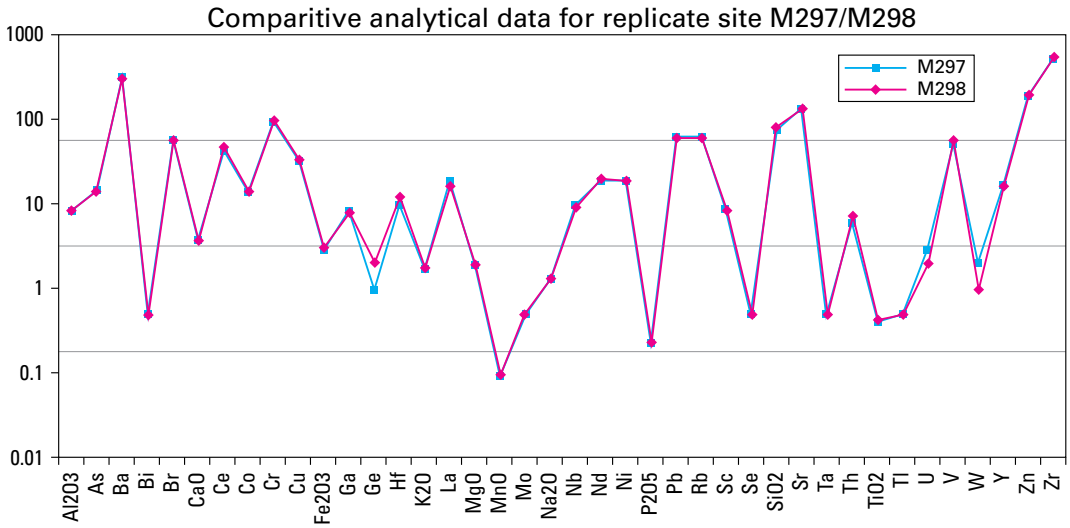
Comparitive analytical data for replicate site M297/M298
M297
M298
1000
100
10
1
0.1
0.01
Al2O3 As Ba Bi Br CaO Ce Co Cr Cu Fe2O3 Ga Ge Hf K2O La MgO MnO Mo Na2O Nb Nd Ni P2O5 Pb Rb Sc Se SiO2 Sr Ta Th TiO2 Tl U V W Y Zn Zr

Appendix 2 Mersey estuarine sediments LOI determinations and sample descriptions

Sample	LOI	Sample Description	Sample	LOI	Sample Description	Sample	LOI	Sample Description	Sample	LOI	Sample Description
	%			%			%			%	
M99 0–10	2.51	East side of	M106 0–10	7.68	Area of eroded	M142 0–10	6.27	Oglet Bank foreshore.	M155 0-10	6.80	Organic soft mud
M99 10–20	2.24	Dungeon Banks.	M106 10–20	6.97	salt marsh	M142 10–20	20.15	Grey/Black mud.	M155 10-20	5.65	adjacent to salt marsh.
M99 20–30	2.04	Sandy mud.	M106 20–30	6.02	on Ince Banks	M142 20–30	6.98		M155 20-30	5.50	North bank of river
M99 30–40	2.48		M106 30–40	6.02	- now a mud flat	M142 30–40	6.33		M155 30-40	5.18	South of old
M99 40–50	1.13		M106 40–50	3.34	Very soft mud.	M142 40–50	5.91		M155 40-50	5.81	Liverpool Airport.
M99 50–60	1.60		M106 50–60	3.65		M142 50–60	5.12		M155 50-60	5.87	
M99 60–70	0.99		M106 60–70	1.93		M142 60–70	3.45		M155 60-70	5.16	
M99 70–80	1.31		M106 70–80	4.05		M142 70–85	3.33				
M99 80–92	0.39		M106 80–90	4.23					M156 0-10	0.63	Rippled sands
			M106 90–100	1.55		M146 0–10	9.00	Mud flat on western	M156 10-20	0.81	sand bank.
M101 0–10	10.54	South end				M146 10–20	8.56	edge of Ince Bank.	M156 20-30	1.00	South of M155.
M101 10–20	9.13	of Icehouse	M108C 0–10	0.81	South Dungeon Banks.	M146 20–30	7.72	Organic-rich mud at	M156 30-40	0.79	
M101 20–30	9.04	Plantation, Hale	M108C 10–20	0.71	Sand bank between	M146 30–40	6.01	surface. Black	M156 40-50	1.04	
M101 30–40	9.60	Very soft mud with	M108C 20–30	0.77	two main channels	M146 40–50	7.04	sand at base.	M156 50-60	1.13	
M101 40–50	9.31	worm burrows on	M108C 30–40	0.86	of R. Mersey.	M146 50–60	6.42		M156 60-70	0.88	
M101 50–60	7.77	surface	M108C 40–50	0.93	Mid-estuary.	M146 60–70	5.09		M156 70-78	0.84	
M101 60–70	3.88		M108C 50–60	0.70	Fine sands with				M156 80-94	0.76	
M101 70–77	2.16		M108C 60–70	0.78	linguoidal rippling	M149 0–10	0.71	Thixotropic rippled			
			M108C 70–80	0.64	minimal algal veneer.	M149 10–20	0.75	sand on flat channel	M157 0-10	0.95	Rippled sands
M102 0–10	6.56	Area of shallow,				M149 20–30	0.62	bed. Fine organic	M157 10-20	0.78	sand bank.
M102 10–20	3.67	creeked soft	M122 0–10	7.33	North west	M149 30–40	0.37	material in mid-core.	M157 20-30	1.17	South of M155
M102 20–30	2.87	muddy sands	M122 10–20	6.35	Dungeon Banks,	M149 40–50	0.59	Mid channel between	M157 30-40	1.18	and
M102 30–40	1.76	thin algae on	M122 20–30	7.18	south of Speke.	M149 50–60	0.56	Stanlow and Ince Banks	M157 40-50	1.23	South of M156.
M102 40–50	3.19	surface.	M122 30–40	5.04	Brown/grey mud	M149 60–70	1.17		M157 50-60	1.00	
M102 50–60	3.01	Wader feeding	M122 40–50	4.21	medium sand at	M149 70–85	1.00		M157 60-70	0.97	
M102 60–70	2.23	Rocks abundant	M122 50–60	5.02	base tip of core.				M157 70-80	1.09	
M102 70–80	2.03	South of Brook Farm,	M122 60–70	1.92		M150 0–10	0.98	Rippled sand in flat	M157 80-90	0.97	
M102 80–90	1.76	Hale.				M150 10–20	0.85	channel bed.	M157 90-100	0.92	
M102 90–100	1.96		M126 0–10	9.28	Centre of Ince Banks.	M150 20–30	0.72	Organic content	M157 100-110	1.11	
M102 100–110	1.34		M126 10–20	9.29	1.2 km north of	M150 30–40	0.73	throughout core			
			M126 20–30	9.24	Stanlow Oil Refinery.	M150 40–50	0.81	depth	M158 0-10	0.81	Rippled sands
M104C 0–10	0.85	Rippled muddy	M126 30–40	8.58	Gey/brown mud.	M150 50–60	0.89	Mid-estuary	M158 10-20	0.92	sand bank.
M104C 10–20	0.76	fine sand.	M126 40–50	7.87		M150 60–70	1.08		M158 20-30	1.23	South of M155,
M104C 20–30	0.52	0.5 km north of	M126 50–58	7.42		M150 70–80	1.16		M158 30-40	0.84	South of M156
M104C 30–40	0.74	Ince Banks				M150 80–90	1.47		M158 40-50	1.13	and
M104C 40–50	0.50	salt marshes.	M131 0–10	1.54	Soft silty fine sand				M158 50-60	1.35	South of M157.
M104C 50–60	0.67		M131 10–20	1.06	algae on surface.	M151 0–10	0.90	Shallow rippled sand	M158 60-70	1.19	Mid-estuary
M104C 60–70	0.86		M131 20–30	0.94	North Ince Banks.	M151 10–20	0.69	in central channel.	M158 70-80	1.11	
M104C 70–80	0.76		M131 30–40	1.01		M151 20–30	0.69	Clean sorted sand	M158 80-90	1.42	
M104C 80–90	0.56		M131 40–50	1.03		M151 30–40	0.81	to depth of core.			
			M131 50–60	0.98		M151 40–50	1.01	Mid-estuary	M160 0-10	0.73	Rippled, dumed bank.
M105C 0–10	1.26	Rippled muddy sands	M131 60–70	0.98		M151 50–60	0.97	South of old	M160 10-20	0.51	Clean sand to depth.
M105C 10–20	1.59	with moderate	M131 70–80	1.06		M151 60–70	1.43	Liverpool Airport	M160 20-30	0.58	Very light organic
M105C 20–30	1.62	algal veneer.	M131 80–91	1.08		M151 70–80	1.40		M160 30-40	0.67	content in centre depth
M105C 30–40	1.38	25 m north of							M160 40-50	1.09	South east of M155.
M105C 40–50	1.14	erosional cliff of							M160 50-60	1.52	
M105C 50–60	1.41	Ince Banks							M160 60-70	0.95	
M105C 60–70	0.97	Small channel							M160 70-80	0.79	
M105C 70–80	1.09	adjacent.							M160 80-90	0.59	
M105C 80–90	1.11								M160 90-99	0.63	

Appendix 3 Salt marsh sampling intervals and sediment type

Hole	Grid reference			Hole	Grid reference			Hole	Grid reference	
WW1	SJ 51729 84551			WW2	SJ 51728 84552			WW7	SJ 51633 84643	
Sample	**Depth in m**	**Sediment type**		**Sample**	**Depth in m**	**Sediment type**		**Sample**	**Depth in m**	**Sediment type**
WW1/01	0.00–0.23	muddy silt		WW2/01	0.00–0.12	mud		WW7/01	2.68–2.94	silty clay
WW1/02	0.23–0.40	muddy silt		WW2/02	0.12–0.30	mud		WW7/02	3.00–3.20	silty clay
WW1/03	0.40–0.60	muddy silt		WW2/03	0.30–0.50	mud		WW7/03	3.20–3.40	silty clay
WW1/04	0.60–0.82	muddy silt		WW2/04	0.50–0.70	mud		WW7/04	3.40–3.60	silty clay
WW1/05	1.00–1.16	sandy silt		WW2/05	0.70–0.88	mud		WW7/05	3.60–3.80	silty clay
WW1/06	1.16–1.40	silty mud		WW2/06	1.00–1.20	silty mud		WW7/06	3.80–3.94	fine sand
WW1/07	1.40–1.60	silty mud		WW2/07	1.20–1.40	silty mud		WW7/07	4.00–4.20	silty clay
WW1/08	1.60–1.80	silty mud		WW2/08	1.40–1.60	silty mud		WW7/08	4.20–4.42	silty clay
WW1/09	1.80–2.00	silty mud		WW2/09	1.60–1.80	silty mud		WW7/09	4.42–4.60	silty clay
WW1/10	2.00–2.12	med/coarse sand		WW2/10	1.80–2.00	silty mud		WW7/10	4.60–4.76	silty clay
WW1/11	2.12–2.30	muddy sand						WW7/11	4.76–4.94	sandy silt
WW1/12	2.30–2.44	muddy sand						WW7/12	5.00–5.24	sandy silt
WW1/13	2.44–2.72	sandy mud						WW7/13	5.24–5.40	silty clay
WW1/14	2.72–3.00	silty/sandy mud						WW7/14	5.40–5.57	silty clay
WW1/15	3.00–3.20	silty fine sand						WW7/15	5.57–5.66	sandy silt
WW1/16	3.20–3.40	silty fine sand						WW7/16	5.66–5.94	silty clay
WW1/17	3.40–3.68	silty fine sand						WW7/17	6.00–6.20	silty clay
WW1/18	3.68–4.00	med/coarse sand						WW7/18	6.20–6.40	silty clay
WW1/19	4.00–4.20	medium sand						WW7/19	6.40–6.56	silty clay
WW1/20	4.20–4.40	medium sand						WW7/20	6.56–6.76	sandy silt
WW1/21	4.40–4.60	medium sand						WW7/21	6.76–6.94	silty clay
WW1/22	4.60–4.86	medium sand								
WW1/23	4.86–5.00	medium sand								

Hole	Grid reference		Hole	Grid reference		Hole	Grid reference	
IB6	SJ 46681 77916		IB7	SJ 45900 77580		IB8	SJ 47555 78114	
Sample	**Depth in m**	**Sediment type**	**Sample**	**Depth in m**	**Sediment type**	**Sample**	**Depth in m**	**Sediment type**
1IB6	0.00–0.10	silt	1IB7	0.00–0.10	silty clay	1IB8	0.00–0.10	silty clay
2IB6	0.10–0.20	silt	2IB7	0.10–0.20	silty clay	2IB8	0.10–0.20	silty clay
3IB6	0.20–0.30	silt	3IB7	0.20–0.30	silty clay	3IB8	0.20–0.30	silty clay
4IB6	0.30–0.40	silt	4IB7	0.30–0.40	silty clay	4IB8	0.30–0.40	silty clay
5IB6	0.40–0.50	silt	5IB7	0.40–0.50	silty clay	5IB8	0.40–0.50	silty clay
6IB6	0.50–0.60	silt	6IB7	0.50–0.60	silty clay	6IB8	0.50–0.60	silty clay
7IB6	0.60–0.70	silt	7IB7	0.60–0.70	silty clay	7IB8	0.60–0.70	silty clay
8IB6	0.70–0.80	silt	8IB7	0.70–0.80	silty clay	8IB8	0.70–0.80	silty clay
9IB6	0.80–0.90	muddy silt	9IB7	0.80–0.90	silty clay	9IB8	1.00–1.10	silty clay
10IB6	0.90–0.96	muddy silt	10IB7	1.00–1.10	silty clay	10IB8	1.10–1.20	silty clay
11IB6	0.98–1.08	muddy silt	11IB7	1.10–1.20	silty clay	11IB8	1.20–1.30	silty clay
12IB6	1.08–1.18	muddy silt	12IB7	1.20–1.30	silty clay	12IB8	1.30–1.40	silty clay
13IB6	1.18–1.28	muddy silt	13IB7	1.30–1.40	silty clay	13IB8	1.40–1.50	silty clay
14IB6	1.28–1.38	muddy silt	14IB7	1.46–1.56	silty clay	14IB8	1.50–1.60	silty clay
15IB6	1.38–1.48	muddy silt	15IB7	1.56–1.66	silty clay	15IB8	1.60–1.70	silty clay
16IB6	1.48–1.58	muddy silt	16IB7	1.66–1.76	silty clay	16IB8	1.70–1.80	silty clay
17IB6	1.58–1.68	muddy silt	17IB7	1.76–1.86	silty clay	17IB8	2.00–2.10	silty clay
18IB6	1.68–1.78	muddy silt	18IB7	2.00–2.10	silt	18IB8	2.10–2.20	silty clay
19IB6	1.78–1.88	muddy silt	19IB7	2.10–2.32	silt	19IB8	2.20–2.30	silty clay
20IB6	1.96–2.16	muddy silt	20IB7	2.32–2.50	silt	20IB8	2.30–2.50	silty clay
21IB6	2.16–2.36	muddy silt	21IB7	2.50–2.86	silt	21IB8	2.50–2.78	silty clay
22IB6	2.40–2.84	muddy silt	22IB7	3.00–3.40	silt	22IB8	2.78–3.00	sandy clay
23IB6	2.96–3.46	sandy silt	23IB7	3.40–3.70	silt	23IB8	3.00–3.30	silty clay
24IB6	3.46–3.96	sandy silt	24IB7	4.00–4.26	silt	24IB8	3.33–3.60	sandy clay
25IB6	3.96–4.42	silty clay	25IB7	4.53–4.96	sandy silt	25IB8	3.60–4.00	medium sand
26IB6	4.42–4.96	sandy silt	26IB7	5.00–5.80	sandy silt	26IB8	4.00–4.32	medium sand
27IB6	4.96–5.56	medium sand	27IB7	5.94–6.21	sandy silt	27IB8	4.36–4.56	medium sand
28IB6	5.56–5.66	medium sand	29IB7	6.21–7.00	fine sand	28IB8	4.56–4.85	medium sand
29IB6	5.66–6.14	medium sand				29IB8	4.85–5.00	fine sand
30IB6	6.14–6.62	medium sand				30IB8	5.00–5.52	medium sand
31IB6	6.62–7.46	medium sand				31IB8	5.52–5.72	medium sand
32IB6	7.46–8.31	medium sand				32IB8	5.72–6.00	medium sand
						33IB8	6.00–6.53	medium sand
						34IB8	6.53–7.00	medium sand
						35IB8	7.00–7.30	medium sand
						36IB8	7.30–7.68	medium sand
						37IB8	7.68–8.00	medium sand
						38IB8	8.00–8.55	medium sand
						39IB8	8.55–9.00	medium sand

Hole	Grid reference			Hole	Grid reference			Hole	Grid reference	
Ince 2	SJ 4668 7730			Ince 3	SJ 4702 7674			Ince 4	SJ 4792 7641	
Sample	**Depth in m**	**Sediment type**		**Sample**	**Depth in m**	**Sediment type**		**Sample**	**Depth in m**	**Sediment type**
INCE 2–1	0.36–0.84	silt		INCE 3–1	0.17–0.65	silty clay		INCE 4–1	0.04–0.59	clayey silt
INCE 2–2	0.84–1.04	sandy silt		INCE 3–2	0.92–1.16	clay		INCE 4–2	0.59–0.94	sandy silt
INCE 2–3	1.30–1.95	silty clay		INCE 3–3	1.16–1.57	clayey silt		INCE 4–3	1.25–1.71	very fine sand
INCE 2–4	2.07–2.81	silty clay		INCE 3–4	3.51–4.07	clayey silt		INCE 4–4	1.71–1.92	sandy silt
INCE 2–5	2.81–3.07	silty clay		INCE 3–5	4.15–5.07	silty clay		INCE 4–5	2.36–2.90	clay
INCE 2–6	3.07–3.86	silty clay		INCE 3–6	5.43–6.07	silty clay		INCE 4–6	4.56–5.07	clay
INCE 2–7	3.86–4.07	silty clay		INCE 3–7	6.07–7.07	silty clay		INCE 4–7	5.29–6.07	silty clay
				INCE 3–8	7.07–8.07	silty clay		INCE 4–8	6.24–7.07	silty clay
Hole	**Grid reference**							INCE 4–9	7.21–7.50	clay
Ince 5	SJ 4862 7613							INCE 4–10	7.50–7.74	clay
Sample	**Depth in m**	**Sediment type**						INCE 4–11	8.48–9.07	medium sand
INCE 5–1	3.32–3.56	sandy silt								
INCE 5–2	3.56–4.07	silty clay								
INCE 5–3	4.22–5.07	silty clay								
INCE 5–4	5.22–6.07	silty clay								

Appendix 4 Example X-ray diffraction traces of orientated <2 µm and <0.5 µm fraction material from sediments in the Mersey Estuary and tributary rivers

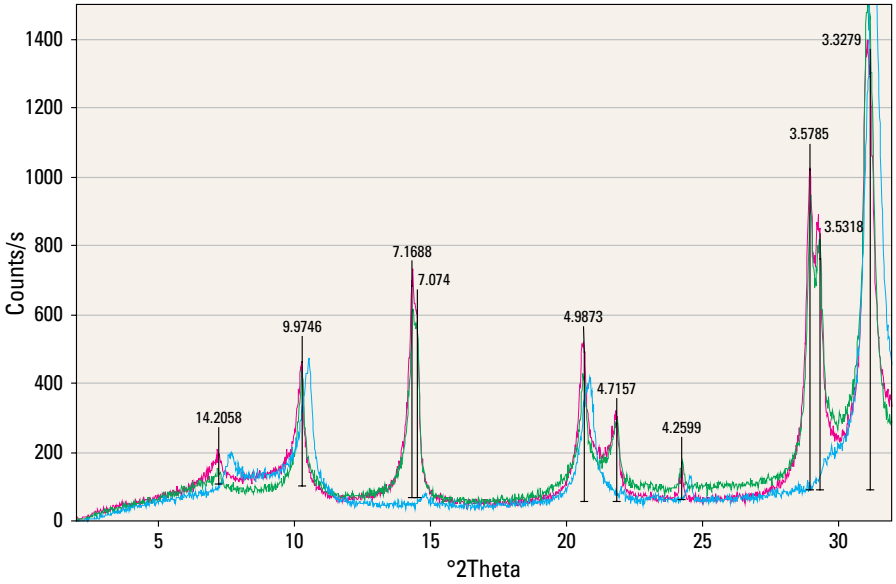

Figure A4.1 Example of typical XRD traces for the <2 µm fraction of Mersey estuary sediment: sample M101, 60–70 cm. Red = air-dried; green = glycolated; blue = heated to 550 ºC.

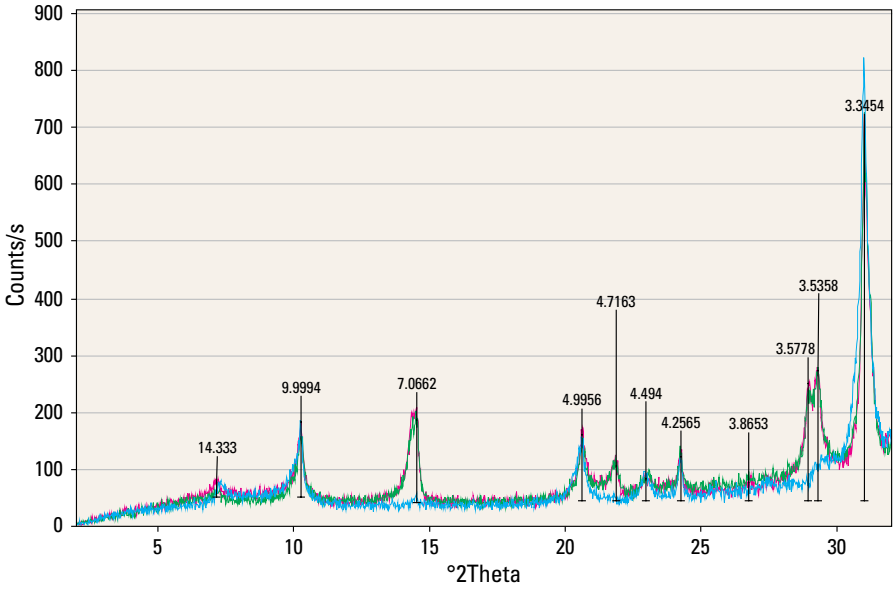

Figure A4.2 Example of typical XRD traces for the <2 µm fraction of Mersey estuary sediment: sample M167, 0–10 cm. Red = air-dried; green = glycolated; blue = heated to 550 ºC.

Figure A4.3 Example of typical XRD traces for the <0.5 µm fraction of Mersey estuary sediment: sample M42, 0 cm. Blue = air-dried; green = glycolated; red = heated to 550 ºC.

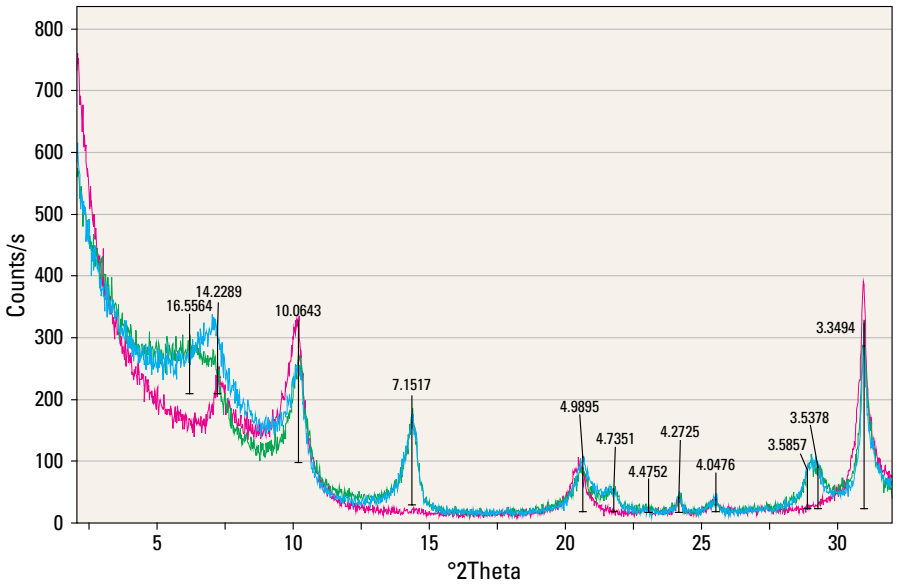

Figure A4.4 Example of typical XRD traces for the <0.5 µm fraction of Mersey estuary sediment: sample M48, 0 cm. Blue = air-dried; green = glycolated; red = heated to 550 ºC.

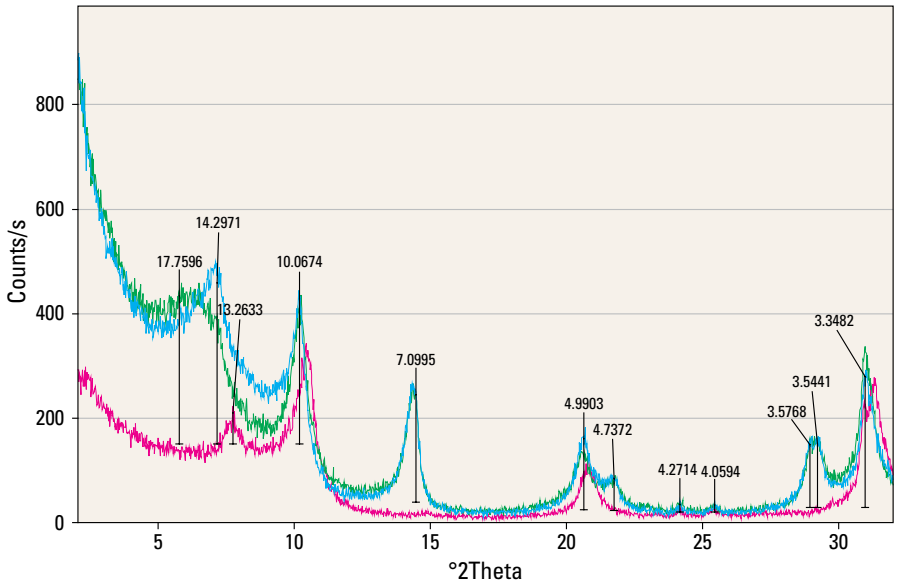

Figure A4.5 Example of typical XRD traces for the <0.5 µm fraction of Mersey estuary sediment: sample M167, 30–40 cm. Blue = air-dried; green = glycolated; red = heated to 550 ºC.

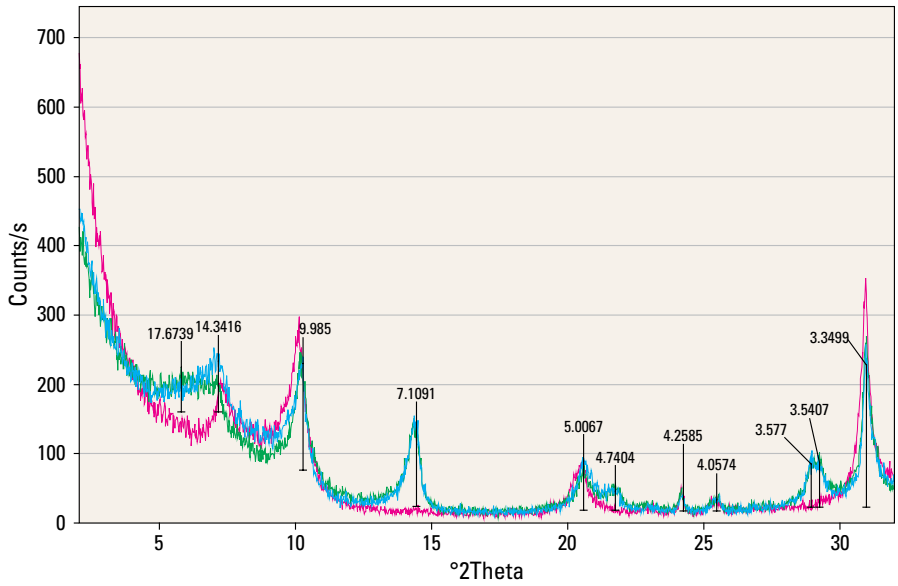

Figure A4.6 Comparison of air-dried XRD tra ces for sample M42, 0 cm: blue = <2 µm; green = <0.5 µm.

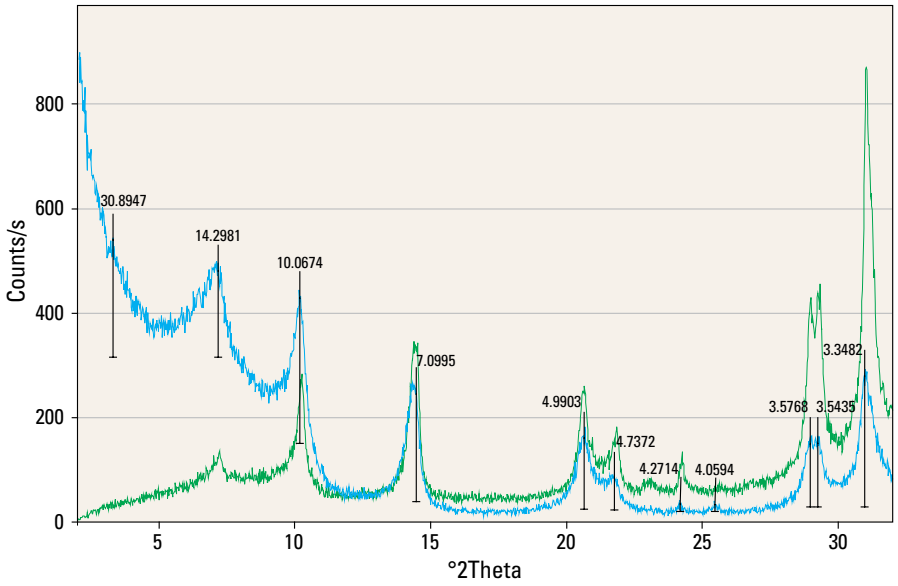

Figure A4.7 Comparison of air-dried XRD traces for sample M48, 0 cm: blue = <2 µm; green = <0.5 µm.

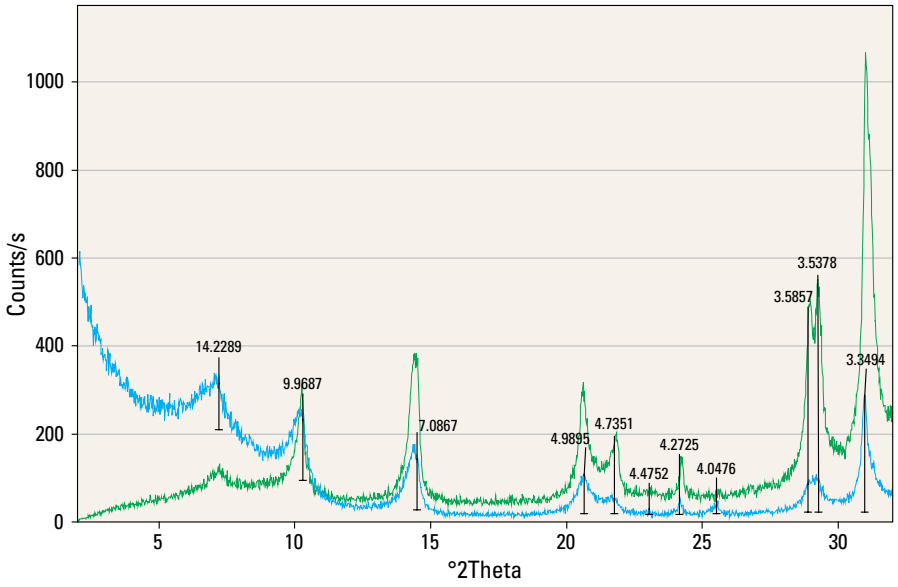

Figure A4.8 Comparison of air-dried XRD traces for sample M167, 30–40 cm: blue = <2 µm; green = <0.5 µm.

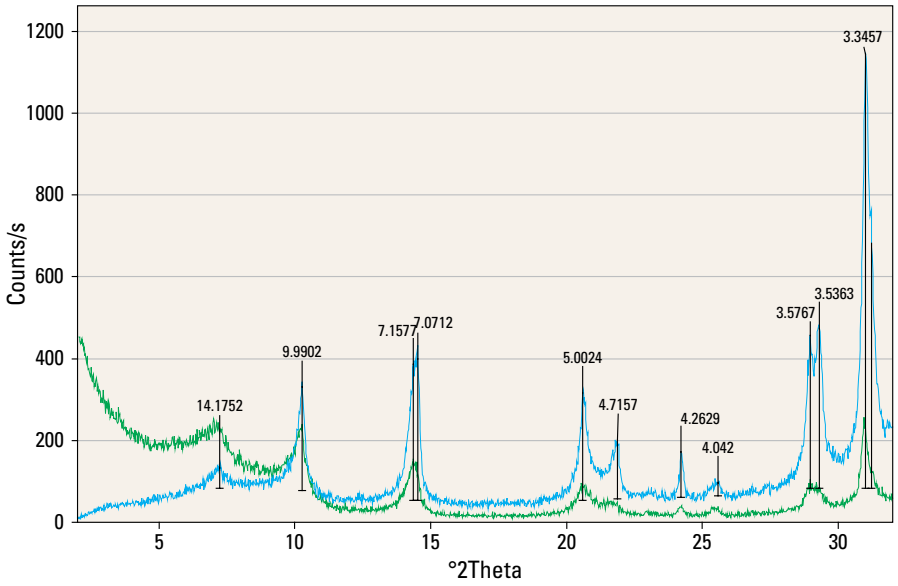

Figure A4.9 Example of typical XRD traces for the <2 µm fraction of river sediment: Irwell Centre River. The catchment of the River Irwell lies entirely in the Carboniferous. Red = air-dried; green = glycolated; blue = heated to 550 ºC.

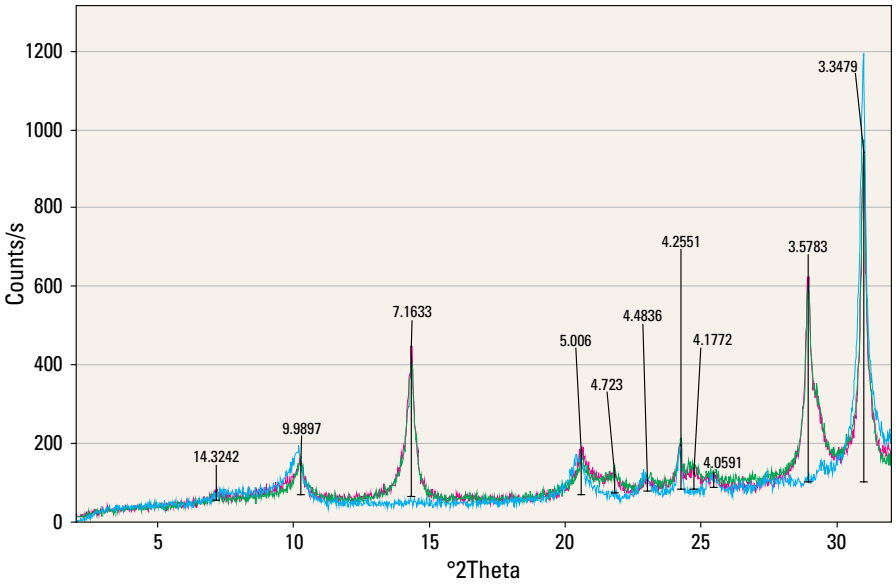

Figure A4.10 Example of typical XRD traces for the <2 µm fraction of river sediment: Weaver. The catchment of the River Weaver lies entirely in the Permo-Triassic Mercia Mudstone Group. Red = air-dried; green = glycolated; blue = heated to 550 ºC.

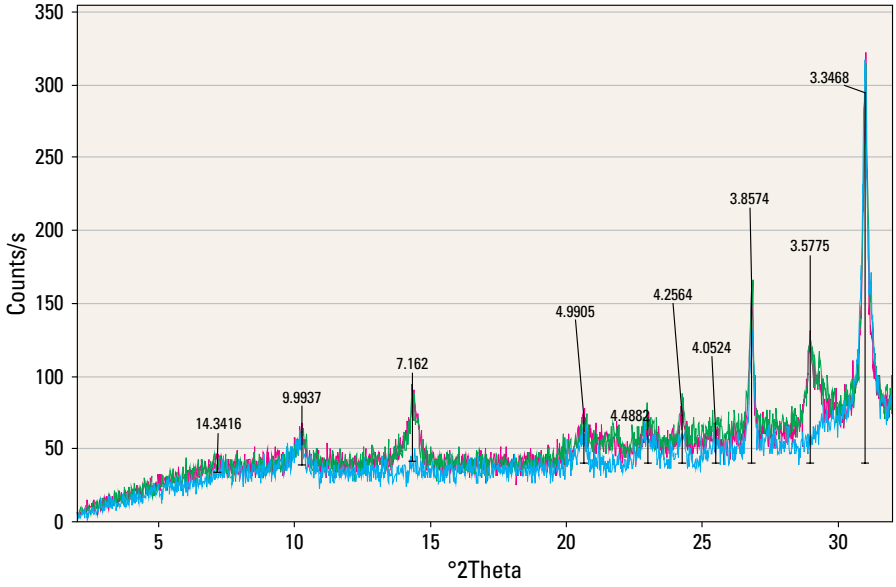

Figure A4.11 Example of typical XRD traces for the <2 µm fraction of river sediment: Mickerbrook. The catchment of the Mickerbrook lies largely in the Permo-Triassic Sherwood Sandstone Group. Red = air-dried; green = glycolated; blue = heated to 550 ºC

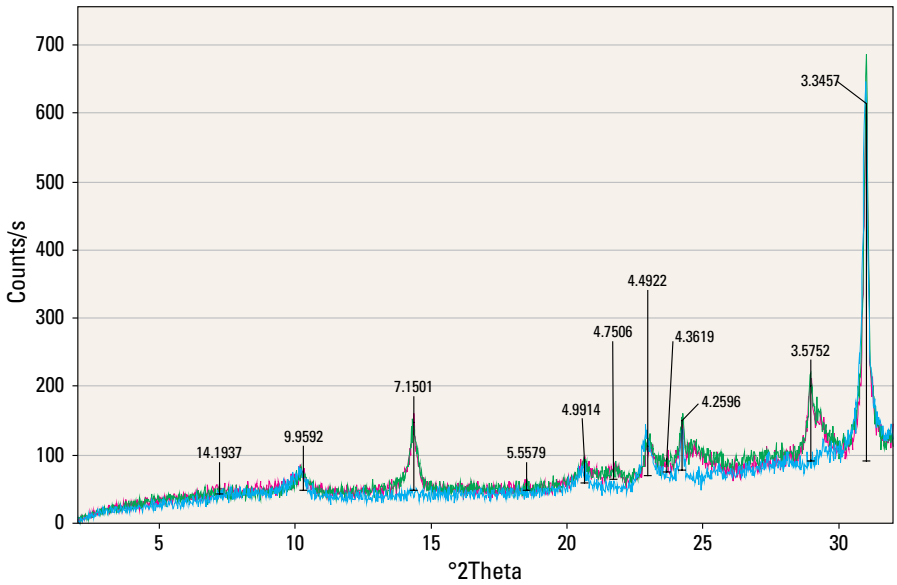

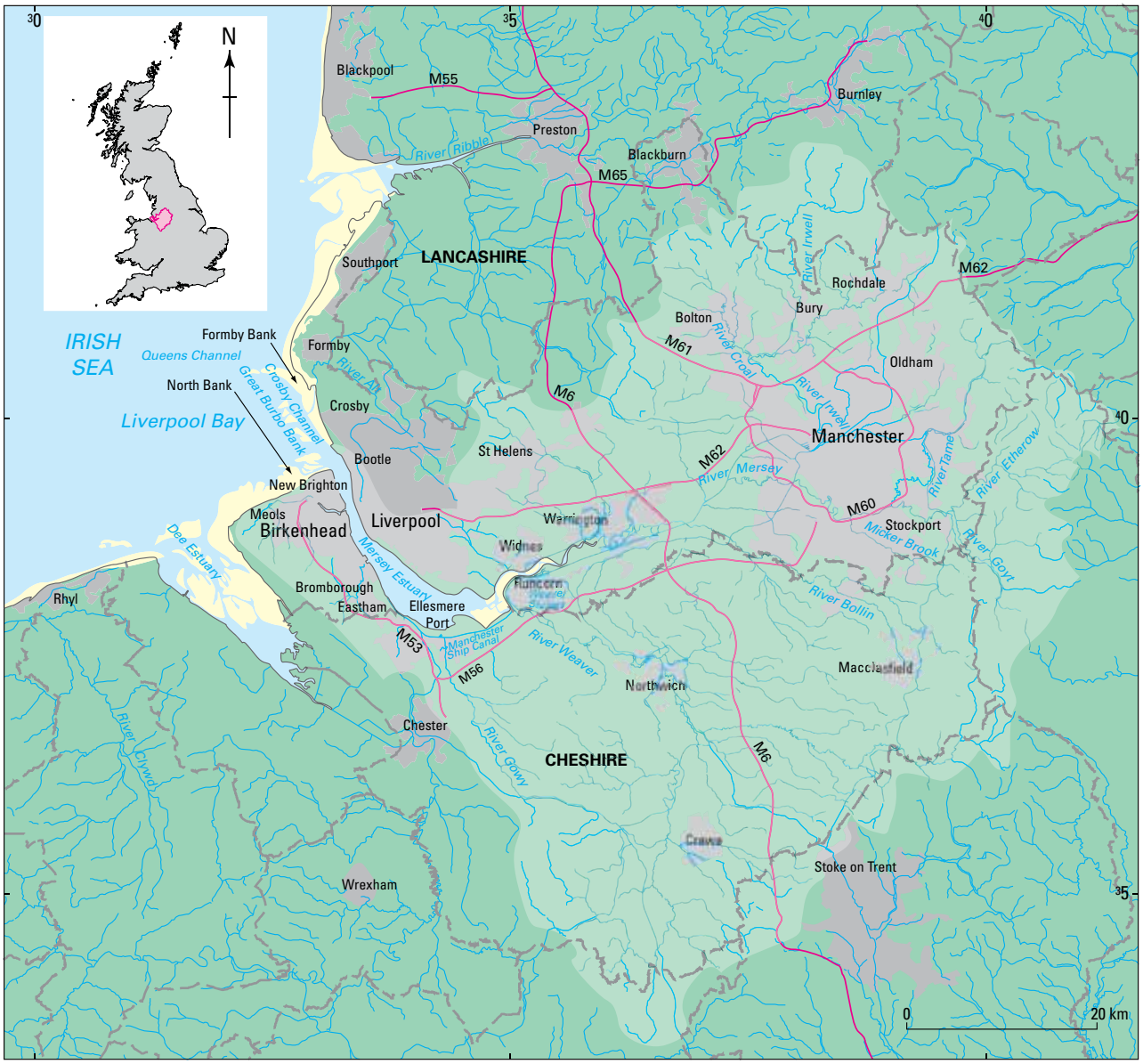

Figure 1.1 Location of the Mersey estuary and catchment basin in north-west England.

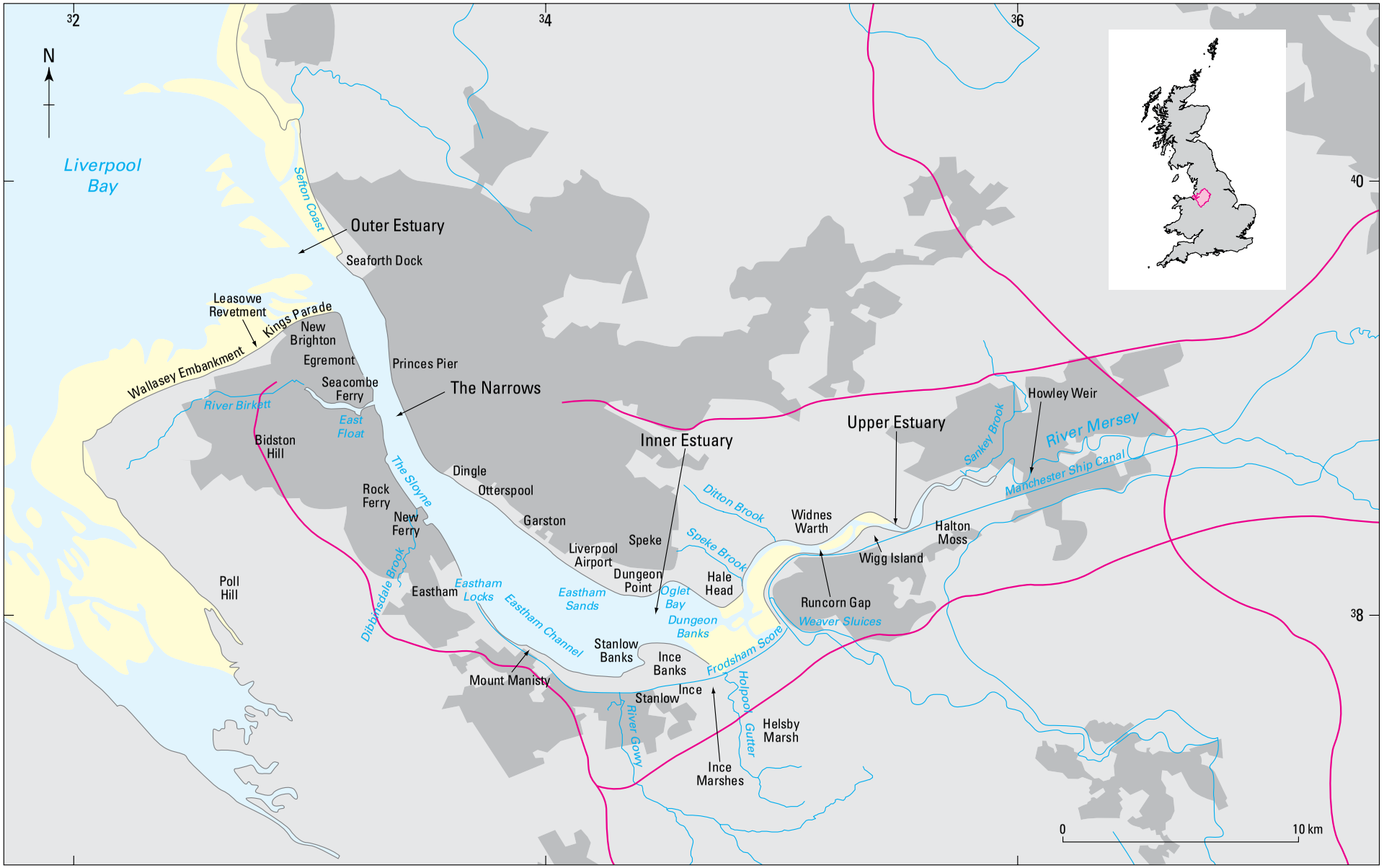

Figure 1.2 Important locations in the Mersey estuary.

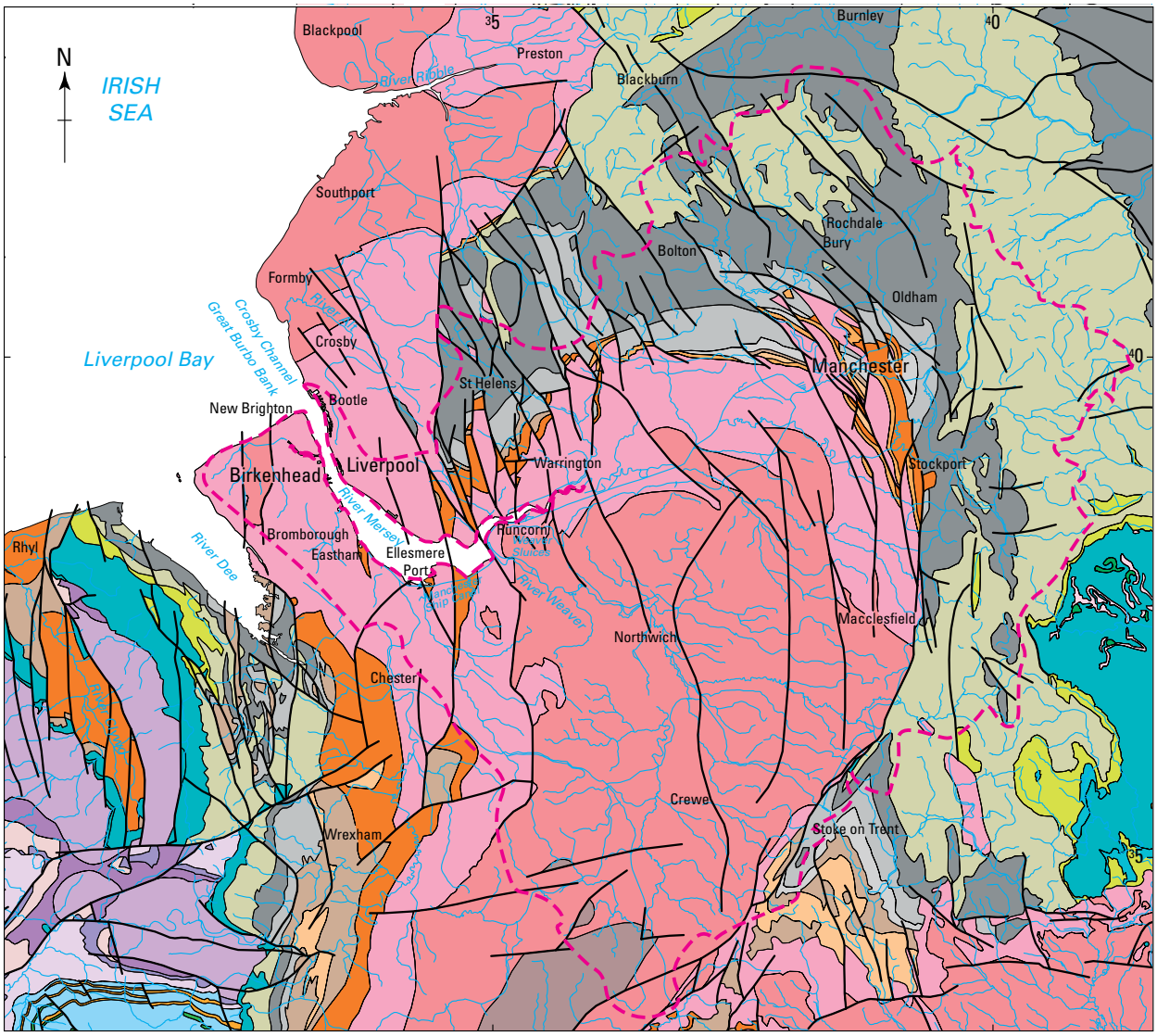

Figure 1.3 Drainage and geology of the Mersey basin (outlined in red).

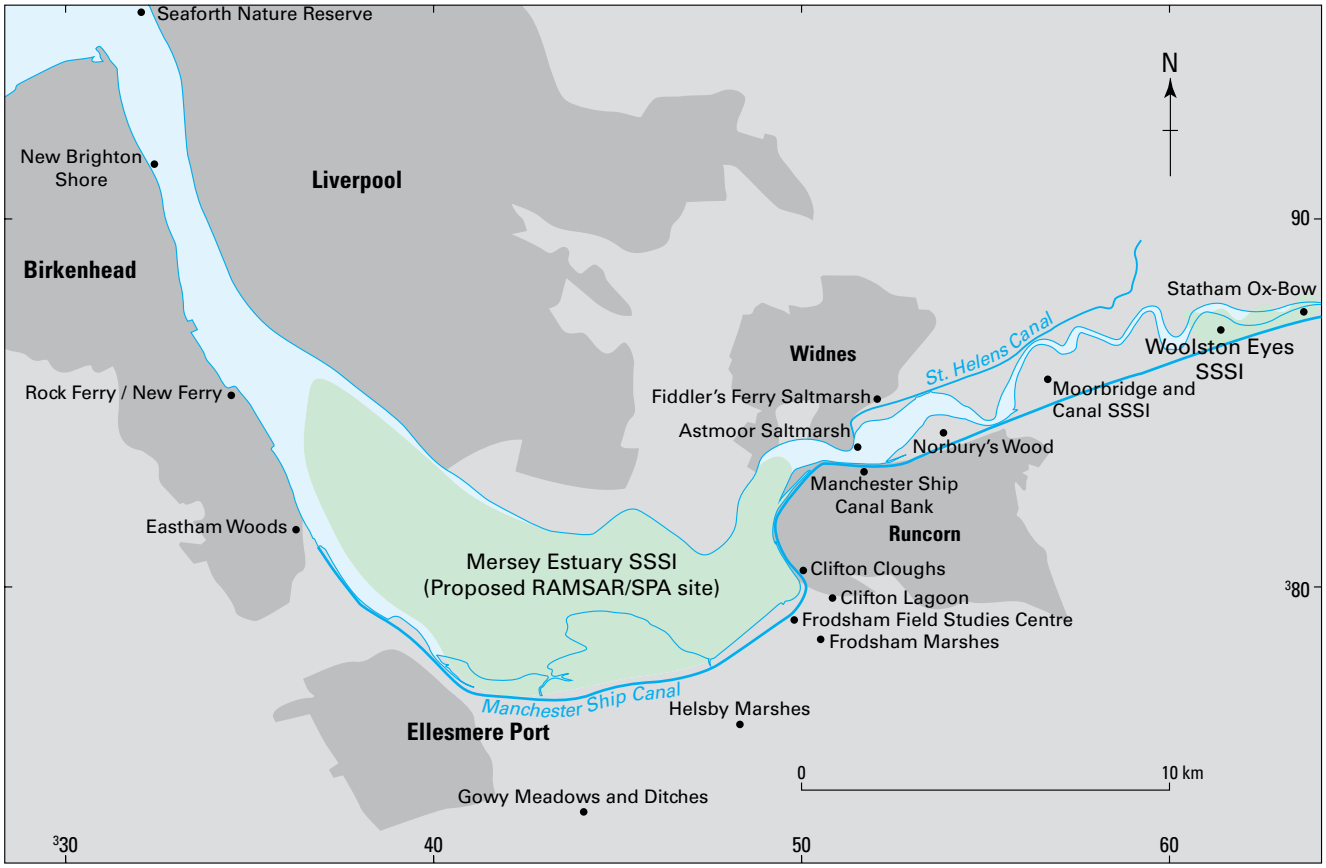

Figure 1.4 Sites of environmental importance in the Mersey estuary.

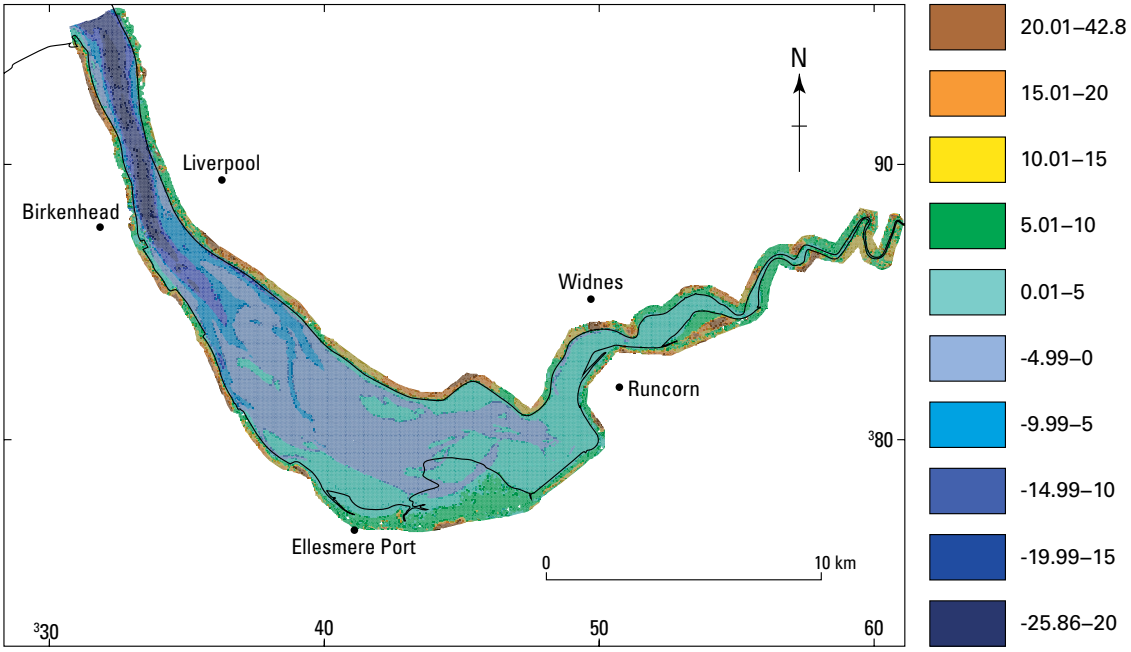

Figure 1.5 Generalised bathymetry of the Mersey estuary. Solid black line represents mean high water on OS maps.

Figure 1.6 Satellite image showing the extent of sand banks in the Inner Estuary at low tide.

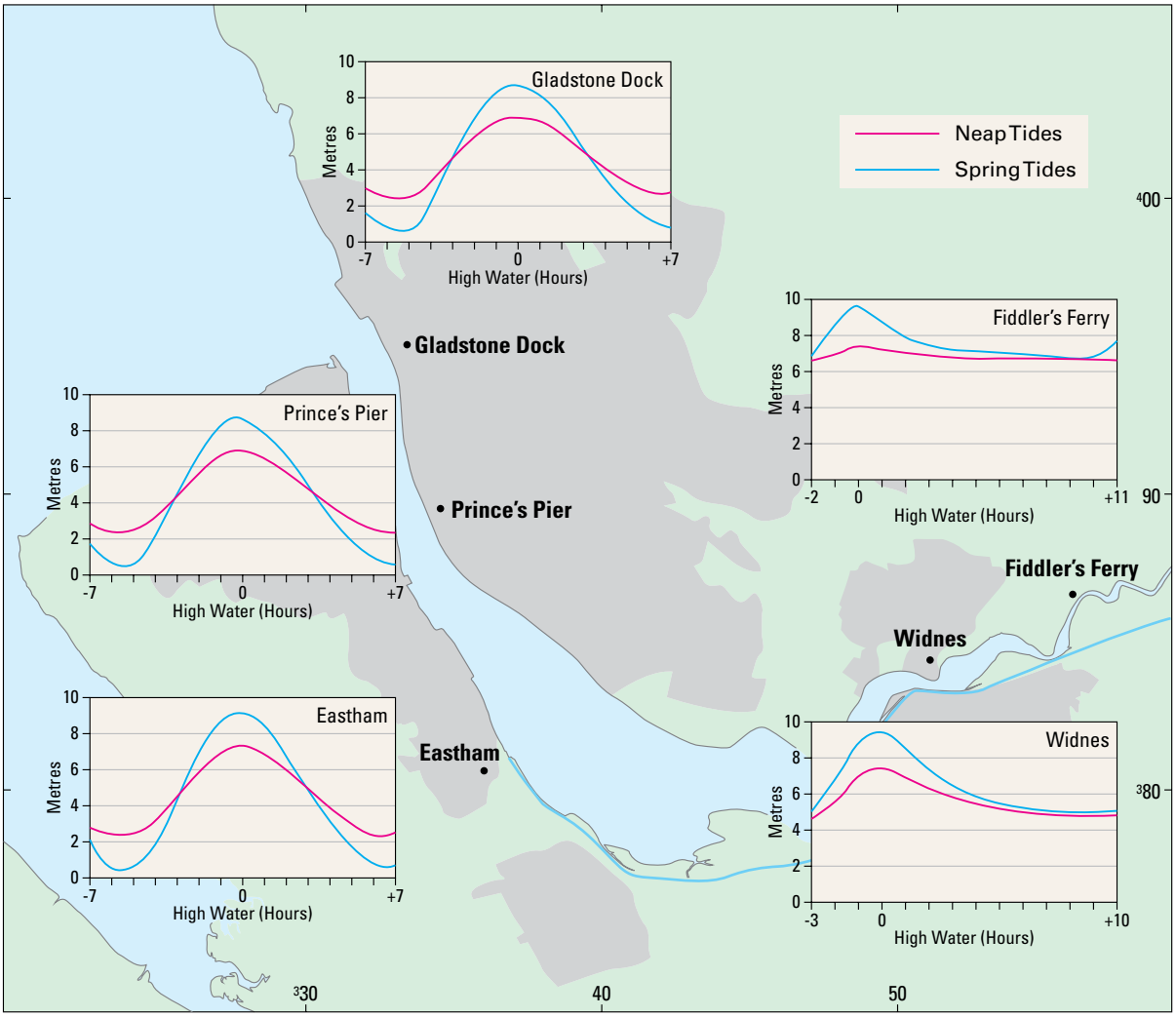

Figure 1.7 Mean spring and neap tidal curves for some Mersey stations.

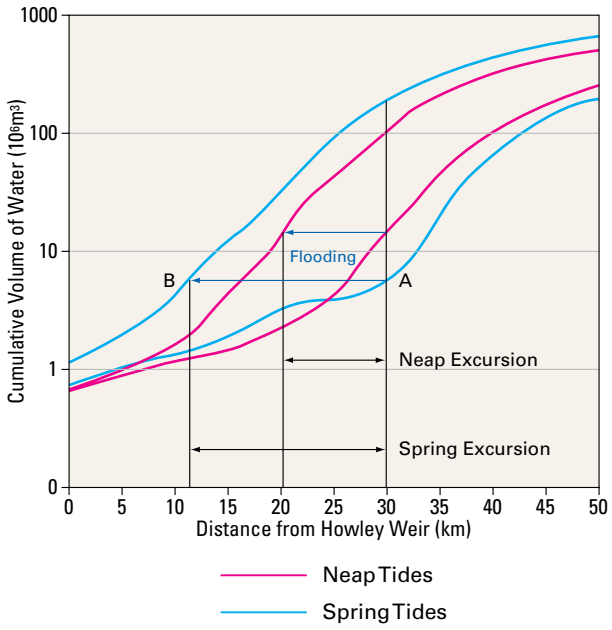

Figure 1.8 Calculated volumes of water seawards of Howley Weir at high and low water for a spring tide of 9.3 m and a neap tide of 7.4 m.

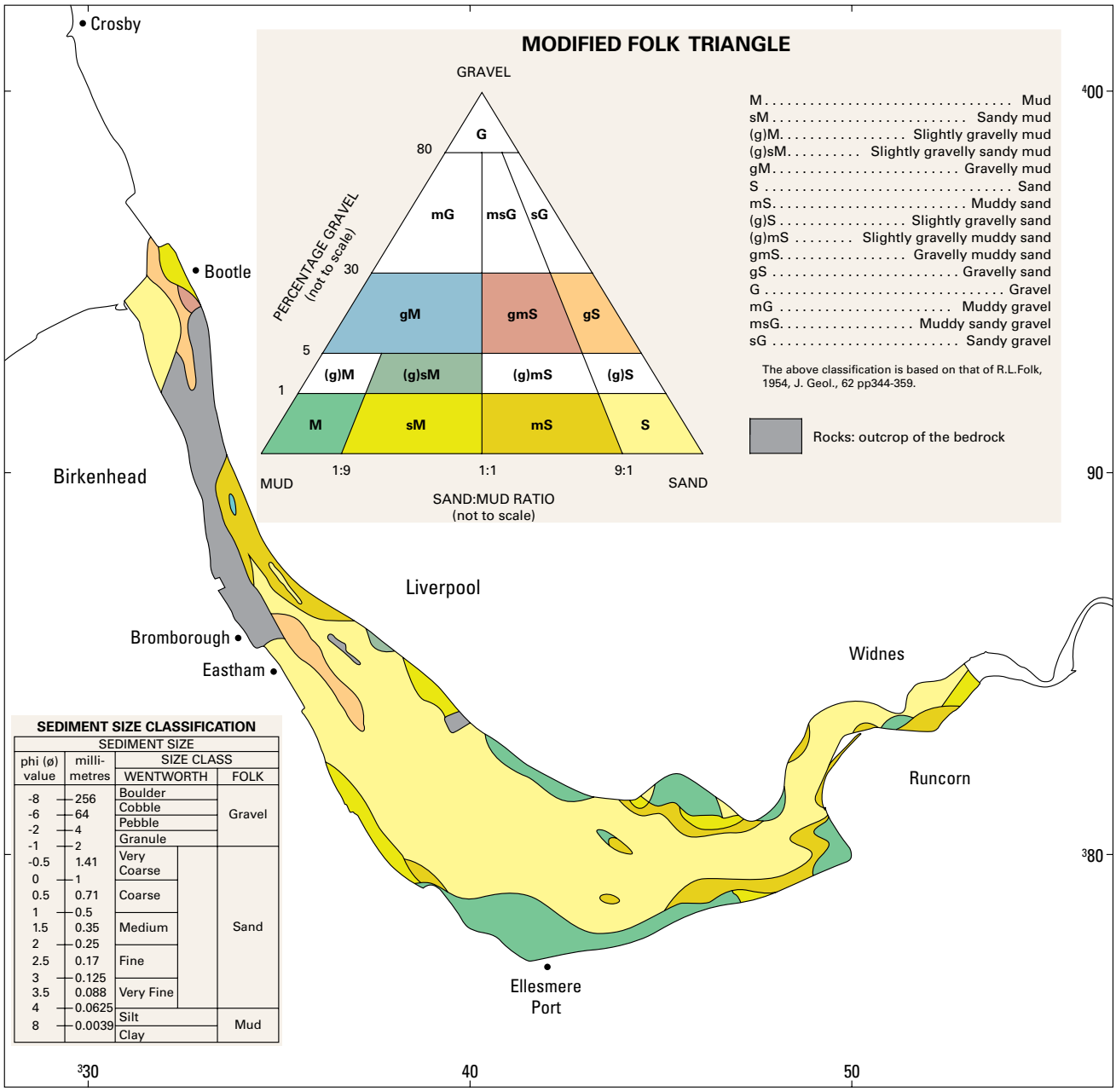

Figure 1.9 Distribution of sediment types in the Mersey estuary.

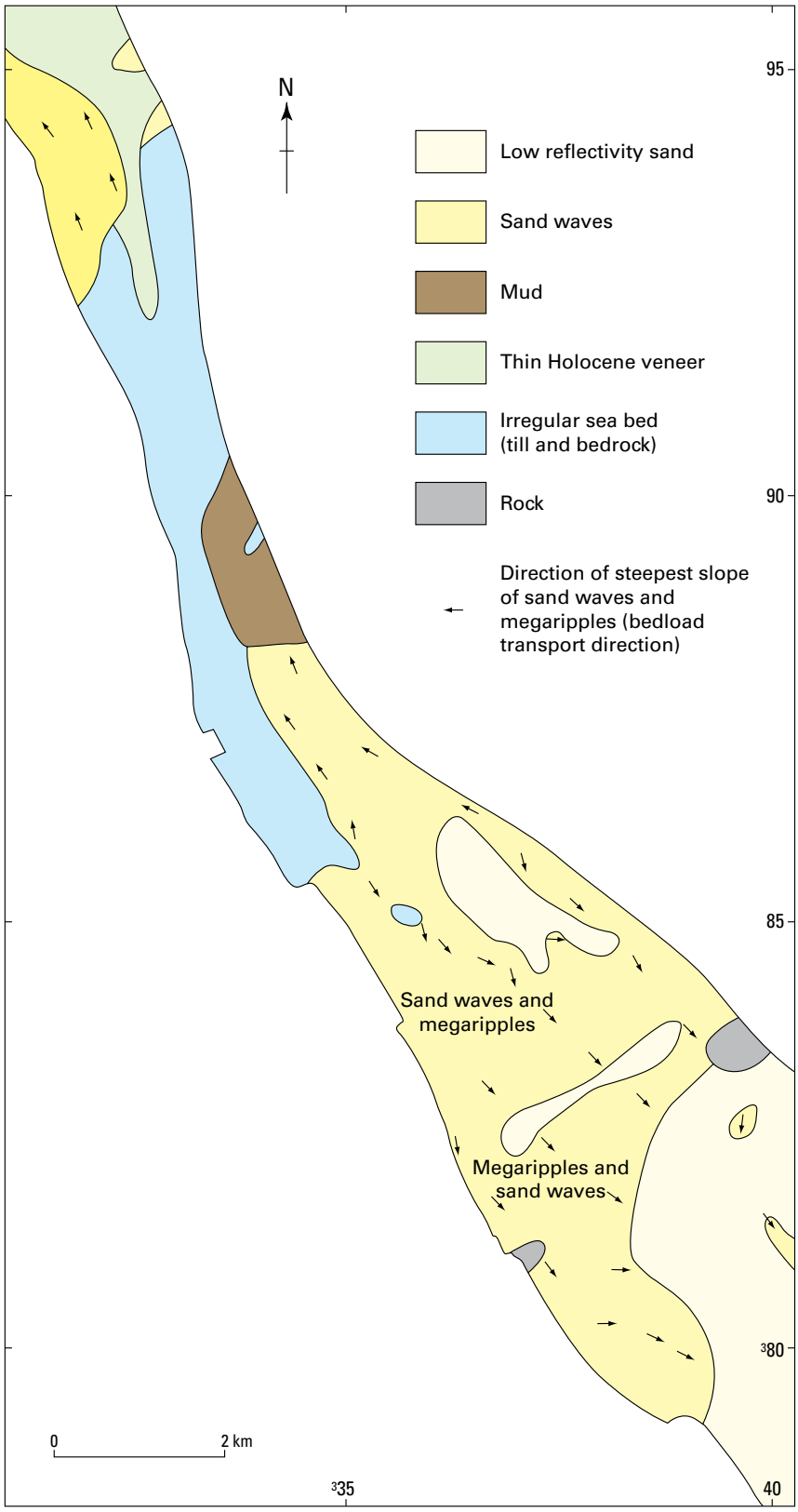

Figure 1.10 Interpretation of side-scan sonar data for the Mersey estuary.

Mersey Low Water Channel 1867-1916

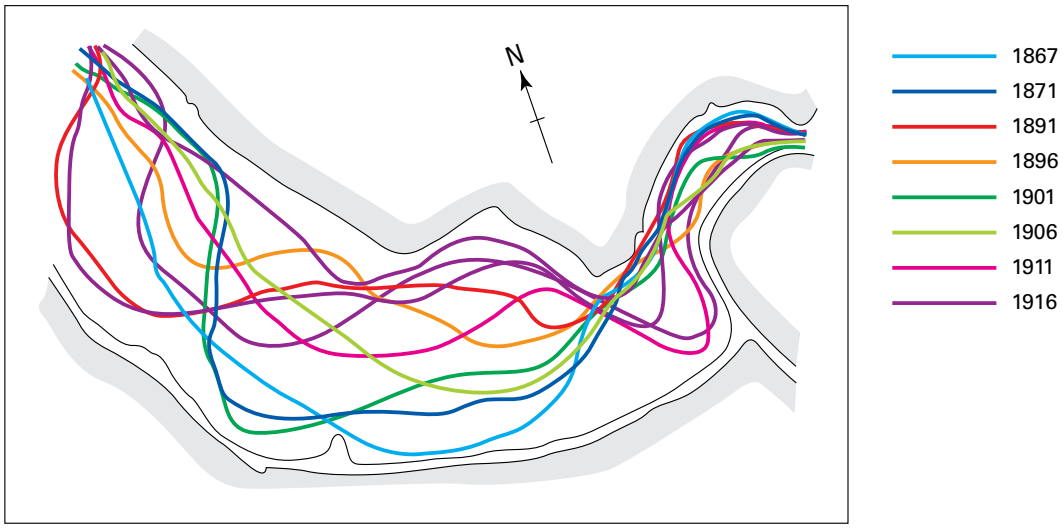

Mersey Low Water Channel 1921-1961

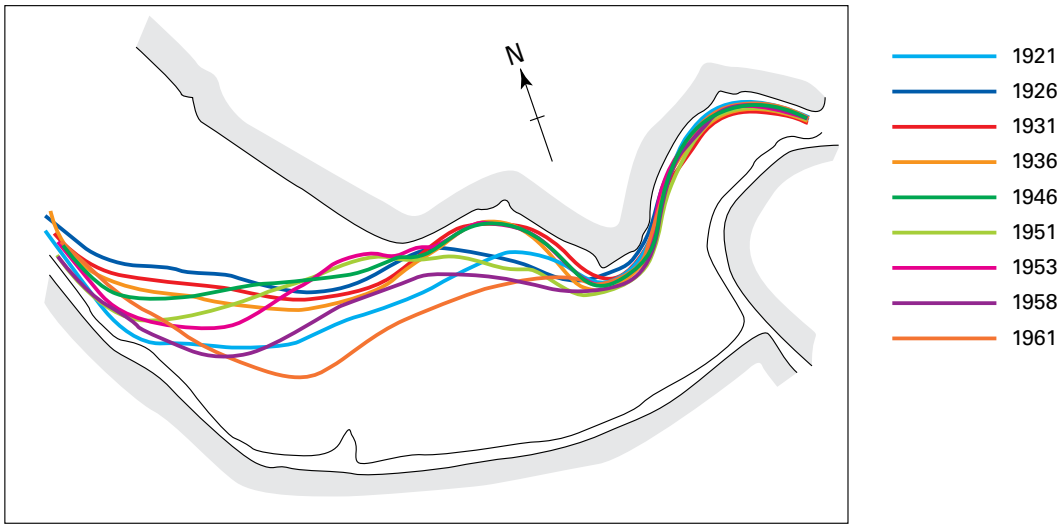

Mersey Low Water Channel 1961-1984

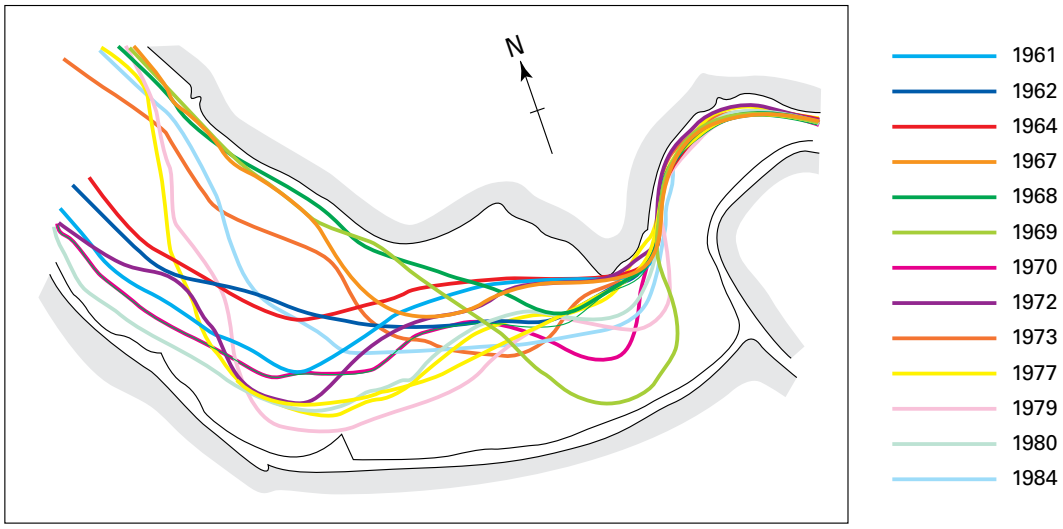

Figure 1.11 Changes in the position of the main channel in the Mersey estuary with time.

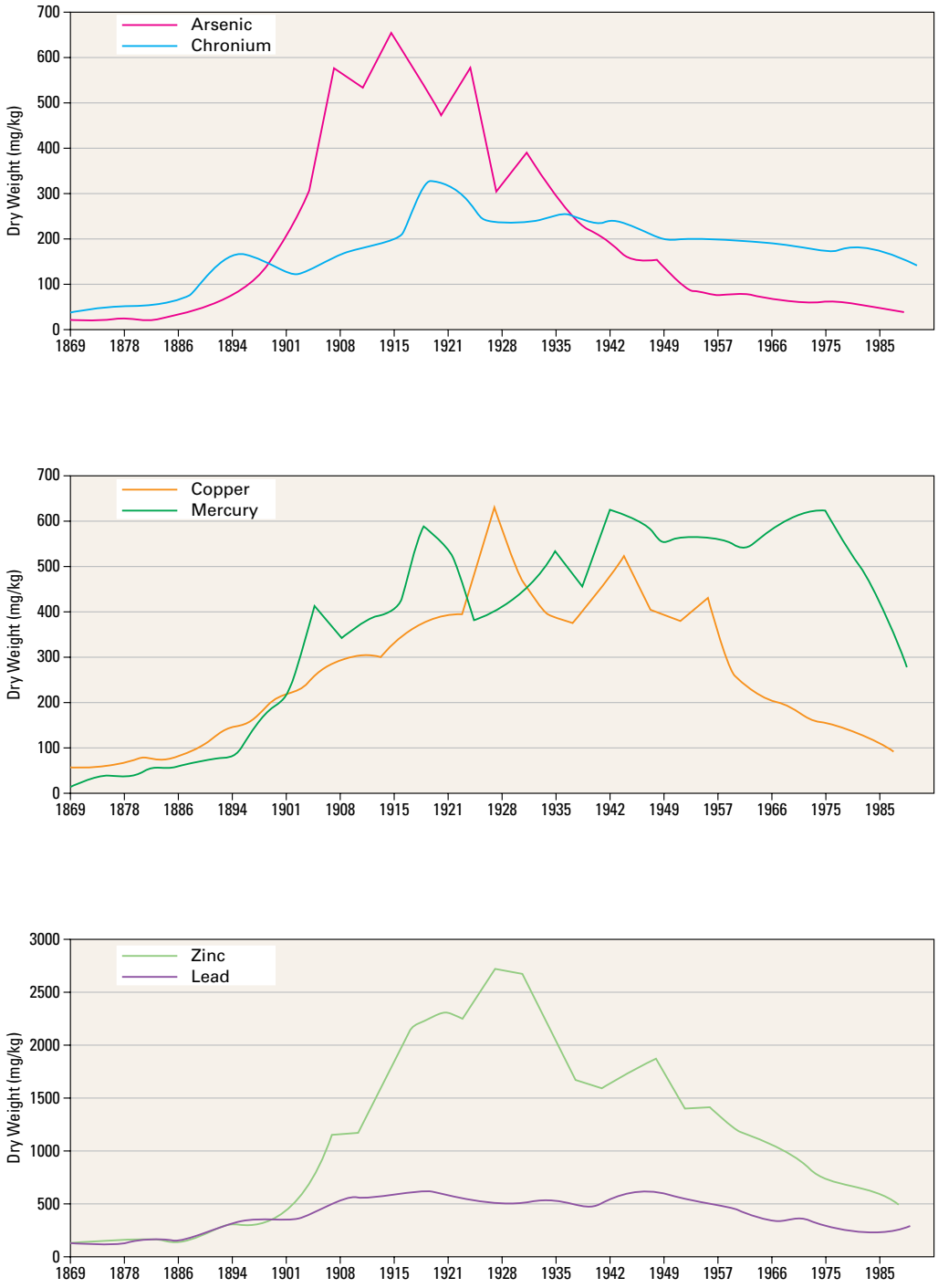

Figure 1.12 Contamination profiles for selected metals in the Widnes Warth core (after NRA, 1995).

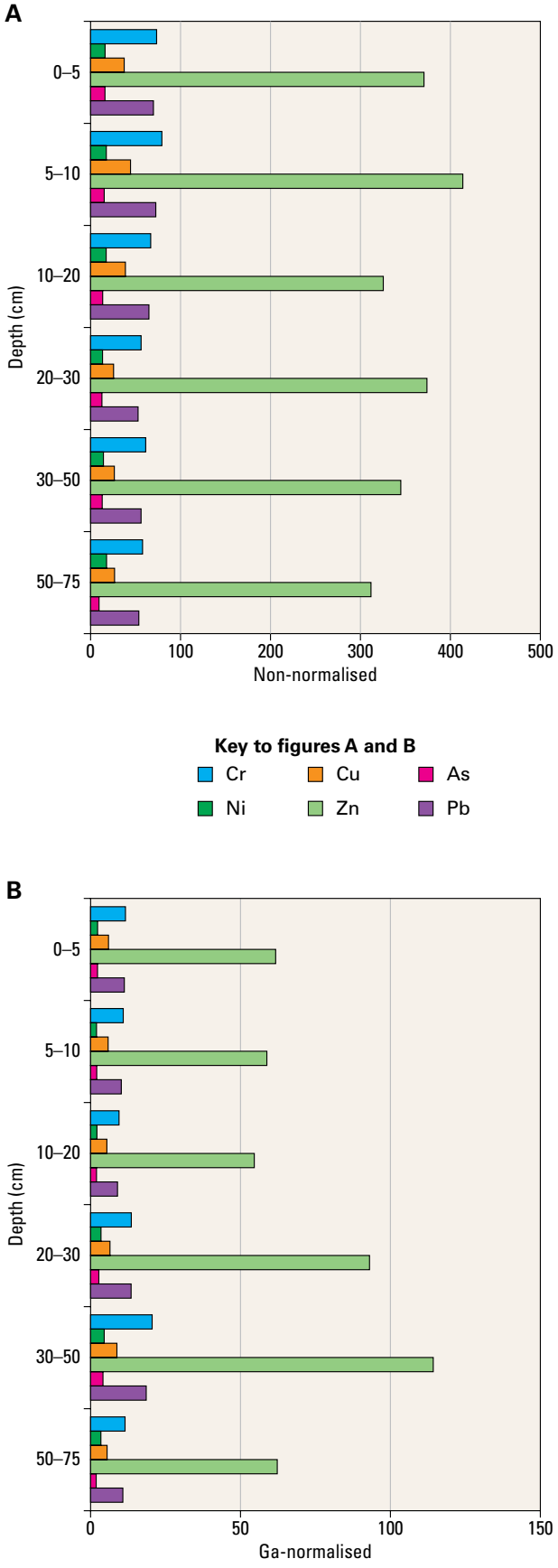

Figure 1.13 Illustration of how normalisation to Ga as a proxy for grain size alters a down-core the profile to show the highest levels of contamination at core depths of 30–50 cm instead of at 5–10 cm in the non-normalised data (after Ridgway et al., 2003).

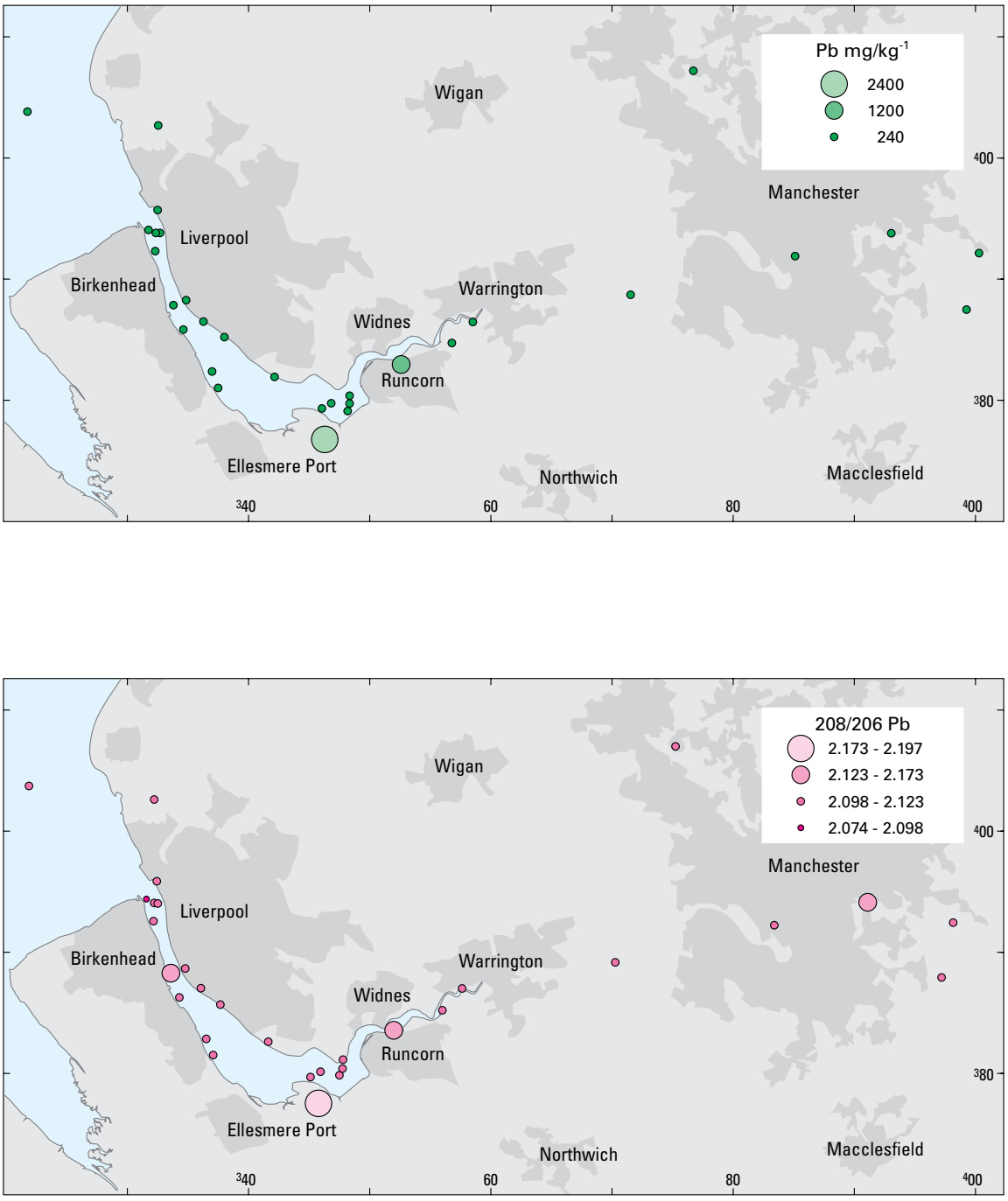

Figure 1.14 Absolute Pb values (top) and Pb isotope data (bottom) for samples from the Mersey estuary (after Ridgway et al., 2003). In the bottom diagram the larger circles depict a greater proportion of petrochemical lead. See text for further explanation.

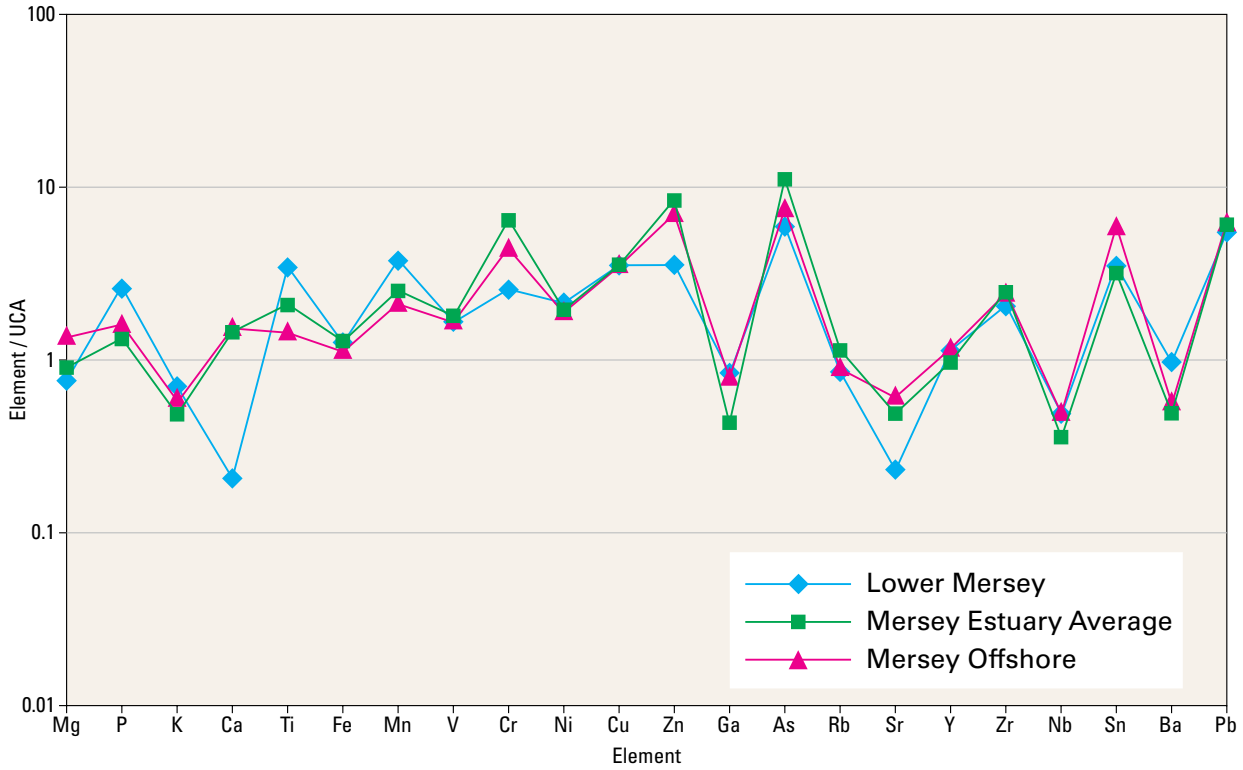

Figure 1.15 Comparison of the average chemistry of 13 surface sediment samples from throughout the estuary (Mersey estuary average) with model values for the catchment (Lower Mersey), based on BGS stream sediment geochemical data (BGS, 1997) (after Ridgway et al., 2003). Values for an offshore sample from Liverpool Bay are also shown.

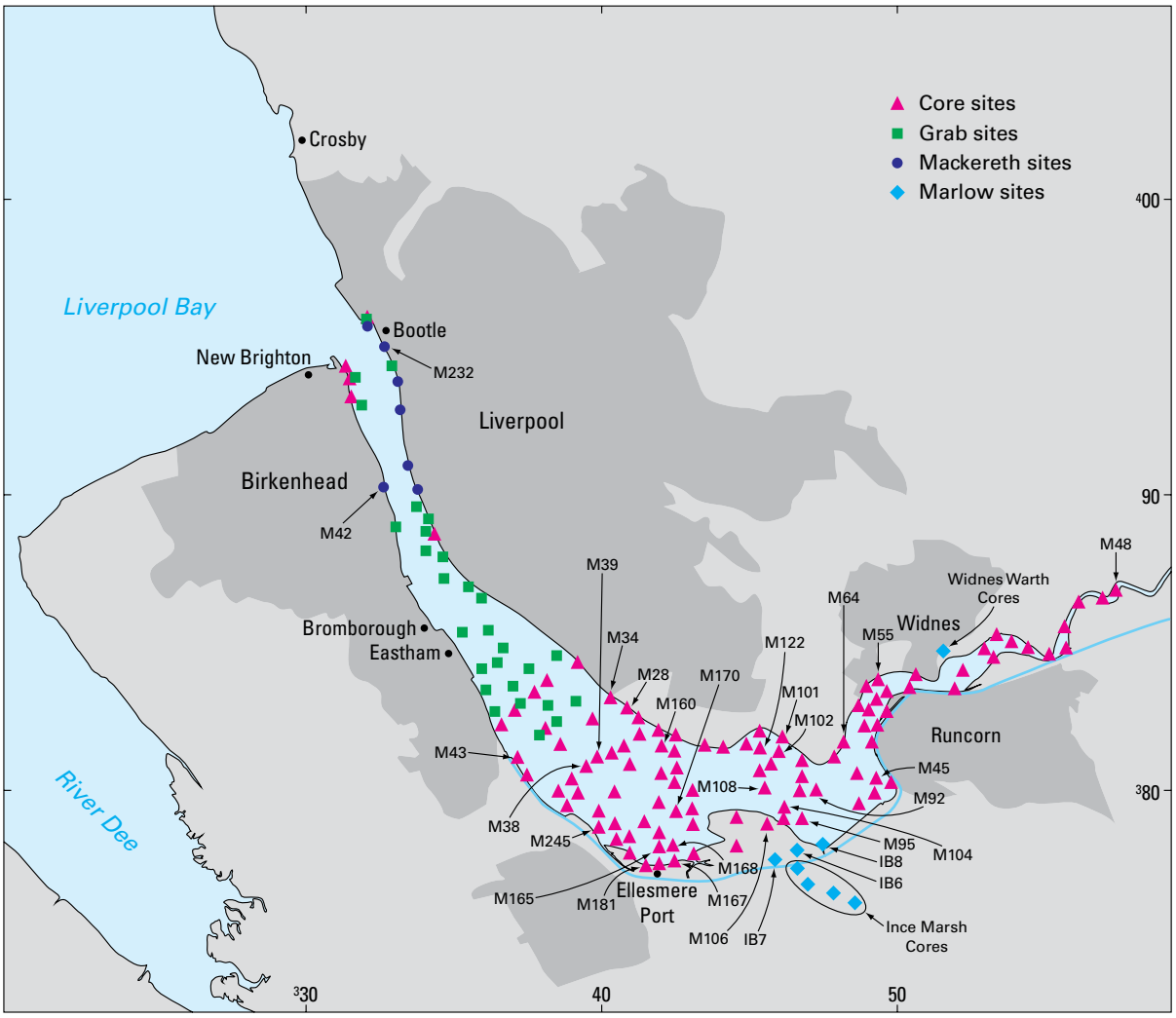

Figure 2.1 Locations of cores and surface samples collected in the Mersey estuary, and described in this report.

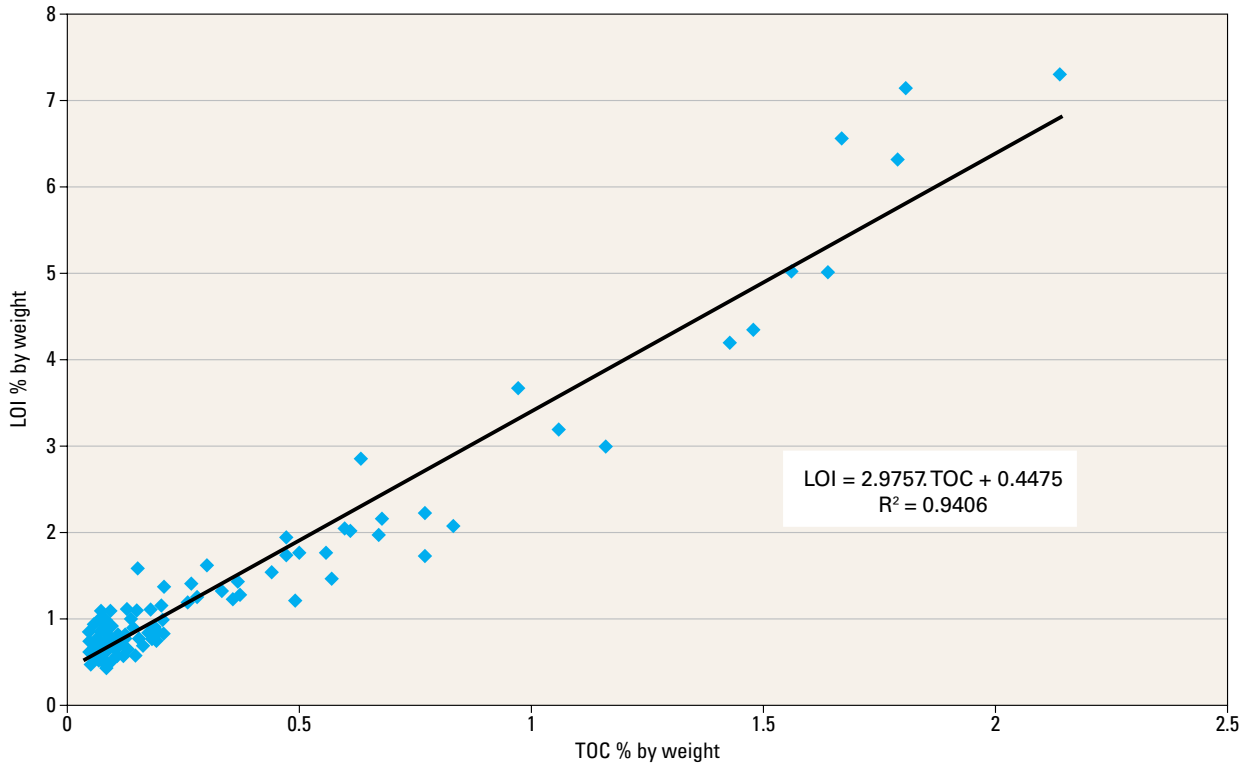

Figure 5.1 Plot of Loss on ignition at 450ºC (LOI) against Total Organic Carbon (TOC), both in weight percent for Mersey samples, showing the strong correlation between the two.

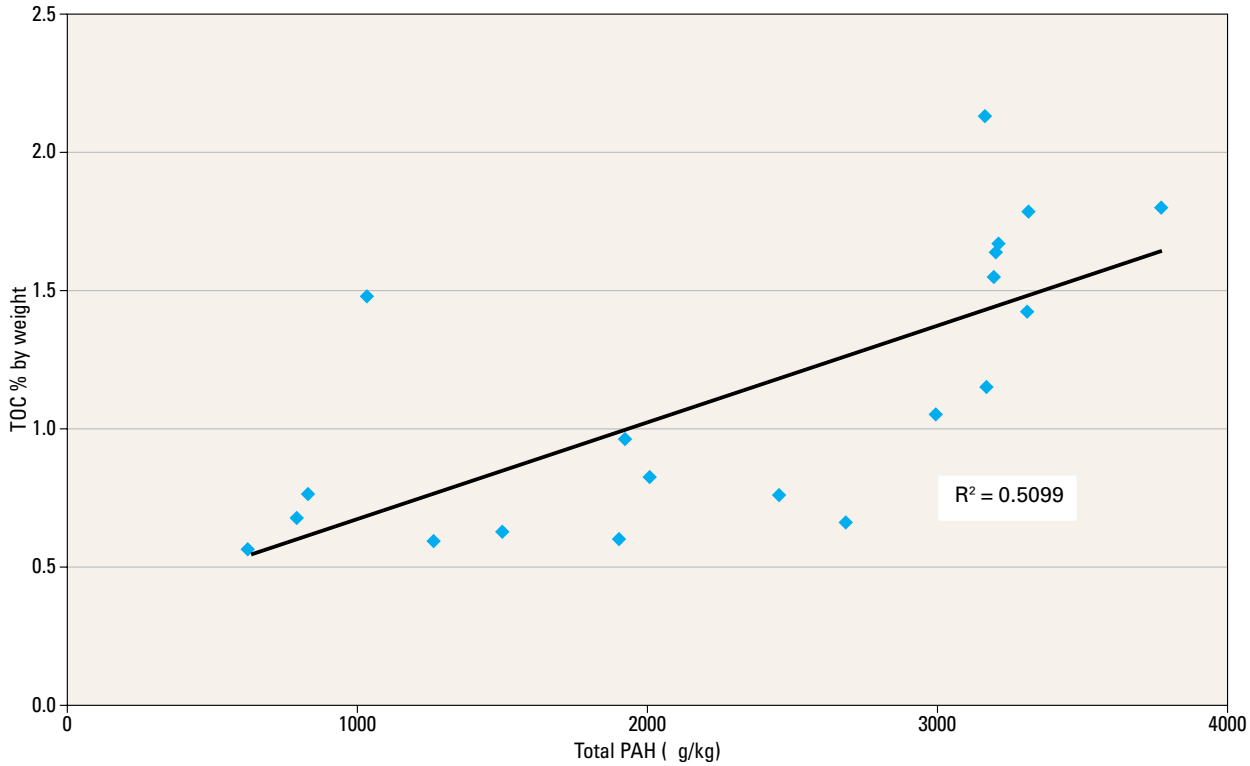

Figure 5.2 Plot of TOC against total PAH concentration for Mersey samples.

Figure 5.3 Contrasting down core PAH profiles for two Mersey cores. Blue = M102, Red = M122.

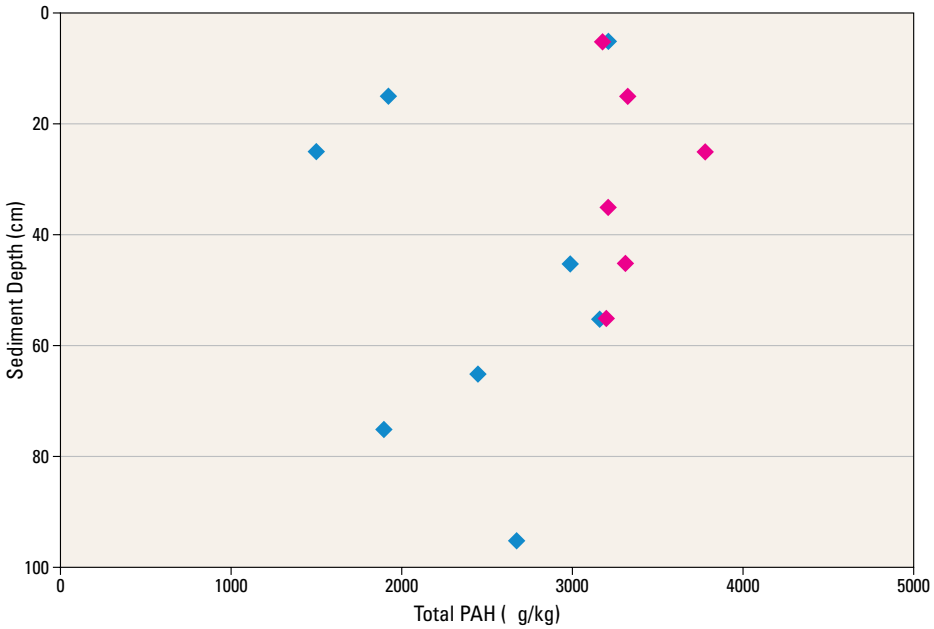

Figure 5.4 Concentrations and distributions of PAHs in Mersey sediments.

Figure 5.4 (cont.) Concentrations and distributions of PAHs in Mersey sediments.

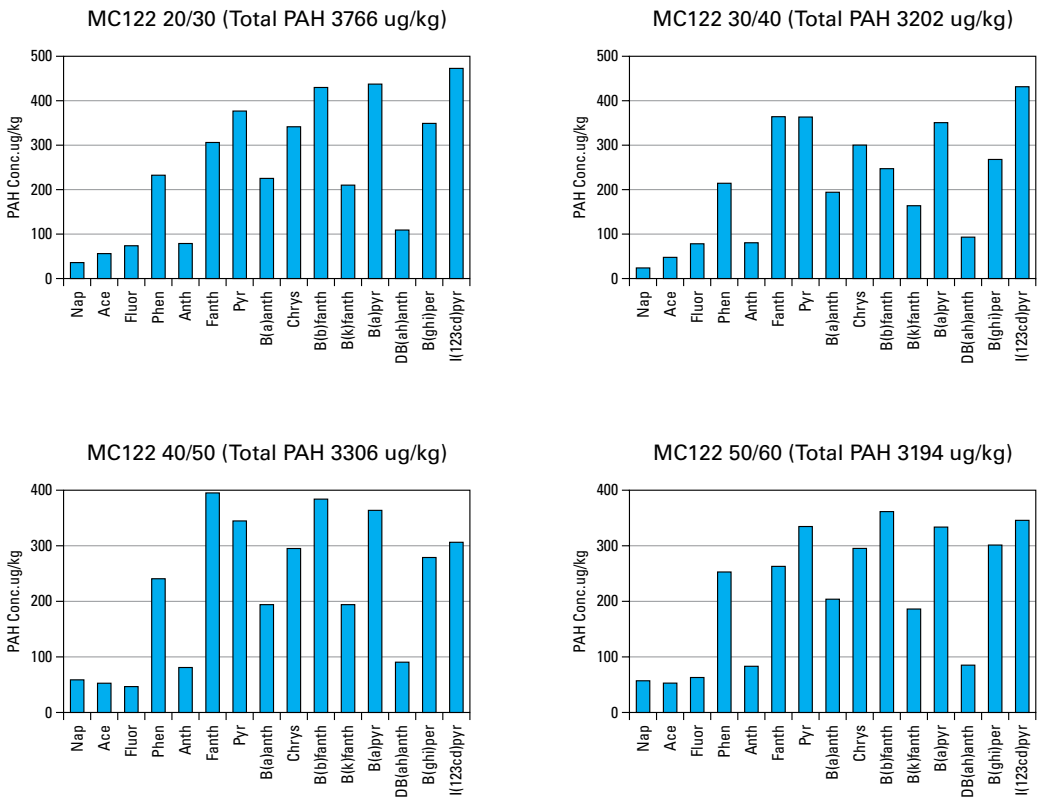

Figure 5.4 (cont.) Concentrations and distributions of PAHs in Mersey sediments

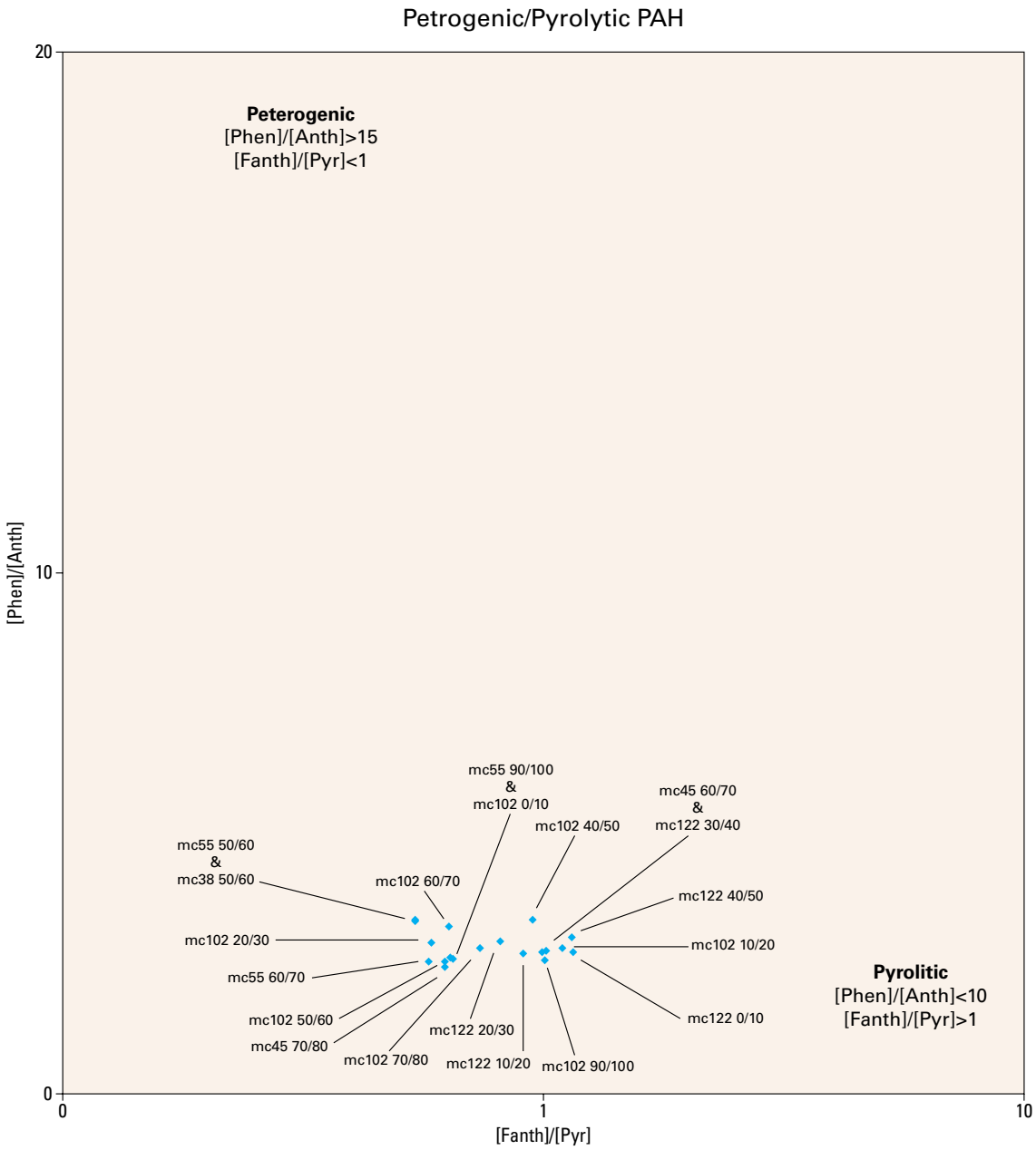

Figure 5.5 Plot of petrogenic versus pyrolitic PAHs for the Mersey samples showing the mainly pyrolitic nature of the analysed samples.

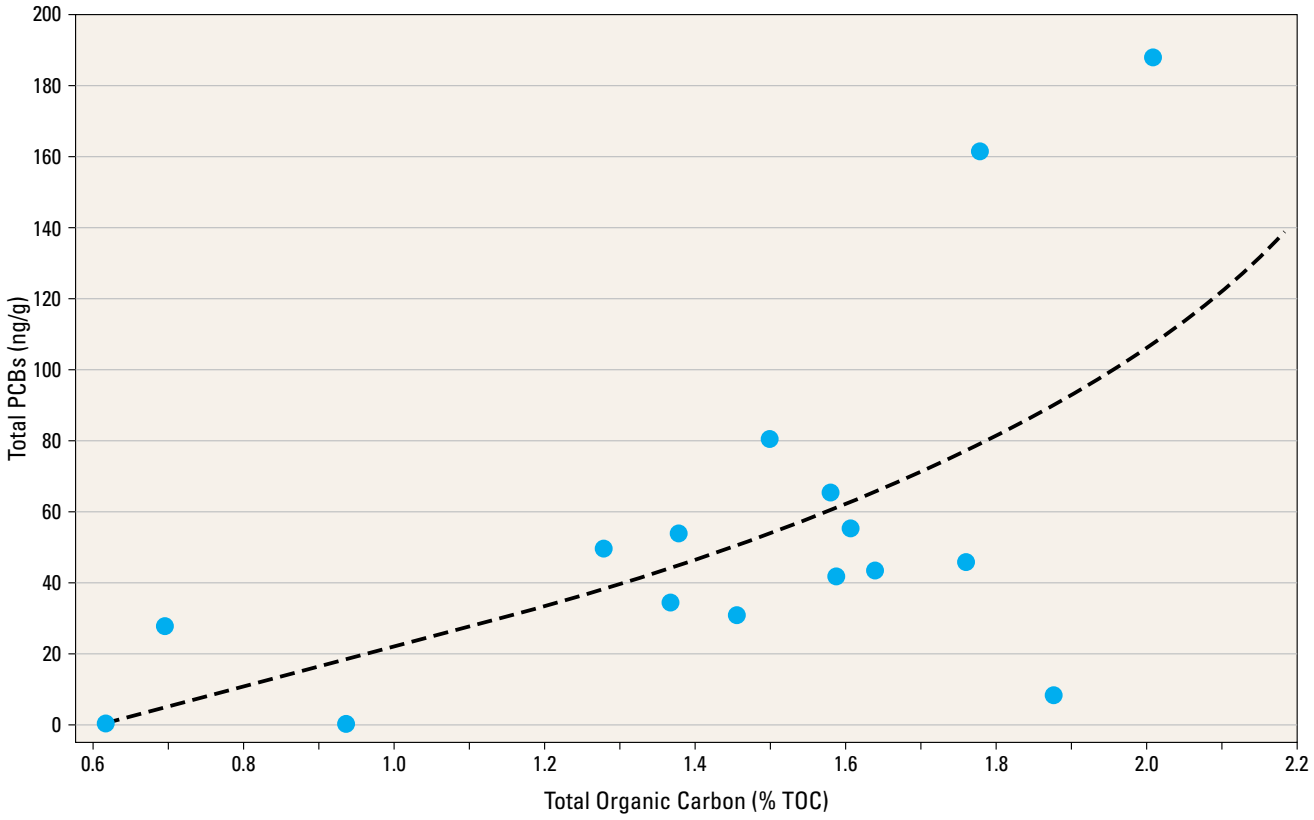

Figure 5.6 Plot of total PCB concentrations from cores M34 and M165 against percentage of organic carbon showing a positive correlation (r2 = 0.44).

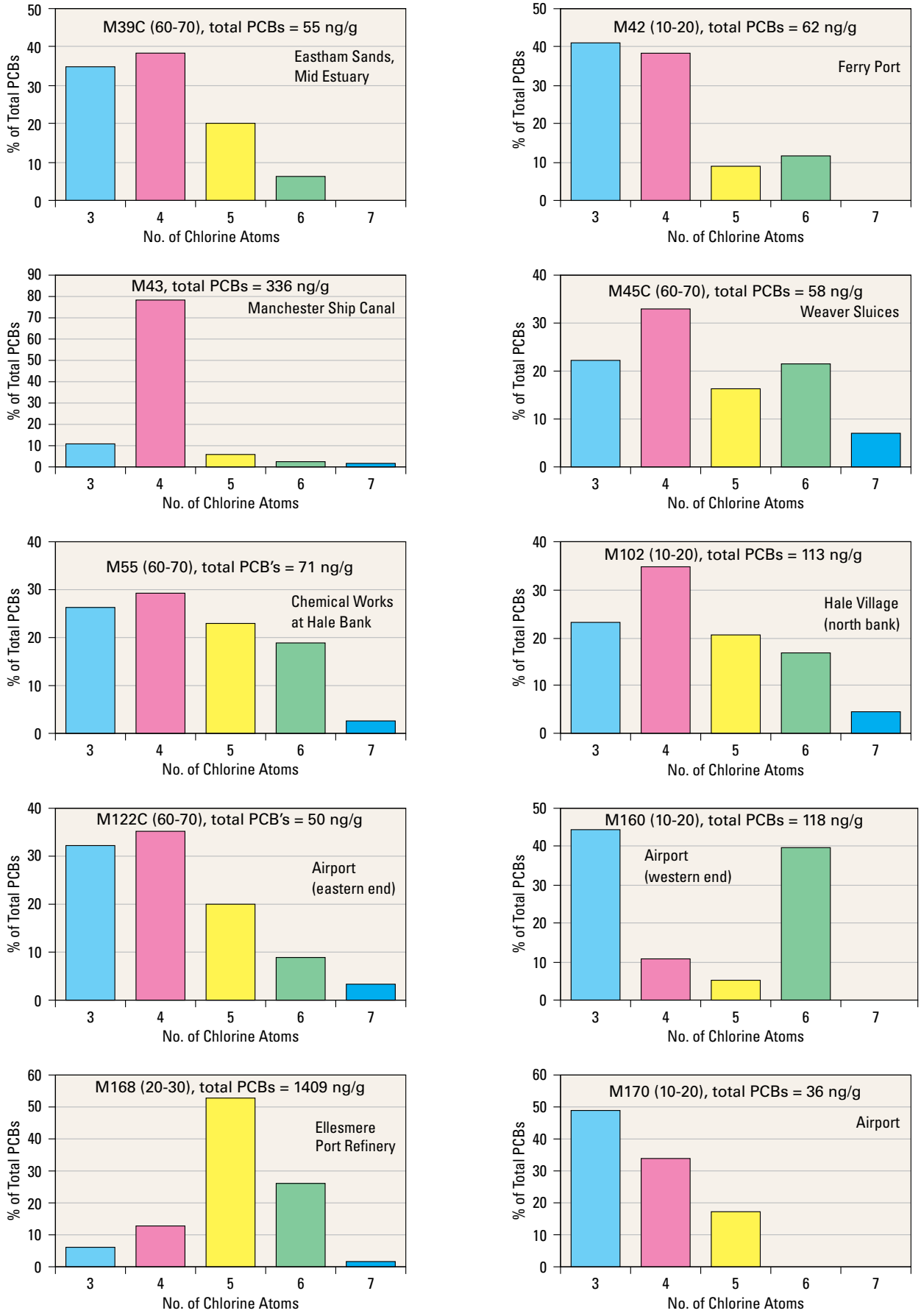

Figure 5.7 Degree of chlorination in PCBs in Mersey estuary sediments from different locations.

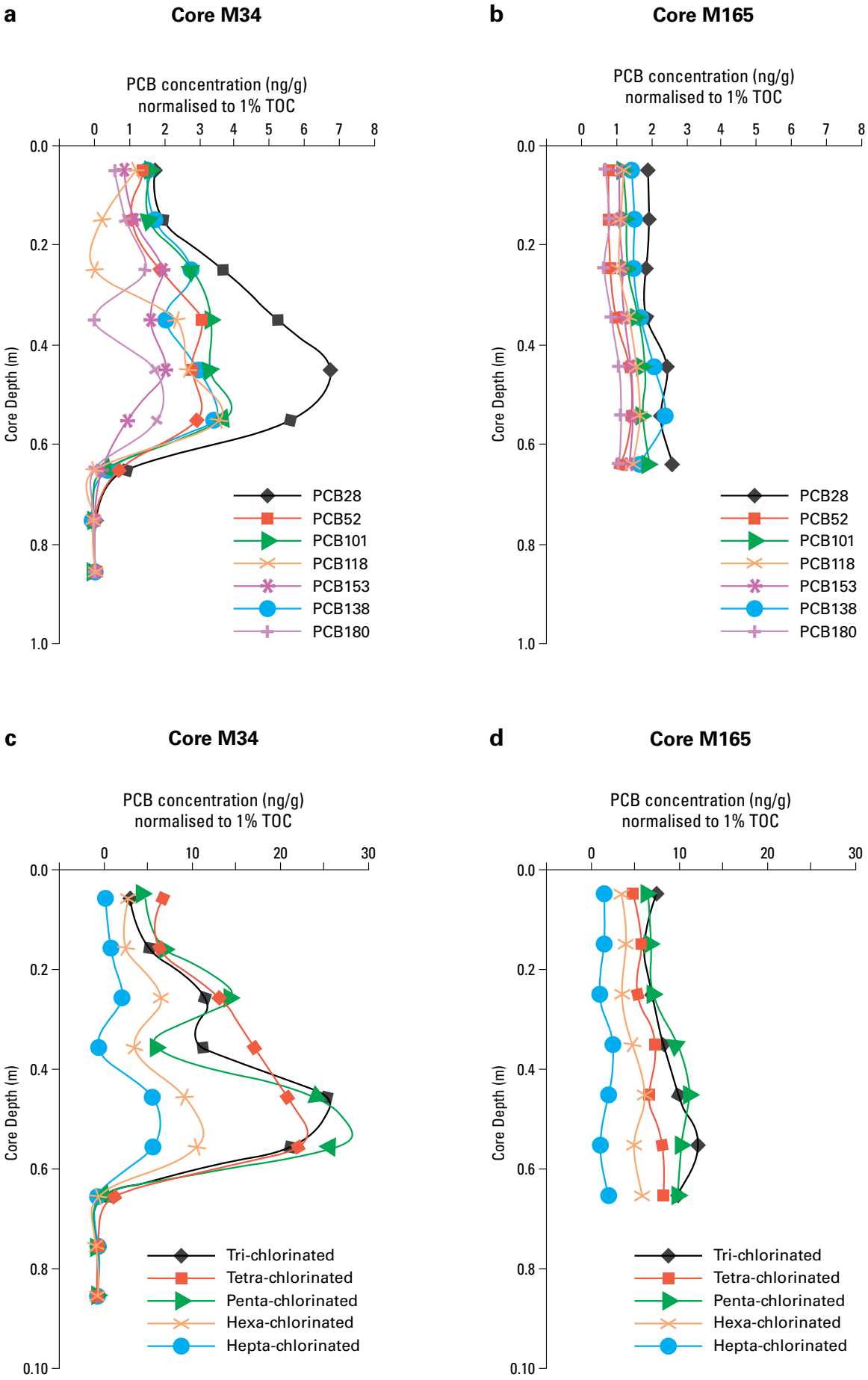

Figure 5.8 PCB concentrations (normalised to 1 per cent TOC) down core. (a) Core M34 individual congeners, (b) Core M165 individual congeners, (c) Core M34 PCBs grouped according to amount of chlorination, (d) Core M165 PCBs grouped according to amount of chlorination. Core M34 shows a distinct peak in PCB concentrations probably as a result of increased PCB use and finally the phasing out of their use. Data presented in Table 5.11 and Table 5.12. See text for further explanation.

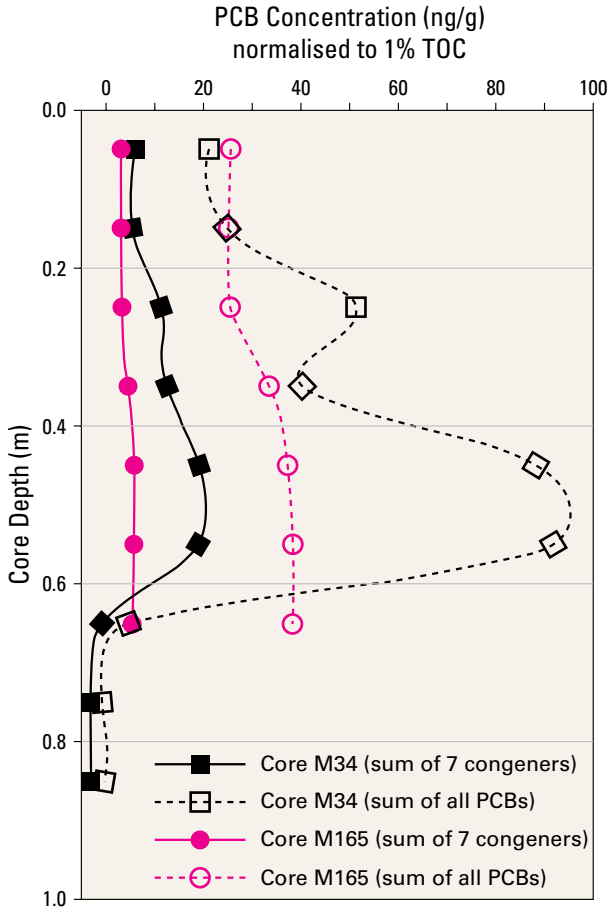

Figure 5.9 Sum of PCB concentrations (normalised to 1 per cent TOC) down core from M34 and M165. Core M34 shows a distinct peak in PCB concentrations probably as a result of increased PCB use and finally the phasing out of their use. Core M165 displays a much smaller increase down core. Data presented in Table 5.11 and Table 5.12. See text for further explanation.

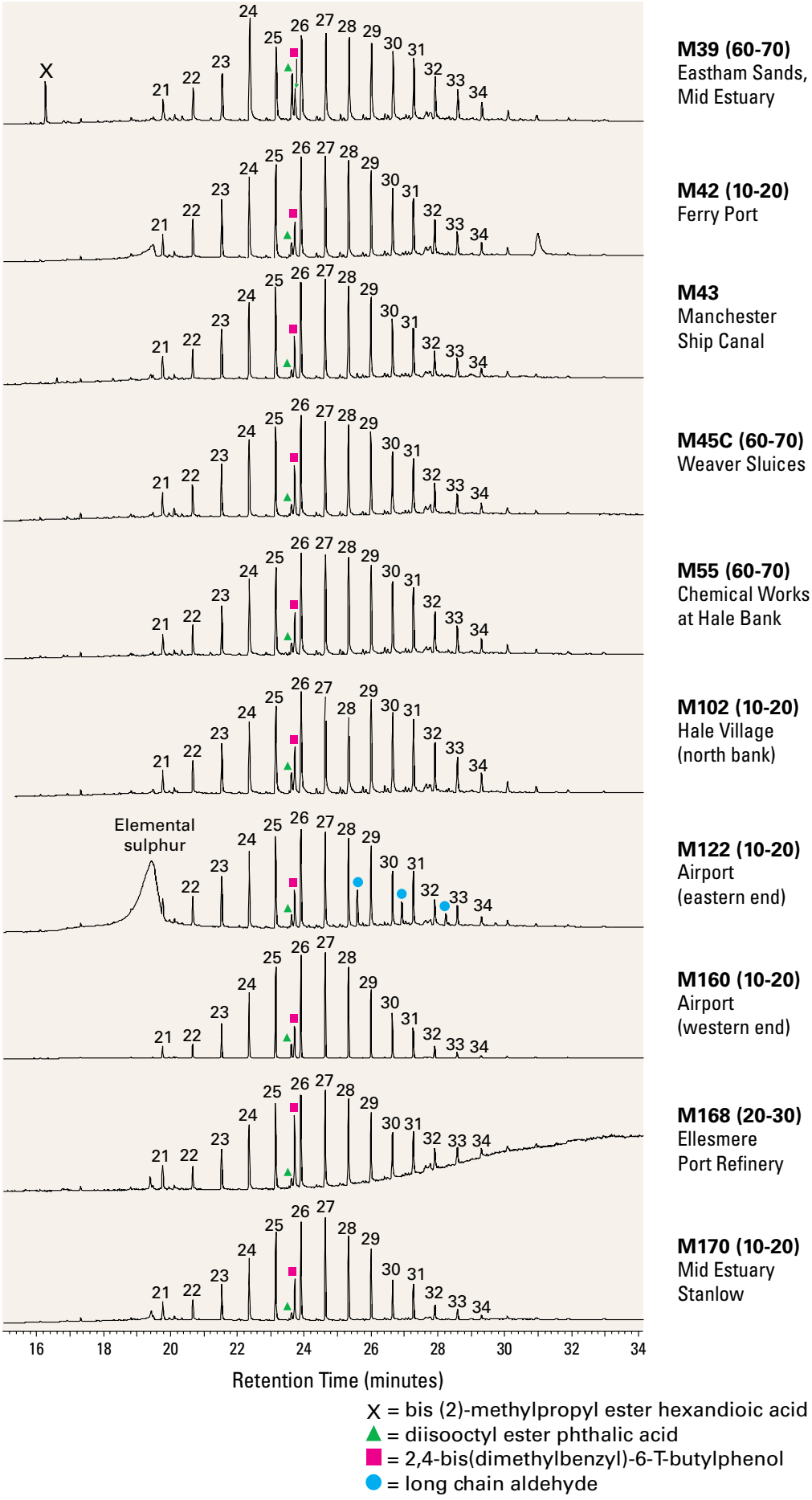

Figure 5.10 Total ion chromatograms of Mersey sediment saturates. n-alkane chain length is given by its number . This shows the distribution of long-chain alkanes. See text for further explanation.

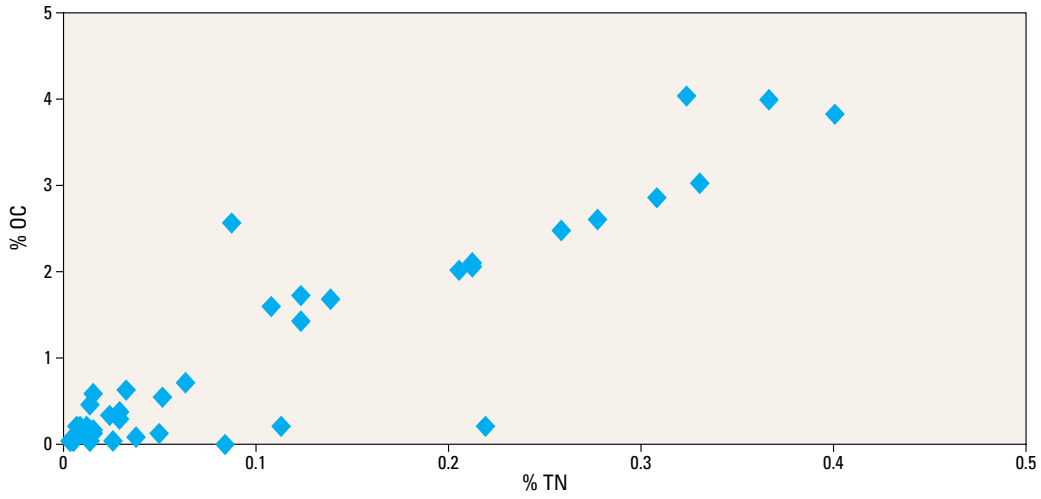

Figure 5.11 Organic carbon (OC) plotted against total nitrogen (TN) content for surface sediments from Mersey estuary. See text for further explanation.

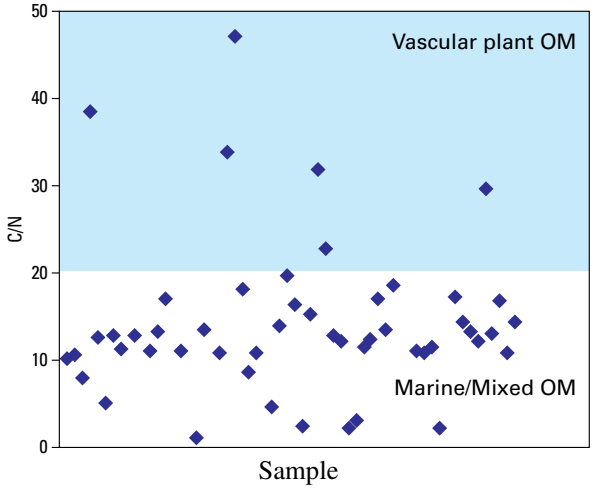

Figure 5.12 Origin of sedimentary organic matter (0–10 cm) in the Mersey estuary based on C/N ratios showing the dominantly marine/mixed nature of the material. See text for further explanation.

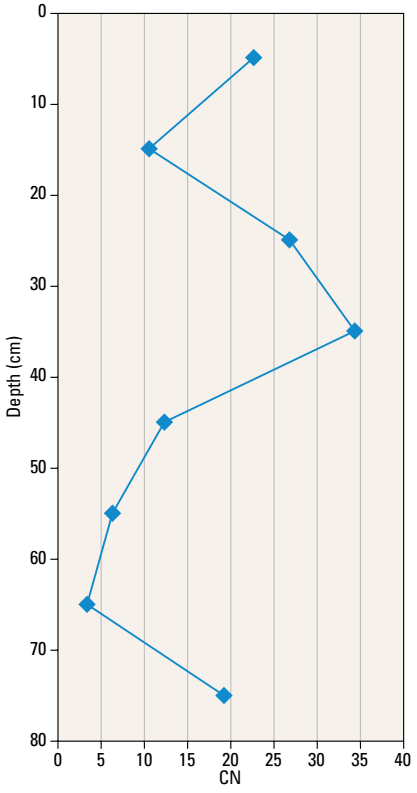

Figure 5.13 Variation in the ratio of carbon to nitrogen content down core M106. See text for further explanation.

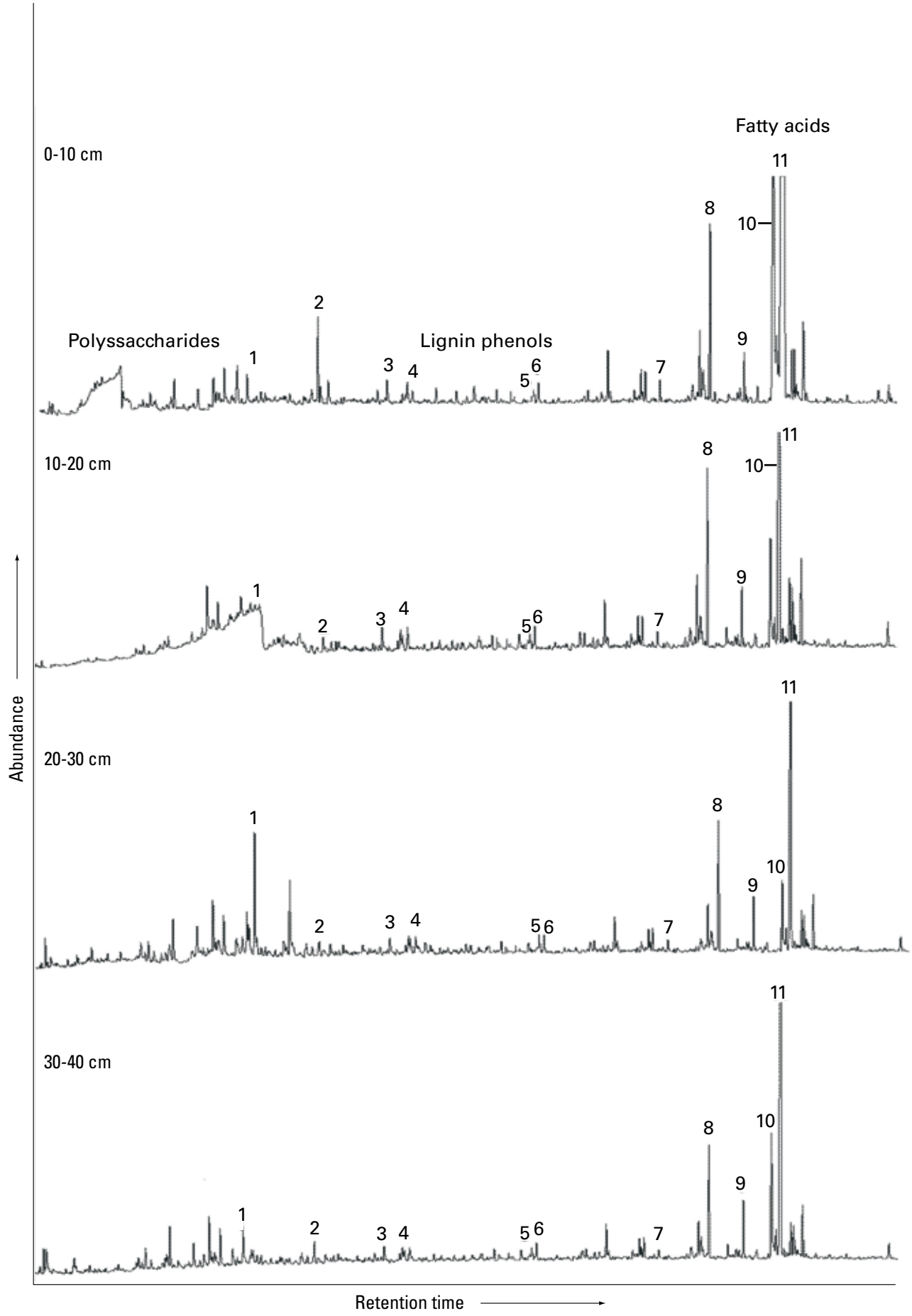

Figure 5.14a Partial chromatogram of the total ion current (TIC) of thermochemolysis products from a core (M106) located on Ince Banks salt marsh. Peak assignments listed in Table 5.14. See text for further explanation.

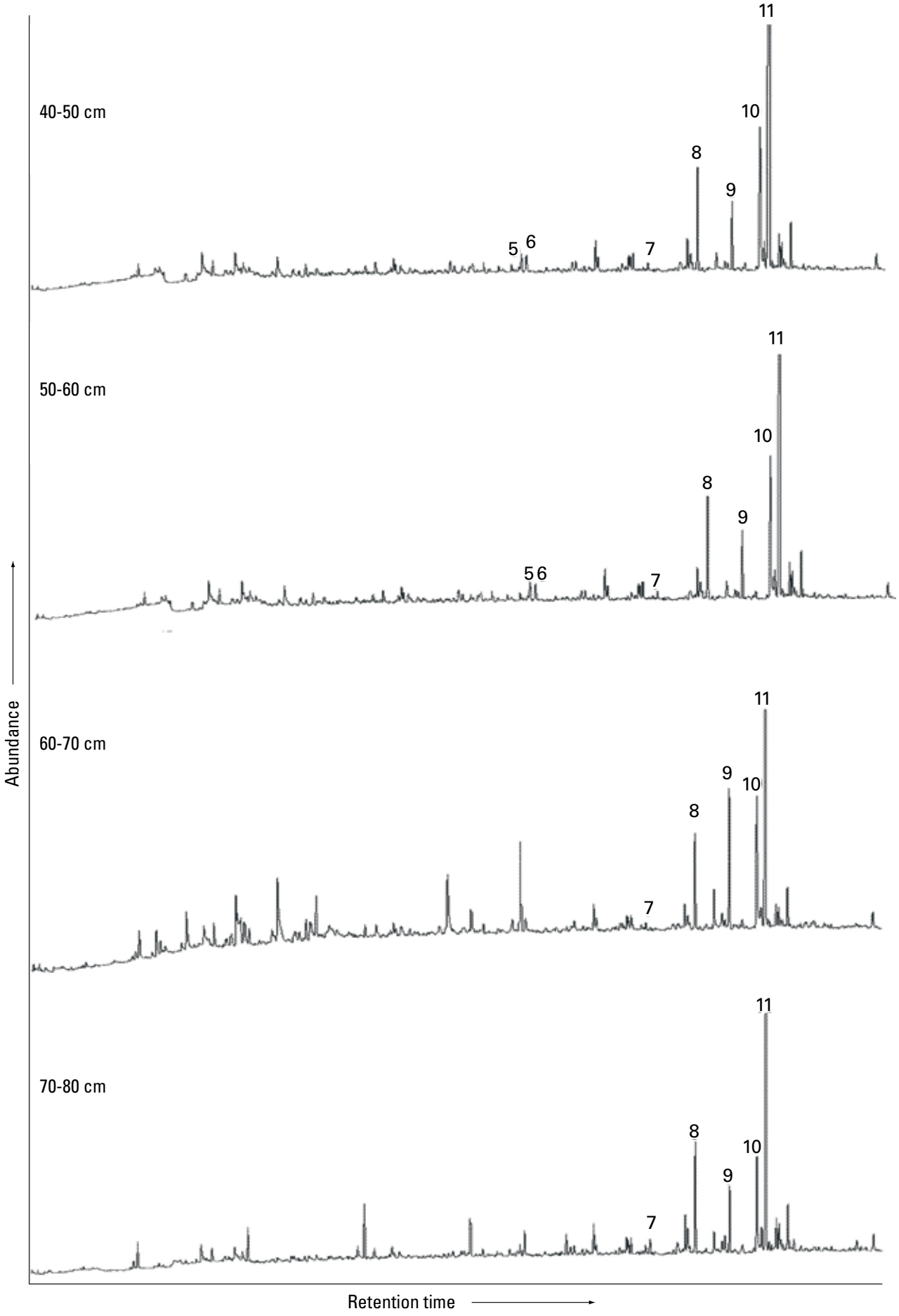

Figure 5.14b Partial chromatogram of the total ion current (TIC) of thermochemolysis products from a core (M106) located on Ince Banks salt marsh. Peak assignments listed in Table 5.14. See text for further explanation.

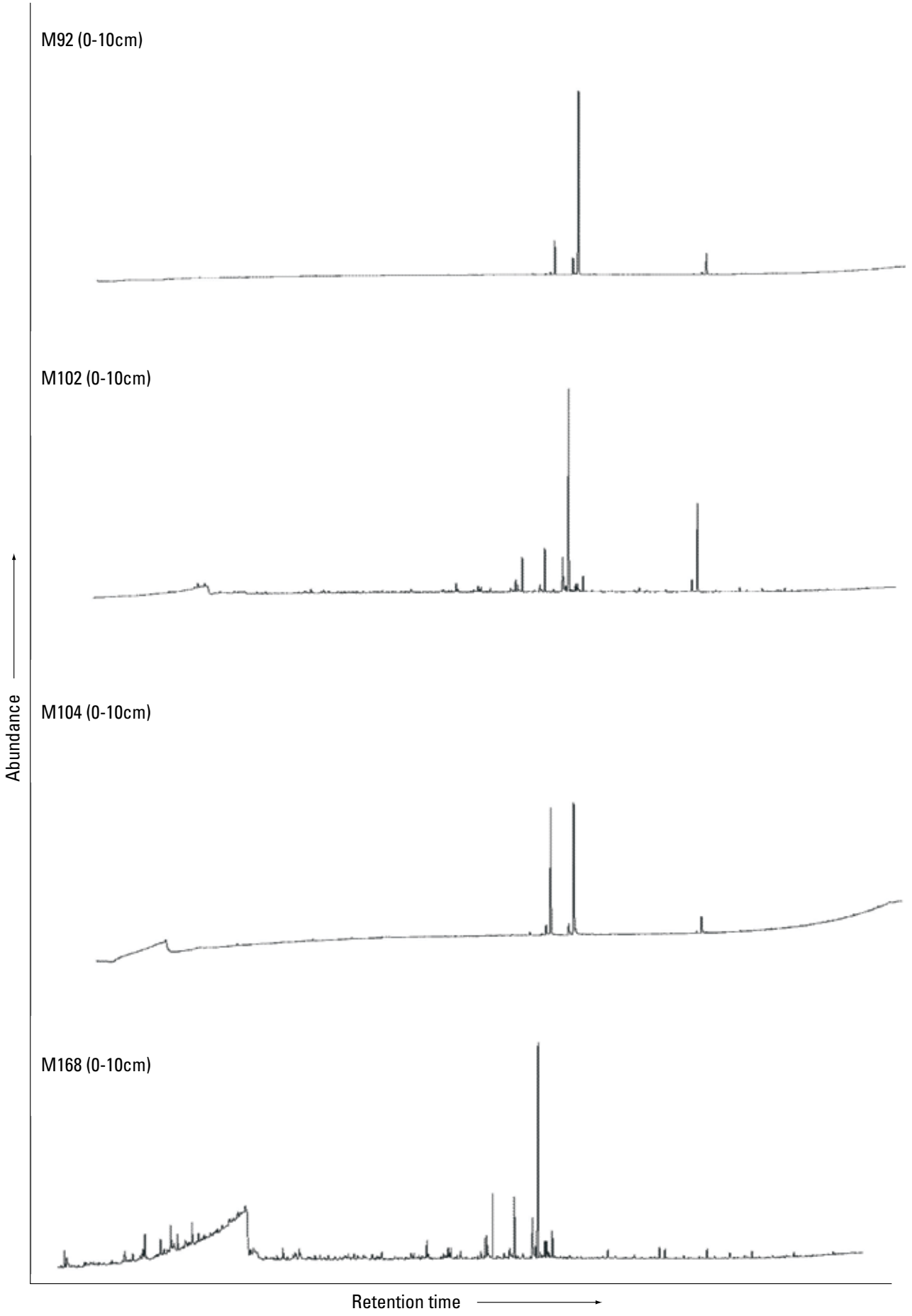

Figure 5.15 Total ion chromatograms of selected surface sediments (0–10cm) up and down stream of Ince Banks (Cores M92, M102, M104, M168). See text for further explanation.

Figure 6.1 Calcium (CaO) in core tops and grab samples.

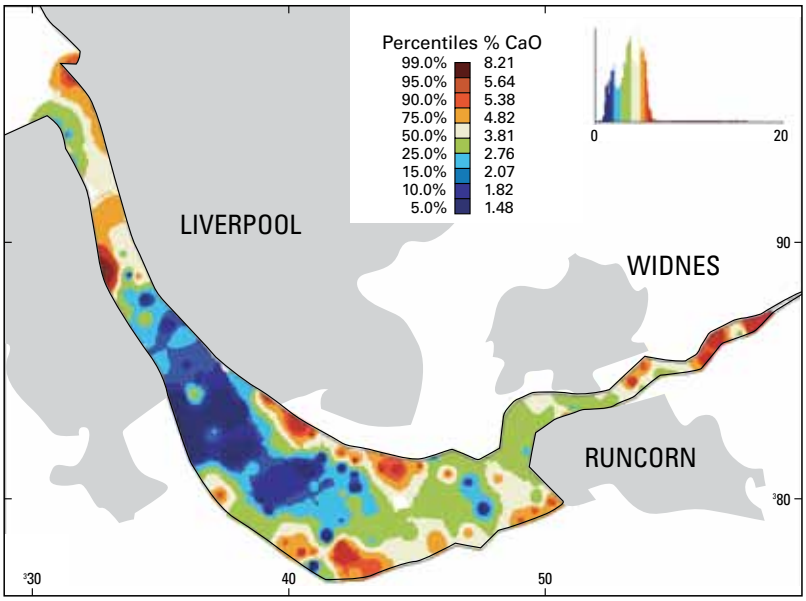

Figure 6.2 Silica (SiO_2) in core tops and grab samples.

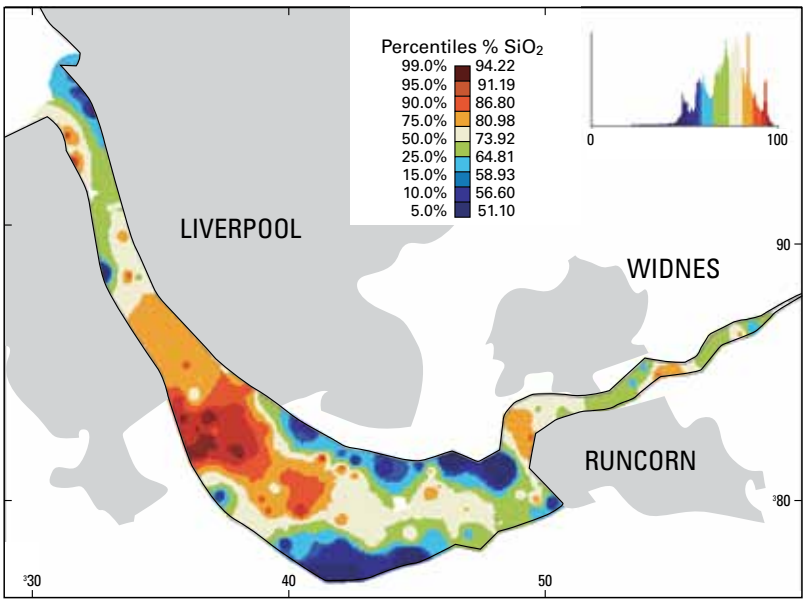

Figure 6.3 Sodium (Na_2O) in core tops and grab samples.

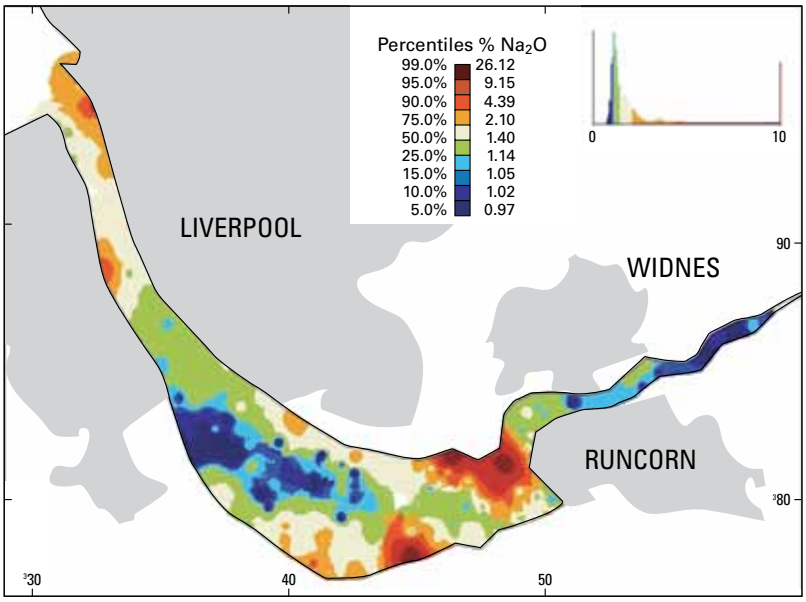

Figure 6.4 Zirconium (Zr) in core tops and grab samples.

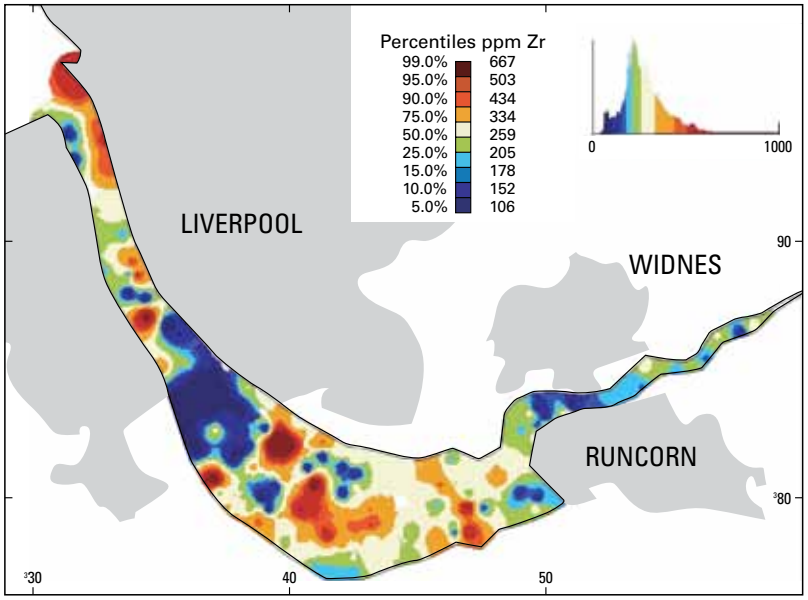

Figure 6.5 Chromium (Cr) in core tops and grab samples.

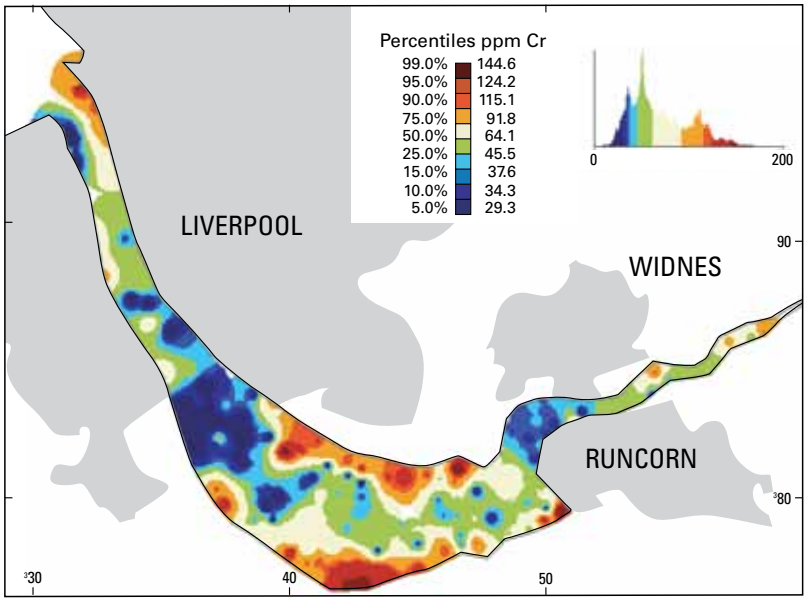

Figure 6.6 Chromium (normalised to Al) in core tops and grab samples.

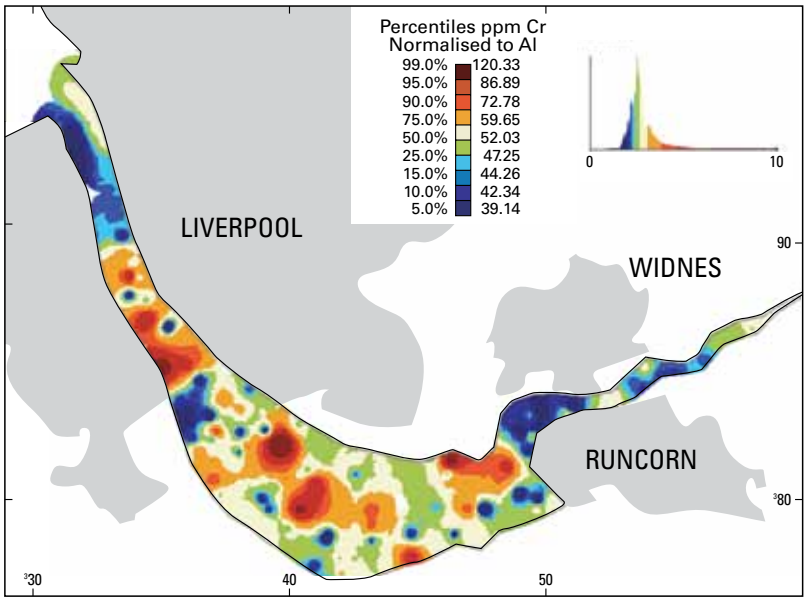

Figure 6.7 Copper (Cu) in core tops and grab samples.

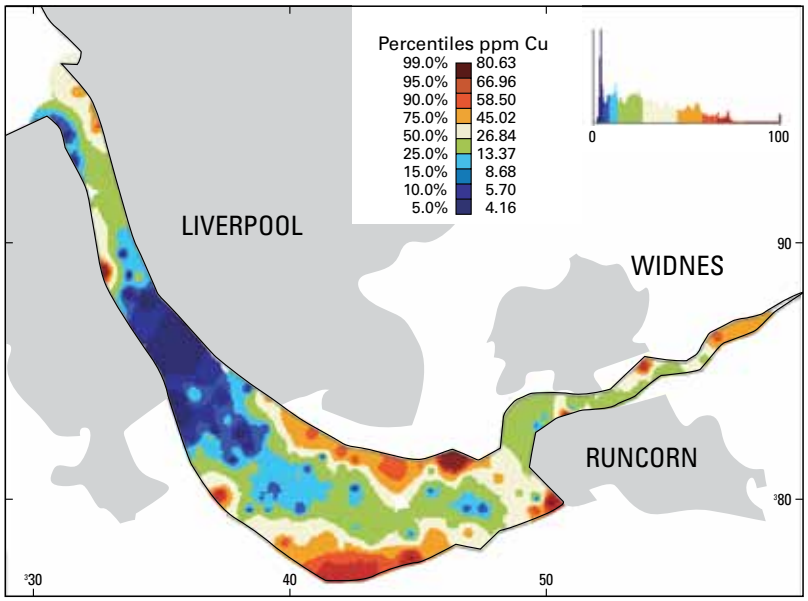

Figure 6.8 Copper (normalised to Al) in core tops and grab samples.

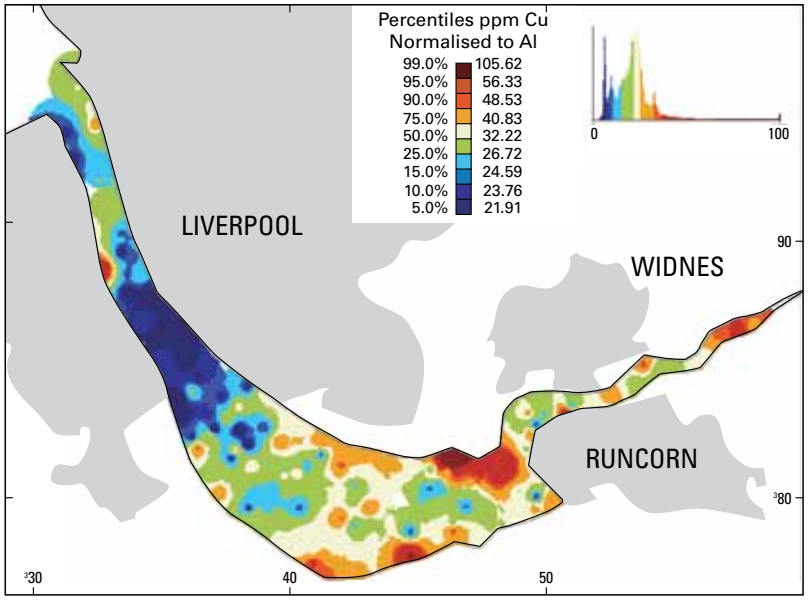

Figure 6.9 Lead (Pb) in core tops and grab samples.

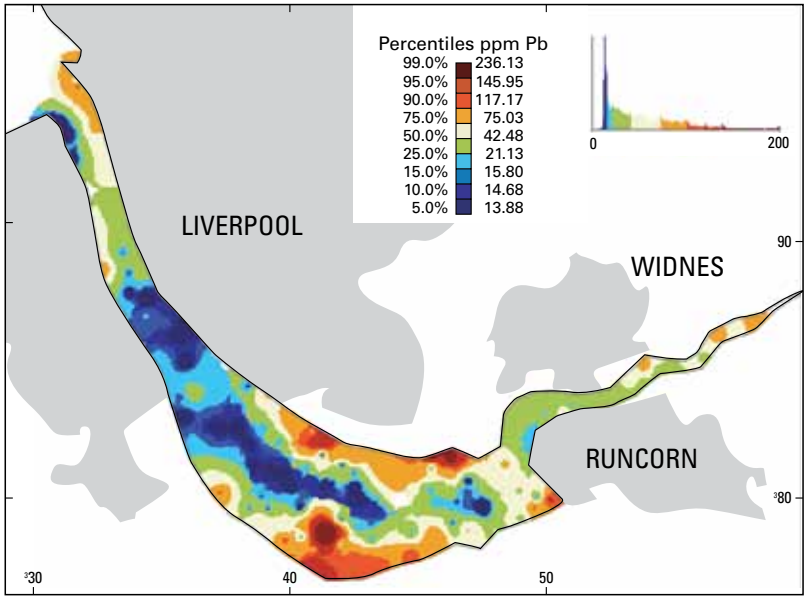

Figure 6.10 Lead (normalised to Al) in core tops and grab samples.

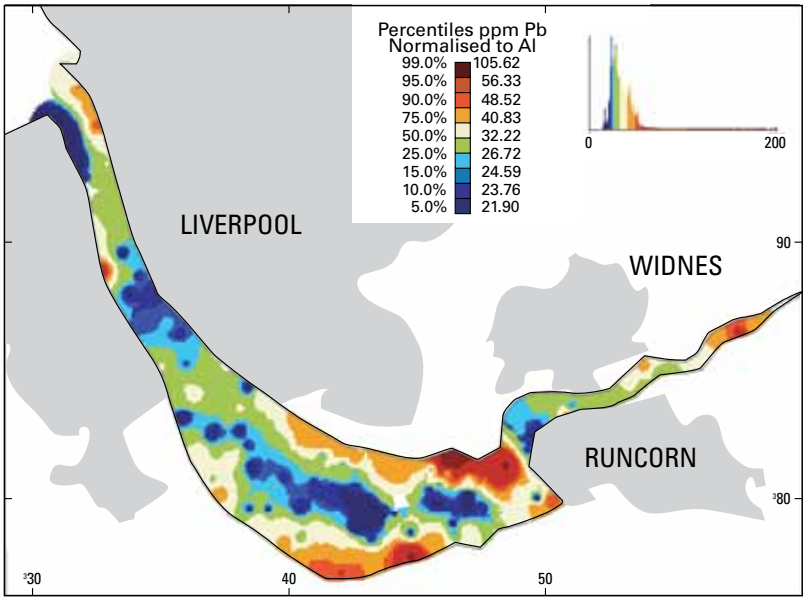

Figure 6.11 Vanadium (V) in core tops and grab samples.

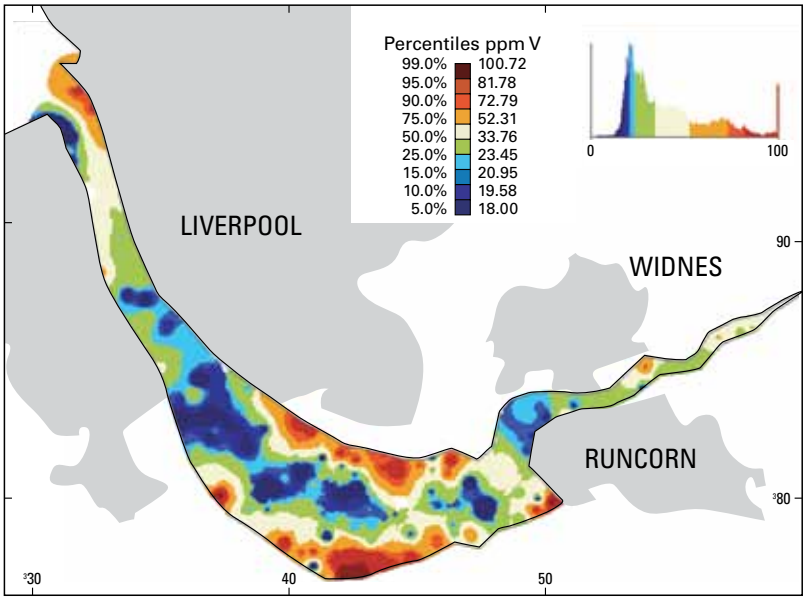

Figure 6.12 Vanadium (normalised to Al) in core tops and grab samples.

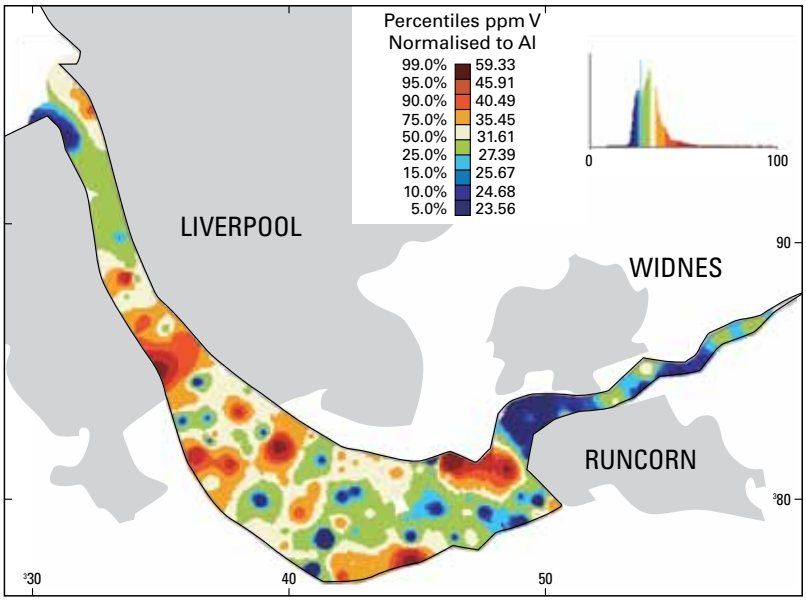

Figure 6.13 Zinc (Zn) in core tops and grab samples.

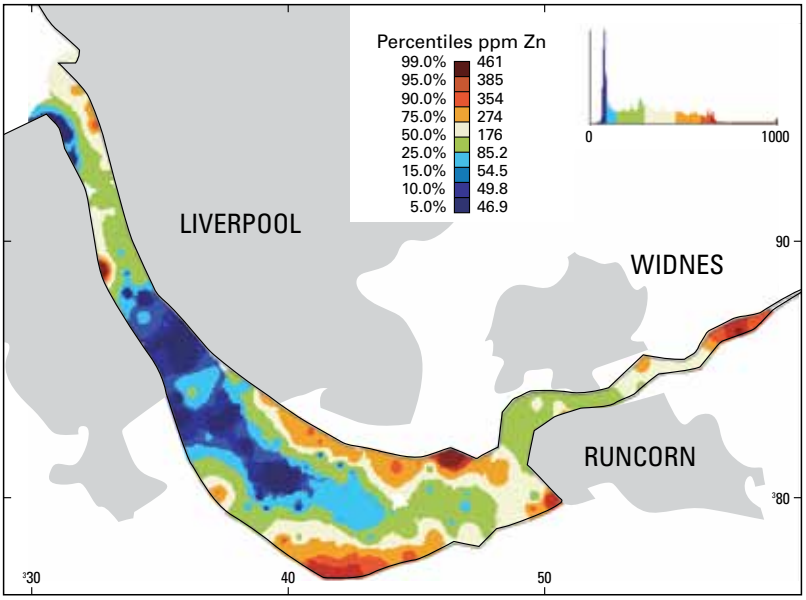

Figure 6.14 Zinc (normalised to Al) in core tops and grab samples.

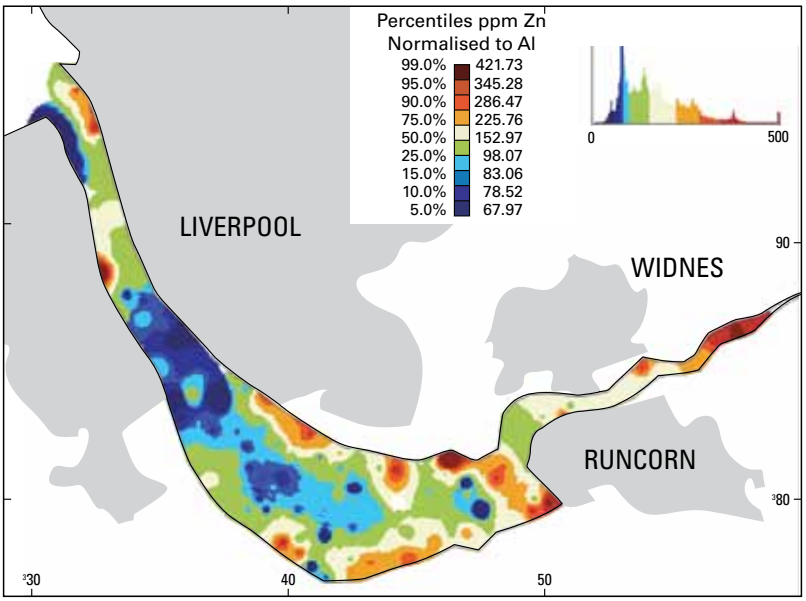

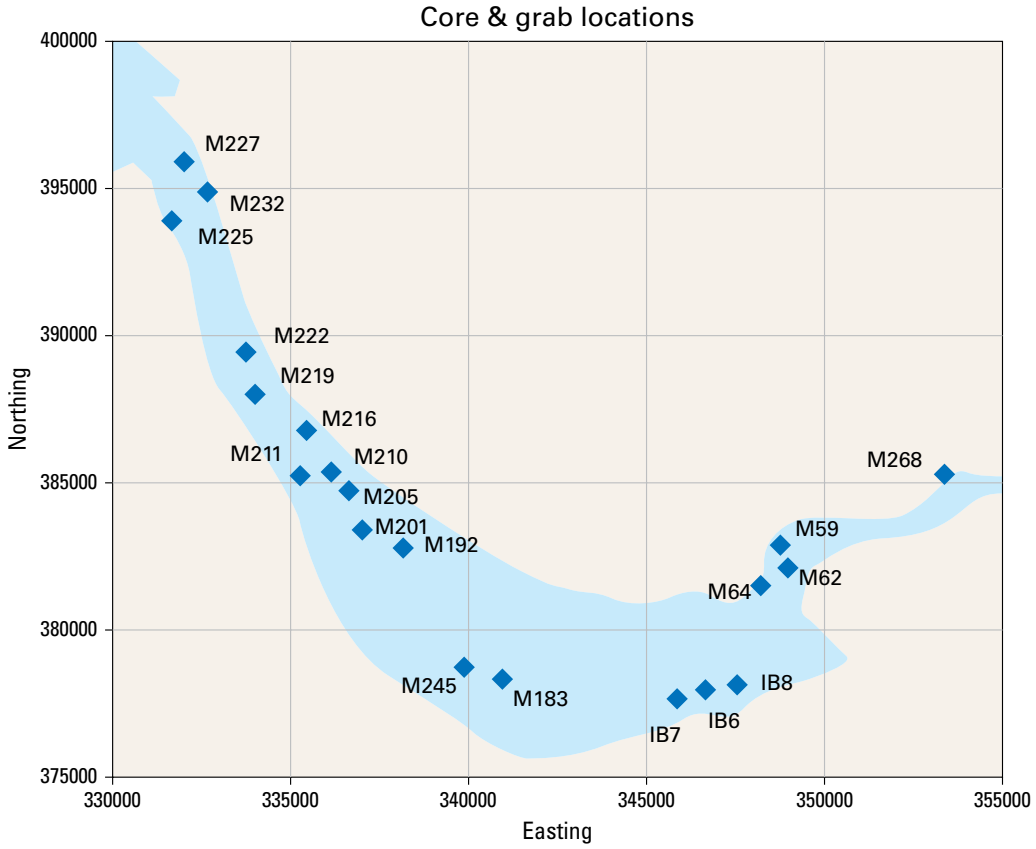

Figure 6.15 Location of core tops and grab samples analysed for mercury (Hg).

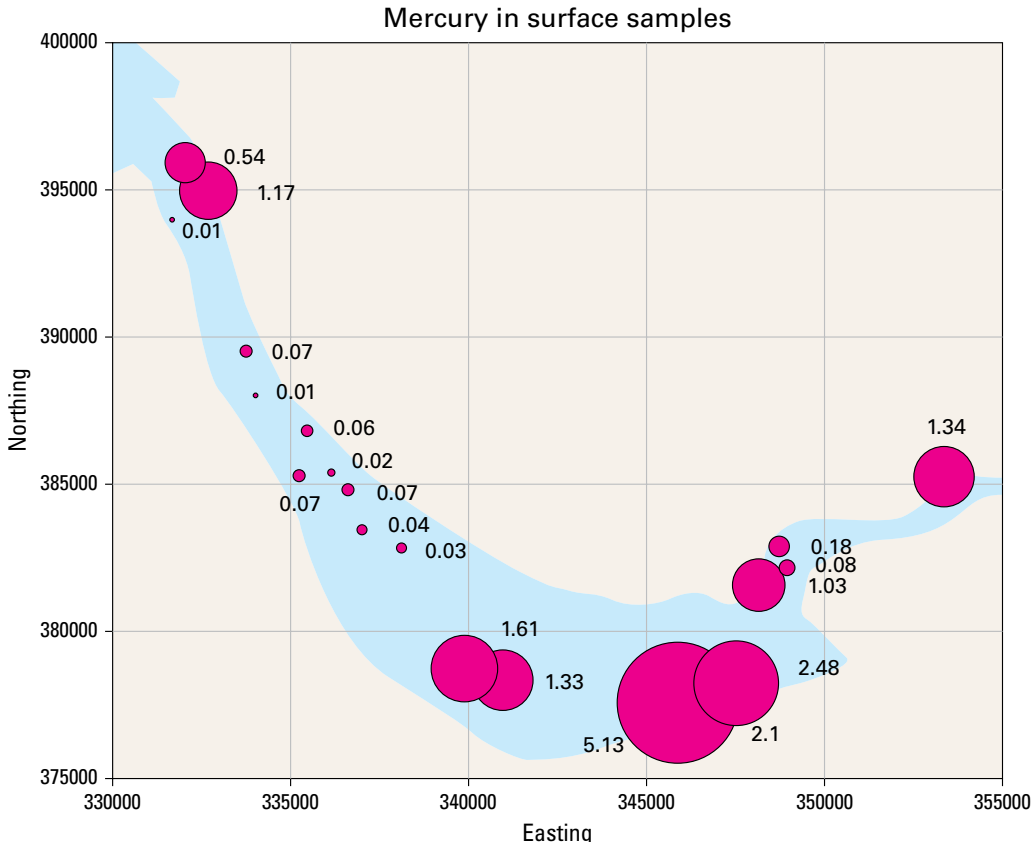

Figure 6.16 Mercury in core tops and grab samples.

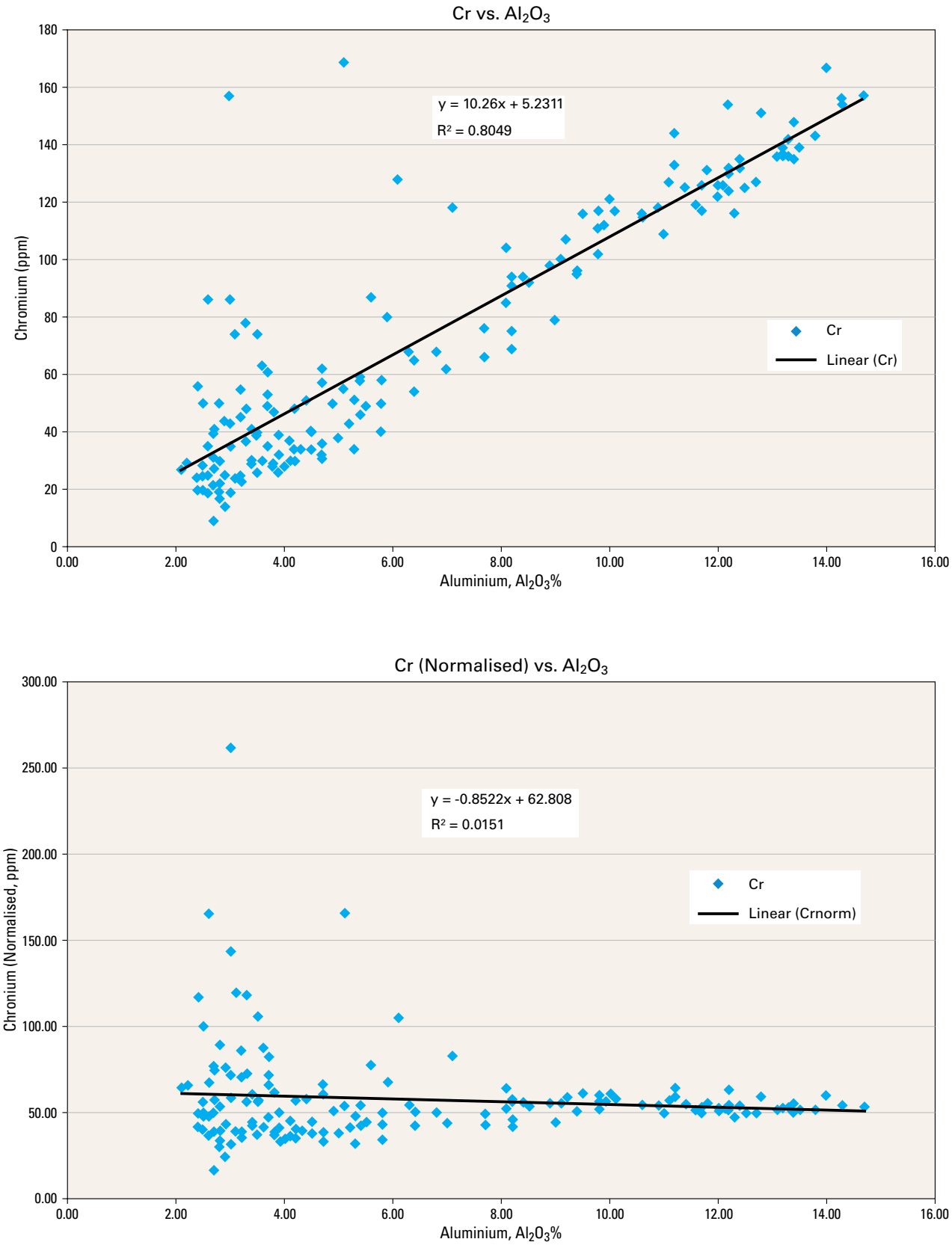

Figure 6.17 Cr v Al_2O_3 and Cr normalised to Al_2O_3.

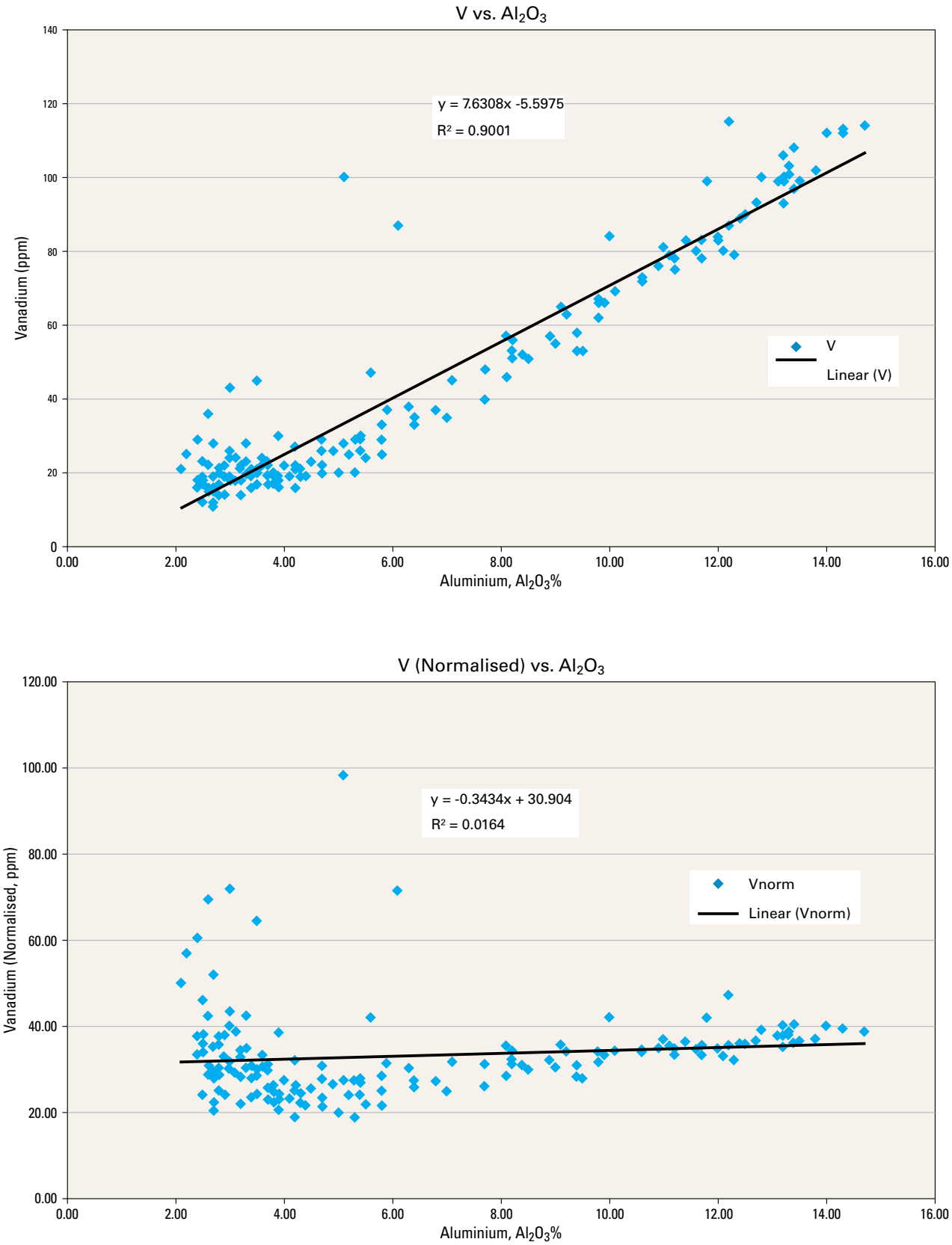

Figure 6.18 V v Al_2O_3 and V normalised v Al_2O_3.

Figure 6.19 Al_2O_3 in core tops and grab samples.

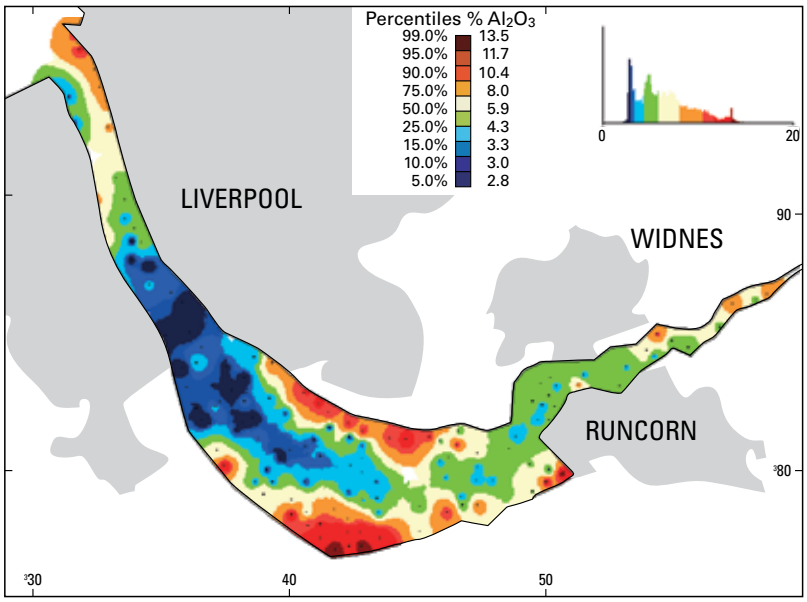

Figure 6.20 As in core tops and grab samples.

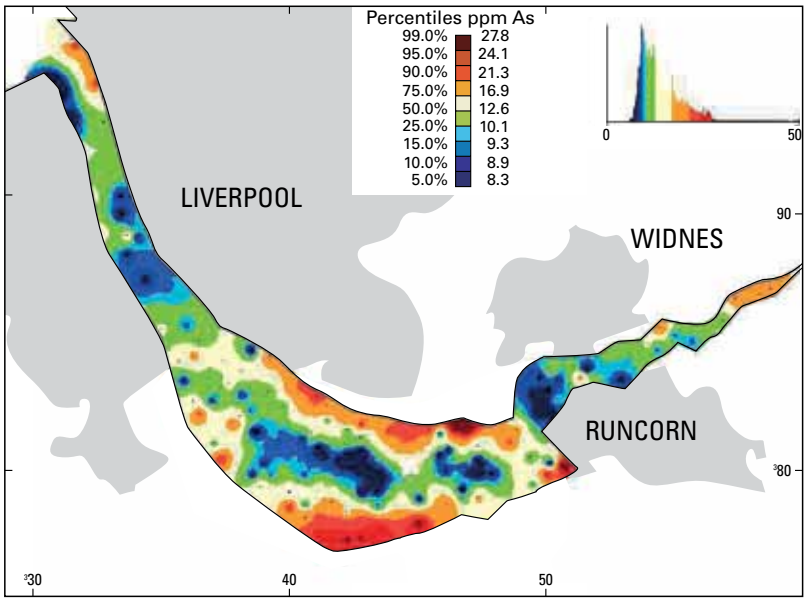

Figure 6.21 Ba in core tops and grab samples.

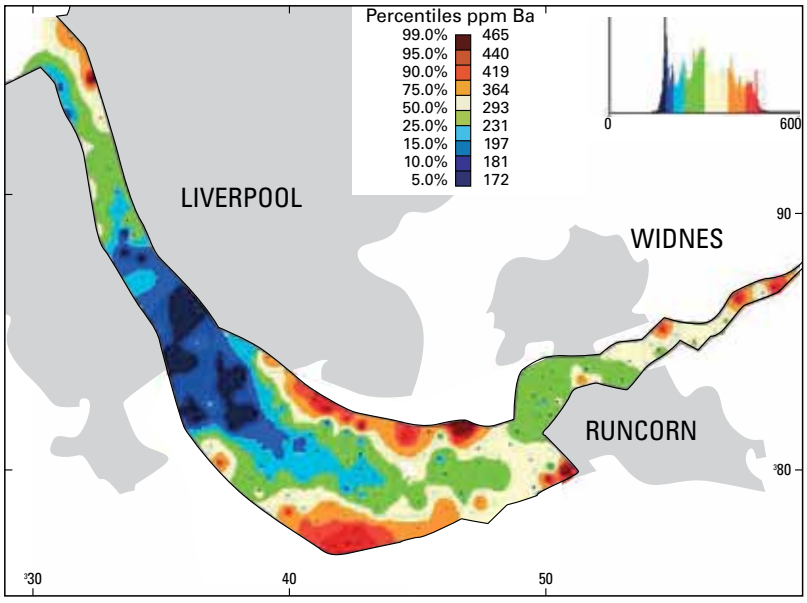

Figure 6.22 Br in core tops and grab samples.

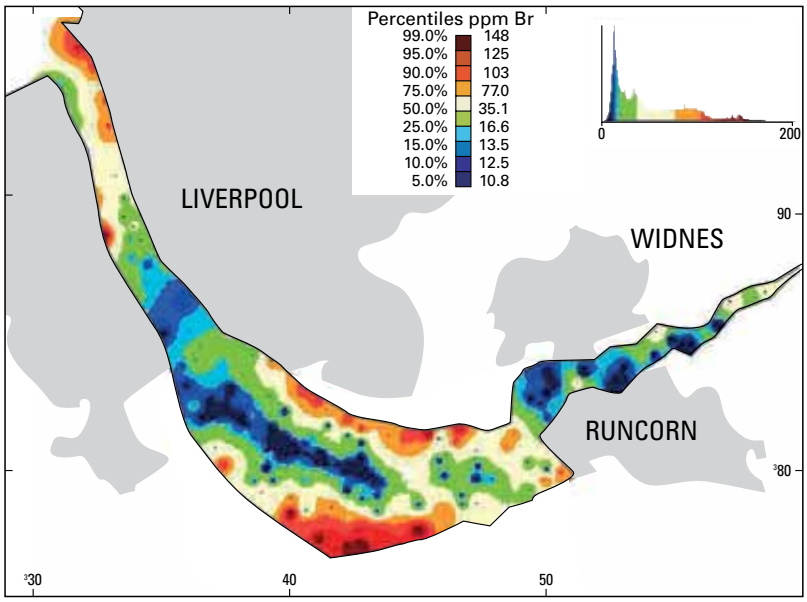

Figure 6.23 Co in core tops and grab samples.

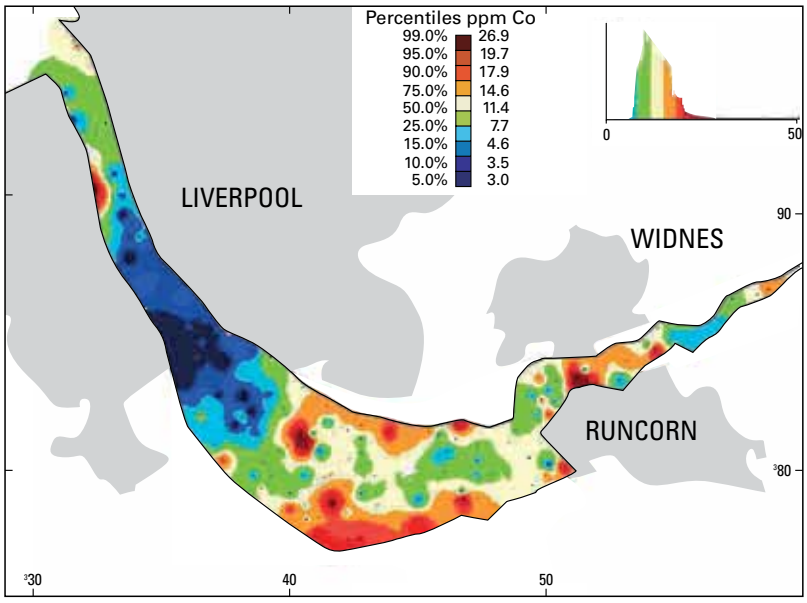

Figure 6.24 Fe_2O_3 in core tops and grab samples.

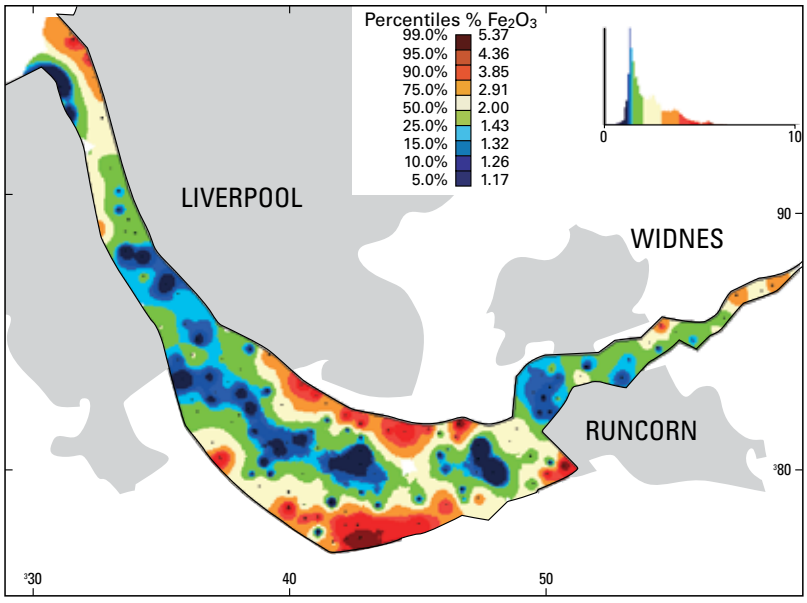

Figure 6.25 Ga in core tops and grab samples.

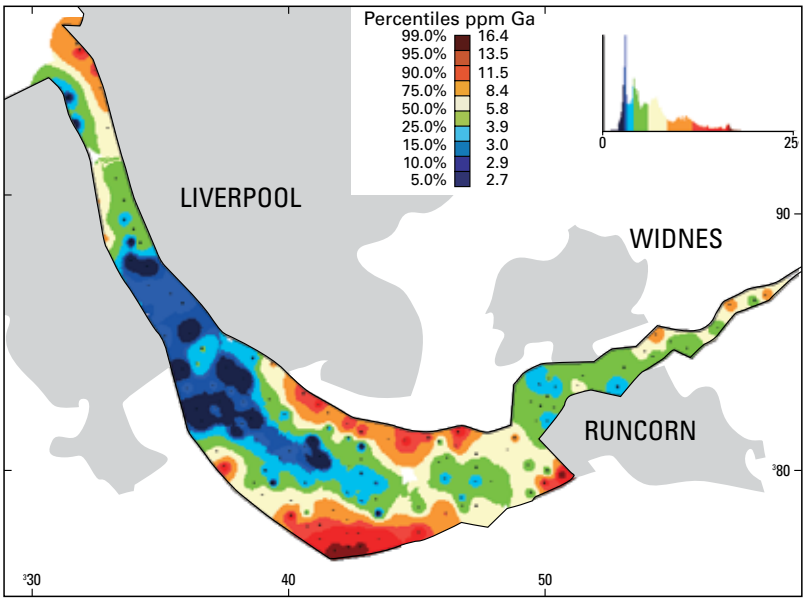

Figure 6.26 Ge in core tops and grab samples.

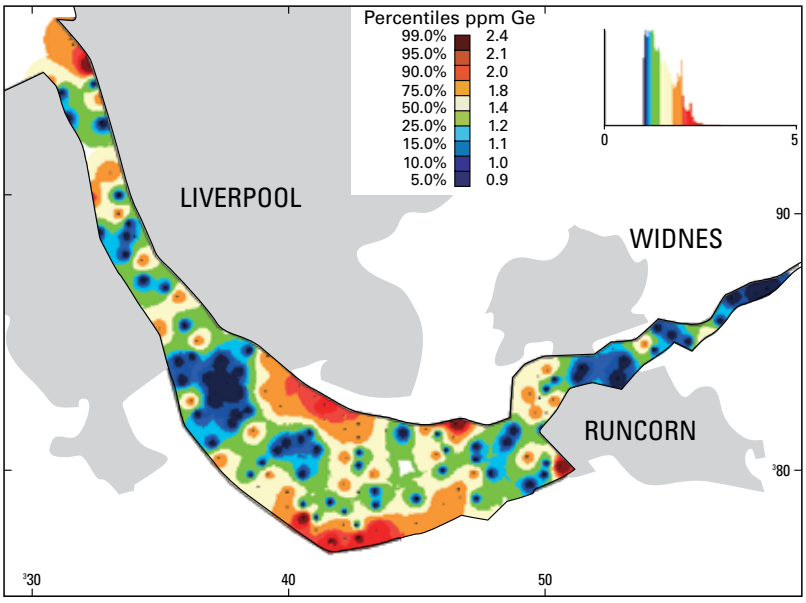

Figure 6.27 K_2O in core tops and grab samples.

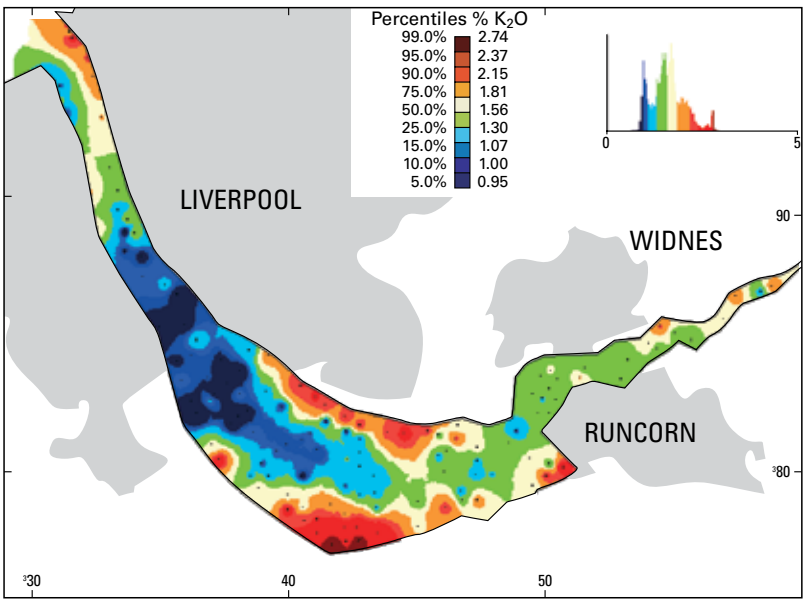

Figure 6.28 La in core tops and grab samples.

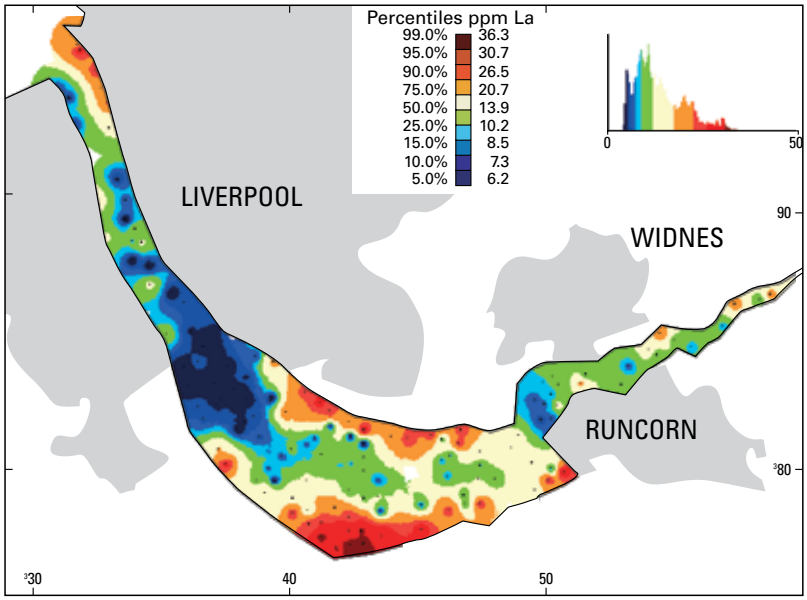

Figure 6.29 MgO in core tops and grab samples.

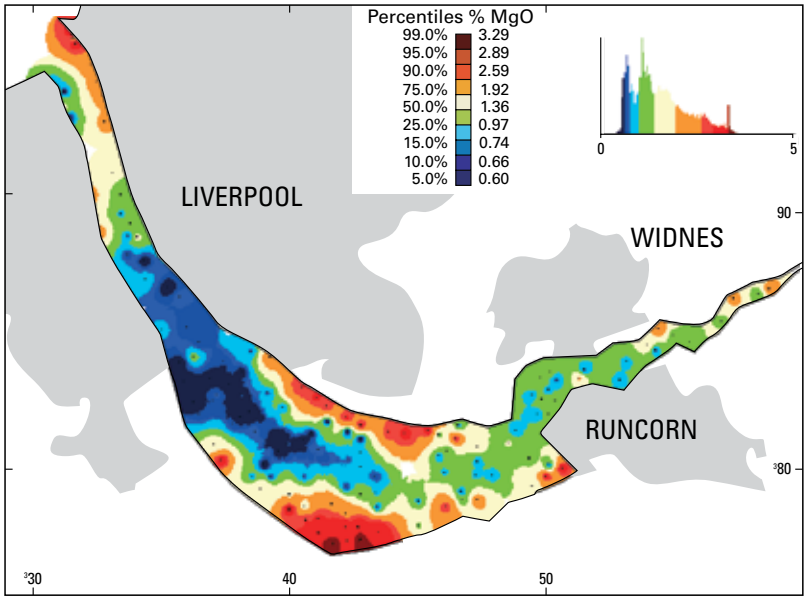

Figure 6.30 Mn in core tops and grab samples.

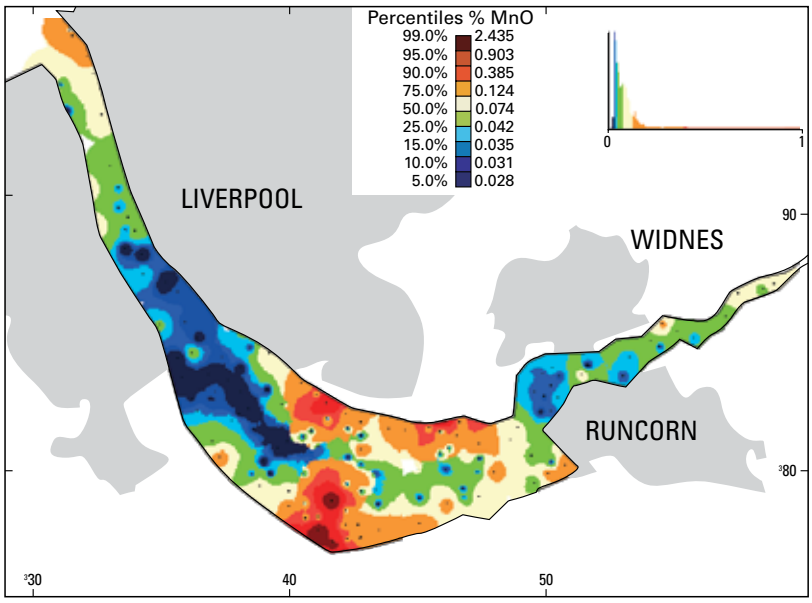

Figure 6.31 Nb in core tops and grab samples.

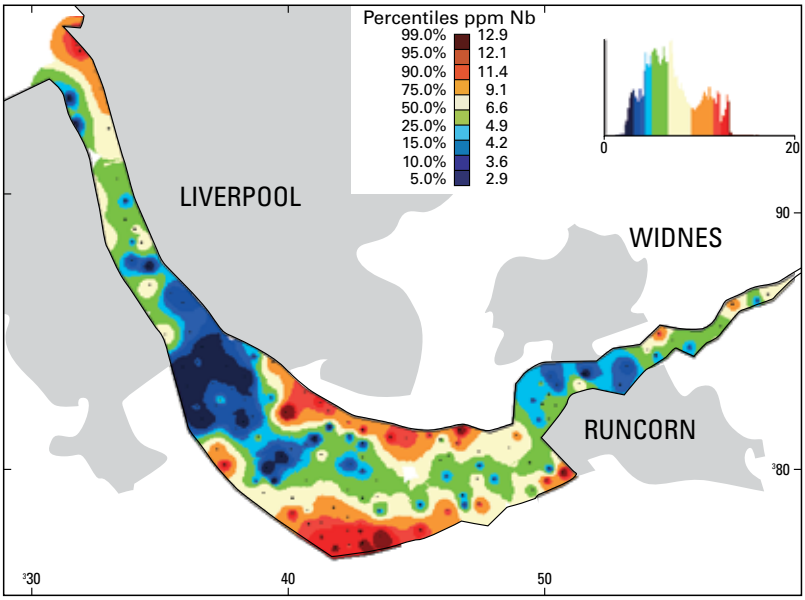

Figure 6.32 Ni in core tops and grab samples.

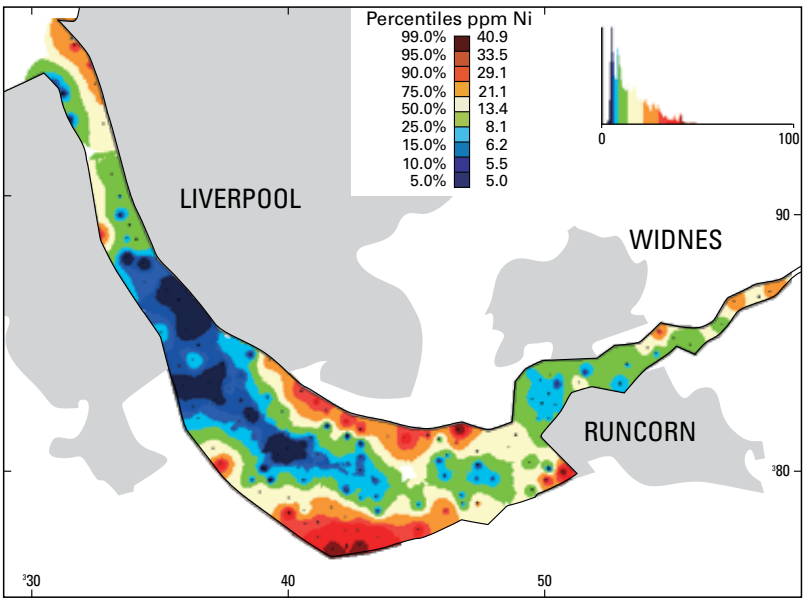

Figure 6.33 Sc in core tops and grab samples.

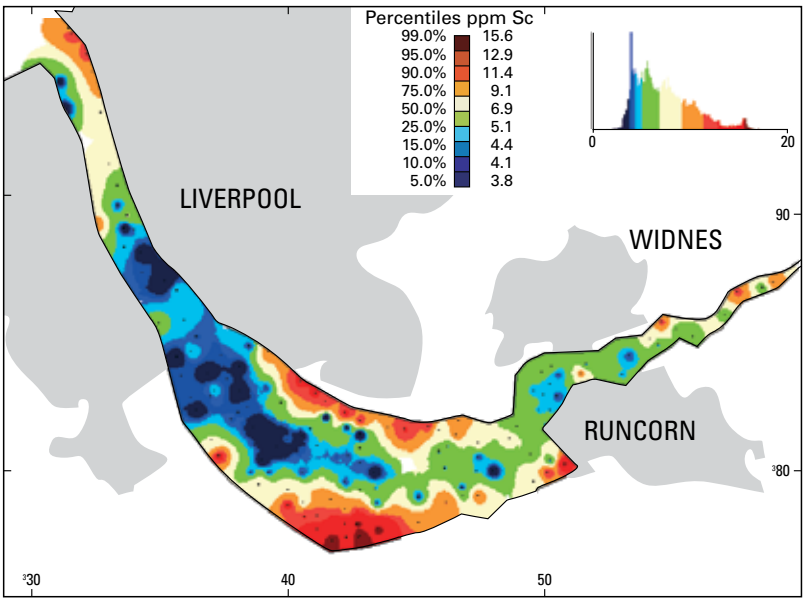

Figure 6.34 Tin (Sn) in core tops and grab samples (includes data from salt marsh cores from Ince Banks and Marshes).

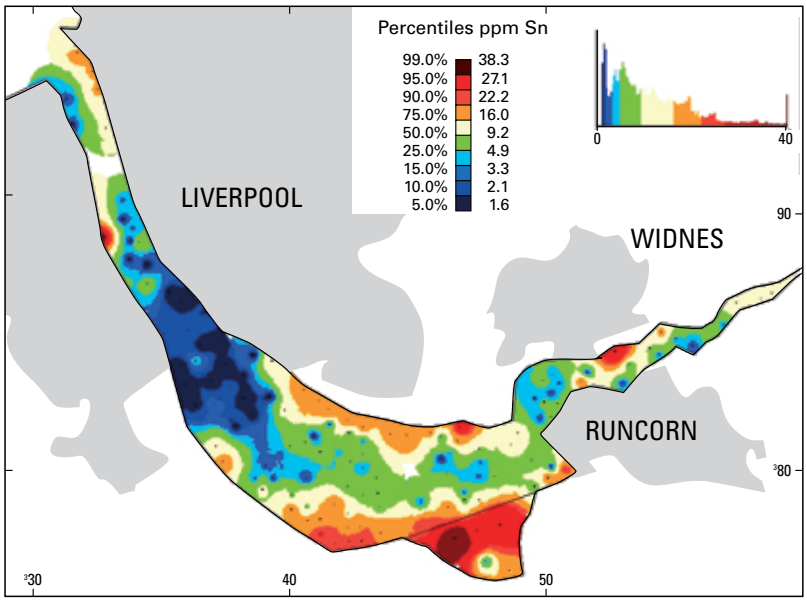

Figure 6.35 Tin (normalised to Al) in core tops and grab samples.

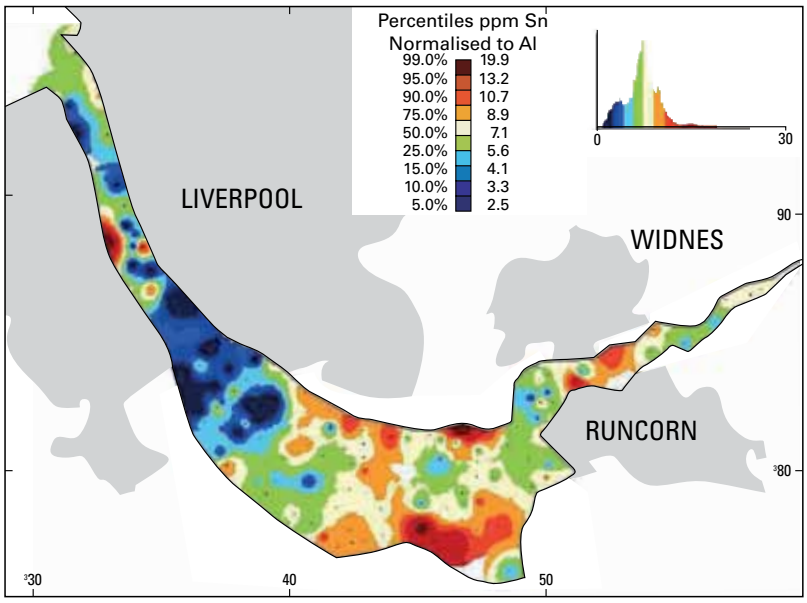

Figure 6.36 Sr in core tops and grab samples.

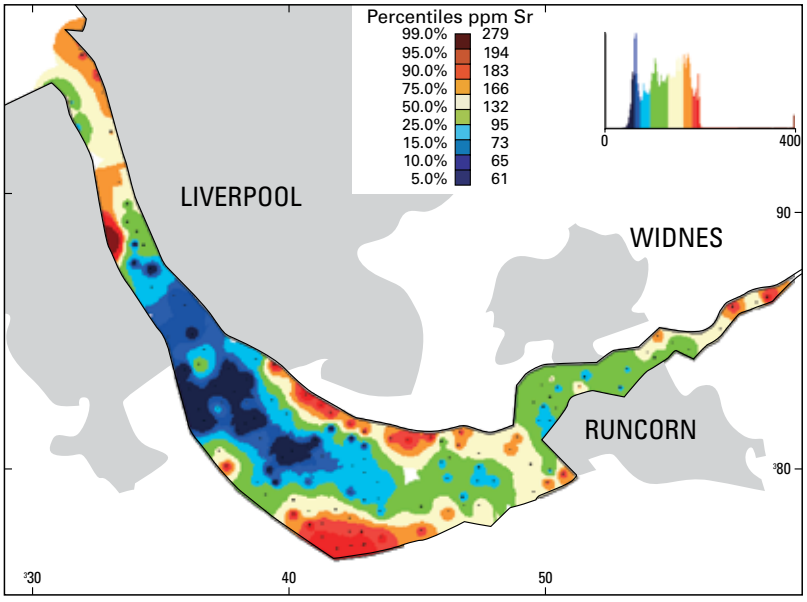

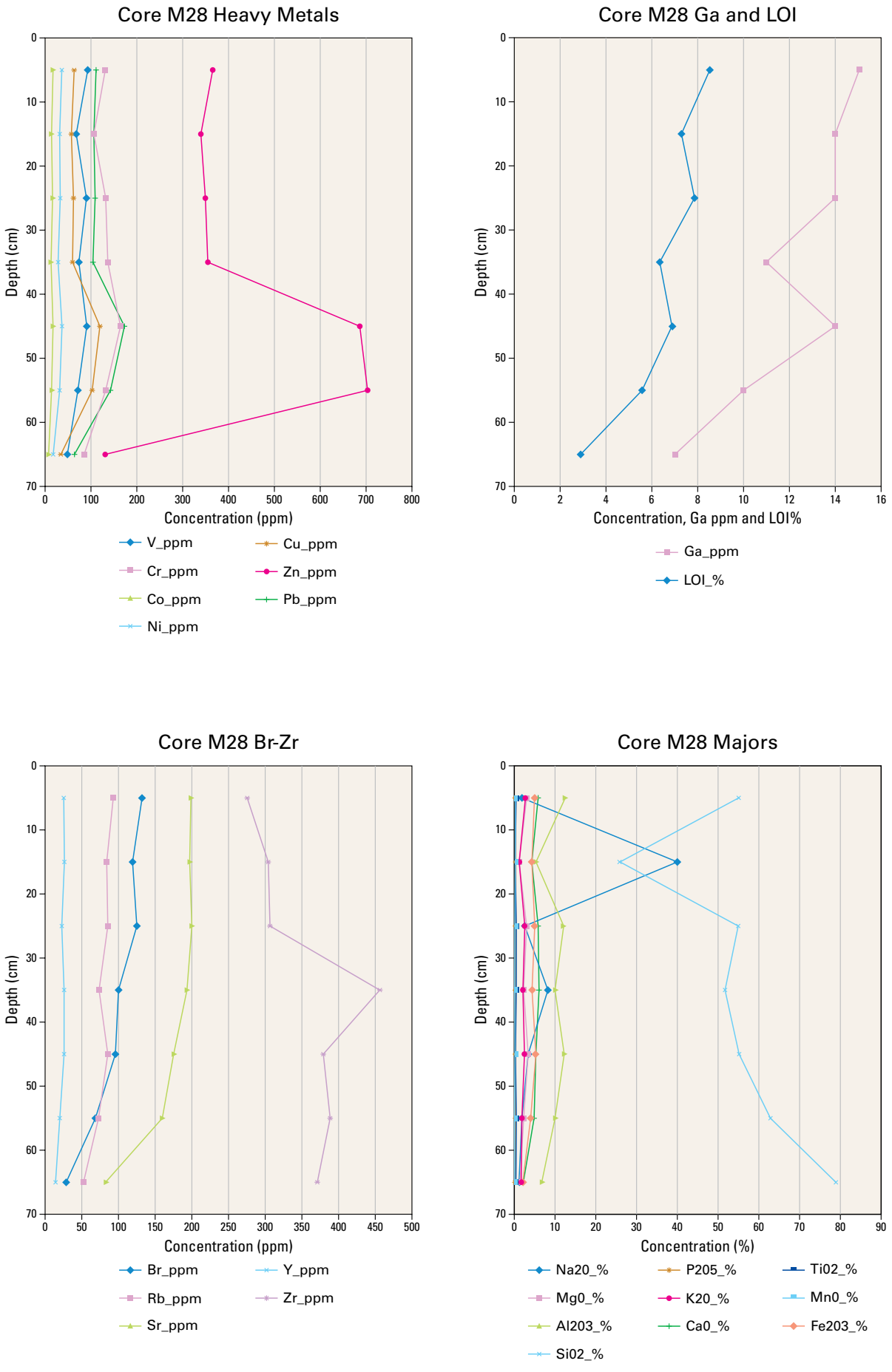

Figure 6.37 Down core profiles for Core M28.

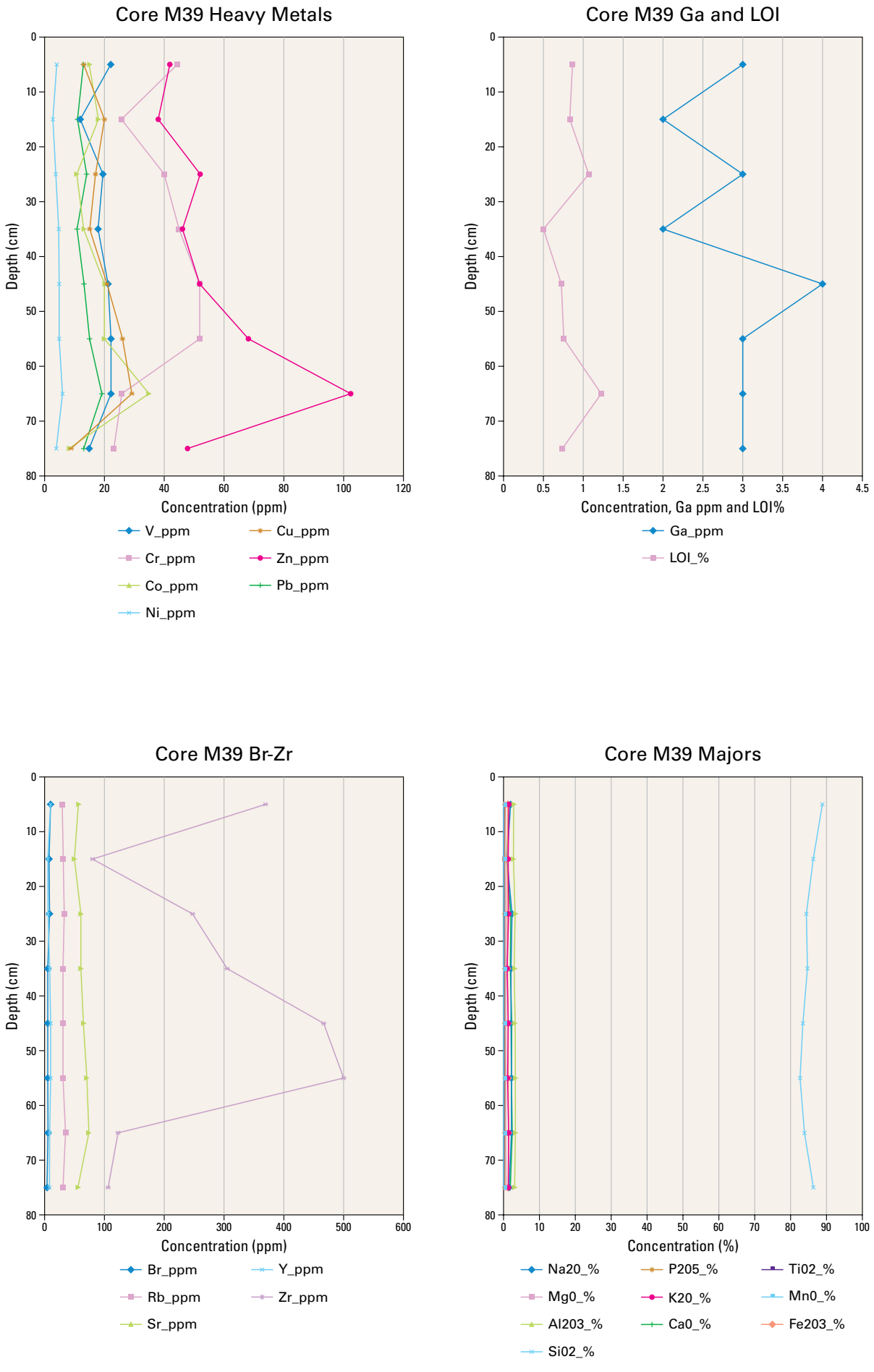

Figure 6.38 Down core profiles for Core M39.

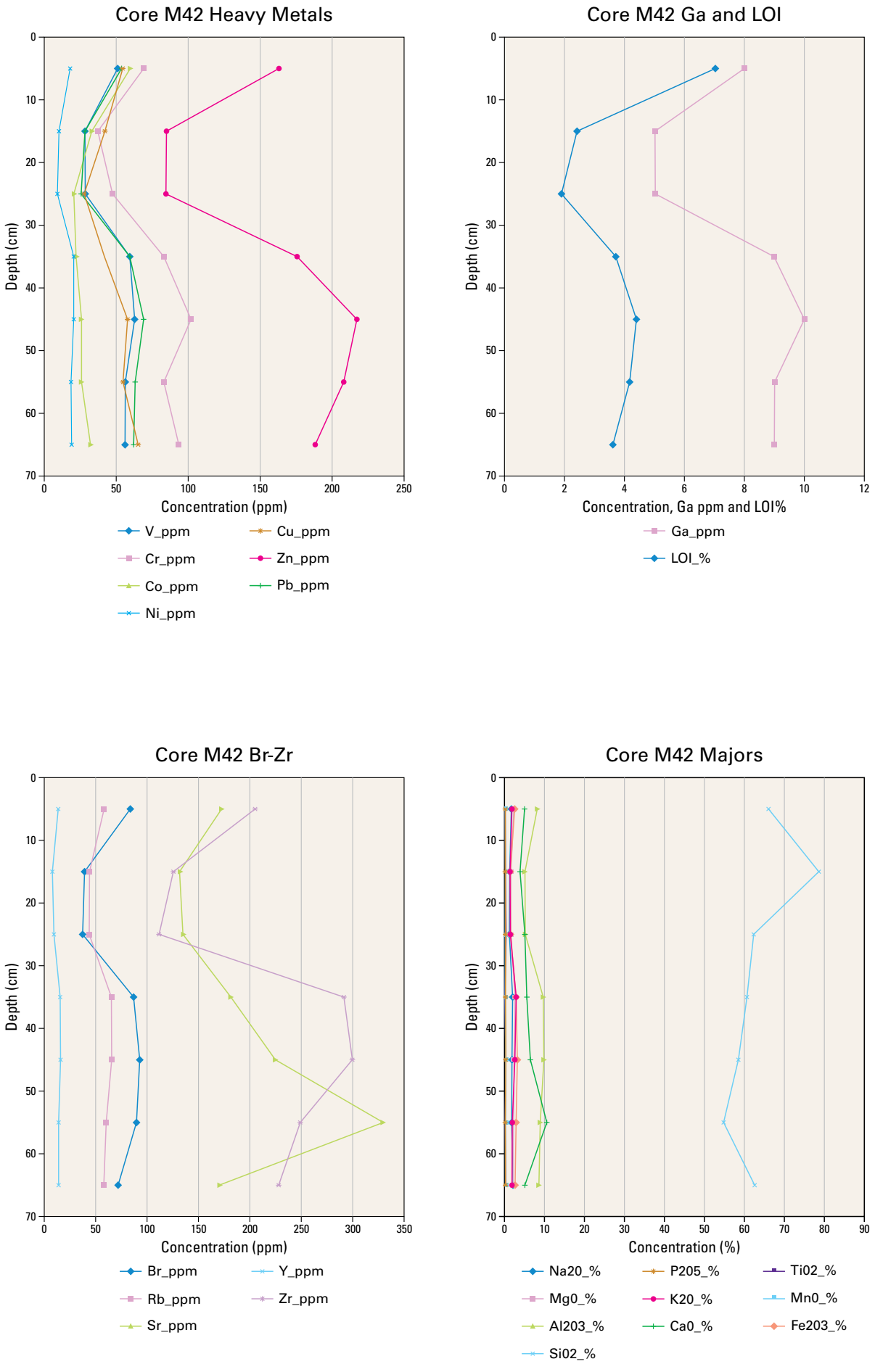

Figure 6.39 Down core profiles for Core M42.

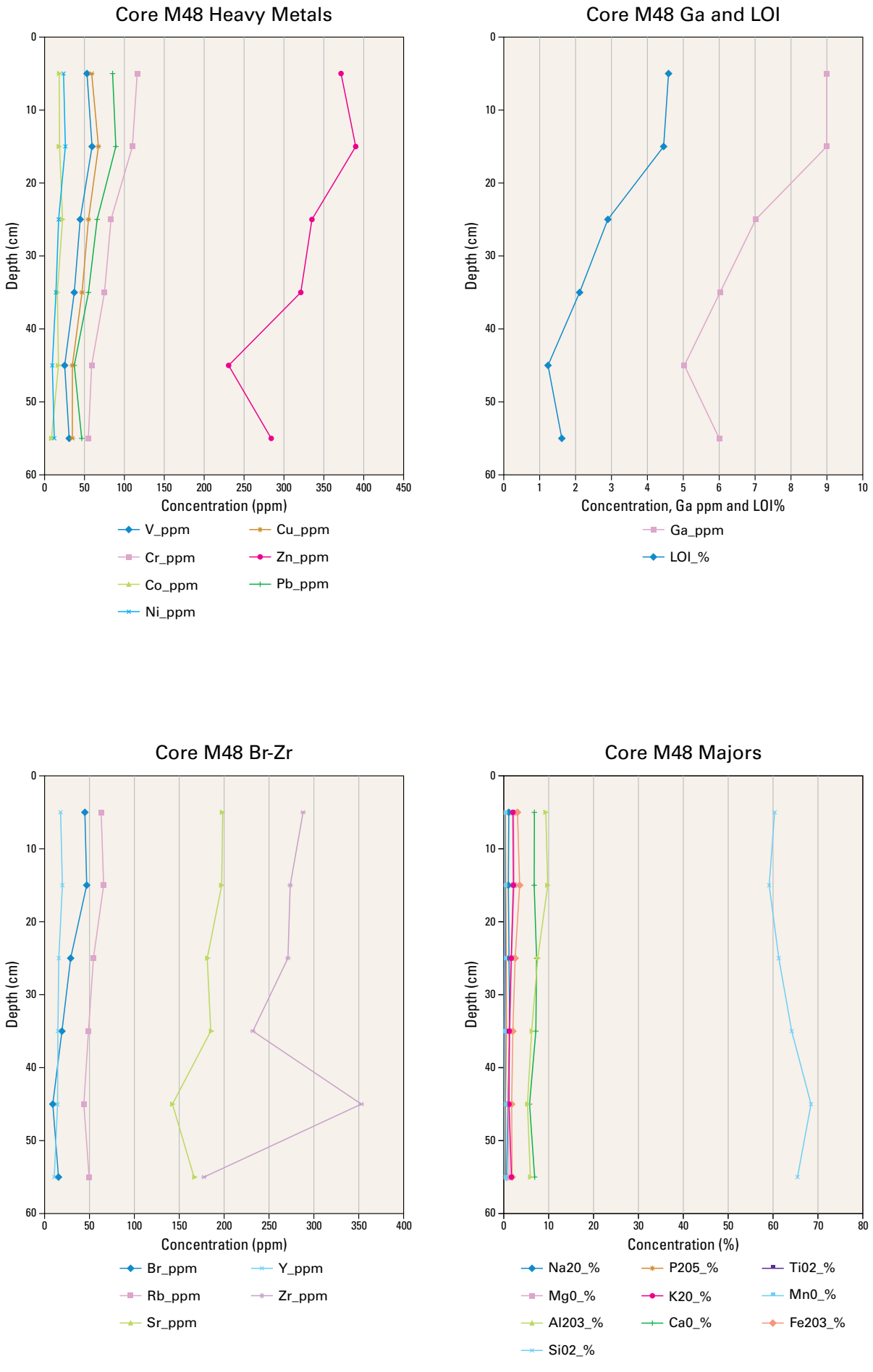

Figure 6.40 Down core profiles for Core M48.

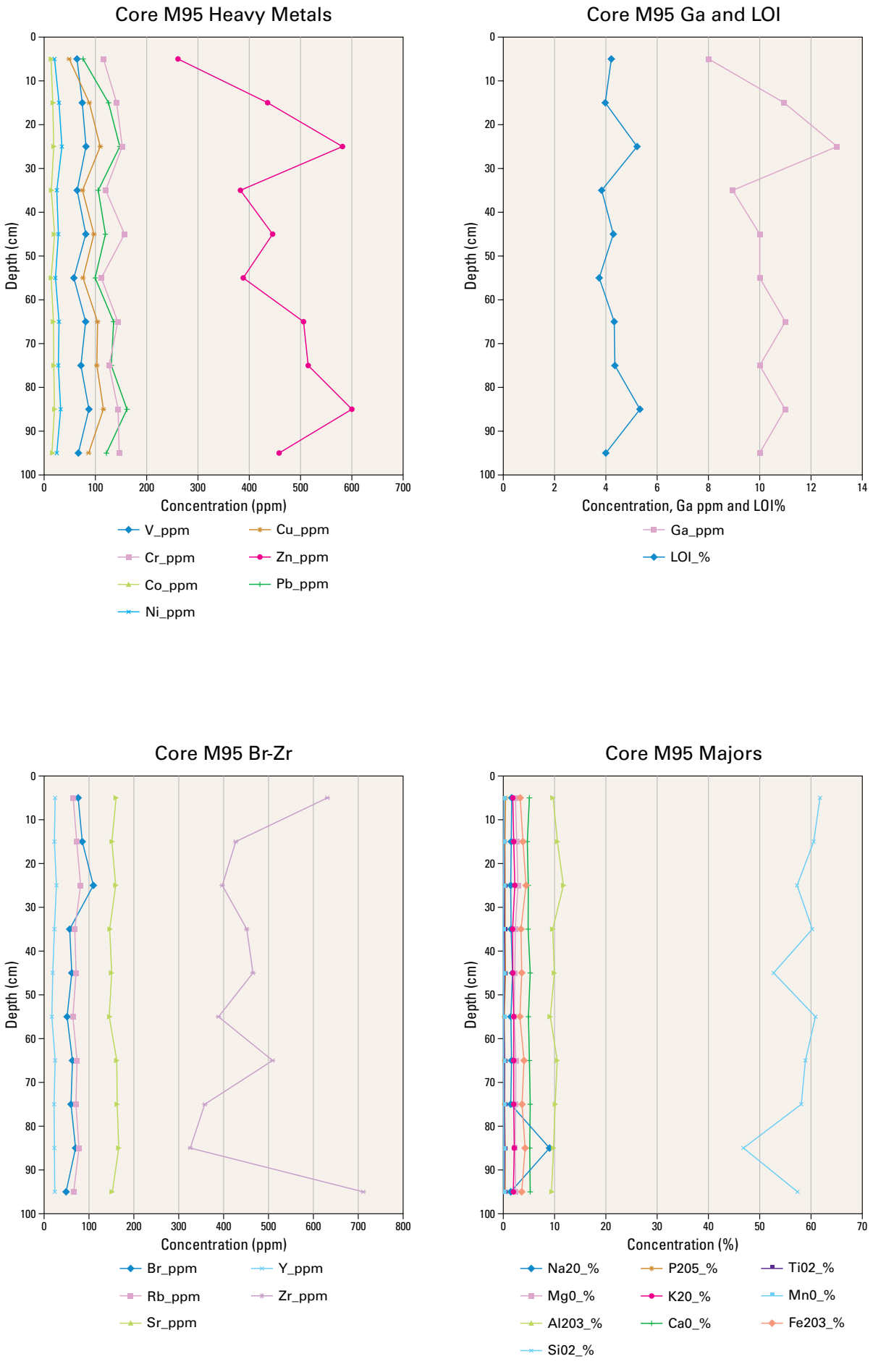

Figure 6.41 Down core profiles for Core M95.

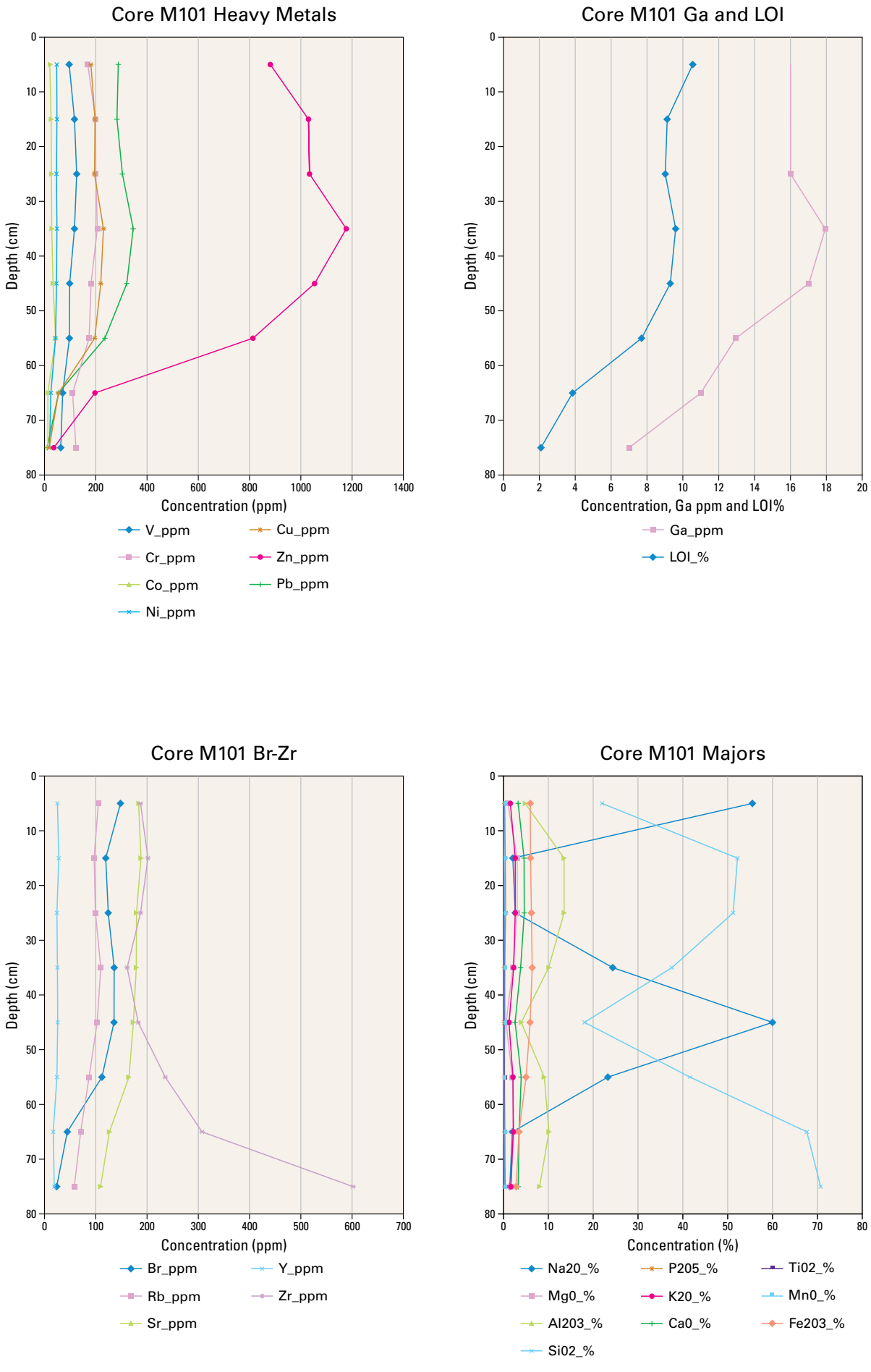

Figure 6.42 Down core profiles for Core M101.

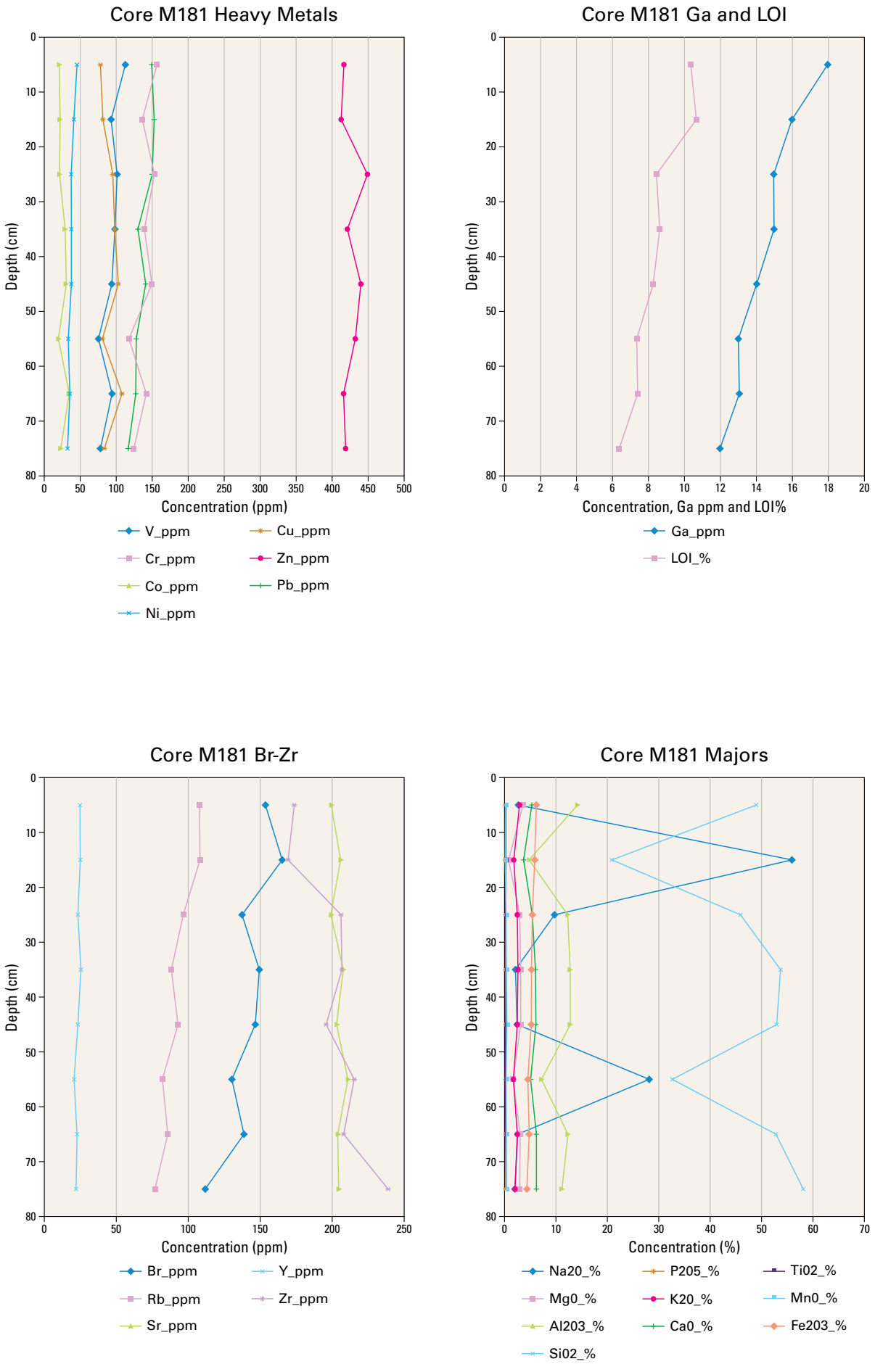

Figure 6.43 Down core profiles for Core M181.

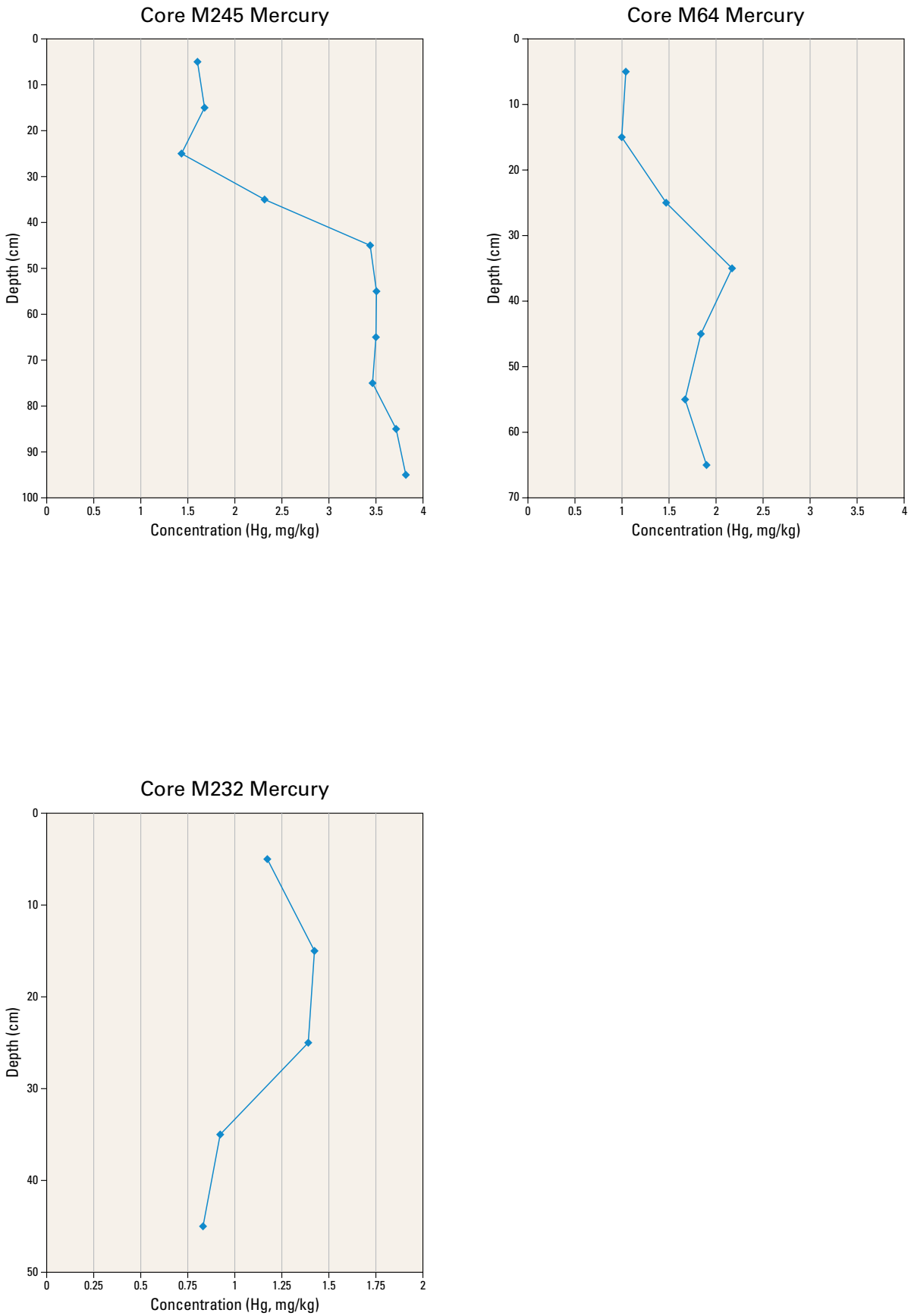

Figure 6.44 Down core profiles for Hg in cores M64, M232 and M245 (see Figure 6.15 for core locations).

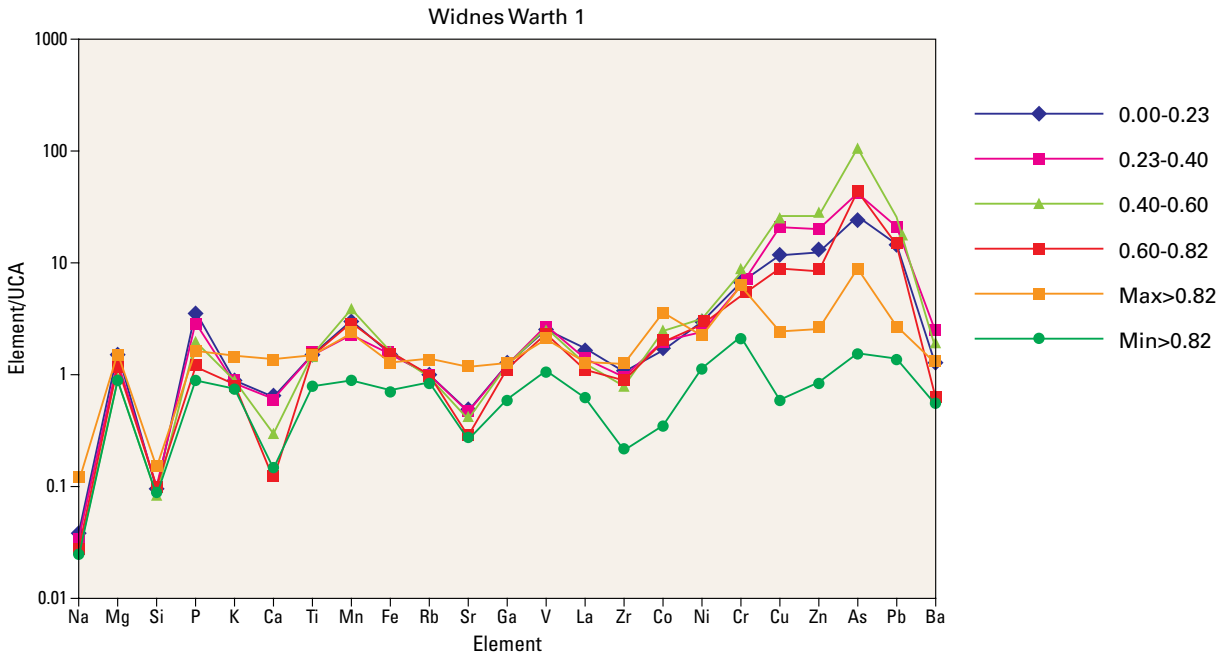

Figure 6.45 Spidergram showing down hole variation in borehole Widnes Warth 1 (normalised to Al to reduce grain-size effects).

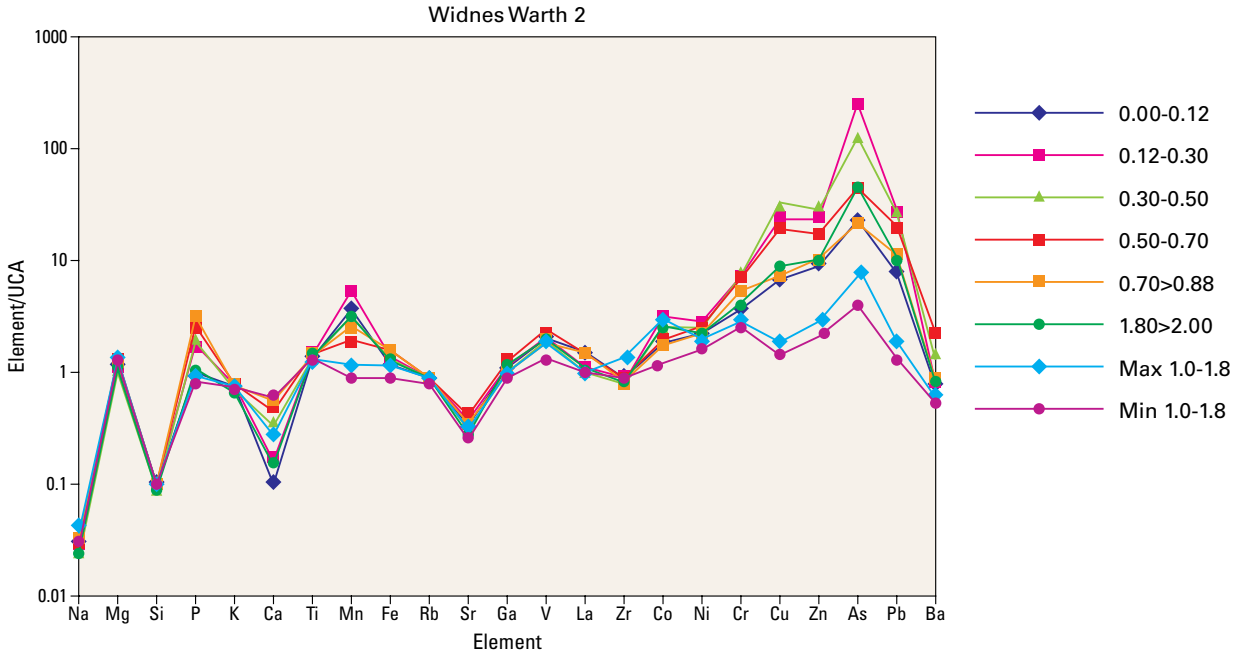

Figure 6.46 Spidergram showing down hole variation in borehole Widnes Warth 2 (normalised to Al to reduce grain-size effects).

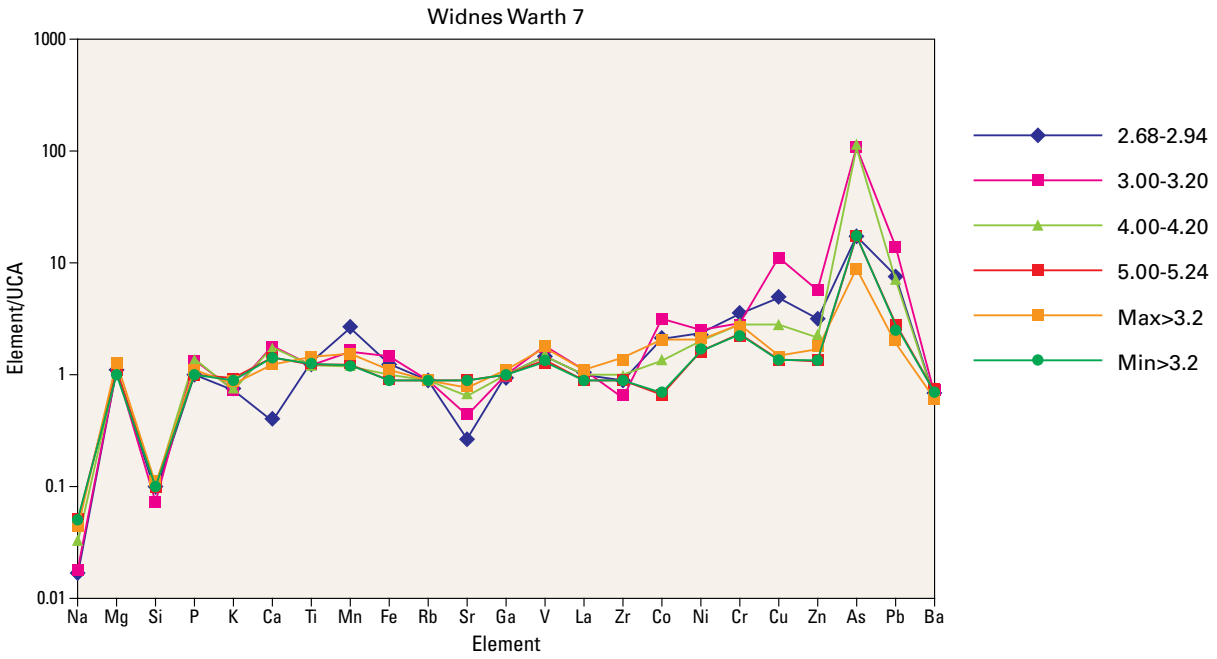

Figure 6.47 Spidergram showing down hole variation in borehole Widnes Warth 7 (normalised to Al to reduce grain-size effects).

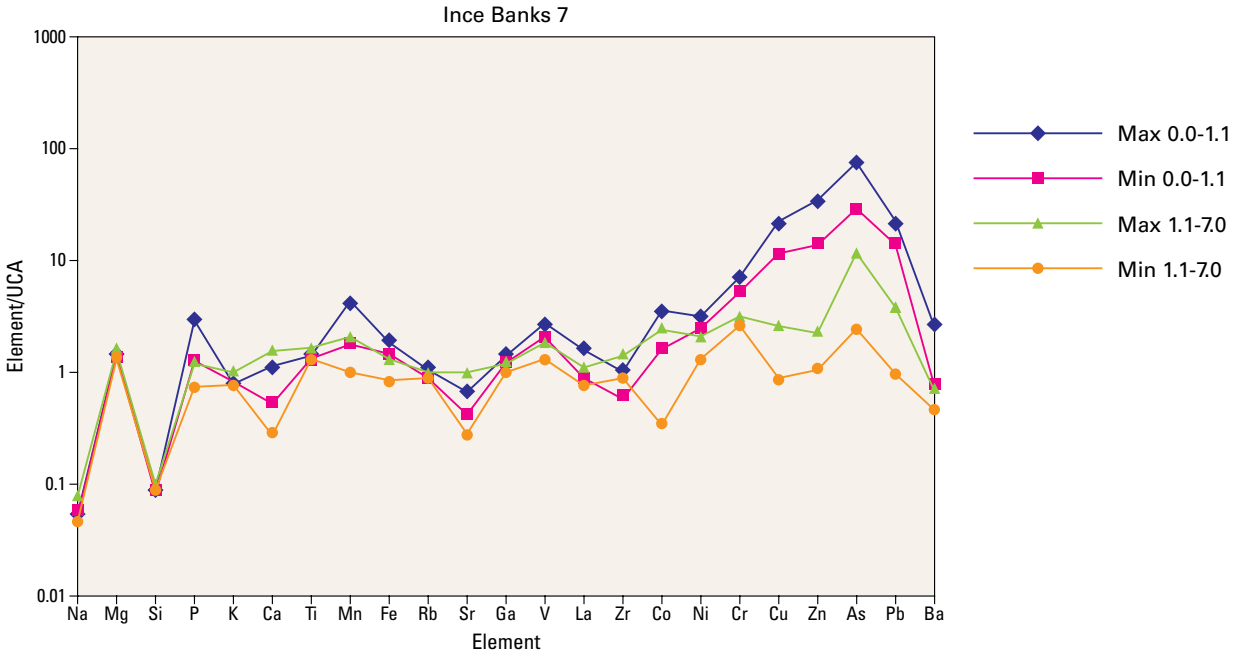

Figure 6.48 Spidergram showing down hole variation in borehole Ince Banks 7 (normalised to Al to reduce grain-size effects).

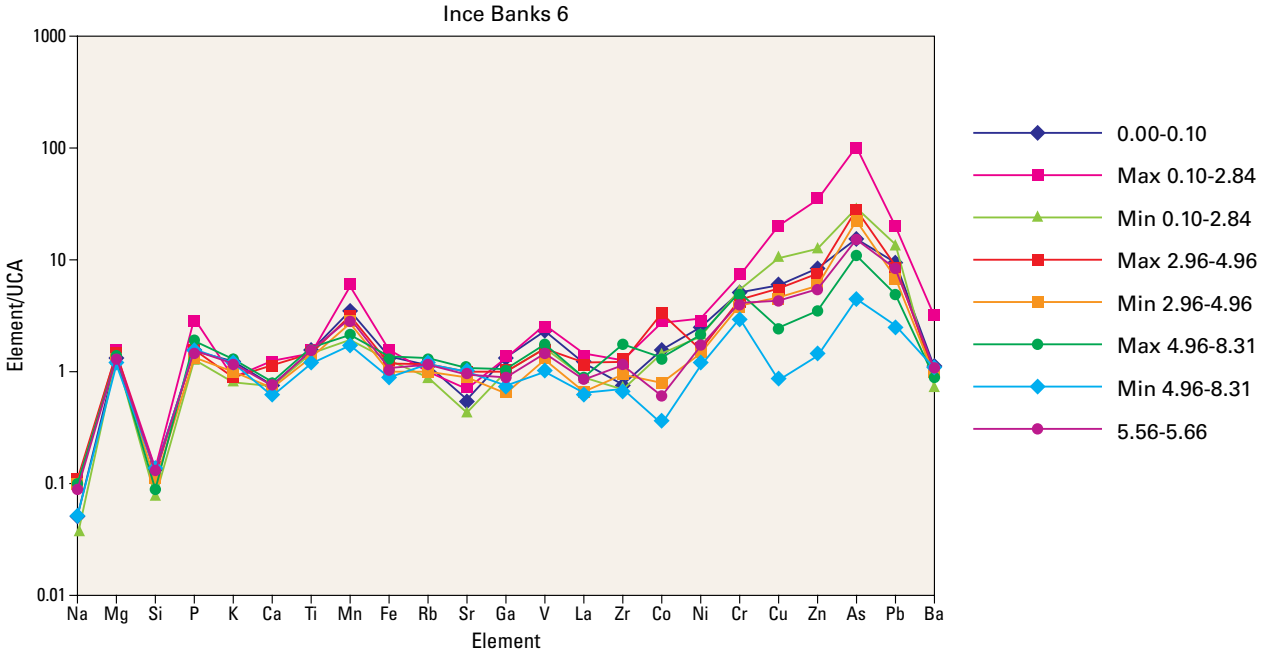

Figure 6.49 Spidergram showing down hole variation in borehole Ince Banks 6 (normalised to Al to reduce grain-size).

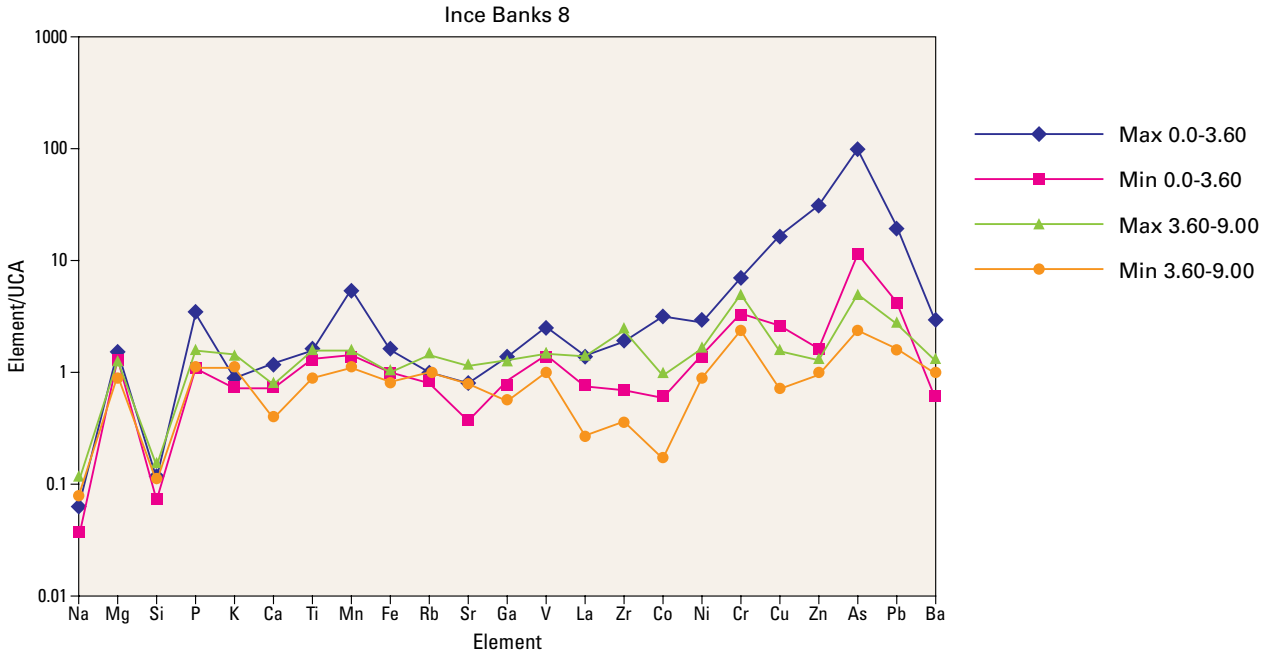

Figure 6.50 Spidergram showing down hole variation in borehole Ince Banks 8 (normalised to Al to reduce grain-size).

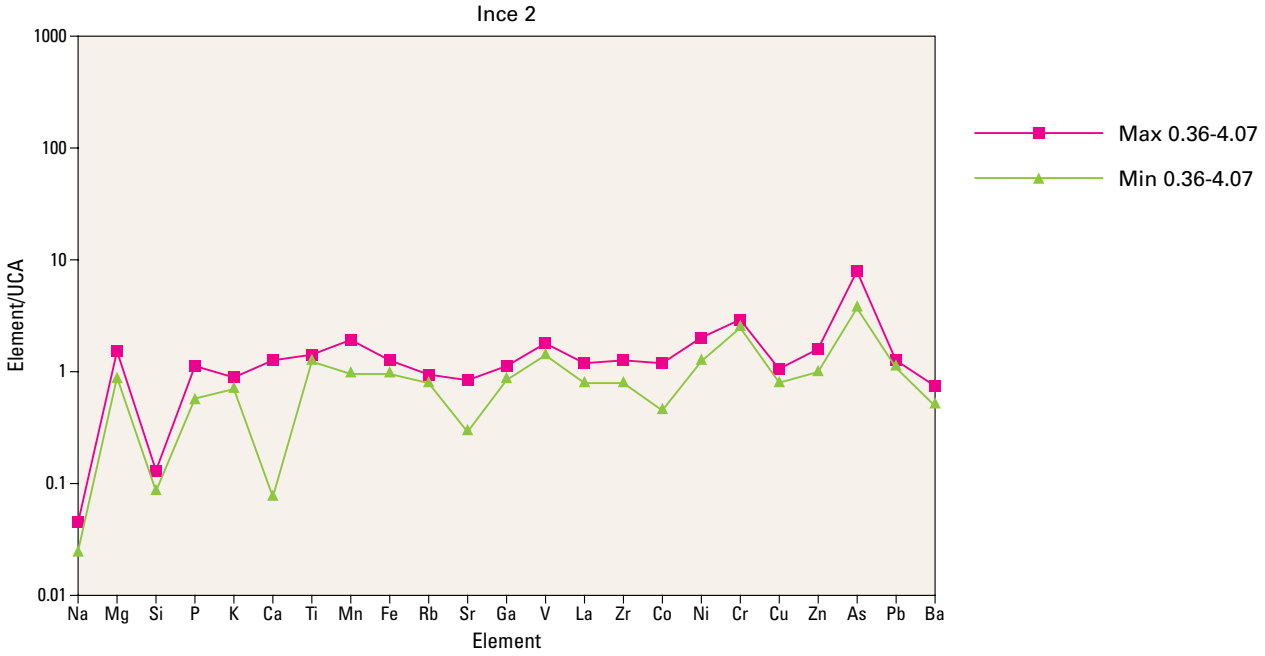

Figure 6.51 Spidergram showing down hole variation in borehole Ince 2 (normalised to Al to reduce grain-size effects).

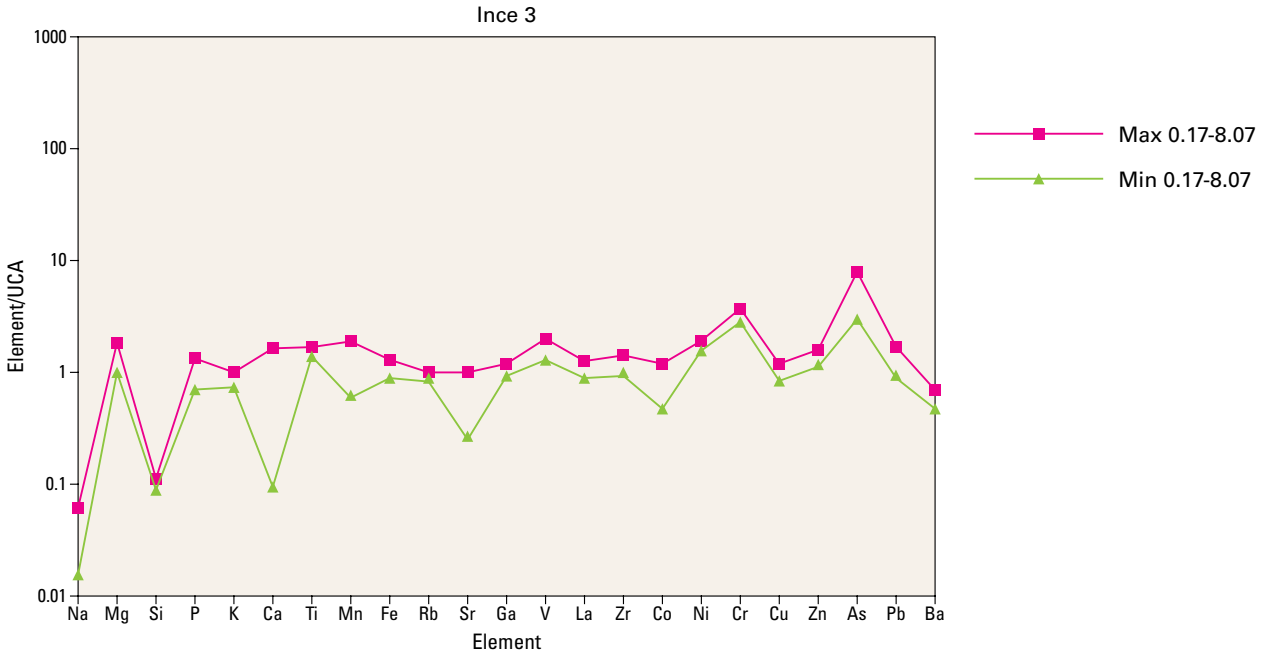

Figure 6.52 Spidergram showing down hole variation in borehole Ince 3 (normalised to Al to reduce grain-size effects).

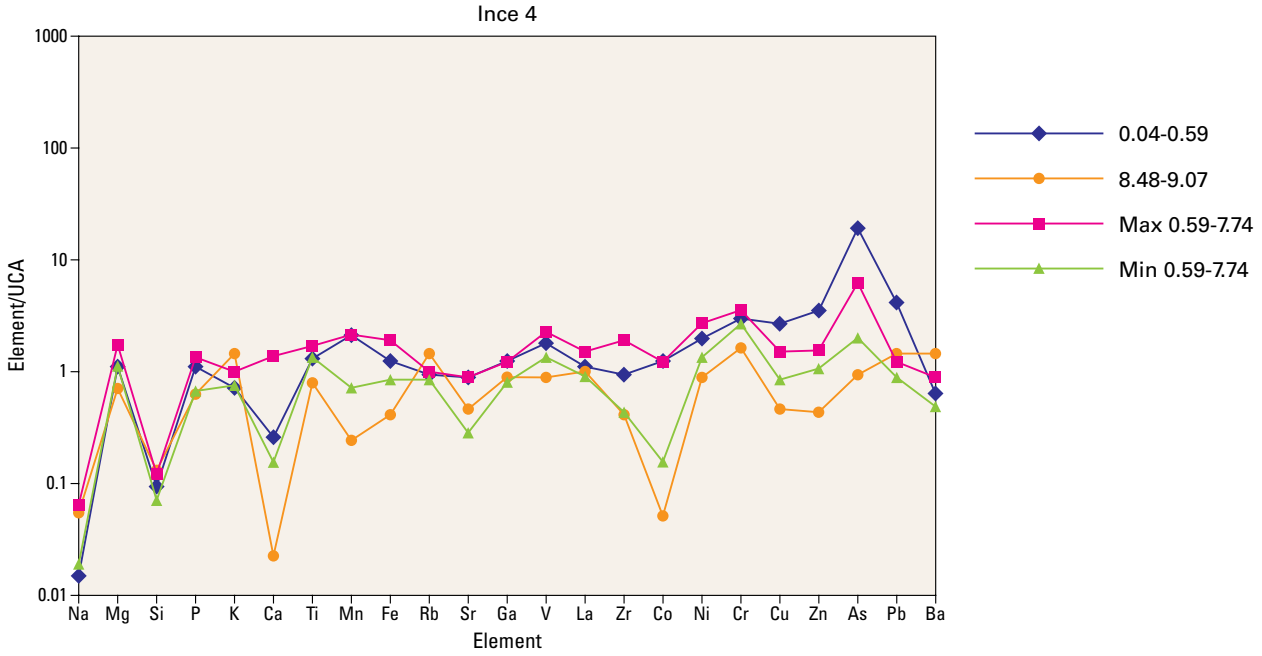

Figure 6.53 Spidergram showing down hole variation in borehole Ince 4 (normalised to Al to reduce grain-size effects).

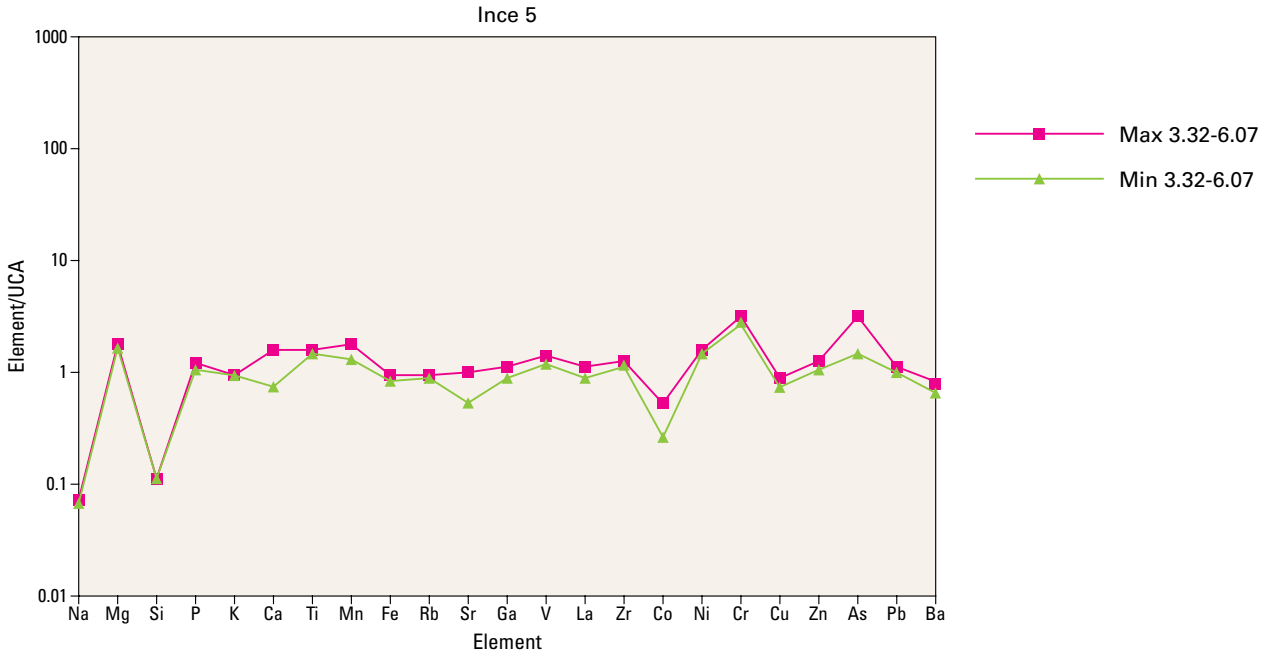

Figure 6.54 Spidergram showing down hole variation in borehole Ince 5 (normalised to Al to reduce grain-size effects).

Figure 6.55 Down core profile for Hg in Widnes Warth core WW1.

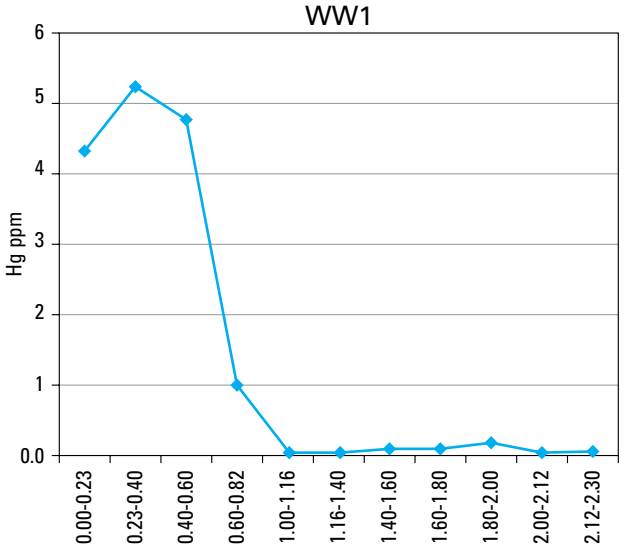

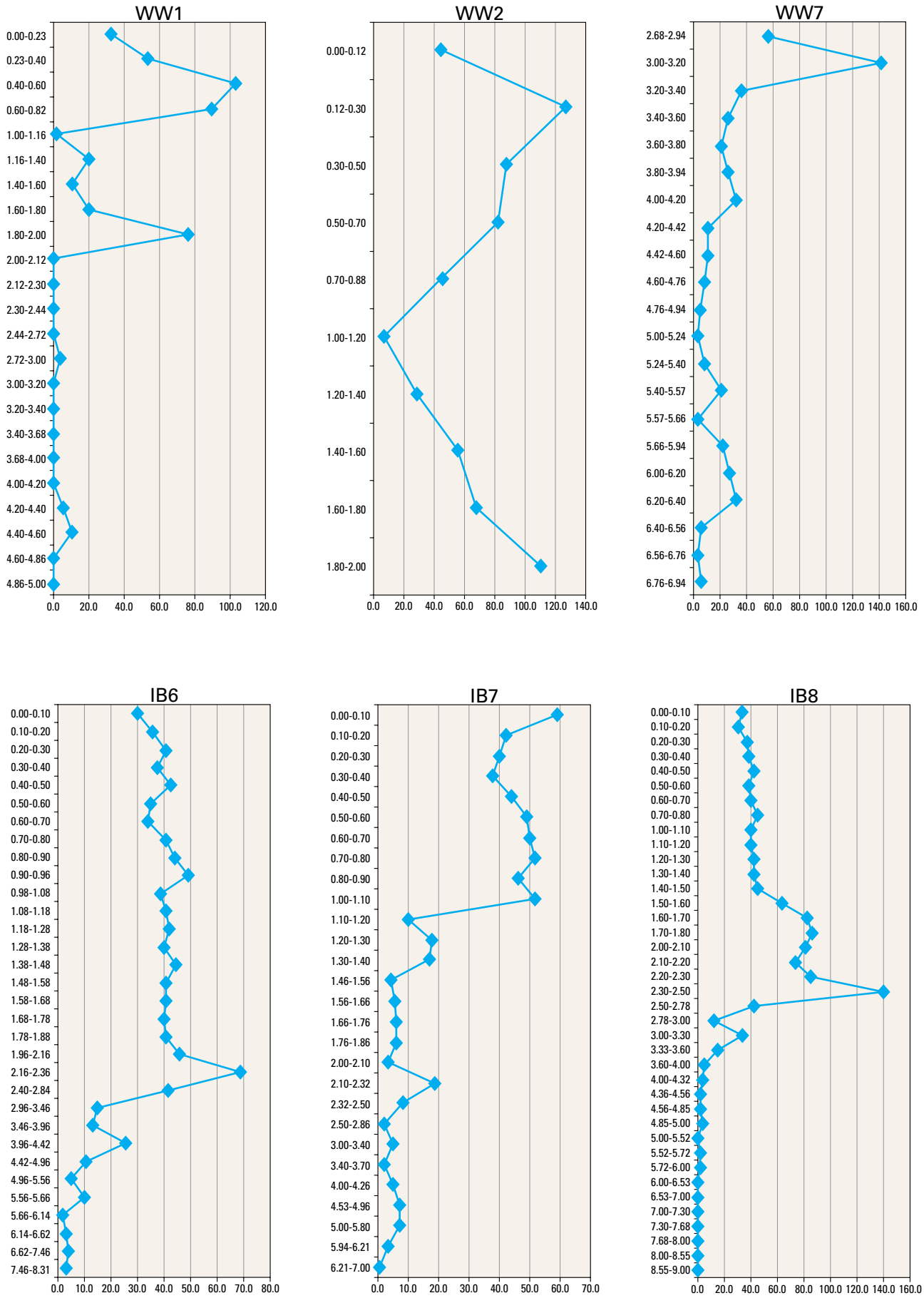

Figure 6.56 Down profiles for Sn in Widnes Warth cores WW1, WW2 and WW7 and Ince Banks cores IB6, IB7 and IB8.

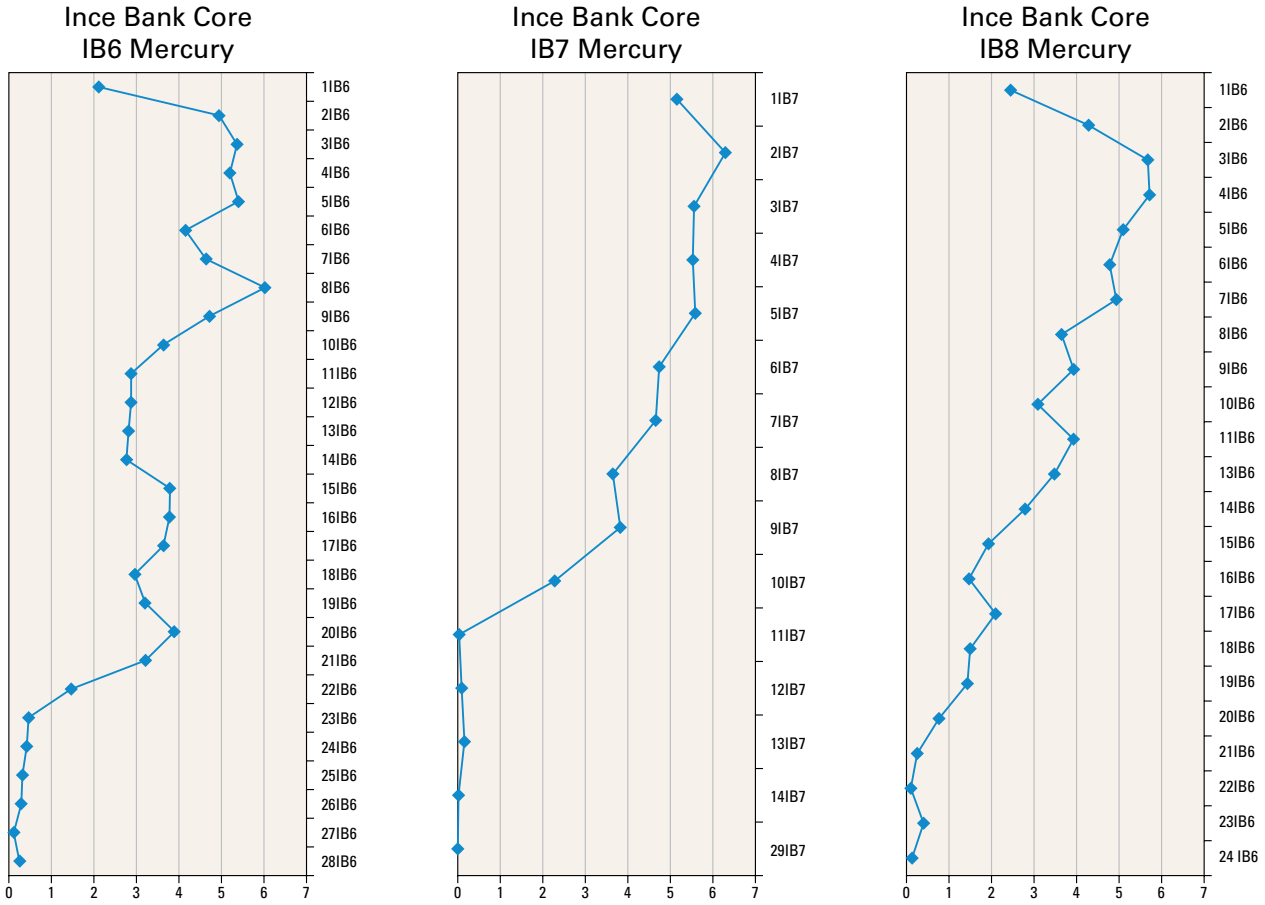

Figure 6.57 Down core profiles for Hg in Ince Banks cores IB6, IB7 and IB8 (see Figure 6.15 for core locations).

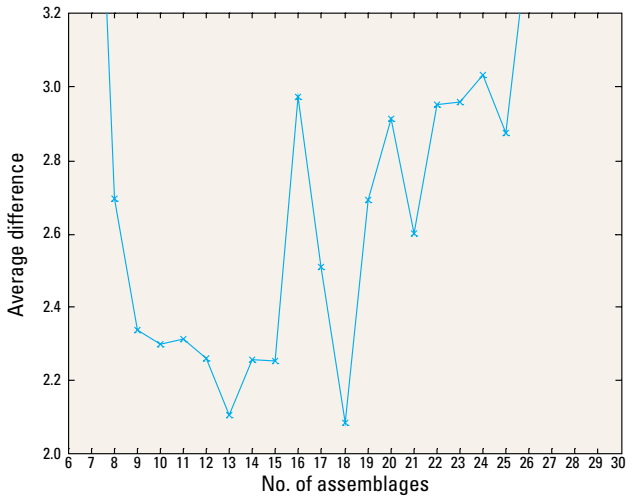

Figure 6.58 Comparison of the average absolute differences between actual and modelled data.

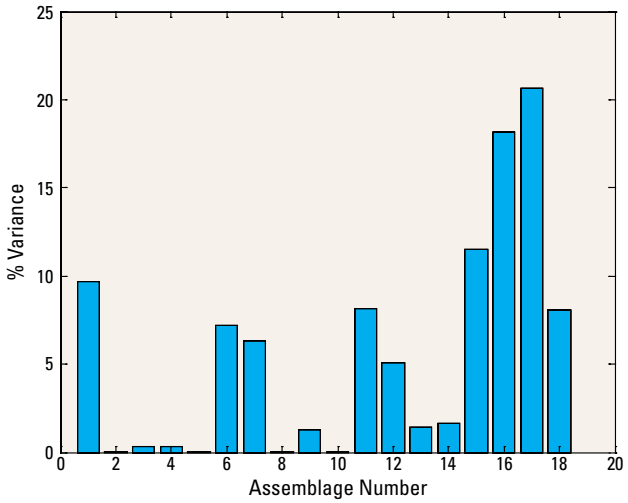

Figure 6.59 Variance in the total element data explained by individual assemblages.

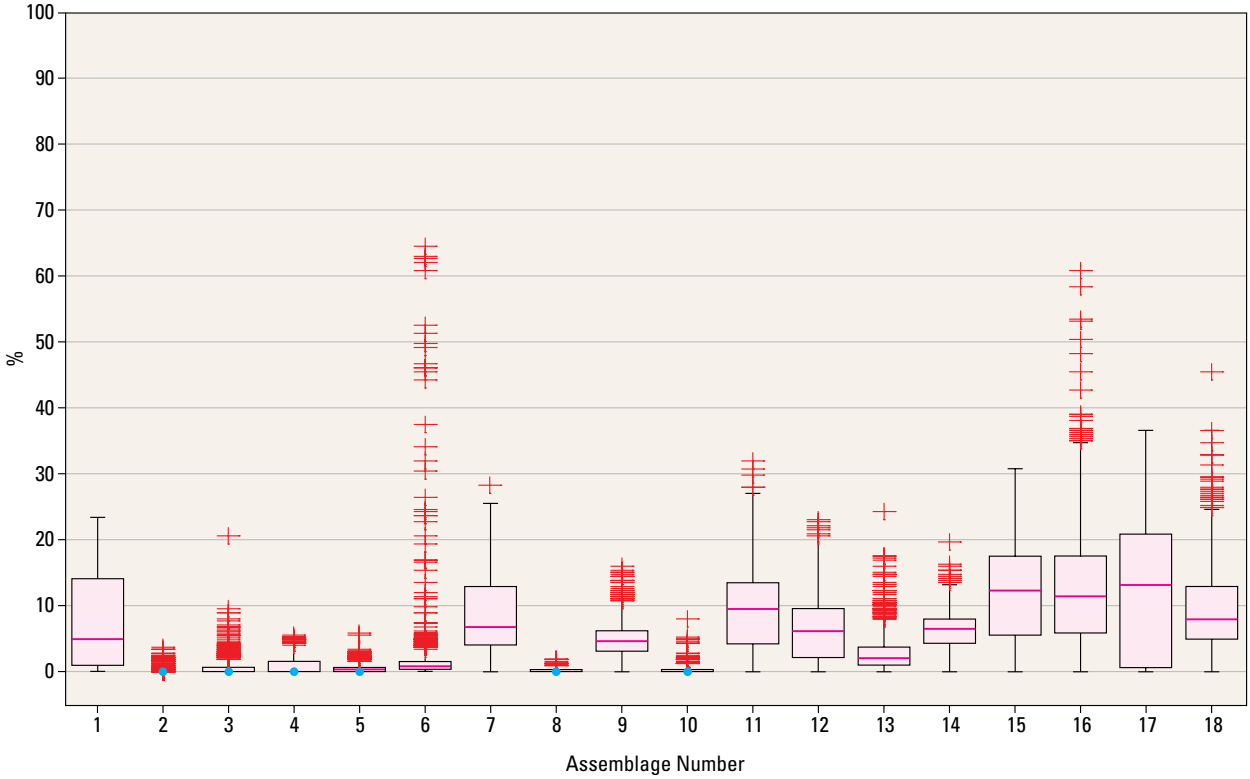

Figure 6.60 Range of masses of each assemblage found in all of the samples.

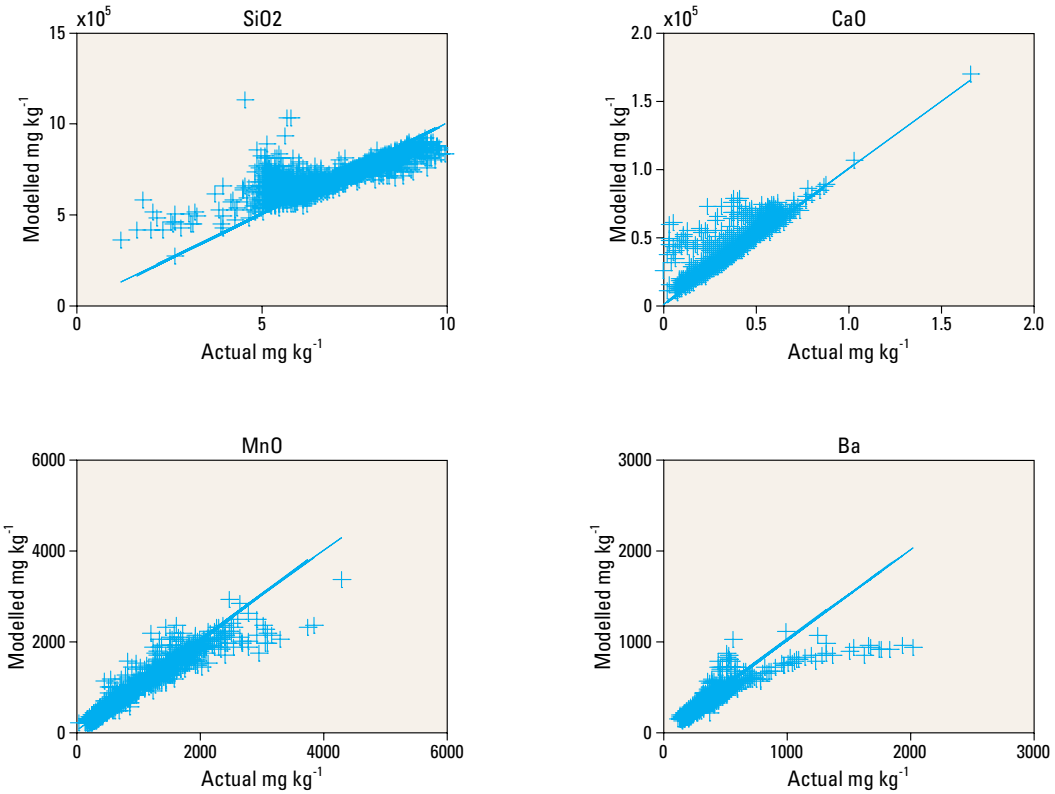

Figure 6.61 Model fit plots for the four worse case elements; Si, Ca, Mn and Ba.

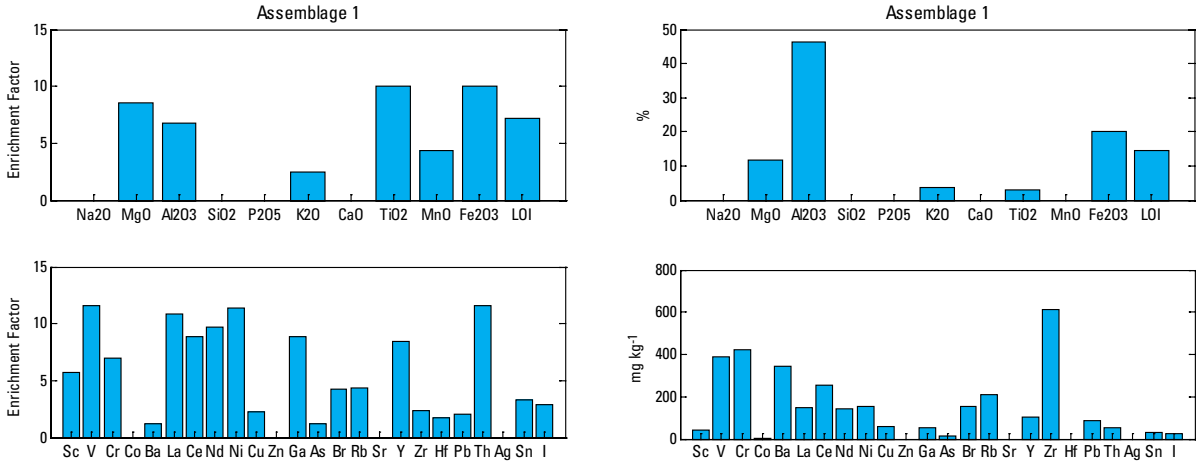

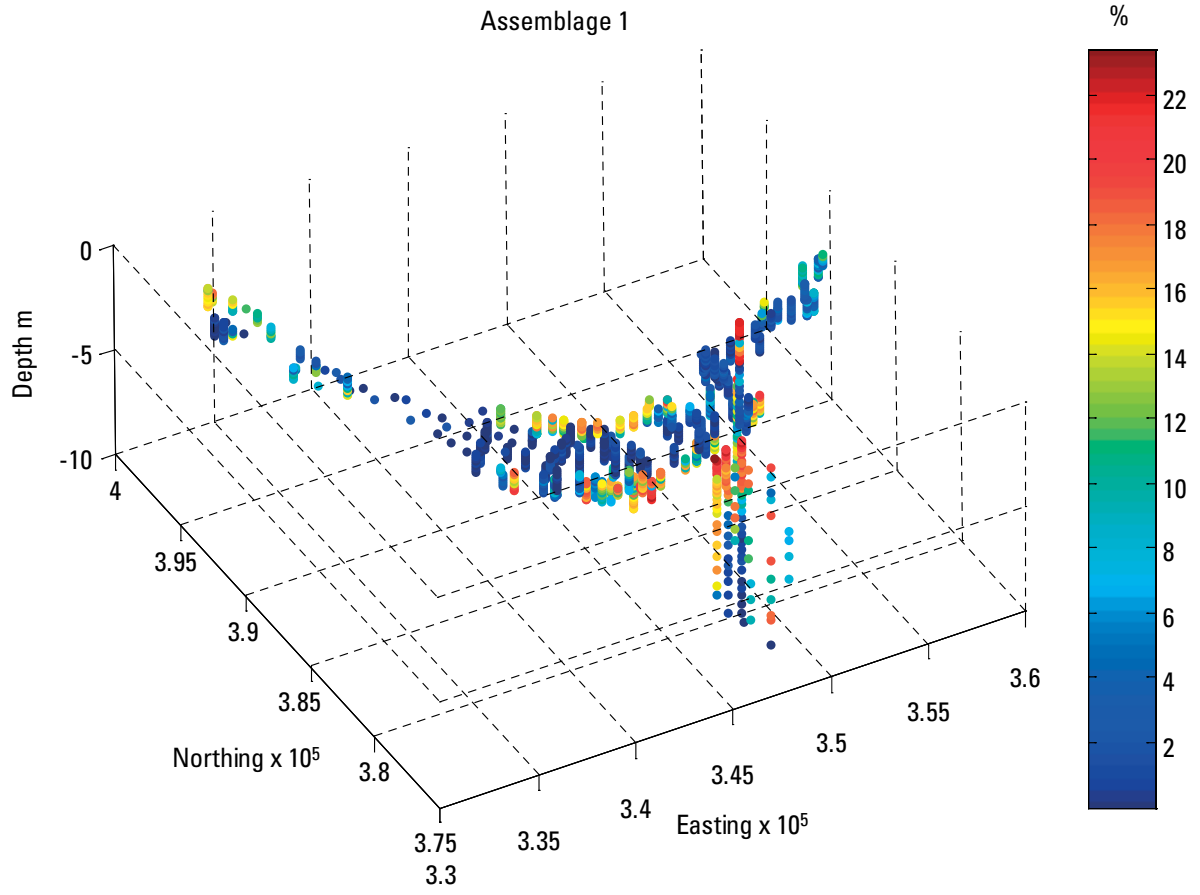

Figure 6.62 Summary of the composition and distribution of Assemblage 1.

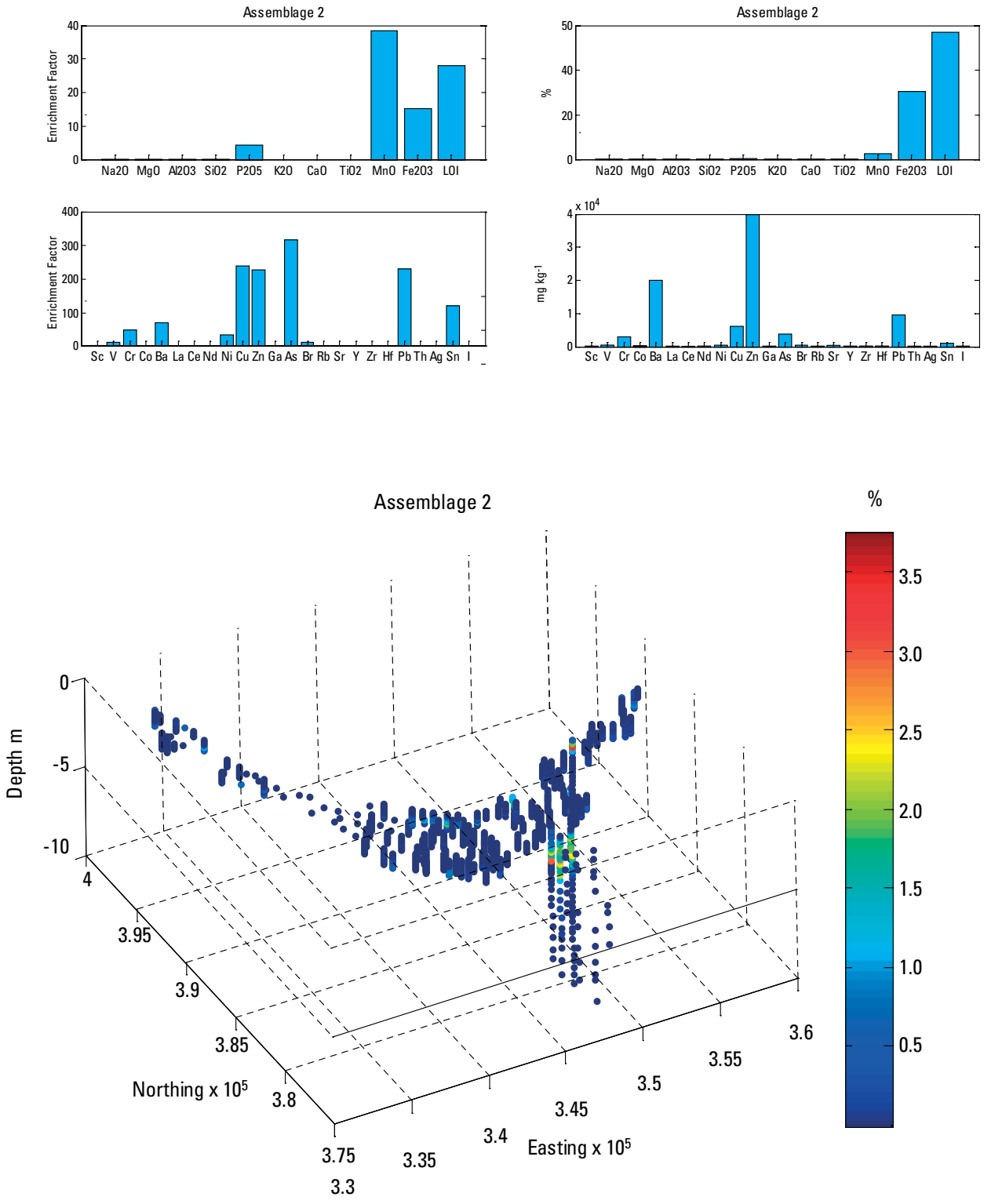

Figure 6.63 Summary of the composition and distribution of Assemblage 2.

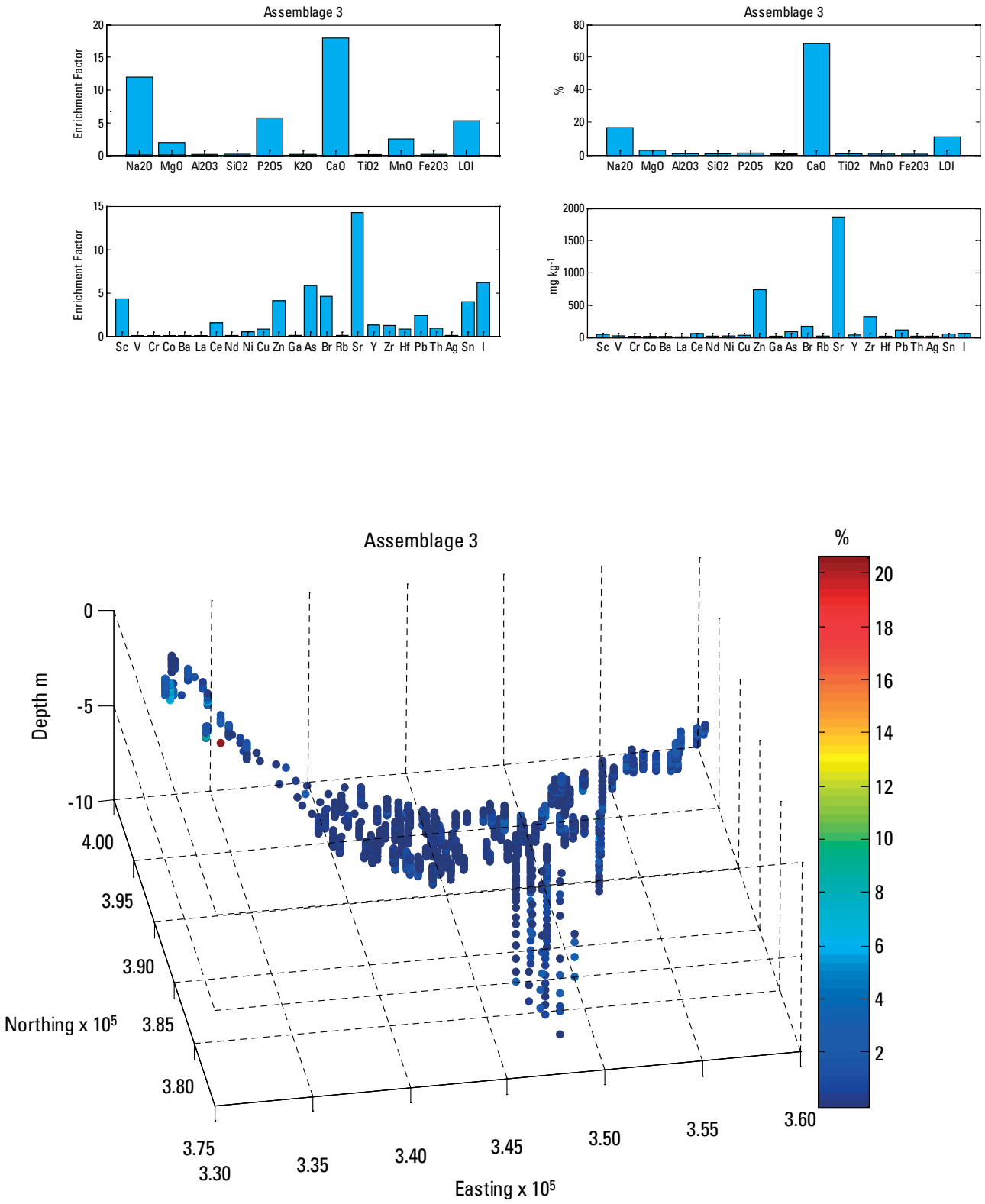

Figure 6.64 Summary of the composition and distribution of Assemblage 3.

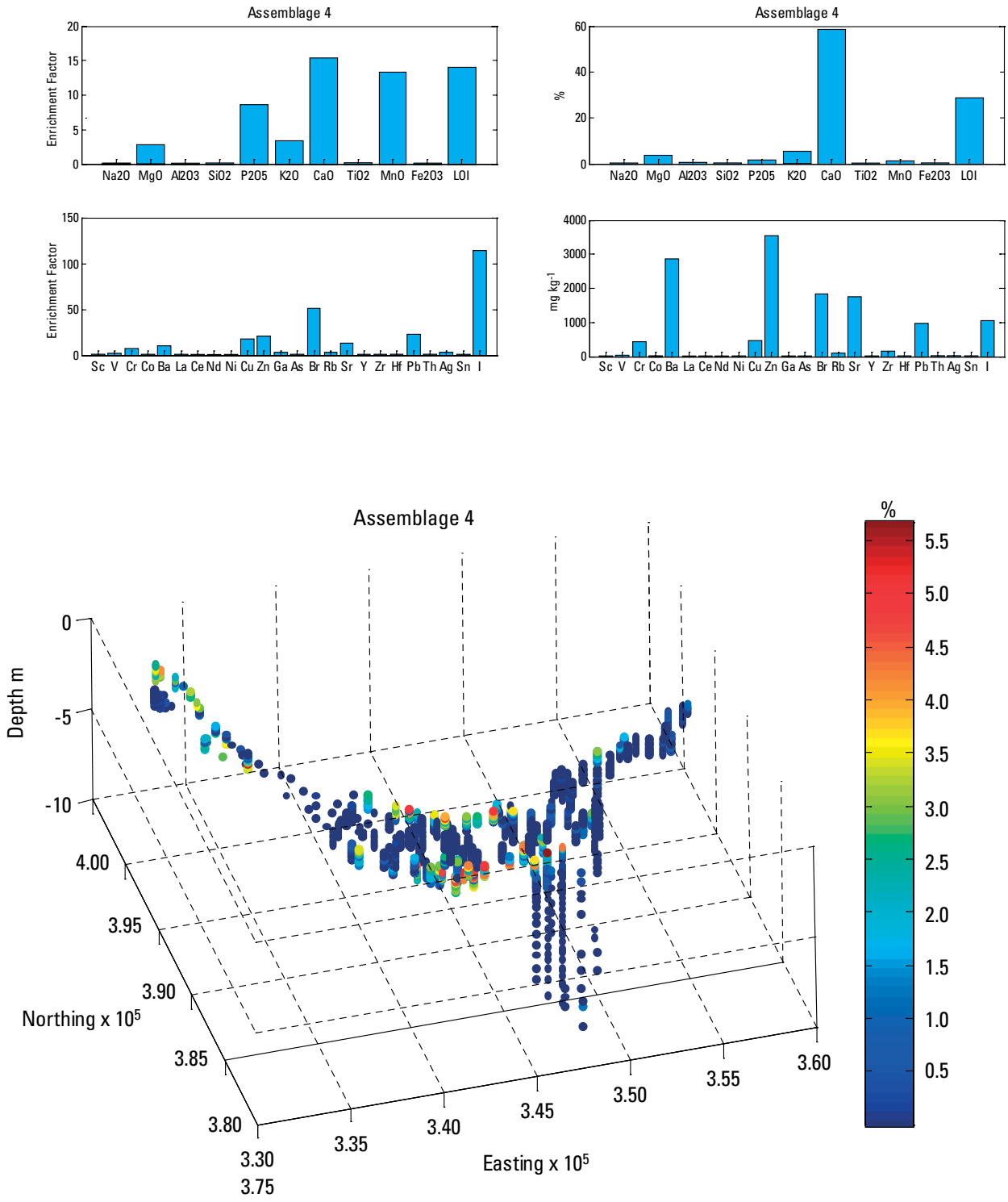

Figure 6.65 Summary of the composition and distribution of Assemblage 4.

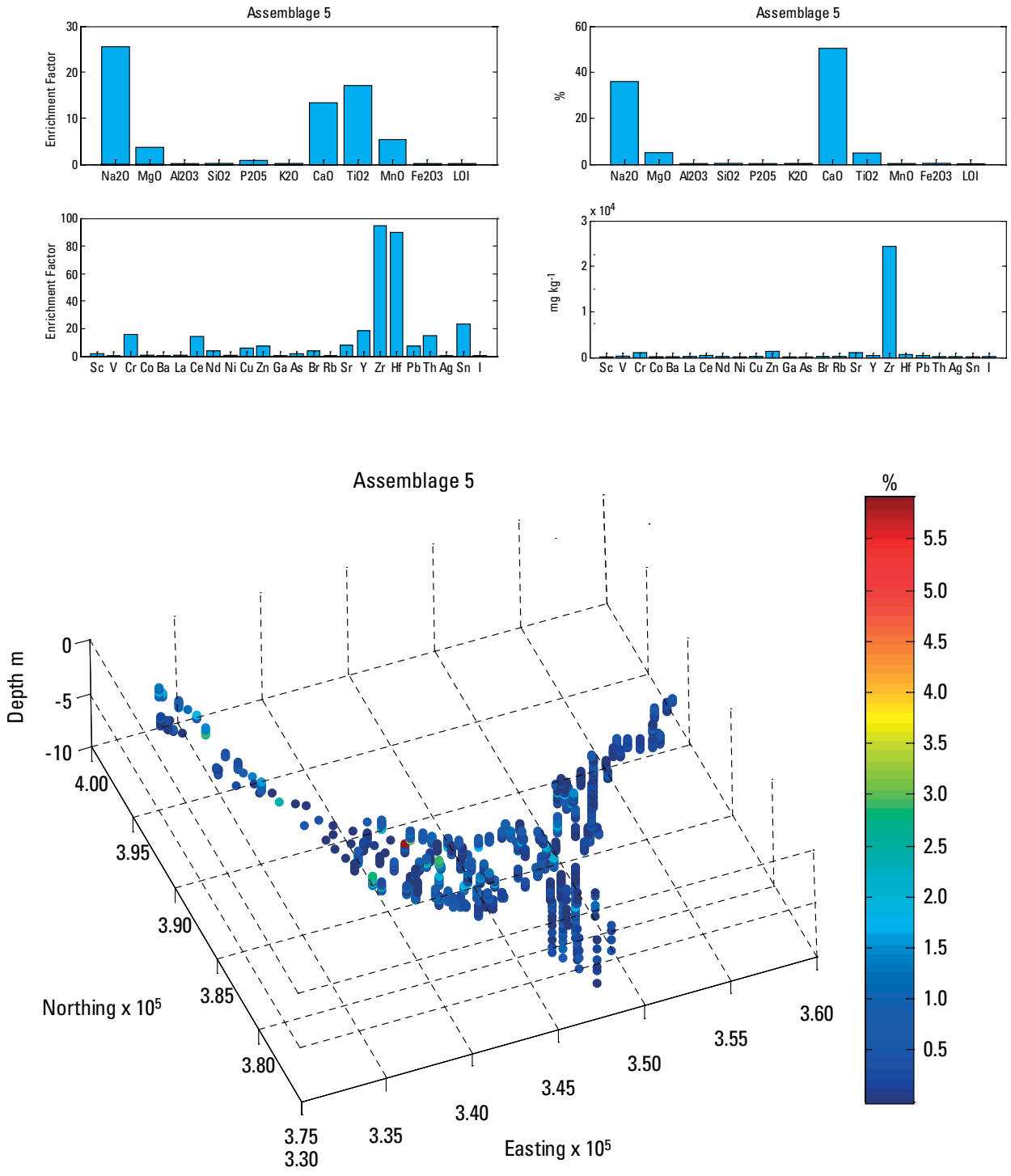

Figure 6.66 Summary of the composition and distribution of Assemblage 5.

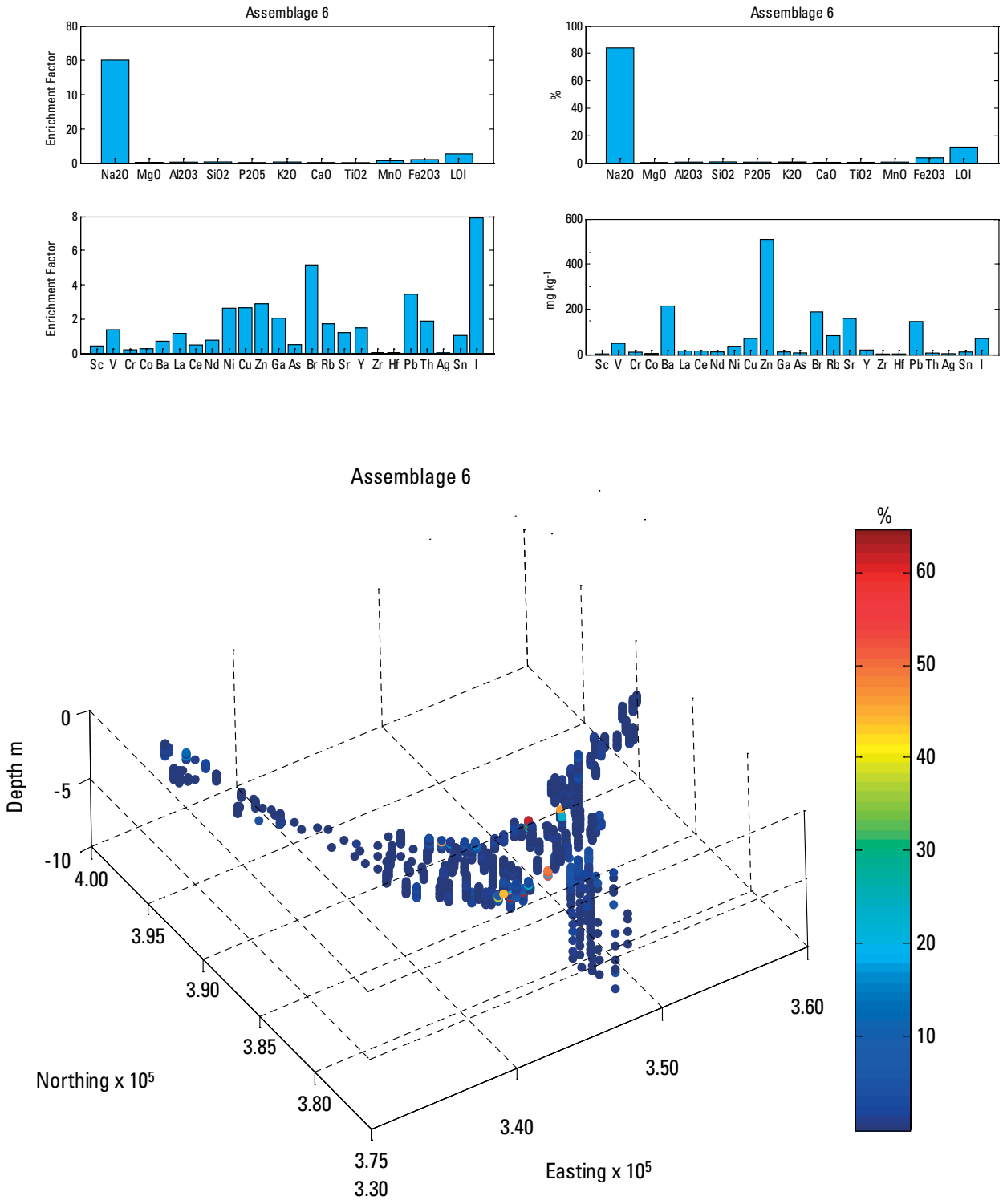

Figure 6.67 Summary of the composition and distribution of Assemblage 6.

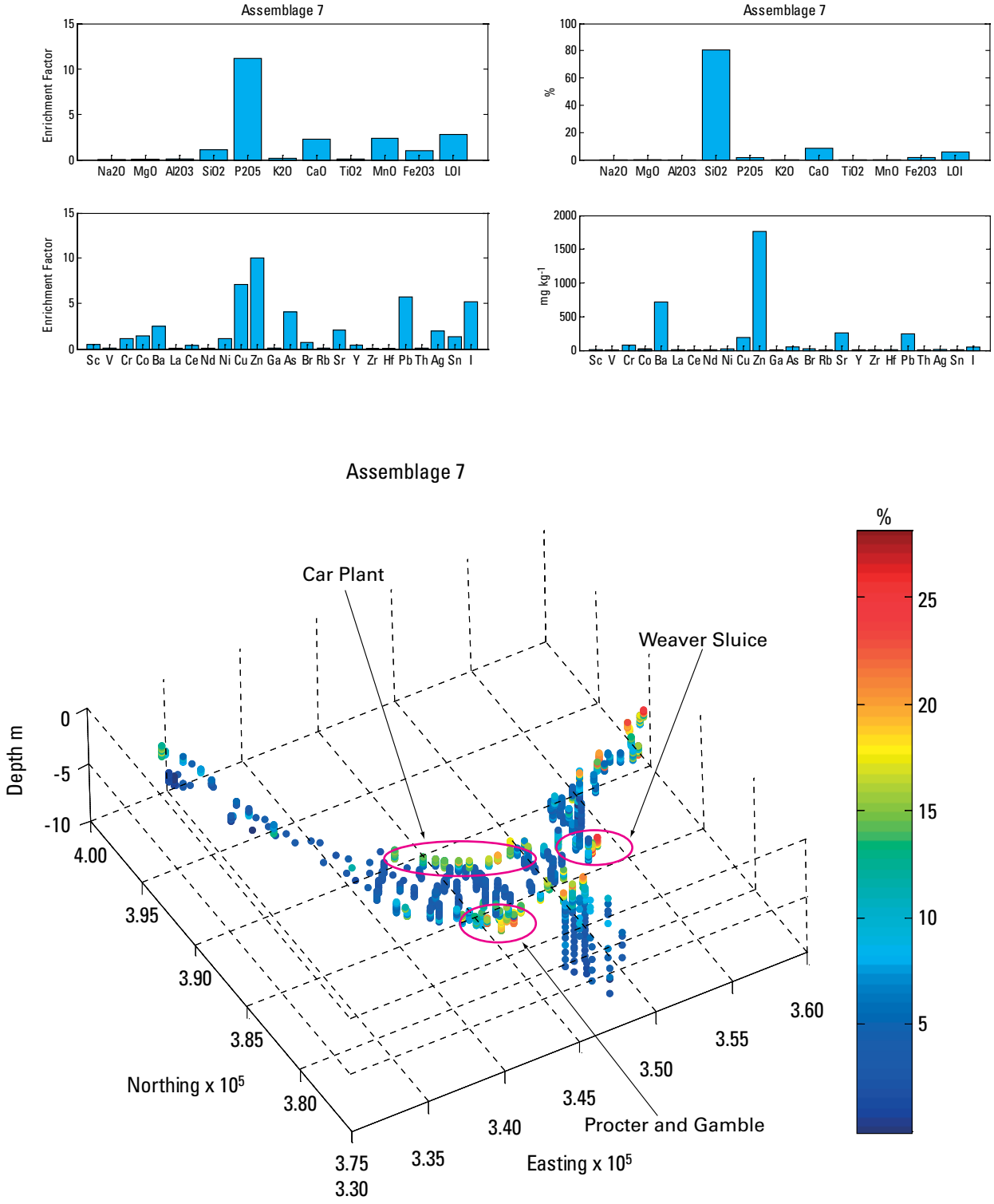

Figure 6.68 Summary of the composition and distribution of Assemblage 7.

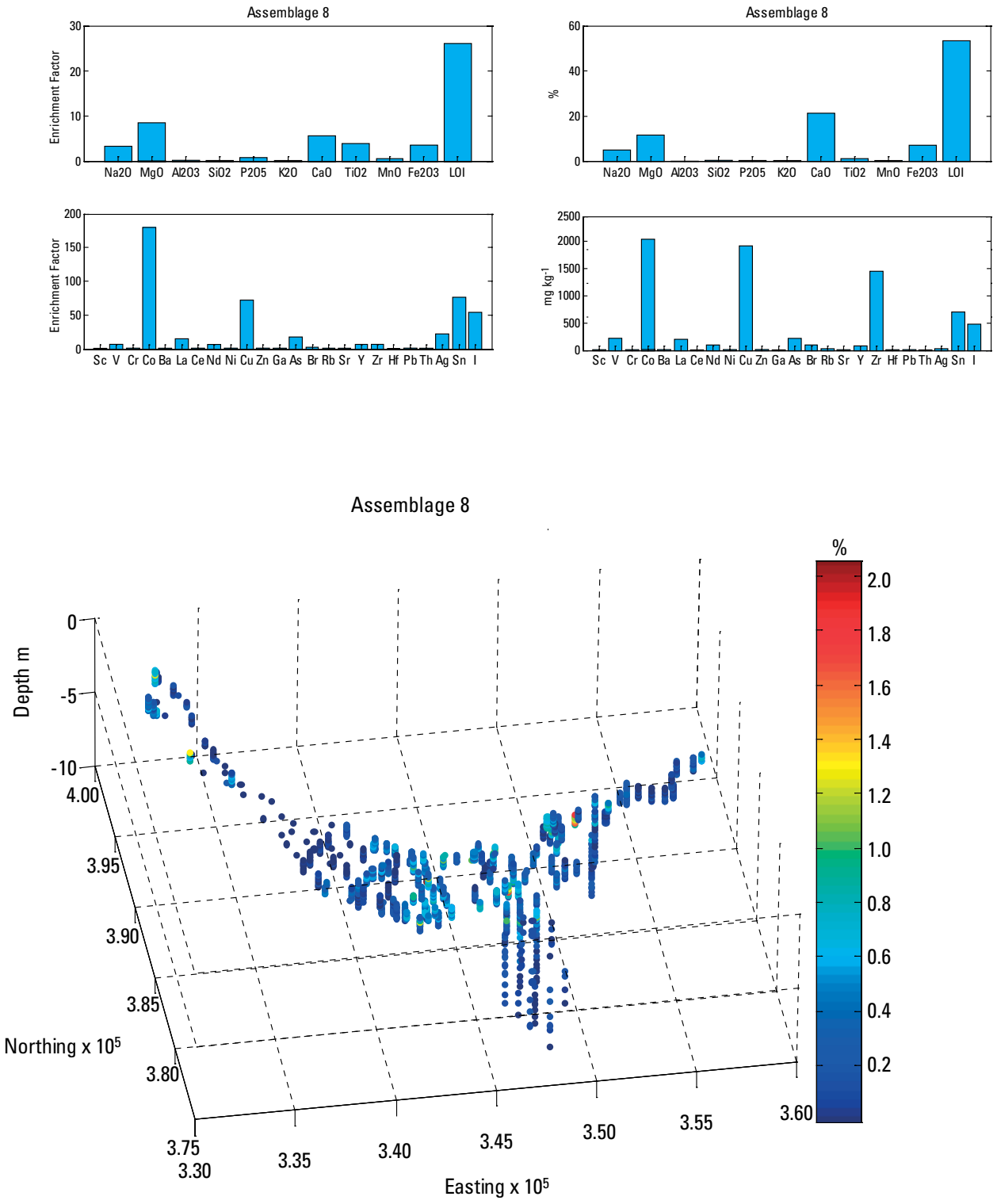

Figure 6.69 Summary of the composition and distribution of Assemblage 8.

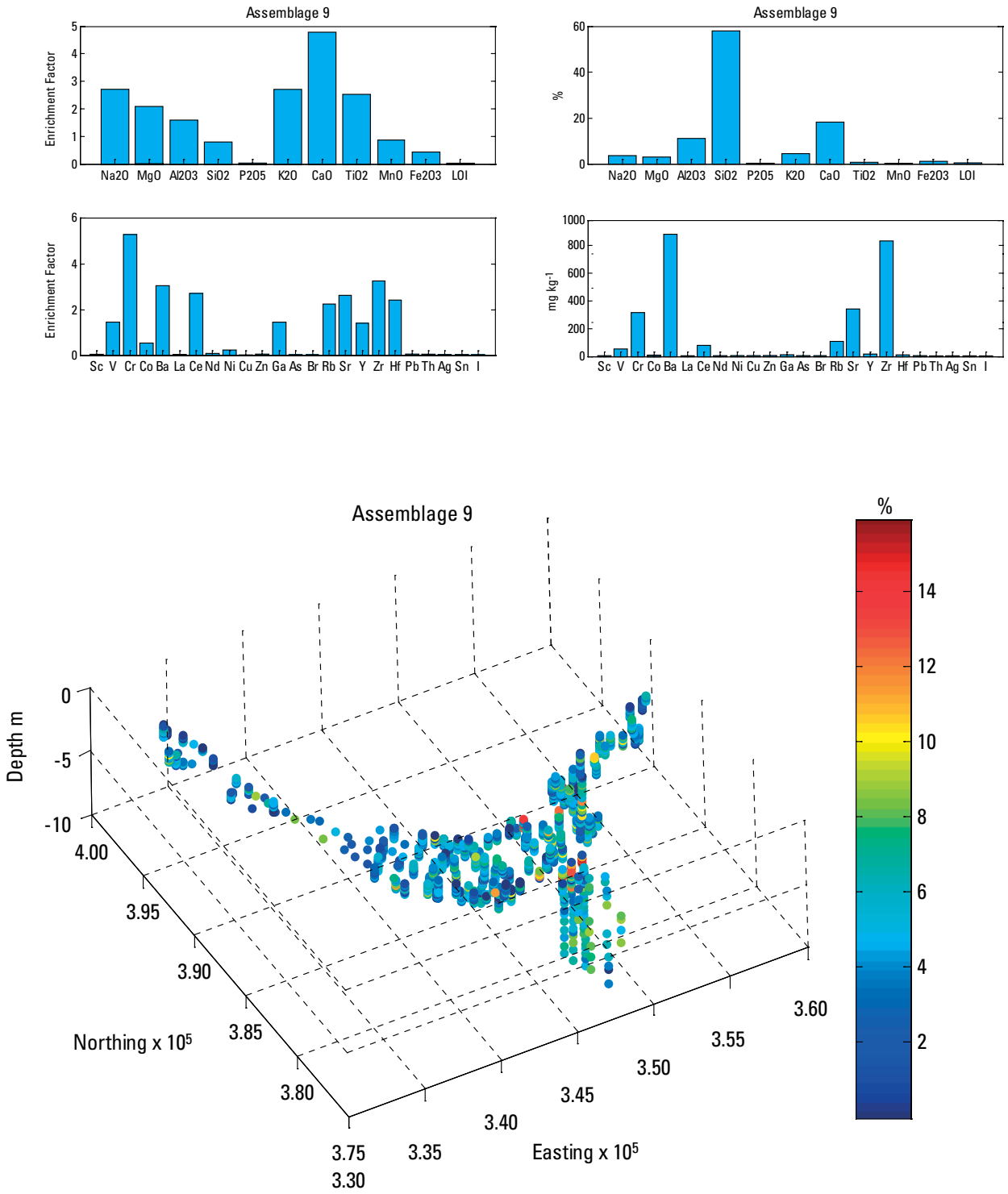

Figure 6.70 Summary of the composition and distribution of Assemblage 9.

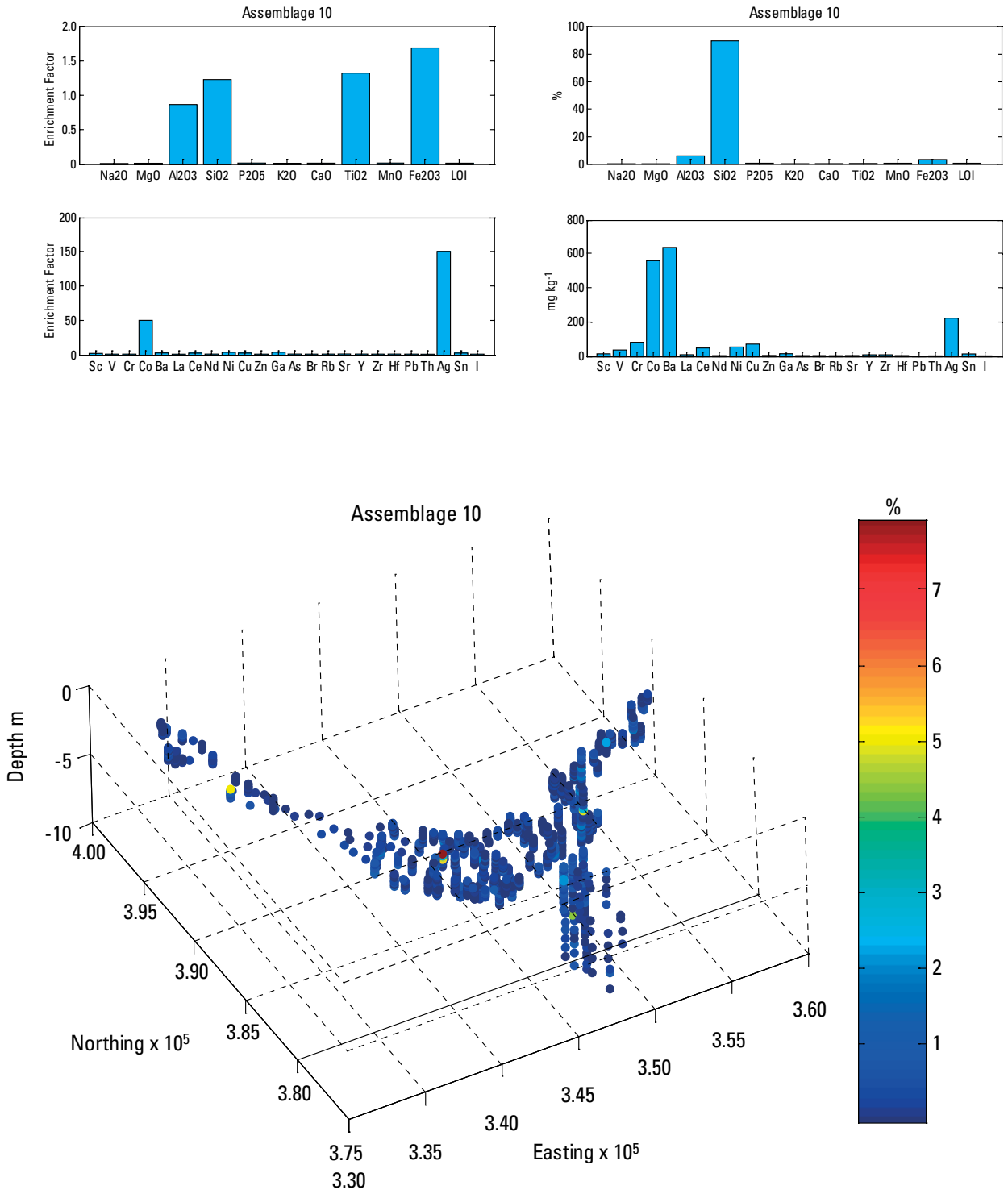

Figure 6.71 Summary of the composition and distribution of Assemblage 10.

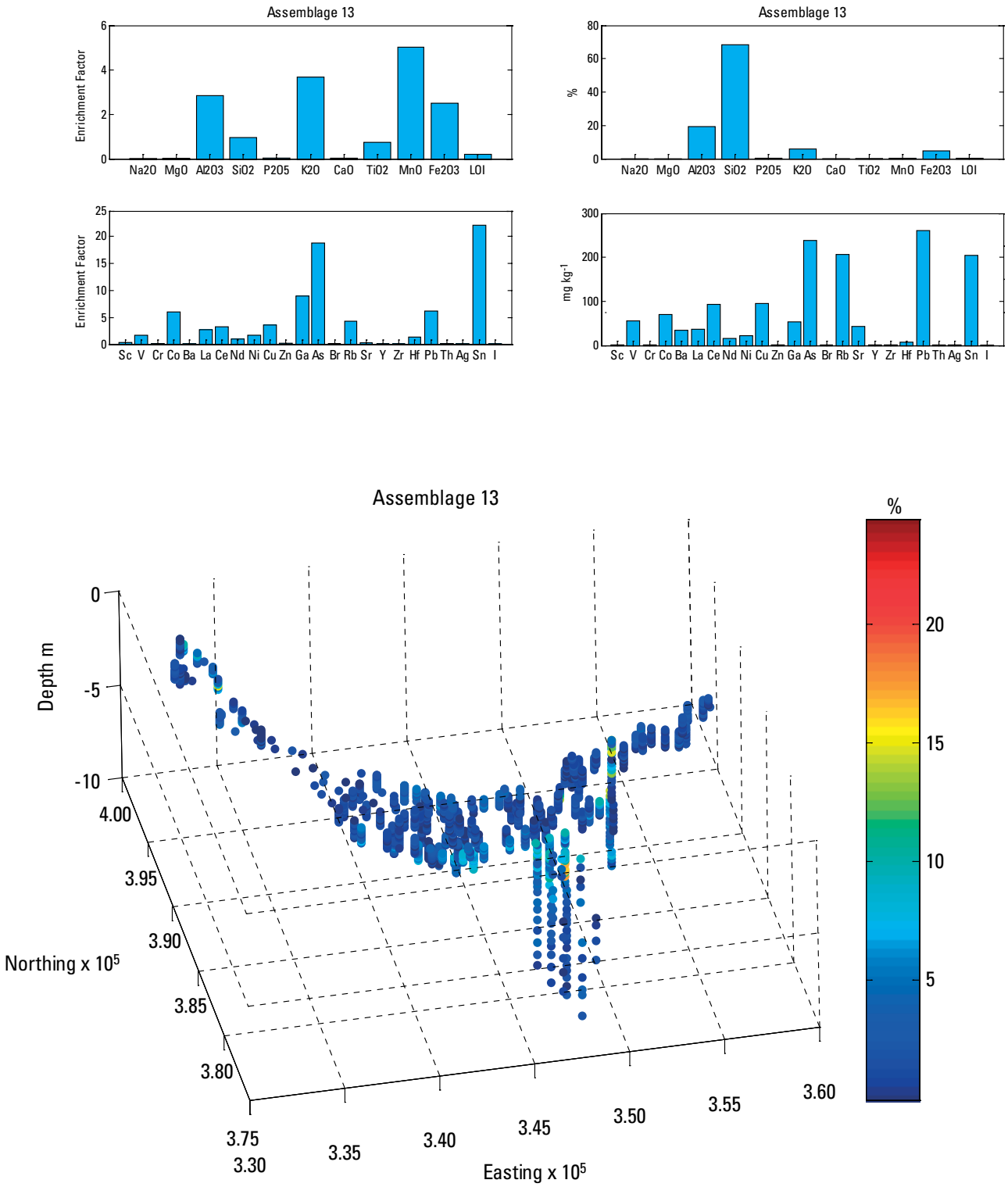

Figure 6.72 Summary of the composition and distribution of Assemblage 13.

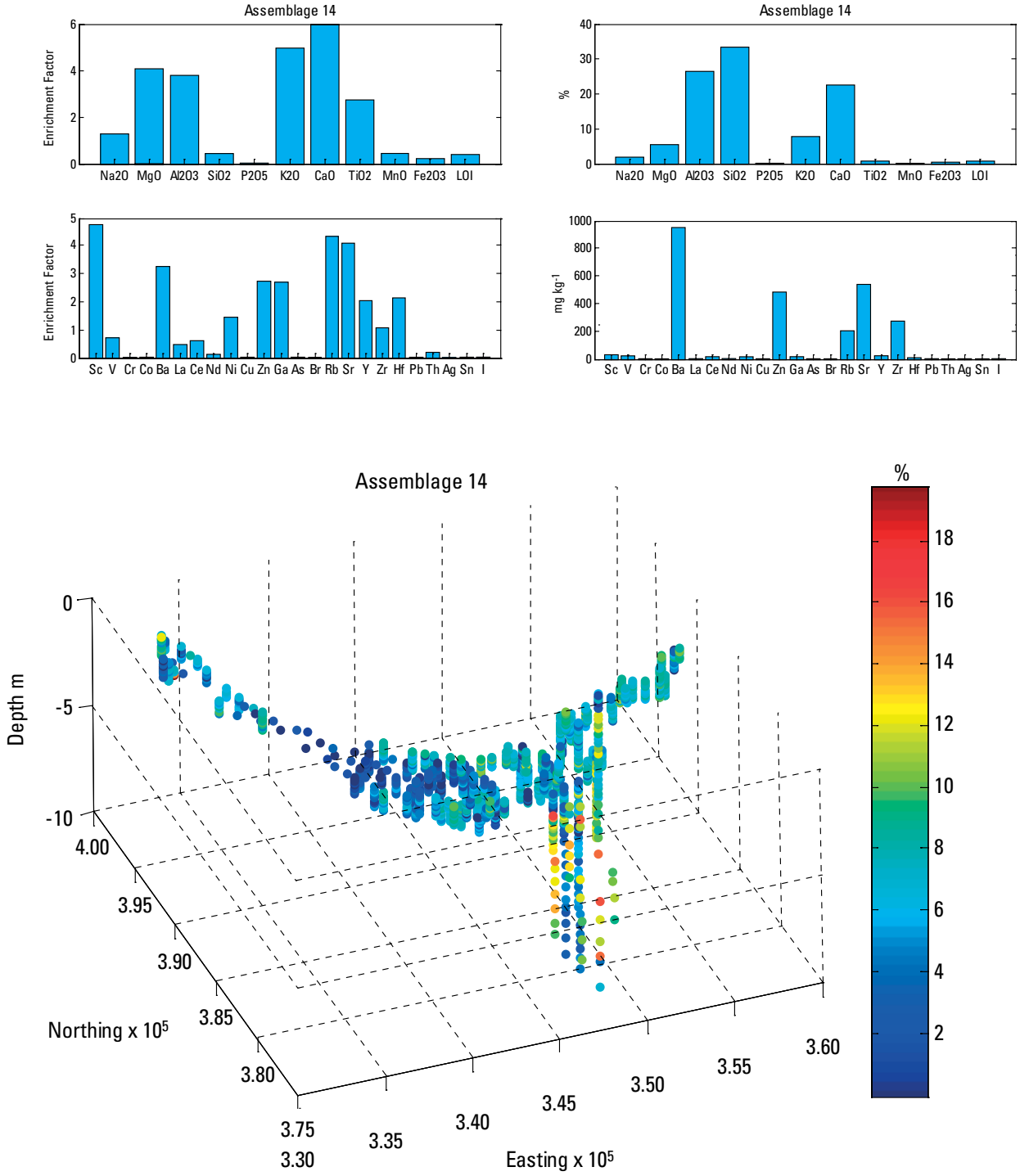

Figure 6.73 Summary of the composition and distribution of Assemblage 14.

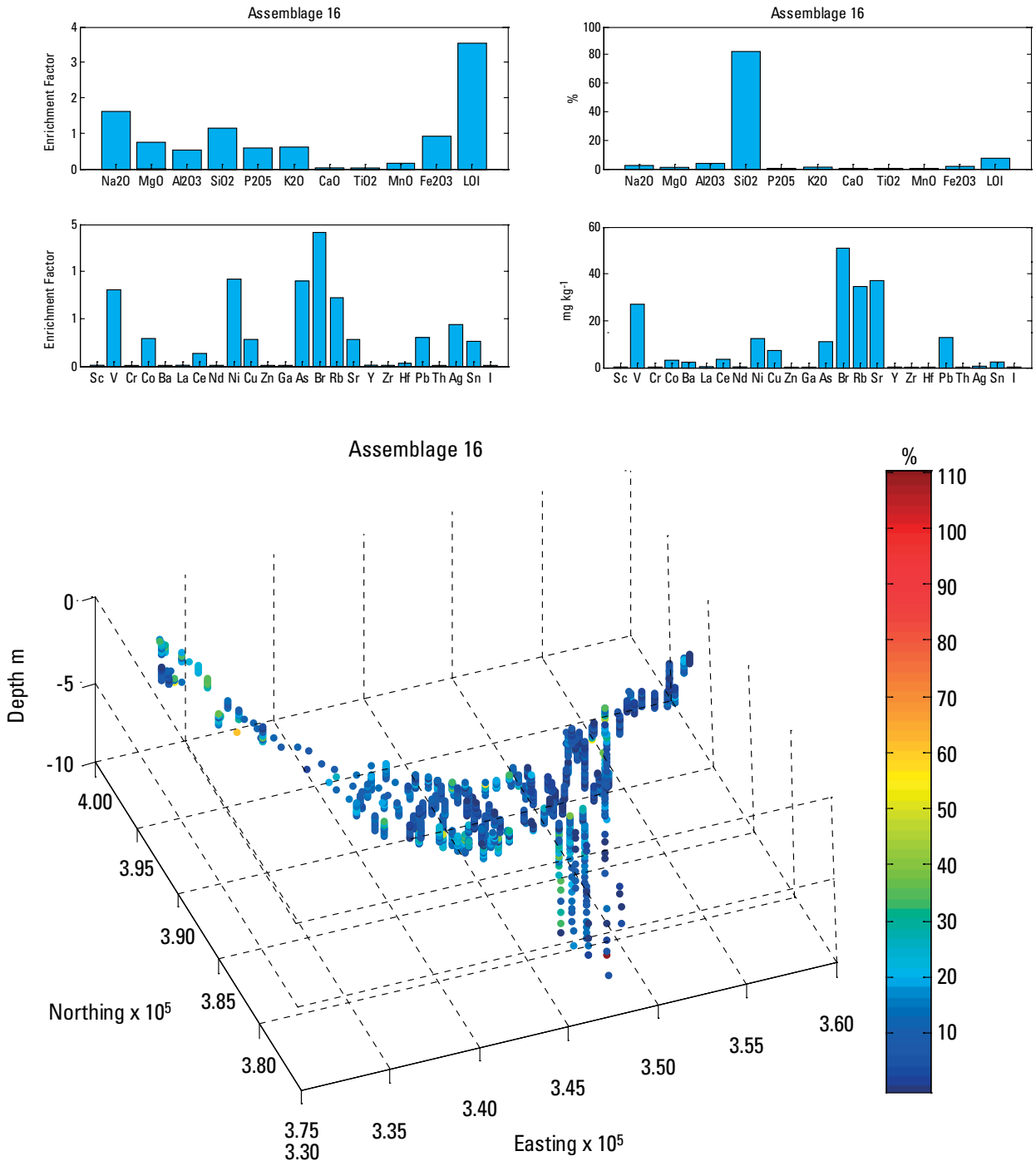

Figure 6.74 Summary of the composition and distribution of Assemblage 16.

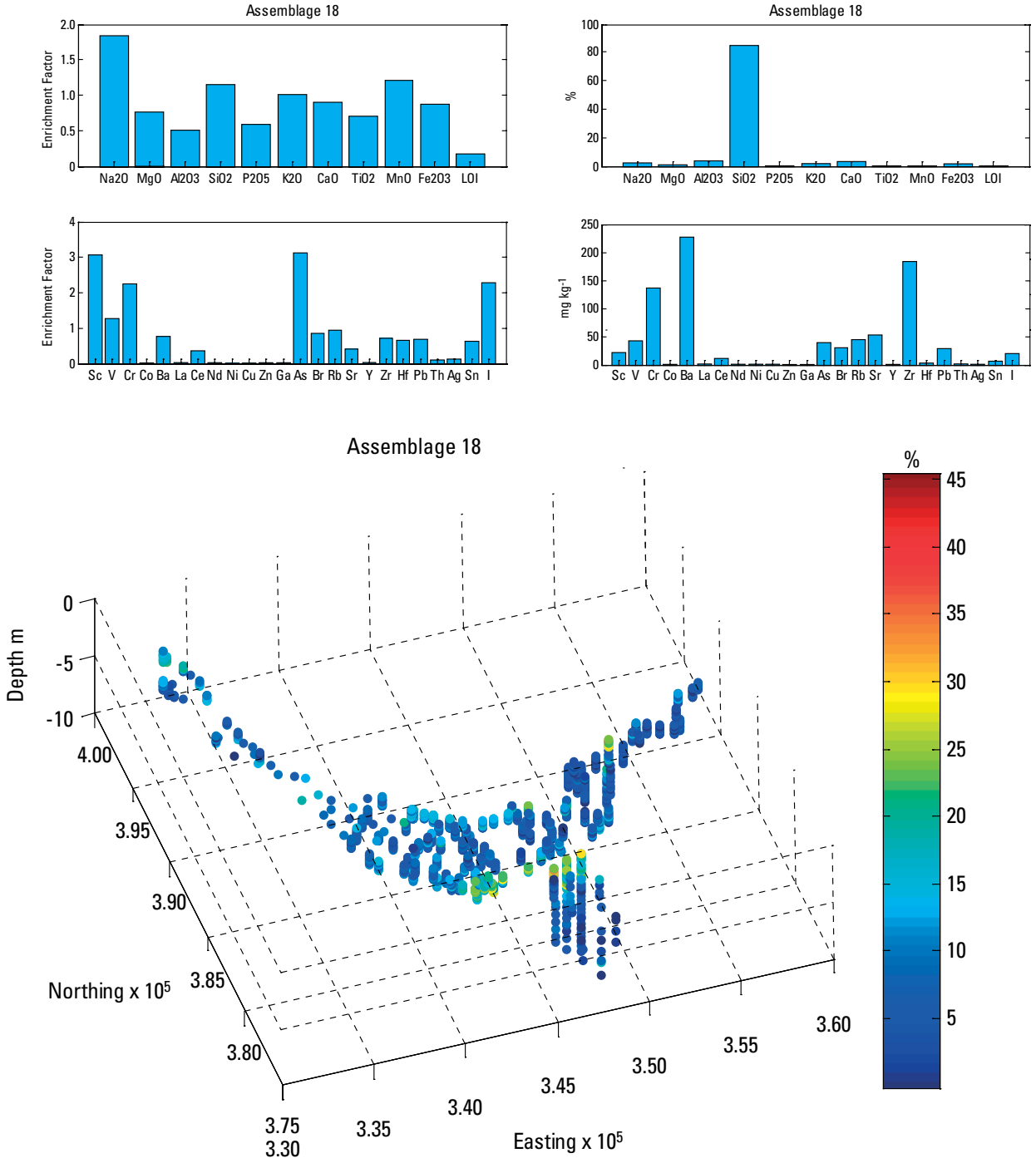

Figure 6.75 Summary of the composition and distribution of Assemblage 18.

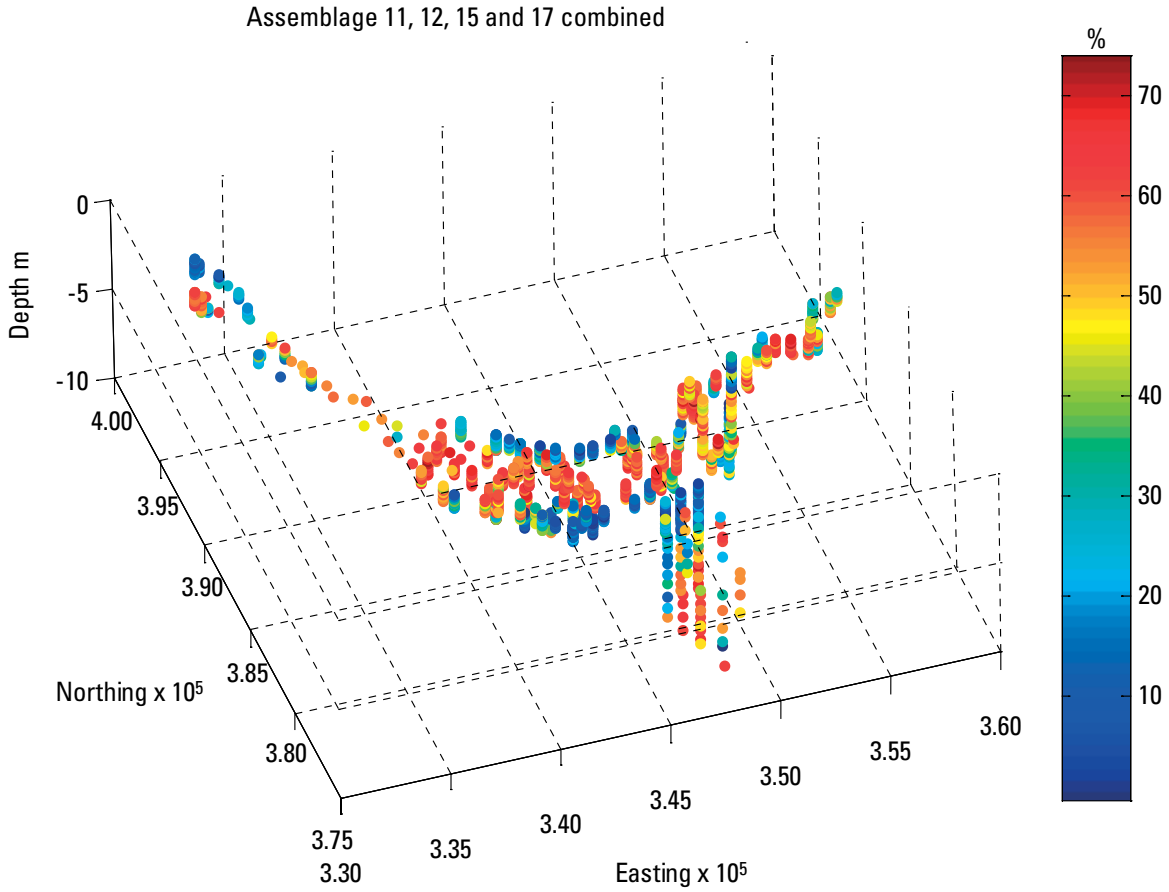

Figure 6.76 Summary of the composition and distribution of Assemblage 11, 12, 15 and 17.

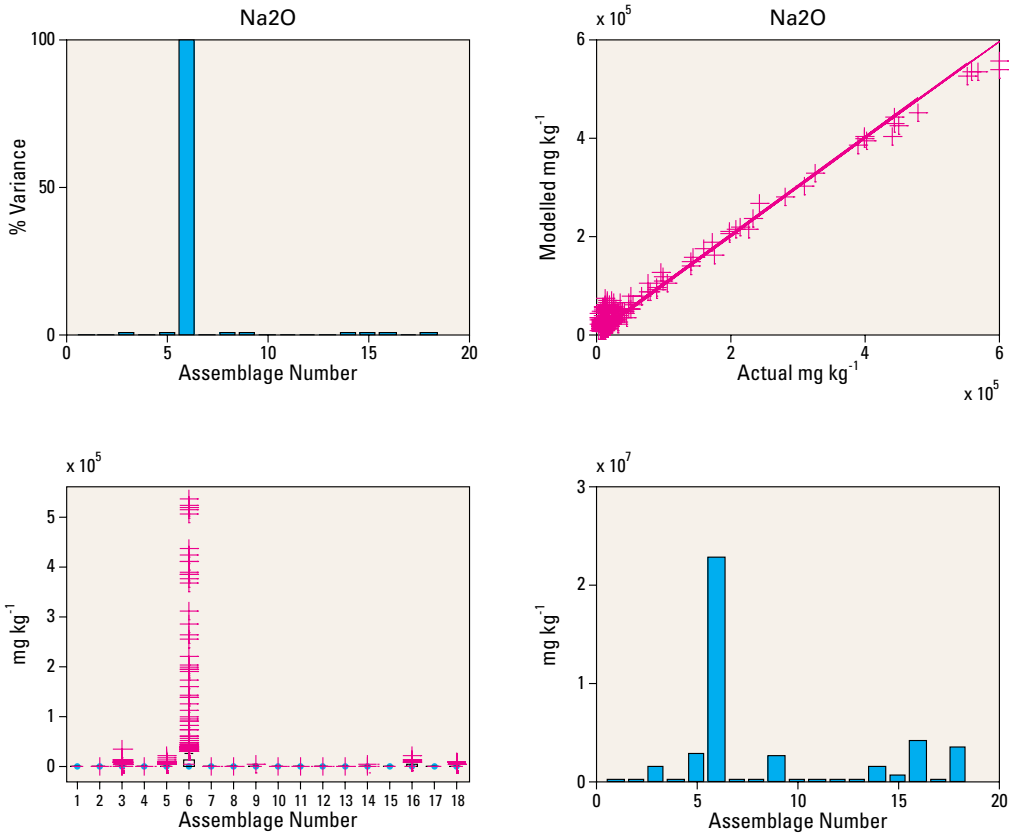

Figure 6.77 Summary of modelled Na data.

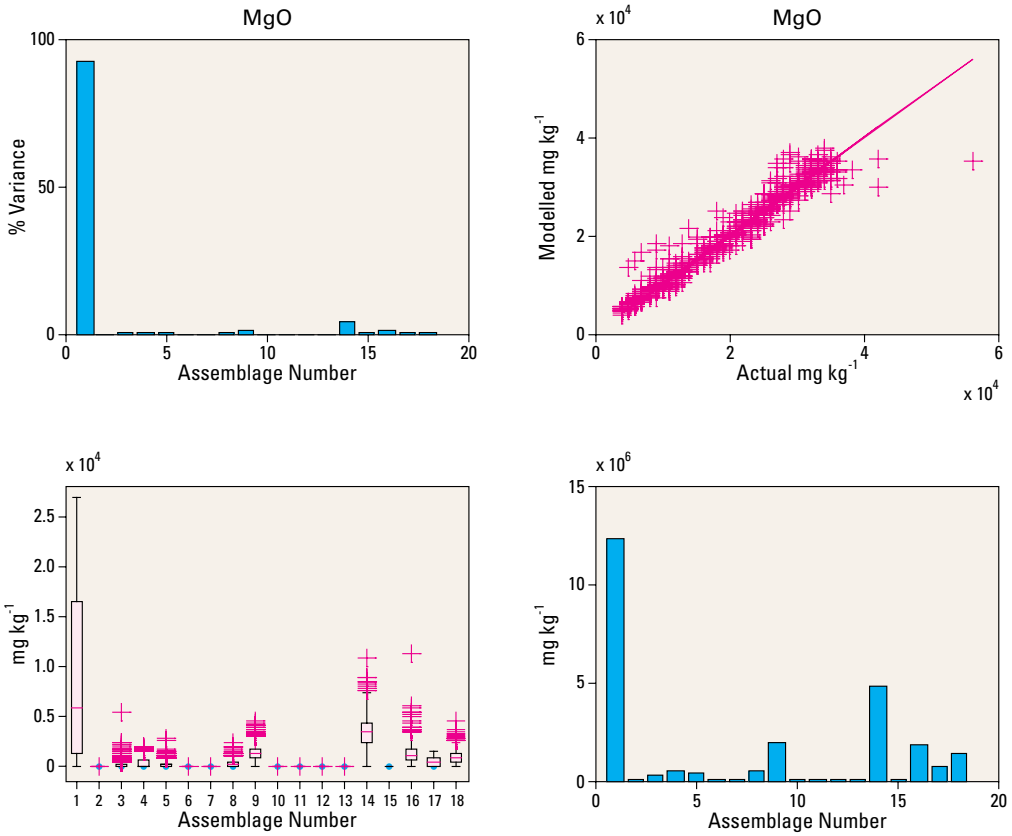

Figure 6.78 Summary of modelled Mg data.

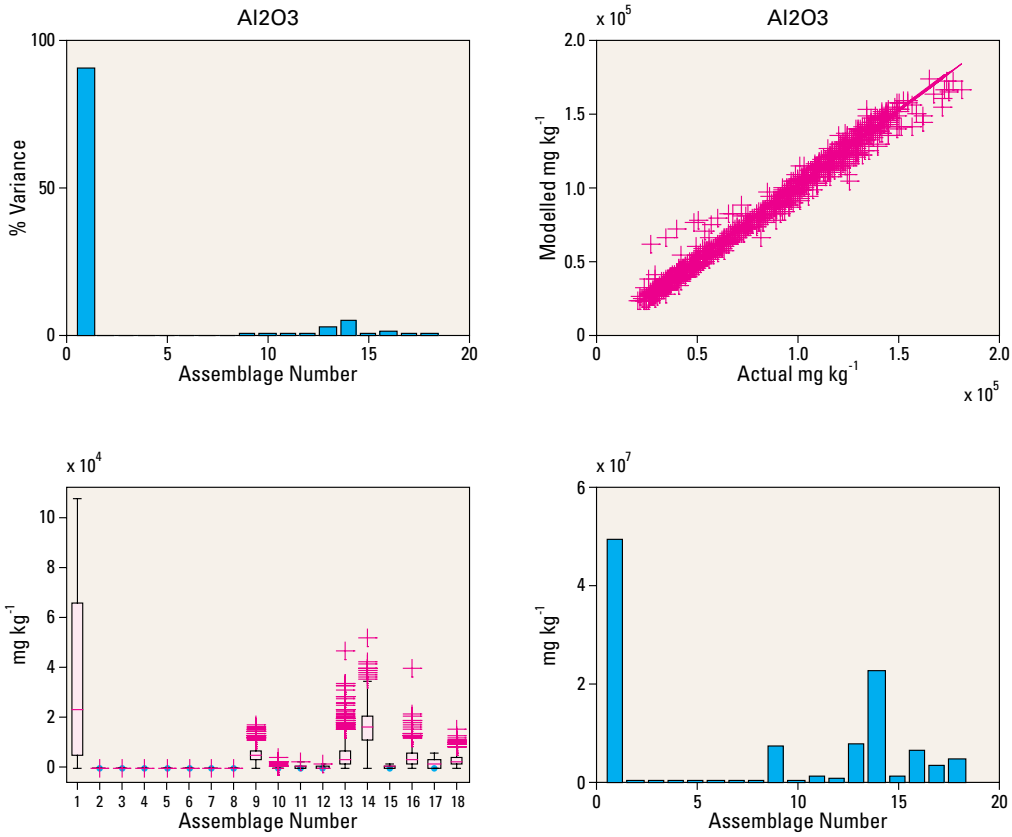

Figure 6.79 Summary of modelled Al data.

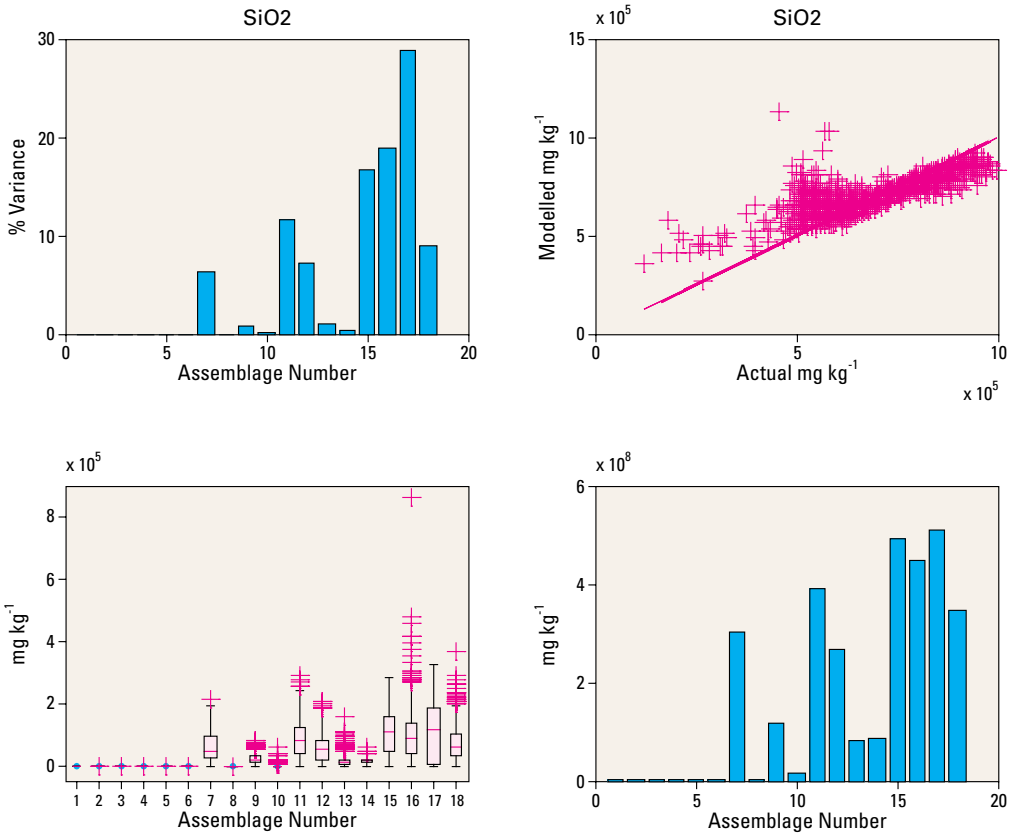

Figure 6.80 Summary of modelled Si data.

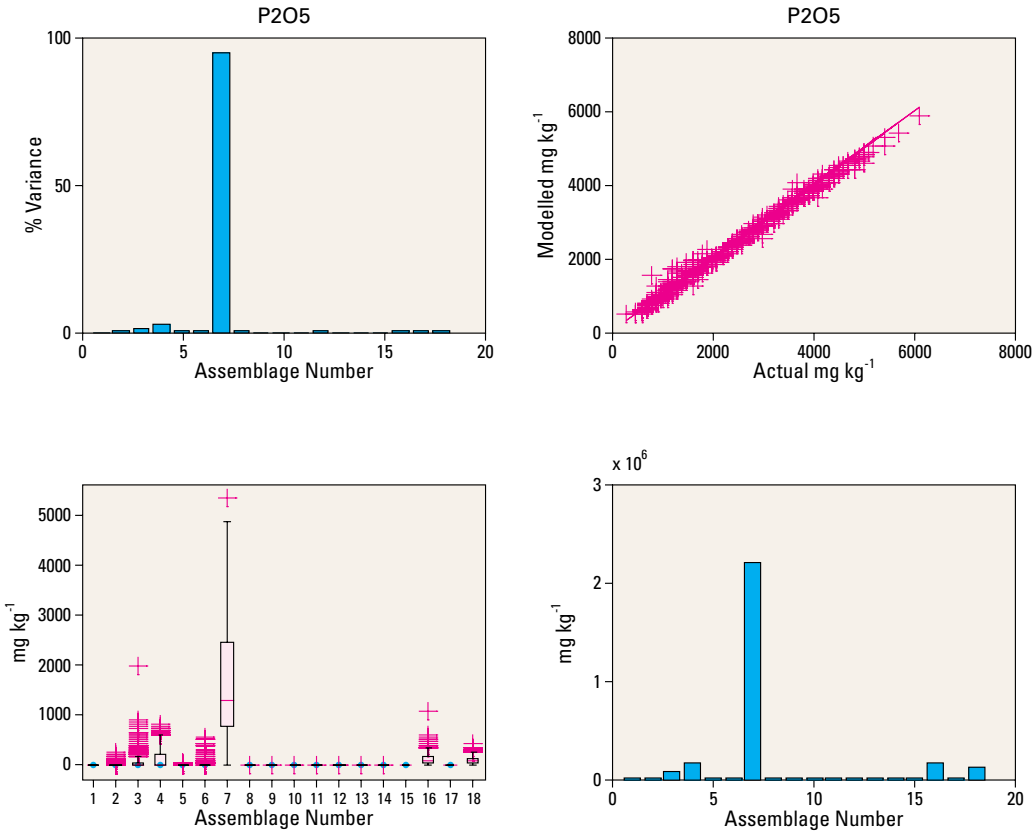

Figure 6.81 Summary of modelled P data.

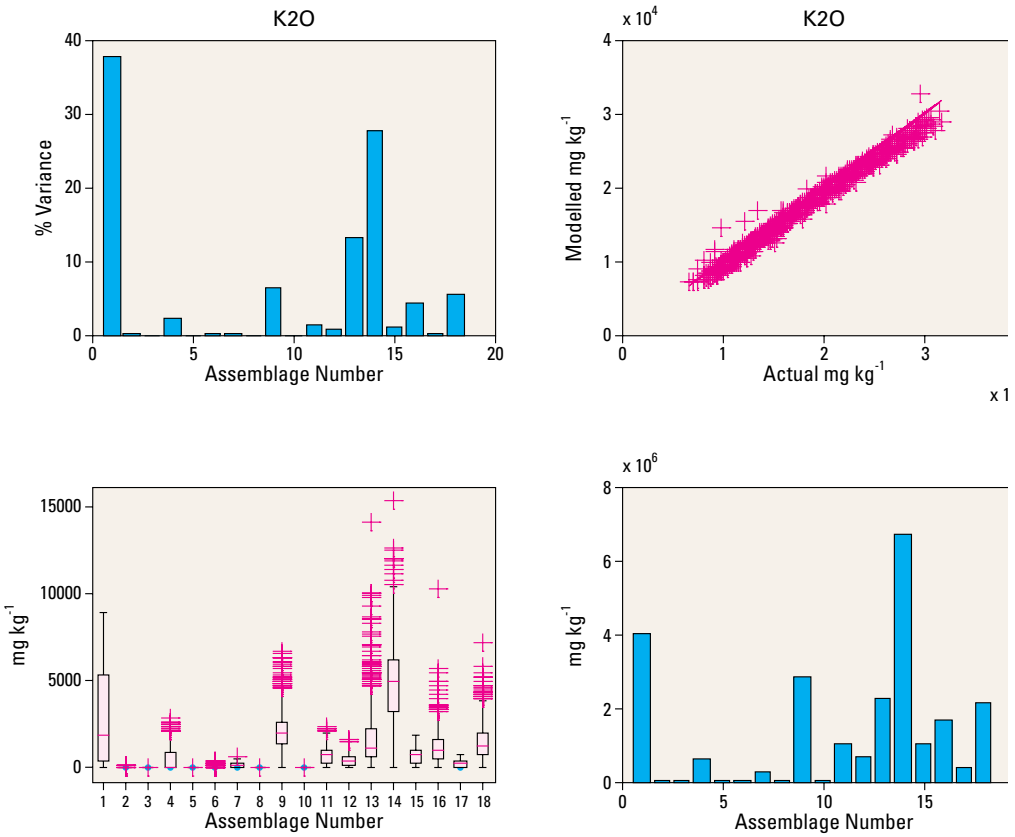

Figure 6.82 Summary of modelled K data.

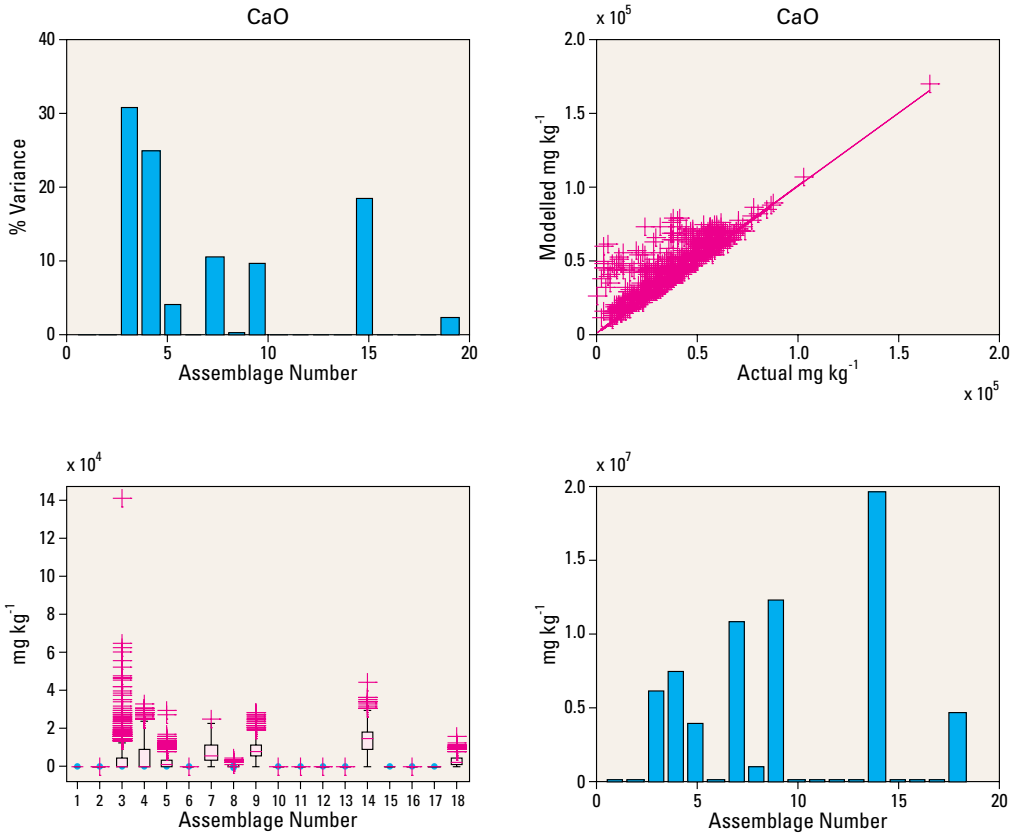

Figure 6.83 Summary of modelled Ca data.

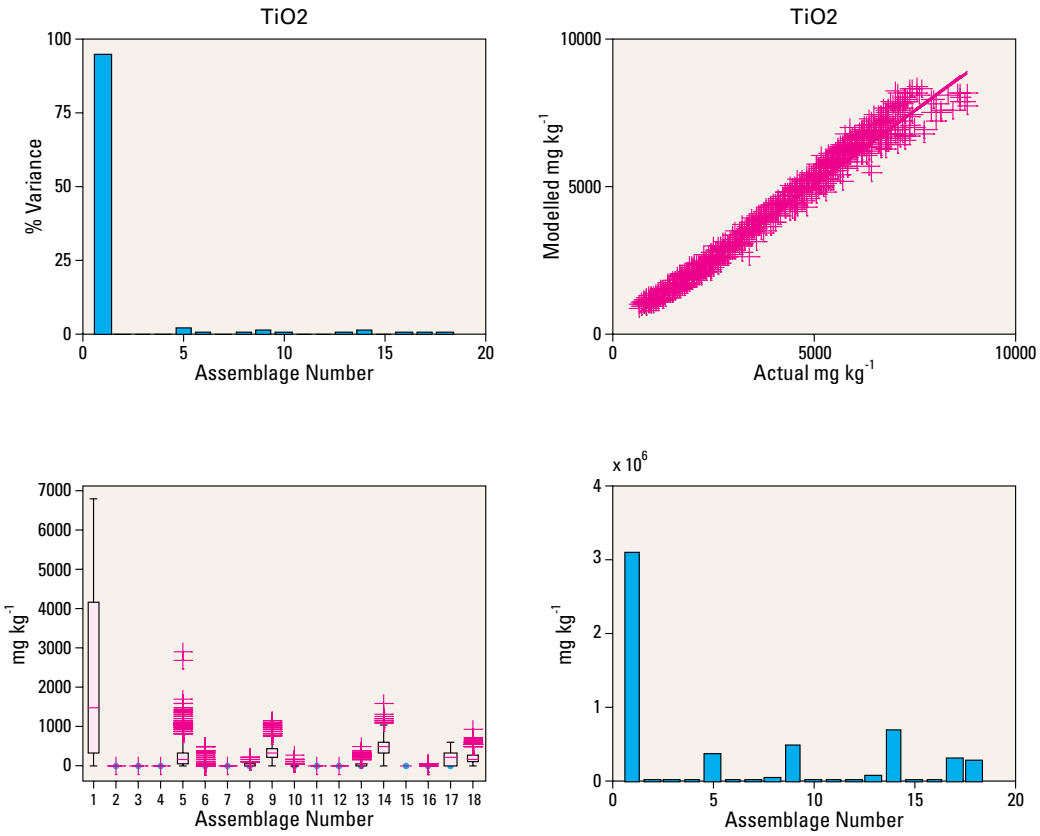

Figure 6.84 Summary of modelled Ti data.

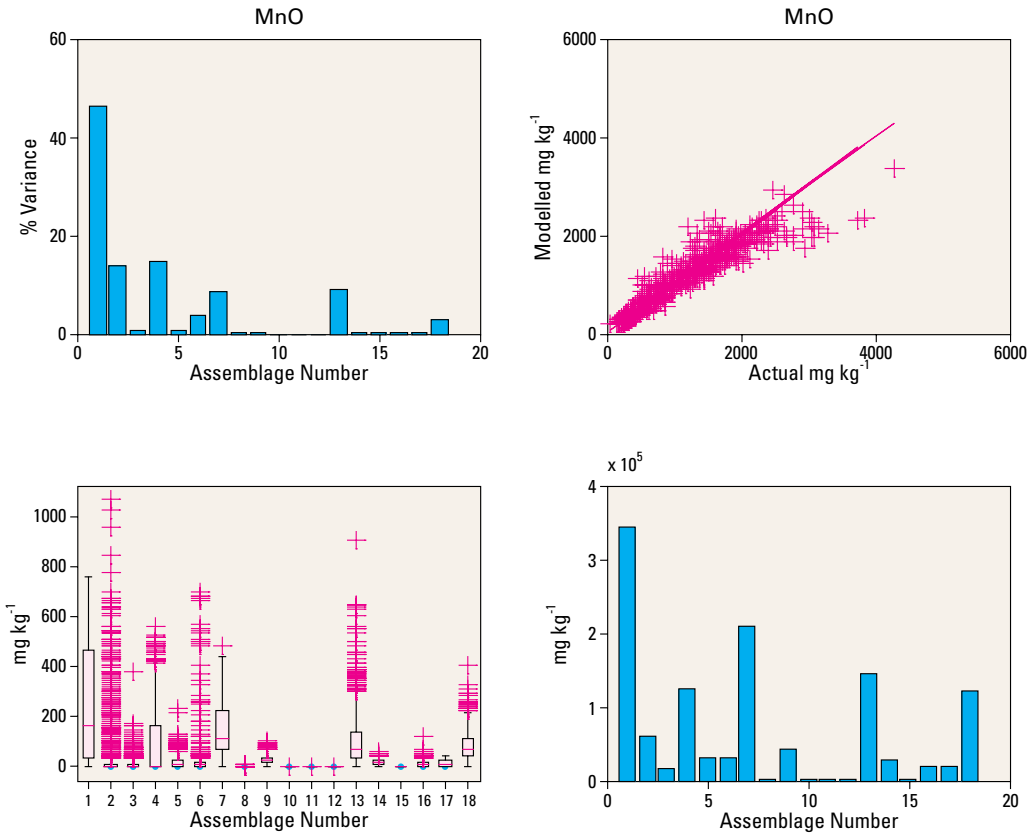

Figure 6.85 Summary of modelled Mn data.

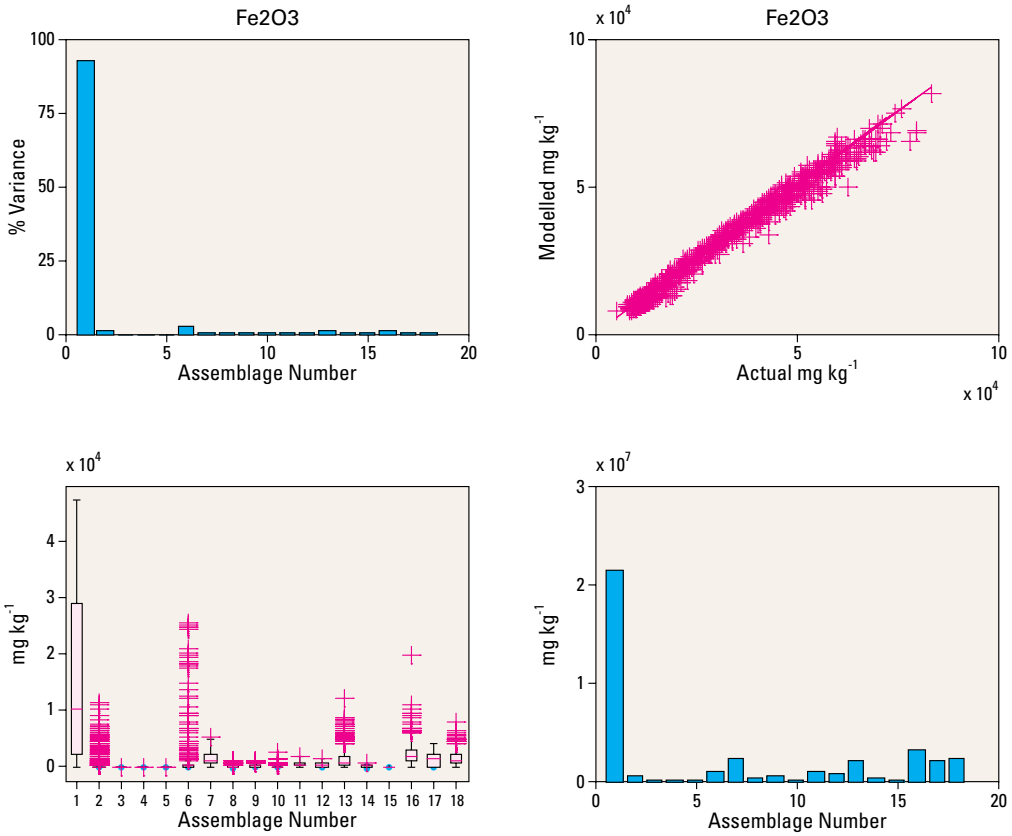

Figure 6.86 Summary of modelled Fe data.

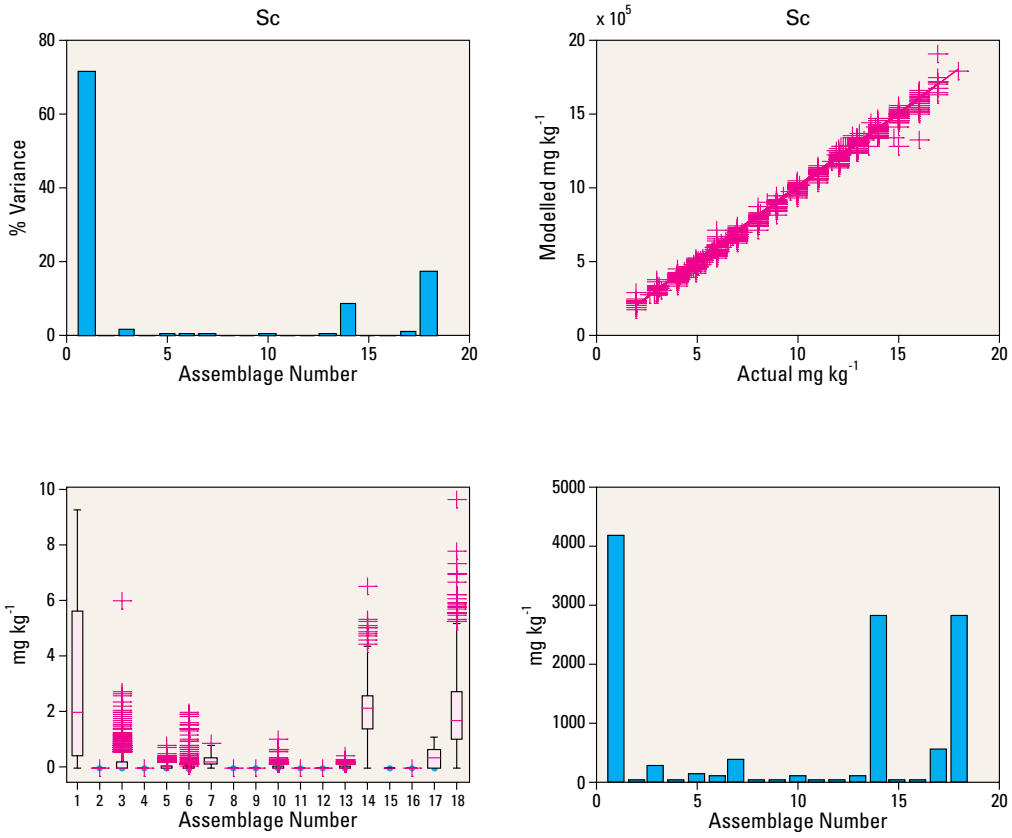

Figure 6.87 Summary of modelled Sc data.

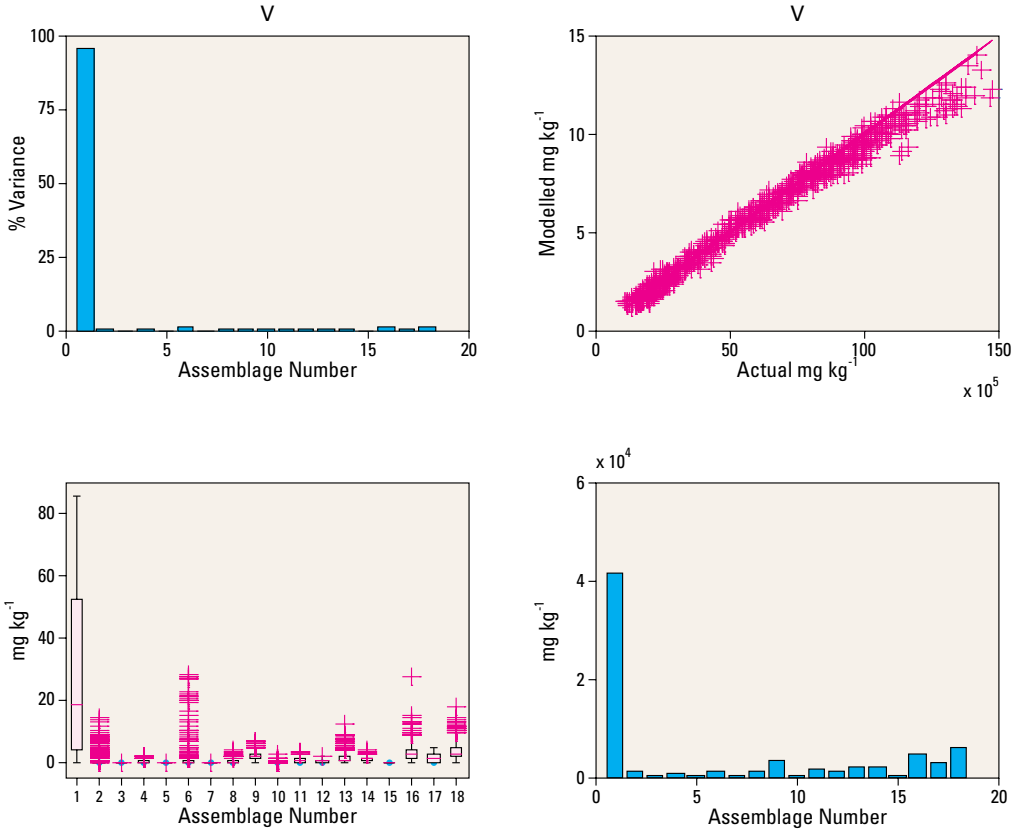

Figure 6.88 Summary of modelled V data.

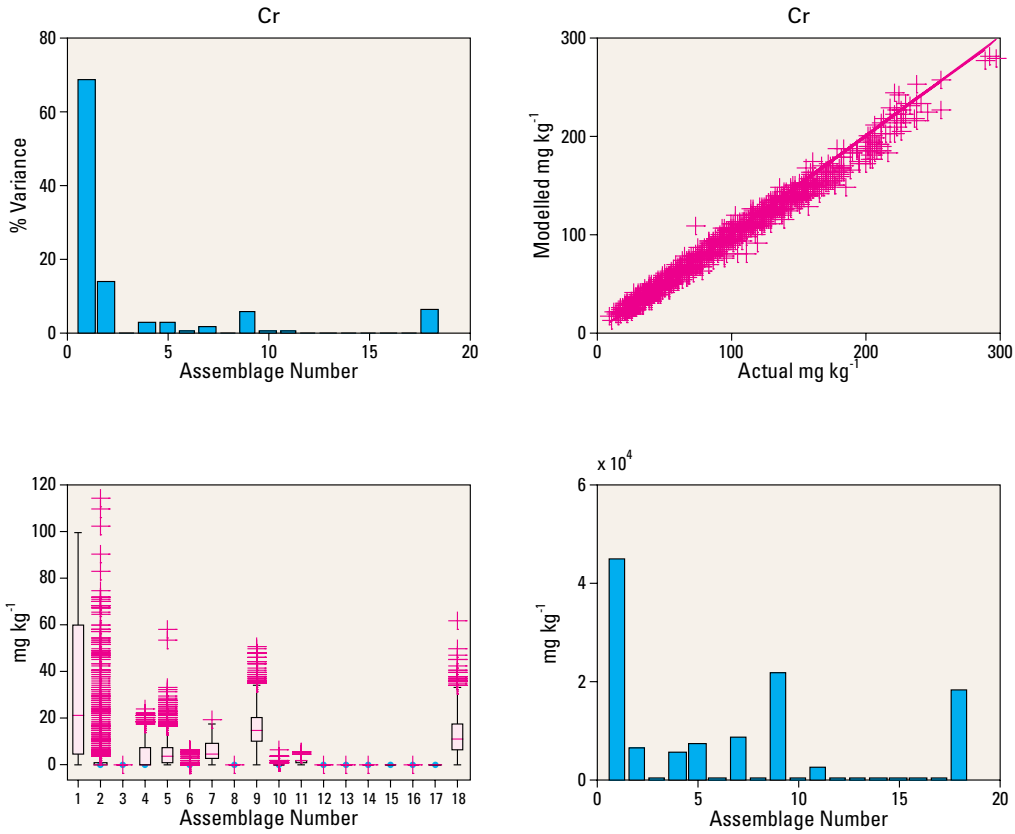

Figure 6.89 Summary of modelled Cr data.

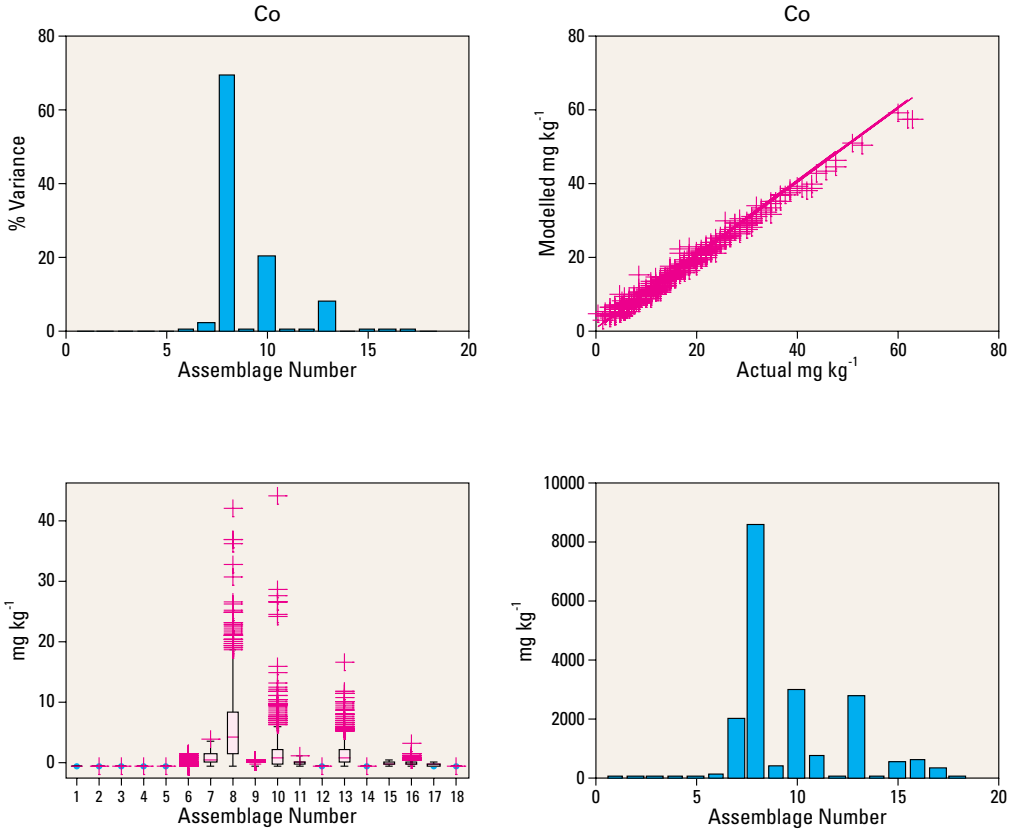

Figure 6.90 Summary of modelled Co data.

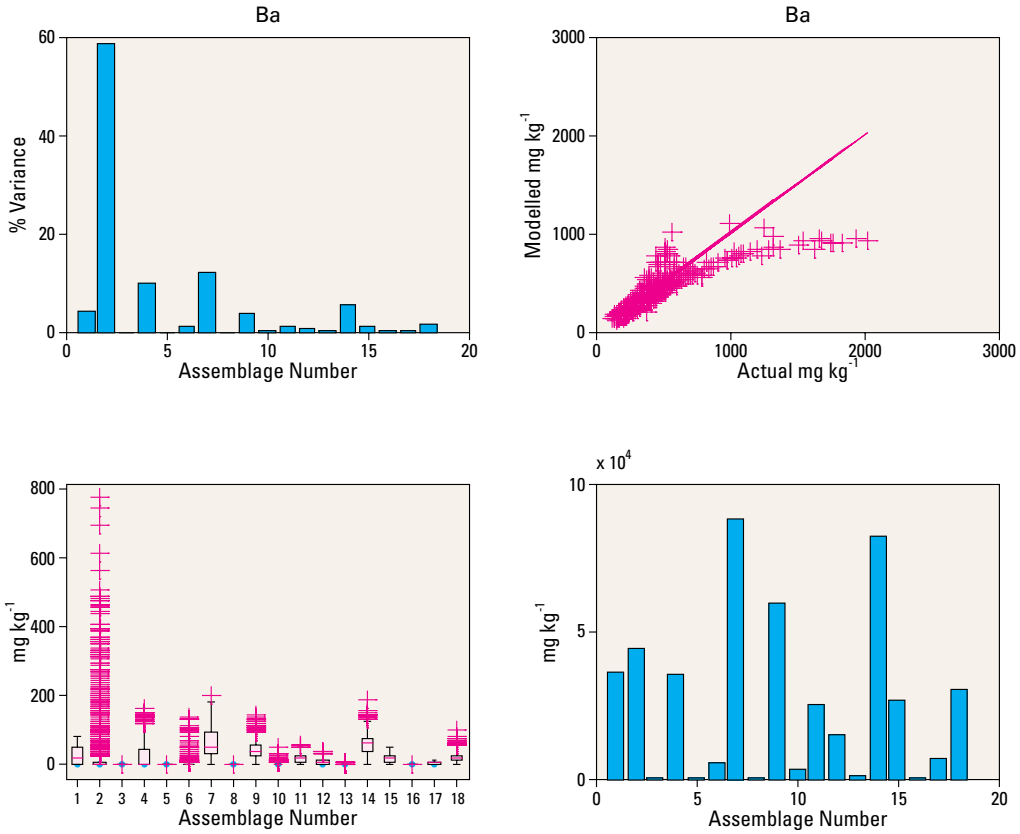

Figure 6.91 Summary of modelled Ba data.

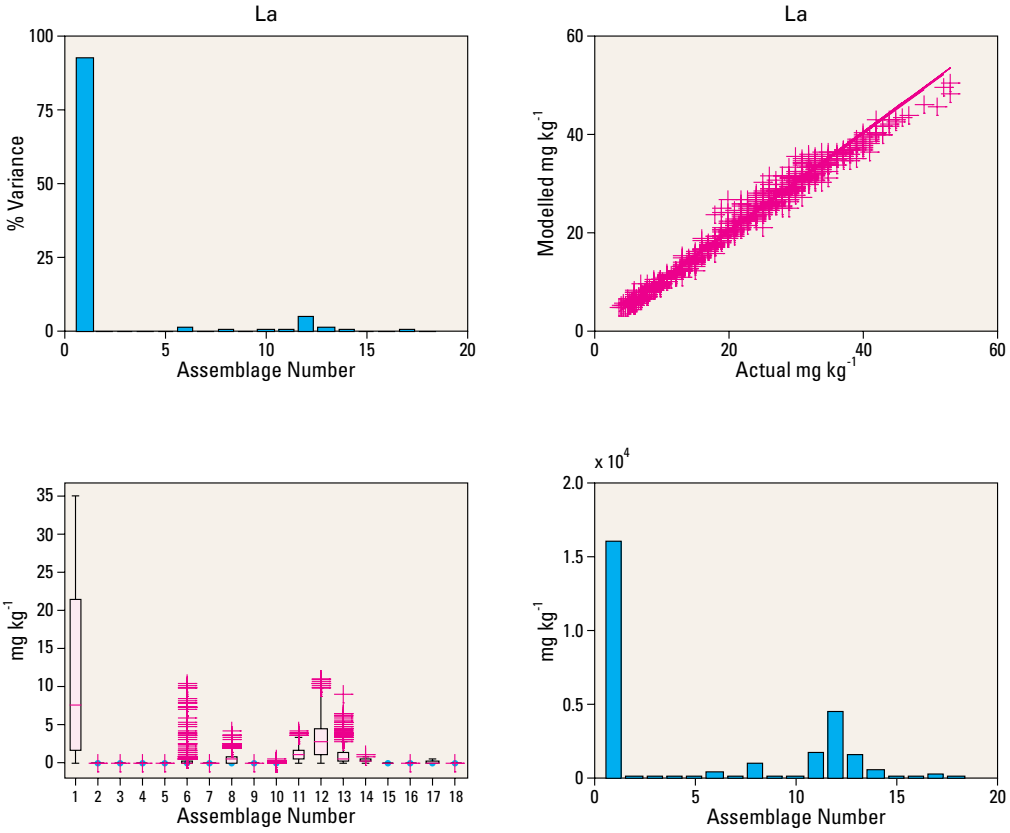

Figure 6.92 Summary of modelled La data.

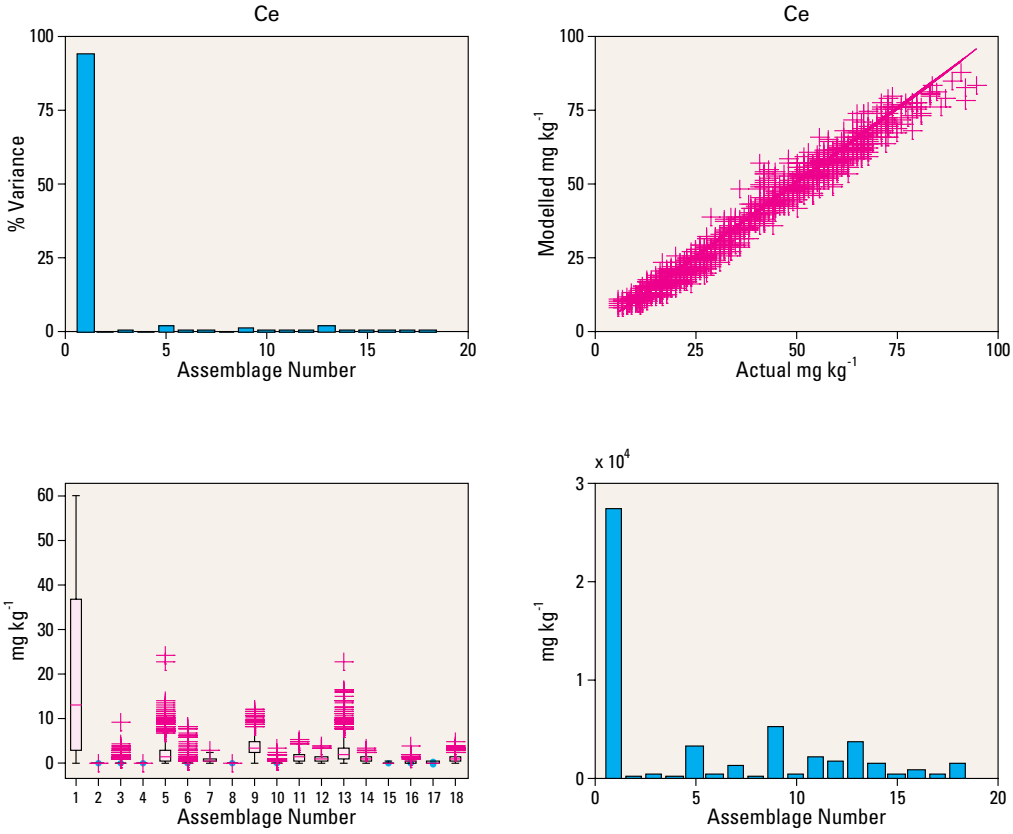

Figure 6.93 Summary of modelled Ce data.

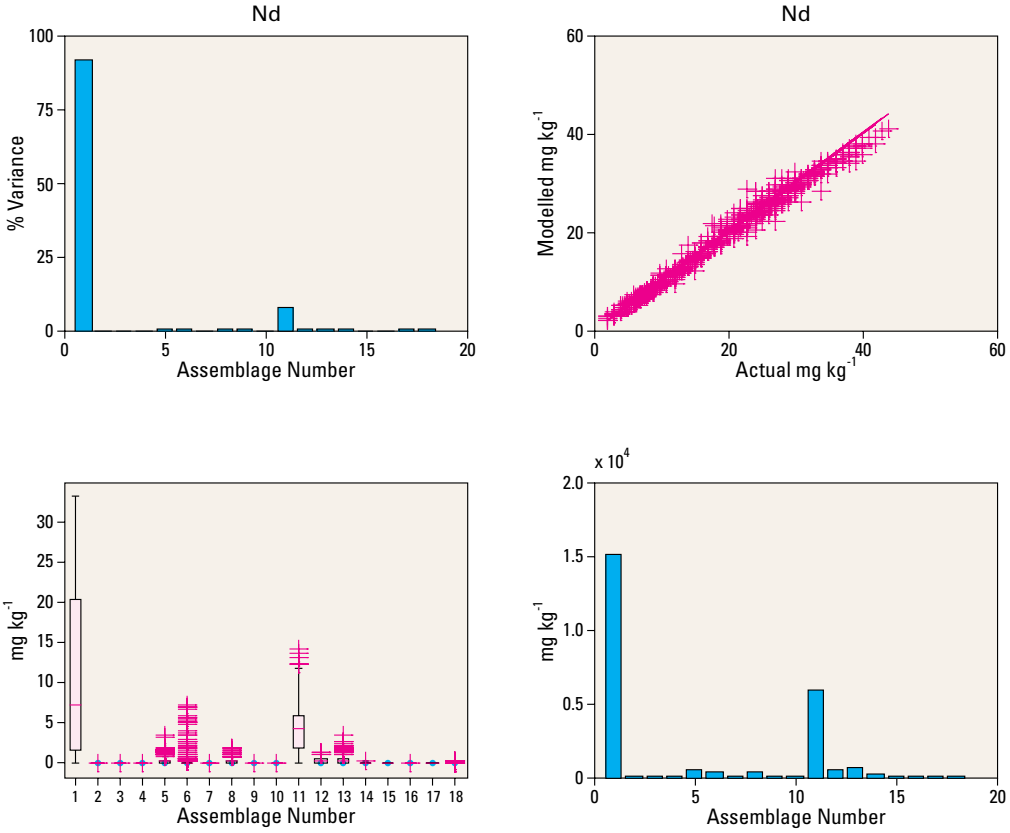

Figure 6.94 Summary of modelled Nd data.

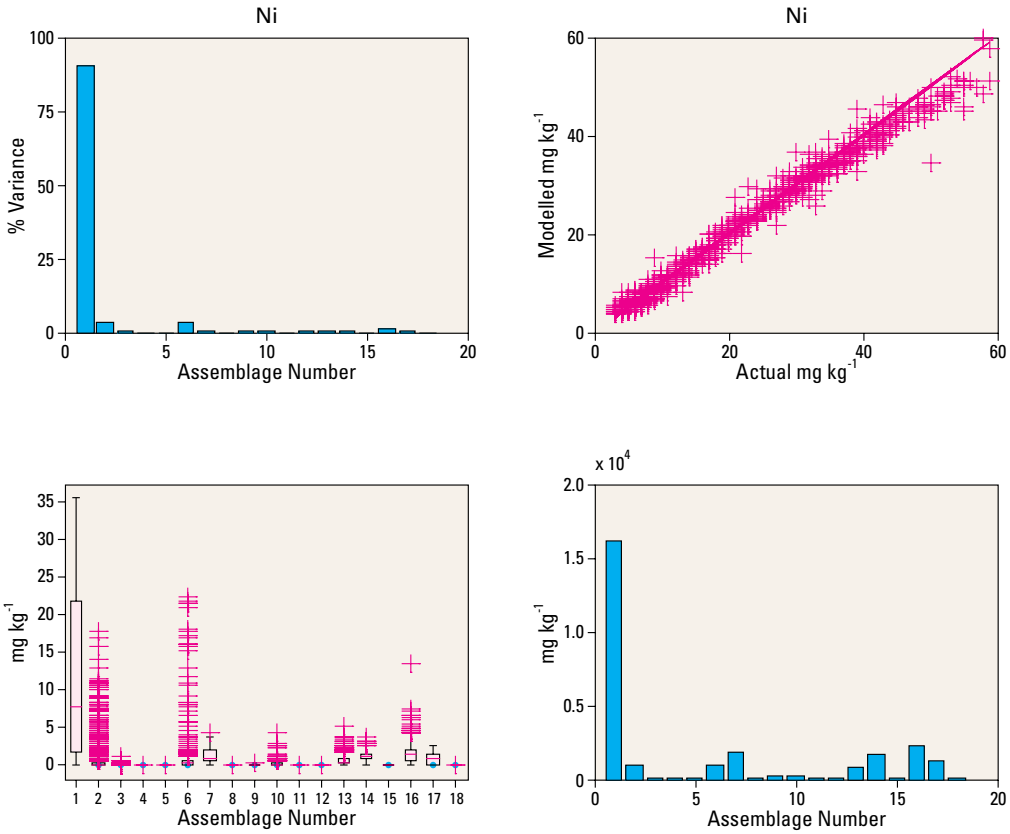

Figure 6.95 Summary of modelled Ni data.

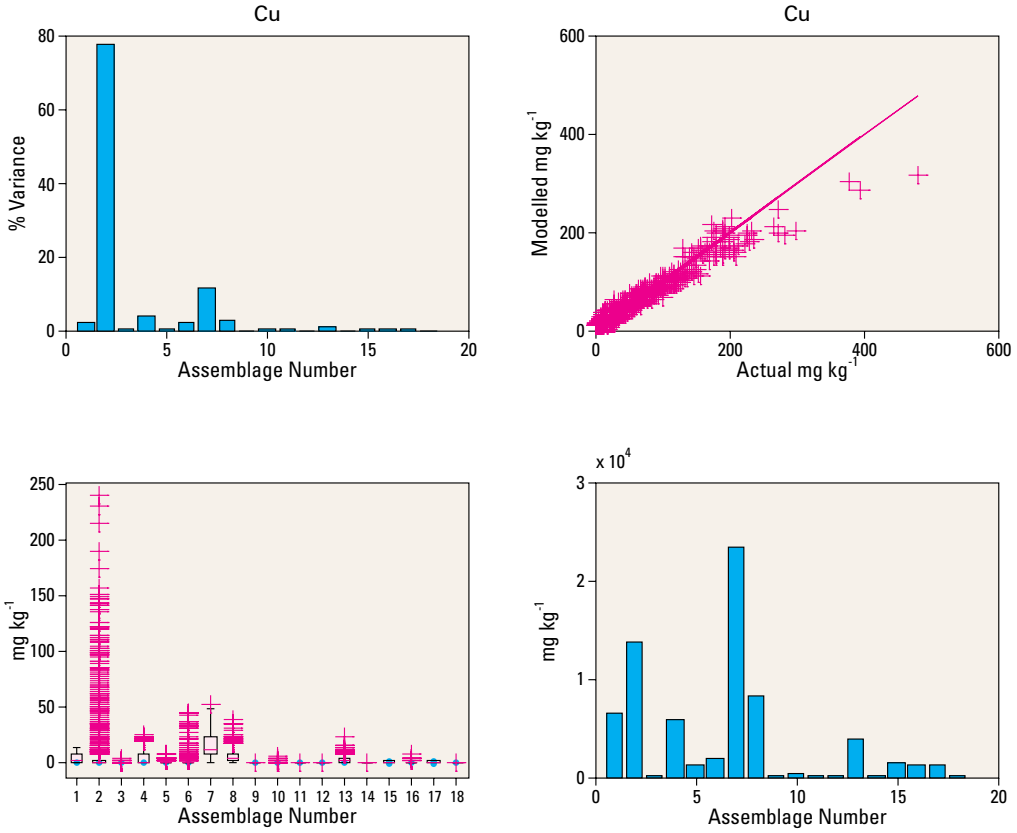

Figure 6.96 Summary of modelled Cu data.

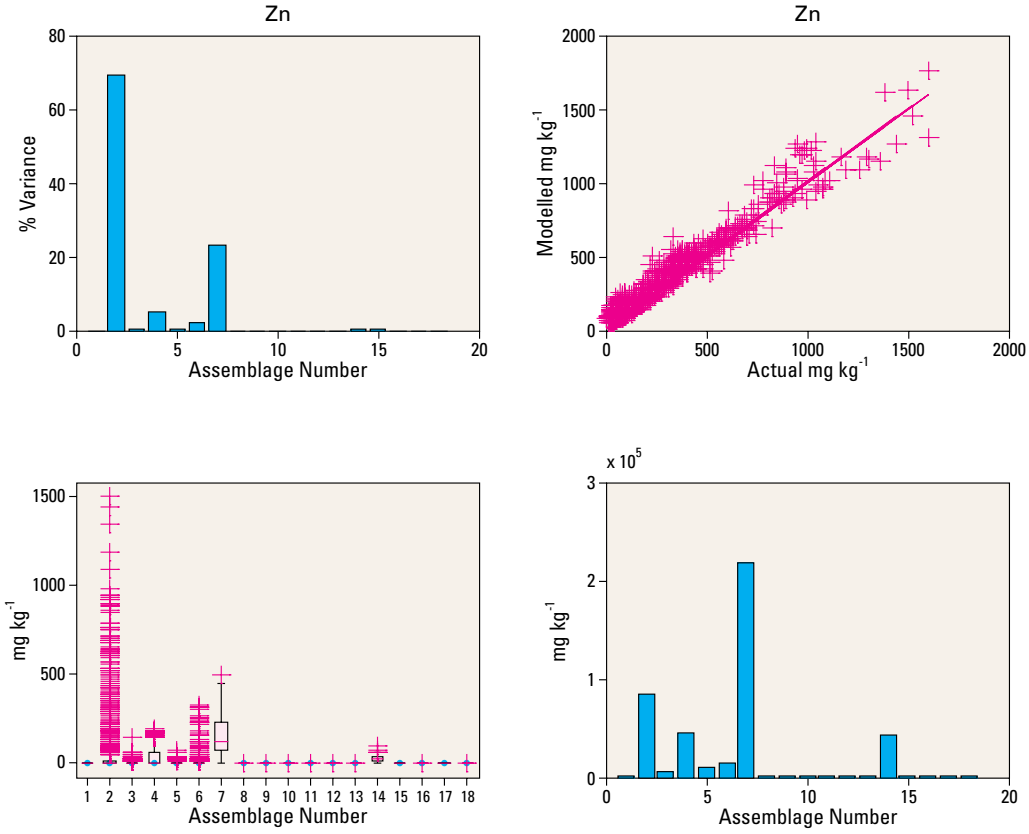

Figure 6.97 Summary of modelled Zn data.

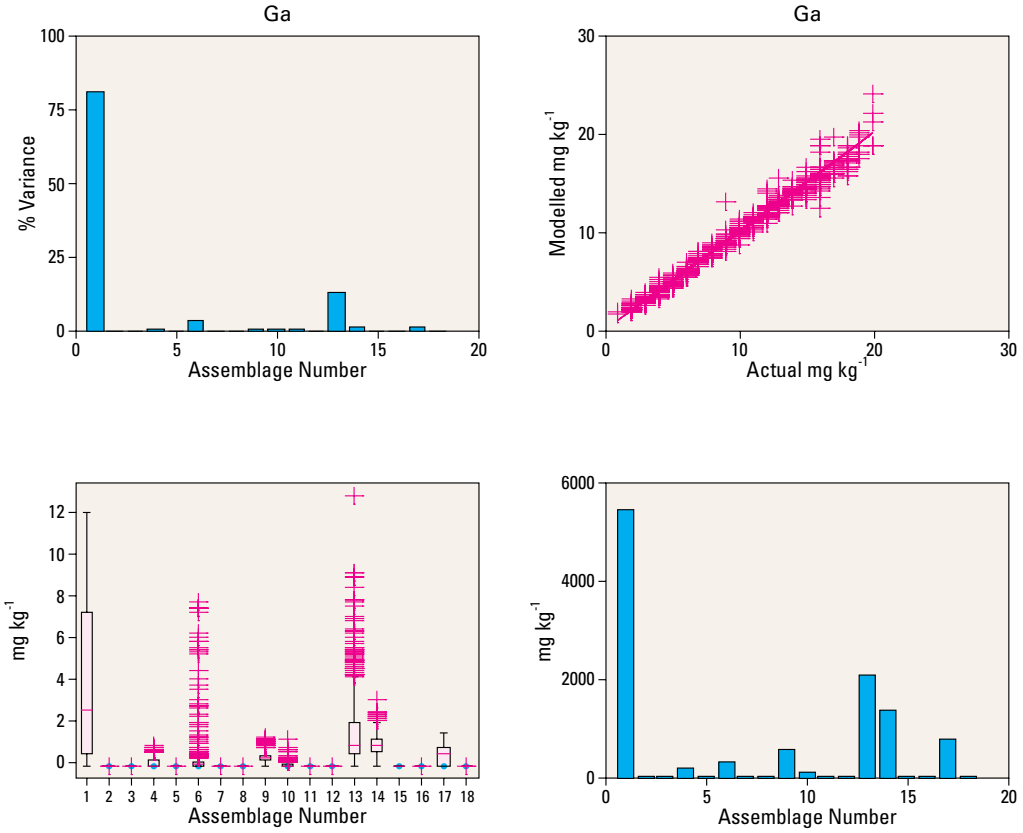

Figure 6.98 Summary of modelled Ga data.

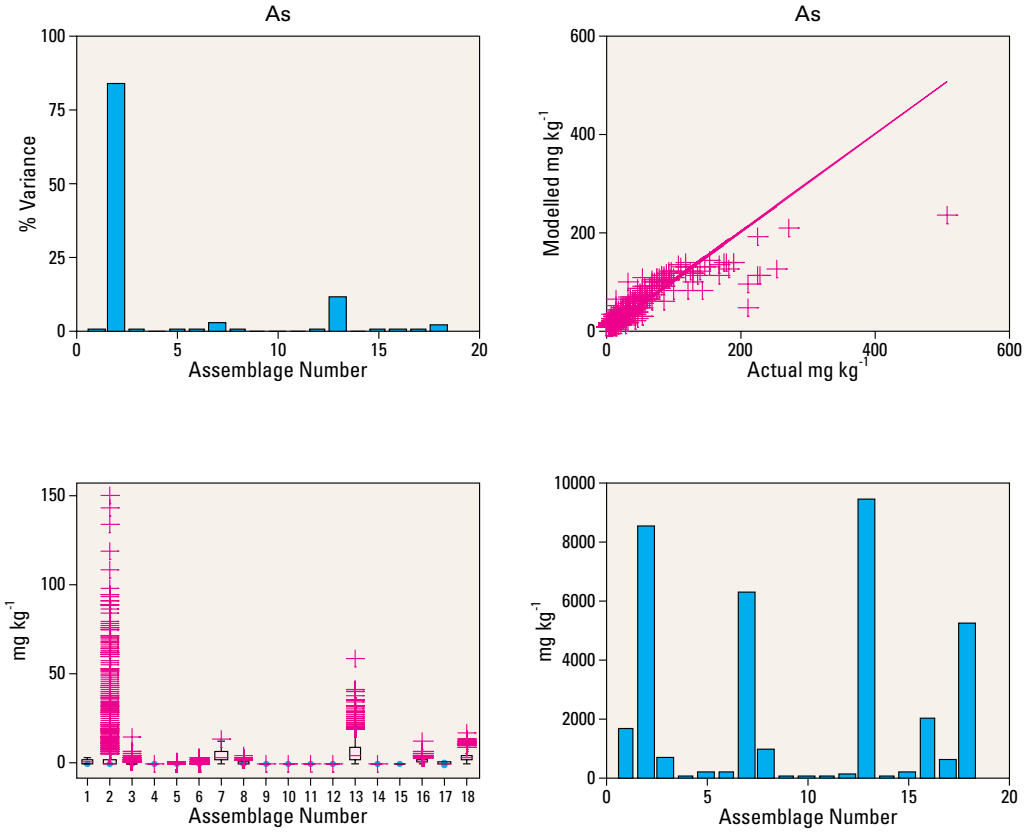

Figure 6.99 Summary of modelled As data.

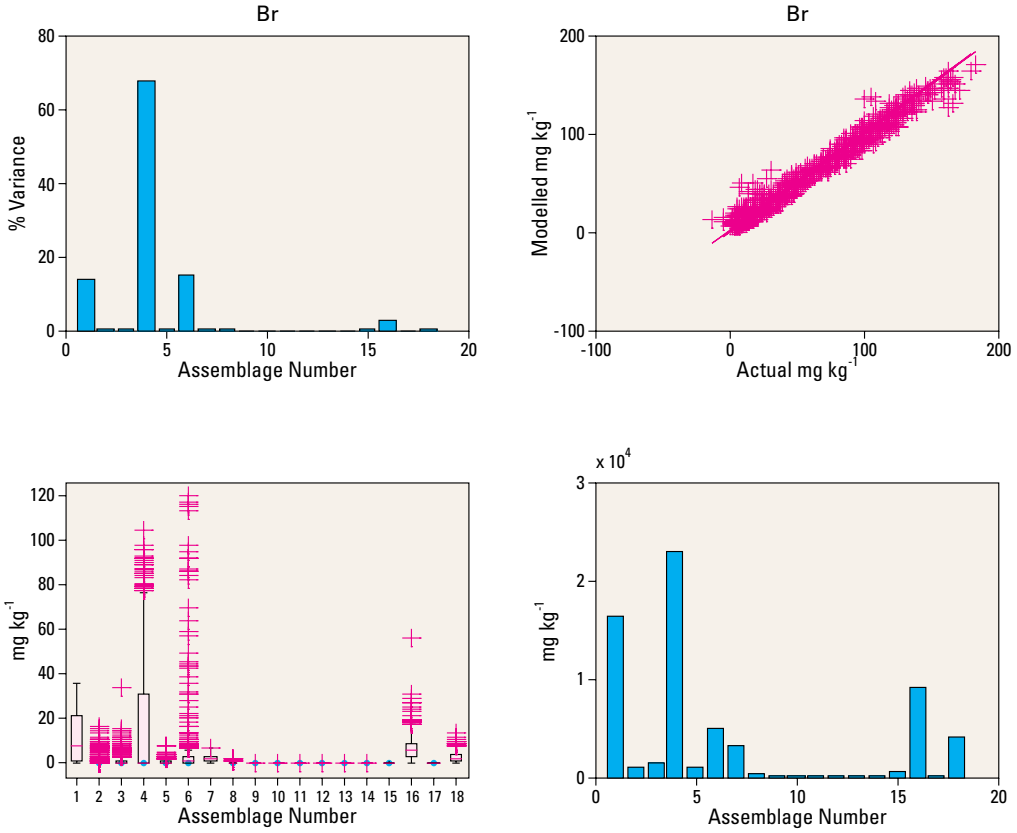

Figure 6.100 Summary of modelled Br data.

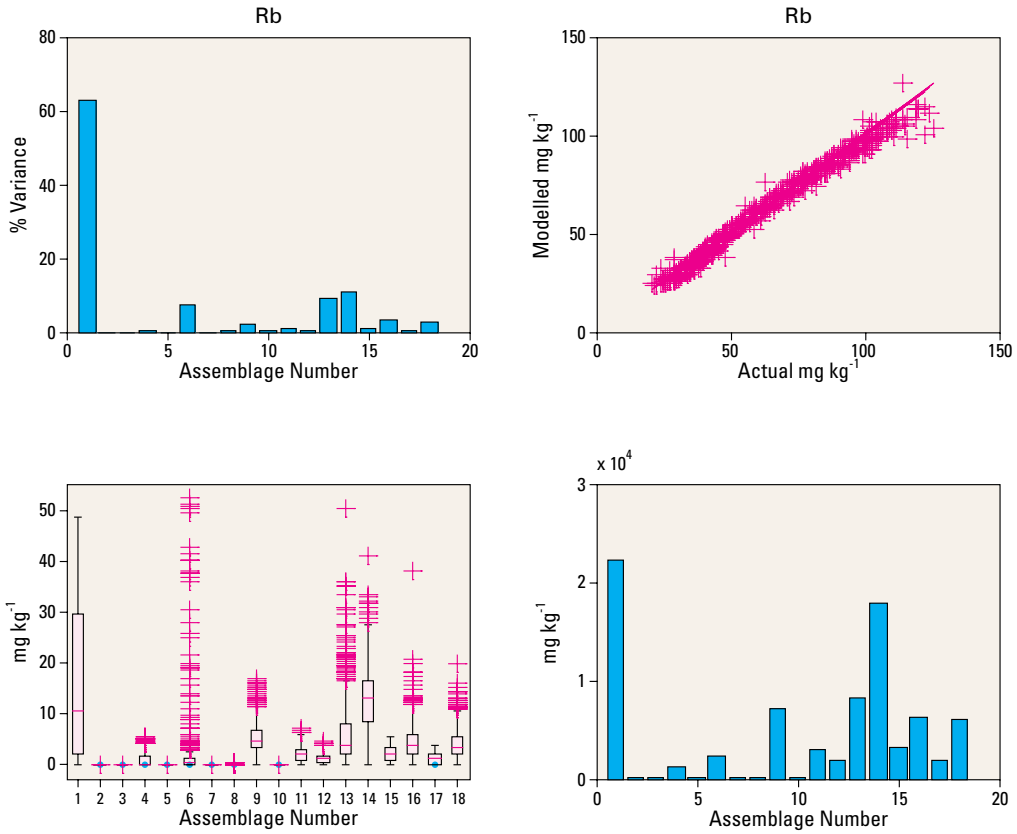

Figure 6.101 Summary of modelled Rb data.

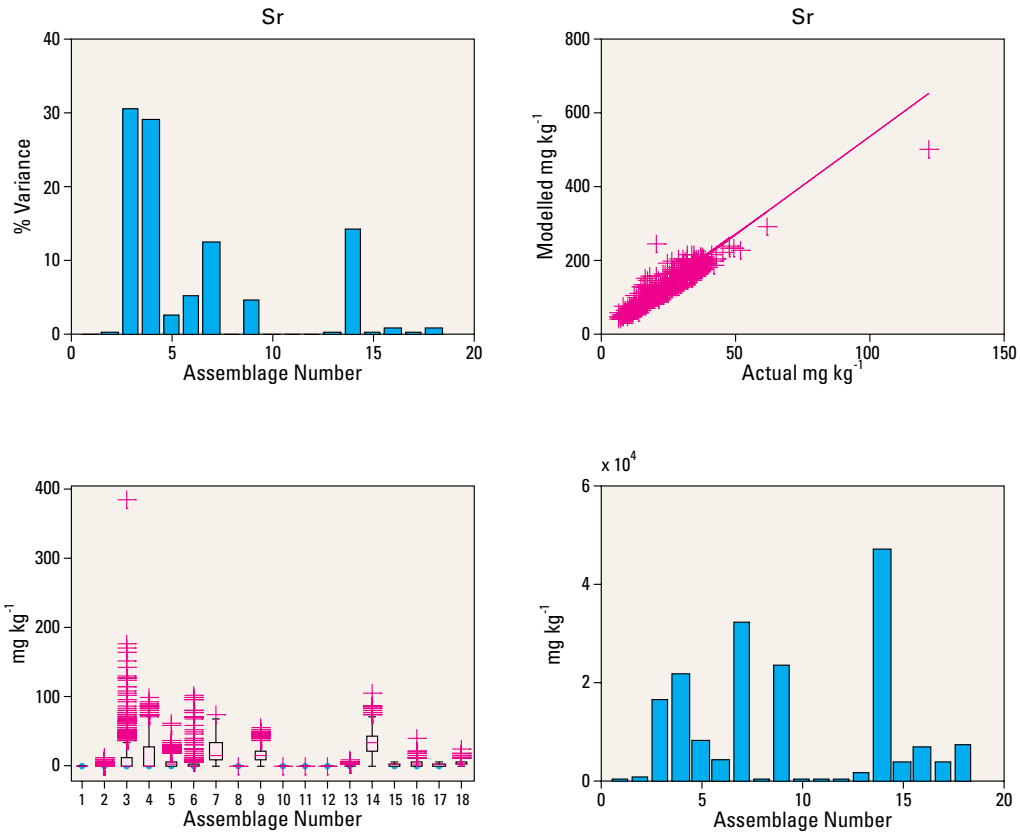

Figure 6.102 Summary of modelled Sr data.

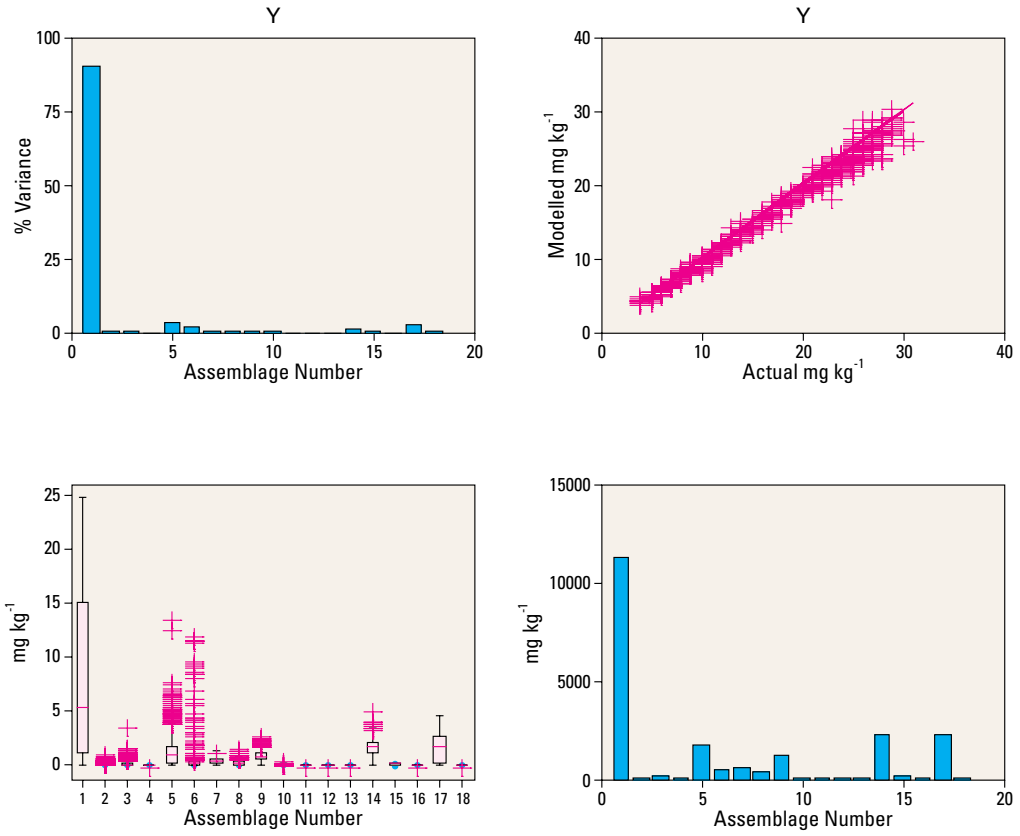

Figure 6.103 Summary of modelled Y data.

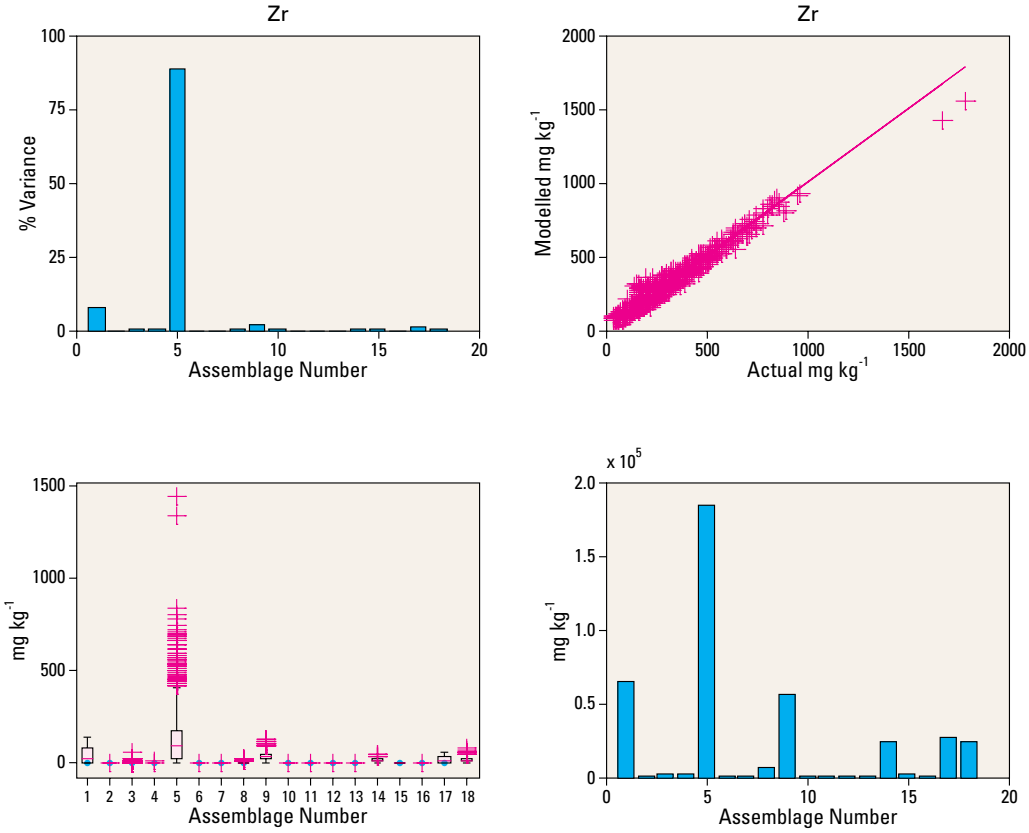

Figure 6.104 Summary of modelled Zr data.

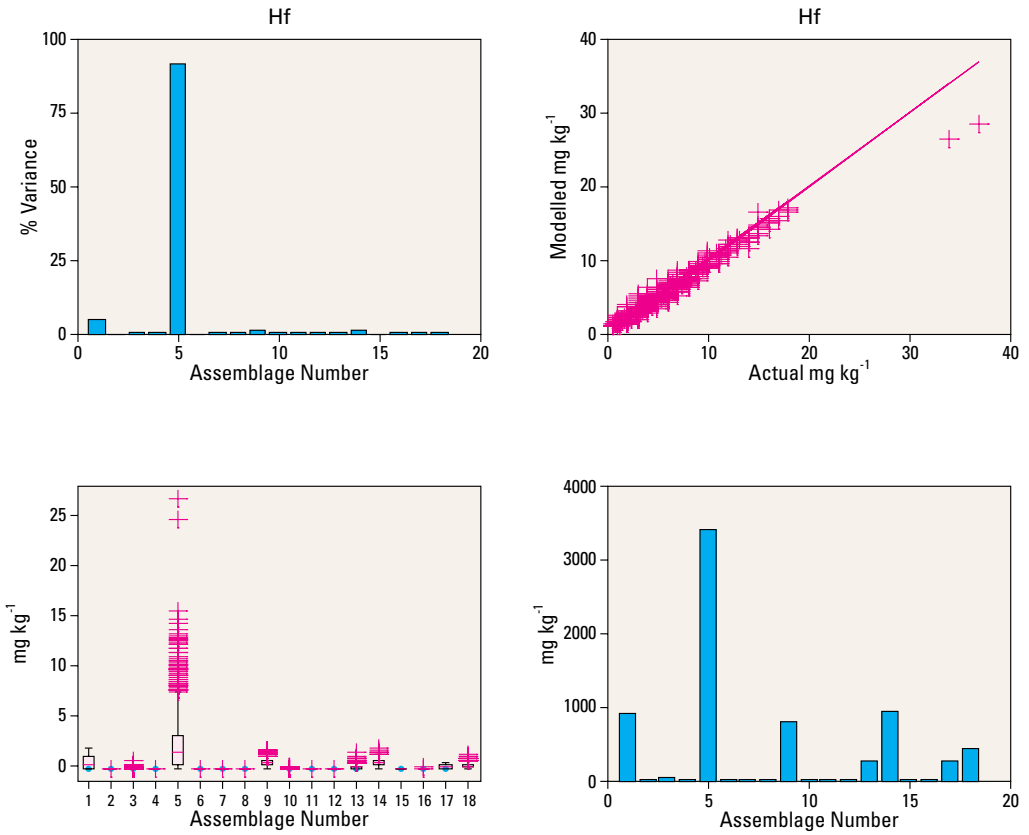

Figure 6.105 Summary of modelled Hf data.

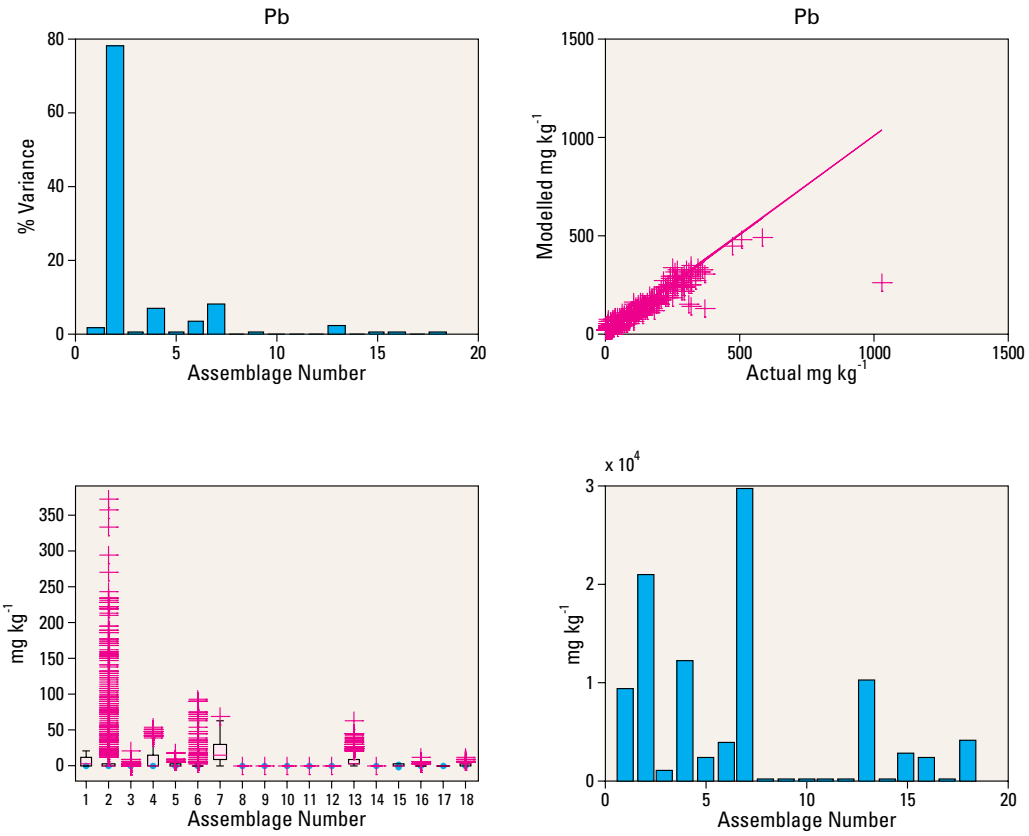

Figure 6.106 Summary of modelled Pb data.

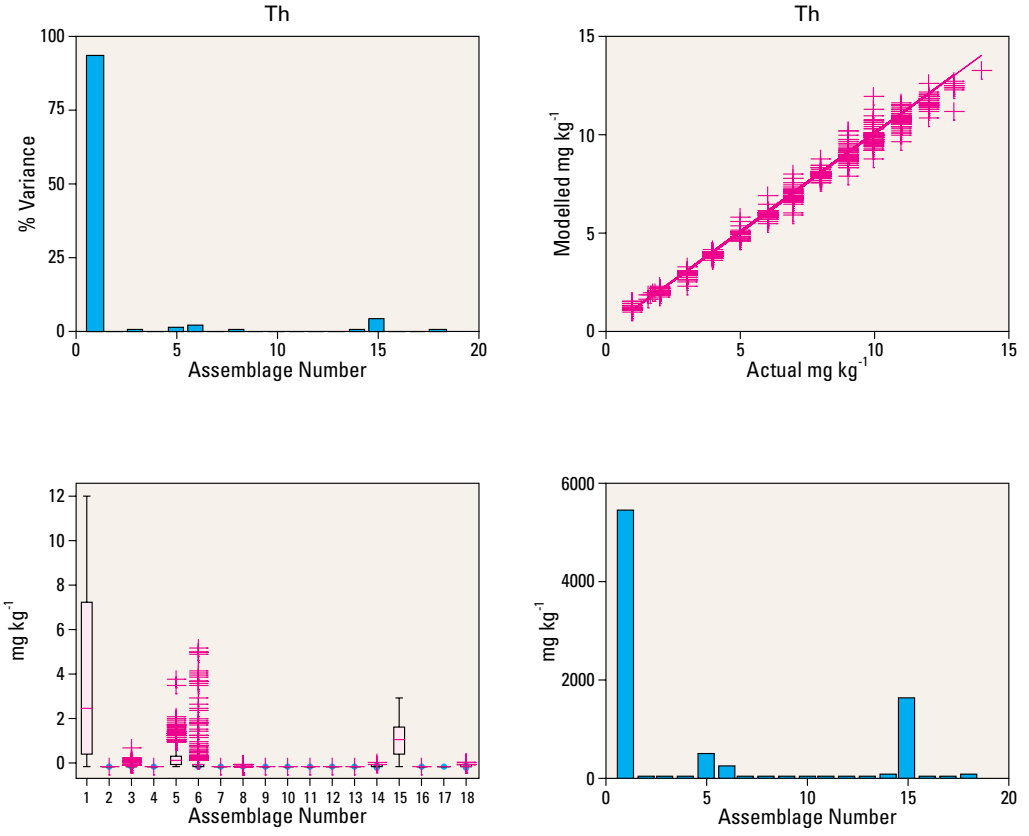

Figure 6.107 Summary of modelled Th data.

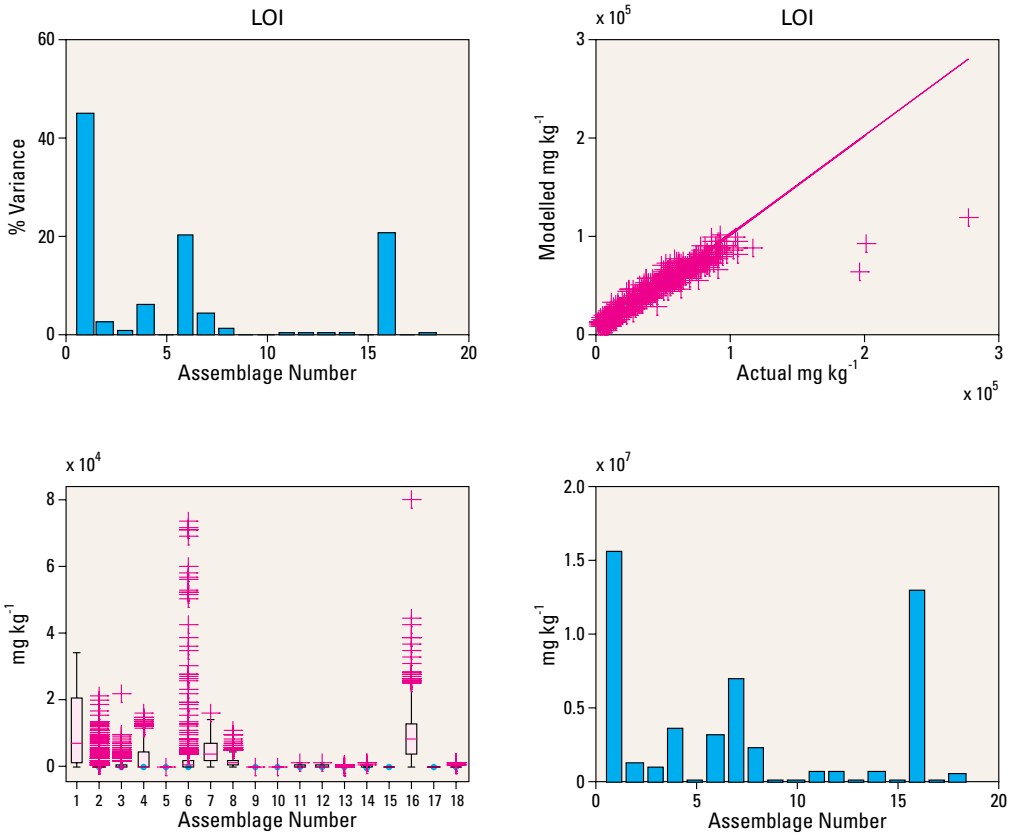

Figure 6.108 Summary of modelled LOI data.

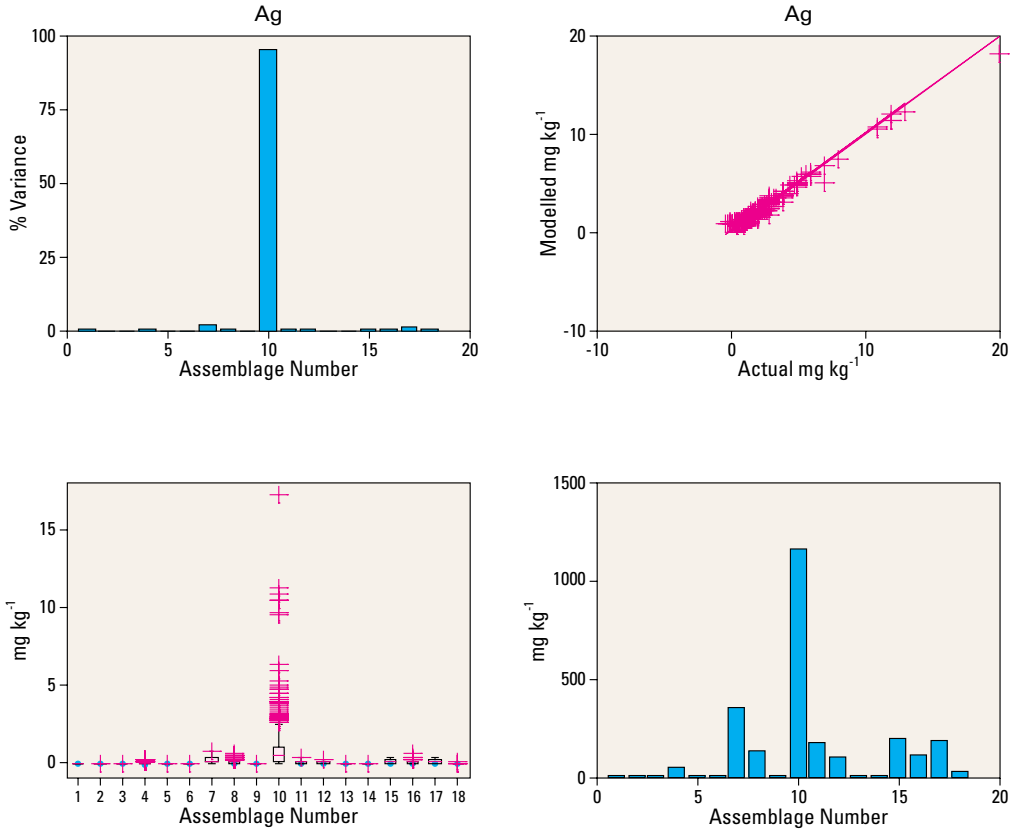

Figure 6.109 Summary of modelled Ag data.

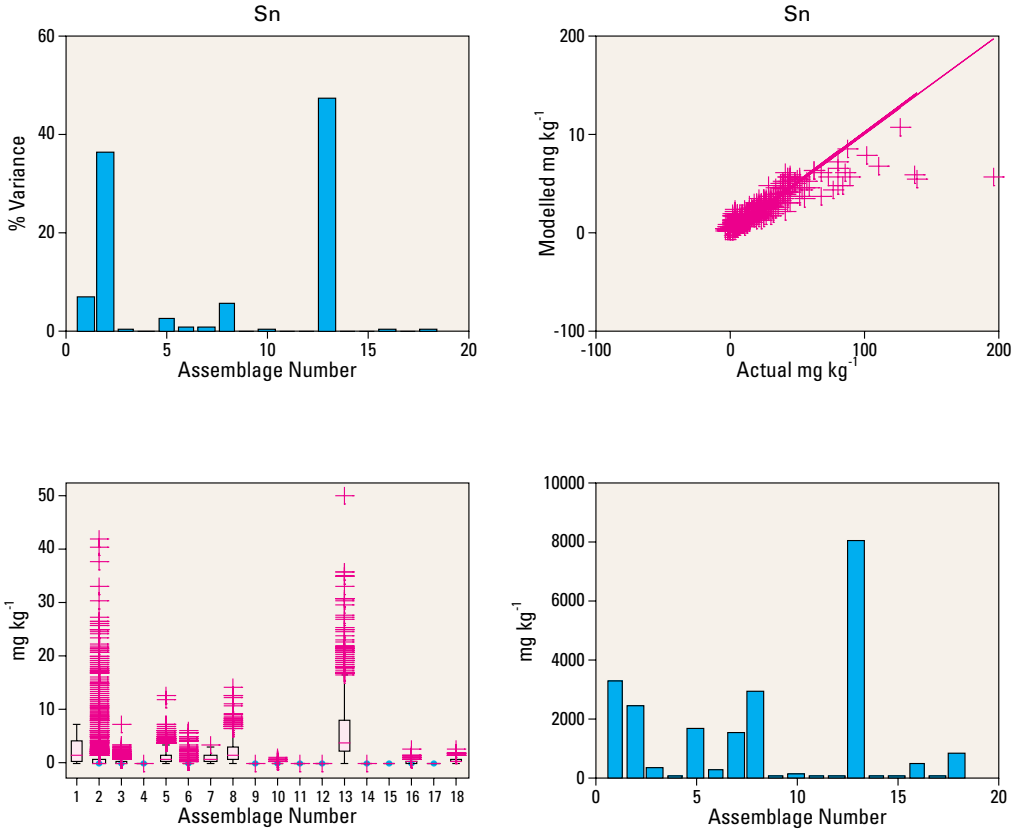

Figure 6.110 Summary of modelled Sn data.

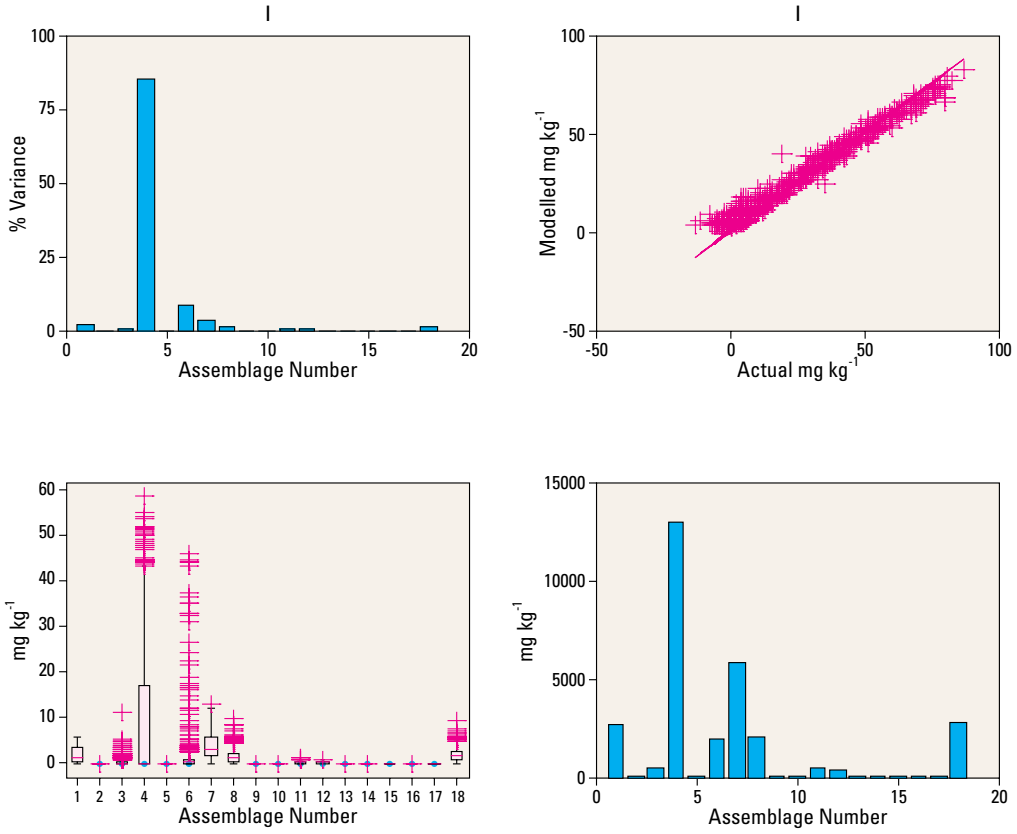

Figure 6.111 Summary of modelled I data.

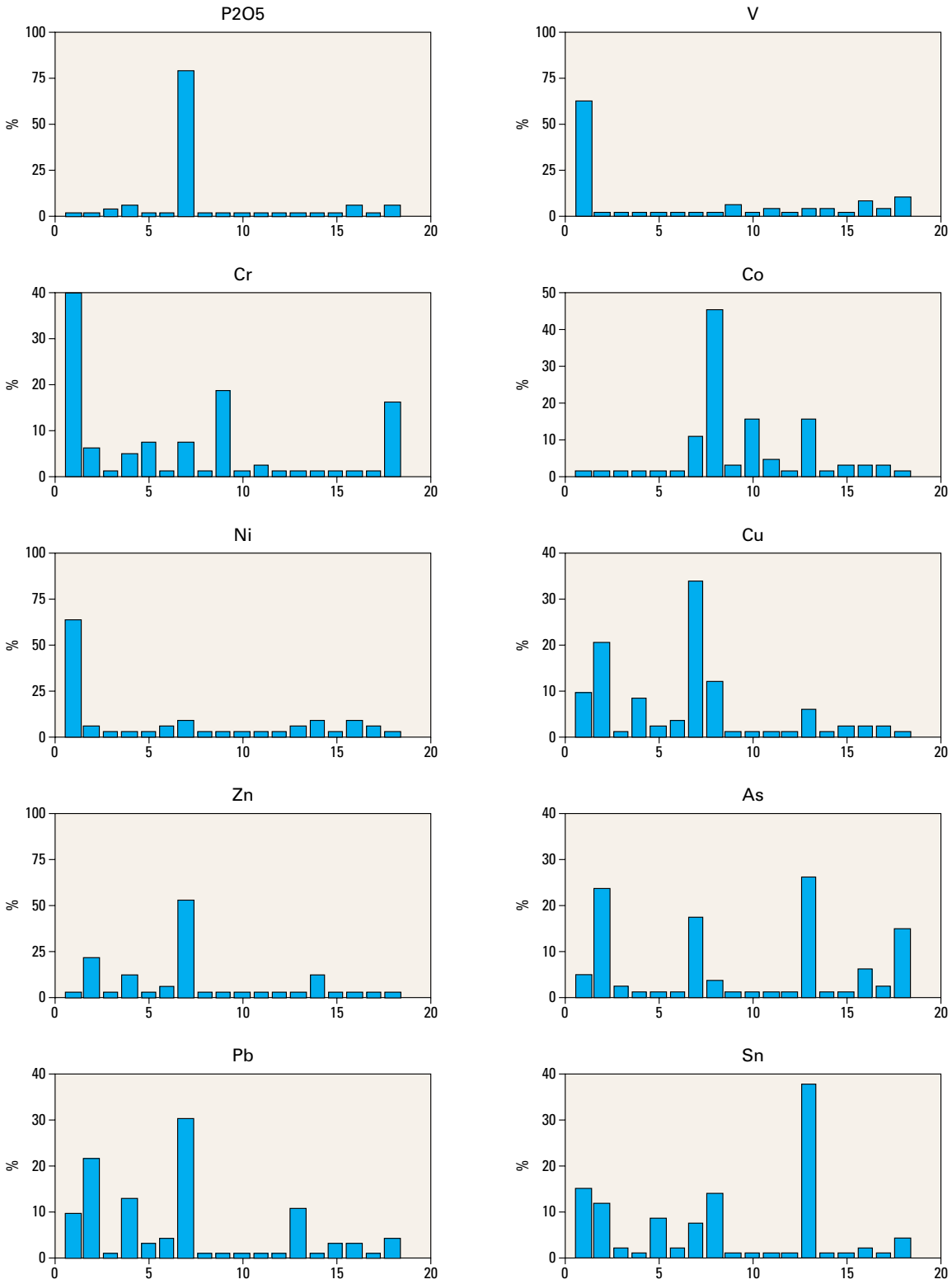

Figure 6.112 Distribution of anthropogenic marker elements between the estuarine assemblages.

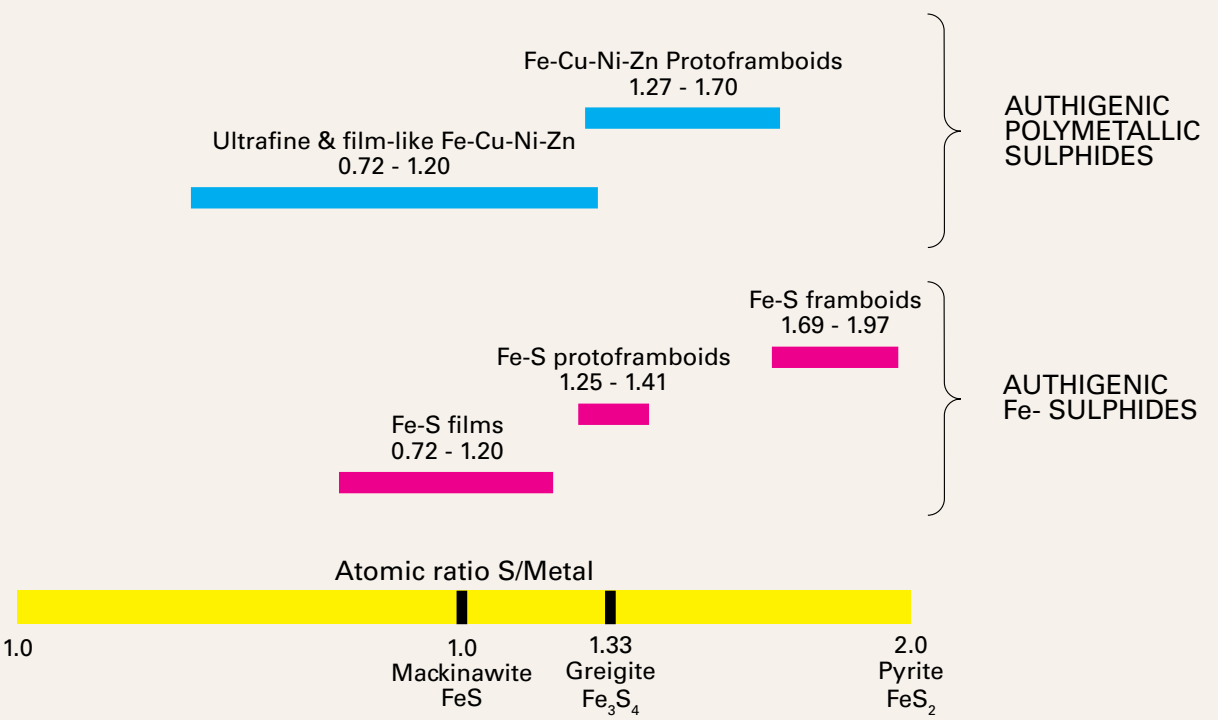

Figure 7.1 Graphical representation of the compositional domains of authigenic iron sulphides and authigenic polymetallic sulphides in the Mersey estuary sediments, and their comparison with stoichiometric iron sulphide minerals.

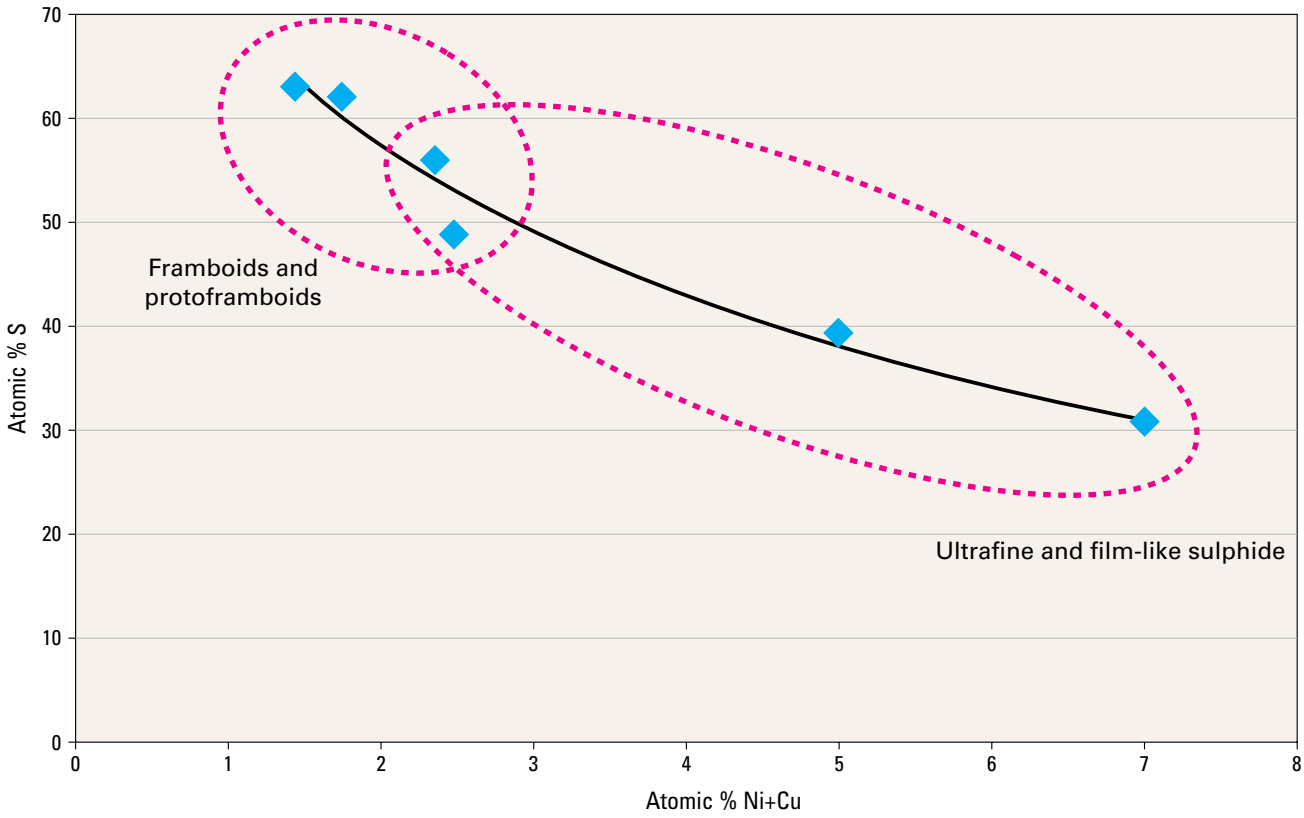

Figure 7.2 Variation in the sulphur content of the authigenic nickel- and copper-bearing iron sulphide as a function of their nickel and copper content. Sample Site M101.

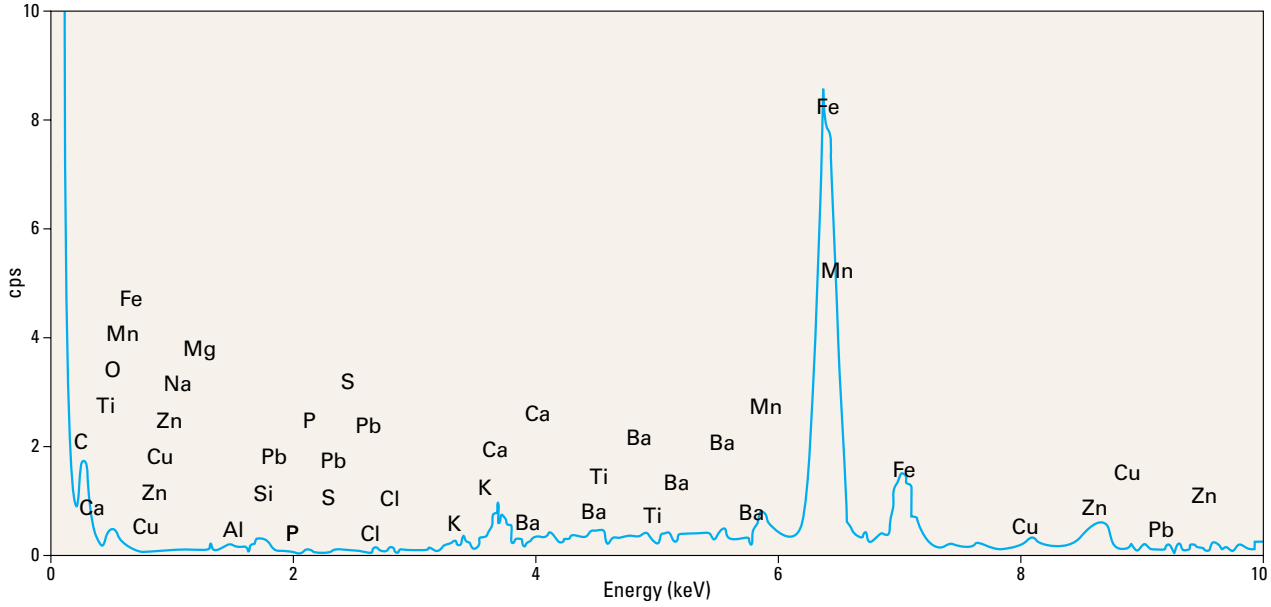

Figure 7.3 EDXA spectrum of spongy iron oxide grain showing significant concentration of Cu and Zn detected. Sample Site M101, 30–40 cm depth.

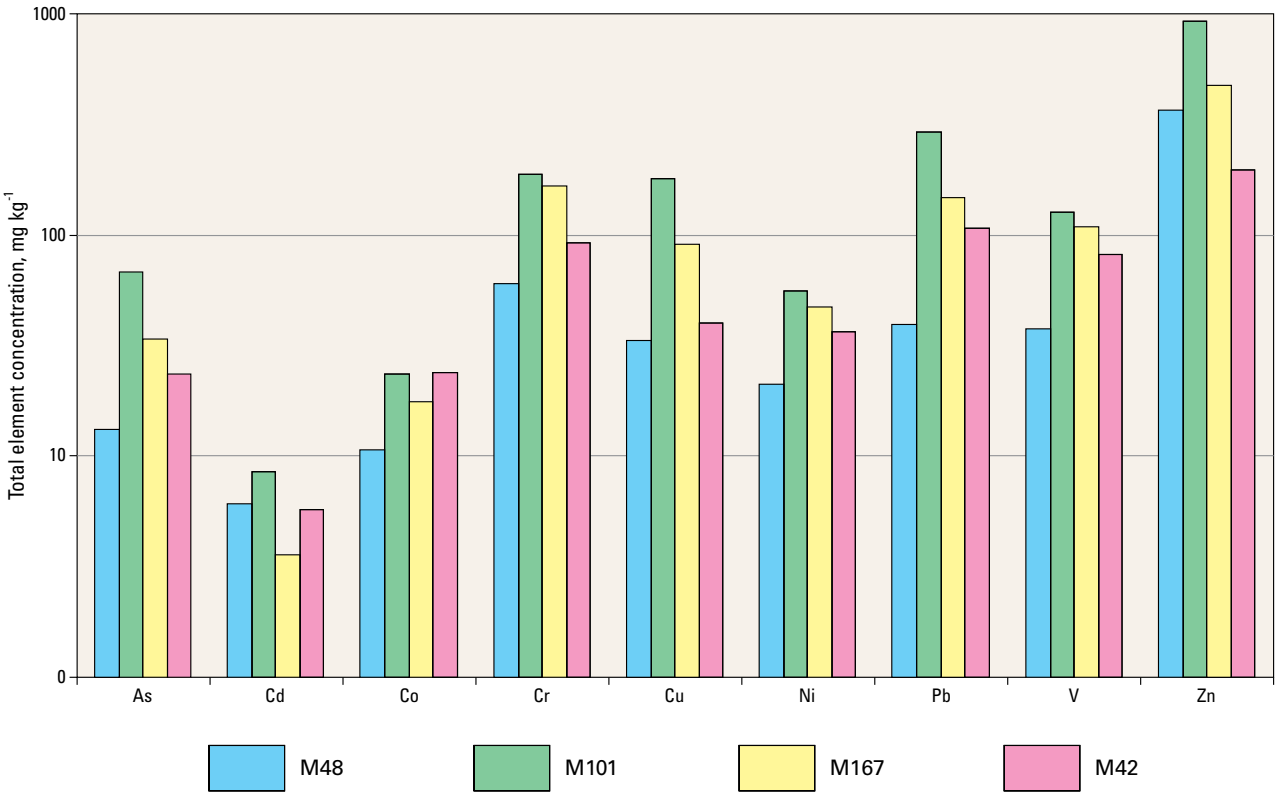

Figure 7.4 Comparison of the selected total element compositions in the core samples.

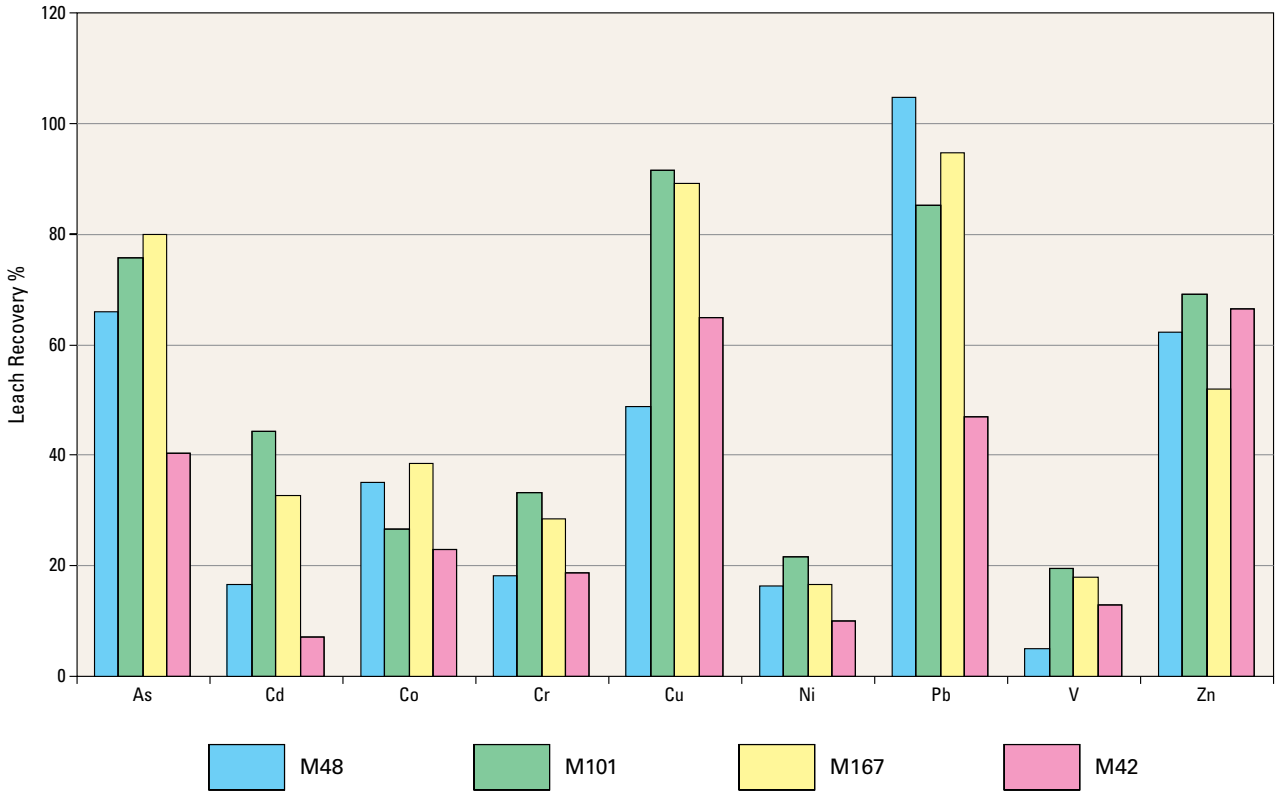

Figure 7.5 Recovery of marker elements from the CISMeD extraction test.

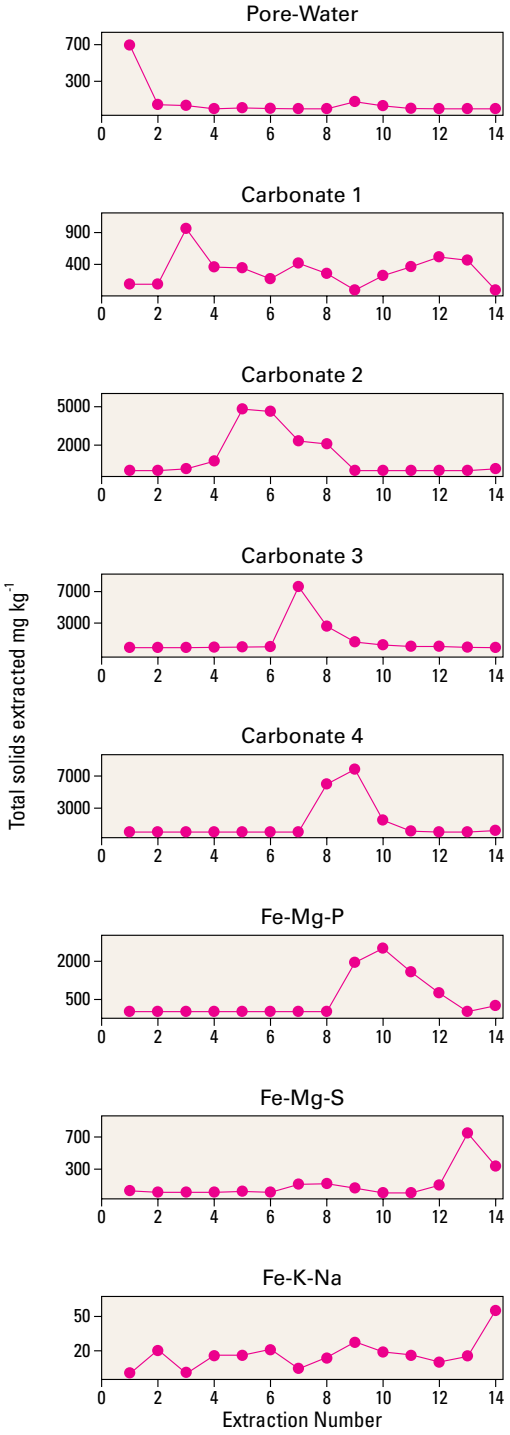

Figure 7.6 CISMeD extraction profiles for core M48.

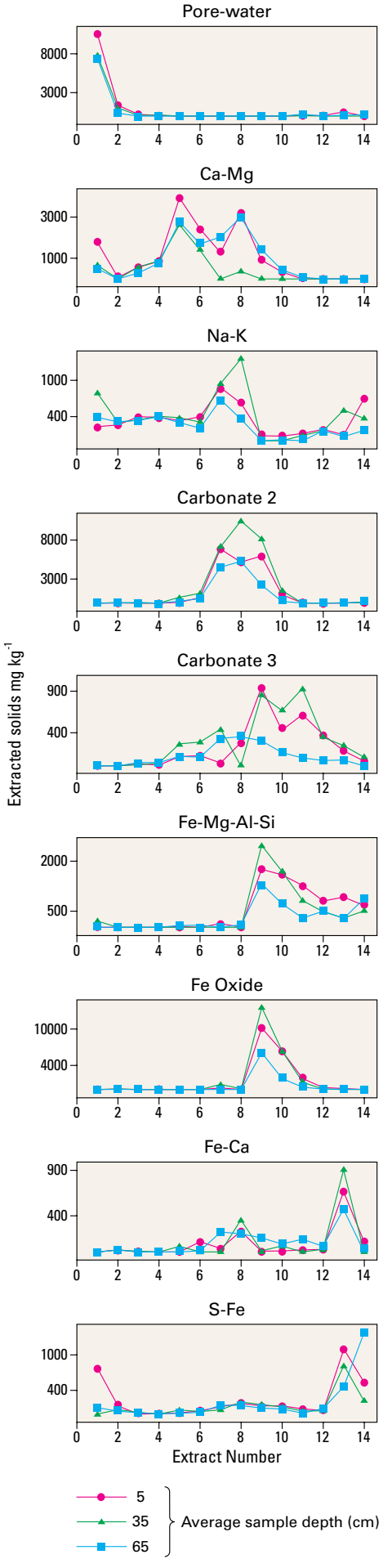

Figure 7.7 CISMeD extraction profiles for core M101.

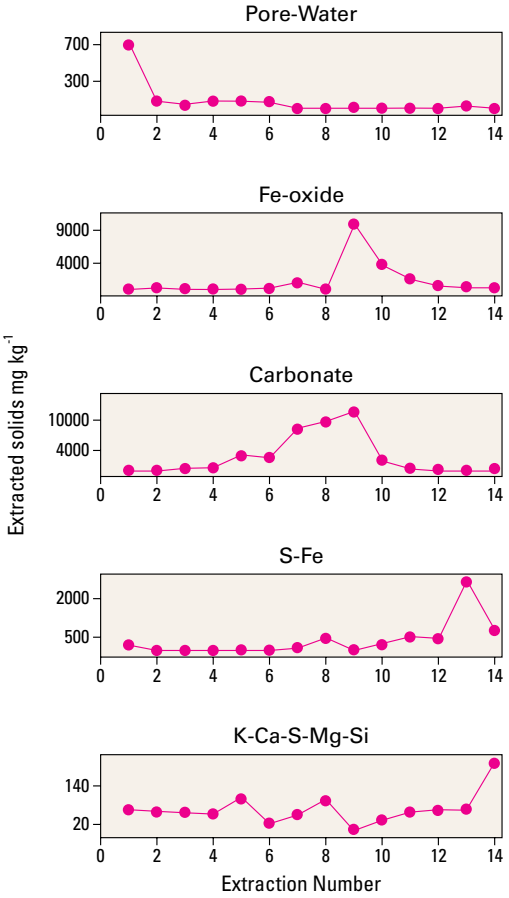

Figure 7.8 CISMD extraction profiles for core M167.

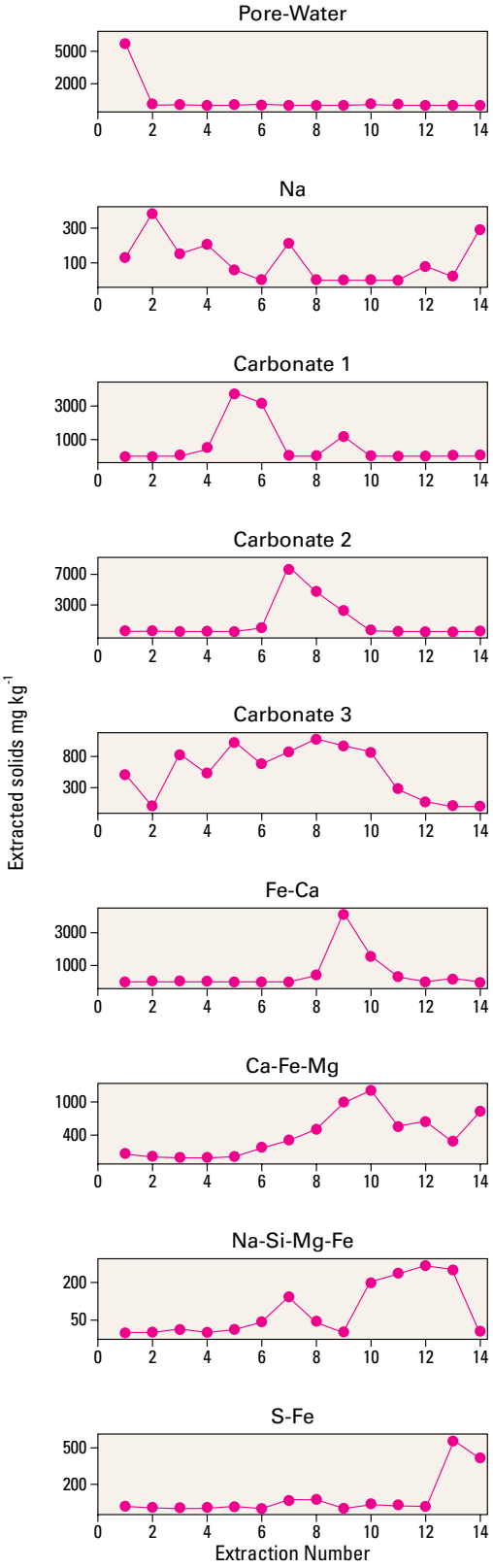

Figure 7.9 CISMeD extraction profiles for core M42.

Plate 2.1 Collection of cores using a hovercraft in the Inner Estuary (P746939).

Plate 2.2 Collection of subtidal samples from the Narrows using a Day grab (P746940).

Plate 2.3 Right: Mackereth corer showing gas bottle, cables and housing (P746941). Left: being used to collect subtidal cores (Clyde) (P746942).

Plate 2.4 Portable vibrocorer in use on an intertidal bank in the Mersey (P746943).

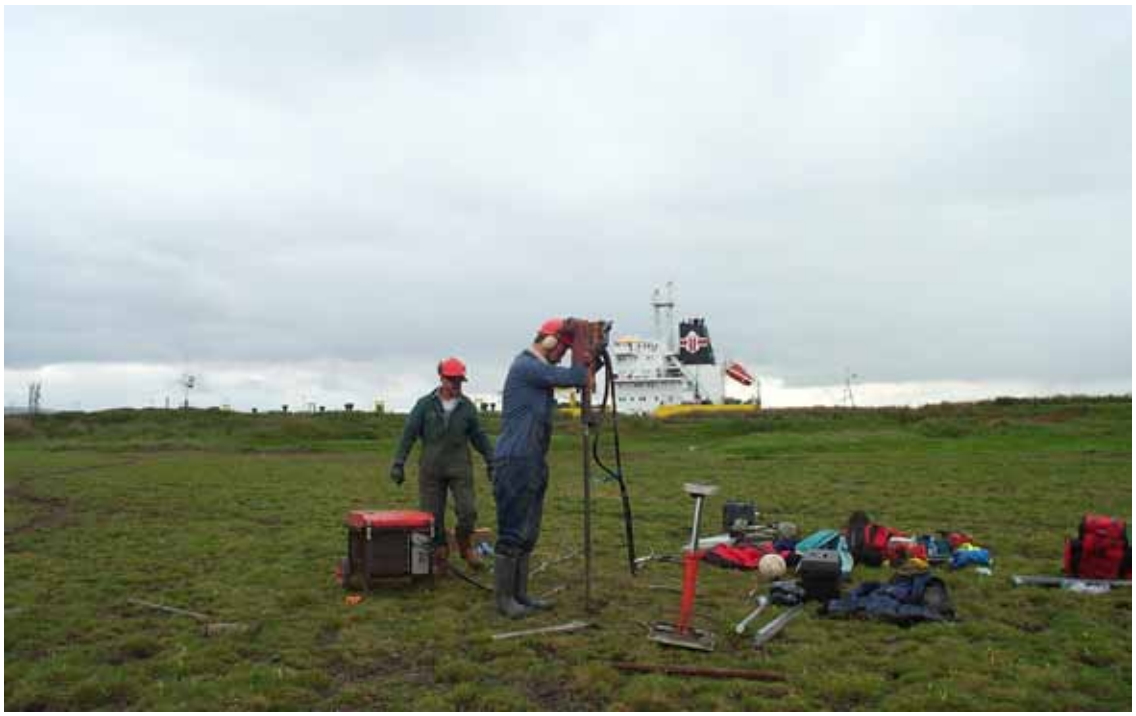

Plate 2.5 The Marlow portable drilling rig in use on Ince Banks (P746944).

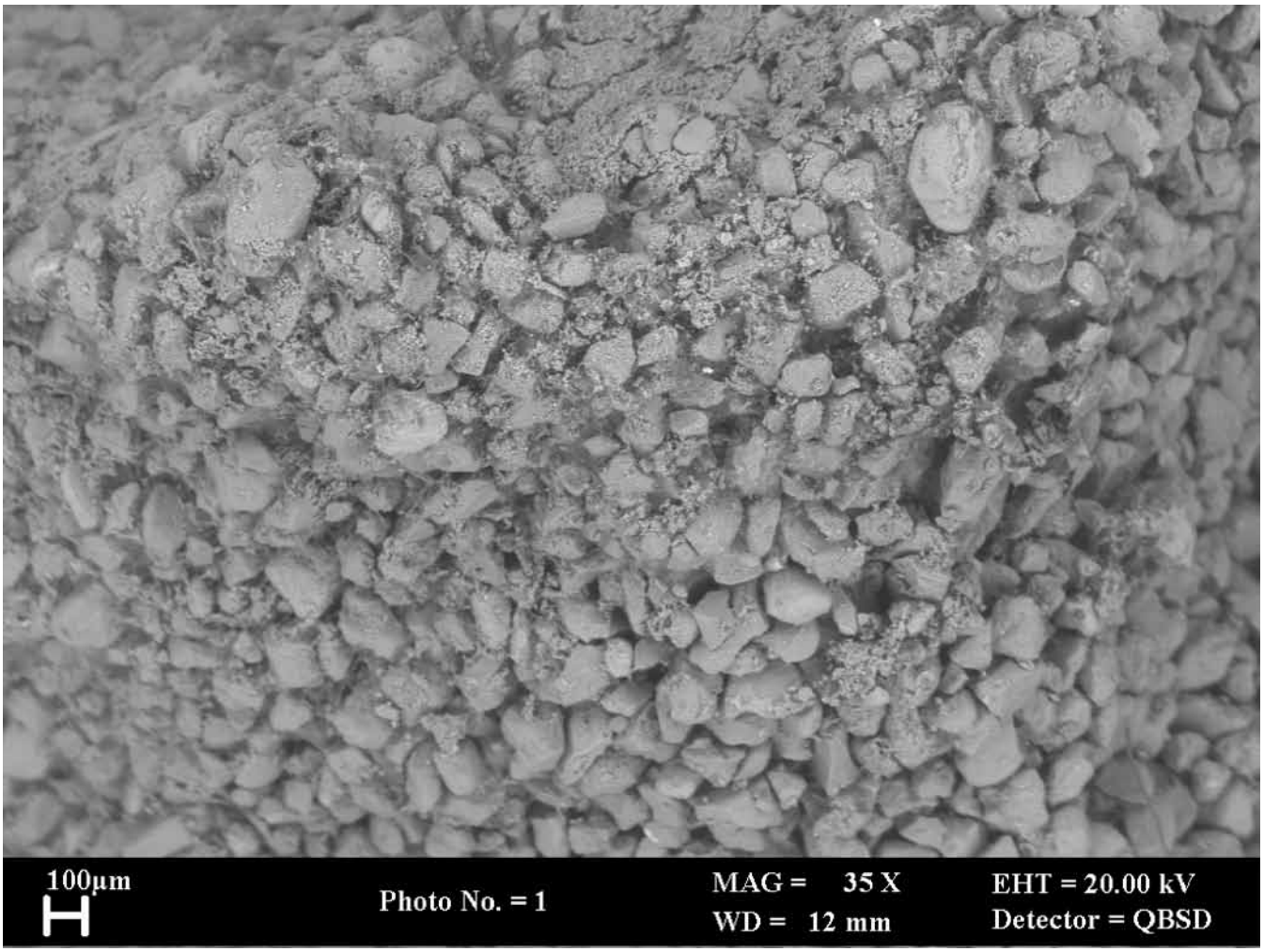

Plate 7.1 Cryogenic SEM image (backscattered electron image) of undisturbed sediment from Site M42 (0–10 cm depth) showing an example of fine muddy sand, composed dominantly of angular grains of detrital quartz. Very little clay grade material appears to be present (P746945).

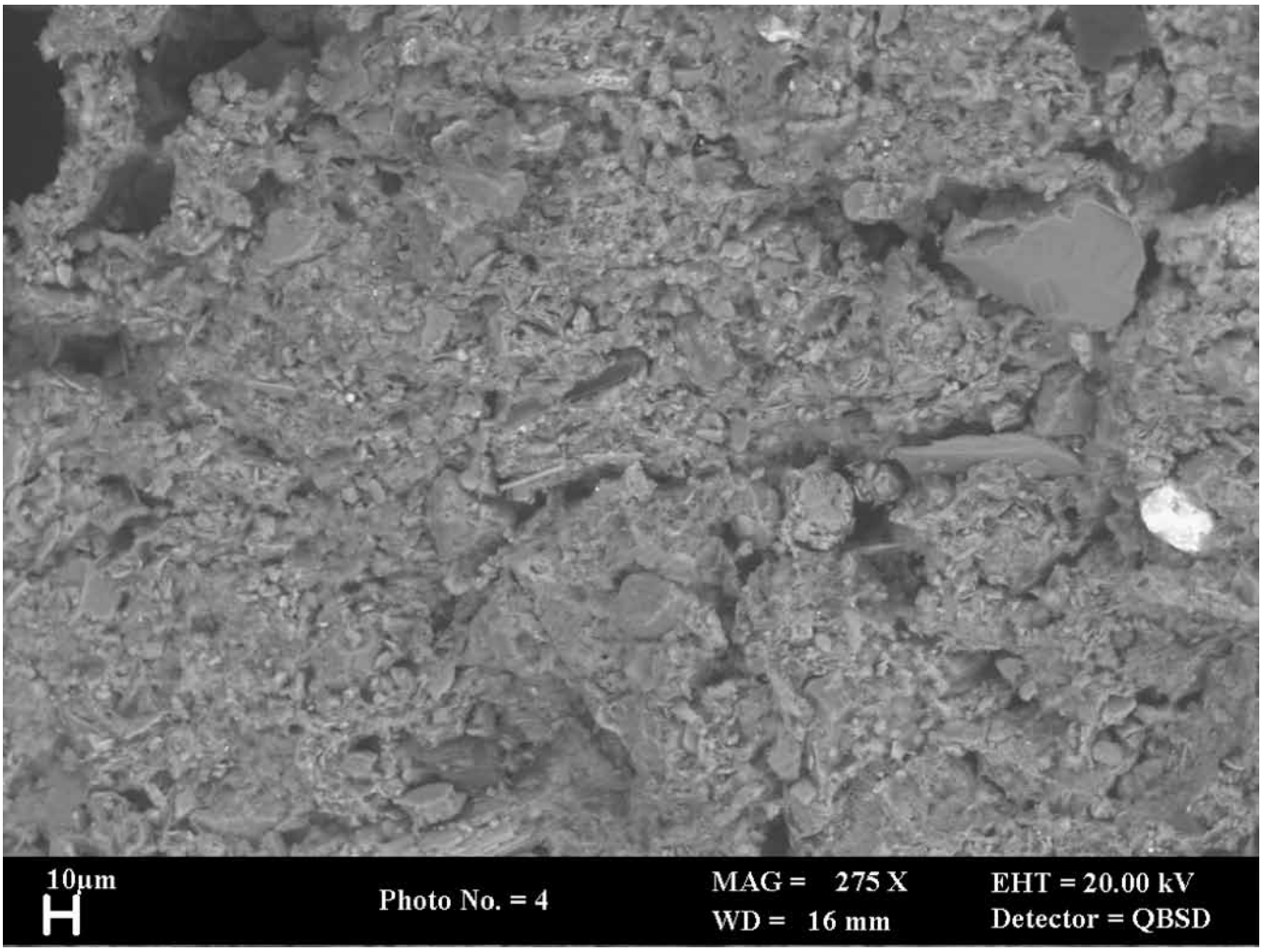

Plate 7.2 Cryogenic SEM image (backscattered electron image) of undisturbed sediment from Site M28 (30–40 cm depth) showing an example of silty mud. Abundant very fine (clay-grade) quartz is present in these sediments (P746956).

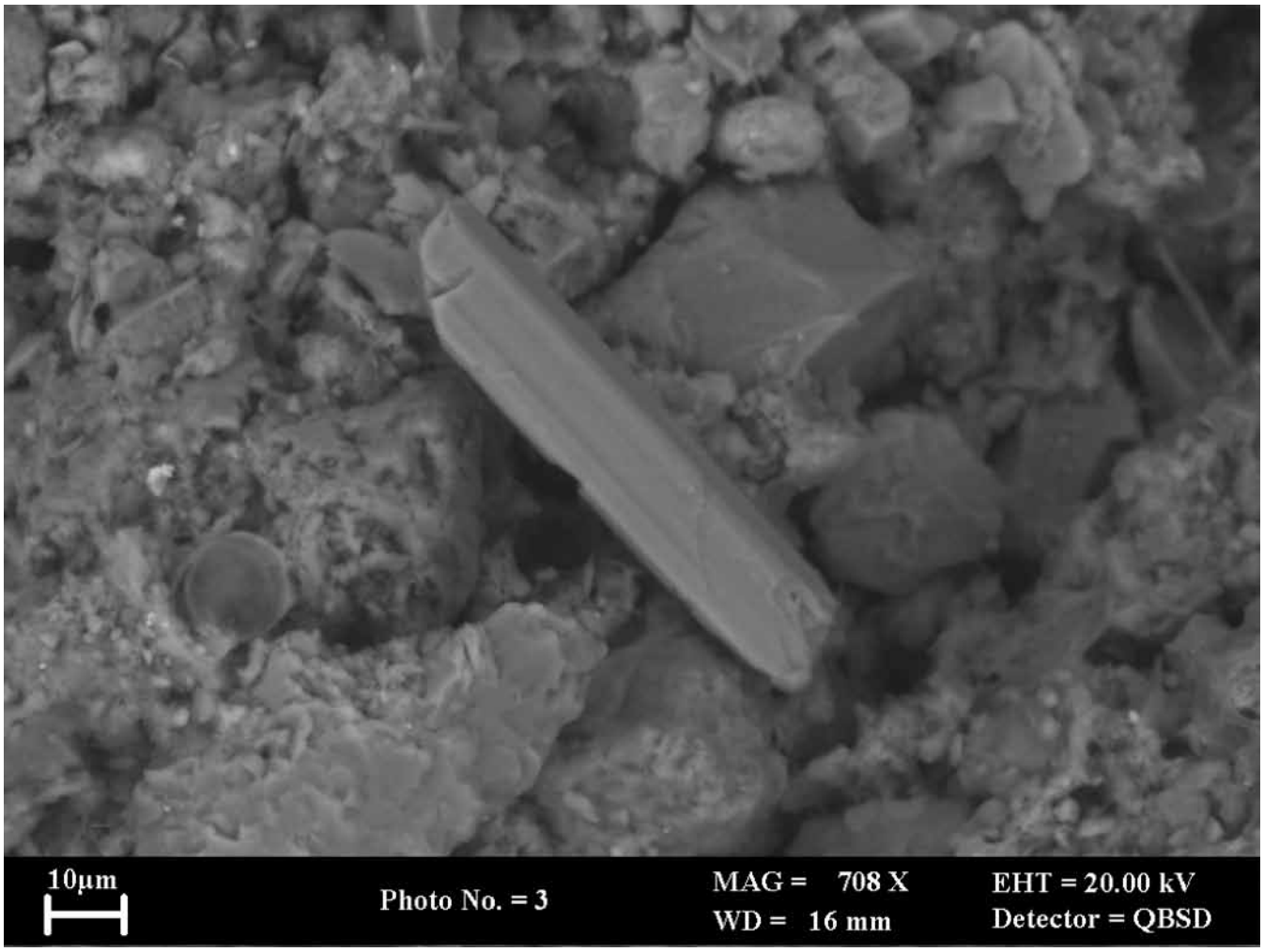

Plate 7.3 Cryogenic SEM image (backscattered electron image) of undisturbed sediment showing typical angular morphology of fine sand- and silt-grade detrital grains. The needle-like grain (centre) is an amphibole grain. Site M28 (30–40 cm depth) (P746963).

Plate 7.4 Cryogenic SEM image (backscattered electron image) of undisturbed sediment showing discoid diatom skeleton. Site M101 (P746964).

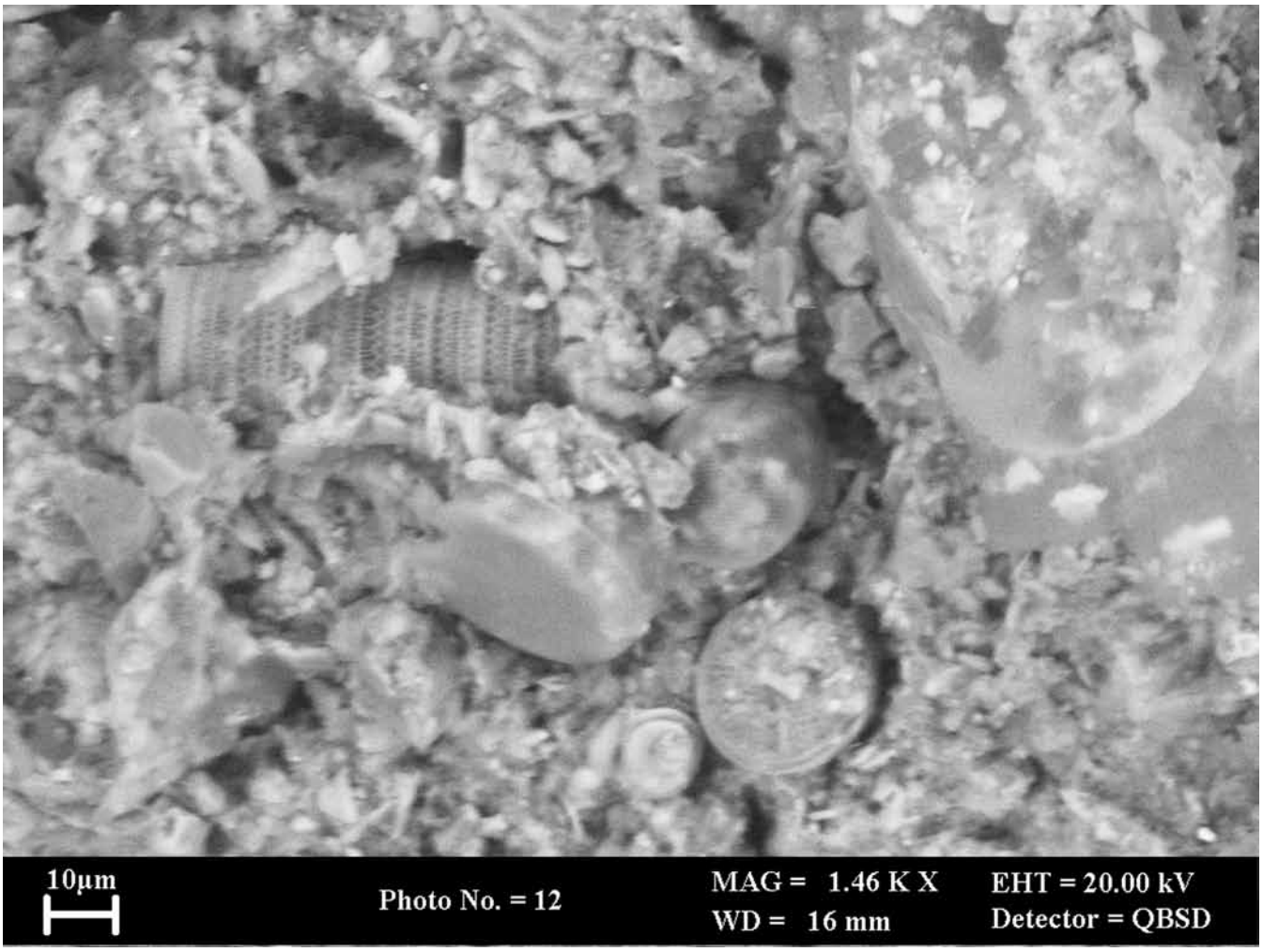

Plate 7.5 Cryogenic SEM image (backscattered electron image) of undisturbed sediment showing abundant cylindrical and discoid diatom skeletons, in silica or quartz-rich mud matrix. Site M101 (P746965).

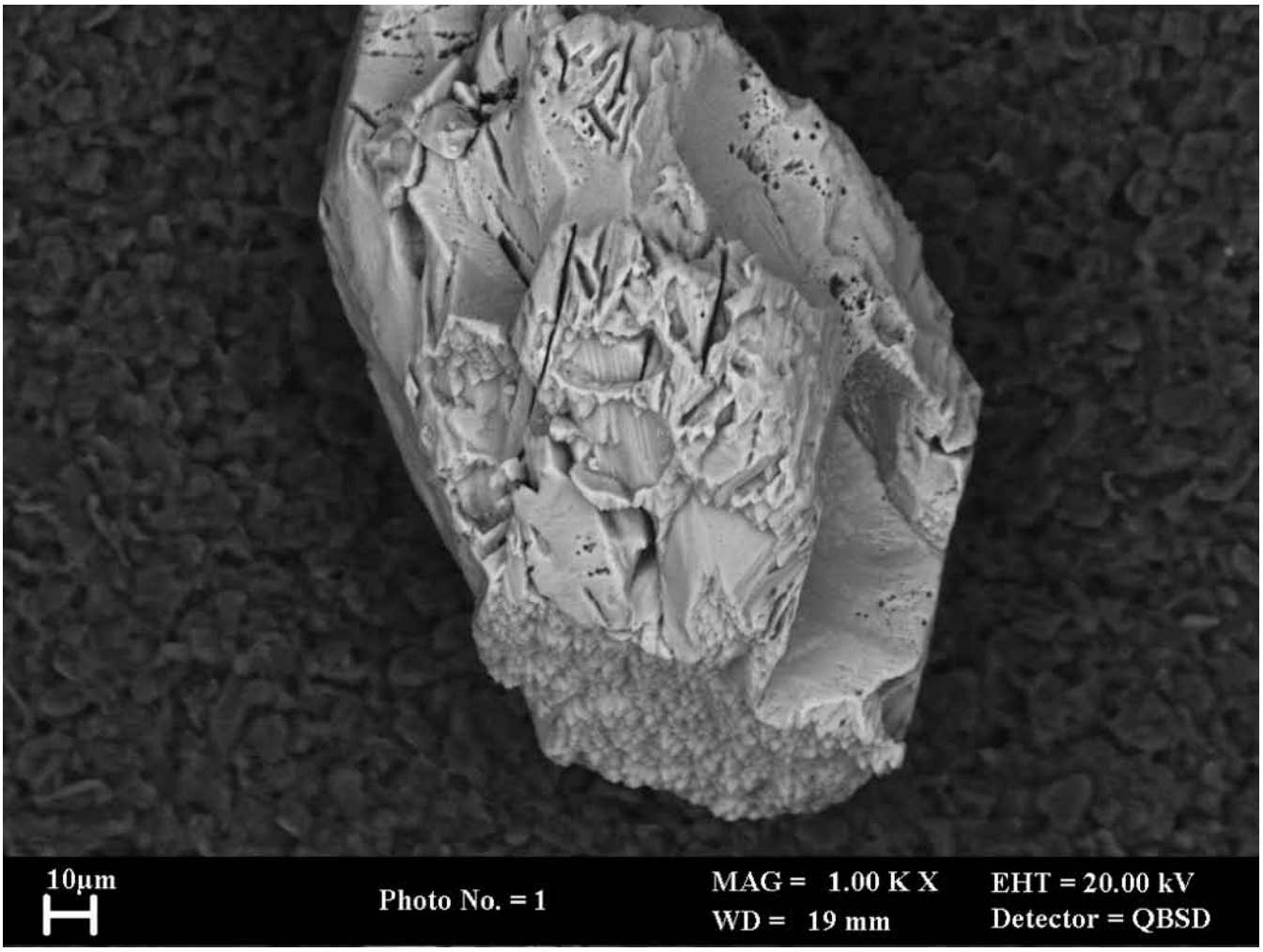

Plate 7.6 SEM image showing amphibole grain from the heavy mineral fraction from sediment at Site M95, Mersey estuary (P746966).

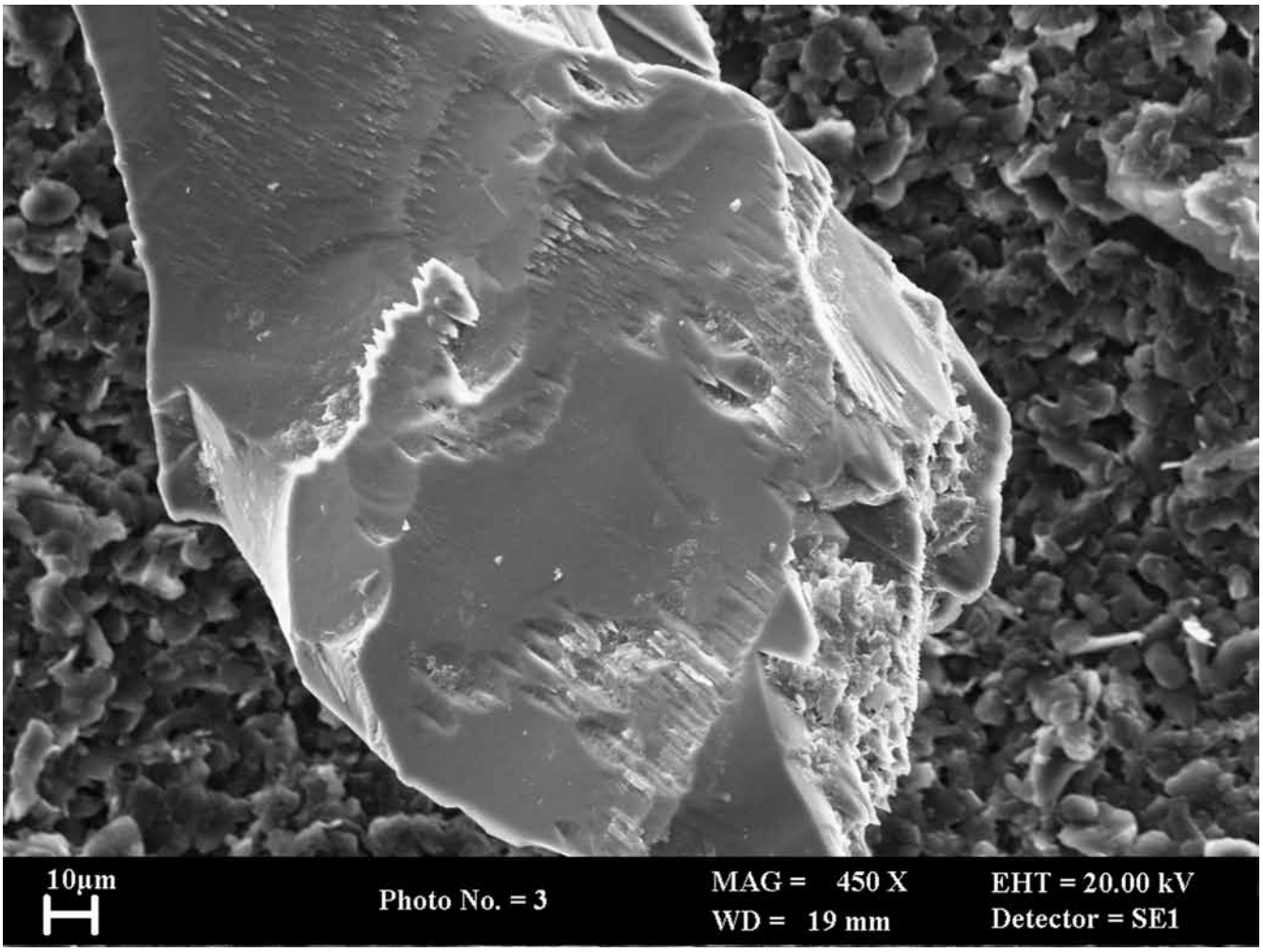

Plate 7.7 SEM image showing very minor etching of a detrital garnet grain from the heavy mineral fraction from sediment at Site M28, Mersey estuary (P746967).

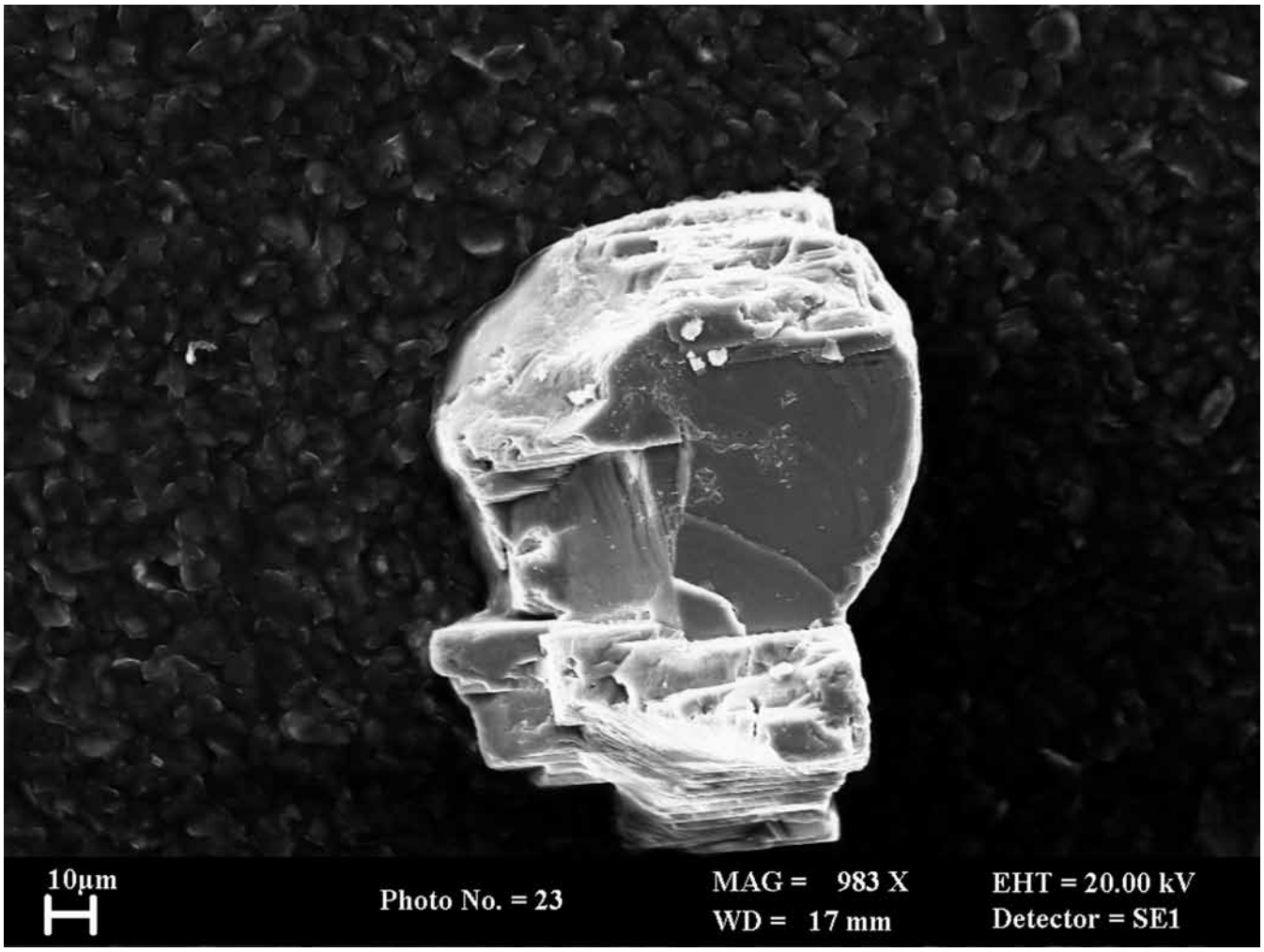

Plate 7.8 SEM image showing angular grain of anhydrite found in a heavy mineral fraction from the sediment at Site M101, Mersey estuary (P746968).

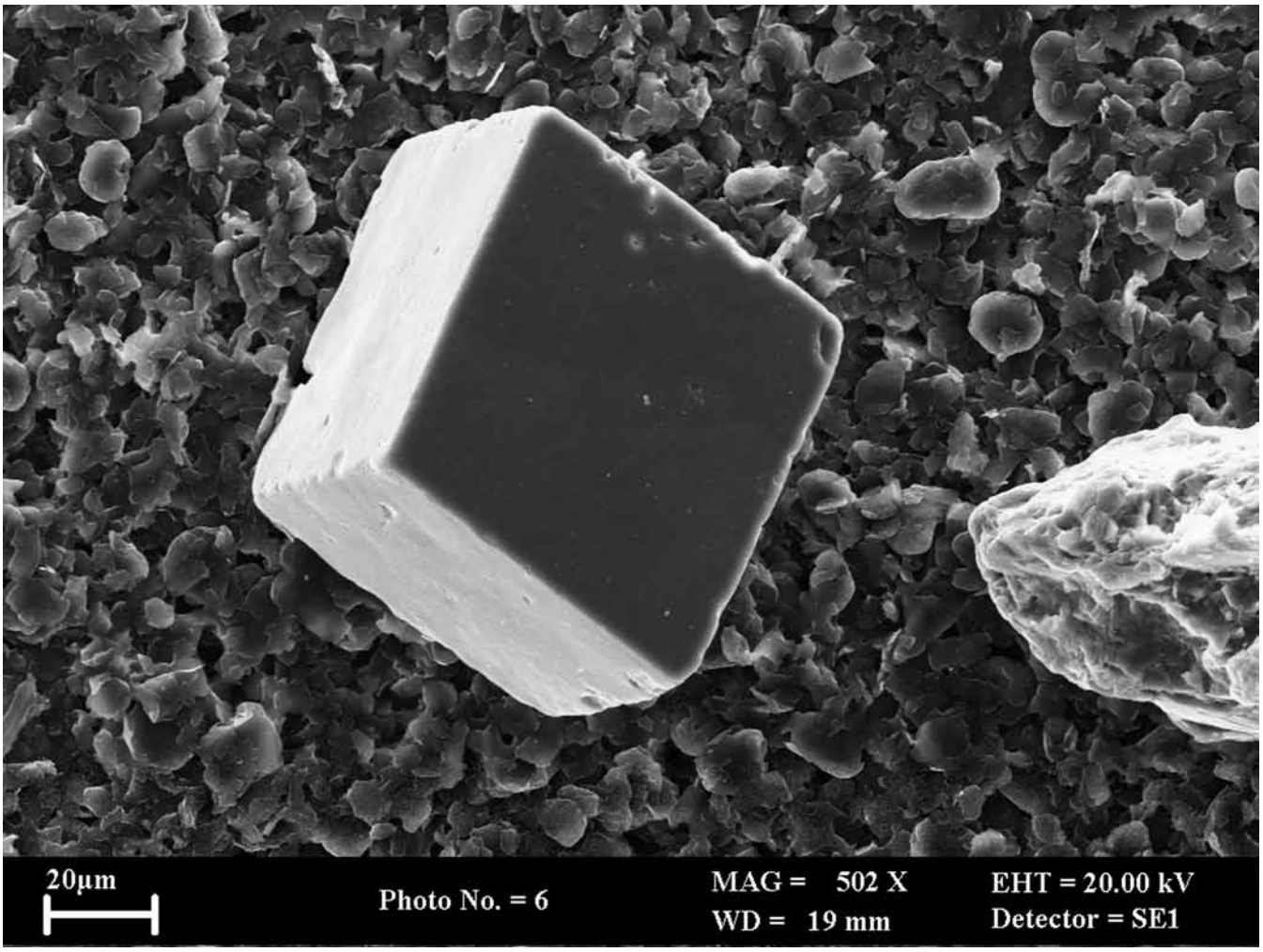

Plate 7.9 SEM image showing fresh, unabraided and uncorroded rhombic crystal of ankerite from heavy mineral fraction in the sediment at Site M42, Mersey estuary (P748671).

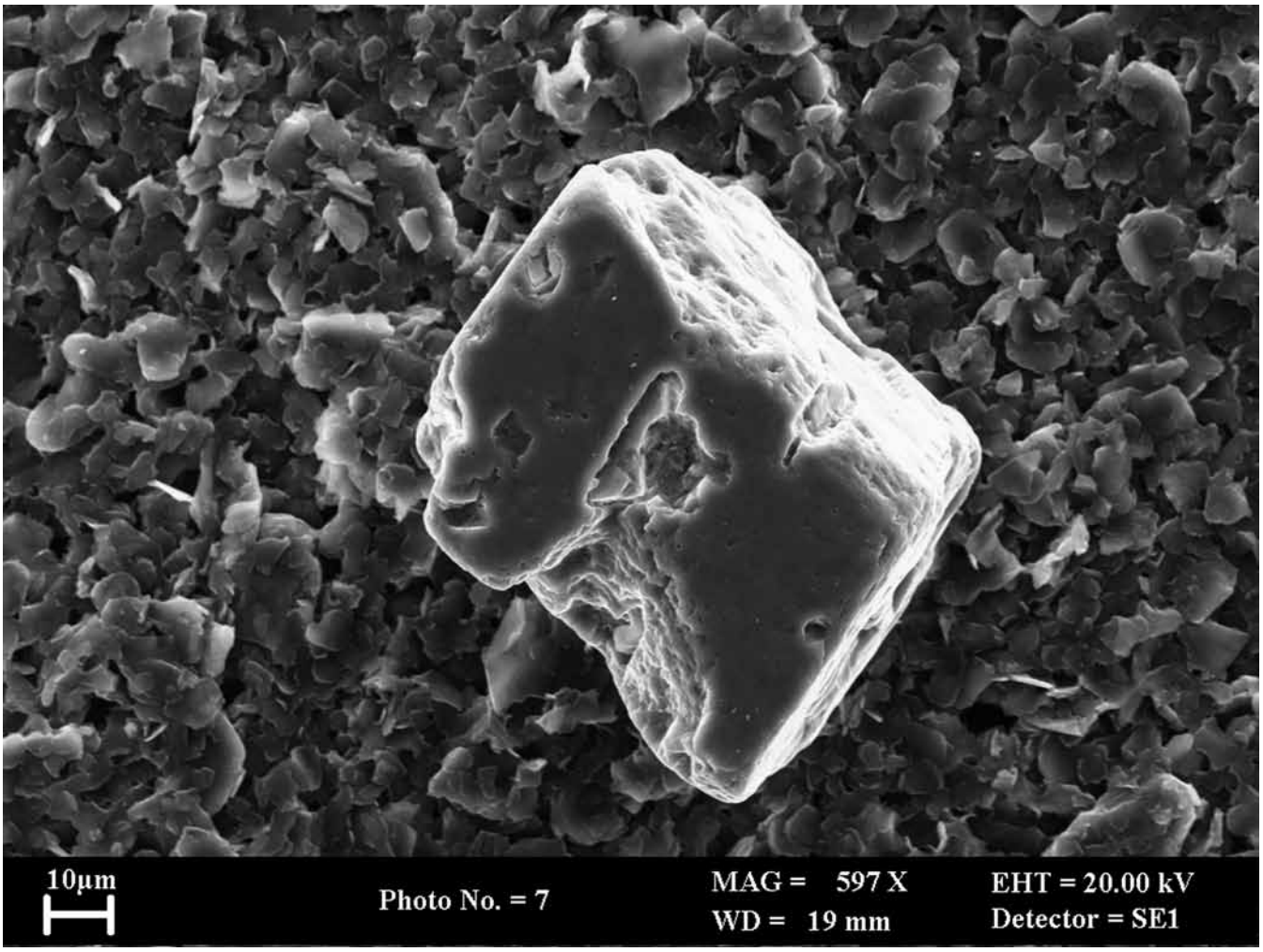

Plate 7.10 SEM image showing a corroded rhombic crystal of ankerite from heavy mineral fraction in the sediment at Site M42, Mersey estuary (P746946).

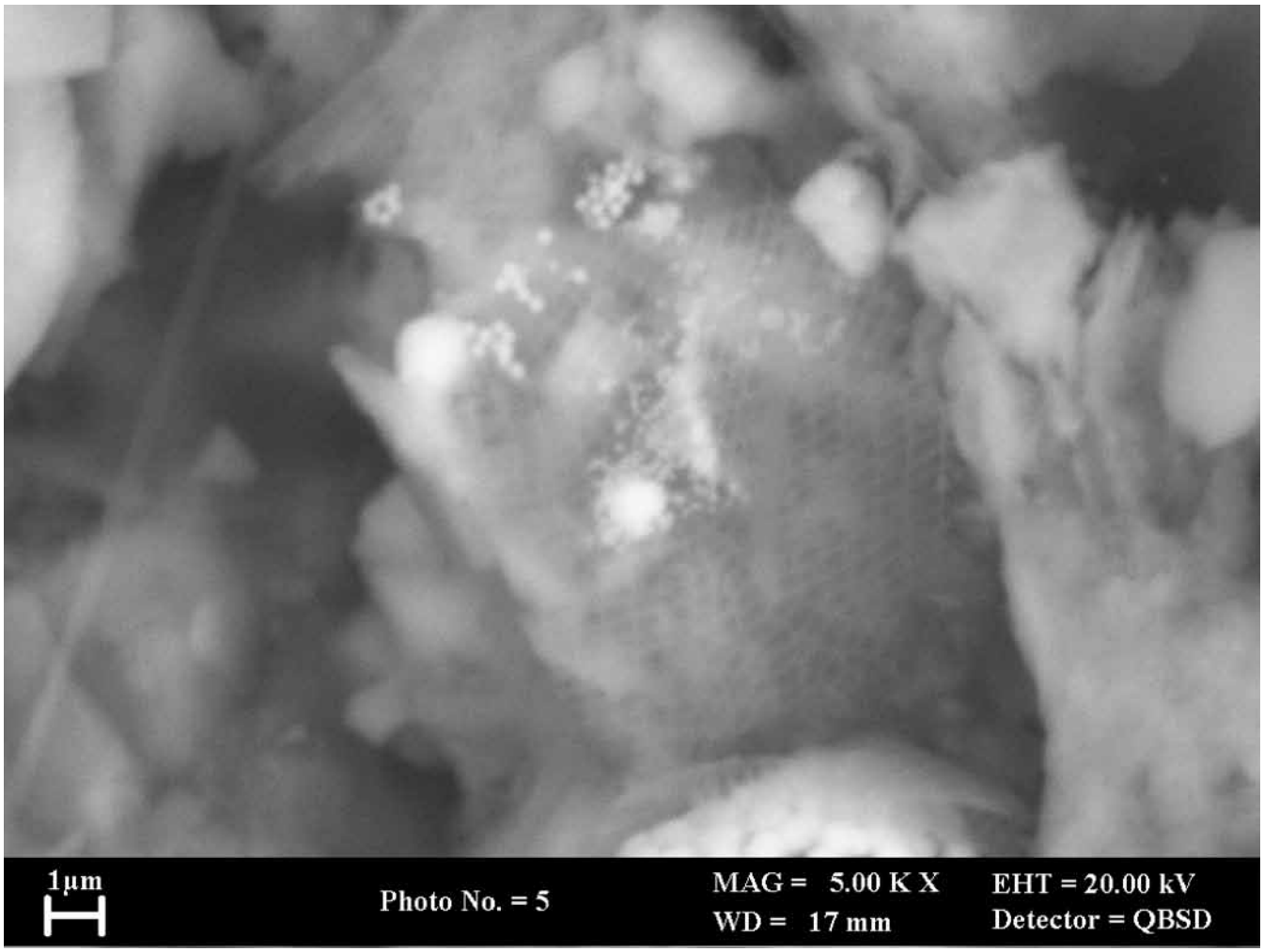

Plate 7.11 Cryogenic SEM image (backscattered electron image) of undisturbed sediment showing a very fine film of authigenic iron sulphide (bright material) coating the fine 'mesh-like' siliceous surface of probable diatom fragments. Site M42, 58–68 cm depth (P746947).

Plate 7.12 Cryogenic SEM image (backscattered electron image) of undisturbed sediment showing spherical iron sulphide protoframboid (with indistinct component crystallites) nucleated on the surface of a detrital quartz particle. Site M42, 0–10 cm depth (P746948).

Plate 7.13 Cryogenic SEM image (backscattered electron image) of undisturbed sediment showing well-developed spherical iron sulphide framboid (with distinct component crystallites) nucleated within the clay matrix. The framboid sits adjacent to fine iron sulphide film developed on siliceous diatomaceous debris (which can be seen just above the framboid in this image). Site M42. 58–68 cm depth (P746949).

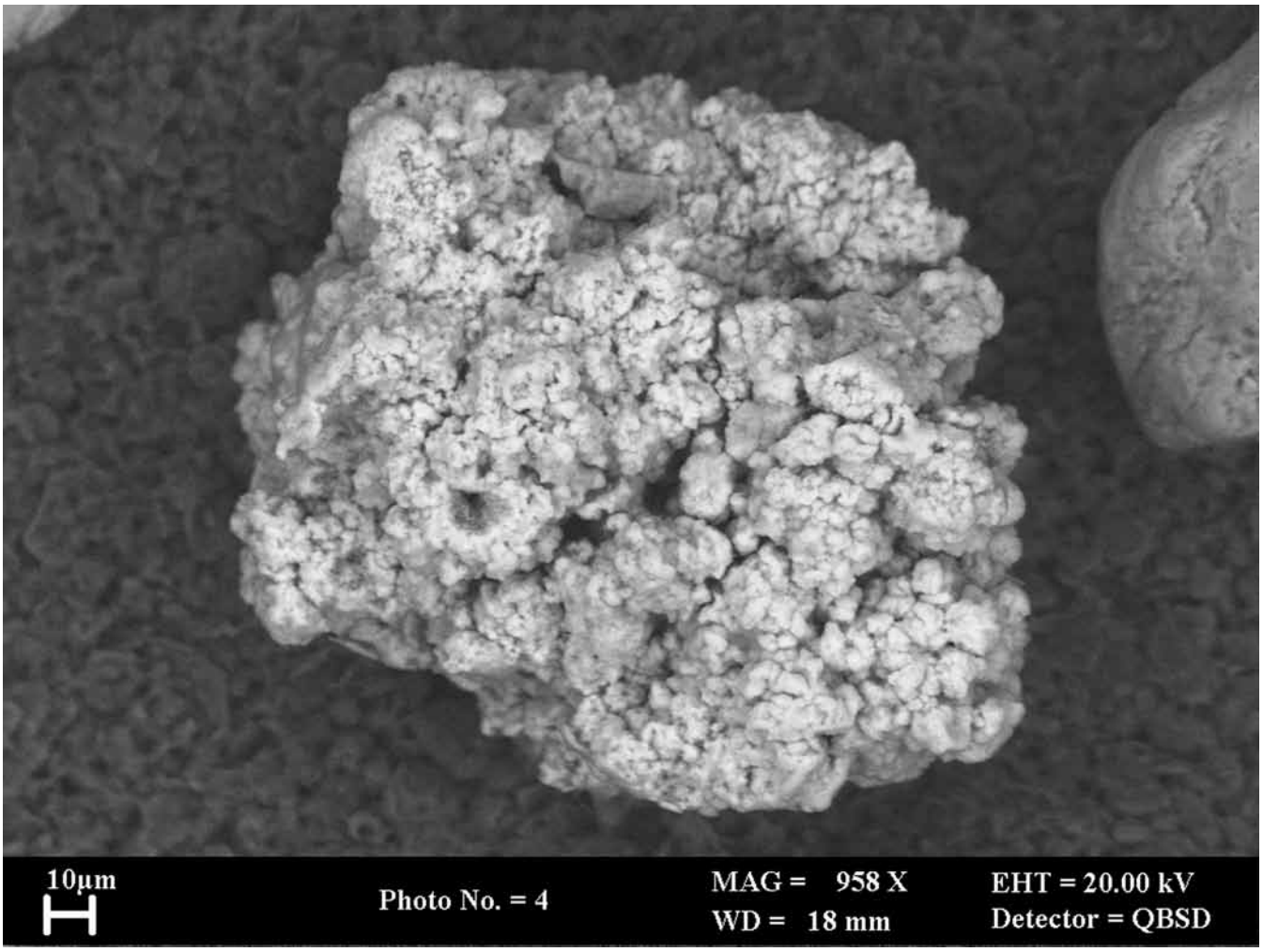

Plate 7.14 SEM image of typical spongy or microporous iron oxide grain encountered in heavy mineral separates from Site M101. 0–10 cm depth (P746950).

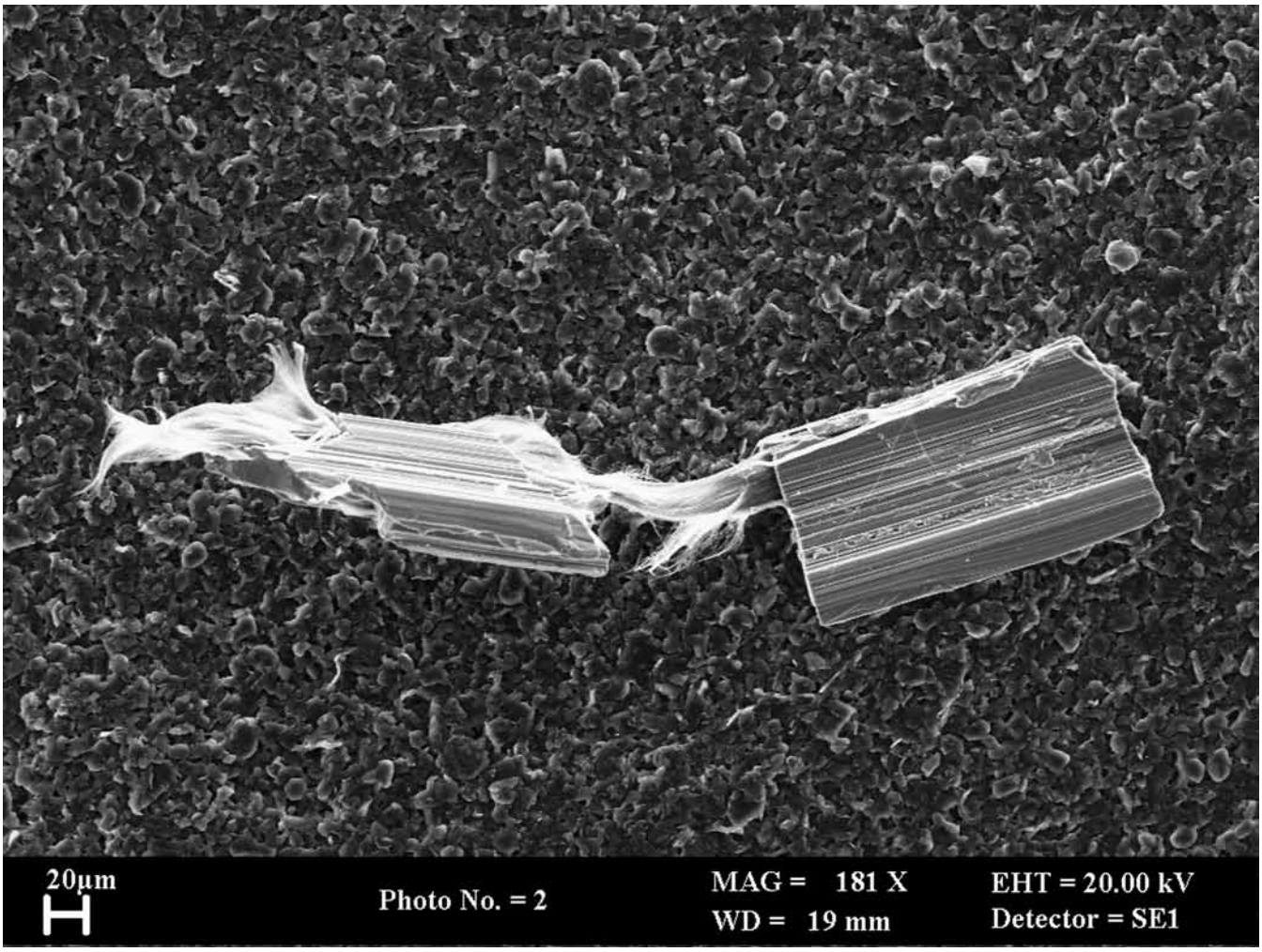

Plate 7.15 SEM image of a fragment of a composite fragment of steel and asbestos found in sediment from Site M42, 58–68 cm depth (P746951).

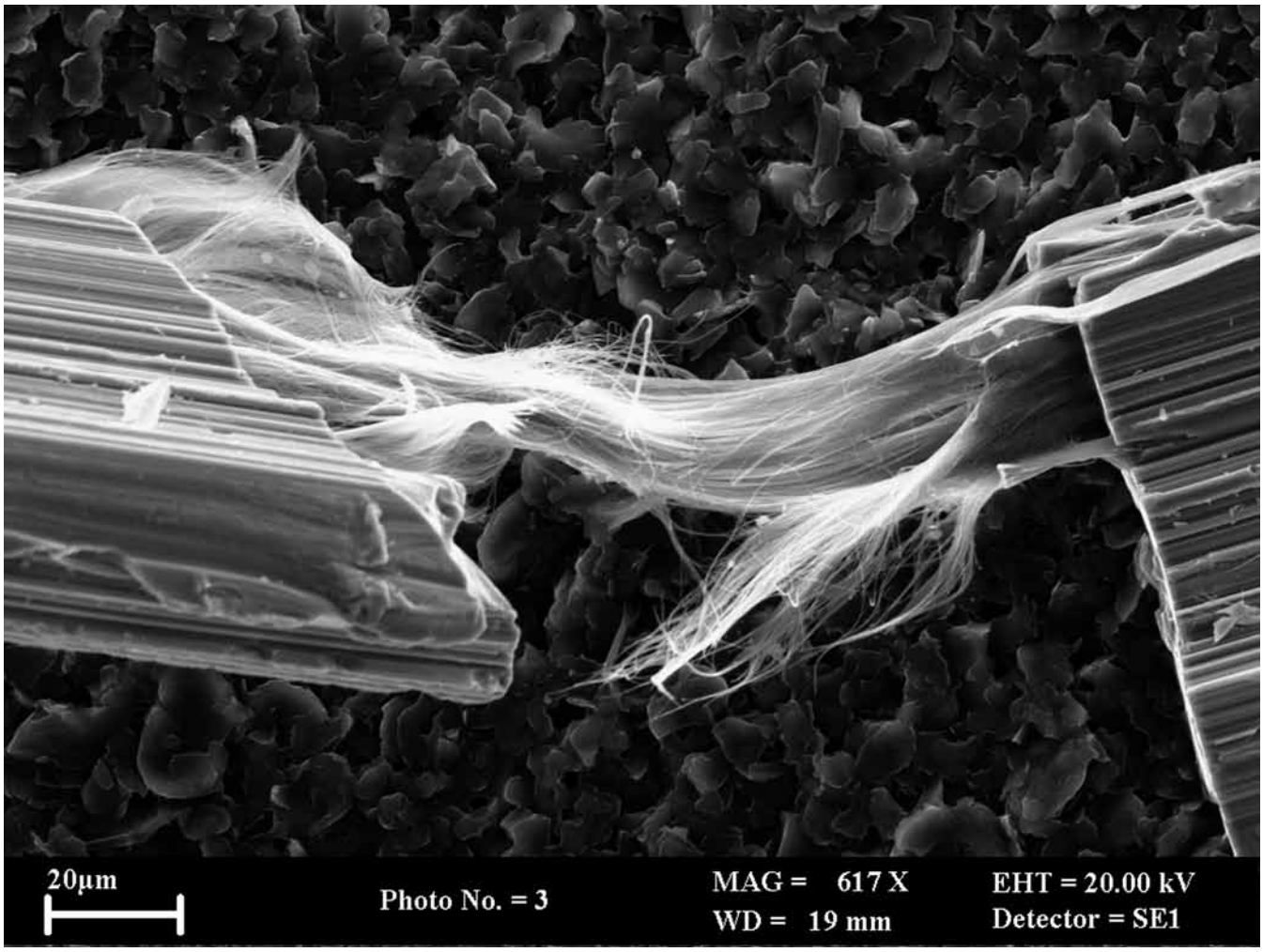

Plate 7.16 SEM image showing detail of fibrous morphology of asbestos within composite asbestos-steel particle seen in Plate 7.15 (P746952).

Plate 7.17 SEM image of a typical grain of sphalerite in heavy mineral separate from Site M101, 30–40 cm depth. The sphalerite grain is angular, and has a fresh, uncorroded and unaltered appearance (P746953).

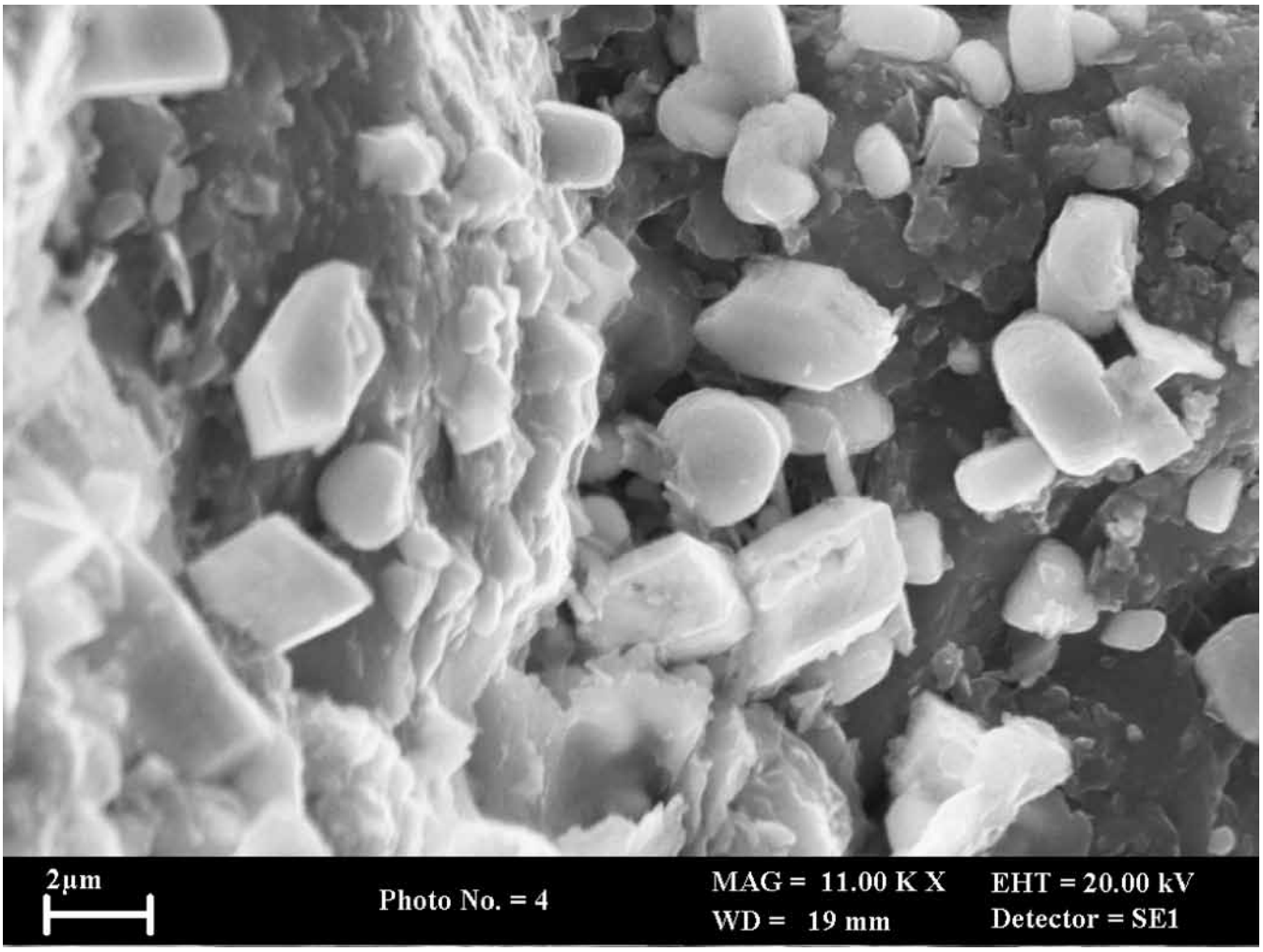

Plate 7.18 SEM image showing small euhedral tin oxide crystals, possibly of authigenic origin, coating a detrital quartz grain. Site M95, 0–10 cm depth (P746954).

Plate 7.19 SEM image showing a Ca-Mg-K-Al- silicate spherule of fly-ash from a heavy mineral separate from sediment at Site M101, 30–40 cm depth. The spherule displays a dendritic crystalline ornamentation on its surface resulting from devitrification (P746955).

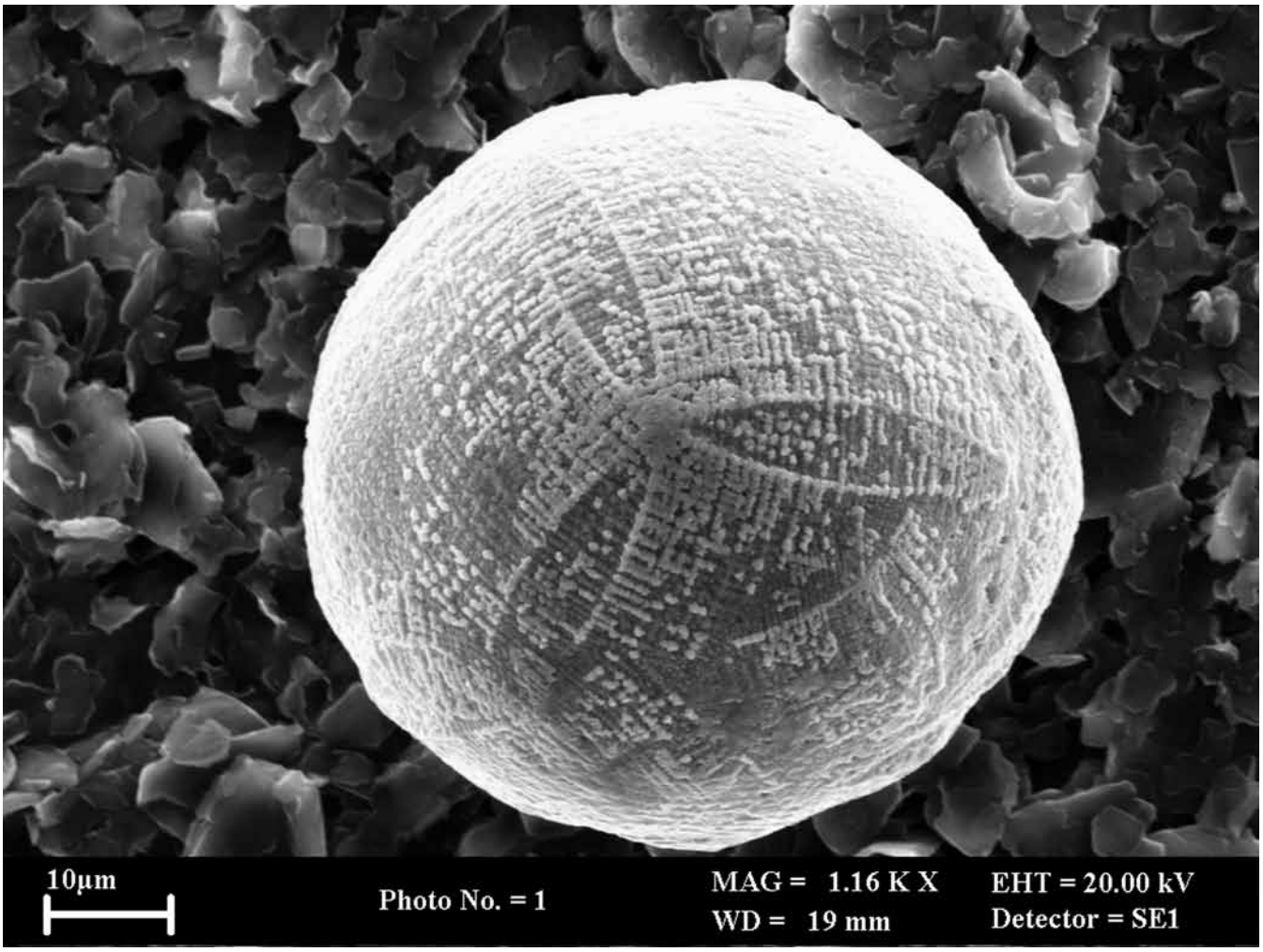

Plate 7.20 SEM image showing a Fe-Al-Ca-P- silicate spherule of fly-ash from a heavy mineral separate from sediment at Site M42, 56–68 cm depth. The spherule displays a crystalline ornamentation on its surface possibly resulting from devitrification (P746957).

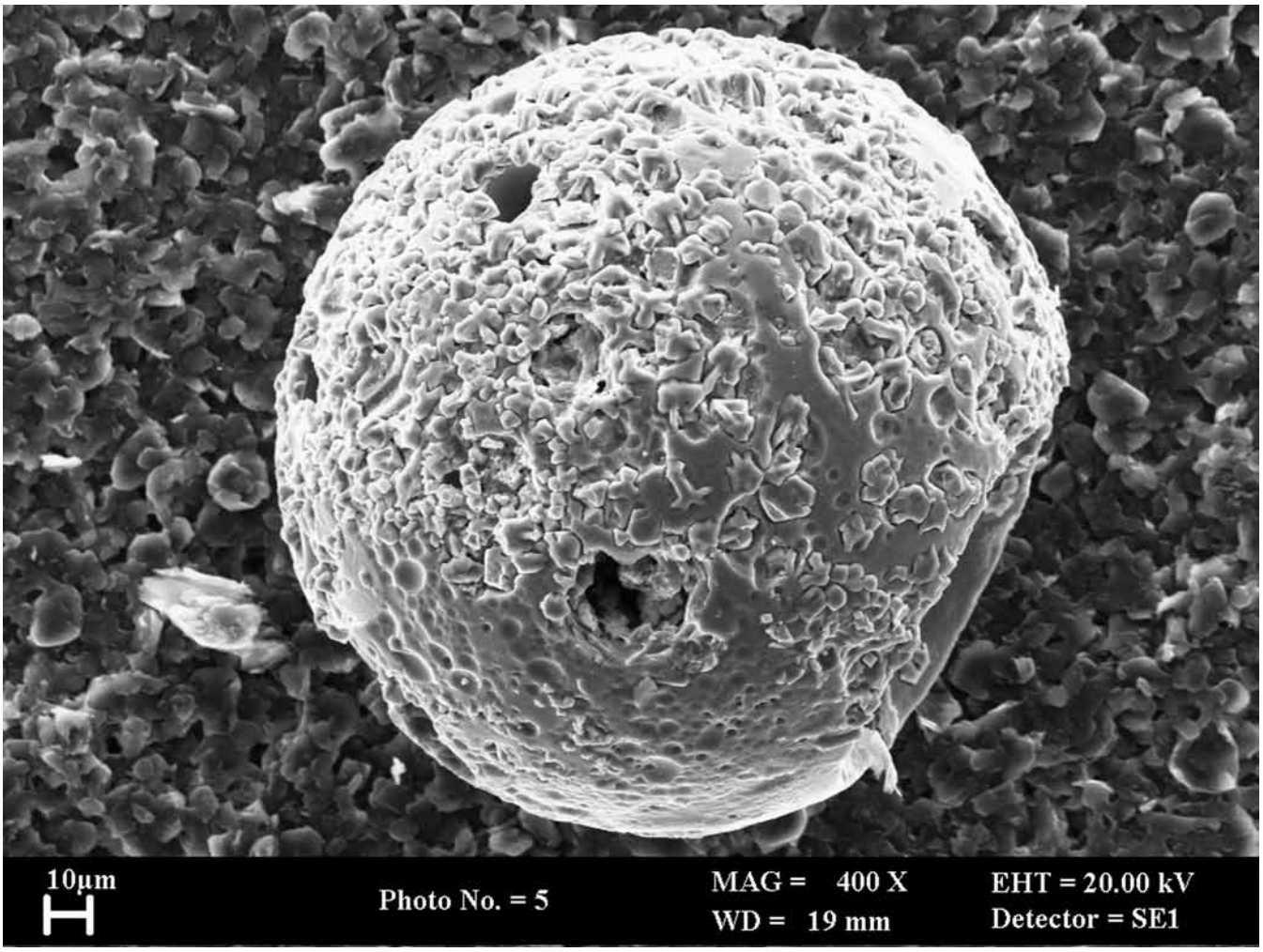

Plate 7.21 SEM image showing a K-Ca-Na-Mg-Al-Fe-Ti- silicate spherule of fly-ash from a heavy mineral separate from sediment at Site M28, 0–10 cm depth. The spherule displays corrosion and etching on its surface resulting from dissolution along the grain boundaries of crystallites (P746958).

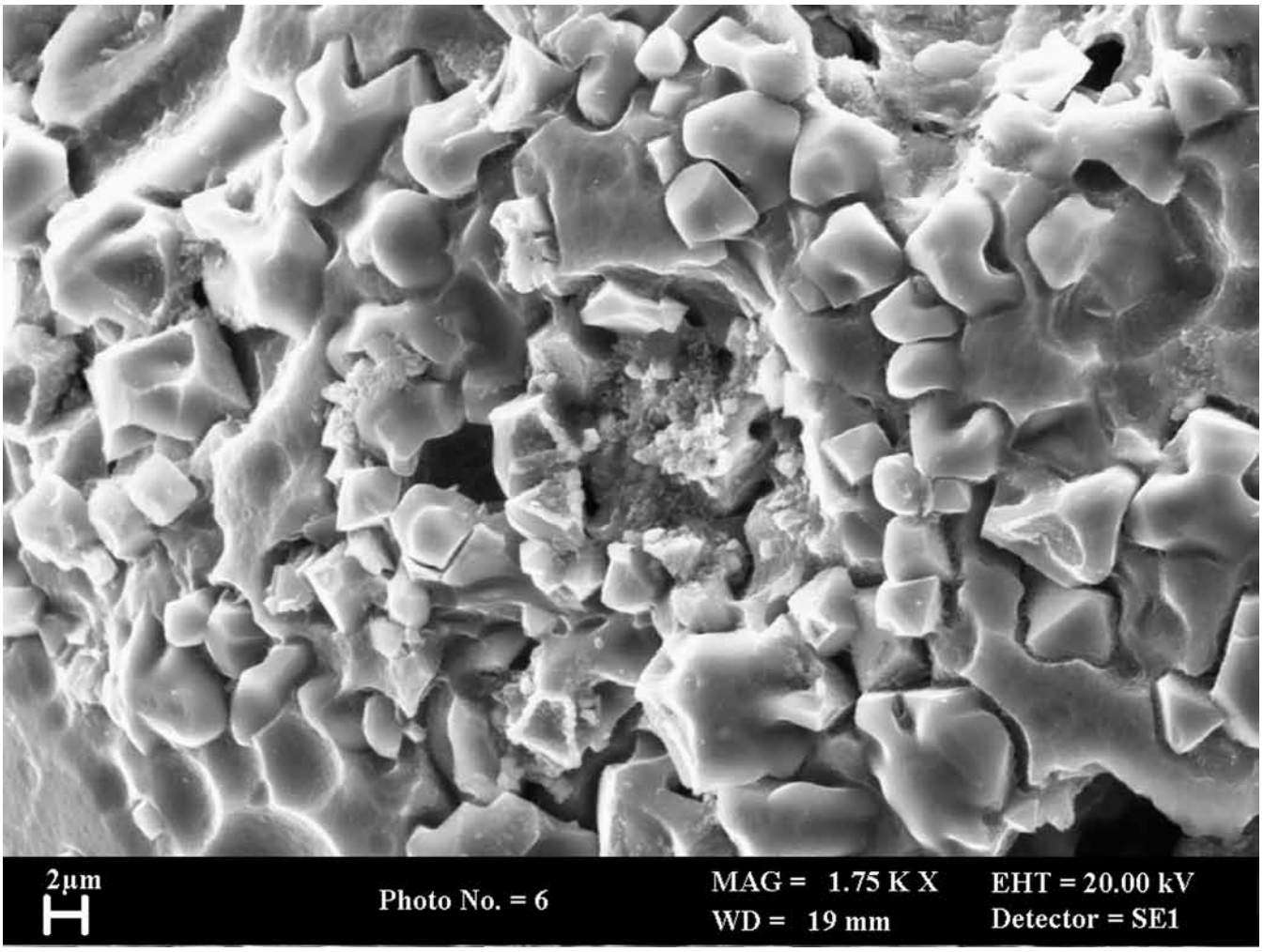

Plate 7.22 SEM image showing detail of the corroded surface of the K-Ca-Na-Mg-Al-Fe-Ti- silicate spherule of fly-ash seen in Plate 21 (Site M28, 0–10 cm depth). The spherule displays corrosion and etching on its surface resulting from preferential dissolution of the glassy silicate matrix along the grain boundaries of Al-Fe oxide crystallite phases (P746959).

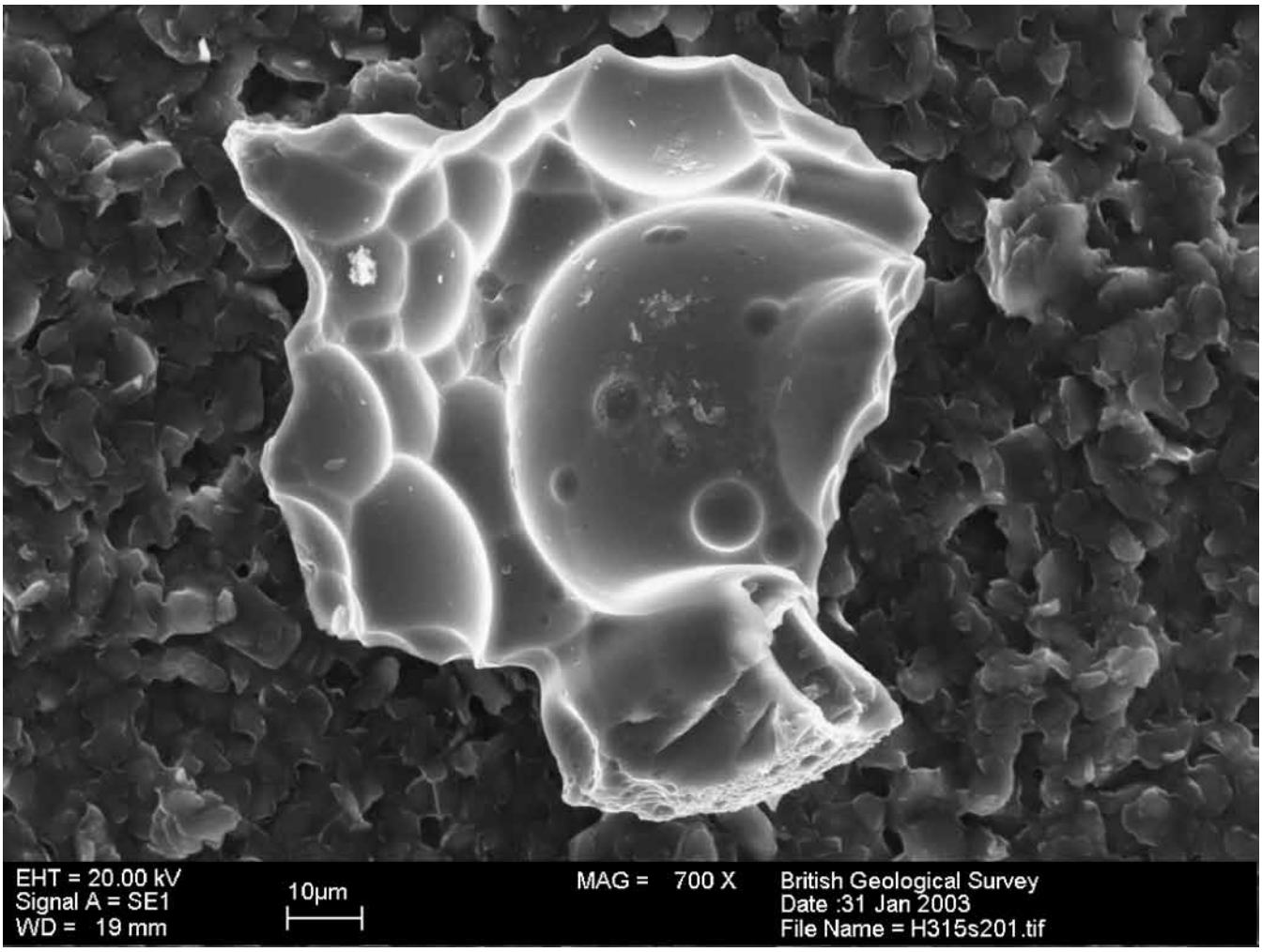

Plate 7.23 SEM image showing secondary spherulitic smectite-like alteration product growing on the surface of an altered glassy slag fragment. Site M101, 0–10 cm depth (P746960).

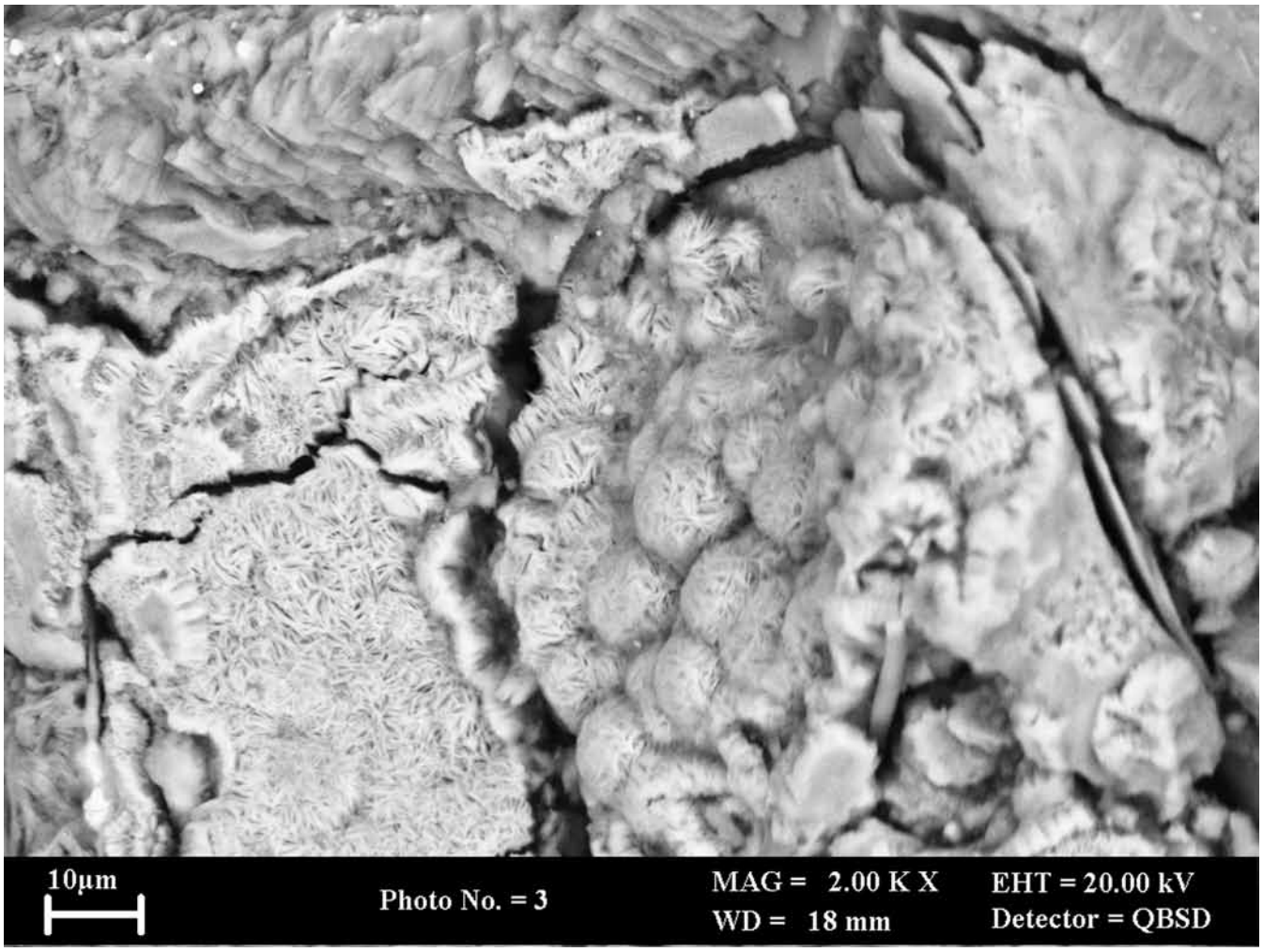

Plate 7.24 SEM image showing secondary spherulitic smectite-like alteration prodct growing on the surface of an altered glassy slag fragment. Site M101, 0–10 cm depth (P746961).

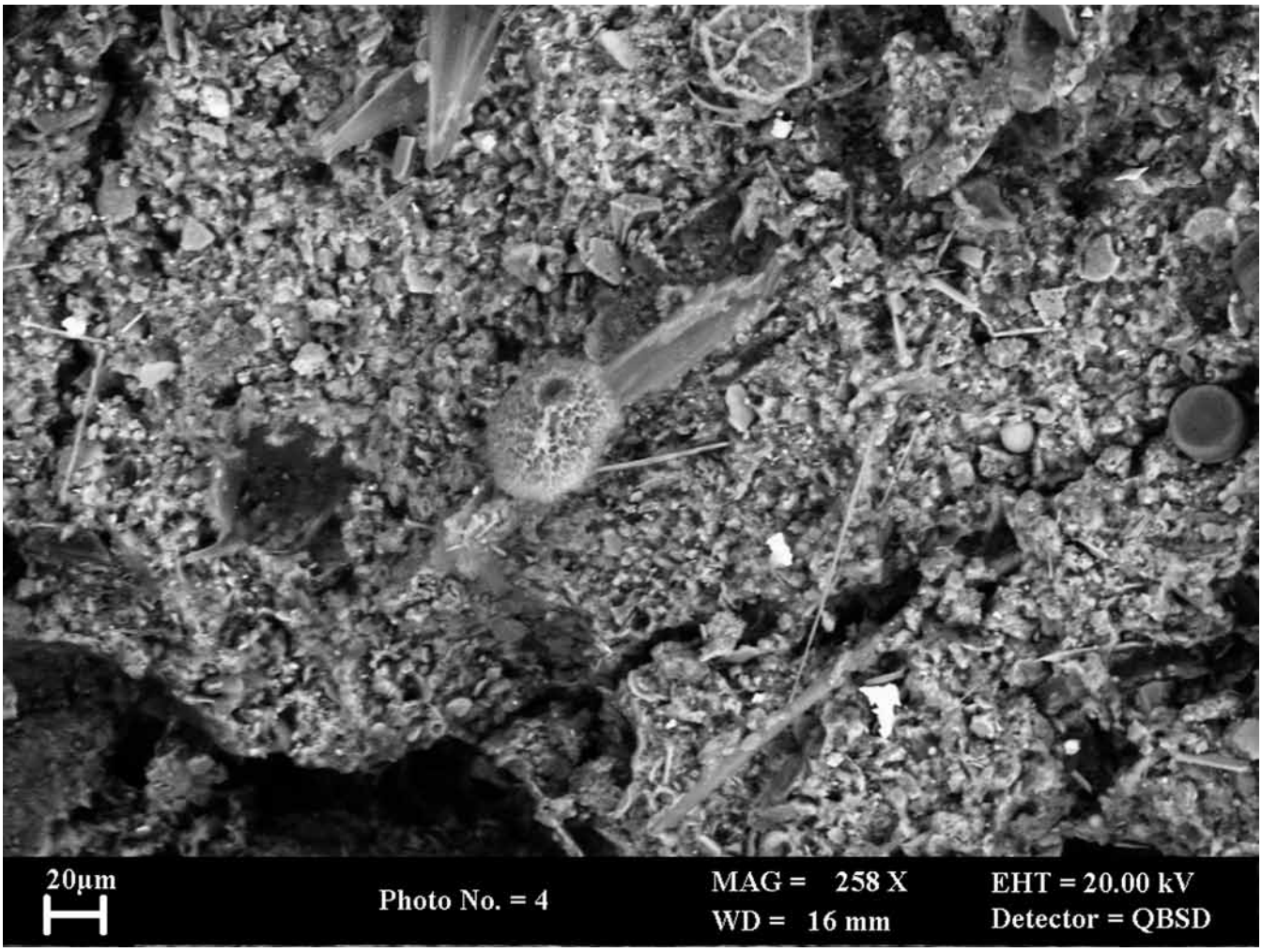

Plate 7.25 CryoSEM image of undisturbed sediment from Site M101 (0–10 cm depth), showing abundant presence of fibrous or asbestiform particles (P746962).